IFIS2016

Bringing Together Theory and Practice

PROCEEDINGS

13-17 June 2016

Belgrade, Serbia

aerodata

precision in special mission

AeroFIS®

Setting the Standard in Flight Inspection

Latest Technology, Advanced Features, Proven Integrity
and Extended Flexibility for Future Expansions.

Key Features:

- Proven Reliability and Availability all over the Globe
- Customized Solutions for Hardware and Software
- Simultaneous multiple Facility Calibration
- Special Features for Military and Civil Customers
- Standard FIS Capabilities plus:
  NPA, RNAV, RNP based on GNSS+DME/DME,
  SBAS/WAAS, GBAS/LAAS, ADS-B,
  Moving Facility Calibration, ...
- Minimum Training Effort
- Maximum Efficiency

Aerodata AG · Hermann-Blenk-Straße 34-36 · 38108 Braunschweig/Germany
Phone: +49 531/2359-0 · Fax: +49 531/2359-158 · E-Mail: mail@aerodata.de

www.aerodata.de

Contents

Session 1 – FIS and Aircraft Technology

Session 2 – Flight Inspection of ILS

Session 3 – Flight Inspection of VOR and SSR

Session 4 – FIS and Aircraft Technology

Session 5 – Flight Validation of ADS-B and Datalink

Session 6 – Safety Concepts and F.I. Organization Certification

Session 7 – PBN (SBAS / GBAS / RNP …)

Session 8 – RFI / EMI

Session 9 – Safety Concepts and F.I. Organization Certification

Session 10 – RFI / EMI

Session 11 – Flight Inspection Standards

Further Publications

IFIS2016

Bringing Together Theory and Practice

Session 1

FIS and Aircraft Technology

Why fabricate a flight inspection aircraft?

José Evânio Guedes Júnior
Flight Inspector Pilot
Department of Airspace Control
Rio de Janeiro, RJ, Brazil
Fax: +55 21 2101
E-mail: evaniojegj@decea.gov.br

ABSTRACT

Noticing that the wear and tear suffered after 13 years of operation, in comparison with same models of aircraft operating in commercial aviation, Brazil realized it would be feasible to invest in a specific platform for flight inspection. An aircraft specially developed for flight inspection would be designed for a reasonable working life considering factors such as the use of the engine at low altitude, structural load due to several go-arounds, particular flight cycle duration and beyond the average amount of landings.

In order to ensure acceptable minimum levels of availability, a flight inspection aircraft must fulfil performance and flying qualities requirements, which are applicable to its special mission. These aircrafts must be capable of, for instance, operating in long ranges, various flight and engine regimes for about 3 uninterrupted hours at low height, allow manoeuvrability in low speeds, operating on short runways and many others.

Reviewing criteria for determining Brazilian option for acquiring an aircraft specific developed for flight inspection, this paper will:

Summarize strategies for reducing cost and improving service of logistics and supply chain management through the study of the advantages of vertical integration of companies;

Present the benefits due to the validation process for certification of flight inspection system onboard, as a new and another type of aircraft.

INTRODUCTION

Do governments make remediable errors in the choice of products? Does the economy "lock-in" to these incorrect choices even when the knowledge that these choices are incorrect is readily available? A path dependence occurs when a minor or fleeting advantage or a seemingly inconsequential lead for some technology, product or standard can have important and irreversible influences on the ultimate market allocation of resources, even in a world characterized by voluntary decisions and individually maximizing behavior[1].

A decision to use a particular system onboard without certification might be a controlling influence for decades. But efficient decisions may not always appear to be efficient in retrospect. So assuming the inferiority of a chosen path is unknowable at the time a choice was made, there will be later acknowledge that some alternative path would have yielded greater wealth, generating costs to effect change and with strong influence on strategic planning.

After 13 years of operation with an independent onboard flight inspection system, Brazil realized it would be feasible to invest in a specific platform for flight inspection, combining the expertise of both manufacturers of the aircraft and the system of flight inspection. At time, the decision-making has been built based in some advantages in designing an aircraft for a reasonable working life considering factors such as the use of the engine at low altitude, structural load due to several go-arounds, particular flight cycle duration and beyond the average amount of landings.

In order to ensure acceptable minimum levels of availability, a flight inspection aircraft must fulfil performance and flying qualities requirements, which are applicable to its special mission. These aircrafts must be capable of, for instance, operating in long ranges, various flight and engine regimes for about 3 uninterrupted hours at low height, allow

[1] LIEBOWITZ, S. J. and MARGOLIS, Stephen E. 1990. "The Fable of the Keys", 22 Journal of Law and Economics.

manoeuvrability in low speeds, operating on short runways and many others.

This paper will summarize strategies for reducing cost and improving service of logistics and supply chain management, through the study of the advantages of vertical integration of companies. Pair of agents who have mutual interest in carrying out a transaction are brought together by a non-bargaining process, out of the market[2]. This reduces obstacles for Government partnership.

Then, in the second part, this article intends to present the validation process for certification of flight inspection system onboard reviewing its benefits.

GOVERNANCE STRUCTURE

A wide range of contractual and organizational phenomena are better understood from the governance structure[3]. There are four common reasons to integrate[4]: setup costs (barriers to entry or allowing price discrimination across customer segments), transaction costs (industry chain have more market power), transaction risks (market is too risky and unreliable) and coordination effectiveness (market is young and the company must forward integrate to develop a market, or the market is declining and independents are pulling out of adjacent stages).

The last one (which is a special case of vertical market failure) of these reasons gives support to the objective pursuit by Government: ensuring the quality of services provided to its citizens. As an essential activity, flight inspection cannot be vulnerable to exploitation by increasingly concentrated suppliers.

Consequently, when Government, as a retailer, decides to contract a new manufacturing business, the idea is get more control over the logistics involved in the operational field. Issues related to bidding procurement processes and any delay in the replacement of spare parts can be reduced through a single logistics support contract.

Besides, joint ventures and strategic alliances allow firms to exchange goods, services, information and expertise while maintaining a formal trade relationship[5]. Companies retain their corporate identities and maximize their potential mutual advantages. A single entity managing the distribution process also has more ability to optimize resource utilization and avoid wasted costs. Therefore, natural conflict in trade relationships can be minimized.

All of these strategies creates opportunities for the companies to distinguish themselves from competitors through effective marketing. The companies, pushing the competitors away from the market, might become stronger and capable to increase efficiency in the provision of public service, in exchange for a long-term contract, partially financed by the state, which is characteristic of large investments such as the acquisition of aircrafts.

Considering adopting a strategy or course of action to non-market channels of resource allocation, the decision-making for integrate or not is basically as below:

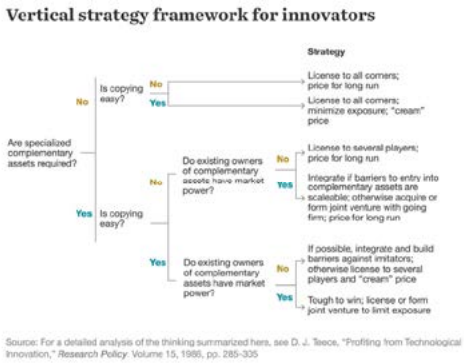

The primary message is: don't vertically integrate unless it is absolutely necessary to create or protect value. Notwithstanding, instruments available to the Government or any other nonmarket forces are scarce resources, so that all can be achieved is a "second-best"[6].

Logistics Supply Support Chain

A logistics supply support chain consists of a set of processes associated with the flow of spares, goods, information, and services. The general idea of logistics is to strategically manage the total flow of this assets. Logistics optimization, therefore, cannot be achieved only from the viewpoint of one firm. It requires total

[2] RUBINSTEIN, A. and and WOLINSKY, A. 1985. "Equilibrium in a market with sequential bargaining" Econometrica.

[3] WILLIAMSON, Oliver E. "Why law, economics, and organization?" UC Berkeley Public Law Research Paper 37 (2000).

[4] "Vertical integration" is simply a means of coordinating the different stages of an industry chain when bilateral trading is not beneficial.

[5] STUCKEY, J. and WHITE, D. "When and when not to vertically integrate". Sloan Management Review, Spring 1993, pp. 71–83.

[6] ARROW, Kenneth J. "The organization of economic activity: issues pertinent to the choice of market versus nonmarket allocation." The analysis and evaluation of public expenditure: the PPB system 1 (1969): 59-73.

optimization of the flow of assets across all firms in the support chain.

By eliminating the intermediate suppliers and profit streams, integration usually offers the lowest total. It also decreases the workload on the Government in terms of quality, purchasing, accounting and project management.

The central theory of economics remains the neoclassical theory, which imparts understanding about price system as resources allocator and a simple model of the business firm[7].

This business firm model structured within a relatively vertical chain characteristic of nonmarket is a didactical method to understand logistical needs of a Government activity that cannot be subject to discontinuities.

Costumers acquire services from companies to increase their expected utility[8], because everybody makes the best decisions by thinking at the margin[9]. Governments, despite of all its bureaucratic specific characteristics, inherent to the management of public affairs, does not act differently.

Thereby, economies of the ability to use large, expensive capital goods had been obvious explanations for the existence of the firm[10]. And the firm is more than a simple efficiency instrument, in the usual scale economies and least-cost factor proportions senses of the term, but also possesses coordinating potential that sometimes transcends that of the market[11].

In terms of logistics, technological indivisibilities have crucial importance, because the laboratory aircraft systems are developed to achieving the final activity, so that all major components are, in some way, linked to the flight inspection system. It is natural, for that reason, that any logistical support contract should be able to contemplate malfunctions solutions outdoors considering not only the aircraft cell components and engines, but as well as the flight inspection system.

A Single Contract: Reducing Transaction Costs

Bureaucracy associated to bidding procurement processes are justified, then, in terms of economies of scale when the average costs falls continually. Firms make decisions that form a part of the solution to the overall resource allocation problem[12].

It is about inputs and outputs and how they relate to the given technology, to each other, and to market forces. This constellation of assumptions and concerns is also focal.

Inside a single firm, there is islands of conscious power in an ocean of unconscious co-operation like lumps of butter coagulating in a pail of buttermilk[13]. Outside the firm, price movements direct production, which is coordinated through a series of exchange transactions on the market. Within a firm, these market transactions are eliminated and in place of the complicated market structure with exchange transactions is substituted the entrepreneur-coordinator, who directs production.

It is clear that these are alternative methods of coordinating production that may be worth Government to maximize its usefulness. The costs of negotiating and concluding separate contracts for each logistics transaction would be certainly more expensive and bureaucratically feasible.

By convention, transaction costs are divided into three general categories: search costs (finding someone with whom to engage in an exchange); bargaining and negotiation costs (concluding the terms of an exchange); and enforcement or monitoring costs (seeing if the terms are adhered to)[14].

But it may be desired to make a long-term contract for the fabrication and the supply of a flight inspection aircraft[15]. This was Brazilian choice. This is due to the fact that security and stability encourage the search for new ways of accomplishing tasks, promote learning and

[7] DEMSETZ, Harold. "The economics of the business firm: seven critical commentaries". Cambridge University Press, 1997, p. 1.

[8] ARROW, K. J. and DEBREU, Gerard. "Existence of an equilibrium for a competitive economy." Econometrica: Journal of the Econometric Society (1954): 265-290.

[9] MANKIW, N. Gregory. "Principles of Microeconomics, (2007).", p. 7.

[10] ULEN, Thomas S. "Coasean Firm in Law and Economics, The." J. Corp. L. 18 (1992), p. 302.

[11] WILLIAMSON, Oliver E. "The vertical integration of production: market failure considerations." The American Economic Review 61.2 (1971), p. 112.

[12] NORTH, Douglass C. “Institutions, institutional change and economic performance”. Cambridge university press, 1990, p. 30.

[13] COASE, Ronald H. "The nature of the firm." Economica 4.16 (1937), p. 388.

[14] ULEN, Thomas S. "Coasean Firm in Law and Economics, The." J. Corp. L. 18 (1992), p. 301.

[15] COASE, Ronald H. "The nature of the firm." economica 4.16 (1937), p. 391.

the exchange of information, and engender trust[16]. And trust is a remarkable efficient lubricant to economic exchange[17].

That is why it is possible to imagine an implicit conceptual frame which by transaction costs are positive in Government long terms contracts:

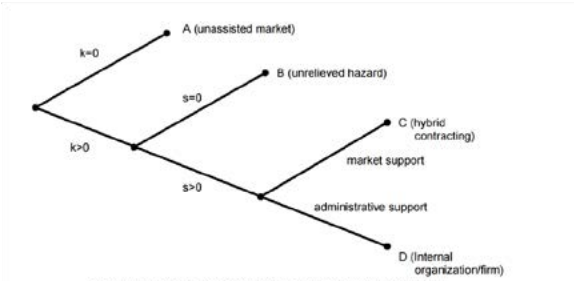

Source: see Williamson, Oliver E. "Transaction cost economics: An introduction."*Economics Discussion Paper 2007-3 (2007).*

Contractual phenomena can be interpreted as variations don a theme. Any issue that arises can be conceptualized as a contracting problem within economizing terms. The combination between semi-formal models and simple contractual schema forms the logic of the best type of contract.

Letting "k' be a measure of asset specificity, so as a Flight Inspection aircraft, the transactions tends to "D", where everything including logistic support chain ("s") is exchanged. In this case, the higher degrees of asset specificity and added uncertainty, the greater needs for cooperative adaptation. Such transactions give rise to bilateral dependencies, in that the parties have incentives to promote continuity.

Contracts concern the future, and therefore there is uncertainty[18]. Thus a long-term contract with the Government allows the entrepreneur to resolve contract disputes with greater autonomy, rather than resort to market trading, as it would be if the State need to deal with multiple suppliers.

The establishment of this autonomy, however, such as continuous monitoring of a governing body of an organization, implies in governance costs. It includes the mechanisms required to balance the powers of the members (with the associated accountability), and their primary duty of enhancing the prosperity and viability of the organization.

In summary, the governance mechanisms point to the abandonment of market rules the greater the specificity of assets, as in the case of manufacturing a laboratory aircraft. The governance cost has to be examined as a variation between the bureaucratic costs associated with the internalized production and the governance mode via market. Therefore, markets as a governance structure give way for hybrids and finally for hierarchies as the level of asset specificity increases as it is illustrated below:

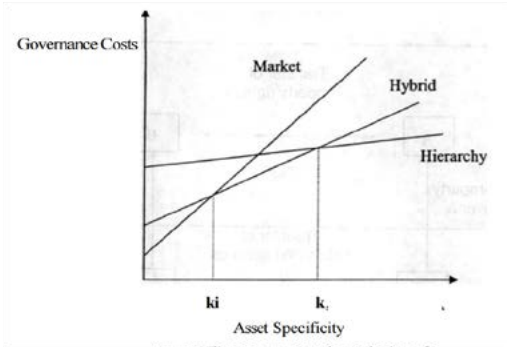

Source: Williamson, O.E. 1996. The Mechanisms of Governance. Oxford University Press. Oxford, p. 109

Although, to understand the existence of this type of governance costs it must be recognized that the hierarchy is a resource employed in a world where knowledge is incomplete and obtained at a high cost, exactly the case of flight inspection system.

Another great advantage of fabricate a flight inspection aircraft is certificate the final product according technical requirements and administrative procedures to ensure the airworthiness and environmental compatibility of parts and appliances, subjected to some specific regulation.

DESIGN AND PRODUCTION ORGANISATION CERTIFICATION

Certification organisms can provide the design and production organization certification and this process demonstrates means and capability to future development of further technologies in flight inspection.

This is because, establishing requirements to be accomplished and demonstrated, certification bodies require the company to follow standards for the implementation of common essential requirements in the field of airworthiness. These standards reflect the state of the art and the best practices, aiming to take into account worldwide aircraft experience and scientific and technical progress.

The need to ensure uniformity in the application of common airworthiness and environmental requirements for aeronautical products, parts and appliances requires that common procedures be followed by the competent authorities of the Government to assess compliance with these requirements. The authorities must develop certification specifications and guidance material to facilitate the necessary regulatory uniformity.

---

[16] POWELL, Walter. "Neither market nor hierarchy." The sociology of organizations: classic, contemporary, and critical readings 315 (2003), p. 304.

[17] ARROW, K. E. "The limits of organization." (1974).

[18] EISENBERG, Melvin Aron. "The limits of cognition and the limits of contract." Stanford Law Review (1995), p. 213.

Therefore, any company applying for a fabricate type-certificated Flight Inspection aircraft shall demonstrate its capability by holding a design organization approval, issued by the authorities.

A Flight Inspection aircraft

Aircraft certification is a critical process because it provides assurance in performing all aspects intended: form, fit, function, producibility, durability, safety and reliability. Structures design and analysis is substantiated by extensive testing. It is the process by which confidence and trust is gained for costumers expect and demand.

The materials and design features of any new or derivative airframe structure will generally be a mixture of existing proven elements and new features being used for the first time. It is essential to validate that the structure and its softwares will perform as intended.

To be considered a flight inspection aircraft some special conditions are required and the authorities shall prescribe special detailed technical specifications and name special conditions. A flight inspection aircraft has novel or unusual design features relative to the common design practices, airworthiness, and the intended use of this airplane is unconventional; unsafe conditions may develop during the flight.

These aircrafts must be capable of, for instance, operating in long ranges, various flight and engine regimes for about 3 uninterrupted hours at low height, allow manoeuvrability in low speeds, operating on short runways and many others.

The applicant shall perform all inspections and tests necessary to demonstrate compliance with the applicable type certification basis and environmental protection requirements. A supplemental type certificate shall include the descriptions and identification required by its special mission.

It must be demonstrated that the flight inspection aircraft meets the applicable certification specifications and accomplish the special mission which for it was designed, any airworthiness provisions not complied with are compensated for by factors that provide an equivalent level of safety and no feature or characteristic makes the product unsafe for the uses for which certification is requested.

The manufacturer of a flight inspection aircraft shall establish an approved production ground and flight test procedure and check-off forms, and in accordance with those forms, test the aircraft produced, as a means of establishing relevant aspects of compliance.

Each production test procedure shall include at least: 1. a check on handling qualities; 2. a check on flight performance (using normal aircraft instrumentation); 3. a check on the proper functioning of all aircraft equipment and systems; 4. a determination that all instruments are properly marked, and that all placards and required flight manuals are installed after flight test; 5. a check of the operational characteristics of the aircraft on the ground; 6. a check on any other items peculiar to the aircraft being tested[19].

Production Organization Approval

The procedure for the issuance of a production organization approval to demonstrate conformity of products, parts and appliances with the applicable design data should contain, with regard to general approval requirements, facilities, working conditions, equipment and tools, processes and associated materials, number and competence of staff, and general organization are adequate to discharge obligations[20].

With regard to certifying staff, authorized by the production organization to sign the documents issued under the scope or terms of approval, a manual shall specify the minimum knowledge, background, including other functions in the organization, and experience of the certifying staff to be appropriate to discharge their allocated responsibilities.

The approval has many benefits, such as perform independent production activities, enabling the development of future projects with the use of different platforms integrated with other flight inspection systems.

The basic principle of enhancing the level of safety of changed aeronautical products is to apply the latest certification specifications for significant design changes to the greatest extent practical. In certain cases, the cost of complying fully with a later certification specification may not be commensurate with the small safety benefit achieved.

These factors form the basis where compliance with the latest certification specification may be considered impractical, thereby allowing compliance with an earlier certification specification. Regardless of which method is used, the process should show that a proposed type- certification basis is able to achieve a positive safety benefit for the overall product.

The process for establishing the type-certification basis for a flight inspection aircraft is an exception proposed.

---

[19] EASA - Commission Regulation (EU) No 748/2012. Point 21.A.127

[20] "The management of regulatory responsibilities through the issuance and oversight of certificates (i.e., pilot, airworthiness, air carrier, repair station, production) has existed and been successful for decades. The concept of a design organization certificate has existed for at least two decades". FLORIO, Filippo De. "Airworthiness: an introduction to aircraft certification". Elsevier, 2010, p. 23.

The steps below present a streamlined approach for making classification whether the change is significant or not significant, and propose an appropriate type-certification basis.

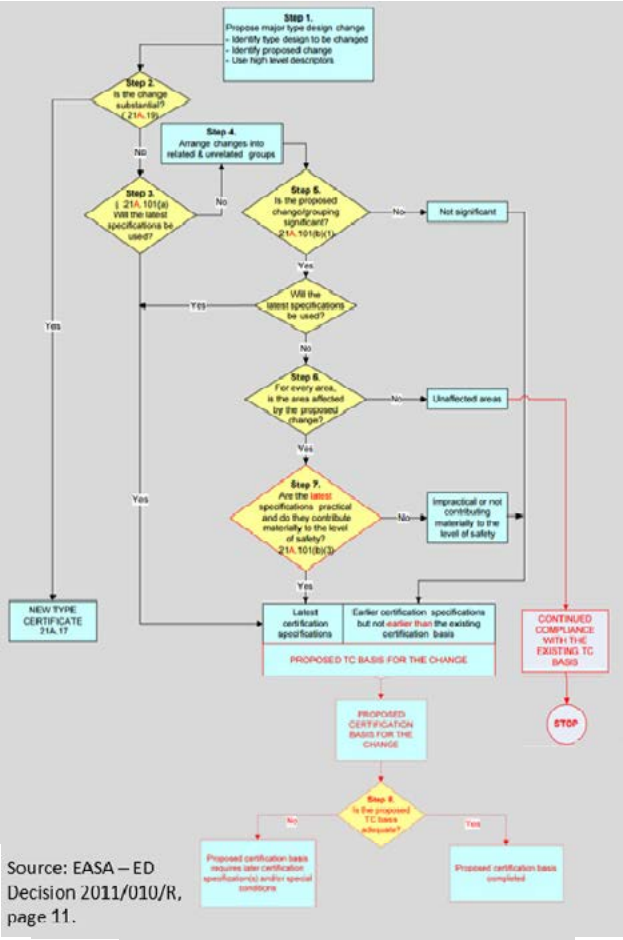

Source: EASA – ED Decision 2011/010/R, page 11.

In this regard, any method used should encourage incorporating safety enhancements that will have the most dramatic impact on the level of safety of the aircraft while considering effective use of resources. This is illustrated below.

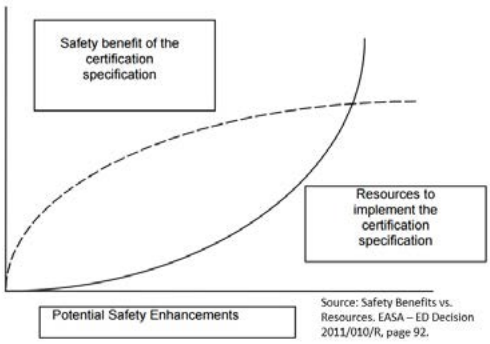

Source: Safety Benefits vs. Resources. EASA – ED Decision 2011/010/R, page 92.

CONCLUSIONS

In 2013 Brazil decided to make a partnership with industry to fabricate a specific platform for flight inspection. At time, the decision-making has been built based in some advantages in designing an aircraft for a reasonable working life considering factors such as the use of the engine at low altitude, structural load due to several go-arounds, particular flight cycle duration and beyond the average amount of landings.

Brazil's Government broke with path dependence for some technology of flight system onboard integration to the airplane basic platform. This was a bold decision considering it had never before been considered to manufacture an aircraft specially designed and certified to operate like a laboratory airplane, which implies obtaining a supplemental type certificate.

The option was made because of many strategies for decreasing cost and improving service of logistics and supply chain management, through the study of the advantages of vertical integration of companies. This reduces obstacles for Government partnership.

The idea was take more control over the logistics involved in the operational field. Issues related to bidding procurement processes and any delay in the replacement of spare parts can be reduced through a single logistics support contract. The costs of negotiating and concluding separate contracts for each logistics transaction would be certainly more expensive than in a one single long-term contact.

Security and stability encourage the search for new ways of accomplishing tasks without concerning about choice of market, promote learning and the exchange of information, and engender trust between companies and the State.

This article also presented the validation process for certification of flight inspection system onboard reviewing its benefits. In order to ensure acceptable minimum levels of availability, a flight inspection aircraft must fulfil performance and flying qualities requirements, which are applicable to its special mission.

These aircrafts must be capable of, for instance, operating in long ranges, various flight and engine regimes for about 3 uninterrupted hours at low height, allow manoeuvrability in low speeds, operating on short runways and many others.

Certificate the final product according to technical requirements and administrative procedures ensures the airworthiness and environmental compatibility of parts and appliances, subjected to some specific regulation. It demonstrates means and capability to future development of further technologies.

This is because, establishing requirements to be accomplished and demonstrated, certification bodies require the company to follow standards for the implementation of common essential requirements in the field of airworthiness.

DISCLAIMER

The views expressed in this paper are those of the author himself only. None of the statements contained in this paper represent an official policy statement of any organism or body of Brazil or any other country, neither reflects the opinion of any international organization.

FUTURE WORK

As has widely been discussed in this article, future studies may include the manufacture and certification of new flight inspection platforms. The manufacture of the first laboratory aircraft certainly has opened door for the certified integration of other basic models to known flight inspection systems. New partnerships between aircraft manufacturers and flight inspection systems makers can better exploit this opportunity.

REFERENCES

[1] ARROW, K. J. and DEBREU, Gerard. Existence of an equilibrium for a competitive economy. Econometrica: Journal of the Econometric Society (1954).

[2] ARROW, Kenneth J. The organization of economic activity: issues pertinent to the choice of market versus nonmarket allocation. The analysis and evaluation of public expenditure: the PPB system 1 (1969).

[3] ARROW, K. J. The limits of organization. (1974).

[4] COASE, Ronald H. The nature of the firm. Economica 4.16 (1937).

[5] DEMSETZ, Harold. The economics of the business firm: seven critical commentaries. Cambridge University Press (1997).

[6] EASA - Commission ED Decision 2011/010/R.

[7] EASA - Commission Regulation (EU) No 748/2012.

[8] EISENBERG, Melvin Aron. The limits of cognition and the limits of contract. Stanford Law Review (1995), p. 213.

[9] FLORIO, Filippo De. Airworthiness: an introduction to aircraft certification. Elsevier, 2010.

[10] LIEBOWITZ, S. J. and MARGOLIS, Stephen E. The Fable of the Keys, 22 Journal of Law and Economics (1990).

[11] MANKIW, N. Gregory. Principles of Microeconomics. (2007).

[12] NORTH, Douglass C. Institutions, institutional change and economic performance. Cambridge University Press (1990).

[13] POWELL, Walter. Neither market nor hierarchy. The sociology of organizations: classic, contemporary, and critical readings (2003).

[14] RUBINSTEIN, A. and and WOLINSKY, A. Equilibrium in a market with sequential bargaining. Econometrica (1985).

[15] STUCKEY, J. and WHITE, D. When and when not to vertically integrate. Sloan Management Review (Spring 1993).

[16] TEECE, D. J. Profiting from Technological Innovation. Research Policy, V. 15 (1986).

[17] ULEN, Thomas S. Coasean Firm in Law and Economics, The. J. Corp. L. 18 (1992).

[18] WILLIAMSON, Oliver E. The vertical integration of production: market failure considerations. The American Economic Review 61.2 (1971).

[19] WILLIAMSON, Oliver E. The vertical integration of production: market failure considerations. The American Economic Review 61.2 (1971).

[20] WILLIAMSON, Oliver E. The Mechanisms of Governance. Oxford University Press. Oxford (1996).

[21] WILLIAMSON, Oliver E. Transition costs: An introduction. UC Berkeley Public Law Research Paper 37 (2000). Economics Discussion Paper (2007).

19th International Flight Inspection Symposium (IFIS), Belgrade, Serbia, June 13-17, 2016

Evaluation of the Suitability of Unmanned Aircraft Systems for Flight Inspection

Mark E. Whittington
Aerospace Engineer
Federal Aviation Administration
Flight Inspection Services
Oklahoma City, Oklahoma, United States
Ph.: +1 405 954 5353
Cell: 1 405-640-8531
Email: mark.e.whittington@faa.gov
Email: markeng101@cox.net

ABSTRACT

This paper is presented as a comprehensive evaluation and discussion of the suitability and associated unique issues with the use of Unmanned Aircraft Systems (UAS) for Flight Inspection (FI). The primary objective of this paper is to stimulate industry interest in the development of this technology for FI. Included is a discussion of the requirements and challenges. This paper also presents potentially innovative means by which to meet FI requirements and to mitigate the associated challenges through the utilization of commercial off-the-shelf (COTS) technologies for UAS FI system development. The research for this paper finds UAS technology has significant potential to become a powerful tool for FI research and use as a FI vehicle.

INTRODUCTION

In recent years the technology of Unmanned Aircraft Systems (UAS) has expanded rapidly. This new and revolutionary technology has profoundly impacted both the military and civilian aerospace communities. This paper examines UAS technologies for the benefits they may provide and the suitability they may have for Flight Inspection (FI). In this paper an applied systems and requirements analysis of FI UAS suitability is presented. In order for UAS to be suitable for flight inspection, it must add value in one or more of the following areas; navigational aid signal measurement and accuracy, flyability, and certification. The desired end result of any value added would be an increase in safety and reduction in FI cost.

UNMANNED AIRCRAFT SYSTEMS TECHNOLOGY

The rapid advancement in UAS technology has been primarily driven by military applications resulting in rapid technological development in the areas of UAS airframes, miniaturization of electronics and communications systems and most recently in the field of UAS autonomy. Military missions are focused on tracking and destroying targets, and to a lesser extent on remote sensing. It is the remote sensing aspect of UAS development that has direct application to FI.

UAS Airframes

Numerous commercially produced unmanned aircraft airframe platforms have been developed for the military. These platforms have been produced in large numbers and fully field tested under harsh real world operational conditions. From these real world operations, advancements have been made in both technology and operational techniques. In anticipation of civilian applications, UAS platforms are being designed with FAA airworthiness certifications for civilian applications [1]. UAS manufacturers are now actively seeking mission package developer partnerships.

Market research finds numerous airframes which have been developed that consist of fixed wing, rotor and tilt rotor designs. The payload capabilities of the various UAS airframes are 10s of lbs. up to 3,000 lbs. The operational range of these airframes is 100s of miles to over 10,000 miles. The cost of these commercially available UAS airframes range from less than 100 thousand USD to over 100 million USD.

Note: Even with the recent increases in battery efficiency, hydrocarbon fuels have sixty times more energy density than batteries. The physical implication of this is a battery must be sixty times the size of a hydrocarbon fuel tank to have the same energy. For this reason only hydrocarbon fueled UAS platforms are considered in this paper.

Figure 1 is a picture of a commercially developed tilt rotor UAS system with a payload capacity of 200 plus lbs., airspeed of 200 plus knots, a maximum altitude of 20,000 ft. and an endurance of 8 hours [2].

Tilt Rotor UAS
Figure 1.

Miniaturization of Electronics

UAS technology advancements have resulted in the development of commercial off–the-shelf (COTS) miniaturization of airborne electronics, such as ruggedized airborne computers, autopilots and airborne sensors. Similar advances have been made in satellite and ground linked communications systems and their associated antennas. An industry product search finds; satellite and ground linked communication systems are now as small as 34 in^3 weighing only 1.7 lbs. (0.77 kg) and Ku satellite antennas have been developed which will fit in a 6.2 in. diameter radome and weigh less than 8 lbs. In addition, miniaturized conformal antenna systems are now available. Inertial Navigation System/Global Positioning System (INS/GPS) flight control systems as small as 95 in^3 and weighing less than 2.2 lbs. (1.0 kg) are now available. Numerous ruggedized computers and data loggers as small as 100 in^3 and weight as little as 3.5 lbs. (1.6 kg) are also available. Each of these products is small enough to fit in one hand. Also found are Light Detection and Ranging (LIDAR) systems weighing as little as 5.35 lbs. (19 kg). Figure 2 is a diagram of an example system, illustrating the component configuration of a FI UAS utilizing the Mission Module concept.

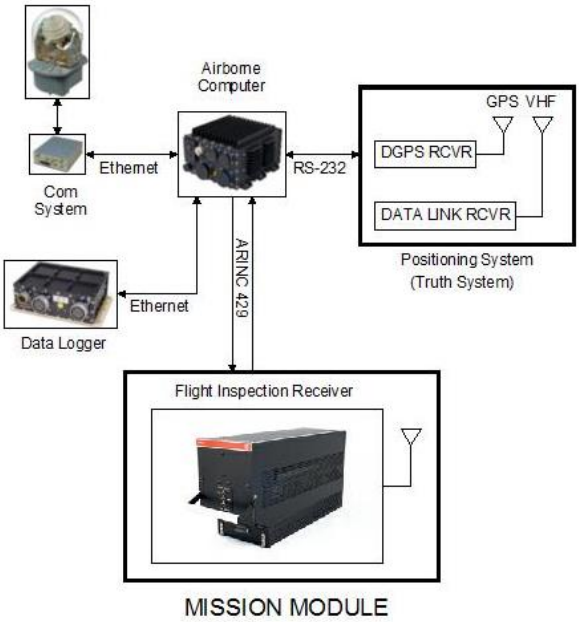

FI UAS System Diagram
Figure 2.

UAS Autonomy

Military UAS platforms have historically been remotely controlled by teams of operators as large as 9 people [3]. This remote control operational approach has diminished due to evolving operational techniques and the development of vehicle health monitoring capabilities. The development of fully autonomous flight and sensor controls has been developed to increased UAS survivability. This autonomous capability includes auto takeoff and landing, as well as autonomous mission flight path and sensor control. An industry product search finds COTS software for mission planning of autonomous flight and sensor payload control. UAS autonomous Airborne Sense and Avoid technology has been developed by industry and flight tested by the National Aeronautics and Space Administration (NASA) [4].

UAS FLIGHT INSPECTION SUITABLITY

FI Requirements

In order for UAS to be suitable for FI applications, the capabilities offered by this technology must be adapted to the requirements of FI. The previously mentioned range of UAS flight platform options and their capabilities have to be matched to the complex requirements of FI Navigational Aid (NavAid) measurement, flyability and certification. The Federal Aviation Administration (FAA) Flight Inspection Services Group is currently responsible for the certification of over 34,000 ground and space based instrument flight procedures supporting the National Aerospace System (NAS). These procedures are certified with 15,000 flight inspections annually. Approaches are inspected every 540 days. Facilities are

found "out of tolerance" on approximately 5 percent of periodic flight inspection missions and as few as 30 facilities are commissioned each year. The results of these FI missions are provided to the FAA Aeronautical Information Services (AIS).

The current flight inspections are accomplished by jet and turboprop powered fixed wing aircraft, which perform numerous complex maneuvers while capturing and verifying the signal integrity of the NavAids within each facility's service volume. These aircraft carry in excess of 600 lbs. of avionic sensors and equipment, making possible the certification of nearly any NavAid in the NAS [5]. This process also requires verification of the flyability of the facilities. The flyability aspect of this mission is highly dependent on flight crew visuals and communication interaction with the facility being certified.

UAS Technical Suitability

The above requirements are truly formidable for any FI UAS with the processes and procedures now utilized by traditional fixed wing FI aircraft. The challenge is to find areas where UAS can add value.

First, it is important to recognize that virtually all of the FI aircraft profiles now flown are a series of race track patterns, straight lines, arcs or orbits in the sky at the precisely located facility being measured. Therefore these flight profiles are in fact programmable. The current straight line or arcing flight paths are due to the flight path limitation of fixed wing aircraft. A rotor or tilt rotor UAS possesses the added capability of both vertical ascent and decent flight paths. These added capabilities make possible more precise 3-dimensional service volume mapping of the signals in space surrounding a facility or service volume, also known as "Service Volume Mapping". Service volume mapping will provide a more accurate picture of the signal accuracy and integrity for each facility and will also aid in identification of signal discrepancies due to environmental issues associated with a facility's unique terrain or architectural construction. Environmental issues associated with topographical sloping or mountainous terrain, water, or even mineral content in the soil are contributors to signal discrepancies. Next it is important to evaluate the current practice and efficiency of transporting all of the equipment necessary to measure and analyze every type of NavAid. Utilizing a "Mission Module" concept which would carry only the systems needed for the FI or facility task being performed would profoundly reduce UAS FI system weight. Taking advantage of existing data link technology to perform FI data analysis on the ground removes the need for the on-board equipment used for human interface and data analysis.

This Mission Module concept, coupled with a data link, would reduce the current payload requirement, which is in excess of 600 lbs. to approximately 50 lbs. A review of current individual navigation receiver systems and associated antennas finds all to be 25 lbs. or less. The currently utilized Global Navigation Satellite System/Differential Global Positioning System (GNSS/DGPS) "Truth System" weight is approximately 11 lbs. [6]. A direct line of sight S-band and/or satellite link communications system weight is approximately 2.5 to 10 lbs. respectively. An airborne ruggedized computer and data logger weighs in at 4 and 3.5 lbs. respectively. The mission specific navigation receiver and antennas could be installed in a rapid change Mission Module. All equipment utilized for analysis would remain on the ground at the other end of the data link for inflight or post flight analysis.

Taking full advantage of the Mission Module concept and data link technology drastically reduces the size and cost for a UAS FI system. The class of UAS required to support a FI mission would cost 3 to 8 million USD, much less than has been spent for a fully equipped manned FI jet aircraft. Discussions with academia and an industry market survey have found a number of suitable research and development UAS platforms. UAS platforms suitable for test and validation of UAS FI technologies would cost less than 100 thousand USD.

UAS FI MISSION DISCUSSION

The technical options of programmability, increased maneuverability, 3-Dimensional Service Volume Mapping and Mission Module capabilities, creates a number of suitable value-added FI mission opportunities for FI UAS. It is important to note that UAS technology is not dependent on eye sight for navigation and therefore is not limited to visual flight rules of daylight or clear weather operation. UAS are capable of flight under conditions when airports are at minimum operations such as late at night or closed due to fog. A segmented and phased approach to integrating UAS technology and its capabilities reduces risk and simplifies operational adaptation. While operating as a highly maneuverable remote sensor, a FI UAS could initially perform the missions identified below.

Facility NavAid Measurement

UAS with Mission Modules consisting of existing FI mission specific navigation receivers, such as the RNA-34BF VOR, ILS and Glideslope receiver, could fly pre-programmed flight paths to capture navigational aid signals in space for any given facility. Data would be captured and or downlinked for real-time or post mission evaluation of the facility's signal integrity. This capability could be utilized by Technical Operations facility maintainers to validate signal integrity following facility maintenance. This capability would represent a vast technical improvement for facility maintainers over the current use of hand held Portable ILS Receivers. FI UAS with these same navigation receiver Mission Modules could be programmed to fly monitor checks to validate a

facility's alarm system. The reduction in the need for standard FI aircraft facility monitor checks would reduce facility disruptions. The results of these interim inspections could be evaluated by FI personnel and fed into the FAA AIS to verify and monitor facility NavAid health. This added data would make possible a "Data Driven" FI dispatch and reliability system. This concept of "Data Driven Inspection" creates an "inspect as necessary" utilization of fully equipped FI aircraft. The potential increases in efficiency could very well reduce the cost of flight inspection and make possible more frequent inspections in the NAS and in countries which now cannot afford periodic FI.

Facility NavAid Service Volume Mapping

The same mission modules used for standard approach NavAid measurement could be employed in developing precision 3-dimensional service volume signal in space mapping of a facility. UAS can precisely fly the boundaries of the service volume for each facility. With this 3-dimensional model, signal anomalies associated with a facility due to NavAid adjustment, terrain, and architecture can be mapped. This modeling would make possible "Precision Commissioning Measurement". All future fixed wing FI aircraft and FI readings could be compared with this base line data.

Facility NavAid Signal Integrity Field Strength Measurement

Utilization of multiple FI UAS vehicles, equipped with a navigational receiver to take measurements at the same time in a series of precise locations within a service volume could provide valuable results. This time stamped multi point signal power density data could be mapped to perform field strength measurement analysis for a facility service volume.

Facility NavAid Signal Uncertainty Measurement

UAS could be utilized to perform repeated measurements at preprogrammed locations within a NavAid facility to build databases for statistical uncertainty measurements. This data would be helpful in building correction algorithms for fixed wing FI signal measurement systems. This type of repeatable precision measurement is not possible with fixed wing aircraft.

Airport LIDAR Mapping

A FI UAS system equipped with a LIDAR Mission Module could provide LIDAR surveys of airport facilities. The periodic comparison of these high precision digital 3-dimensional maps could be used to detect airport obstructions such as new building or tower construction and vegetation. The digital database from these surveys would aid in the development of precise simulator models for facility flyability verification. See Figure 3 for a LIDAR image of an airport [7].

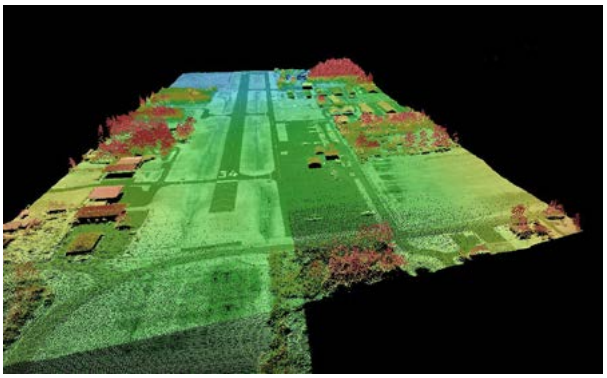

Airport LIDAR Map
Figure 3.

Commercial UAS Procedure Approval

The overwhelming pressure to permit the use of UAS by commercial operators in the NAS will soon result in a whole host of commercial applications. Each of these UAS applications will require the development and approval of flight procedures for their use. It is not practical to validate these procedures with traditional fixed wing FI aircraft. The use of FI UAS with GNSS coverage measurement capability will be required to certify the validity of these new procedures for UAS NAS integration. This "Pathfinder FI Mission" is a near term added responsibility for the FI community. It also represents potential for a significant growth market in the FI community.

UAS FI INFRASTRUCTURE INTERFACE

A significant challenge for UAS FI is how best to interface such a system with the existing FI infrastructure. At present FI is conducted by fixed wing aircraft which are dispatched to facilities in support of facility personnel needing FI assistance in a commissioning or periodic certification. The first question is whether the FI UAS would be transported to facilities where its services are needed or stationed in close proximity to be used for periodic maintenance and inspection support. The next question is would the UAS be operated by the facility's NavAid maintenance personnel or by the current FI operations organization? Workload and proximity of adjacent facilities as well as UAS airframe capabilities will dictate the best deployment method for UAS FI vehicles. The best method for operational control of these systems will be driven by the level of autonomous capability of the UAS FI system.

As previously discussed the results of any UAS FI procedure performed would be input to the FAA AIS data base for evaluation. This data would be used to determine the need for FI checks to be performed by fully equipped aircraft. An ideal scenario is for relatively low cost and highly autonomous UAS FI systems to be located at or near facilities to help maintain the service volume. It can also be argued that ground transporting regionally located UAS flight inspection systems is more cost effective than

dispatching a large jet to a facility. The benefit would be more frequent checks of the NavAid service volume and reduced workload for fixed wing FI aircraft. Increased verification of NavAid signal integrity is correlated directly to flight safety. The economic benefit of FI UAS is highly dependent on the procedures and policies developed to best implement available UAS FI technologies. The final answer to each of these, and many more questions, will be dictated by the actual level of value added to FI by FI UAS.

UAS FI CHALLENGES

In order for UAS to be utilized in a beneficial way as a flight inspection tool, a number of challenges will need to be addressed. The least of these challenges is technical. FI policy and procedures will require change to take full advantage of the added capabilities UAS technology offers. At present, the greatest challenge is regulatory policy for UAS operation in the NAS.

UAS FI Technical Challenges

In discussions presented previously in this paper, it is clear that many of the technical challenges associated with UAS systems have been addressed by the maturity of this technology. The scope and scale of the integration effort for FI avionics can be mitigated through the use of the FI Mission Module concept. The greatest technical challenge for utilizing UAS for FI is programming the flight paths for each NavAid measurement procedure. Flight path programming will dictate the level of autonomy with which these vehicles can be operated. The normal challenges of Airframe and FI system integration such as antenna location and propeller modulation will impact UAS airframe selection. But once again the Mission Module concept minimizes the number of antennas installed on the UAS and reduces the size and cost of the vehicle required.

UAS FI Flyability

Certifying the Flyability of a facility represents a significant challenge for UAS FI systems. However these issues can be to some degree addressed through the comparative analysis of the precision facility mapping obtained with a FI UAS LIDAR Mission Module. Going further, combining precision LIDAR facility mapping and FI data coupled with flight simulation techniques may meet the flyability requirement.

FI UAS Policy and Procedure

The utilization of UAS systems for use in FI will change current NavAid facility signal measurement and certification procedures. Initially FI UAS technology may aid in research and development of more accurate and economic FI systems. If technical and economic advantages for the use of UAS technology are operationally developed and demonstrated, FI policy and procedure changes will be required to fully integrate FI UAS as tool for FI.

UAS NAS Integration

At present a significant obstacle in utilizing UAS technology for FI are the FAA regulatory restrictions for operation of UAS in the NAS. The pressure from industry to take full advantage of UAS technology commercially is overwhelming. The technical concerns associated with operation of unmanned aircraft are steadily being addressed by industry. For example, industry has recently developed and has flight tested Sense and Avoid technologies which give UAS flight platforms the ability to autonomously avoid other aircraft. The FAA has a mandate to develop regulations, policies, procedures, guidance material, and training requirements for UAS operations in the NAS [8]. Industry and the FAA are working with the Radio Technical Commission for Aeronautics (RTCA) special committee SC-228 to develop Minimum Operational Performance Standards for UAS. Similar efforts are under way with the American Society of Testing and Materials (ASTM). ASTM Committee F38 is addressing issues related to design, performance, quality acceptance tests, and safety monitoring for unmanned air vehicle systems. The European Organization for Civil Aviation Equipment (EUROCAE) is on a similar path with Working Group 73 to facilitate the insertion of UAS in all classes of airspace. In the United States UAS are required to obtain Airworthiness certificates under Federal Airworthiness Certification Standard (FAR) Part 23, Subpart D. However, without a flight crew and interior related design considerations, notable portions of the FAR Subpart D requirement do not apply. The use of FAR 21.17B, which permits an equivalent level of safety, reduces irrelevant certification burdens. The pending "Consensus Standards" changes to FAR 23 promoting innovation, rapid change and implementation of technology, are expected to further simplify UAS certification. At present there are 14 applications to the FAA for UAS Type Certification in the United States. Clearly it is not a question of if UAS will integrate with airspace, but when this will occur.

CONCLUSIONS

In review of the topics discussed in this paper it can be concluded that UAS technology may very well offer a paradigm shift in flight inspection. At a minimum the added maneuverability and repeatability for positioning accuracy with UAS within NavAid service volumes will be a beneficial tool for signal measurement accuracy and 3-dimensional modeling. The programmability and potential for autonomous signal capture and measurement may revolutionize FI through improvements in efficiency and economy. The economic benefits if realized will make possible increased FI. It can be argued that increased FI correlates directly to added safety of those served by the NAS.

RECOMMENDATIONS

FI has the disadvantage of being highly technical, yet controlled by complex international regulations. Therefore a staged and incremental approach to verifying and implementing the benefits of UAS technology is necessary. Fortunately the technology of UAS is reasonably mature and many COTS options exist. Forward thinking Academic institutions have recognized the long term paradigm shift UAS technology represents. These institutions have developed advanced curriculums which are researching and developing advanced technologies in this field. Industry is already capitalizing to the tune of many billions of USD on UAS technology. Industry has produced technologies and systems which are waiting for sensor package developers. With these facts in hand, the question now is how best to proceed with FI UAS integration, development and implementation.

The first recommendation is to partner with academia and industry. These partnerships can assist in development of processes and procedures applicable to FI and UAS integration and provide assistance in validation of these processes and procedures. Areas of interest include but are not limited to:

1. Further research and identify suitable UAS FI mission opportunities.
2. Identify and recommend FI procedures changes necessary to implement UAS FI.
3. Study the FI mission impact and economics of the various FI UAS deployment options.
4. Research and validate UAS flight path precision capability.
5. Development of FI UAS programmable flight path models.
6. Evaluate signal in space data mapping software.
7. Develop or locate image sensors for Precision Approach Path Indicator Mission Module.
8. Development of a FI UAS Radio Frequency Interference (RFI) Mission Module.
9. Development or selection of a UAS platform to perform proof of concept testing and validation.
10. Identification of suitable Airframes for FI UAS.

ACKNOWLEDGMENTS

The following individuals shared their expertise and made innovative contributions to the development of this paper:

James Field
James Wilson
Dewayne McMurtrey
Samuel Colasanti

REFERENCES

[1] General Atomics Aeronautical, http://www.ga-asi.com/certifiable-predator-b

[2] Textron Industries, Bell Helicopter

[3] Aviation Week, 12-25 October 2015, Eyes Wide Shut, commentary.

[4] NASA, 23 June 2015, http://www.nasa.gov/press-release/nasa-partners-test-unmanned-aircraft-systems

[5] FAA Flight Inspection Services Maintenance and Engineering Group, Engineering Order 06-28-16, 24 November 2015.

[6] FAA Flight Inspection Services Maintenance and Engineering Group, Engineering Order 03-07-16, 27 September 2016.

[7] Global Navigation Sciences, http://www.globalnavigationsciences.com/services.html

[8] U.S. Department of Transportation, Federal Aviation Administration, Integration of Civil Unmanned Aircraft Systems (UAS) in the National Airspace System (NAS) Roadmap, First Edition-2013.

A Robust Runway Zebra Crossing Detection Algorithm in Visual-based Flight Inspection System

Xiaoyan. Luo
Dr.
Beihang University
Beijing, China
Fax: +86 10 82339078-8058
E-mail: luoxy@buaa.edu.cn

Xiaofeng. Shi
Associate Professor.
Beihang University
Beijing, China
&
University of Saskatchewan
Saskatoon, Canada
Fax: +86 10 82338906
E-mail: shixiaofeng@buaa.edu.cn

Liangyu. Zhou
Beihang University
Beijing, China
E-mail: 2650003512@qq.com

ABSTRACT

Visual-based navigation system is a main development direction for the low altitude flight since the optical sensors are common equipments on the aircrafts. The visual information from airborne cameras can provide additionally intuitive details, which can aid the flight inspection system to make it more convincible and accurate.

In order to accurately locate aircraft, the robust runway zebra crossing detection is very important. However, the object detection from aerial images is known as one of the most difficult problems due to the low-quality images and complex scenes. The general steps have 1). Enhance the low-quality images based on some shudder or imaging parameter assumptions. 2). Define the object properties in terms of visual views. The first step could lead to important information loss, and the second step cannot make sense in different conditions.

In this paper, we investigate how to design a robust runway zebra crossing detection algorithm for flight inspection system. The detection algorithm can handle the imaging divergence under different inspection conditions such as insufficient light at night or different airport conditions. Considering that only the low-rank property of zebra crossing is kept always, the patch comparison is through the image sequences. From the similar patches, the low-rank matrix is constructed via some matrix representation methods. The low-rank matrix can be viewed as basic image feature, which can be used to detect the Runway zebra crossing characteristics. Finally, the runway zebra crossings information can generate the location of plane. The simulation results demonstrate that the proposed detection algorithm can play an effective performance to get the plane information in the flight inspection system.

INTRODUCTION

In traditional flight inspection system, we calculate the location coordinates of the aircraft via Global Positioning System (GPS). As we know, the positioning accuracy is limited if there is no differential GPS (DGPS) station. Unfortunately, the DGPS instruments are not installed in or near the most common airports. In fact, we usually require temporary artificial installation of DGPS to finish the verification. However, this will

cause a demand for the workers in airport, which is difficult for the airports in highlands. In addition, the performance of DGPS could be distorted by many factors such as the ground radio signals in airport and the effects of the ionosphere.

Considering the advantages of optical sensors (i.e. common equipment with low weight and power consumption), the visual orientation from optical videos is relatively popular [1-2]. Based on the onboard cameras without other additional hardware, the visual system not only has the ability to avoid obstacles [3], but also obtains the accurate location information [4]. Inspired by this, we investigate how to perform the flight inspection task aided by the visual sensors. In visual-based flight system, it is an important step to detect the runway zebra crossing, which can be used to guide the location of aircraft.

Therefore, in this paper, we focus on automatically detect the position of runway zebra crossing, which can mark the time to trigger the calculation of positioning. The significance of this method is to avoid the operating requirement for pilot in previous mode, and then improve the timeliness of the system and reduce the risk of flight safety.

OUR PROPOSED METHOD

To analyze the feasibility of visual-based flight inspection, detecting the runway zebra crossing area from the front-view camera is a good start point. In this paper, we aim to detect the runway zebra crossing from the video captured by the Gulfstream 450 airplane, which has an enhanced vision system with front-view camera, rear-view and top-front-view three cameras. In our proposed method, we combine the analyses on image and low rank property on video to detect zero crossing area. The flow is shown in Figure 1. The detail parts will be described in the following subsections.

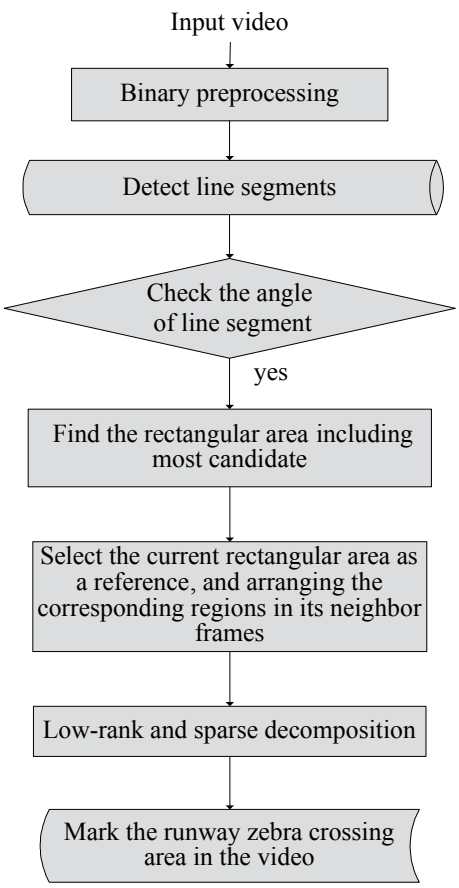

Figure 1. The Flow of Our Algorithm

Binary Preprocessing

Since the runway area is constructed by some cement material, it holds lighter reflective property than the surrounding lawn. We can simply generate a binary image for the current video frame to find the airplane whether the airplane has been in viewable area for runway. Given one frame image I, its output binary image B is based on comparison between its luminance and one threshold. For the greater pixels, the value are replaced by 1(white), otherwise the values are set as 0 (black), which can be formed as the following.

$$B(i,j)=\begin{cases}1, I(i,j)>255\cdot\alpha \\ 0, others\end{cases} \quad (1)$$

where (i, j) means one pixel position and α denote the luminance factor which is between 0 and 1.

(a) The input image at video frame 924

(b) The Binary image

Figure 2. The Binary Image of Video Frame.

Figure 2 gives an example with luminance factor $\alpha = 0.55$, which can obviously distinguish the runway area from the surroundings. For the runway area, the

light pixels are dense. Therefore, we can select these dense light regions as runway area, where the zebra crossing could exist.

Line Segment Detection

Considering the edge characteristic of runway zebra crossing, we utilize line segment extraction as one preprocessing step. Line segment detection is a basic step for many object detection applications. Therefore, there are many line detection methods have been proposed. Recently, von Gioi et al. developed a linear-time Line Segment Detector (LSD), which includes three steps: search line-support regions from pixels, approximate line segment for each line-support region, and validate line segment based on the number of false alarms [5].

Generally, the aircraft flies along the center axial of the runway, so the zebra crossing also extends according to the axial direction of the aircraft, i.e. the imaging vertical centerline of the front-view camera. Therefore, based on the angle of the line segment, we can pick up the potential edges of zebra crossing.

For one line segment, its two endpoints are denoted as (i_1, j_1) and (i_2, j_2) in coordinates. Then its angle can be calculated as

$$\theta = \arctan\left(\left|\frac{j_2 - j_1}{i_2 - i_1}\right|\right) \tag{2}$$

which is in $[0,\ 90°]$. The larger the value is, the more the line segment is in vertical direction. If we set $35°$ as a threshold, the potential zebra crossing can be pick out when $\theta \geq 35°$. To handle the potential candidates, we use a rectangular to box them.

Taking the video frame 960 as an example, the line segment detection, the angle filtering result, and the boxed rectangular are seen in Figure 3.

Low-rank and Sparse Decomposition

From Figure 2, we can observe that the aircraft wheels are in the field of front-view camera. It can cause some difficulty to detect the whole zebra crossing. Therefore, the parallel characteristic of zebra crossing edges will expire in the blocked area of wheels. On the other hand, the perspective view is not always effective to capture clear edges like Figure 3. Considering that the potential areas should shown low rank property with zebra crossing, we select the rectangular area with better detection result as a reference to analyze corresponding regions in neighbor frames.

Assuming the reference region is pulled into one column vector as x_i at frame i, its forward and backward t-neighbors at same coordinates can be respectively denoted as $x_{i-1}, \cdots x_{i-t}$, and $x_{i+1}, \cdots x_{i+t}$,

(a) Line segments detected by LSD

(b) Angle filtered result

(c) The boxed rectangular

Figure 3. The Line Segment Analysis at Frame 960.

in the term of vectorization. These vectors can be matrixed together as

$$M = [x_{i-t}, \cdots, x_{i-1}, x_i, x_{i+1}, \cdots, x_{i+t}] \tag{3}$$

In the potential zebra crossing areas, it is low rank if the zebra crossing exists, while the others vary in sparse model. Therefore, the integrated matrix can be decomposed as

$$M = L + S,\ s.t.\ L \text{ is low rank and } S \text{ is sparse} \tag{4}$$

This can be solved by Robust Principal Component Analysis (RPCA) [6]. The problem is converted as

$$\min\ rank(\mathrm{L}) + \|S\|_0,\ \ s.t.\ M = L + S \tag{5}$$

where $\|*\|_0$ denotes the l_0-norm. This is intractable in polynomial-time, so it can be replaced by its convex relaxation as follows:

$$\min\ \|L\|_* + \lambda \|S\|_1,\ \ s.t.\ M = L + S \tag{6}$$

where $\|*\|_*$ and $\|*\|_1$ represent the nuclear norm and the the l_1-norm of matrix, and λ is a weight to control the sparse matrix. After decomposing the matrix M, the L can be viewed as stable zebra crossing areas no matter the luminance, the view change, and even the image

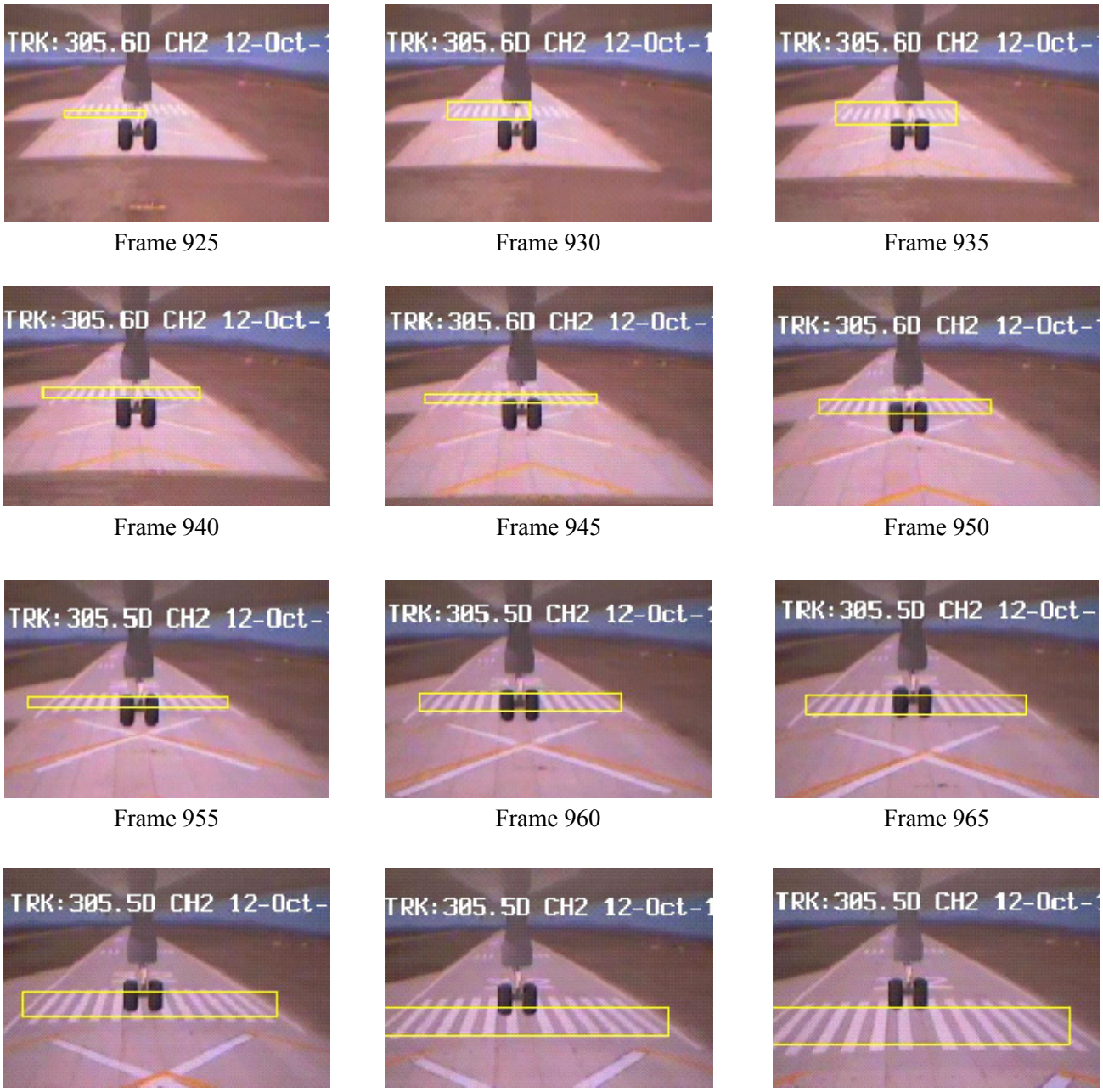

Frame 925 Frame 930 Frame 935

Frame 940 Frame 945 Frame 950

Frame 955 Frame 960 Frame 965

Frame 970 Frame 975 Frame 980

Figure 4.TheClose-up Views of Detection Result.

noise. Therefore, it is a robust detection method for the runway zebra crossing.

EXPERIMENTAL RESULT

In this subsection, we use the captured video by the onboard front-view camera of Gulfstream 450 airplane to test our detection method. We input the whole video, and generate the binary image from the first frame image. If the lighter region is larger than 75% of the image resolution, we set this region as runway area, and then the line segment detection is performed in the regions. After obtaining the candidate rectangular of zebra crossing, it is selected as reference frame. Via RPCA, we can get the low rank component from the neighbor regions, which can be marked as stable zebra crossing regions. The results can be shown in Figure 4. From it, we can observe that the detection result is fixed on the stable area of runway zebra crossing area no matter how the view angle changes. Therefore, it is robust to estimate the position of aircraft in the future visual-based flight inspection system.

CONCLUSIONS

In this paper, we design an automatical runway zebra crossing detection method. This method utilized the line characteristic as a basic feature of zebra crossing, and the low rank as an advance property to aid the detection for the forward and backward frames. This can handle the imaging divergence and the capture view changes. The simulation results demonstrate that the proposed detection algorithm can play an effective performance to get runway zebra crossing information, which can

further aid the flight inspection system. Moreover, this method has no requirement about image resolution, so the original airborne camera without installing special equipment can meet the image capture.

FUTURE WORK

In our method, we detected the zebra crossing in the captured whole video. It is a post-processing system. In the future, we should improve it in real time, which can be feasible in the flight inspection system. In addition, the localization algorithm and precision of crossover point is also our future consideration.

ACKNOWLEDGMENTS

The authors would like to appreciate Mr. Xiaoqiang Li and Yongchao Wang, who give us much help and discussion about the detection framework.

REFERENCES

[1] M. K. Kaiser, N. R. Gans, and E. Dixon, "Vision-based estimation for guidance, navigation, and control of an aerial vehicle," IEEE Transactions on Aerospace and Electronic Systems, vol. 46, no. 3, pp. 1064-1077, 2010.

[2] C. D. Larson, "An integrity framework for image-based navigation systems," Doctoral Dissertation in Air Force Institute of Technology, 2010.

[3] J. Candamo, R. Kasturi, D. Goldgof and S. Sarkar, "Vision based on-board collision avoidance system for aircraft navigation", *Proceedings of SPIE*, vol. 6230, 2006.

[4] J. Zhang, W. Liu, and Y. Wu, "Novel technique for vision-based UAV navigation," IEEE Transactions on Aerospace and Electronic Systems, vol. 47, no. 4, pp. 2731-2741, 2011.

[5] R. G. von Gioi, J. Jakubowicz, J.-M. Morel, and G. Randall, "LSD: A fast line segment detector with a false detection control," IEEE transactions on pattern analysis and machine intelligence, vol. 32, No. 4, pp. 722-732, April 2010.

E. Cand`es, X. Li, Y. Ma, and J. Wright, "Robust principalcomponent analysis?," Journal of the ACM, vol. 58, no. 3, pp.1–37, 2011.

Standardized semi-automatic check of FIS aircraft antennas

Rolf Seide
Senior Manager
Competence Center Flight Inspection
Aerodata AG
Hermann-Blenk-Straße 34-36
D-38108 Braunschweig, Germany
Phone: +49 – (0)531-2359-133
Fax: +49 – (0)531-2359-222
Internet: http://www.aerodata.de
E-mail: seide@aerodata.de

ABSTRACT

After installation of Flight Inspection antennas on aircraft, the performance should be validated showing their real data in the aircraft environment. The typical technical data from simple datasheets should not be taken for any field strength calculation in the flight inspection, because these do not fulfill ICAO requirements on accuracy of the systems.

To improve the long-term stability of aircraft antenna data, in certain intervals antenna data should be re-tested. A semi-automatic system to shorten measurement time and the possibility to decrease the number of human errors is very helpful and cost-effective.

This presentation shows practical solutions to validate these antenna data after installation in a semi-automatic way.

Additionally some results showing insufficient antenna data and the effect on flight inspection results will be discussed.

INTRODUCTION

After installation of Flight Inspection antennas on Calibration Aircraft the RF performance must be tested in practice on the real aircraft in real RF-environment. A theoretical or simple copy-data-sheet approach will not result in the error budget as required by ICAO. Gain and pattern of AFIS antennas have the same influence on the "Signal-in-Space" measurements then the calibration of an AFIS receivers.

The typical set-up for this measurement is a stationary fixed TX antenna with a NAV/GS Band transmitter and the aircraft with the antenna under calibration on ground at a certain distance slowly turning 360° and recording the received signal level. This procedure is repeated for several antennas and frequencies.

One main parameter is the horizontal pattern on different frequencies. These data consists currently of about 8000 data-points in the NAV- and 2000 in the GS band.

Manual data collection has a risk of misarranging them in the files, and if one entry in the log is wrong, the cause cannot be investigated later anymore.

If data are collected in an automatic mode within the Flight Inspection System, files could be replayed and analyzed similar to standard FIS records.

HISTORY

Control of the transmitter for the reference NAV TX signal was done manually with order from the aircraft to the TX station by telephone, requiring additional personnel at the TX station.

In general, this procedure is technically usable, but has a higher human failure rate and needs more personnel and time then necessary. It is too complex to use it as a standard re-check procedure in normal operation.

Block diagram

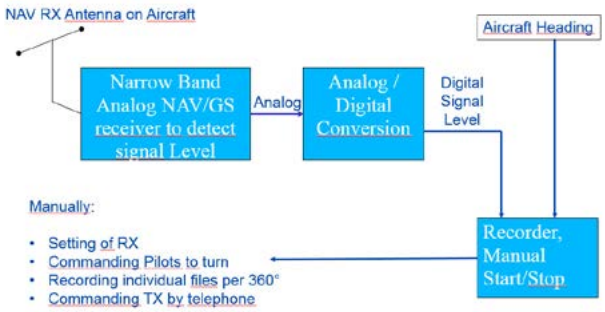

Figure: Block diagram Aircraft Manual Mode

Manual Operation

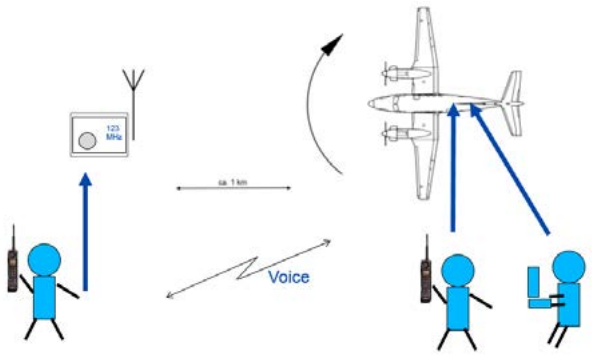

Figure: Set-up for Manual Calibration

3 Persons are required for manual operation:

- Operator recording data at AFIS (aircraft)
- Radio Operator and mission coordinator on board (aircraft)
- Radio Operator switching transmitter (ground)

NEW SYSTEM

The automatic version establishes a bi-directional data-link from the aircraft to the reference TX. The operator is guided step-by-step through all procedures like performing a flight inspection.

The software automatically controls the transmitter and the receiver.

Data is collected and files are clearly labeled for later replay, if necessary.

Automatic Operation

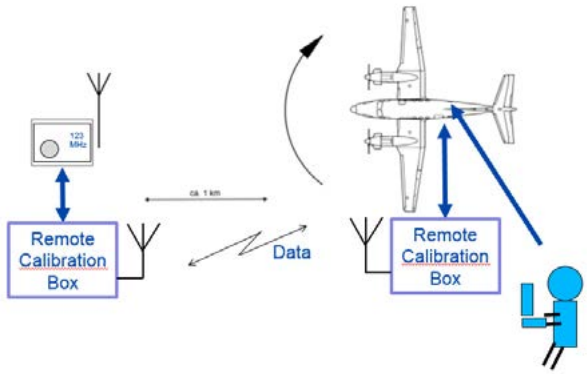

Figure: Set-up for Automatic Calibration

Only 1 Person is required for automatic operation:

- Operator, recording data at AFIS and coordinating mission (aircraft)

Block diagram Aircraft

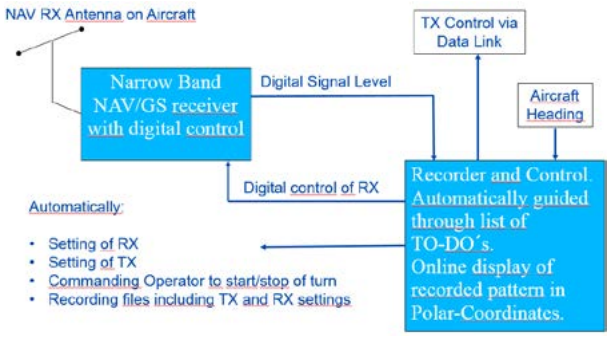

Figure: Block diagram Aircraft Automatic Mode

Pictures

Figure: Transport Box with Data Link and Computer

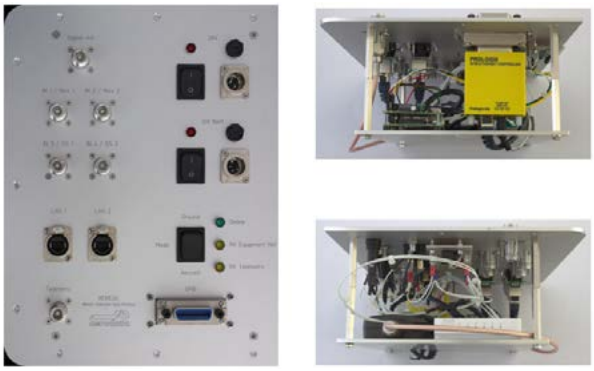

Figure: Frontpanel and Internal wiring

The control panel holds all connectors to interface the AFIS, the RX and control the TX.

DETAILS

Modem and Data link

A standard 1 Watt UHF-telemetry MODEM was selected as data link between NAV reference transmitter station (fixed on ground) and aircraft (mobile on ground). Data rate was set to 9600 baud, bidirectional.

Practical tests of the radio data link were performed to optimize

- Latency of Data Packages
- Error Rate
- Total system delay

to get shortest response times for switching the transmitter settings.

A test vehicle (van) was used to simulate an aircraft taxiing.

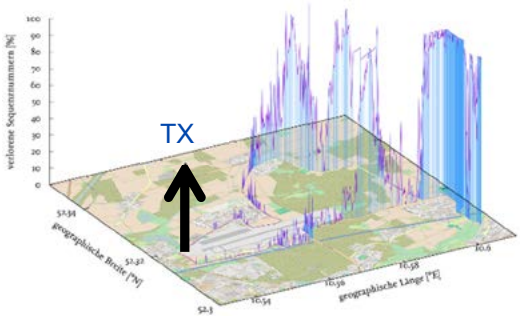

Figure: Data Error Rate around the data link transmitter antenna on ground

One string for transmitter control can be sent, decoded and acknowledged in about 400 ms, depending on the number of data (Full set or only delta to last transmission)

Equipment, Computer, Aircraft

A small COTS computer was installed, based on a RASPBERRY PI system. These computers have a street-price of only 35 US$.

It was upgraded to support Dual Ethernet and GPIB control lines to interface between the

- Flight Inspection System
- The Receiver
- The Modem to control the TX

The computer is programmed to support the control parameters, handshake and error correction of the MODEM signals.

Equipment, Computer, Stationary

The hardware of the interface box is identical to the aircraft installation.

Instead of the receiver (in aircraft), the stationary transmitter is controlled by the computer.

Radio License and local Interference

A local Radio license is required to transmit NAV band reference signals as well as telemetry data to control the transmitter.

Bundesnetzagentur
für Elektrizität, Gas, Telekommunikation, Post und Eisenbahnen

Frequenzzuteilung
mit Ausstellungsdatum: 22.09.2015

Gemäß § 55 in Verbindung mit § 58 Telekommunikationsgesetz wird / werden hiermit

1 Daten des Zuteilungsinhabers

Aerodata AG
Hermann-Blenk-Str. 34 - 36
38108 Braunschweig

HRB 5217
AG Braunschweig

unter der

Zuteilungsnummer: 02 55 5834

die Frequenz/en

108,1 MHz; 109,0 MHz; 110,0 MHz; 111,0 MHz; 112,0 MHz; 113,0 MHz; 114,0 MHz; 115,0 MHz; 116,0 MHz; 117,0 MHz; 117,9 MHz; 329,0 MHz; 330,0 MHz; 331,0 MHz; 332,0 MHz; 333,0 MHz; 334,0 MHz; 335,0 MHz; 335,9 MHz

Figure: Radio License

Local interference while NAV calibration was found on

117.90 MHz: NAV-Calibration-frequency, (low power) with
117.95 MHz: local GBAS TX (50 Watt, burst packages).

This interference influences the quality of the data and should be detected by the operator as early as possible to avoid recording low-quality data (Human experience!)

OPERATIONAL ASPECTS

Turn Rate of aircraft under calibration

To get a smooth antenna plot, one measurement should be recorded at least every 0,5°, resulting in 720 Steps per circle.

A turn rate of 3 minutes per 360 degrees can be handled by the pilots. (2 degrees per second). Slower turn is not possible with the aircraft on ground.

This results in 4 measurements per second.

If several frequencies could be measured within one turn, time would be saved.

But with the system as installed today, a dynamic frequency hopping including measurement is not possible in time. This gives room for future designs and could reduce operating costs and taxy-time of the aircraft under calibration.

RESULTS

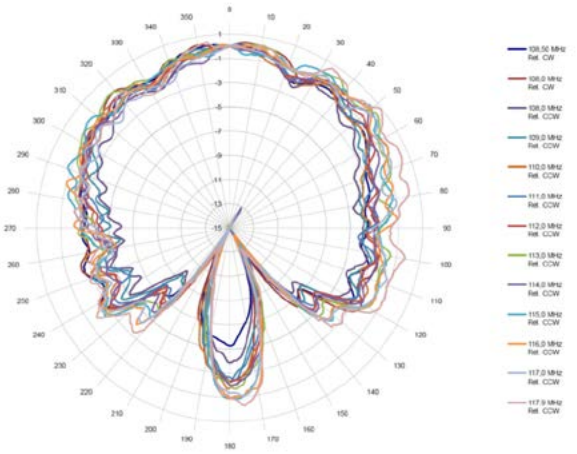

Figure: NAV Band plot of a perfect installation

This plot with 13 frequency lines was taken in about one hour, requiring only one pilot and one operator on board.

The recorded antenna pattern data can be automatically exported to the AFIS as antenna correction data.

DETECTED FAILURES

The following example shows a failure, which is not obvious and hard to detect by other procedures.

This plot is typical, if one-half of an antenna is not 100% serviceable, a phasing problem at a coupler occurs or the wiring has been repaired unqualified.

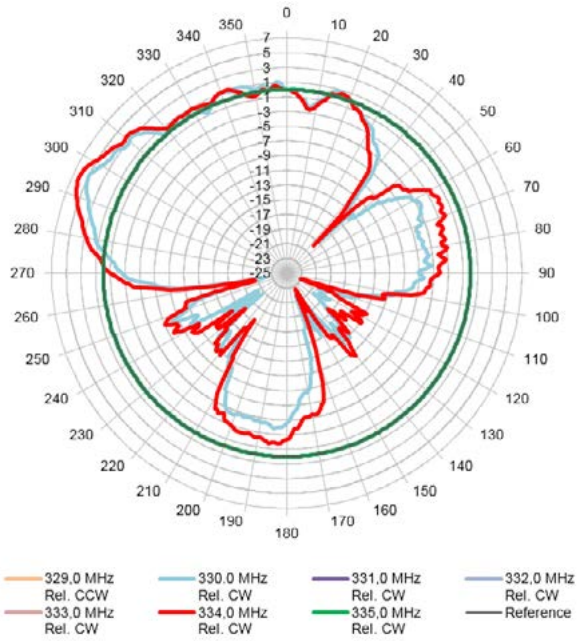

Figure: Antenna diagram of a faulty antenna system

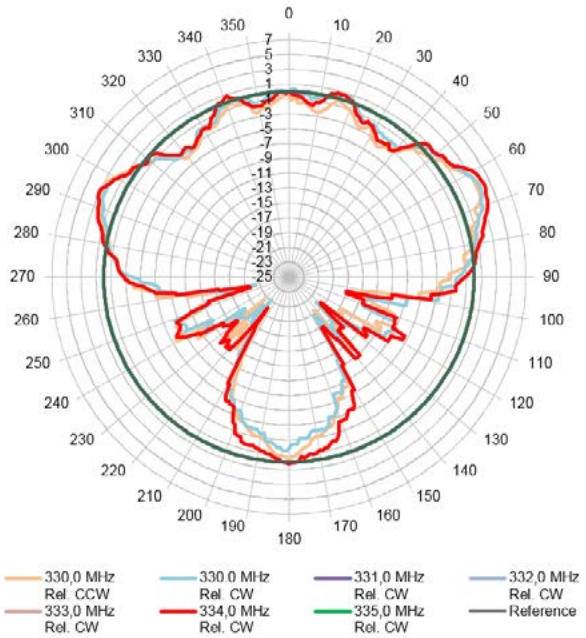

Figure: Antenna diagram after repair

RECOMMENDATIONS

Checking antenna performance on regular basis on ground is required, to ensure constant quality of signal strength measurements according to the allowed error budget according to ICAO regulations.

The shorter the intervals, the higher are the possibilities of detection incorrect values in flight. This finally reduces errors and saves time and money by avoiding repeating of calibration runs.

With a (semi-)automatic and fully-into-the-FIS-integrated system, also trend monitoring can be achieved and failures may be detected before measurement errors add up to unwanted quantities.

FUTURE WORK

The (Semi-) automatic antenna pattern determination can be used in the future for

- Calibration of new installed aircraft antennas (Full set of data)
- Scheduled re-check of antenna parameters (Full set of data)
- Simplified spot-check on shorter intervals , down to spot checks before leaving base or prior to each mission (on ground)
- Simplified spot-check on shorter intervals (in the air)

Exploiting Communication Technologies to Enhance Flight Inspection Capability and Productivity

Carl J. Rieger
Avionics Engineer
Flight Inspection Services
Federal Aviation Administration
Oklahoma City, OK, United States
Fax: +1 405 954 4740
E-mail: carl.rieger@faa.gov

ABSTRACT

With the increasing availability of communication technologies for aircraft, there is the ability to implement a Connected Aircraft. The Connected Aircraft can provide the capability for communication to, from, and/or within the aircraft. These communications can be utilized to enhance flight inspection (FI) capability and productivity.

This paper will present some communication technologies selected for use in the Federal Aviation Administration's (FAA) Flight Inspection Connected Aircraft. A brief description of the type of information and coverage area is provided. In addition, specific examples shall illustrate the capability and productivity enhancements that are realized in terms of maintenance, operations, and engineering.

INTRODUCTION

As communication technologies advance, and with equipment and services becoming readily available, updates to an aircraft's communications can be implemented to enhance flight inspection capability and productivity. However, if care is not taken, an operator may be burdened with the high cost of redundant equipment and ballooning monthly service fees.

This paper presents the process that the Federal Aviation Administration's (FAA) Flight Inspection Services (FIS) utilized to establish and prioritize communication requirements, evaluate equipment, and to determine non-recurring equipment and recurring monthly subscription cost. The realized outcome is a "Connected Aircraft" that provides benefits in terms of maintenance, operations, and engineering.

CONNECTED AIRCRAFT REQUIREMENTS

In establishing the Connected Aircraft requirements, many aspects were taken into consideration. In addition to the data itself, several other factors were considered. Table 1 contains a condensed version of requirements identified for FIS aircraft. These requirements were defined on the necessity of the data, and not on the capabilities of available equipment or current practices. A short description of these requirements is provided.

The FAA operates numerous different types of aircraft for FI activities. In some cases, a requirement is dependent upon the aircraft type due to operating limitations and/or operational area. In the cases where this is true, different requirements were defined for different aircraft types. Coverage refers to the geographical area where communications will occur. This is a significant driver in the selection of a communication pathway, such as cellular or Wireless local area network (LAN) (WIFI). For phase of flight, communications can occur inflight, on the ground, or both. Direction refers to the data flow referenced to the aircraft; down is the transfer of data from the aircraft, and up is the transfer of data to the aircraft. Frequency refers to how often data will need to be transferred to or from the aircraft.

In addition to establishing the communication requirements, a priority was determined and assigned to each requirement. The priorities were assigned by the significance of the data, as well as, the presence of an existing solution. This prioritization allowed for a phased implementation approach and provided an input for a cost-benefit analysis. Additional details, regarding cost-benefits, are included below.

Table 1. Communication Requirements for FIS Aircraft

REQUIREMENTS						
Priority	**Data**	**Aircraft**	**Coverage**	**Inflight / Ground**	**Direction**	**Frequency**
1	Event Based Monitoring	All	Global	Ground	Down	Each Flight
2	Engine Trend	Jets	Global	Ground	Down	Weekly
		Turboprop	Home Station	Ground	Down	Weekly
3	FOQA	All	Home Station	Ground	Down	Weekly
4	Administrative Tasks	All	Home Station	Ground	Up / Down	As Needed
5	FI Computer VNC	All	N/A	Inflight	Within	As Needed
6	Aircraft Locating	All	Global	Inflight / Ground	Down	5 minutes
7	Messaging	All	Global	Inflight / Ground	Up / Down	As Needed
8	AFIS Data Downlink	All	Global	Ground	Down	Each Flight
9	AFIS Data Uplink	All	Home Station	Ground	Up	As Needed
10	Avionics Database	All	Global	Ground	Up / Down	7 days
11	Flight Plans	All	Global	Ground	Up	Each Flight
12	Maintenance Logbook	All	Home Station	Ground	Down	As Needed

A detailed diagram of the Connected Aircraft communications was developed from the requirements and is contained in Appendix 1. This diagram shows the flow of data to, from, and within the aircraft, as well as, the preferred communications.

EQUIPMENT EVALUATION

Upon definition of the communication requirements, an initial Connected Aircraft Architecture was created. Extensive research was performed on the existing aircraft capabilities, in addition to the available equipment and related certifications and approvals.

Architecture

Ideally, the Connected Aircraft would have a single gateway/router to provide communications to and from the aircraft, and also be capable of routing data to the correct aircraft system. The initial Connected Aircraft architecture, which illustrates a single gateway/router, is shown in **Figure 1**. However, with numerous proprietary systems and communications protocols, an existing solution was not available, and the development of such a gateway/router was determined to be cost prohibitive.

Equipment Availability

The Connected Aircraft project plan included the following risk register item:

"The technology and subsequently the equipment available for wireless data transfer in the aircraft have been rapidly changing over the past few years. Due to the time required for system design, prototyping, and contracting and acquisition, there is a risk the technology and equipment may change during that time." [1]

This risk was assigned a probability 3/5 of occurring with an impact severity of 4/5. Over the course of the equipment evaluations, this risk did occur as numerous products became available during the evaluation period, were in development, or were removed from the market. As an impact example, a selected Connected Aircraft product was still in development and did not become available for the initial aircraft installation. Consequently, provisional wiring was installed to accommodate installation at a later date.

Certifications and Approvals

Existing equipment certifications and approvals were considered and weighted during the equipment evaluations. FIS has the ability to implement aircraft changes under a supplemental type certification (STC). However, such STC changes greatly increase the installation cost and approval time frame.

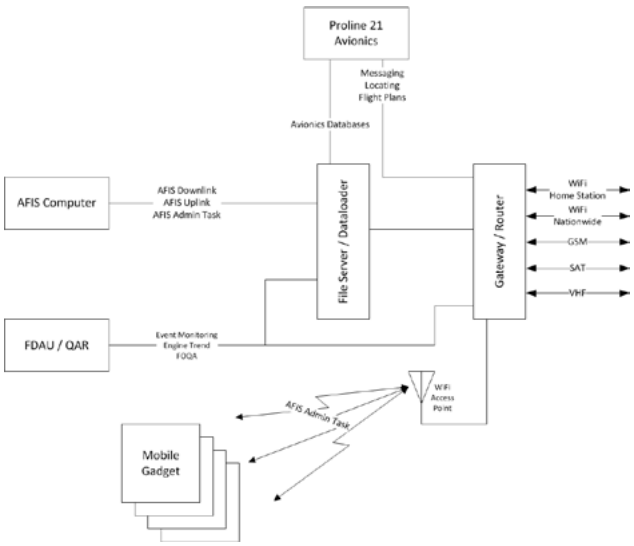

Figure 1. Initial Connected Aircraft Architecture

COST

Since a single gateway/router did not exist to fulfill the Connected Aircraft communication requirements, different combinations of equipment were compared in terms of requirement fulfillment, non-recurring equipment cost, non-recurring development cost, and recurring subscription cost. Table 2 provides one example of an equipment matrix which illustrates the requirements met, overall cost on a per aircraft basis, and any non-recurring cost incurred. This matrix was repeated for numerous equipment combinations for comparison.

In addition to comparing the cost of various equipment options, an analysis was performed for each requirement to ensure the benefits outweighed the cost. If it was determined that it did not, the requirement was not addressed in the final design. A requirement not addressed, can be implemented at a later date either through technological advances or reduced equipment or subscription cost.

Table 2. Equipment Option Matrix Example

Option 1 Requirement	Event	Engine	FOQA	FI Admin	FI Down	FI Up	Locating	Messaging	Databases	Flight Plans	EGPWS	Logbook	Unit Cost	Monthly Recurring	NRE	Software	STC
Priority	1	2	3	4	5	6	7	8	9	10	11	12					
Wireless Flight Data Device	✓	✓	✓										$65,000	$500	$300,000	$6,060	
WiFi Bridge				✓	✓	✓						✓	$20,000				
Satcom							✓	✓		✓			$37,775	$833			
Wireless Database Device									✓				$25,000	$208			✓
Cost Per Aircraft													**$147,775**	**$1,541**			
NRE Cost															**$300,000**	**$6,060**	

CONNECTED AIRCRAFT

The final Connected Aircraft design realized benefits in terms of maintenance, operations, and engineering. Examples in each of these areas are provided.

Maintenance Benefits

Prior to the Connected Aircraft, flight data used for Event Monitoring, Engine Trend Monitoring, and Flight Operations Quality Assurance (FOQA), was manually collected by maintenance personnel from the aircraft. This task was usually accomplished once per week, typically on a Friday afternoon, when aircraft returned from a week's mission. This data was then uploaded to the maintenance intranet for processing. With the Connected Aircraft connectivity, the flight data is automatically transferred after each flight. This not only removes the burden from maintenance personnel and the errors that are prone to occur in a manual operation, but provides a more reliable and timelier processing of flight data. This timelier processing allows for earlier detection of exceedances and prompt notifications that a maintenance action may be required.

Maintenance activities, such as database updates, that required the transfer of data to the aircraft, necessitated the use of a memory device such as a universal serial bus (USB) memory stick. With the Connected Aircraft, the aircraft's FI LAN can connect with the maintenance intranet. This connectivity removes the need carry data to or from the aircraft, as the data can be accessed directly from the aircraft's LAN, much in the same way as it can be accessed from an office computer.

Operations Benefits

Similar to the transfer of flight data, the Connected Aircraft automatically downloads FI data/results after each flight. Previously, the FI mission specialist was required to transfer the FI data/results to a USB memory stick prior to landing as the FI system is powered down during this phase of flight. If unable to transfer prior to landing, the FI system must be powered and the FI data/results retrieved prior to the aircraft being shut down. Once the FI mission specialist has transferred the FI data/results onto a USB memory stick, it still requires the FI mission specialist to manually upload to FI data/results repository. The Connected Aircraft transfers the FI data/results, along with the flight data, automatically upon landing with no interaction required from the FI mission specialist.

In another example of a manual operation, the FI mission specialist typically places a mission's required data on a USB memory stick and carries it to the aircraft prior to a FI mission. Comparable to the maintenance activities, the mission specialist is now capable of accessing this data directly on the aircraft.

With the Locating and Messaging capabilities, the Connected Aircraft provides communication between the aircraft and Flight Inspection Central Operations (FICO). In addition, FICO is continually kept apprised of the aircraft's location.

Engineering Benefits

As engineers are well aware, operations always has a list of new technologies or capabilities they need to enhance their performance of FI activities. One example would be to provide the pilot the ability to fly a Tactical Air Navigation (TACAN) flight inspection mission in relation to the information displayed on the FI system. The Connected Aircraft's cabin WIFI provides the ability for the pilot, using a carry-on device such as a tablet computer, to establish a virtual network connection (VNC) with the FI system. In this manner, the necessary information is available to the pilot without the need to install additional equipment and wiring, thereby reducing the engineering requirements. A portion of a Temporary Flight Inspection Guidance (TFIG) for a TACAN procedure, utilized by the FAA's FIS, is included in Appendix 2 as reference.

CONCLUSIONS

Just as in our personal lives, technological advances are increasing the availability of equipment and infrastructure to keep us connected with the world around us. However, if not properly planned, a user can be saddled with a system(s) that does not meet their requirements, is inflexible and unable to meet future needs, or requires an exorbitant amount of redundant equipment and/or subscription cost.

Care must be taken with the installation of additional Radio Frequency (RF) equipment, and with the use of Personal Electronic Devices (PED). Compliance with RTCA's certification guidance [2][3][4] and FAA's Advisory Circulars [5][6] should be verified for Electromagnetic Compatibility (EMC).

With proper planning and implementation, the transition from a person's office, be it maintenance or operations, to an aircraft environment can be seamless, thereby increasing productivity and effectiveness in executing FI activities.

REFERENCES

[1] FAA, "Connected Aircraft Project Plan", Version 1.5, September 2, 2015.

[2] RTCA, "Certification Guidance for Installation of Non-Essential, Non-Required Aircraft Cabin Systems and Equipment", RTCA-DO 313, October 2, 2008

[3] RTCA, "Aircraft Design and Certification for Portable Electronic Device (PED) Tolerance", RTCA-DO 307 Change 1, December 16, 2008

[4] RTCA, "Aircraft Design and Certification for Portable Electronic Device (PED)Tolerance", RTCA-DO 307, October 11, 2007

[5] FAA, "Certification Guidance for Installation of Non-Essential, Non-Required Aircraft Cabin System and Equipment (CS&E)", AC 20-168, 07/22/2010

[6] FAA, "Use of Portable Electronic Devices Aboard Aircraft", AC 91.21-1C, 05/07/2015

APPENDIX 1

Connected Aircraft with Priorities, Preferred Communications, and Coverage.

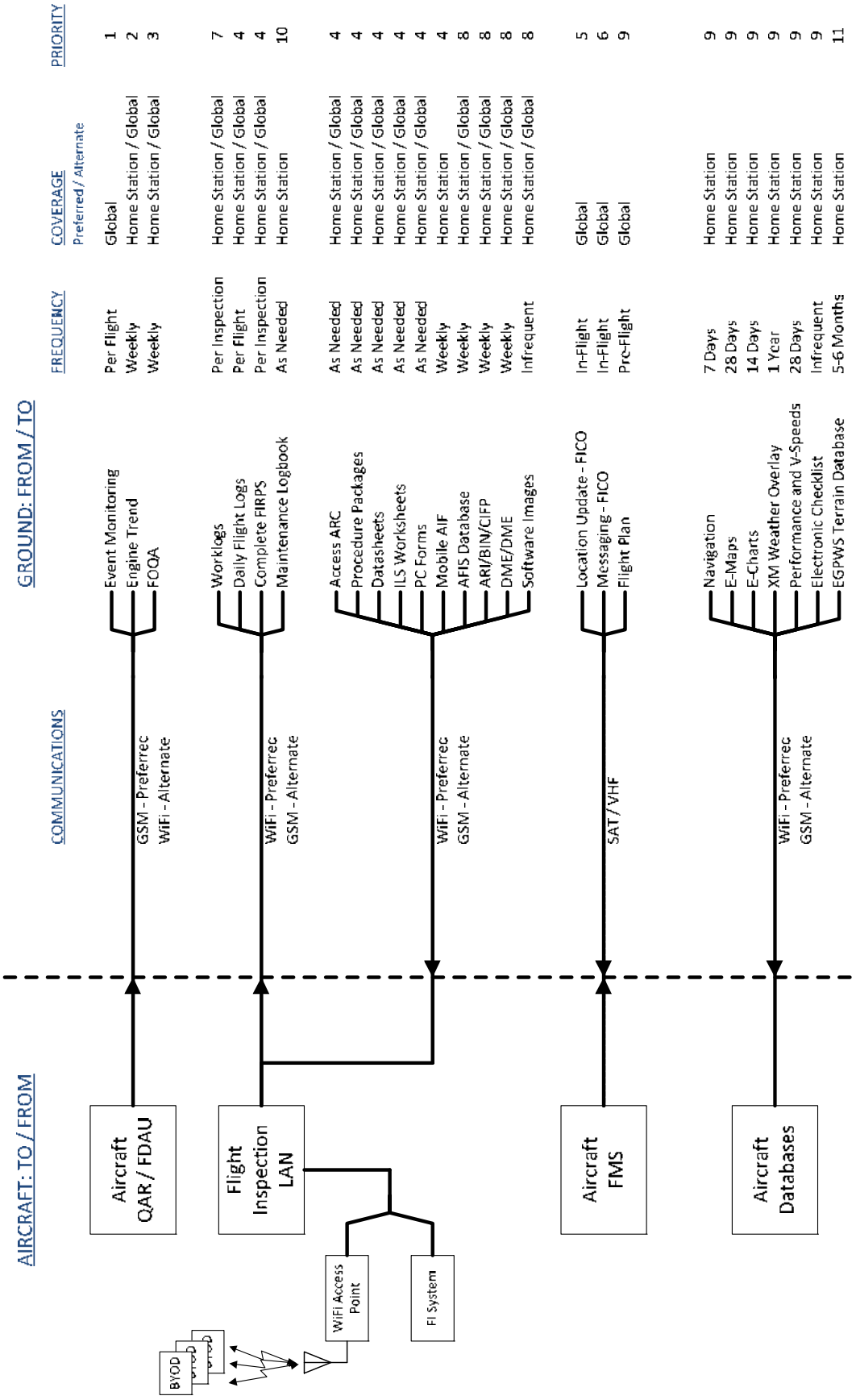

APPENDIX 2

Temporary Flight Inspection Guidance (TFIG) – TACAN Procedure Inspection

TFIG #63 (ORIG - 01/15/2014)

Subject: CL-605 TACAN Procedures

TACAN procedures are completed in the CL-605 using a TACAN HSI displayed on a carry-on device. Data from the AFIS TACAN receiver is used to create a TACAN HSI on AFISView which is then shared with the carry-on device using cabin WiFi and screen sharing software.

Limitations:

1. TACAN Procedures may only be conducted in VMC for flight inspection.
2. Do not use the carry-on device on any approach with the intent to land.
3. Using the carry-on device to view data for other inspection types is approved; however the Mission Specialist must disable VNC anytime AFIS workstation performance becomes unacceptably slow. To disable, select "Stop TightVNC Service" from the Start Menu.

System operation has been demonstrated to work with the following Operating Systems and applications: Windows (Tight VNC Viewer), iOS (Mocha VNC Lite), and Android (androidVNC). The carry-on device must be connected to the cabin WiFi using SSID "********". The client should be configured to connect to IP Address 192.168.2.49 and password "********".

Operational Procedures:

1. If VNC server on AFIS workstation is not already running, select "Start TightVNC Service" from the Windows Start Menu.
2. On AFISView select Nav Map Display / RMI and ensure the TACAN bearing pointer (magenta) is selected.
3. On the carry-on device, ensure connected to cabin WiFi.
4. Open the VNC client application and connect to the AFIS workstation.
5. Pan and/or zoom so that the TACAN HSI is displayed as desired.
6. Place the carry-on device in a location that can be viewed while flying the TACAN procedure.
7. Mission specialist will select RADIN or RADOUT and OBS per standard practices. The course value in the top left of the HSI changes if the aircraft is inbound or outbound to the selected OBS. During inbound runs, the TACAN HSI course will automatically change to the inbound course when the aircraft heading is within 90° of the inbound course.

CAUTION: It is highly recommended that the carry-on device be tested on the ground and/or low workload time well before being needed for a TACAN procedure inspection.

Real-Time Data Acquisition and Time Synchronization

Maik Ritter
System Engineer
Aerodata AG
Hermann-Blenk-Straße 34-36
38108 Braunschweig, Germany
Phone: +49 531 2359 246
Fax: +49 531 2359 222
E-mail: ritter@aerodata.de

ABSTRACT

Flight inspection has to deal with a lot of data that is simultaneously delivered by many different kinds of sensors to the flight inspection system. This includes but is not limited to reference position data (e.g. aircraft GPS and ground based telemetry), primary aircraft data (e.g. attitude, heading and pressure altitude) and of course the data delivered from the dedicated flight inspection receivers such as NAV/LLZ/GP, DME, GPS, GBAS, etc.

This paper presents a deeper look into the importance of real-time data acquisition and time synchronization in order to meet the required accuracies of flight inspection results. Furthermore it discusses known drawbacks of current system implementations and provides ideas and solutions to overcome these.

The paper gives an overview of today's data acquisition and signal processing technology and how it can help to improve the real-time data acquisition and time synchronization in a cost efficient automatic flight inspection system. Special attention is given to the operation of this equipment in a rugged and airborne environment.

INTRODUCTION

The key elements for a successful and meaningful Flight Inspection (FI) are accuracy, precision and repeatability regarding the Navigational Aid (NavAid) signals that are inspected (see definition for accuracy and precision in Figure 1). Some of those signals have to obey harder constraints regarding accuracy and precision than others but in the end, the operator of a Flight Inspection System (FIS) expects to get the same results from the same facility if the FI aircraft is flying the same procedure (e.g. a center ILS approach) two times directly one after the other. Only if this condition is fulfilled, the FI operator can rely on the readings from the system when he comes back for a periodic check of the same facility half a year later and realizes that something has changed. It must be trusted, that this change is caused by the facility itself or by the surrounding environment but not by the FIS itself.

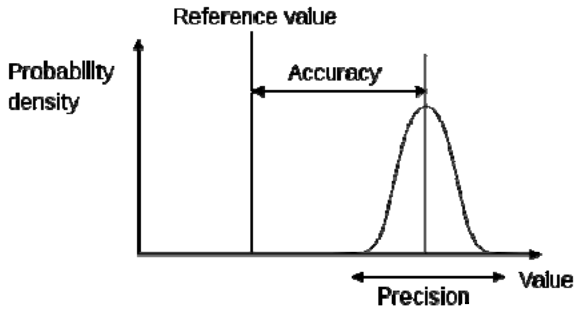

Figure 1 (Source: Wikimedia, Image by Pekaje [4])

In order to achieve the required precision of the FI measurements, dedicated and calibrated sensors are used. Those sensors can be subdivided into the receivers of the NavAid signal, the position reference sensor signals and the primary aircraft sensors such as barometric pressure probes and aircraft attitude and speed parameters.

In order to achieve the required accuracy of the FI measurements, the aforementioned sensor data from many different sub-systems have to be aligned in a way that they complement one another to form accurate measurements at well-defined locations like the ILS points or the coverage limit lines. A critical parameter for this alignment task is time. More precise, the point in time, when data from each sensor arrives at the FIS data acquisition inputs. Only if each dataset gets a time stamp of its point of arrival in the FIS, it is possible to align all the recorded data for the accurate measurements because it is known e.g., at what speed and attitude the aircraft has been at what position when a certain data value was recorded. Only with this information constantly available throughout the whole inspection run, it is possible to get repeatedly reliable results for the condition of a NavAid.

Assumed that the FIS is equipped with precise sensors such as calibrated flight inspection receivers and corrected GNSS data for position reference, a part must be added that assures that all data is aligned for further processing in the FIS software. This part should be a real-time data acquisition device that most likely is a Computer system that is dedicated for the task.

"REAL-TIME" – A DEFINITION

A flight inspection system should at least contain a real-time computer for data acquisition. The term "real-time" very often confuses people because one tends to think that is has to be an incredible fast computer system with the latest and most expensive hard- and software available in it. That is not the case.

The definition for a real-time computer system is generally that it is dedicated to a certain task and that it guarantees the completion of the required actions within a defined period. The length of the period, that the system guarantees to meet, depends on the requirements under which the system was designed. The requirements under which a flight inspection real-time system should be designed can be derived from [1] and [2]. From these requirements, one has to derive the number and types of inputs and processing intervals for each data type.

The term real-time can be divided further into different classes, namely hard-, firm- and soft-real-time.

Hard real-time means that the system fails completely and without recovery if the timing requirements for the task were not met once.

Firm real-time means that the system continuous to run after the missing of the timing requirements, but that the results can be regarded as useless for at least a certain amount of time after the miss. However, the system can recover and continue to work as required.

Soft real-time allows timing misses with just a degradation of the results, but still usable. This can be achieved, by e.g. recognizing the miss and interpolating the data between valid values from correct measurements.

An FIS real-time system can be placed between firm and soft real-time requirements. However, presumed a careful system design, today, it should be easily possible to reach hard real-time capability without disproportional effort.

REAL-TIME COMPUTERS IN THE PAST

In the past, limitations had to be implemented in the real-time system in order to meet processing power and data storage limits of the then available hardware. E.g. it was determined that the flight inspection data acquisition runs at a general update rate of 10Hz. This update rate had not been sufficient for all data inputs such as A429 labels for localizer or glide path deviations. In such a case, the data update rate has ben raised to 50Hz or more.

On other parameters such as AGC, only one data set per 10Hz time slice has been used and all other data of the same type was skipped.

Additionally, due to less integrated circuitry of the digital parts such as processors, memories and interface controllers it was hard to implement all required interfaces on one Printed Circuit Board (PCB). Each interface PCB had its own processor that had to be synchronized with the other boards processors for a decent time stamping. All shared resources had to be carefully arbitrated in order to not accidently loose data or lock the data transmission completely. Such arbitration took processing power from the then available CPUs that were already occupied by the task of FIS data acquisition and preprocessing. Programmable Logic Devices (PLD) or dedicated integrated circuits to support the CPU had been available, so that CPU support for e.g. Direct Memory Access (DMA) or bus arbitration could have been effectively implemented. However, additional dedicated chips took valuable space on the PCBs and additional effort for the design of the hardware. Special care on many aspects of digital design had to be taken. This included power estimation, functional logic analysis and thermal considerations in order to guarantee a stable digital design over the complete specified temperature range of the real-time computer

Considering the definition for real-time from the last section, those computers, having all these limitations, could be regarded as real-time capable as well. This is because the specification and the design defined the periods for the data acquisition with respect to the available hardware and with a focus on the most important parameters. Although not very convenient for all imaginable applications, the most important requirements were covered and so that system could have been declared as "real-time".

REAL-TIME COMPUTERS TODAY

Today, such limitations described in the last section should not exist anymore. A state of the art processing and data storage hardware should be able to handle all flight inspection data without the need for compromises.

The general processing period should be increased to 100Hz and beyond. There are parameters and operations for which 10Hz is even in theory not enough. Considering the Nyquist theorem, it is not possible to decode station identification Morse codes with a sample rate of just 10Hz. Additionally, Inertial Navigation System (INS) attitude signals should at least be sampled with 50Hz.

The modern technology should not force the hardware developer to decide which parameter on which input is more important in order to give this a higher priority or

a better time resolution. Today, the hardware should be able to process all data that is available on a theoretically basis. This means, if the system offers e.g. 20 A429 inputs, it should also guarantee that all of these inputs could be connected to other devices that transmit data at the highest rate defined by the A429 standard. This approach should also be used for all available UARTs and additional data communication interfaces. In the past, due to the above mentioned restrictions, data got lost which is just not acceptable today, in a modern system.

Handling the input messages at the fastest defined data rate does not only mean the raw data itself but additionally the timing information that the real-time computer adds to each data set. For A429 this means that for each 32bit data word, a timestamp data word is added processed and recorded along the message raw data. For UART data, it should be possible to time stamp each 8bit UART word that reaches the system.

Analog and digital inputs should be sampled such that the highest expected data signal frequencies can digitally processed according to Nyquist laws. Again, additional memory space must be considered for time stamp information.

Special low latency inputs should be provided for synchronization to a highly accurate timing information

source such as the Pulse Per Second (PPS) signal from a Global Navigation Satellite System (GNSS) receiver. Such a signal should be used as absolute reference in order to recognize clock drift of the digital system or even as Phase Locked Loop reference input in order to prevent clock drift at all.

Why is it important to have accurate time stamping and sufficient data sampling available? As discussed in the introduction, the accuracy of flight inspection results highly depends on the comparison between sensor and position reference data. This data must be aligned in time for the best results.

TIME SYNCHRONISATION

The need for time synchronization or alignment between sensor data and position reference is due to the movement of the measurement system. This system is installed in an aircraft (A/C) that is constantly moving at different speeds. **Error! Reference source not found.** shows what effect the movement of the aircraft could have on the accuracy of the sensor data. It shows the covered distance vs. the A/C speed. The blue marked fields show the typical FIS

Table 1 Covered Distance vs A/C Speed

A/C Speed (kn)	A/C Speed (Kmh)	Distance per Second (ft)	Distance per 100ms (ft)	Distance per 10ms (ft)	Distance per Second (m)	Distance per 100ms (m)	Distance per 10ms (m)
100	185.2	168.78	16.88	1.69	51.44	5.14	0.51
110	203.72	185.66	18.57	1.86	56.59	5.66	0.57
120	222.24	202.54	20.25	2.03	61.73	6.17	0.62
130	240.76	219.42	21.94	2.19	66.88	6.69	0.67
140	259.28	236.29	23.63	2.36	72.02	7.2	0.72
150	277.8	253.17	25.32	2.53	77.17	7.72	0.77
160	296.32	270.05	27	2.7	82.31	8.23	0.82
170	314.84	286.93	28.69	2.87	87.46	8.75	0.87
180	333.36	303.81	30.38	3.04	92.6	9.26	0.93
190	351.88	320.68	32.07	3.21	97.74	9.77	0.98
200	370.4	337.56	33.76	3.38	102.89	10.29	1.03
210	388.92	354.44	35.44	3.54	108.03	10.8	1.08
220	407.44	371.32	37.13	3.71	113.18	11.32	1.13

maneuvering speed for a King Air flight inspection A/C. It shows that in a 10Hz based data acquisition system, the distance covered in one data acquisition time slice (100ms) is about 27ft or 8.2m. This means, if the sensor data and position reference data is misaligned by just one time slice (because data is sampled at the beginning and at the end of the time slice), the error for the underlying data processing would be already too high for almost all requirements of [1] and [2].

The situation would be even worse if the offset between the sensor and position reference data would jitter from time slice to time slice. Figure 2 illustrates the above mentioned problems.

In the best case, an experienced flight inspector would recognize that something is wrong with the acquired data but in the first place, he would most likely not suspect the FIS to be the cause for the behavior. This

means a lot of time must be spend on investigation of the issue and finally figuring out that the cause is the misalignment introduced by the FIS. The worst-case scenario of course would be that the data would be accepted because it was trusted that the FIS is working correctly.

Even if everything is aligned perfectly, in a 10Hz only system, it would not be sufficient to use the sensor data and position reference from the same time slice. It could happen that one datum was recorded at the beginning of the time slice and the other at the end. This would introduce almost the same amount of error as if they were a time slice apart. This is the reason why the 10Hz system (and even a 100Hz system, too) performs some "oversampling" on certain parameters in order to get additional data inside a time slice boundary.

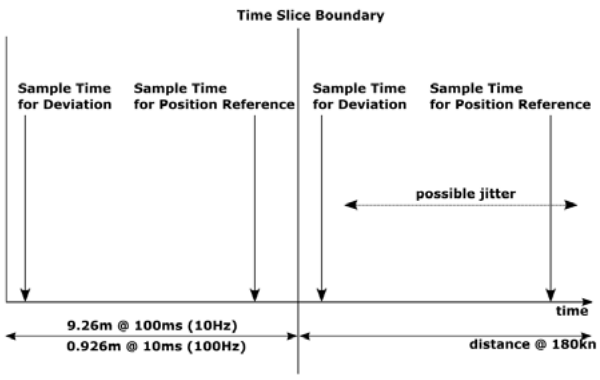

Figure 2 Distances inside Time Slices between samples @ different Sample Rates

The given examples and **Error! Reference source not found.** shows extreme views on the subject. Since flight inspection of an ILS e.g. does not focus on high accuracies in distance but in horizontal and vertical angels of deviation, the effects of A/C speed are not that big like **Error! Reference source not found.** implies. However, examples should give an estimate about the dimensions of possible systematic errors.

TIMING RELATED ERROR -EXAMPLES

Given is an FI A/C that is flying a centerline approach with 180kn. We assume that the glide path deviation from the FI receiver and the deviation from the reference position are sampled at the beginning and at the end of the time slice respectively. The real glide path angle is 3°.

The different times in sampling the deviations give a slant range error of about 9m between the point where both, the measured and the reference deviations are sampled and time stamped. Now, by looking at the glide slope angle that is calculated by using these values, one gets a result of about 2.99° instead of 3°.

This result does not look like a big error. However, [2] states that the uncertainty for a CAT III glide path has to be 0.3% of the nominal glide path angle which in fact is 0.009°. The conclusion is that only because of insufficient time alignment, the uncertainty budget is already consumed, leaving no reserve for additional systematic errors.

An additional example of timing related errors would be to look at orbit flights around a VOR. If two flights are performed in both clockwise and counter clockwise direction and the system is error prone to timing issues, one would get different results on bearing error calculations for each direction. The amount of error could even vary with different A/C speeds.

The goal for a modern real-time computer must be to minimize all systematic errors as far as possible. Being a digital system, there is no way to completely get rid of all timing related errors, but today, it is possible to minimize them to a degree, where the real-time computer system is much better than the connected sensors. A deeper look at this fact is provided in the conclusions and future work section.

MODERN FI REAL-TIME COMPUTER DESIGN

A modern FI real-time computer has to provide a high degree of parallelization concerning the data acquisition. Each input to the system has to have the same priority so that no data is delayed before it gets time stamped. All inputs should be able to operate at their specified data rates without any compromise. All data must be time stamped and recorded for future use. It is not the real-time computer to decide which data is more important than other. This decision is left to a higher system level.

The real-time system uses a lot of very special and non standard interfaces such as A429 in combination with analog and digital inputs and outputs. The combination of all these interfaces is not very common and it is hard to just buy them off the shelf. Especially if the requirement is that all have to be time stamped with regards to the same time base.

Being used in an aircraft, it has to obey additional requirements like little power consumption, weight and robustness against vibrations and different temperatures. Using Commercial off the Shelf (COTS) equipment is just not possible and would soon lead to system failure.

The computer has to minimize the emission of Electromagnetic Interference (EMI) which can be a critical factor if operating at several hundred Megahertz (MHz).

Referring the example from the last section, one should consider to increase the general operation speed to either 100Hz or to the maximum speed of individual interfaces.

For the sake of completeness (not important for the topic of real-time, of course), the computer should fit into a standard Line Replaceable Unit (LRU) housing in

order to avoid extra mechanical development and verification testing.

REAL-TIME COMPUTER HARDWARE

A real-time data acquisition computer for flight inspection can be regarded as an embedded system. An embedded system is designed to perform pre-defined tasks with very specific requirements (functional and time constraints). Compared to a general purpose computer (such a desktop PC), the developing team of an embedded system knows exactly what the tasks are and therefore, the hardware selection can be very easy because it has not to be discovered the most powerful hardware for all imaginable purposes, but only the hardware that best fits the requirement. Additionally, because the requirements do not change very rapidly, an embedded system lifetime is much longer than the lifetime of a general purpose computer. Once developed and tested thoroughly, it can be a reliable working horse for years without the need to change or redevelop something.

Today, the perfect hardware for a flight inspection real-time computer is easily available. This hardware is a so-called System on Chip (SoC), which is a multi-core Central Processing Unit (CPU) combined with memory controllers, communication interfaces (such as Ethernet and UART), Serial Peripheral Interfaces (SPI) and I2C for interfacing external devices, general purpose IOs in one housing. This facilitates the development of a computer PCB at a great amount because there are no interconnections between all those components to be concerned about if they were all in separate chips.

The latest and most important feature (regarding the development of an FI real-time computer) in SoC advancement that took place in the last couple of years is the integration of a full-fledged Field Programmable Gate Array (FPGA) into the device.

The FPGA is a PLD that can be used to integrate all the interfaces custom protocols (e.g. A429), data acquisition and time synchronization. It is perfectly suited for parallelization of all computer interfaces so that there is no delay on any input of the system between data arrival and time stamping. Since everything in the FPGA can be designed as clock synchronic circuitry, it is even possible to compensate for any delay that is caused by the data acquisition because it is easy to calculate delay times by just counting the clock ticks that occurred between data arrival and time stamping. The FPGA is the main feature of the real-time computer that guarantees that the real-time requirements are finally met constantly and repeatedly.

Given a decent FPGA design in a Hardware Description Language that is supported by third party simulation tools, it is possible to design and simulate the whole design in order to constantly check against the specifications of the system. FPGA vendors provide development tools that make sure that timing constraints (here: the digital timing between clock synchronous registers in the digital FPGA design) are met for all specified temperatures. The developer of the digital system has not to consider difficult PCB design for layouts that have to support system clocks between 25MHz up to 1 GHz because it is all contained in one device, the SoC.

SoCs are also preferable when it comes to EMI testing of the final real-time computer before installing it into the A/C. Since most of the high clock rates are generated with Phase Locked Loops (PLL) inside the SoC, the radiation of disturbing emissions is limited to a very low amount.

SoCs like the one pictured in Figure 3 offer dedicated hardware for Direct Memory Access (DMA) that makes it easy and error save to transfer the collected data between processing units. This happens fully automatically without the need for the CPU to intervene.

The multicore CPU of the SoC is an ARM based processor that is also commonly used in millions of mobile phones and embedded systems, all around the world. This guarantees that software-, development- and debug-tools are constantly developed, maintained and improved, making it a future-save platform.

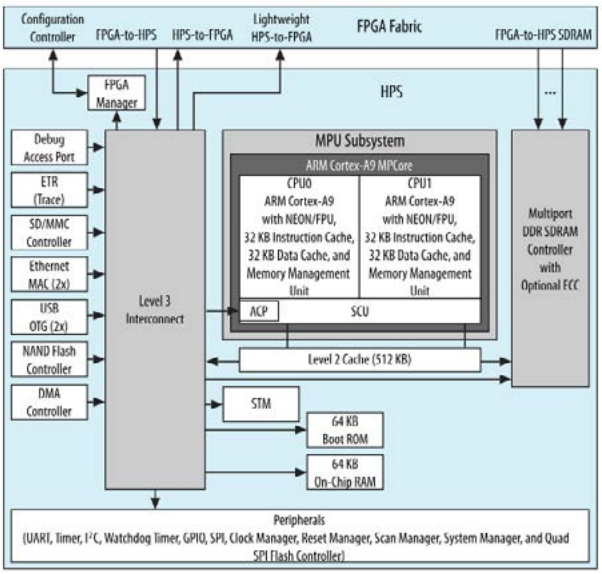

Figure 3 SoC Block Diagram

Based on the specifications and design considerations above, a CPU/FPGA board can be developed that is pictured in Figure 4.

The specs for such a system read as follows:

- Dual ARM Cortex A9 CPU @ 800MHz
- 1GB DDR3 RAM with ECC
- 1000BASE-T, IEEE 802.3 Ethernet

- SD-Card Interface
- UART Interface
- JTAG Interface
- SPI/I2C interfaces for Real-Time Clock and Hardware Monitor connection
- Co-Processor FPGA linked via 2 x 3.125Gbps transceiver links
- SoC-FPGA with 110k Logic Elements, 5.5MB Onchip RAM
- Co-FPGA with 150k Logic Elements, 6.8MB Onchip RAM

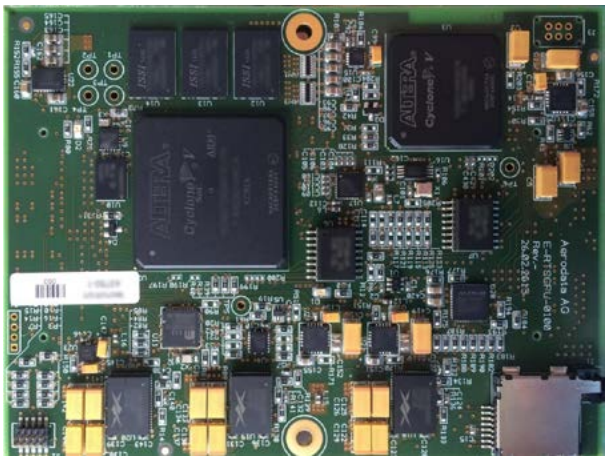

Figure 4 Real-Time Computer Processing Board

Reading the specs for the system, one could assume that this is not a very highly sophisticated computer system, which is true if you compare the specs to a modern desktop computer. However, one has to keep in mind that the real-time computer is built for a special purpose that can be easily achieved with this hardware. It still has enough processing resources and I/Os left to add additional functionalities for future use. Compared to a desktop computer system, it is easy to maintain, and uses only a fraction of the power.

For the complete system, it still lacks interface boards for signal level adjustments of the different interfaces and for analog to digital and digital to analog converters. Additionally, a power supply board and backplane for the connection of all boards to form the complete system have to be added. The only consideration in terms of real-time have to be made for external level adjustment and interface protocol chips that may introduce latencies for the FI signals. Those latencies are normally in the nano or micro seconds range so that they can be neglected after careful consideration of the influence on the signal.

Finally, everything is fitted into an airworthy housing. Figure 5 shows an example LRU of an FI real-time computer that is ready for operation.

Figure 5 Airworthy Real-Time Computer

REAL-TIME COMPUTER SOFTWARE

The software for a real time computer like it is described here does not have to obey the requirements of being real-time capable because the aforementioned hardware has already taken care of the real-time sensible part of the system. All interface data is already time stamped and can therefore be further processed in a manner without any real-time restrictions. The only requirement that has to be verified is that the constant data stream that is delivered from the FPGA can be processed before it is send to a higher level system that will display the data to the FI operator.

So what does this further processing include and why is it necessary?

Further processing can

- configure interfaces to set up correct speeds and data formats according to the needs for the current FIS, where the computer is installed in.
- pre filter data that is processed by the FPGA but will never be used (e.g., data from unconnected interfaces). This way, memory devices that are used to store the inspection data will not overflow with useless data.
- calculate position reference data from the positioning sensors. This data is used for the final inspection results calculations on the higher order system as well as for a possible flight guidance that is used during flight inspection to steer the A/C on the programmed procedure path. Since the flight guidance connects to primary A/C interfaces via the computers interfaces, the calculations are best performed on the real-time computer itself.
- tune FI receivers to the currently selected and inspected facilities.

- accumulate the time stamped data and sends it to the higher level computer via a defined protocol that is based on Ethernet.
- perform system monitoring and fault reporting in the case of a failure.

Since the CPU is a standard ARM CPU and the real-time requirements for the software are quiet low, the operation system that should be considered first is Linux. The advantages are that it is widely used and supported by a huge developing community. It is open source so that custom adjustments are possible to integrate. Many tools and concepts for the embedded use case are available and field proven. Additionally, it has a well-defined, well-documented and stable Application Programming Interface (API) that facilitates programming user applications.

A real-time kernel would also be available for Linux. Since it is already stated that there are no real-time requirements for the Operation System, this is only mentioned for completeness. The integration of real-time capabilities in the Linux kernel is a complex task and much harder than to implement it in hardware (say, the FPGA).

The user application can then be programmed in order to perform the above mentioned software functionalities. Additionally, device drivers have to be developed that interface the FPGA components to the user application.

QUALIFICATION OF AN FI REAL-TIME COMPUTER

The FI real-time computer operates in a harsh environment regarding vibrations and temperatures. It has to be qualified for this environment with respect to the operational use and under safety considerations. The environment should not be the cause for a failure of the system since the flight inspection must be aborted immediately when the device fails.

Additionally, the device must not put the A/C or crew in danger in case of e.g. a cabin decompression or because of its electromagnetic emission.

It is recommended to perform the following tests to insure safe and reliable operations in the flight inspection aircraft:

Table 2

Qualification	RTCA/DO-160G
Power Input	Section 16, Cat. B
Voltage Spike	Section 17, Cat. B
Audio Frequency Susceptibility	Section 18, Cat. B
Radio Frequency Susceptibility	Section 20, Cat. R
Radio Frequency Emission	Section 21, Cat. M
Temperature	Section 4, Cat. A4
Temperature Variation	Section 5, Cat. C
Humidity	Section 6, Cat. A
Shock	Section 7, Cat. A
Vibration	Section 8, Cat. SC, SL
Decompression	≤ 35.000ft

ADDITIONAL CONSIDERATIONS

After covering the problematic of real-time data acquisition and time synchronization in a FIS in the preceding sections and giving an example on real-time computer design, it should be mentioned that there are additional aspects to consider. By referencing [3] it becomes clear that a well designed real-time data acquisition computer is only half the way to a perfect time synchronization.

Many sensors such as flight inspection receivers have complex filtering and data processing algorithms implemented so that the output signal from those sensors has a certain time delay compared to the occurrence of the signal in free space. Especially in a very dynamic environment, which flight inspection due to the flying aircraft at a mostly bumpy flight level certainly is, it is mandatory to either know those delays for each receiver and parameter in order to compensate for them in the FIS or one should consider moving the time stamping of the data into those sensors.

One approach for a distributed time synchronization would be the Precision Time Protocol (IEEE 1588) that defines a time synchronization over Ethernet in the sub-microsecond range. Since this approach would imply redevelopment of many subsystems of the FIS, other means should be developed to compensate for sensor delays, which is up to the flight inspection system designer to implement.

RECOMMENDATIONS

Time synchronization of flight inspection data is a sometimes underestimated field, that, if wrongly or not sufficiently performed, can lead to many effects in the flight inspection results. If timing issues would not be even considered as cause for these effects, maybe ground stations that in reality perform correctly would get limitations while not being responsible for anything.

Flight inspection system manufacturers should review their system design for flaws regarding the time

synchronization and should consider to design a proper data acquisition computer if none is already present in their system. As stated above, this would not compensate for individual sensor delay, but once the sensor delay is known, would increase accuracy and repeatability of flight inspection results.

Flight inspection system operators should be aware of the problems that an insufficient time synchronization could cause and should apply this knowledge when they are faced with strange measurement results. Maybe it is not the facility but the FIS that is causing the problems.

REFERENCES

[1] ICAO, July 2007, International Standards and Recommended Practices, Annex 10 to the Convention on International Civil Aviation, Volume IV, Surveillance an Collision Avoidance Systems, 4th Edition, http://www.icao.int

[2] ICAO, 2000, Manual on Testing of Radio Navigation Aids, Volume 1, Testing of Ground-Based Radio Navigation Systems, Doc 8071, 4th Edition

[3] Alf W. Bakken, IFIS paper 2010, How to save time and money on ILS flight inspection using correct methods and input data, Time Synchronisation Error Between Reference Signal and ILS Signal

[4] Pekaje, Accuracy and precision, image, Wikipedia: The Free Encyclopedia, viewed 29 April 2016, https://commons.wikimedia.org/wiki/File:Accuracy_and_precision.svg

IFIS2016

Bringing Together Theory and Practice

Session 2

Flight Inspection of ILS

ILS Critical and Sensitive Areas: ICAO NSP and Eurocontrol Developments

Gerhard E. BERZ, Valeriu VITAN
EUROCONTROL
Brussels, BELGIUM
E-mails: gerhard.berz@eurocontrol.int
valeriu.vitan@eurocontrol.int

Leonardo CANON (see note)
CIMPA SAS
Toulouse, FRANCE

Guillaume CAMBON, Laurent EVAIN
Airbus SAS and Airbus ProSky (respectively)
Toulouse, FRANCE
E-mails: guillaume.cambon@airbus.com
laurent.evain@airbus.com

Antonino ITALIANO, Rodolfo GUIDI
IDS Ingegneria Dei Sistemi S.p.A.
Pisa, ITALY
E-mails: a.italiano@idscorporation.com
r.guidi@idscorporation.com

ABSTRACT

The ICAO Navigation Systems Panel has finalized the update to the ILS Critical and Sensitive Area (CSA) guidance material in Annex 10. It is expected that ICAO will publish a State Letter on this matter during 2016. The update includes a consistent set of example tables for both Localizer and Glide Path that address different vehicle and aircraft categories including very large aircraft. The guidance material seeks to provide a globally applicable and safe set of materials while allowing for local optimizations. The paper will present an overview of the material and some explanations of the process, thoughts and intentions that led to its current form.

The updated guidance is building on a coordinated effort of several parties over several years. During this time, most studies focused on the Localizer, since it has the greatest airport impact. Only a limited amount of work was done on the Glide Path until recently. After the general overview and introduction of the new CSA guidance, the paper will further explain the studies conducted through a cooperation between Eurocontrol and Airbus Prosky on the ILS Glide Path, going into further technical details about how the simulations were conducted and what criteria were applied. Thereafter, an additional study was conducted by Eurocontrol and IDS to see if optimizations of the Glide Path antenna could lead to operational improvements and a reduction of the CSA. The paper will present an overview of these results also.

Since one clearly accepted element of the CSA guidance material is that simulation capabilities need to be verified through actual ground and air measurements, it is expected that both the general overview of the updated CSA guidance material and the related simulation studies will be of interest to the flight inspection community.

INTRODUCTION

The introduction of very large aircraft (such as the Airbus A380) triggered the need to review the Annex 10 [1] guidance material on ILS critical and sensitive areas. Due to the evolution of the operational environment, improvements in ILS technology, and the difficulty to recover the technical details of the initial material, a complete overhaul was needed. An initial change proposal [2] was presented by ICAO for review by its member States in 2008 (Amendment 84). The proposal was rejected due to potentially unacceptable operational impacts. After considerable rework and consultation with operational experts, a new change proposal has been completed now. The rework included a significant effort on the ILS glide path, which will be the main focus of this paper. The paper will first provide an overview of the underlying principles in the updated guidance material, second explain how the associated glide path simulations have been conducted and used to generate the associated guidance material tables and third, how the results have been used to evaluate potential optimizations of ILS glide path antennas.

PRINCIPLES OF UPDATED GUIDANCE MATERIAL

Guidance material is published in the so-called Annex 10 green pages as non-binding, advisory material. However, some States elect to treat guidance material almost at the same level as standards. In order to write guidance material that is helpful, it is necessary to go into a certain level of detail. Such details are often only one possible way of achieving the objectives which are required by the standards. Consequently, the words need to be carefully chosen to not give rise to too prescriptive interpretations in order to maintain

flexibility but still provide useful guidance. It is peculiar to note that the Annex 10 guidance defines critical and sensitive areas as only one possible method of protecting ILS operations from multipath interference, whereas all other ICAO documents dealing with ILS use those terms exclusively.

Operational Objectives

A concern that was expressed by operational stakeholders during the ICAO State Letter consultation was that the updated CSA dimensions were too restrictive, due to the example tables indicating larger areas than before. The main argument used was that in normal operations, the current areas were considered to be sufficient. However, what may be considered operationally acceptable may not necessarily meet minimum ICAO standards. Avionics have implemented additional, non-standardized filtering to ensure smooth ILS services, and more generally, it is normal that operational equipment exceeds the minimum requirements with a margin. ICAO guidance material, on the other hand, cannot be in contradiction with the standards that it supports. Consequently, the objective of the guidance material on ILS CSA remains to protect the standards given in the white pages, i.e., the alignment and structure tolerances given in Annex 10. Even if in some cases, operational experience may suggest that the margin between minimum standards and actual performance is too large, in other cases it has been shown that exceeding the ILS tolerances as specified can lead to detrimental effects.

The initial Amendment 84 version of the guidance material update included changes to the definitions of the critical and sensitive areas with operational implications. One specific concern was the introduction of a 2NM limit relating to the transition between critical and sensitive area protection, which caused an issue for high capacity airports with advanced low visibility procedures. The new amendment proposal thus returns to the original definitions, and instead adds a discussion on operational and technical trade-offs when determining protection segments. The objective of the rewrite was to publish, in line with the global nature of Annex 10, generic, globally valid material, while leaving full flexibility for local optimization. In other words, while the expert group working on the example tables made an effort to produce areas that were as small as possible, it clearly does not mean to exclude any further, local improvements.

Another important aspect to help ensure operational acceptance is an application note at the beginning of the new material. It reminds readers that if existing CSA have been shown to be safe, no further action is needed as a consequence of the updated Annex 10 guidance. While the text has been updated, all the well-established principles of CSA protection remain the same. All that has been added is a (hopefully) better description of current industry and air navigation service provider (ANSP) practice.

ILS CSA Protection Segments

The established CSA definitions describe what is done operationally. However, they do not specify how they should be determined technically. From an operational point of view, a common interpretation is that the critical area should protect aircraft in the entire coverage volume down to at least the Cat I decision height, while the sensitive area should protect low visibility operations from the Cat I decision height down to the runway. A common technical view is that critical area disturbances affect the entire approach, while a sensitive area disturbance is typically a locally limited disturbance. Those two views don't necessarily align.

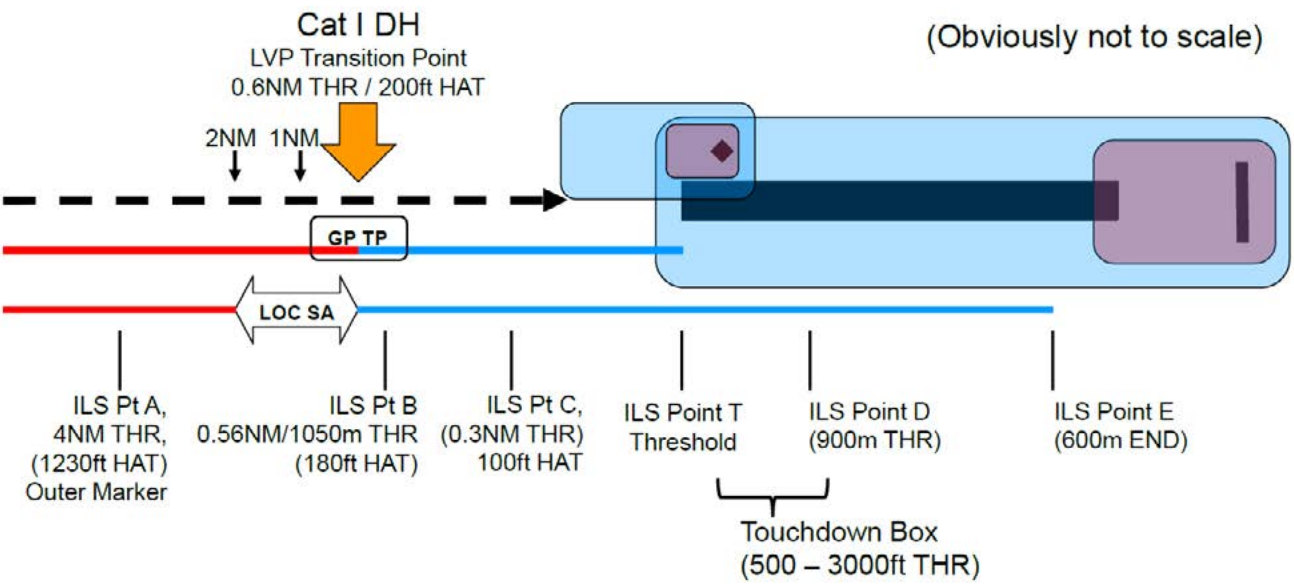

Figure 1. ILS CSA Protection Segments for Localizer and Glide Path

Moreover, protecting the localizer critical area all the way to the Cat I decision height typically results in unacceptably large critical areas which overlap the stop end of the runway. While the previous guidance made an implicit assumption that critical area sizes never overlap operational areas, the new material recognizes that in some cases, management of aircraft movements in relation to the critical area may be necessary.

Many States have found that relaxing the transition point between localizer critical and sensitive area protection segments to 2NM before the threshold results in CSA that can be better managed operationally. The guidance material does not prescribe the selection or application of protection segments. They are illustrated in figure 1 (critical area and corresponding approach protection segment in red, sensitive area in blue). To illustrate the flexibility in choosing protection segments in CSA assessments, the transition point is not the same between the localizer and the glide path. A transition in line with the operational ideal has been chosen for the glide path mainly because CSA protection zones for the glide path can be accommodated more easily – they do not suffer from the stop-end runway overlap issue and are only creating capacity issues when runway line-up operations need to pass directly in front of the glide path antenna on a mixed-use runway (landings and take-offs).

Purpose of CSA Example Tables

"A picture is worth a thousand words" is a saying that applies, unfortunately in a mostly undesired sense, to the example tables. The NSP considered deleting the example tables completely, since many environmental assumptions need to be made such that only very few, if any, runways will fit the simulation parameters. Finally, it was decided to retain the tables, but to explicitly specify their purpose. Firstly, they provide a rough order of magnitude indication of CSA dimensions. It remains very possible that local CSA will be significantly larger or smaller, but in that case it would be sensible to understand the reasons. Second, they serve as a benchmark to verify simulation tools. Third, they should serve as a trigger for further study in airport construction projects: if the CSA table indicates, for example, a potential conflict with a planned runway exit, it is recommended to undertake further, more detailed studies to ensure airport compatibility. Conversely, what should not be done is to just blindly apply the example CSA tables to an existing runway and compare them directly with existing CSA dimensions. Any such comparison needs to take into account all differences between the stated simulation assumptions and the local conditions.

One good way to illustrate the potential discrepancy between the example tables and real conditions is to consider the aircraft tail height used in grouping size classes. The simulations assume a flat runway, which will be encountered only very rarely in reality. One tail height boundary, between the medium and the large size class, is at 14m. It will not require any atypical terrain unevenness to elevate an aircraft with a 13m vertical tail height into the next larger tail height group from an ILS signal reflection scenario point of view.

The example tables have been generated to provide a comprehensive set of examples in terms of ILS antenna types, ILS categories and aircraft orientations. While the given examples are considered to be globally representative, they are not meant to cover each and every scenario, especially when it comes to installations using special or advanced antenna designs.

ILS GLIDE PATH CSA SIMULATIONS

While the recent work on the localizer material was mainly conducted by DSNA, Eurocontrol conducted a cooperative study with Airbus, using the ELISE tool, for the glide path. This allowed the use of Airbus computing resources, since glide path simulations are more demanding due to the higher wavelength of the carrier signal. ELISE is a tool that has been used in conjunction with a number of verification test campaigns, allowing good confidence in the glide path simulation results.

Agreement of Simulation Parameters and Assumptions

The glide path CSA study was conducted in two phases. The first phase served to analyze simulation parameters, so that they could be agreed in preparation for the full simulations in the second phase. Among the findings of the first study phase are that the meshing of the 3D aircraft shape at one sixth of the wavelength is sufficient, and that it is acceptable to run all simulations at a glide path frequency in the middle of the band (332.0 MHz was used). It was also decided to use the middle of the vertical tail as a reference point, and worst case orientations other than zero and 90 degrees to the runway axis were derived.

A bit of a surprise were questions on the interpretation of ILS tolerances. The ILS glide path structure tolerances apply to the mean glide path, allowing for some curvature, especially below ILS point B. Annex 10 guidance specifies that "*Analysis of ILS glide path bends should be made using as a datum the mean glide path and not the downward extended straight line.*" (Attachment C, 2.1.5). One practice to establish the mean path above ILS point A and below ILS point B is to use a graphical average [3]. Different approaches may exist in how to evaluate a graphical average numerically. Because it was simpler, conservative and not causing significant disadvantages, it was decided to use the nominal 3 degree glide path as a reference to evaluate both alignment and structure tolerances.

Evaluation of the structure tolerances further involves a sliding window of ±20 seconds. However, when evaluating sensitive area impact starting at 0.6NM

(approximately corresponding to the 200ft Decision Height), only 20 seconds of approach to the threshold remain available at an aircraft speed of 105 knots. In other words, a full 40 second sliding window can no longer be evaluated. Consequently, it was decided to use 2 consecutive seconds of total tolerance exceedance as an equivalent to the sliding window criteria (95% of 40 seconds).

For the aircraft on the ground causing multipath reflections, the medium category used a Tupolev 204 (largest tail height within category), the large category used a Boeing 747-400, and the very large category an Airbus A380. Given that the medium size aircraft category covers quite a significant diversity, airports could take advantage of further optimizations if the largest aircraft that can or will operate on their runways are smaller than the Tu-204. For the small aircraft / large ground vehicle category, initially a rectangular box, 4m wide, 12m long and 6m high was used. While this was judged to be an acceptable simplification initially, this box produced larger areas than the medium aircraft category in some cases. Consequently, the results were reworked using a 3m wide, 12m long and 4m high box. This more closely matches the largest ground vehicle that can be encountered at an airport, the so-called ARFF (Airport Rescue and Fire Fighting vehicle). These results were further verified against a Beech 1900D as a typical example of small aircraft with a tail height below 6m.

Simulation Results

Figure 2 shows a typical ELISE simulation result. The grid represents all simulation points, sampled at 25m laterally and 50m longitudinally. The dark orange color indicates areas where either the alignment or structure tolerances are exceeded, but only very briefly, such that the sliding window tolerance is still respected. The dark red / burgundy color indicates areas where the sliding window criterion is violated. The software extrapolates the colors between the sample points, so no attention or electromagnetic rigor should be attached to the color graduations between sample points. The grid points represent aircraft tail locations where multipath or other propagation effects cause a signal disturbance to an approaching aircraft. Looking at the number of points and multiplying them by the number of scenarios for all aircraft size classes at a 15cm mesh, aircraft orientations, ILS categories and antenna types can give an appreciation of the computational burden this implies when using an exact method of resolution of the corresponding propagation equations. It should consequently not be surprising that some simplifications needed to be made.

One surprise was to see how far out both the critical and sensitive areas can extend: more than 800m for a medium aircraft and up to 1400m for an A380 in front of a Null-reference antenna. While the situation improves significantly for M-type arrays, airports with adjoining runway or taxiway operations will need to consider this. In some cases, this led to some additional simulation runs being necessary to ensure that the stop end of the tolerance exceedance could be confirmed. Cases were added both on the far end in front of the antenna and behind the antenna as necessary. The overlap over the runway and onto the other side was also evaluated.

The choice of the Cat I decision height or 0.6NM before threshold as a transition point between glide path critical and sensitive area protection caused the critical area to be slightly larger than the sensitive area in almost all cases. This highlights the fact that depending on protection segment choices, the typical notion of the sensitive area being larger than the critical area may not hold true. In the guidance material example, this can enable a single protection area concept and will lead to simplified operational management.

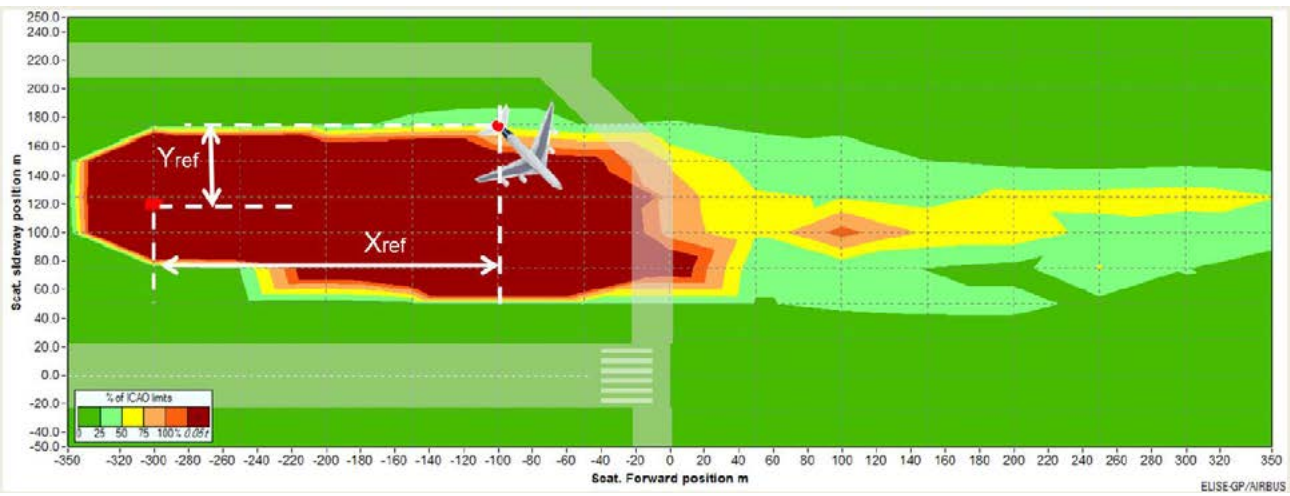

Figure 2. Example Simulation Result (Cat II/III critical area, Medium aircraft, M-Type antenna)

Deriving Keep-Out Areas

For the localizer, deriving keep out areas to allow the determination of hold lines is simpler than for the glide path. There, the dominating aircraft orientation for the sensitive area is perpendicular, with the tail of the aircraft pointing towards the runway. Parallel to the runway orientations have little impact and non-parallel, non-perpendicular orientations only add to the perpendicular areas. The fact that the localizer is centered on the runway axis is also helpful in relaxing geometry constraints. In the case of the glide path, the reflection geometry gets compressed into a relatively small space, with a smaller margin between the antenna and the adjoining taxiway. Annex 14 constraints have been taken into account in the analysis – this ensures that for example, keep out areas will always provide wingtip clearance (i.e., the CSA dimensions ensure that the aircraft will not hit the glide path antenna mast). Given the limited "exposure area" in terms of length along the runway, care was taken to minimize CSA overlap into typical parallel taxiway distances.

Initially, the non-parallel, non-perpendicular orientations were termed "worst case" orientations. However, that was found to be a tricky term: in some cases, parallel or perpendicular orientations could be more constraining that those with oblique angles. Also, "worst case" can be applied to either the magnitude of the signal distortion or the impact on airport keep-out areas. Finally, the term "other orientations" was adopted to denote the turn to line up in 15 degree increments as well as the perpendicular orientation where the tail of the aircraft points towards the runway – this latter case being rarer than the typical line up with the nose towards the runway.

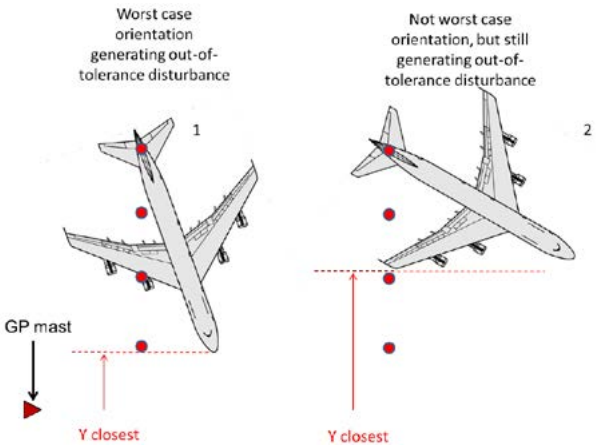

Figure 3: Keep-Out Area Derivation

Keep out areas were then derived taking into account ALL orientations which cause out of tolerance signals, and depending on the corresponding aircraft orientation, the largest value was chosen. This is illustrated in figure 3, using an example of a lateral y value. Depending on aircraft geometry, there are fixed angles where either the wingtip, the nose or the tail determine this distance. Because this distance limit is still causing out of tolerance signals, a buffer in line with the sampling steps was added to ensure in-tolerance signals when the keep out area is respected (25m laterally, 50m longitudinally). It turned out to be impossible to properly take aircraft orientations into account by any other method, such as starting from a point that is just outside of the out-of-tolerance areas, as shown by the example aircraft location in figure 2.

The above process illustrates that while there is a generally valid logic that larger aircraft cause larger keep-out zones, typically driven by the vertical tail, there can be some surprising non-linearities. For example, it is possible that an A380 has a smaller keep-out area than a B747, simply because the critical orientation is with the nose towards the runway, putting the A380 tail farther away due to its greater length.

ILS GLIDE PATH ANTENNA OPTIMIZATION STUDY

Once the ILS CSA work was nearing completion, a related study was started to address a long-standing question on glide path coverage requirements. Some years ago, Eurocontrol lead an Annex 10 localizer coverage standards change to accommodate a reduced coverage volume [4]. The objective was to allow specific localizer array designs to be in compliance with Annex 10 that significantly reduce exposure to clearance multipath (since course multipath can be addressed by larger arrays without causing standards compliance issues). The Annex 10 change allows reduced field strength at low altitudes at the far out, ±35 degree coverage edges, as long as approach profiles ensure that coverage is not operationally used in those areas. The change accommodates both specific designs as well as current installations which may struggle to provide coverage at the extreme edges. The same logic can be applied to the ILS glide path: the ±8 degree lateral coverage does seem rather excessive given that glide path use occurs after being established on the localizer, which has a lateral guidance sector of not more than about ±3 degrees.

The question that was to be addressed by the study was if significant benefits can be obtained when relaxing the ±8 degree lateral glide path coverage requirement. Given that updated results on glide path CSA were available, it made sense to evaluate if any antenna system changes could significantly reduce the CSA dimensions – laterally as needed and longitudinally. An additional objective was to improve the far out coverage. During the operational studies conducted by Eurocontrol to support the localizer changes [5], it was discovered that with increasing use of continuous descent approaches, it is becoming quite common for aircraft to establish themselves on the glide path at distances far beyond the formal 10NM coverage. Being able to focus the glide path beam more than is common today was expected to achieve this, thereby aligning system service provision with the evolution of the operational use.

Design Targets

To simplify the analysis, only the critical area for an A380 in parallel or perpendicular orientations was evaluated to assess CSA benefits. For the lateral critical area target limit, a value of 45m, referenced to the glide path mast, was used. This limit is 10 meters lower than the limit computed by the Airbus simulations and provides 5m wing tip clearance for an A380. For the longitudinal limit, the optimum would be 230m (300m glide path setback, minus half-width of taxiway and wingspan). This would allow an A380 to line up right in front of the glide path antenna without any problems. Since this is clearly not possible, an alternate optimum was derived. Figure 4 illustrates how a distance of 575m prevents excessive penetration of the first Fresnel ellipsoid by the A380 tailfin. While the impact on a line up taxiway right in front of the glide path mast is unavoidable, at least the potential impact on adjoining airport operations is minimized. The 575m are an improvement over the 700m for the M-array and the 1450m for the Null-Ref derived in the Airbus CSA study. Depending on airport layout, the adjoining movements could actually result in more operational complications than the line up on the runway that the glide path is serving, since this only comes into play when the glide path is both on the line-up side and the runway is being used in mixed operations.

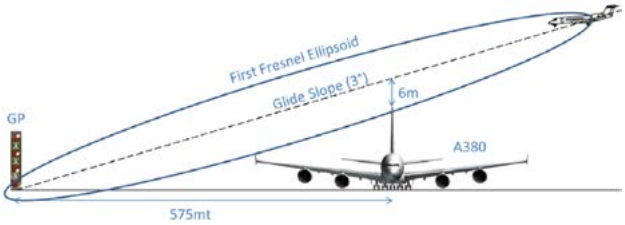

Figure 4: Desired Longitudinal CSA Limit

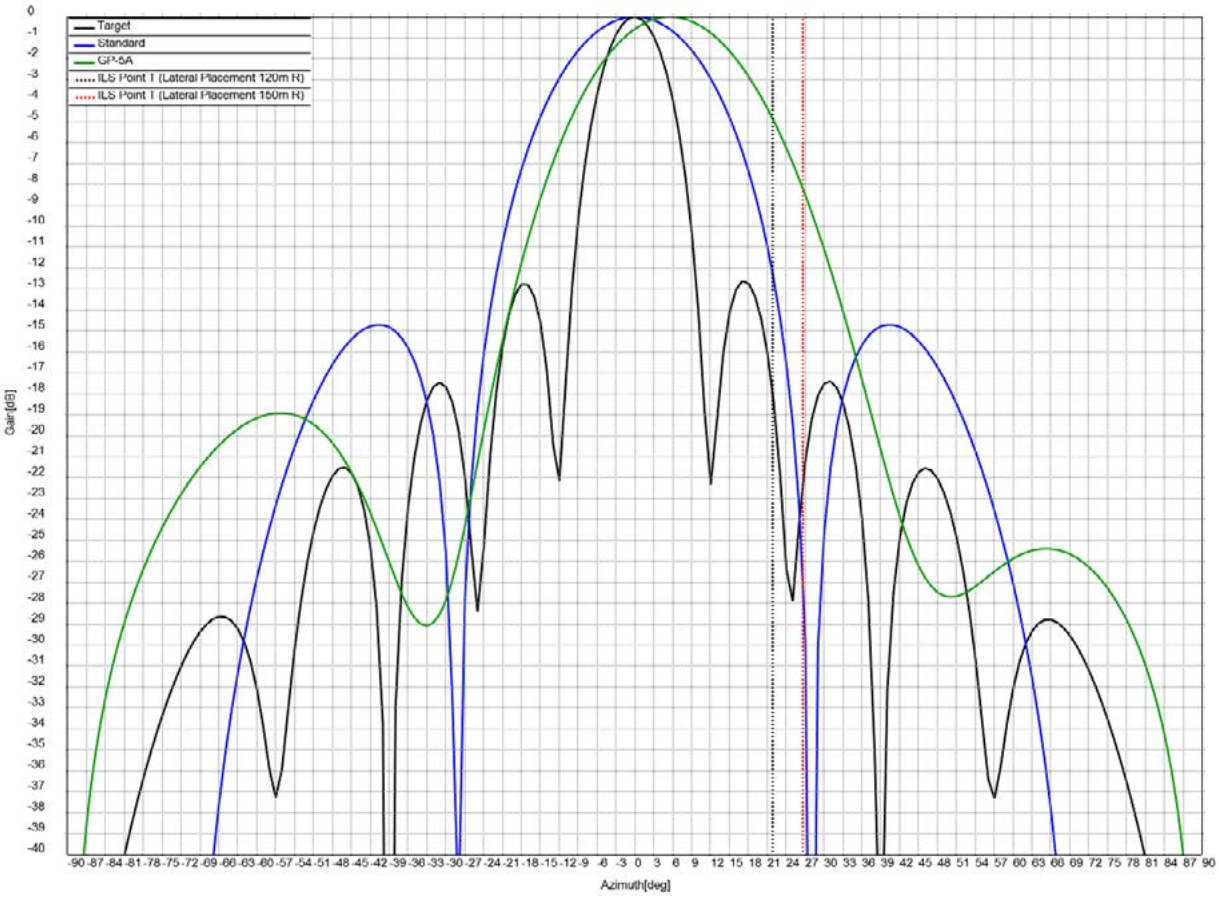

Figure 5: Gain Pattern Comparison

For the far out coverage – which is expected to be in conflict with the longitudinal CSA reduction – two metrics were used. Inside a ±3 degree sector, minimum field strength was assessed either in terms of range or elevation angle. The maximum range was evaluated at 0.45θ with a target of 25NM. The minimum elevation angle was evaluated at 25NM with a target of 0.45θ or 1.35 degrees for a nominal 3 degree glide path.

Finally, it was recalled that the ±8 degree coverage sector does have a supporting rationale linked to the final phase of the approach. Depending on glide path antenna offset, the 8 degrees will provide coverage to a point on the centerline below the half-way point between the Cat I decision height and the threshold. This corresponds to where auto-land systems typically stop using the glide path and switch to the radio altimeter in preparation for

the flare maneuver. Consequently, sufficient and stable threshold coverage was added as a design target.

Approach

Since a few optimization methods are already known, such as tilting the antenna or off-setting some elements, the study aimed to identify potential benefits as free from constraints as possible. Obviously, the design needs to be physically realizable, taking into account the constraints of a frangible mast – increasing antenna directivity by adding lateral width or vertical height must remain within moderate limits. Some manufacturers stated a strong preference for keeping the Kathrein antenna element. This is due to the element being a mass-produced antenna that is also used in telecom applications, and thus it comes at a very affordable price in the generally price sensitive ILS market. However, given that the target design was to serve challenging installations, this was not kept as a necessary constraint.

Target Antenna Gain Pattern

Eurocontrol contracted IDS to analyze glide path antenna optimizations. IDS used their EMACS software tool, which has an advanced suite of propagation modelling capabilities. IDS analyzed different options for antenna elements in terms of the number of dipole columns and their spacing. Log-periodic antennas were also evaluated. The largest panel analyzed contained 12 columns at 72cm spacing, resulting in a panel width of almost 9m. Further analysis focused on up to 8 elements resulting in a somewhat more reasonable width of less than 6m. Finally, an initial design (referred to as "target") with log-periodic antennas was identified as shown in figure 5. The black pattern is the new target pattern, while the blue trace is the standard M-type using Kathrein elements, and the green pattern corresponds to the GP-5A antenna panel from Watts Antenna Company. Also shown is the location of the runway threshold in azimuth angle as seen from the glide path antenna mast, for both a 120m and a 150m offset.

The GP-5A represents an already somewhat proven design for CSA optimization – it has been found to enable line up at normal holding points, allowing large aircraft to proceed ahead of the glide path antenna mast on the parallel taxiway, thereby reducing line-up times. Consequently, this antenna design was used as a benchmark. When looking at the GP-5A pattern, it can be observed that gain on the left side is reduced with respect to the standard pattern, limiting illumination of the nearby taxiway. On the right hand side, the asymmetrical pattern has greater gain than the standard one, ensuring stable coverage in threshold region.

The black target pattern has greater cut-off that leads to improved performance in terms of lateral limit of CA and far-out coverage but, on the other hand, it shows sharp nulls that are far from optimal when looking at the needs of increasing threshold coverage and keeping phase stability along the entire approach path. To overcome this problem, IDS initially proposed the use of four frequencies instead of two frequencies. This would create an additional beam tilted towards the runway, capable of increasing phase stability and threshold coverage. Finally, IDS modeled the elements using the method of moments and a heuristic search algorithm called MACCO or "Memetic Ant Colony Constrained Optimization" to determine phase and amplitude. This was realized on a 4m wide element using 2 by 6 thick dipoles, without needing to use four frequencies. The final version is expected to perform better in terms of monitoring and coupling effects and have better phase stability and threshold coverage. The design has a main beam which points slightly towards the runway (0.5 degrees), has a maximum gain of 15dB, a side lobe level of -18dB and a front-to back ratio of at least 17dB, while being stable over the entire glide path frequency range. The resulting pattern (referred to as "optimal") is shown in figure 6, in comparison with the "target" pattern.

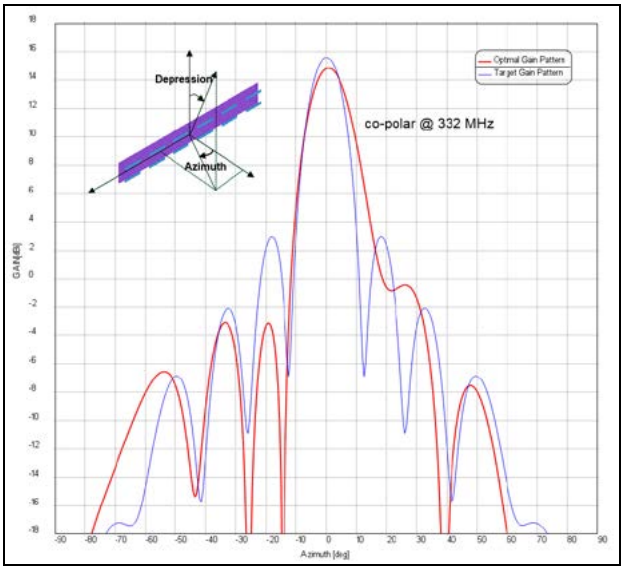

Figure 6: Optimized GP Antenna Pattern

While this optimized antenna panel already performs well, a fourth antenna panel is needed to reduce the longitudinal limit of CA, leading to a mast height of 17,5m. This modified M-array requires an offset of at least 130m to avoid impinging the inner transitional Annex 14 [6] surface. The bottom-most and third element are fed with CSB, SBO and CLR signals, while the second element is fed with CSB and SBO, and the fourth, top element with SBO. An increment of course transmission power is required for the modified M-array system to keep an unchanged calibration of the DDM signal. The optimized antenna panel in itself and the fourth panel can be used individually or in combination.

Assessment of Results

The comparison of the antenna designs in accordance with the developed metrics is given in table 1, considering the standard M-array system and the GP-5A as a reference. It can be seen that the optimized design developed by IDS for the antenna panel improves performance in all aspects when using four optimized

antenna panels. The M-array system assessed uses Kathrein antennas, a course power of 5W and a clearance power of 0.5W. The same power settings are used in the GP-5A. For the optimized IDS antenna design, course power had to be increased to 12,5W, while clearance power could be kept at 0.5W.

Recognizing that a 17m high antenna supporting four 4m wide panels is a rather significant antenna change, the design constraints were reviewed with the aim to produce a more cost-effective antenna panel, while still maintaining most of the benefits. The longitudinal critical area limit, which is for a 90 degree orientation (aircraft perpendicular to runway) turned out to be a significant constraint, while the potential benefits proved not to be all that impressive – both 600m and 700m are quite large values. Given how rare such runway configurations are with an exactly perpendicular adjacent runway, it was decided to drop this criterion. Retaining the lateral critical area criterion and near and far coverage objectives, a "sub-optimal" antenna panel design was produced. The sub-optimal panel has a width of 2,7m and merges the best features of the Kathrein element (better far out coverage) and the GP-5A (better lateral CSA and good threshold coverage). However, the performance turns out to be quite similar to the benchmarks. This shows that it is difficult to significantly improve glide path performance when staying within the constraints of a typical M-array mast.

Table 1: Antenna Performance Assessment

Performance			Results	
CA	Lateral limit for 0° orientation		Kathrein	50m
			GP-5A	45m
			Optimal	**45m**
	Longitudinal limit for 90° orientation		Kathrein	700m
			GP-5A	700m
			Optimal	**600m**
Far Out Coverage		Maximum Range @0.45θ	Kathrein	≈12NM
			GP-5A	≈10NM
			Optimal	**≈15NM**
		Minimum Elevation @25NM	Kathrein	1.80° (0.600θ)
			GP-5A	2.05° (0.683θ)
			Optimal	**1.67° (0.556θ)**
Threshold Coverage		Minimum Field Strength below CAT I DH	Kathrein	-52.26 dBV/m
			GP-5A	-39.05 dBV/m
			Optimal	**-35.96 dBV/m**

Of course a lot of work would still be needed to get from a simulated design to a production ready, fully proven antenna. While the new optimal IDS antenna design certainly has very good performance, the benefits are not very convincing, especially when contemplating the complexities of the higher mast. One detail finding that was surprising was that the reduction of the sidelobe levels did not lead to significant benefits. So even if the ±8 degree lateral coverage requirement is excessive for far out coverage, it remains difficult to realize a stable antenna design that is more directional while respecting or improving on existing performance objectives. The positive aspect of this finding is that current glide path designs are not that far from the ideal. Consequently, Eurocontrol decided to not pursue any further development in this area at this time. Nonetheless, manufacturers are encouraged to continue studying antenna design optimizations since it has been shown that a lot can be done with relatively simple means such as asymmetric patterns using appropriate phase and amplitude feeding.

Impact on Future Standards Development

The results of the IDS study were presented to the 22nd meeting of the Eurocontrol Navigation Steering Group (NSG) in April 2016. The NSG agreed with the conclusion that given the limited benefits, further development of an optimized glide path antenna was not required. However, given the fact that especially asymmetric designs may struggle to meet the ±8 degree lateral coverage requirement, the NSG recommended that the matter be brought to the attention of the ICAO Navigation Systems Panel for further evaluation. Eurocontrol plans to do this in 2016.

CONCLUSIONS

This paper gave a comprehensive overview of Eurocontrol efforts in ILS sustainment through its ICAO NSP activities in recent years. While a significant effort on ILS localizer coverage optimization concluded some years ago, the main recent activity was the contribution to the Critical and Sensitive Area guidance material update. The paper gave an overview of the principles and methods used in the CSA effort, especially with respect to the glide path, building on the cooperation with Airbus. For example, it was shown that deriving keep out areas (for placing taxiway hold lines) based on simulation results is not a trivial matter.

A further study was undertaken with IDS on glide path antenna optimization, where corresponding metrics and methods were developed and shown. The study built on the CSA results, but also added additional criteria originating from the work on localizer coverage optimization. While no dramatic improvements were identified, it was shown that some optimization potential does exist, which is relevant primarily for airports where

the ILS glide path mast is on the same side of the runway as aircraft line up operations.

During 2015, an outreach activity on ILS CSA was conducted, to explain the material especially to operational stakeholders, in the hopes that the new Annex 10 amendment will be accepted by States. This paper represents another contribution in this regard, but with more technical background. Airport stakeholders have requested the development of additional guidance. It is recognized that a lot of information does get lost when compiling extensive technical studies into a few pages of guidance material. It is hoped that this further guidance can be generated in the coming years.

RECOMMENDATION

It is hoped that the information in this paper will be useful for flight inspection organizations involved in ILS CSA assessments and ILS optimization projects. In view of the plan to generate further guidance material on ILS optimization in the future, readers of this paper are invited to bring any relevant feedback on these matters to the attention of Eurocontrol.

DISCLAIMER

This paper contains no official EUROCONTROL or ICAO position, and does not constitute any endorsement of a particular company or product. All intellectual property, copyrights and trademarks of specific products mentioned remain with their respective owners.

ACKNOWLEDGMENTS

EUROCONTROL gratefully acknowledges the helpful comments received from Alf Bakken and Thor Breien from INDRA NAVIA and from John Johnson from Watts Antenna Co. Thanks also go to Christophe Dehaynain from the French DSNA/DTI for a fruitful cooperation during the revision of the ILS CSA guidance material.

NOTE

Leonardo Canon has left the company CIMPA, which was supporting Airbus in the ILS CSA simulation tasks.

REFERENCES

[1] ICAO, July 1996, Radio Navigation Aids, International Standards and Recommended Practices, Annex 10 to the Convention on International Civil Aviation, Volume 1, 6th Edition

[2] S. Dale Courtney, June 2008, Determination of ILS Critical and Sensitive Areas: A Comparison of Flight Measurement versus Simulation Techniques, Proceedings of the 15th International Flight Inspection Symposium, Oklahoma City, USA

[3] FAA, April 2015, United States Standard Flight Inspection Manual, Order 8200.1D

[4] H. Demule, G. Berz, A. Bakken, June 2008, Evaluation, Design, Commissioning and Certification of a ±15° Reduced Coverage Localizer, Proceedings of the 15th International Flight Inspection Symposium, Oklahoma City, USA

[5] G. Berz, M. Amherd, October 2007, The Power of Recorded Flight Data Analysis to support ILS Sustainment Studies, Proceedings of the 26th Digital Avionics Systems Conference, Dallas, USA

[6] ICAO, July 2013, Aerodromes: Aerodrome Design and Operations, International Standards and Recommended Practices, Annex 14 to the Convention on International Civil Aviation, Volume 1, 6th Edition

19th International Flight Inspection Symposium (IFIS)

Belgrade, Serbia, 13-17 June 2016

NEW ILS LOCALIZER ULTRA-WIDE ANTENNA SYSTEM WILL INCREASE LVP LANDING CAPACITY IN ZURICH

Hervé Demule
Navigation Engineer, Project Manager
Skyguide, Swiss air navigation services
Geneva, Switzerland
E-mail: herve.demule@skyguide.ch

Laurent Evain
Product Manager Simulations
Airbus ProSky
Toulouse, France
E-mail: laurent.evain@airbus.com

ABSTRACT

End 2014, the Instrument Landing System (ILS) Localizer on the main landing runway 14 of Zurich Airport has been replaced by the new ultra-wide NORMARC 32-element antenna system.

Thanks to its very narrow beam and the fact that its sensitivity to signal reflection is significantly decreased, the equipment has very small or nearly no sensitive area. The paper presents the simulations of the Zurich 14 Localizer Critical and Sensitive Areas (CSA) using the advanced 3D modelling ILS prediction software ELISE developed by the Airbus Group and the ENAC.

Besides, the "Optimised Operation" concept as explained in EUR Document 013 (European Guidance Material on All Weather Operations at Aerodromes) was originally addressed to MLS and GBAS operations. This concept applied to ILS operations with the introduction of a new Landing Clearance Line (LCL) will enable to set new criteria for the management of landing and exiting aircraft.

Finally, by analyzing the last two LVP seasons (more than 1500 LVP landings), the direct effect of the introduction of these new LCL has been studied and assessed: the LVP spacing between two landing aircraft (till Heavy category) can be reduced from 6 NM to 5 NM. This will allow ultimately an improvement of capacity in LVP by around 17 %, which will translate into an important operational benefit for the Airport, Controllers and Airspace users.

INTRODUCTION

The increased air traffic volume has resulted in a more demanding situation for handling of the traffic flow. However, restrictions given by the ILS Localizer Critical and Sensitive Area (CSA) size result in traffic constraints during Low Visibility Situation (LVP), which would be avoided if a smaller CSA were implemented.

End 2014, the new Instrument Landing System (ILS) composed of an ultra-wide aperture type of Localizer on the main landing runway 14 of Zurich Airport has been released for CAT III operations.

Thanks to the fact that its sensitivity to signal reflection is significantly decreased, this ultra-wide aperture Localizer has nearly no ILS sensitive area. And thus the separation minima in Low Visibility Procedures (LVP) will be reduced . This will allow ultimately an improvement of capacity in LVP, which will translate into important operational benefits for the Airport, Controllers and Airspace users.

The width of the Localizer antenna system is the only factor, which can be applied to reduce the size of the CSA. The purpose of this paper is twofold: first, it demonstrates that significant improvements in airport operations can be gained by replacing existing Localizer antenna systems with a Ultra-wide antenna system. Secondly, it shows that an airport site-specific analysis of the CSA using advanced airport environment simulation software like ELISE could also significantly reduce the size of the CSA and bring operational benefits.

THE NEW ULTRA-WIDE LOCALIZER NM7332A PERFORMANCES

The replacement project

In collaboration with AIRBUS ProSky and Indra Navia AS, Zurich airport (FZAG) and skyguide launched in 2013 a feasibility study in order to assess the size of the CSA of the new localizer 14 Zurich (in particular the new NM 7232A), and evaluate the potential gain for airport operations. Among several localizer types (and different antenna heights), the results of the ELISE study clearly showed the benefits of the NM 7232A, with an antenna height of 3 meters. Thus, the replacement project has been launched for a realization phase in 2014, according to the following the schedule:

- Building phase in February and March 2014
- Mechanical installation in April 2014
- Ground commissioning in May 2014
- Flight check in June 2014
- CAT III certification phase from June to December 2014
- CAT III Clearance for Operation in December 2014.

Figure 1 shows a picture of the new installed localizer NM 7232A in Zurich RWY 14.

Figure 2 illustrates the very clean course structure of the new localizer, measured during the commissioning flight check. It confirms its insensitivity to signal reflections and its big margin relative to CAT III requirements. Since December 2014, no outage has been reported and its MTBO higher than 16'000 hours confirms the expectations in term of continuity of service and stability.

Figure 1 Picture of the Indra NM7232A, seen from behind

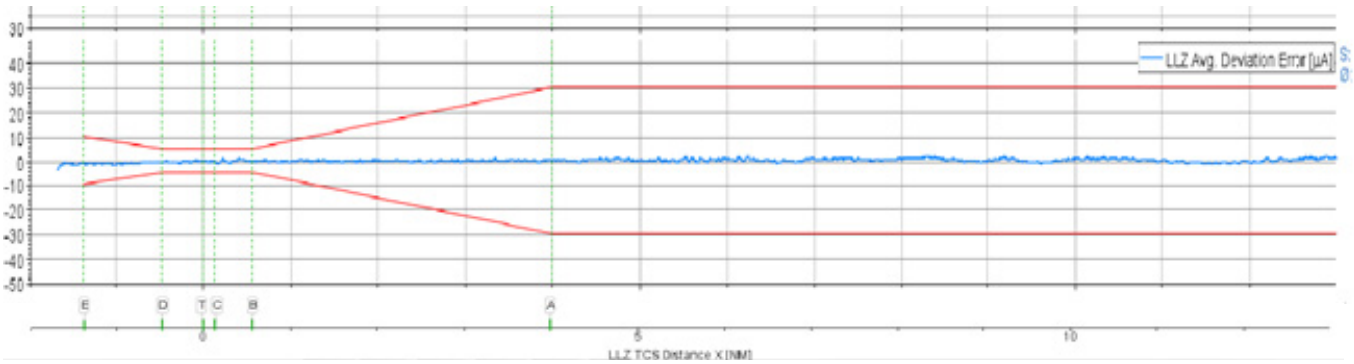

Figure 2 CAT III course structure (measured during commissioning flight check)

ILS Protection Areas on ground

The protection areas of the ILS 14 signal at ZRH were computed with the support of ELISE (Exact Landing Interference Simulation Environment) software, which is developed by the Airbus Group in collaboration with the French National Civil Aviation University (ENAC). The ELISE software uses advanced 3D technologies to assess the impact of an object on the Instrumental Landing System (ILS) signal received by the following aircraft in final approach. The simulations conducted with ELISE are based on the "Method of Moments" (MoM), which is the reference method for the analysis of the propagation of the electromagnetic waves. For the purpose of accuracy and reliability, the MoM has been applied on the entire 3D model of aircraft. The defined protection areas are:

- 2D Localizer Critical Area on ground (LCA): this is an area where the aircraft on ground creates an out-of-tolerance disturbance on CAT III signal before 1 or 2 NM

in the landing direction (i.e. from the beginning of the approach - 10 NM - to 1 or 2 NM from the runway threshold).

- 2D Localizer Sensitive Area on ground (LSA): this is an area where the aircraft on ground creates an out-of-tolerance disturbance on CAT III signal from 1 or 2 NM from runway threshold to Point E on the runway (600 m before the runway end).

The assessment of the Localizer Critical Area shall be based on a late landing clearance at 1 NM (conservative area vs. 2 NM). The assessment of Localizer Sensitive Area shall be based on a nominal landing clearance at 2 NM (conservative area vs. 1 NM).

The Runway 14 layout and aircraft routings (as shown on Figure 3 and Figure 4) has been modelled in ELISE.

Figure 3 Runway 14 ZRH layout

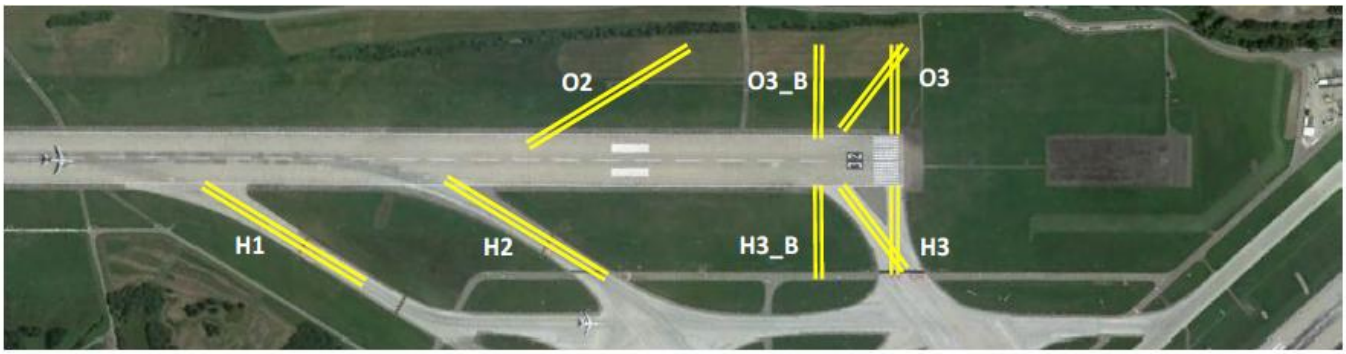

Figure 4 Aircraft routing on exiting taxiways

<u>Localizer Critical Areas on ground</u>

The following figures represent the CA simulations for different types of aircraft:

- Figures 5 and 6 for "medium" size aircraft (Airbus A321and Tupolev Tu204)

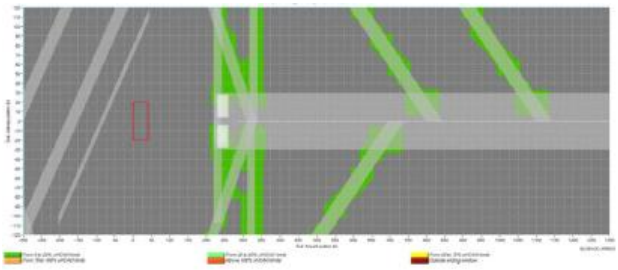

Figure 5 Localizer Critical Area for Airbus A321

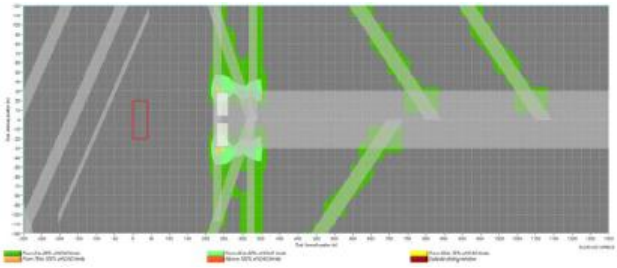

Figure 6 Localizer Critical Area for Tupolev Tu204

- Figure 7 for "heavy" size aircraft (Boeing 747)

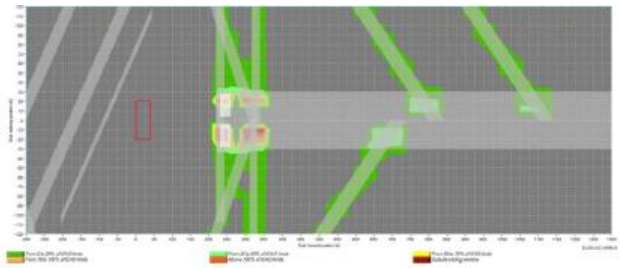

Figure 7 Localizer Critical Area for Boeing 747

- Figure 8 for "super heavy" size aircraft (Airbus A380)

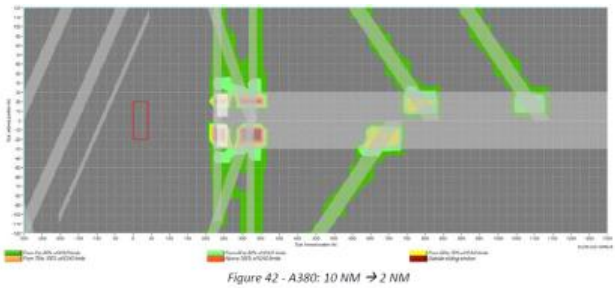

Figure 8 Localizer Critical Area for Airbus 380

Except for the "super heavy" class, the simulations demonstrate that the LCA do not penetrate the runway. The exception of Airbus A380 on the last taxiway H3 has been assessed and accepted by the operations based on the following arguments:

- With less than 0.3% of the traffic, the use of H3 is already considered as an exception.
- With only two Airbus A380 movements per day, "super heavy" aircraft are also considered as exceptions.

<u>Localizer Sensitive Areas on ground</u>

The following figures represent the LSA simulations for different types of aircraft:

- Figures 9 and 10 for medium (Airbus A321 and Tupolev 204)

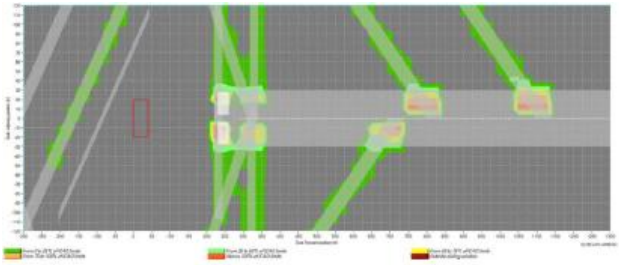

Figure 9 Localizer Sensitive Area for Airbus A321

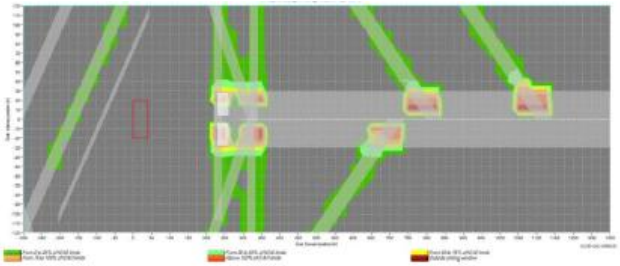

Figure 10 Localizer Sensitive Area for Tupolev Tu204

- Figure 11 for heavy (Boing 747)

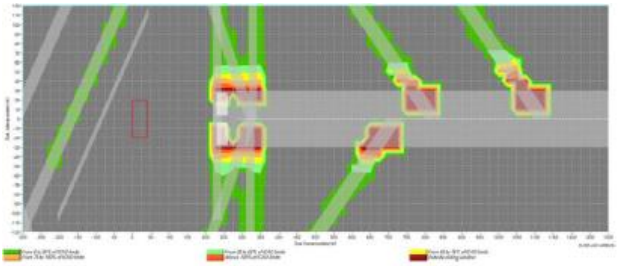

Figure 11 Localizer Sensitive Area for Boeing 747

- Figure 12 for "super heavy" size aircraft (Airbus A380)

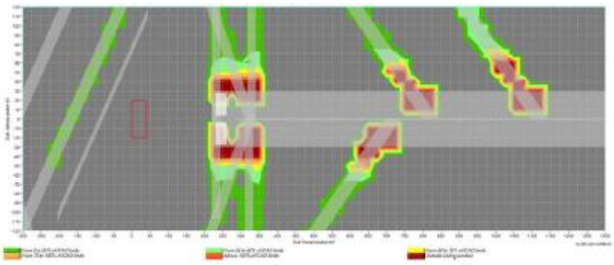

Figure 12 Localizer Sensitive Area for Airbus A380

Table 1 summarizes the results of the simulations of the Localizer Sensitive Areas on ground. Their maximal widths referenced to the runway centerline are:

- +/- 30 m for "medium" size aircraft
- +/- 50 m for "heavy" size aircraft
- +/- 70 m for super heavy size aircraft

Aircraft	Approaching aircraft distance range (reference THR)	Lateral distance between RWY CTL and end of LSA						
		H3	H3B	O3	O3B	H2	O2	H1
A321	2 NM to Point E (idem for 1 NM to Point E)	30 m		30 m				
Tu-204	2 NM to Point E (idem for 1 NM to Point E)	30 m	30 m	30 m	30 m	20 m		20 m
747-400	2 NM to Point E (idem for 1 NM to Point E)	40 m	40 m	40 m	40 m	40 m	40 m	50 m
A380	2 NM to Point E (idem for 1 NM to Point E)	50 m	50 m	50 m	50 m	60 m	50 m	70 m

Table 1 LOC 14 Widths of the Localizer Sensitive Area on ground (reference aircraft tail end)

THE OPTIMISED OPERATION CONCEPT FOR LVP CONDITIONS

Documented by [2] EUR Doc 013 "European Guidance Material on All Weather Operations at Aerodromes", the Optimised Operations concept has been developed to reduce the impact of LVP on runway capacity. It specifically addresses the case of a landing aircraft following a landing aircraft on a runway equipped with a precision approach landing aid that has a very small sensitive area, or no sensitive area in the vicinity of the runway. Initially dedicated and particularly applicable to MLS and GBAS, this concept can also be applied to high performance ILS, with very small sensitive area.

The capacity of a runway in Low Visibility Procedures is limited by a number of factors. There are two factors that are addressed in this concept. The first is the location of the CAT II/III holding positions and the second is the position at which ATC give landing clearance to arriving aircraft.

The Optimised Operations concept allows a maximization of the runway capacity (because the spacing between the aircraft on final approach is reduced), provided that the runway is equipped with following technology approach and landing aids:

- Precision approach landing aid with no or very small sensitive area;
- Surveillance system to monitor aircraft on final approach; and
- A-SMGCS (Advanced Surface Movement Guidance and Control System).

It states that a Landing Clearance Line (LCL) is to be defined and displayed on the A-SMGCS to identify to the controller the point the aircraft vacating the runway must have reached in order to issue landing clearance to a subsequent landing aircraft. Therefore, to fully optimize LVP operations, the sensitive area should not extent beyond the Landing Clearance Line:

- 77.5 m from the runway centerline for “super heavy” size aircraft
- 60 m from the runway centerline for “heavy” size aircraft aircraft and smaller

Current operations

In current operations, issuing landing clearance is based on the preceding landing aircraft being clear of the Localiser Sensitive Area (further than the CAT II/III stopbar) at which point ATC issue landing clearance to the following landing aircraft, subject to the following aircraft being no closer than 2 NM from the threshold (may exceptionally be reduced to 1 NM). This in turn defines the final approach spacing between these aircraft, which must be sufficient to allow time for the preceding aircraft to vacate the LSA before the following aircraft reaches 2 NM from touchdown.

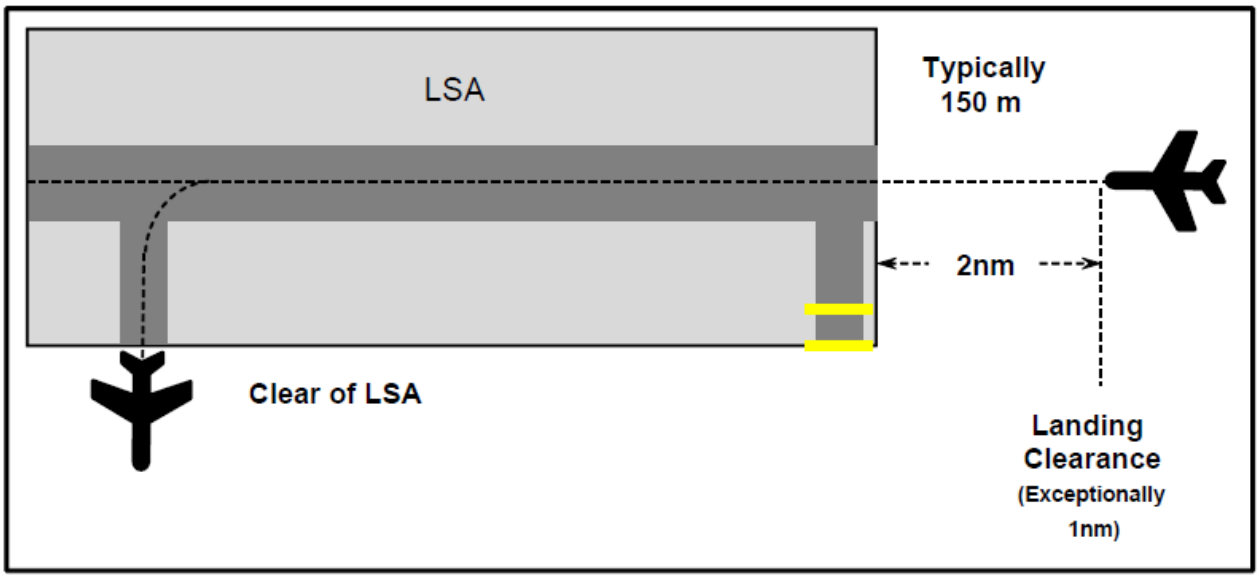

Figure 13 Requirements in current operations

Future operations

According to the Optimized Operations concept, a new criterion can be applied: instead of the current CAT II/III stopbar, a Landing Clearance Line (LCL) is defined. This line is not marked on the airfield by any signs or markings. It is only displayed on the A-SMGCS to identify to the controller the point the aircraft vacating the runway must have reached in order to issue landing clearance to a subsequent landing aircraft. For "heavy" size aircraft or smaller, this LCL can be positioned at a distance of 60 m from the centerline, on condition that the (half-) width of sensitive area of the landing aid is smaller than 60 m. **For ZRH 14 and its new localizer performances, as the maximal (half-) width of the sensitive area for "heavy" size aircraft is +/- 50 m, this criterion is applicable and a LCL at 60 m can be considered**.

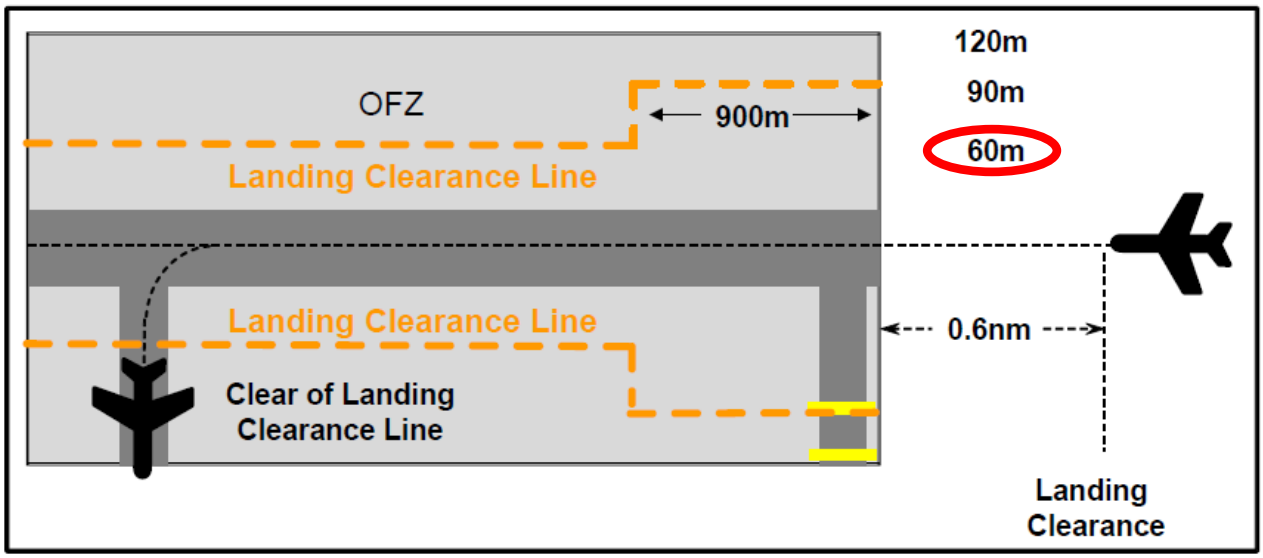

Figure 14 Future requirements for "heavy" size aircraft aircraft and smaller

FROM TECHNICAL PEFORMANCES TO LVP OPERATIONAL BENEFITS

As the Optimised Operations concept with this new LCL criterion (at 60 m) can be applied in ZRH 14 for "**heavy" size** aircraft or smaller, the questions to be answered are:

- What is the operational benefit in term of reduction of the spacing between two landing aircraft?
- From the current CAT II/III stopbar to the future LCL: as Runway 14 in Zurich is the main landing runway during LVP (without any take-off), what is the impact of the change of the exiting criterion?

The current LVP traffic situation

In order to assess the current situation, a statistical analysis of the last two LVP seasons, with more than 1,500 LVP landings, has been conducted

The general taxiway distribution during LVP for exiting aircraft is the following one:

- 67 % on H1,
- 33 % on H2
- Marginal on H3 (0.3 %)

As "super heavy" size aircraft (Airbus A380) only represent 1% of the traffic and are subject to special spacing rules due to wake turbulence, they are considered as exceptions and are not affected by this study and change. Thus, the reduction of LVP spacing in ZRH 14 will affect all the aircraft categories but the "super heavy" and will represent 99% of the traffic. The goal is to set **one single new rule for (nearly) all aircraft**.

The current LVP spacing

As illustrated by the histograms on Figures 15 and 16, the current LVP spacing is **5.6 NM** after an aircraft exiting on H1 and **6.0 NM** after an aircraft exiting on H2 (with a variance of 0.8 NM).

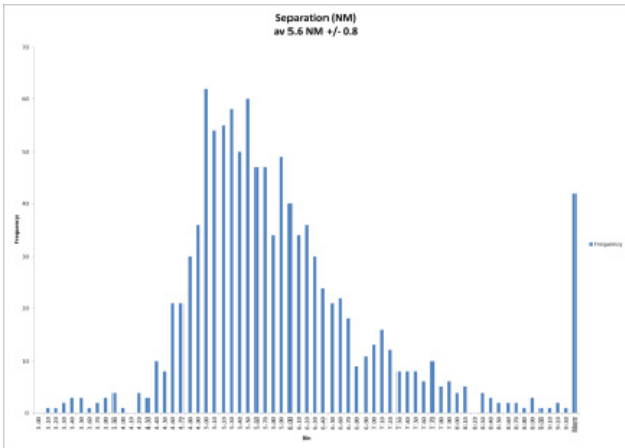

Figure 15 Spacing after an aircraft exiting on H1

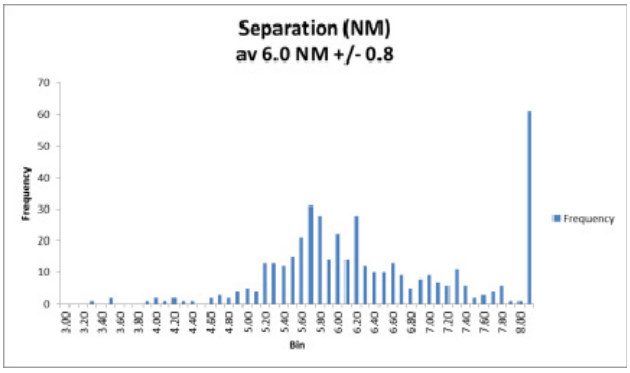

Figure 16 Spacing after an aircraft exiting on H2

In order to better understand the reason behind this current LVP spacing of approximately 5.6 NM to 6 NM, the next step of the study consists in assessing the position of aircraft #2 (the following aircraft) relative to the threshold when aircraft #1 (the preceding aircraft) passes the CAT II/III stopbar:

- For H1: the position of aircraft #2 is **2.1 NM** from threshold, when aircraft #1 passes the CAT II/III stopbar (with a variance of 0.7 NM).
- For H2: the position of aircraft #2 is also **2.1 NM** from threshold , when aircraft #1 passes the CAT II/III stopbar (with a variance of 0.8 NM).
- This position of 2.1 NM from the threshold (just before the nominal Landing Clearance Delivery Point at 2 NM) justifies a posteriori the current spacing of approximately 5.8 NM.

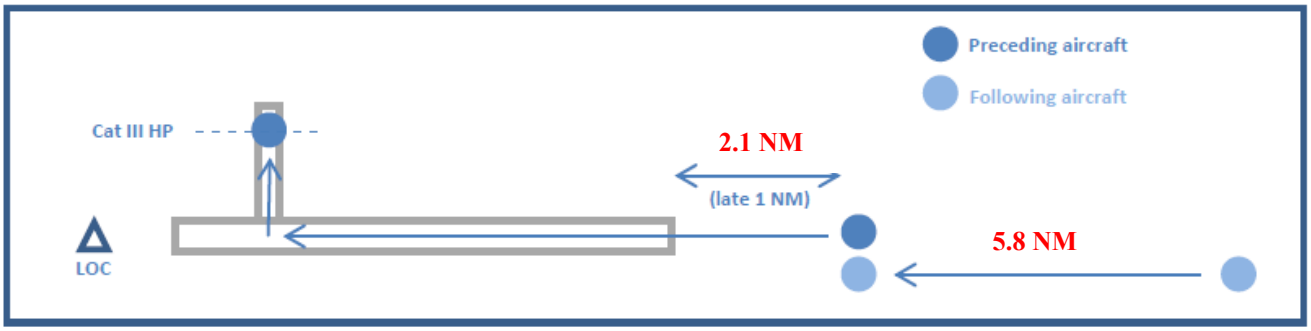

Figure 17 Current LVP operation at ZRH 14

<u>A new criterion for a new spacing</u>

In the today situation, the orthogonal distances from centerline of the current CAT II/III stopbars are the following ones:

- 170 m on H1; and
- 130 m on H2 and on H3.

In order to assess the possible reduction of the spacing between two aircraft, the same methodology has been applied with the new LCL criterion (at 60 m) instead of the CAT II/III stopbar. It consists in assessing the position of aircraft #2 (the following aircraft) relative to the threshold when aircraft #1 (the preceding aircraft) passes the LCL:

- For H1: the position of aircraft #2 is **2.9 NM** from threshold, when aircraft #1 passes the LCL (with a variance of 0.7 NM).

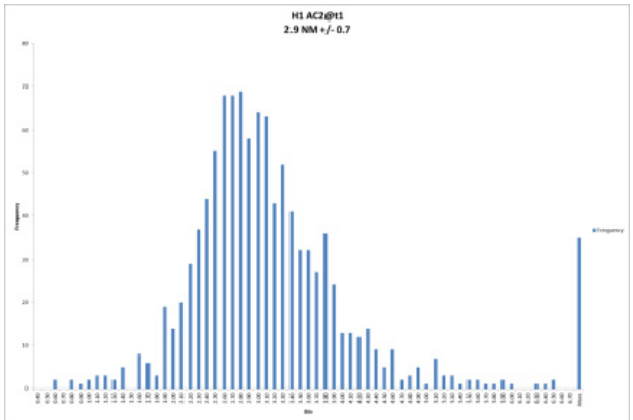

Figure 18 AC #2 position when AC #1 crosses LCL

- For H2: the position of aircraft #2 is **2.8 NM** from threshold ,when aircraft #1 passes the LCL (with a variance of 0.7 NM).

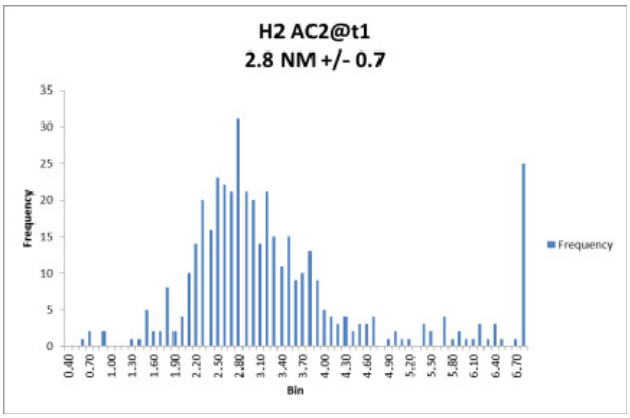

Figure 19 AC #2 position when AC #1 crosses LCL

- **Thus, this criterion change from CAT II/III stopbar to LCL can be converted into a spacing reduction of approximately 0.8 NM**

Based on this statistical study**, the chosen future target for LVP spacing will be 5 NM.**

LOCALIZER AND GLIDE PATH CRITICAL VOLUMES FOR MISSED APPROACH EVENTS

Localizer Critical Volume

The first 2D part of the study has demonstrated that the localizer sensitive area on ground for "heavy" size aircraft does not extend beyond 50 m from the runway centerline and that it is compatible with a LCL at 60 m.

However, for non-nominal situations, experience has shown that an aircraft that performs a take-off or a missed approach or a balked landing (overflying the localizer) could cause an out-of-tolerance disturbance to the following aircraft, which is in the final approach.

Thanks to the new advanced technologies of ILS signal modelling with ELISE, it is now possible to compute the Localizer Critical Volume (LCV) in 3 dimensions, including the vertical limits. The LCV is a 3D volume where the aircraft in flight (after a missed approach or a take-off) creates an out-of-tolerance signal to the following approach in approach.

The Figures 20 and 21 illustrate the LCV for "medium" size and "heavy" size aircraft with 5 NM spacing. The triangles in yellow or trapeze in red indicate an out-of-tolerance disturbance. It means that an aircraft at this position in X and Z might create an out-of-tolerance disturbance for the following aircraft in approach at 5 NM behind.

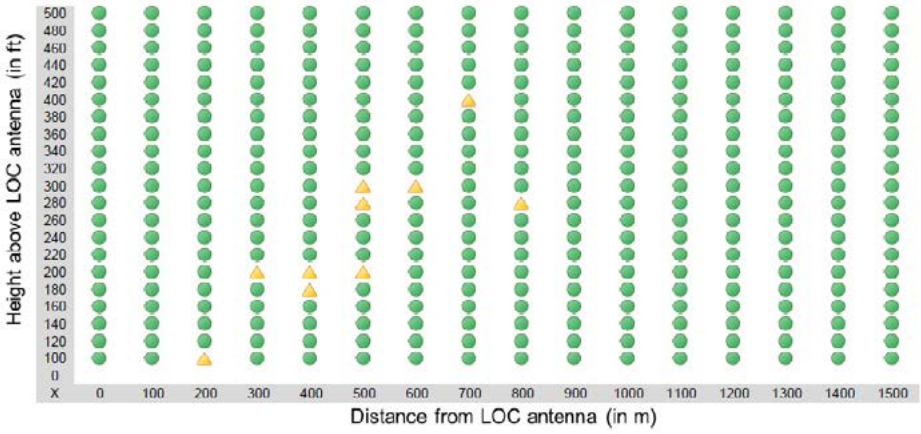

Figure 20 Static LCV for "medium" size aircraft with 5 NM spacing

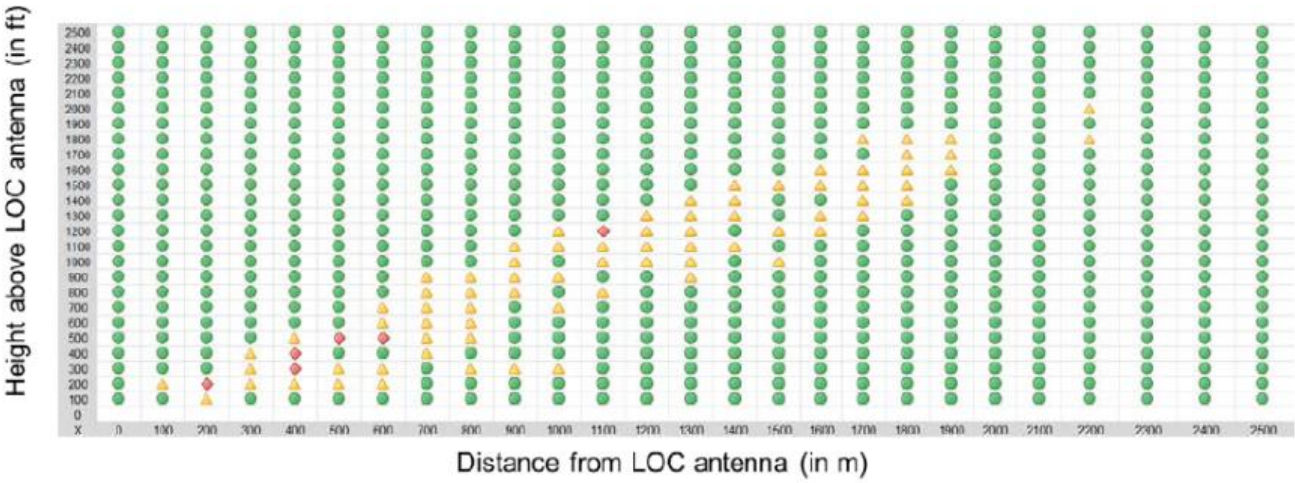

Figure 21 Static LCV for "heavy" size with 5 NM spacing

A link between the climb gradient and the minimum horizontal safe distance from the runway threshold to start the missed approach/balked landing (due to out-of-tolerance disturbances) can be determined.

The dynamic LCV is a protection volume that takes into account the movement of both aircraft:

- The first aircraft that overflies the localizer antenna, which causes the disturbance; and
- The second aircraft that follows the approach, which receives the disturbance.

The aim of this 3D study is to determine at which distance from the runway threshold a "heavy" size aircraft, which triggers a go-around or a missed approach, would not create an out-of-tolerance disturbance to the second aircraft. The analysis considers a large scope of climb gradients for the first aircraft that performs a go-around: from a minimum of **2.5 % as specified in PANS-OPS** manual to a maximum of around 30 %. The PANS-OPS value of 2.5 % is very conservative and, in practice, modern aircraft achieve much higher climb rates. A typical missed approach climb gradient experienced on airports is in **the order of 15 %** to 20 %. The analysis also considers that the first aircraft could deviate up to 200 m from the runway centerline when overflying the localizer antenna. However the simulations show that the biggest disturbances are within 100 m from the runway centerline.

The corresponding dynamic LCV for "heavy" size aircraft is illustrated by the Figure 22.

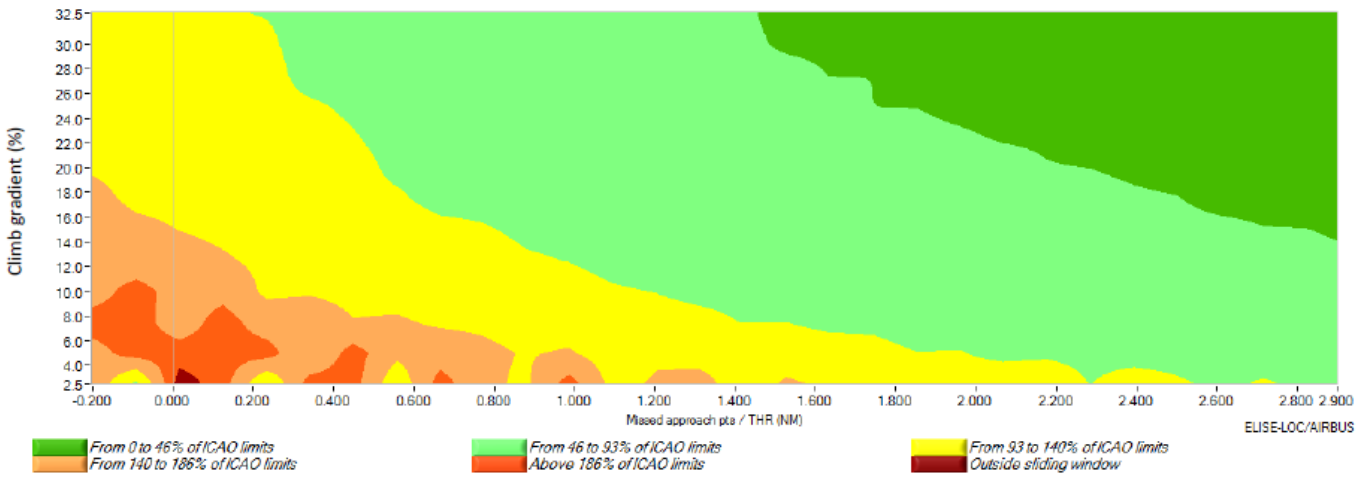

Figure 22 Dynamic LCV for "heavy" size aircraft with 5NM spacing

It can be noticed that the distance at which the first out-of-tolerance disturbances occur at the minimum **2.5 % climb gradient is 2.8 NM** from the runway threshold. For a typical 15 % climb gradient, it can be seen that the distance at which the first out-of-tolerance disturbances occur is 0.8 NM from the runway threshold with 5 NM final spacing.

As a conclusion for LCV, if Aircraft #1 performs a go-around, it can create an out-of-tolerance disturbance just when overflying the LOC antenna (i.e. -1.8 NM from threshold). The out-of-tolerance disturbance could be located on the entire approach because Aircraft #1 is in the localizer critical volume. Then, whatever the spacing between Aircraft #1 and Aircraft #2 is, Aircraft #2 might also perform a go-around (because Aircraft #2 would receive an out-of-tolerance disturbance caused by Aircraft #1). With a 5 NM final spacing, Aircraft #2 would be located 3.2 NM from the threshold (5 NM – 1.8 NM); and the values of **2.8 NM** indicate that Aircraft #2 would never create an out-of-tolerance signal to Aircraft #3 because Aircraft #2 will never penetrate the localizer critical volume even at minimum 2.5 % climb gradient (3.2 NM > 2.8 NM).

In conclusion, if pilots of Aircraft #1 perform a go-around for whatever reason, it might also trigger a go-around of pilots of Aircraft #2 (whatever the spacing between Aircraft #1 and Aircraft #2 is). But, with a 5 NM spacing, Aircraft #3 will never be affected and would land normally.

Glide Path Critical Volume

The aim of this study is to assess the impact on the **glide path** signal caused by an aircraft, which performs a go-around. Thanks to the new advanced technologies of ILS signal modelling with ELISE, it is also possible to compute the Glide Critical Volume (GCV) in 3 dimensions, including the vertical limits. The GCV is a 3D volume where the aircraft in flight (after a missed approach or a balked landing) creates an out-of-tolerance signal to the following approach in approach. The static GCV above the glide path antenna is computed for the reference "heavy" size aircraft (Boeing 747). It consists in a protection volume with the following assumptions:

- The first aircraft (which causes the disturbance) is static, but located at multiple positions along its trajectory of go-around; and
- The second aircraft that follows the approach (which receives the disturbance) is in movement, with a reference speed of 145 kts, at an average separation of 5 NM behind the first aircraft.

This analysis is based on a 3D modelling of the first aircraft, so the simulations have been performed using a Boeing 747 aircraft with a typical pitch angle of 15 °, as observed for go-around events. The aim is to determine the minimum safe height above the glide path antenna and the minimum safe distance in front the threshold for which the first aircraft would no longer create out-of-tolerance disturbances on the signal received by the following aircraft. The static GCV corresponding to the "heavy" size aircraft is illustrated by Figure 23 below. The triangles in yellow and trapezes in red indicate an out-of-tolerance disturbance: it means that an aircraft at this position in X and Z would create an out-of-tolerance disturbance for the following aircraft in approach at around 5 NM behind.

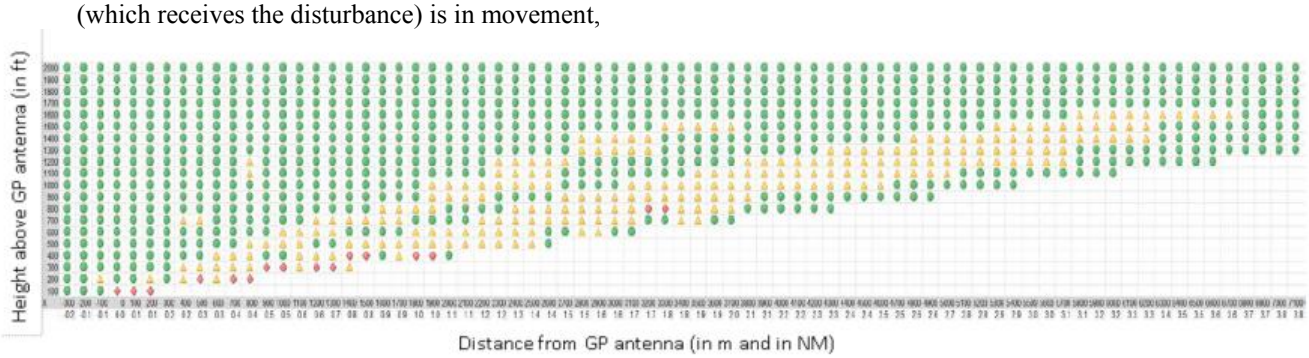

Figure 23 static GCV for "heavy" size for 5 NM spacing

As for the analysis of the LCV, a link between the climb gradient and the minimum horizontal safe distance from the runway threshold to start the missed approach/balked landing (due to out-of-tolerance disturbances) can be determined. The green line (below) determines the boundary distance at which it is safe to start the missed approach/balked landing at a given climb gradient. As it is logical, when the climb gradient increases, the minimum horizontal safe distance is smaller. This link is illustrated by Figure 24 below.

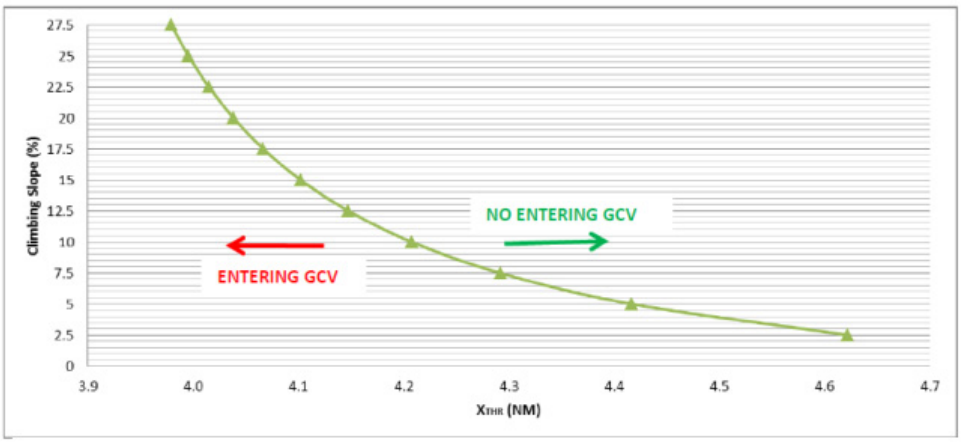

Figure 24 Link between the climb gradient and the minimum horizontal safe distance for "heavy" size aircraft

The distance at which the first out-of-tolerance disturbances occur (at the **minimum 2.5 % climb gradient) is 4.6 NM** from the runway threshold. For a typical 15 % climb gradient, it can be seen that the distance at which the first out-of-tolerance disturbances occur is 4.1 NM from the runway threshold, which is not significantly different than for 2.5 % climb gradient.

As a conclusion for GCV, if Aircraft #1 performs a go-around, it can create an out-of-tolerance disturbance just when overflying the GP antenna (i.e. -0.2 NM from threshold). The out-of-tolerance disturbance could be located on the entire approach because Aircraft #1 is in the glide critical volume. Then, whatever the spacing between Aircraft #1 and Aircraft #2 is, Aircraft #2 might also perform a go-around (because Aircraft #2 would receive an out-of-tolerance disturbance caused by Aircraft #1). With a 5 NM final spacing, Aircraft #2 would be located 4.8 NM from the threshold (5 NM – 0.2 NM); and the values of **4.6 NM and 4.1 NM** indicate that Aircraft #2 would never create an out-of-tolerance signal to Aircraft #3 because Aircraft #2 will never penetrate the glide path critical volume (4.8 NM > 4.6 NM).

In conclusion, if pilots of Aircraft #1 perform a go-around for whatever reason, it might also trigger a go-around of pilots of Aircraft #2 (whatever the spacing between Aircraft #1 and Aircraft #2 is). But, with a 5 NM spacing, Aircraft #3 will never be affected and would land normally.

CONCLUSIONS

Since end of 2014, the new Instrument Landing System (ILS) composed of an ultra-wide aperture type of Localizer on the main landing runway 14 of Zurich Airport has been released for CAT III operations.

Thanks to the fact that this ultra-wide aperture Localizer has a very small sensitive area for “heavy” size aircraft (smaller than +/- 50 m from centerline), the Optimized Operations concep for LVP operations is applicable with a Landing Clearance Line located 60 m from the runway centerline.

By analyzing the last two LVP seasons (more than 1,500 LVP landings), the direct effect of the introduction of this new LCL has been studied and assessed: the LVP spacing between two landing aircraft (till Heavy category) can be reduced from 6 NM to 5 NM.

For non nominal situations with missed approach events, the analysis concludes that, if pilots of Aircraft #1 (medium or heavy) perform a go-around for whatever reason, it might also trigger a go-around of pilots of Aircraft #2 (medium or heavy) due to localizer or glide path disturbances whatever the spacing between Aircraft #1 and Aircraft #2 is (because the disturbance on localizer or glide path signals caused by Aircraft #1 can affect the entire approach). However, with 5 NM spacing (and 6 NM spacing), Aircraft #3 (of any size) will never be affected and would land normally. Therefore, the 3D technical study concludes that go-around is a recurrent phenomenon limited to two aircraft and that there is no difference in managing go-around events between 6 NM spacing and 5 NM spacing.

From 15.09.2016, the spacing between two consecutive landing aircraft in Low Visibility Procedures will effectively be reduced to 5 NM for ILS 14 approaches in Zurich. This will allow ultimately an improvement of capacity in LVP (from 24 to 28 landings per hour), which will translate into important operational benefits for the Airport, Controllers and Airspace users.

REFERENCES

[1] ICAO, July 2006, International Standards and Recommended Practices, Annex 10 to the Convention on International Civil Aviation, Volume 1, Radio Navigation Aids, 6th Edition, Attachment C para. 2.1.9.1 http://www.icao.int

[2] EUR Doc 013 "European Guidance Material on All Weather Operations at Aerodromes", 4th Edition, ICAO European and North Atlantic Office, September 2012

Using Multi Frequency Point Calibration Method on NAV Receiver to Improve Flight Inspection Quality of Localizer Signal Strength

Li Wang

Flight Inspector
Flight Inspection Center of CAAC
Chaoyang District, Beijing, China
E-mail: wangli040@163.com

Mao Ge

Flight Inspector
Flight Inspection Center of CAAC
Chaoyang District, Beijing, China
E-mail: simone_10031@aliyun.com

ABSTRACT

A novel calibration method, named multi frequency point calibration (MFPC) method, is proposed to improve the accuracy and the consistency of the onboard flight inspection system (FIS) on checking the signal strength of the localizer (LOC). Compared with the current single frequency point calibration (SFPC) method, MFPC method requires us to make the calibration of LOC receiver signal strength on every frequency point. Based on this method we can improve original one dimensional single frequency point signal strength compensating table, which is formed by the SFPC method, to a two dimensional multi frequency point signal strength compensating table, which has compensation corresponding to every frequency point used by the LOC. And MFPC method could make the FIS get a more accurate result on checking the signal strength of the LOC, and then improve the consistency of the FIS on checking the signal strength of the LOC. By computing the expectation and calibration uncertainty of the test result, we found that: compared with the SFPC method, the MFPC method can improve the accuracy and the consistency of the signal strength of the LOC on flight inspection practice.

INTRODUCTION

Coverage of the LOC is a very important profile on the flight inspection of the instrument landing system (ILS) [1, 2]. The result helps pilots and flight procedure designers to confirm the available area of the LOC signal.

On the commissioning flight inspection of the 02R# ILS (IDM/108.5*MHz*) which is installed at GuangZhou BaiYun airport in southern China,, two flight inspection aircrafts received different signal strength of the LOC. Figure 1 is the signal strength curve of the LOC received by aircraft A, and figure 2 is the signal strength curve of the LOC received by aircraft B.

From figure 1 and figure 2 we could easily find that, the signal strength of LOC received by aircraft A is 8~9 *dBm* smaller than that received by aircraft B. This situation would lead to different conclusions on the same facility. The conclusion of the LOC coverage profile is restricted after the flight inspection by aircraft A. However, the conclusion is unrestricted after the flight inspection by aircraft B. Therefore the flight check results seriously affected the flight inspection conclusion of the LOC.

Aiming at the above-mentioned phenomenon, maintainers of the flight inspection system (FIS) primarily considered that it was caused by the difference of the gain between different navigation (NAV) antennas and the difference of the loss between different cables which is used to connect the NAV receiver and the NAV antenna. But after the measurement we discovered that those factors could not cause such a big influence. Therefore, we switch our focus to the calibration of the NAV receiver. After the test, we found that, the accuracy of the calibration to the NAV receiver of the FIS on LOC signal strength decides the accuracy and the consistency of the flight inspection practice on LOC coverage directly.

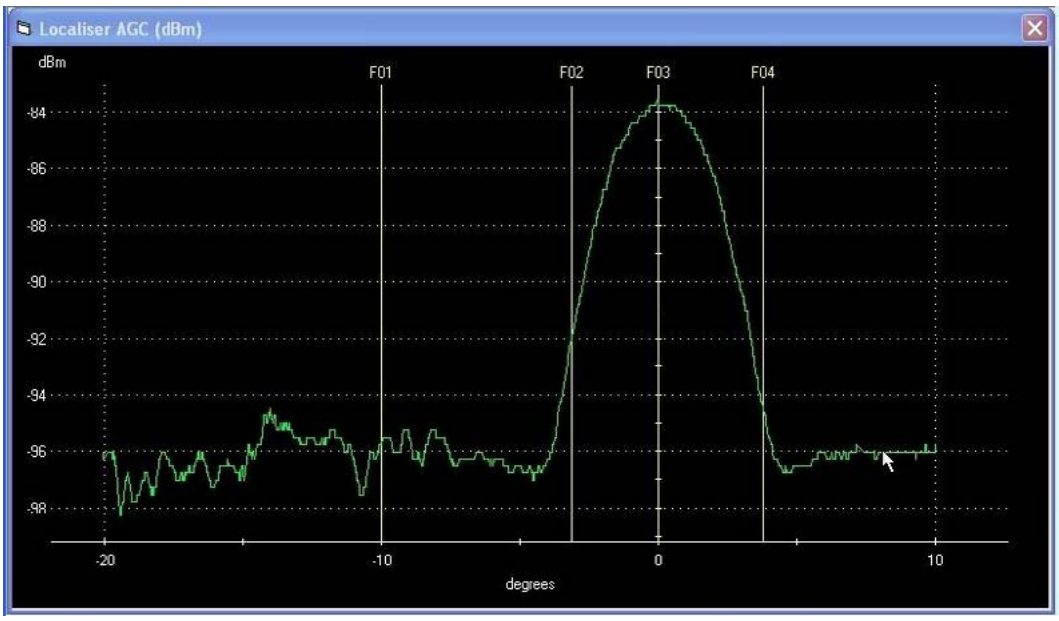

Figure 1. Signal Strength Curve of The LOC Received by Aircraft A

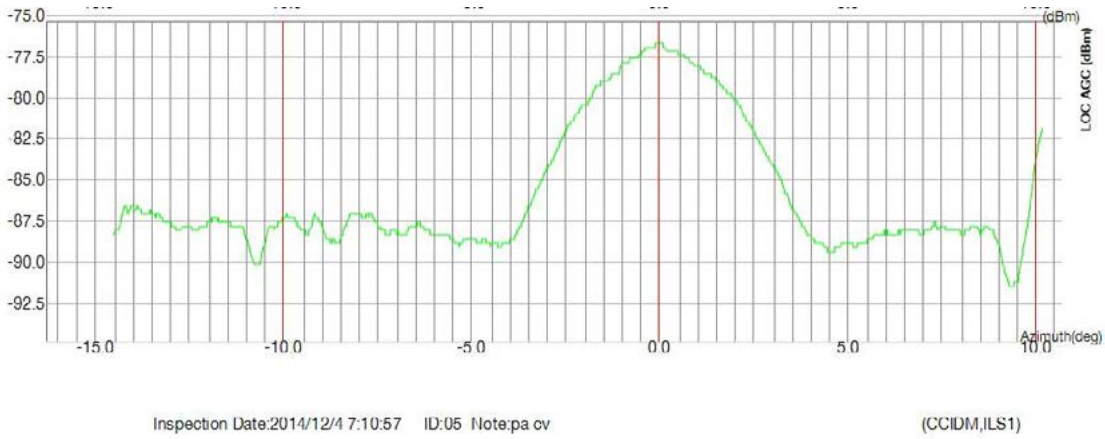

Figure 2. Signal Strength Curve of The LOC Received by Aircraft B

The current calibration method to the NAV receiver of the FIS on LOC signal strength is single frequency point calibration (SFPC) method, this method is to select a special frequency point as the carrier frequency of the LOC standard signal to calibrate the NAV receiver of the FIS on LOC signal strength, and then the system will form a one dimensional single frequency point signal strength compensating table, which only selects LOC signal strength as reference, to compensate the signal strength of the received LOC signal. Based on the SFPC method, a novel calibration method, namely multi frequency point calibration (MFPC) method, is proposed in this paper. After the calibration by this method, the FIS will form a two dimensional signal strength compensating table, which is not only selecting LOC signal strength as reference but also selecting LOC signal carrier frequency as reference, to compensate the signal strength of the received LOC signal. Test results show that compared with the SFPC method, the MFPC method could improve the accuracy and the consistency of the result on checking the signal strength of the LOC obviously.

The rest of this paper is organized as follows. **The second part** introduces the current SFPC method and the test result of the LOC signal strength on several selected frequency points after the calibration by the SFPC method. **The third part** introduces the MFPC method, the test result of the LOC signal strength on former selected frequency points after the calibration by the MFPC method, and the analysis of the flight inspection results based on the multi frequency point signal strength compensating table. Analysis and comparison on the expectation and the calibration uncertainty of the two test results are presented in **the fourth part**. At last, we conclude this paper and put forward our recommendations.

THE SFPC METHOD AND THE TEST RESULT OF THE LOC SIGNAL STRENGTH

The SFPC Method

The SFPC method [3] is a single frequency point calibration method. It is used to calibrate the NAV

receiver of the FIS on LOC signal strength, and is recommended by the manufacturer. In this method, a standard LOC signal, whose carrier frequency is 110.9 *MHz*, is produced by the standard signal generator, and is sent to the FIS through the calibration port. Figure 3 shows the interconnection set-up required for LOC receiver signal strength calibration. By operating the system calibration software, the FIS maintainers sample the signal strength of the standard LOC signal, and the injected signal strength ranges from -50 *dBm* to -110 *dBm* in 5 *dB* steps. Comparing the received signal strength to the standard signal strength, the system forms a one dimensional single frequency point signal strength compensating table. Table 1 is the compensating table of the FIS of aircraft A calibrated by the SFPC method. Table 2 is the compensating table of the FIS of aircraft B calibrated by the SFPC method.

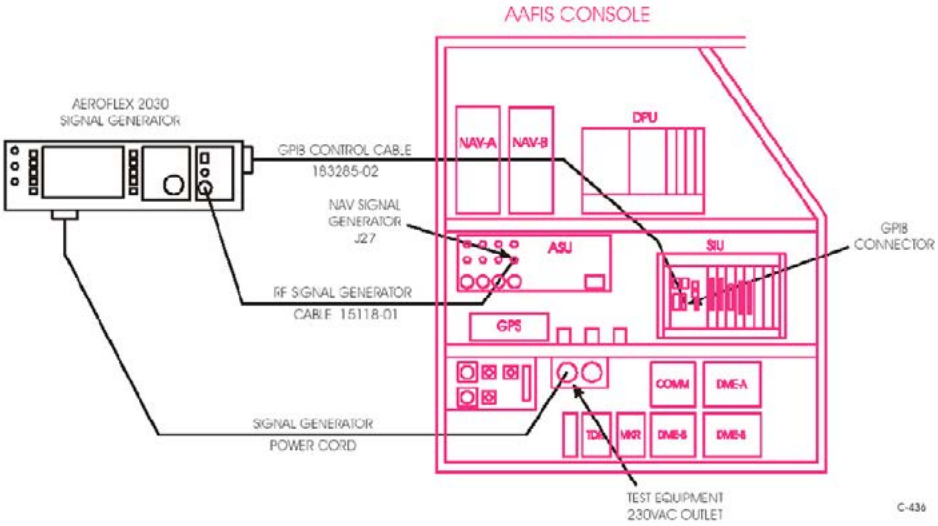

Figure 3. LOC Receiver Calibration Interconnect Diagram

Table 1. Compensating Table of The FIS of Aircraft A Calibrated by The SFPC Method

S. S. / Freq.	-50.0	-55.0	-60.0	-65.0	-70.0	-75.0	-80.0	-85.0	-90.0	-95.0	-100.0	-105.0	-110.0
110.9	2.25	1.75	1.50	0.50	1.00	1.00	2.18	2.00	1.75	1.53	1.00	0.25	-3.00

Table 2. Compensating Table of The FIS of Aircraft B Calibrated by The SFPC Method

S. S. / Freq.	-50.0	-55.0	-60.0	-65.0	-70.0	-75.0	-80.0	-85.0	-90.0	-95.0	-100.0	-105.0	-110.0
110.9	3.00	5.25	5.32	5.50	5.75	5.75	5.65	5.00	5.00	5.25	5.66	6.00	6.75

During the flight inspection, the FIS compensates the received LOC signal strength by referring to the one-dimensional single frequency point signal strength compensating table.

The advantage of this method is the simple and convenient operation. It uses only one frequency point to calibrate the LOC receiver signal strength of the FIS, and eventually forms a one dimensional single frequency point signal strength compensating table to compensate the received LOC signal strength with the signal strength value as a reference.

The shortage of this method is that, the received result of the LOC receiver would be different in response to different LOC signal frequencies, but the compensating quantity is the same. This would increase the system error of the flight inspection result of the LOC signal strength.

The Test Result of The LOC Signal Strength after The Calibration by The SFPC Method

The carrier frequency of LOC is 108.1 ~ 111.95 *MHz*, the space between the two carrier frequencies is 0.05*MHz*, and only use those frequency points that the number after the decimal point is odd . In order to achieve full coverage of the frequency, six carrier frequencies, 108.1 *MHz*, 108.7 *MHz*, 109.1 *MHz*, 110.1 *MHz*, 110.9 *MHz*, and 111.9 *MHz*, are selected as the test frequency points to do the LOC signal strength test after the FIS NAV receiver was calibrated through the SFPC method. The testing signal strength points are -50 *dBm*, -55 *dBm*, -60 *dBm*, -65 *dBm*, -70 *dBm*, -75 *dBm*, -80 *dBm*, -85 *dBm*, -90 *dBm*, -95 *dBm*, -100 *dBm*.

After calibrating the NAV receiver of the FIS on LOC signal strength by the SFPC method, we use the previous six standard signals one by one to do the LOC

signal strength test of the NAV receiver. We compared the test result with the original standard signal strength, table 3 is the compared result, and figure 4 is the corresponding line chart. The horizontal axis of the chart represents the signal strength, the unit is *dBm*. The vertical axis represents the difference of the signal strength, the unit is *dB*. The data in the table or the chart is the difference of the signal strength between the test result and the original standard signal. The difference is more close to zero shows that the measured signal strength more close to standard signal strength.

Table 3. Compared Result of The Test after The Calibration of The SFPC Method

S. S. / Freq.	-50	-55	-60	-65	-70	-75	-80	-85	-90	-95	-100
108.1	-12.75	-13.06	-13	-12.83	-12.66	-12.9	-12.88	-13.04	-13.53	-15	-10
108.7	-7.37	-7.25	-7.22	-7.25	-6.82	-7.15	-7.37	-7.61	-7.48	-7.65	-10
109.1	-3.61	-3.68	-3.5	-3.89	-3.75	-3.03	-3.44	-3.68	-3.92	-3.88	-3.82
110.1	0.24	0.28	0.26	0.5	0	0	0.35	0	0	0.3	0
110.9	0.48	0.28	0.26	0.5	0.28	0	0.35	0	0	0.3	0.28
111.9	-0.56	-0.79	-0.75	-0.56	-0.75	-0.61	-0.59	-0.79	-0.78	-0.8	-0.88

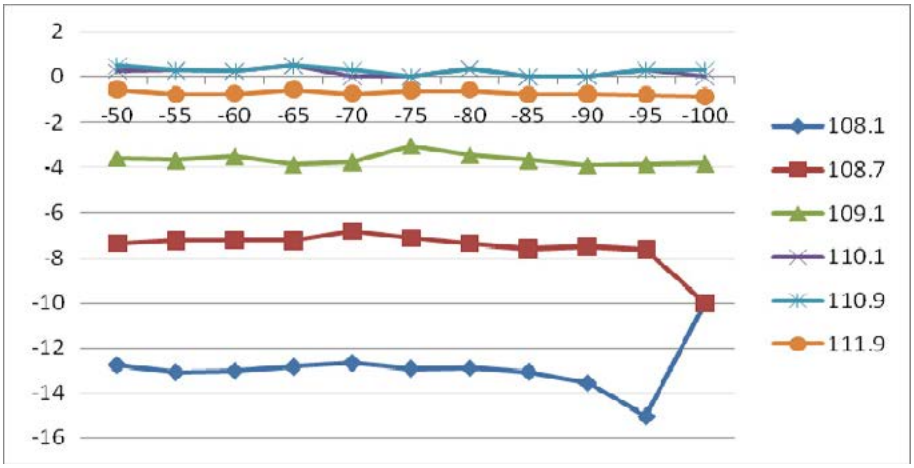

Figure 4. Corresponding Line Charts to Table 3

From table 3 and figure 4 we could see that, when the LOC signal has different carrier frequencies, the NAV receiver will have different results on signal strength. And when the difference between carrier frequencies is narrow, the received results are close; when the difference between carrier frequencies is wide, the received results are more different, and the biggest difference could reach to 13~15 *dB*. So if the NAV receiver is calibrated by the SFPC method, the conclusion of the flight inspection may be affected seriously.

THE MFPC METHOD AND THE TEST RESULT OF THE LOC SIGNAL STRENGTH

The MFPC Method

The MFPC method is a multi frequency point calibration method which is used to calibrate the LOC receiver signal strength of the FIS. The interconnection set-up and the injected signal strength range of the MFPC method are the same as that of the SFPC method. The difference between the MFPC method and the SFPC method is the carrier frequency of the standard LOC signal, and based on that, the FIS forms a two dimensional signal strength compensating table. In order to avoid different results in response to different LOC signal frequencies, the MFPC method extends the injected signal frequency from a single frequency point to multiple frequency points, that is, using *MHz* as unit, selects the number that the first decimal place is odd as the carrier frequency, calibrates the NAV receiver of the FIS on LOC signal strength respectively. The MFPC method could also select all 40 carrier frequencies, which are used by ILS, as the carrier frequencies of the calibration signal. On the current research, the NAV receiver of the FIS of aircraft A is calibrated by the MFPC method of 20 carrier frequencies, and the NAV receiver of the FIS of aircraft B is calibrated by the MFPC method of 40 carrier frequencies. After the calibration, the FIS forms a two dimensional signal strength compensating table. This table not only selects LOC signal strength as reference, but also selects LOC signal carrier frequency as reference. Table 4 is the compensating table of the FIS

of aircraft A calibrated by the MFPC method, table 5 is the compensating table of the FIS of aircraft B calibrated by the MFPC method. So, during actual flight inspection, referring to the received carrier frequency and signal strength of the LOC signal, the FIS finally gets the LOC signal strength result according to the two dimensional signal strength compensating table.

Because this two dimensional signal strength compensating table has compensation corresponding to every frequency point used by the localizer, the MFPC method could make the FIS get a more accurate result on checking the signal strength of the LOC, and then improve the accuracy and the consistency of the FIS on checking the signal strength of the LOC.

Table 4. Compensating Table of Aircraft A Calibrated by The MFPC method

S. S. / Freq.	-50.0	-55.0	-60.0	-65.0	-70.0	-75.0	-80.0	-85.0	-90.0	-95.0	-100.0	-105.0	-110.0
108.10	14.50	14.50	14.50	15.00	15.25	15.00	14.75	14.73	14.25	12.00	7.00	2.00	-3.00
108.30	12.50	12.00	12.00	12.00	13.00	13.00	12.75	12.50	12.05	11.50	7.00	2.00	-3.00
108.50	10.00	10.00	10.00	10.00	10.50	10.75	10.37	10.25	10.00	9.50	7.00	2.00	-3.00
108.70	9.50	9.25	9.20	8.75	8.75	9.75	9.73	9.50	9.50	8.63	7.00	2.00	-3.00
108.90	7.75	7.00	6.93	7.00	6.75	7.73	9.70	7.50	7.25	6.88	6.25	2.00	-3.00
109.10	5.50	5.25	5.38	5.25	5.00	5.28	5.75	5.75	5.60	5.27	4.60	2.00	-3.00
109.30	4.50	4.35	4.15	3.75	3.53	3.75	4.50	4.50	4.50	4.00	3.25	2.00	-3.00
109.50	3.72	3.27	3.12	3.00	2.50	2.75	3.75	3.75	3.50	3.17	2.50	1.50	-3.00
109.70	3.00	2.75	2.50	2.25	2.00	2.25	3.00	3.02	2.90	2.50	2.00	1.25	-3.00
109.90	2.12	1.50	1.25	1.40	0.95	1.00	2.25	2.00	1.75	1.65	0.97	0.00	-3.00
110.10	1.85	1.50	1.25	1.00	0.97	1.00	1.75	2.00	1.75	1.25	1.00	0.25	-3.00
110.30	2.00	1.75	1.50	1.17	1.00	1.00	1.93	2.00	1.75	1.50	1.00	0.25	-3.00
110.50	1.50	1.25	1.00	0.50	0.50	0.50	1.25	1.50	1.25	0.75	0.48	-0.50	-3.00
110.70	1.75	1.50	1.25	0.75	0.75	0.75	1.53	1.75	1.50	1.00	0.73	-0.20	-3.00
110.90	2.25	1.75	1.50	0.50	1.00	1.00	2.18	2.00	1.75	1.53	1.00	0.25	-3.00
111.10	5.75	5.75	5.50	5.50	5.75	5.75	6.00	6.22	5.75	5.50	5.12	2.00	-3.00
111.30	4.50	4.50	4.65	4.25	4.00	4.65	4.75	4.75	5.00	4.25	3.50	2.00	-3.00
111.50	3.75	3.50	3.50	3.25	2.75	3.00	3.75	3.75	3.75	3.30	2.75	1.92	-3.00
111.70	3.25	3.15	2.75	2.50	2.55	2.37	3.25	2.72	3.25	2.75	2.75	1.38	-3.00
111.90	2.75	2.50	2.25	2.00	1.75	1.75	2.75	2.25	2.50	2.25	1.76	0.75	-3.00

Table 5. Compensating Table of Aircraft B Calibrated by The MFPC Method

S. S. / Freq.	-50.0	-55.0	-60.0	-65.0	-70.0	-75.0	-80.0	-85.0	-90.0	-95.0	-100.0	-105.0	-110.0
108.10	1.75	2.00	2.25	2.25	2.11	2.22	1.75	1.75	2.00	2.00	2.25	2.75	4.25
108.15	1.94	2.19	2.38	2.38	2.27	2.35	1.98	1.89	2.13	2.13	2.38	2.88	4.31
108.30	2.50	2.75	2.75	2.75	2.75	2.75	2.68	2.33	2.50	2.50	2.75	3.25	4.49
108.35	2.56	2.83	2.81	2.81	2.81	2.84	2.84	2.40	2.56	2.58	2.81	3.37	4.60
108.50	2.75	3.06	3.00	3.01	3.00	3.12	3.29	2.60	2.75	2.83	3.00	3.75	4.91
108.55	2.81	3.04	3.06	3.07	3.06	3.16	3.22	2.64	2.75	2.87	3.00	3.69	4.78
108.70	3.00	3.00	3.25	3.25	3.25	3.25	3.00	2.76	2.75	3.00	3.00	3.51	4.40

108.75	2.81	2.85	3.13	3.19	3.21	3.20	3.01	2.72	2.70	2.97	3.04	3.51	4.45
108.90	2.25	2.39	2.75	3.00	3.09	3.06	3.03	2.59	2.57	2.90	3.16	3.52	4.60
108.95	2.31	2.48	2.79	2.94	3.00	3.00	2.89	2.51	2.55	2.80	3.10	3.41	4.50
109.10	2.50	2.75	2.92	2.75	2.75	2.83	2.50	2.26	2.50	2.50	2.92	3.10	4.21
109.15	2.31	2.56	2.69	2.56	2.62	2.69	2.38	2.13	2.38	2.38	2.74	2.95	4.04
109.30	1.75	2.00	2.00	2.00	2.22	2.25	2.00	1.75	2.00	2.00	2.19	2.52	3.50
109.35	1.94	2.24	2.25	2.25	2.29	2.31	2.19	1.94	2.17	2.21	2.33	2.70	3.69
109.50	2.50	2.96	3.00	3.00	2.50	2.50	2.78	2.50	2.69	2.85	2.75	3.25	4.25
109.55	2.44	2.82	2.94	3.00	2.65	2.64	2.84	2.52	2.66	2.86	2.85	3.32	4.34
109.70	2.25	2.39	2.75	3.00	3.09	3.06	3.03	2.59	2.57	2.90	3.16	3.52	4.60
109.75	2.44	2.56	2.88	3.06	3.22	3.11	3.02	2.63	2.72	2.92	3.18	3.57	4.69
109.90	3.00	3.07	3.25	3.25	3.61	3.25	3.00	2.75	3.18	3.00	3.25	3.73	4.95
109.95	3.00	3.18	3.31	3.40	3.64	3.38	3.19	2.88	3.22	3.09	3.31	3.90	4.97
110.10	3.00	3.50	3.50	3.84	3.75	3.75	3.76	3.25	3.33	3.38	3.50	4.42	5.00
110.15	2.81	3.22	3.31	3.63	3.58	3.58	3.58	3.09	3.14	3.26	3.42	4.19	4.90
110.30	2.25	2.39	2.75	3.00	3.09	3.06	3.03	2.59	2.57	2.90	3.16	3.52	4.60
110.35	2.44	2.96	3.28	3.44	3.57	3.59	3.52	3.07	3.01	3.30	3.65	4.01	5.03
110.50	3.00	4.66	4.89	4.75	5.00	5.21	5.00	4.50	4.35	4.50	5.14	5.50	6.32
110.55	3.00	4.75	4.92	4.88	5.04	5.22	5.06	4.56	4.45	4.56	5.16	5.56	6.37
110.70	3.00	5.00	5.00	5.25	5.16	5.25	5.25	4.75	4.75	4.75	5.25	5.75	6.52
110.75	3.00	5.06	5.08	5.31	5.30	5.38	5.35	4.81	4.81	4.88	5.35	5.81	6.58
110.90	3.00	5.25	5.32	5.50	5.75	5.75	5.65	5.00	5.00	5.25	5.66	6.00	6.75
110.95	2.25	3.94	4.02	4.19	4.39	4.44	4.30	3.73	3.69	3.94	4.33	4.69	5.81
111.10	0.00	0.00	0.12	0.25	0.31	0.50	0.27	-0.07	-0.25	0.00	0.32	0.75	3.00
111.15	0.11	0.08	0.22	0.31	0.42	0.56	0.41	0.00	-0.19	0.06	0.42	0.81	3.00
111.30	0.42	0.33	0.50	0.50	0.75	0.75	0.86	0.22	0.00	0.25	0.72	1.00	3.00
111.35	0.44	0.39	0.50	0.56	0.75	0.75	0.87	0.23	0.06	0.28	0.73	1.04	3.00
111.50	0.50	0.60	0.50	0.75	0.75	0.75	0.92	0.25	0.25	0.37	0.75	1.15	3.00
111.55	0.50	0.57	0.55	0.75	0.78	0.81	0.93	0.25	0.25	0.34	0.80	1.15	3.00
111.70	0.50	0.50	0.69	0.75	0.87	1.00	0.96	0.25	0.25	0.25	0.96	1.14	3.00
111.75	0.52	0.51	0.73	0.81	0.90	1.06	0.97	0.31	0.31	0.31	1.00	1.17	3.00
111.90	0.57	0.55	0.84	1.00	1.01	1.25	1.00	0.50	0.47	0.50	1.12	1.25	3.00
111.95	0.75	0.75	0.87	1.00	1.25	1.25	1.25	0.50	0.50	0.75	1.23	1.50	3.00

The Test Result of The LOC Signal Strength After The Calibration of The MFPC Method

After the calibration to the NAV receiver of the FIS on LOC signal strength by the MFPC method, we select four of the six test carrier frequencies, whose test results of the SFPC method are obviously different, to do the LOC signal strength test, in order to not only minimizing work load of the test, but also showing the superiority of the MFPC method. The four carrier frequencies are 108.1 *MHz*, 108.7 *MHz*, 109.1 *MHz*, and 110.9 *MHz*. After the test, we compared the test result with the original standard signal strength. Table 6 is the compared result of the test after the calibration by the MFPC method, and figure 5 is the corresponding line chart of table 6.

From table 6 or figure 5 we could see that, comparing with the inputted LOC signal strength, the NAV receiver gets almost the same result when the carrier

frequencies are different, the difference between the received signal strength and the inputted signal strength is in 1*dB*. From table 3 and table 6 we could conclude that, compared with the SFPC method, the MFPC method could improve the accuracy and the consistency of the signal strength of the LOC on flight inspection practice obviously.

Table 6. Compared Result of The Test after The Calibration of The MFPC Method

S. S. / Freq.	-50	-55	-60	-65	-70	-75	-80	-85	-90	-95	-100
108.1	0.26	0.25	0.5	0.45	0.48	0.26	0.26	0.48	0.28	0	0
108.7	0.51	0.53	0.71	0.27	0.25	0.42	0.48	0.26	0.75	0.46	0
109.1	0	0	0.37	0.26	0.26	0.5	0.23	0.25	0.1	0.29	0.4
110.9	0.48	0.28	0.26	0.5	0.28	0	0.35	0	0	0.3	0.28

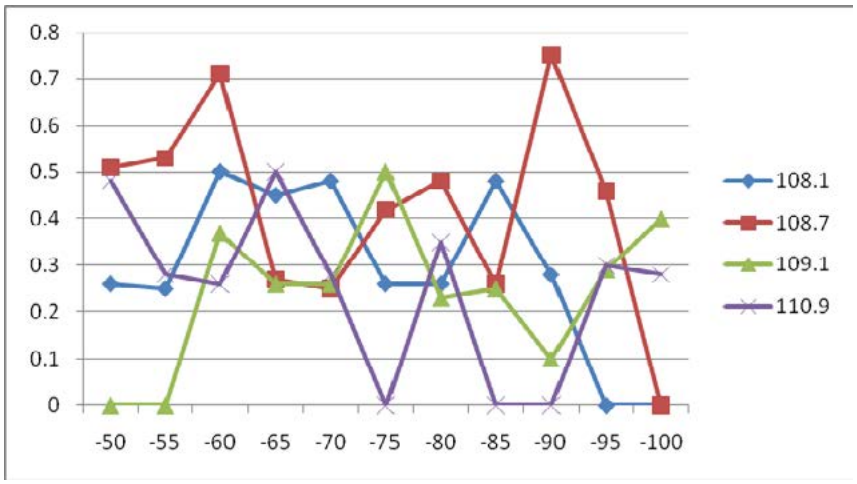

Figure 5. Corresponding Line charts to Table 6

<u>The Analysis of The Flight Inspection Results Based on The Multi Frequency Point Signal Strength Compensating Table</u>

Table 7 is the comparison of the multi frequency point signal strength compensating table of the FIS of aircraft A and that of aircraft B on frequency 108.5 *MHz* and 110.9 *MHz*. From table 7 we could see that, the signal strength compensating quantity of aircraft A on 108.5 *MHz* and -95 *dBm* is 6.7 *dB* more than that of aircraft B, and the signal strength compensating quantity of aircraft A on 110.9 *MHz* and -95 *dBm* is 3.3 *dB* less than that of aircraft B. Summarizing the two results, when the NAV receiver is calibrated by the SFPC method, the LOC signal strength compensating quantity of the aircraft A is 10 *dB* less than that of the aircraft B approximately. This result is coincidence with what we mentioned before in the paragraph INTRODUCTION, that is, the signal strength of LOC received by aircraft A is 8~9 *dBm* less than that received by aircraft B. This result could help us to prove that, on the flight inspection of the LOC signal strength at that airport, the problem that different flight inspection aircrafts had different result is caused by the SFPC method. Therefore, the MFPC method would overcome the shortcomings of the SFPC method, and improve the accuracy and the consistency of the signal strength of the LOC on flight inspection practice.

Table 7. Comparison of The Multi Frequency Point Signal Strength Compensating Table

Aircraft	S. S. / Freq	-50.0	-55.0	-60.0	-65.0	-70.0	-75.0	-80.0	-85.0	-90.0	-95.0	-100.0	-105.0	-110.0
A	108.5	10.00	10.00	10.00	10.00	10.50	10.75	10.37	10.25	10.00	9.50	7.00	2.00	-3.00
	110.9	2.25	1.75	1.50	0.50	1.00	1.00	2.18	2.00	1.75	1.53	1.00	0.25	-3.00
B	108.5	2.75	3.06	3.00	3.01	3.00	3.12	3.29	2.60	2.75	2.83	3.00	3.75	4.91
	110.9	3.00	5.25	5.32	5.50	5.75	5.75	5.65	5.00	5.00	5.25	5.66	6.00	6.75

COMPARISION AND ANALYZATION OF THE TEST RESULT ON EXPECTED VALUE AND CALIBRATION UNCERTAINTY

The expected value of the test results in the paper is the average value of the test results, the closer it gets to the standard value, reflects the more accurate measurement of the FIS becomes. Uncertainty [4, 5] is a measure of the degree of uncertainty due to the measurement errors. It is an indicator of the quality of the measurement results, which reflects the closeness between the actual measurement result and the true value, that is, the consistency of the measurement results. Calibration uncertainty includes type A uncertainty, type B uncertainty, synthesis uncertainty and extended uncertainty.

The type A uncertainty is

$$u_A = s = \frac{\sum_{i=1}^{n}(A_i - \overline{X})^2}{n-1}$$

Where,

$$\overline{X} = E = \frac{\sum_{i=1}^{n} A_i}{n}$$

Where, E is the expected value of the test results, and A_i is the test result of the LOC signal strength.

The type B uncertainty is

$$u_B = \frac{U}{\kappa}$$

Where, $U = 0.15$, is the signal strength uncertainty of the signal generator. $\kappa = 2$, is the expansion factor.

The synthesis uncertainty is

$$u_C = \sqrt{u_A^{\ 2} + u_B^{\ 2}}$$

The expanded uncertainty is

$$u = 2u_C$$

Bring test results to the above formulae separately, we could obtain the expectation E_S and the calibration uncertainty u_S of the test results after the calibration of the SFPC method, and the expectation E_M and the calibration uncertainty u_M of the test results after the calibration of the MFPC method. Table 8 shows the E_S and the E_M of the test results corresponding to different signal strength in test. Table 9 shows the u_S and the u_M of the test results corresponding to different signal strength in test.

Table 8. E_S And E_M of The Test Results

Signal Strength	E_S	E_M
-50.00	-53.93	-49.69
-55.00	-59.04	-54.74
-60.00	-63.99	-59.54
-65.00	-68.92	-64.63
-70.00	-73.95	-69.68
-75.00	-78.95	-74.71
-80.00	-83.93	-79.67
-85.00	-89.19	-84.75
-90.00	-94.29	-89.72
-95.00	-99.46	-94.74
-100.00	-104.07	-99.83

Table 9. u_S and u_M of The Test Results

Signal Strength	u_S	u_M
-50.00	10.51	0.44
-55.00	10.57	0.40
-60.00	10.53	0.37
-65.00	10.62	0.26
-70.00	10.12	0.24
-75.00	10.34	0.41
-80.00	10.58	0.25
-85.00	10.47	0.37
-90.00	10.76	0.60
-95.00	12.01	0.36
-100.00	9.64	0.38

From table 8 we could see that, the expectation of the test results obtained after the NAV receiver was calibrated by the MFPC method is close to the standard value, and the average signal strength error is within 0.5 dB; the expectation of the test results obtained after the NAV receiver was calibrated by the SFPC method is far from the standard value. From these results we could conclude that, the accuracy of the test on the signal strength of the LOC could be improved obviously after using the MFPC method. From table 9 we could see that, the calibration uncertainty of the SFPC method is bigger than that of the MFPC method under different test signal strength. And this result shows that, compared with the SFPC method, the MFPC method

could improve the consistency of the signal strength of the LOC on flight inspection practice.

Comprehensive the above analysis and the test result of table 8 and that of table 9 we could conclude that, compared with the SFPC method, the MFPC method could get a good result on improving the accuracy and the consistency of the signal strength of the LOC on flight inspection practice.

CONCLUSION

In order to improve the accuracy and the consistency of the onboard FIS on checking the signal strength of the LOC, a novel calibration method, namely MFPC method, is proposed. Through expanding the carrier frequency of the standard LOC signal which is used on calibration practice from one point to multi points, the MFPC method makes the compensating table formed by the FIS from one dimension to two dimensions, and then makes the FIS get a more accurate result on checking the signal strength of the LOC. The analysis on the expectation and the calibration uncertainty of the test results shows that, the MFPC method could improve the accuracy and the consistency of the signal strength of the LOC on flight inspection practice.

RECOMMENDATIONS

Sincerely hope the FIS producer could pay attention to the MFPC method, and make the FIS obtain a more accurate and more consistent result on checking the signal strength of the LOC.

REFERENCES

[1] CAAC, 2014, Flight Inspection Management Rule of Communication Navigation and Surveillance Facility of Civil Aviation, CCAR-86.

[2] CAAC, 2010, Flight Inspection Rule, MH2003-2000.

[3] RVA AEROSPACE SYSTEM LTD, SYSTEM OPERATING INSTRUCTIONS, AAFIS-2, CHINA.

[4] CFI, Nov. 2008, The Calculation Rule of CFI, CFI-AJGF-01.

[5] CFI, May 2009, The Calculation of the Uncertainties of the Flight calibration values, CFI-AJGF-02.

IFIS2016

Bringing Together Theory and Practice

Session 3

Flight Inspection of VOR and SSR

A benchmark study on measurement and simulation techniques for navigation systems and multipath propagation

Björn Neubauer
Institute for Electromagnetic Compatibility, TU Braunschweig
Schleinitzstr. 23, 38106 Braunschweig, Germany
Fax: +49(0)531/391-7724
E-mail: b.neubauer@tu-bs.de

Georg Zimmer, Dr. Robert Geise
Institute for Electromagnetic Compatibility, TU Braunschweig
Schleinitzstr. 23, 38106 Braunschweig, Germany
Fax: +49(0)531/391-7724
E-mail: {g.zimmer, r.geise}@tu-bs.de

ABSTRACT

Due to the intended abandoning of the nuclear energy the generation by wind turbines has experienced a growing interest ever since. This can be recognized by the huge investments made in wind farms. At the same time the flight safety must not be affected. That is to say that reflections of navigation signals, e.g. (Doppler)VOR or radar, at the wind turbines are not allowed to falsify/distort the intended information. In order to avoid safety impairing constellations the ICAO recommends to individually investigate the cases whenever intended wind turbines are to be set up within a 15 km radius of a (D)VOR ground station.
Numerous studies exist on that topic, based both on flight inspection measurements and simulations. However, focusing on individual scenarios, they lack a fundamental basis for a comparison and validation and hardly all relevant scenario parameters are specified in detail. By means of a scaled model measurement setup such a fundamental set of results is provided under well-controlled, reproducible and completely specified boundary conditions for a rotating wind turbine as one of the most complicated object in the context of multipath propagation and navigation systems, e.g. radar or VOR.
Several aspects are addressed separately, such as functionality, i.e. can simulation tools adequately describe moving/rotating objects inducing Doppler shifts. Another aspect is complexity, which deals with the degree of approximation according to the object's size. Additionally, sensitivity is investigated, that is how results change with small variations of input parameters, such as rotational speed, blade orientation, etc.
Finally, results are related to newest flight inspection studies and techniques.

INTRODUCTION

Multipath propagation in the context of navigation systems, e.g. radar or (D)VOR, is a demanding and challenging topic due to the very complex boundary conditions. Whereas in some cases a solely static scattering scenario needs to be considered, e.g. building facades reflecting instrument landing system signals, rotating wind turbines are dynamic scatterers leading to a time-dependent propagation channel.

Several numerical studies exist on that topic [1–4] where the rotational motion of the wind turbines can be considered a very crucial part within the simulations, the validation of which is a highly argued issue in the community. Especially for this matter the contribution at hand provides a fundamental basis.

Flight inspection measurements on VOR disturbances and wind turbines [4, 5] provide valuable sample studies but hardly describe all relevant boundary conditions to their full extent, such as a detailed operational state of the wind turbines or even wind farm. Consequently, it is difficult to relate current work of numerical studies to these measurement results. By means of scaled

measurement the scope of this contribution is to provide scenarios with wind turbines under well controlled boundary conditions for comparison in the community, initiating a benchmark study on this very complex topic.

In particular, for planning approval procedures of wind farms, flight inspection measurements can only give results on the initial level of bearing errors due to existing terrain topology proving a margin for wind turbines to be built, but can not assess their actual impact in advance. The latter needs to be done by numerical studies or by scaled measurements as presented in this contribution. Which provides a study of an isolated generic wind turbine without the influence of additional boundary conditions, such as terrain effects or buildings.

This contribution is organized as follows. The fundamental principle of scaling in scattering theory is explained in the next section. After that the scaled measurement setup is briefly discussed and related to existing literature. Finally, measurement configurations and corresponding results are given.

SCALED MEASUREMENTS IN SCATTERING THEORY

The features of an object determining the scattering behavior with respect to electromagnetic (em) waves are its state of motion, conductivity, shape and size. The conductivity may depend on the frequency, however can be considered infinite as soon as the structure consist of metal. In this context the electrical object's size as ratio between its dimensions and the wavelength, is the solely relevant measure. A very intuitive example is the $\frac{\lambda}{2}$ dipole. Its radiation pattern always stays the same, if its length corresponds to half a wavelength.

That means that an object being shrank by a factor K_{SC} does not alter its electrical size as long as the frequency is increased by the same factor as quite obvious in the following formula:

$$c_0 = \left(\frac{\lambda}{K_{SC}}\right) \cdot (f \cdot K_{SC}). \tag{1}$$

Mathematically the scaling concept for metal-like objects can analytically be proven be fundamental theorems of the spatial Fourier transform [6].

The scaling concept is well established in the context of military radar and signature analysis of aircraft as well as for analysis of antenna performance installed on aircraft [7]. Previous work of the authors deal with the application of this concept to other navigation systems and objects, e.g. wind turbines or large taxiing aircraft [8]. Fundamental advantages yielded by the concept of scaled measurements are essentially the full control of the environment and the nearly unlimited availability.

Measurements presented in this contribution refer to the scale of 1:144 that transfers VOR frequencies in VHF band to 15.9 GHz.

For the case of a rotating wind turbine both time variant scattering amplitudes and probable frequency shifts due to Doppler effects are considered in measurements presented here.

Doppler shifts in the scaled environment

Does scaling a scattering scenario influence the Doppler shift? Given that the speed of light c is way greater than the remaining velocities involved relativistic effects don't need to be taken into account. Given an emitter and a receiver with the relative velocity v with respect to on another the received/obtained frequency is given by

$$f_R = \frac{1}{1 \mp \frac{v}{c}} f_E. \tag{2}$$

The Doppler shift $f_{DS} = \Delta f$ is calculated by

$$f_{DS} = f_R - f_E = \frac{1}{1 \mp \frac{v}{c}} f_E - f_E = \cdots = \frac{\pm v}{c \mp v} f_E \overset{c \gg v}{\approx} \frac{\pm v}{c} f_E \tag{3}$$

The tangential velocity of a (scaled) wind turbines rotor blade is given by $v_t = 2\pi f_{rot}\left(\frac{r}{K_{SC}}\right)$ with f_{rot} the rotation frequency of the blades and r the distance to the axis of rotation. Inserting v_t in (3) yields:

$$f_{DS} = \frac{\pm 2\pi f_{rot}\left(\frac{r}{K_{SC}}\right)}{c} (f_E K_{SC}) = \frac{\pm 2\pi f_{rot} r}{c} f_E \tag{4}$$

This derivation exhibits that the scaling of the wind turbine does not alter the Doppler shift.

Scaled Measurement Setup

The emitted (D)VOR signal has a bandwidth of only 20 kHz, thus it is very narrowband. Consequently, sounding a time-dependent propagation channel, e.g. rotating wind turbines, by measurements can be done at continuous wave. The validation of this particular concept as well as corresponding hardware requirements, especially at scaled higher frequencies are presented in [9]. A summarizing sketch of this setup is given in Fig. 1.

Basically, two propagation paths are relevant: a direct intentional propagation path and a scattered one that can be time-dependent due to rotating wind turbines.

In [8] the abstracting concept of simplifying any navigation system into these relevant propagation paths is demonstrated. Both the ideal and the scattered propagation path are measured quasi-simultaneously in 0.47 s intervals using an alternating timing scheme of emitting antennas corresponding to these paths, indicated in Fig. 2 with the colors red and blue.

The characteristics of propagation channel are measured at an intermediate frequency of 100 kHz which is by far high enough to sample the time-dependency of the channel.

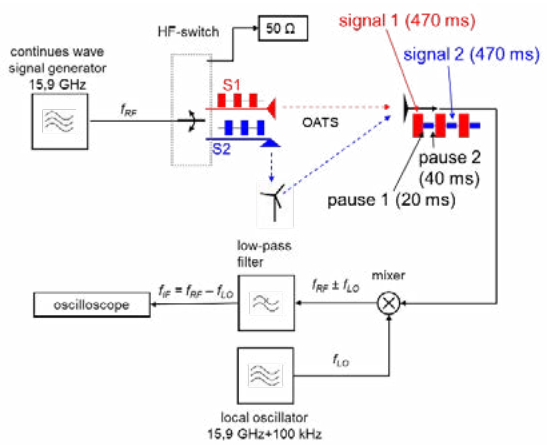

Figure 1. Hardware setup with the scaled measurement environment.

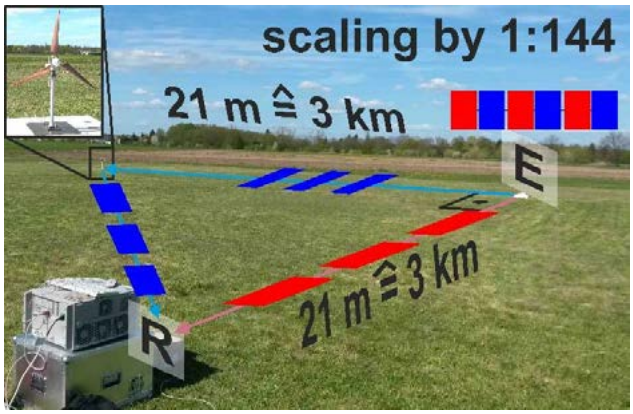

Figure 2. Measurement setup on the OATS: Emitter E, wind turbine and Reciever R form an isosceles triangle.

The measurements are conducted at an open area test side (OATS) with a metallic mesh in the ground. Emitter (E), receiver (R) and the wind turbine (WT) do form an isosceles and right-angled triangle, whilst the pair WT-R lies on the hypotenuse and E-R, E-WT on the catheti as depicted in Fig 2. Both catheti measure 21 m which corresponds to 3 km due to the scaling of 1:144. Both horn antennas of the emitter are 11.5 cm above the conducting ground, one directly facing the wind turbine for the scattered path, the other points to the receiver for the ideal propagation path. The receiving patch antenna is 15 cm above ground and faces the emitter.

Due to confidentiality of individual blade designs, thus limited availability to a wide community that may be interested in comparing numerical results with the measurement results presented here, generic rotating blade structures are chosen, such as follows.

In total five different wings types, as presented in Fig. 3, are installed. The rectangular shape serves as mount for adhesive copper foil and consists of 20 mm thick Rohacel. Rohacel behaves like air with respect to EM waves. The wings K I and K II are taken from Kosmos experiment boxes [10, 11] and metalized with copper foil as well.

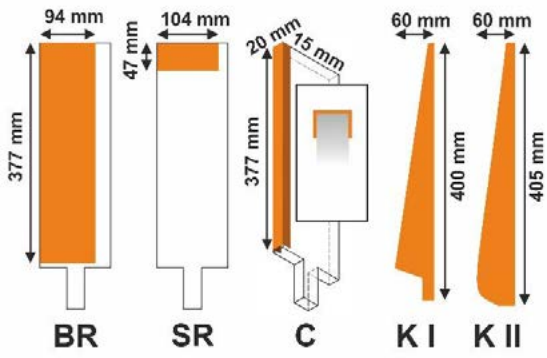

Figure 3. Measured wings: BR = big rectangle, SR = small rectangle, C = C-shaped edge, K I and K II = Kosmos experiment box I and II.

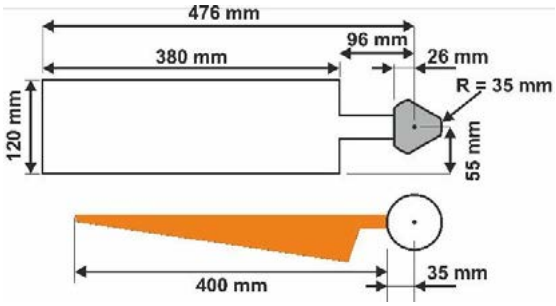

Figure 5. Dimensions of the Rohacell-mounting for copper foil BR, SR and C and its plastic-pickup. The pickup, white, of both K I and K II has a radius of 35 mm.

The hub of the miniature WT is 57 cm above the ground. The wing length with respect to the hub is given in Fig. 5.

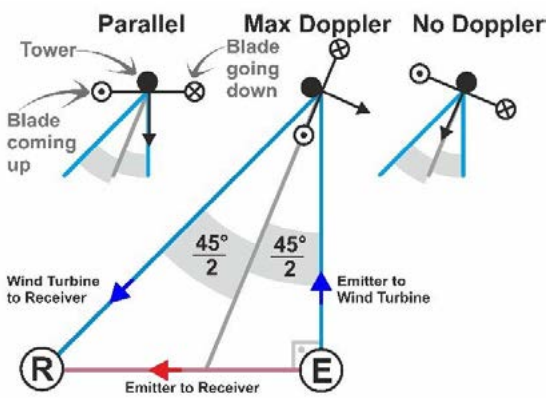

Figure 6: Bird's eye view: Orientation of the rotor blade's plane of rotation.

Three different planes of rotation — Parallel, Max Doppler, No Doppler — visualized in Fig. 6 are chosen. In the parallel constellation the plane of rotation is parallel to the line between E-R. Max Doppler: The plane

of rotation is in line with the bisectrix, which in turn leads to the wings having the same relative motion with respect to the emitter as to the receiver. No Doppler: The plane of rotation is perpendicular to the bisectrix between E and R. Hence as much as a wing moves towards E it moves away from R and vice versa. Therefore a change of the frequency at R cannot be expected. Tab. 1 summarizes the different Doppler shifts for the presented orientations.

Table 1. Calculation of the Doppler shift; f_{rot} rotation frequency of the blades, r distance to the hub, c speed of light, f_E frequency of the emitter.

	f_{DS}
Parallel	$\frac{\pm 2\pi f_{rot} r \cos(45°)}{c} \cdot f_E$
Max Doppler	$\frac{\pm 2 \cdot 2\pi f_{rot} r \cos(22.5°)}{c} \cdot f_E$
No Doppler	$\frac{+2\pi f_{rot} r \cos(67.5°) - 2\pi f_{rot} r \cos(67.5°)}{c} \cdot f_E = 0$

Measurement results are assessed two-fold. On the one hand Doppler spectra that occur due to the motion of the wings are shown in frequency domain. On the other hand time-dependent amplitude variations are presented in time domain.

In Tab. 2 all 72 parameter constellations which have been measured are given. Each setting of which the Doppler spectrum at the intermediate frequency is presented is denoted by an "F". "A" marks the constellations of which the analysis of the amplitude is shown further below.

Measurement Results with Respect to Doppler Spectra

In Fig. 7 to 14 the relative amplitude in dB versus the Doppler shift to the intermediate frequency in Hz is plotted for the constellations named above. The peak the scattered path is normalized to the peak of the direct path, whilst the ratio is given in dB. The vertical black line marks the maximal Doppler shift and the green one the minimal one calculated with the equations given in Tab. 1. The tachometer displays the frequency the blades rotate with per minute and the state of the wing is visualized by the inset to the right of the peak.

In Fig. 7 the spectra gained from the constellation with the empty Rohacell mounts rotating with $f_{rot} = 22.2\ min^{-1}$ in the parallel orientation is shown. In this constellation only static scatterer are present, such as the tower of the wind turbine.

Table 2. Measured constellations. "F" denotes parameter constellations of which the frequency spectrum is presented and discussed. "A" indicates constellations where the effect of amplitude modulation on a VOR-receiver is offered.

		$\frac{0}{min}$	$\frac{20}{min}$	$\frac{22.2}{min}$	$\frac{71.4}{min}$
Parallel	empty holder			F	
	big rectangle				
	small rectangle				
	C-edge				F
	Kosmos I			F, A	F
	Kosmos II				F
Max Doppler	empty holder				
	big rectangle				
	small rectangle				
	C-edge			A, F	A, F
	Kosmos I				
	Kosmos II				
No Doppler	empty holder				
	big rectangle				
	small rectangle				
	C-edge				
	Kosmos I				
	Kosmos II				A, F

No Doppler shift is detected, which meets the expectations, since the blades bear no reflecting metal surface.
Fig. 8 and 9 display the spectra for the C-edge in the Max Doppler orientation rotating at $f_{rot} = 22.2\ min^{-1}$ and $f_{rot} = 71.4\ min^{-1}$. Clearly visible are the Doppler shifts to the left of the peak. The plateaus start and end well-nigh at the calculated values.
In all figures only negative Doppler shifts are visible which are attributed to the movement of the wing above the hub with a relative motion both away from the receiver and the emitter. The reason for this is that due to

the conducting ground only the upper half of the wind turbine is significantly illuminated. Similarly, the radiation characteristics of the wind turbine is also affected by the ground.

Fig. 14 shows components in the spectrum that can not be attributed to Doppler shifts of the wind turbine. Such components can be associated with other environmental dynamic occurrences, but are rarely seen and can easily be identified. The different blade shapes are clearly visible in the Doppler spectra. Whereas the C-edge of the wing have a plateau-like shape in the spectrum, the shapes Kosmos I and II show the varying cross sections of the wing associated with different relative velocities and Doppler shifts. If the influence of Doppler shift is to be investigated in flight inspection measurements both the theoretical considerations and the measured results suggest a corresponding scenario as presented in Fig. 6.

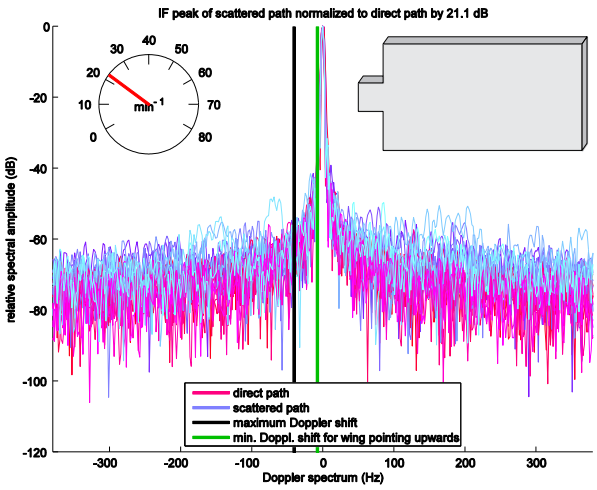

Figure 7. Doppler spectrum of the scenario Empty Holder, 22.2 min^{-1}, Parallel.

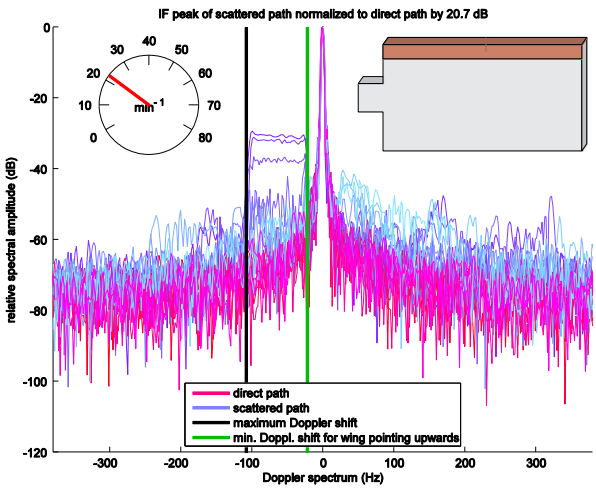

Figure 8. Doppler spectrum of the scenario C-edge, 22.2 min^{-1}, Max Doppler.

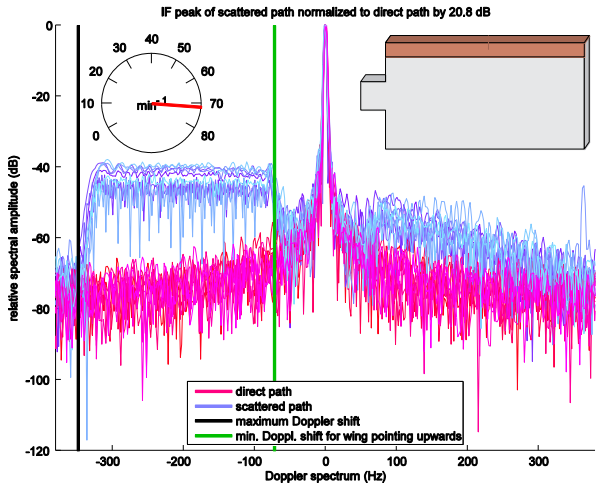

Figure 9. Doppler spectrum of the scenario C-edge, 71.4 min^{-1}, Max Doppler.

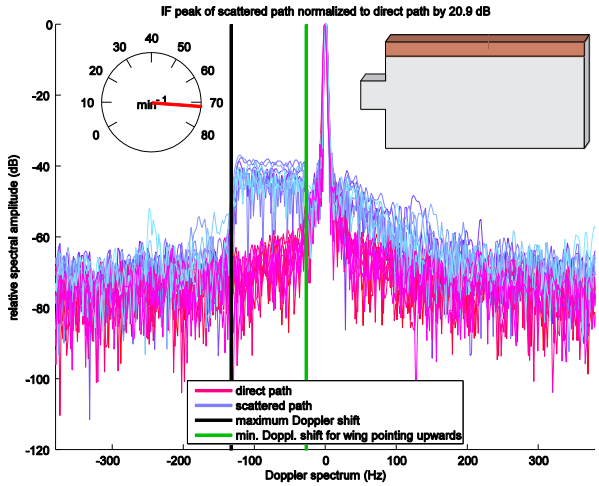

Figure 10. Doppler spectrum of the scenario C-edge, 71.4 min^{-1}, Parallel.

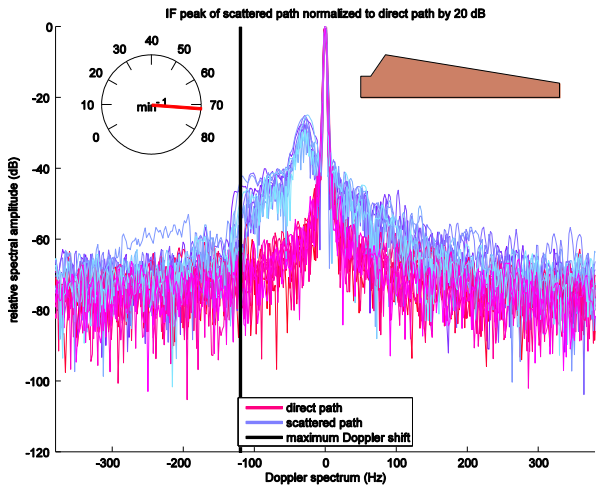

Figure 11. Doppler spectrum of the scenario Kosmos II, 71.4 min^{-1}, Parallel.

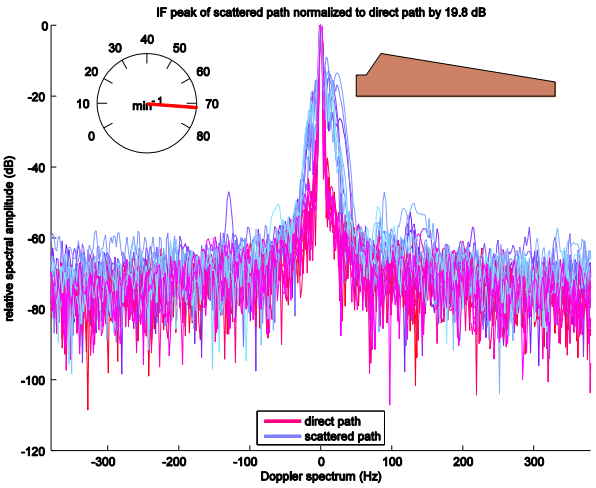

Figure 12. Doppler spectrum of the scenario Kosmos II, 71.4 min^{-1}, No Doppler.

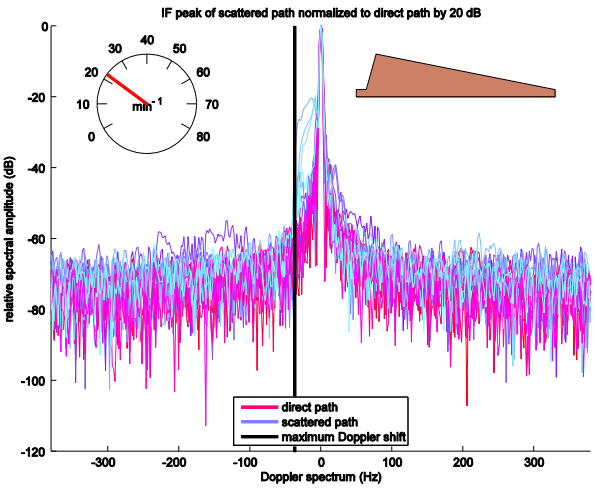

Figure 13. Doppler spectrum of the scenario Kosmos I, 22.2 min^{-1}, Parallel.

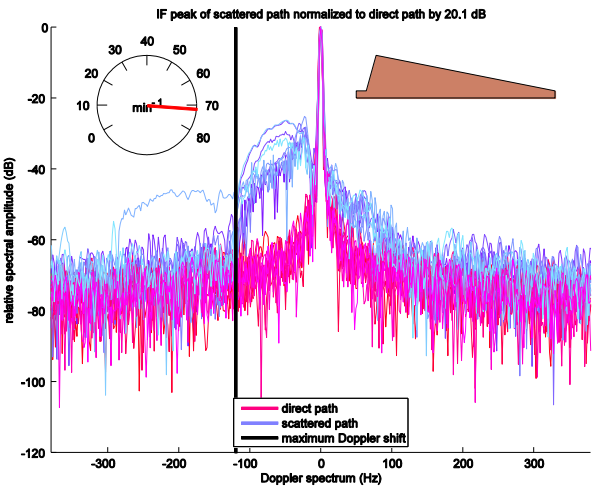

Figure 14. Doppler spectrum of the scenario Kosmos I, 71.4 min^{-1}, Parallel.

An intrinsic property of the rotating blades is the random blade position range within a given measurement time. However, the Doppler shift strongly depends on this particular blade position. For example, if the blade is moving through the upright position (12 o'clock), then the Doppler shift has its maximum. A minimum occurs for the 3 and 9 o'clock positions. Consequently, it is necessary to adapt the measurement intervals depending on the rotational speed. For example:

A measurement interval of 1 s is not suitable for a rotational speed of 20 min^{-1} for a three-blade rotor, that is 60 times the same blade orientation per minute. Thus such a measurement interval would always sample the same blade configuration.

Measurement Results with Respect to Time-Variant Amplitude

The time-variant propagation channel with rotating wind turbines may cause an additional amplitude modulation the AM component of the VOR may be sensitive to.
This effect of amplitude modulation is measured with the navigation receiver EVS 300. Fig. 15 illustrates how scaled measurements, post-processing and the test setup for feeding the EVS are related. Previous work of the authors deals with an EMI characterization of navigation receiver with respect to such multipath interferences. A sophisticated description of a corresponding measurement setup and its validation is presented in [12] and is only described briefly here.
The (D)VOR signal is generated by an arbitrary wave form generator (AWG). According to the two propagation paths measurement setup at the OATS both the intentional (D)VOR signal and the scattered signal are superposed at the receiver's input stage.
The signal of the AWG is split over a direct path with no attenuation and a scattered path with a voltage-controlled variable attenuator ZX73-2500 allowing the implementation of an AM-modulated channel.
As the scope of this analysis is only the effect of the amplitude modulation, the bearing error resulting from of static scatterers for the FM component according to [13] is not taken into account.

The direct path is assumed to have no additional modulation by the channel, otherwise it would be a noise effect of the environment which is not the scope of the contribution.

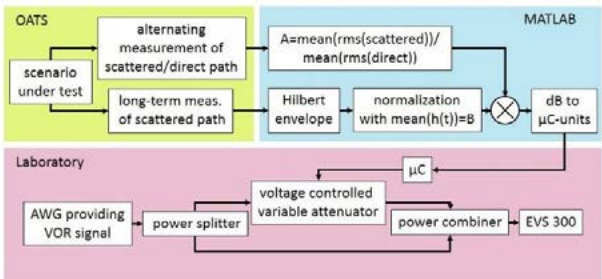

Figure 15. Measurement setup for determination of bearing errors due to AM-modulated scatterers.

Two measurement modi are conducted at the OATS to assess AM disturbances. A first one is necessary to relate the scattered amplitude to the ideal propagation path. This is done with short measurement intervals of half a second. In Fig. 15 it is referred to as alternating measurement. A second one measures the scattered path solely with a larger observation time of 10 s labeled long-term measurement.

In the post-processing the measured signals in the intermediate frequency band is demodulated with a Hilbert envelope $h(t)$ in Matlab according to [14] using the built-in function "hilbert". To normalize the signal $h(t)$, it is divided by its mean value B. With this normalization the signal becomes unit less. Exemplarily, Fig. 16 shows quantities of these individual post-processing steps.

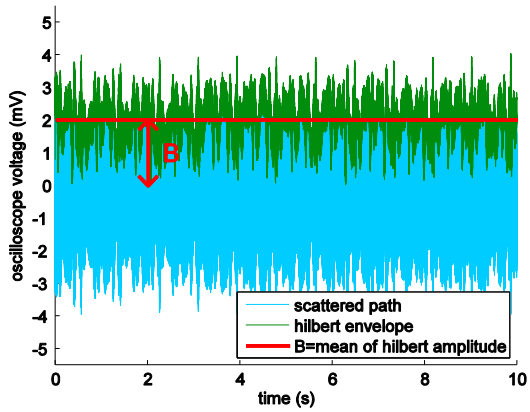

Figure 16. Post-processing quantities of measured data. The scenario is Kosmos II, 71.4 min^{-1}, No Doppler.

The attenuation value for the scattered path in the AWG setup is taken from the alternating measurement results that yield the factor A as ratio between the ideal and the scattered propagation path according to:

$$A = \frac{\sqrt{\frac{1}{T}\int_0^T U_{sc}^2(t)dt}}{\sqrt{\frac{1}{T}\int_0^T U_{dir}^2(t)dt}}\,, \qquad (5)$$

where U_{sc} and U_{dir} are the voltages measured with the oscilloscope of the scattered and the direct paths, respectively.
Thus A, transferred to the dB scale, determines the operating point of the variable attenuator. Therefore the necessary attenuation $a(t)$ of the variable attenuator is:

$$a(t) = -20\log_{10}\left(\frac{A}{B}h(t)\right). \qquad (6)$$

As the attenuator is voltage-controlled where the control voltage is generated by a microcontroller, the attenuator must be calibrated. This is done by measuring a look-up table to relate byte values in the µC to the attenuation in dB.

Fig. 17-21 show the time dependent amplitude of the scattered path as realized with the external variable attenuator. The insets display the rotational speed of the wind turbine as measured at the OATS and the standard deviation of the bearing error as received with the EVS. With the scenario C-edge, 22.2 min^{-1}, Parallel, a standard deviation of the bearing errors of 0.31° is measured; see Fig. 17.
As presented in [12], the bearing error of the (D)VOR is very sensitive if the channel modulation frequency is around 30 Hz. For example, as it can be seen in Fig. 8 that in the measured spectrum of the intermediate frequency band there are sideband components at 30 Hz below the IF.

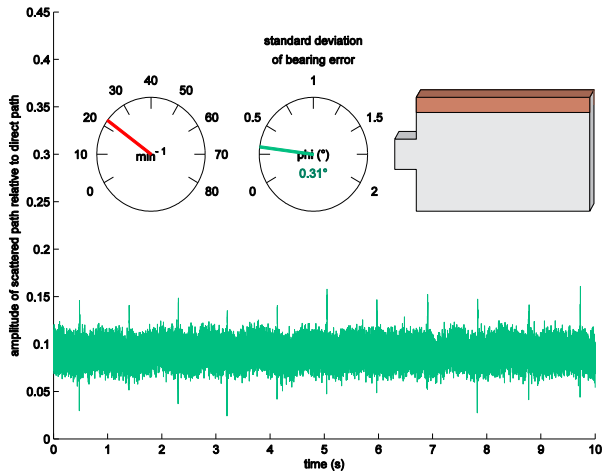

Figure 17. The scenario is C-edge, 22.2 min^{-1}, Parallel.

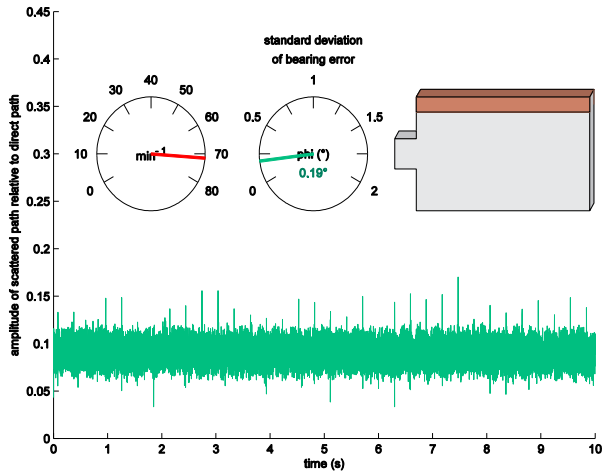

Figure 18. The scenario is C-edge, 71.4 min^{-1}, Parallel

For a higher rotational speed there is are no significant bearing error to be detected (Fig. 18). In the spectrum, due to the increased speed, there are no components at ±30 Hz to be recognized (Fig. 9). The standard deviation of the bearing errors is 0.19°, which can be considered as noise, mainly due to incomplete removal of the carrier with the Hilbert envelope, followed by subsampling of the microcontroller. Standard deviations of the bearing

error of around 0.2° are also detected due to this effect for the static measurements.

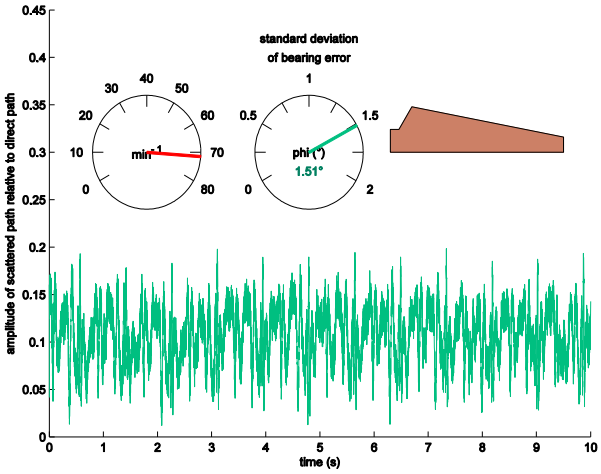

Figure 19. The scenario is Kosmos II, 71.4 min^{-1}, No Doppler.

An example for significant bearing errors of a very generic wind turbine is shown in Fig. 19 for the scenario Kosmos II, 71.4 min^{-1}, No Doppler with a standard deviation of 1.51°, due to the channel amplitude modulation. It is a scenario where the blade orientation is such that no Doppler shifts occur because the relative velocities of the blades with respect to receiver and emitter are equal but of opposite sign. It is therefore a typical example for a scenario where significant bearing errors occur without any Doppler shift, but solely due to the amplitude modulating characteristic of the channel.

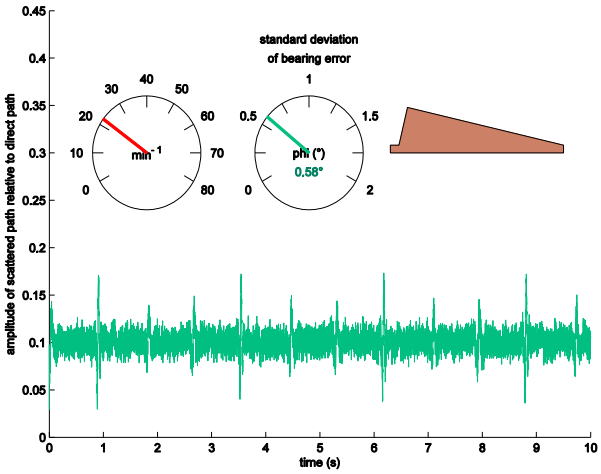

Figure 20. The scenario is Kosmos I, 22.2 min^{-1}, Parallel.

The scenario presented in Fig. 19 has a high rotational speed. Another scenario with a more realistic speed of 22.2 min^{-1} is Kosmos I, Parallel, given in Fig. 20. It also shows bearing errors with a standard deviation of 0.56°.

As a result, the effect of a rotating wind turbine on the bearing error of a VOR due to amplitude modulation may dependent on the shape of the wing, rotational speed and orientation of the wind turbine.

CHALLENGE

Several results are presented of scaled measurements in the context of (D)VOR disturbances. They are meant to provide a fundamental validation bases for simulation tools also aim to include the dynamic behavior of rotating wind turbines. The set of configurations and available measurement data given in Tab. 2 can be used as a benchmark study to compare different numerical methods. Once numerical results for any of the mentioned scenarios are provided, authors offer a comparison with their measured results.
Authors would also appreciate if other scaled measurements are conducted for constellations given in Tab. 2.

CONCLUSIONS

Regardless the actual navigation system measurement results of wind turbines in terms of Doppler spectra and time-dependent amplitudes are presented. The particular influence on a navigation system, e.g. VOR or radar or weather radar can be assessed individually. However, the mandatory characterization of moving scatterers is given here and could be used as validation bases for numerical software tools.

For the VOR case the influence of the amplitude modulated characteristics of a rotating wind turbine is exemplarily investigated.

An additional important part for analyzing errors in navigation systems due to multipath propagation must address the navigation receiver characteristics. It may be interesting to use the measured and the proposed measurement setup to investigate different navigation receivers.

RECOMMENDATIONS

For future flight inspection measurements authors recommend to record the operational state of wind turbines, at least with the parameters blade orientation and rotational speed. Such data is mandatory for reproducibility with simulation tools and scaled measurements.

ACKNOWLEDGMENTS

This work was supported by the German Ministry for Economic Affairs and Energy under Grant 0325831, project min-VOR-Win.

REFERENCES

[1] C. Morlaas, M. Fares, and B. Souny, “Wind turbine effects on VOR system performance,” IEEE Transactions on Aerospace and Electronic Systems, vol. 44, no. 4, pp. 1464–1476

[2] C. Morlaas, A. Chabor, and B. Souny, “Propagation model for estimating vor bearing

error in the presence of windturbines – hybridation of parabolic equation with physical optics," Antennas and Propagation (EuCAP), 2010 Proceedings of the Fourth European Conference on, pp. 1–5,.

[3] G. Greving and L. N. Spohnheimer, "Recent Issues in Performance Prediction and Flight Inspection Measurements" 2014, 16.-20. June IFIS, Oklahoma City, USA.

[4] "Validation of Ohio University NAVAID Performance Prediction Model (OUNPPM) Mathematical Model for Signal Interference in VOR Systems Caused by Wind Turbine Farms," AJP-7B3, 2010. 10. June.

[5] J. Bredemeyer, "Further expertise on the interaction between wind turbines and DVOR facilities of the air navigation services," 2015, 17.April, https://www.schleswig-holstein.de/DE/Fachinhalte/W/windenergie/Downloads/fortfuehrendesGutachtenWindenergie_engl.pdf?__blob=publicationFile&v=2

[6] H. D. Lüke, Signalübertragung: Grundlagen der digitalen und analogen Nachrichtenübertragungssysteme. ISBN 3-540-65197-7, Berlin, Heidelberg: Springer, 1999.

[7] T. Macnamara, Introduction to antenna placement and installation., ISBN 978-0-470-019818, Chichester, West Sussex, U.K, Hoboken, NJ: Wiley, 2010.

[8] R. Geise, B. Neubauer, and G. Zimmer, "Analysis of Navigation Signal Disturbances by Multipath Propagation – Scaled Measurements with a Universal Channel Sounder Architecture," Frequenz, no. 11-12, pp. 527–542.

[9] R. Geise, G. Zimmer, B. Neubauer, Distortion of Modulated Signals by Time-Variant Channels - Measurement Concepts and Algorithms, EuCAP 2016, 11.-15. April, Davos, Schweiz

[10] "Kosmos II: Kosmos Experiment Box Windenergy," http://www.kosmos.de/produktdetail-909-909/wind_energie-7687/

[11] "Kosmos I: Kosmos Experiment Box Windenergy," http://www.buch.de/shop/home/rubrikartikel/ID27177365.html?ProvID=10910555

[12] R. Geise, O. Kerfin, G. Zimmer, B. Neubauer, and A. Enders, "Investigating EMI-Characteristics of Navigation Receivers," ESA Workshop on Aerospace EMC, Valencia, Spain, 2016.

[13] S. Anderson and R. Flint, "The CAA Doppler Omnirange," Proc. IRE, vol. 47, no. 5, pp. 808–821, 1959.

[14] M. R. Schroeder, Computer speech: Recognition, compression, synthesis ; with introductions to hearing and signal analysis and a glossary of speech and computer terms., ISBN 3-540-64397-4, Berlin: Springer, 1999.

Real-time SSR Pulse Analysis and Spectrum Protection Monitoring

Maik Ritter
System Engineer
Aerodata AG
Hermann-Blenk-Straße 34-36
38108 Braunschweig, Germany
Phone: +49 531 2359 246
Fax: +49 531 2359 222
E-mail: ritter@aerodata.de

Christopher Dean
Chief Technical Services Engineer
AeroPearl Pty Ltd
GPO Box 884
Hamilton Central
Brisbane, QLD 4007, Australia
Phone: +61 7 3860 0618
Fax: +61 7 3216 3164
E-mail: cdean@aeropearl.com.au

ABSTRACT

Measurement and analysis of SSR performance has largely been made on the basis of the flight inspection aircraft playing the role of a co-operative, calibrated target, able to generate high quality truth data for accuracy analysis purposes. This is a time consuming process and real time assessment of SSR performance and coverage is often not possible onboard the aircraft itself.

Additionally, with classic and Mode S RADAR, Multi-Lateration Systems and TCAS adding to the 1030 MHz RF environment new technology was required to be developed and integrated into the flight inspection system for SSR pulse analysis and interference detection.

This paper presents the methods used for such analysis in the past and how they led to the development of new technology able to complete this analysis, airborne and in real time. The hardware/software concept and realization into the airborne system is presented.

The effectiveness of the system in the context of SSR flight inspection and additional considerations for the use of monitoring spectrum protection with regards to EU Regulation No 1207/2011 is considered. Several use-cases are presented, including examples where the capabilities offered by the technology were key to understanding complex interactions in the 1030 MHz RF environment and resolving issues observed in SSR performance.

INTRODUCTION

Flight Inspection of Secondary Surveillance Radar (SSR) systems differs from conventional flight inspection for ILS/VOR or DME. A flight inspection aircraft is equipped with sophisticated measurement equipment in order to measure, analyze and record data literally “on the fly” and present the results during the inspection to the operator of the Flight Inspection System (FIS). Graphics, alpha numerics and results are presented for parameters that are not displayed on primary flight instruments. Reports are prepared by the system to automatically decide if a facility parameter is inside a predefined tolerance.

With the help of dedicated flight inspection receivers and equipment such as oscilloscopes and spectrum analyzers, the operator has many means to examine the signals from ground Navigational Aids (NavAid) in the air, which is not possible with general aviation aircraft.

Many parameters of the FIS are digitized and recorded during a flight inspection. This way, the condition of a NavAid can be documented and, in the case of an error, be investigated later on ground by replaying the recorded inspection.

For an experienced Flight Inspector, it is possible to see developing problems with a facility, that maybe in tolerance during the ongoing flight inspection but, because some slight deviations on the signal, may fail in the near future. This is possible because the Flight Inspector is supported by a system that presents an inside view of the navigation data of a NavAid.

All this is not possible for SSR signals when the flight inspection aircraft is not equipped with dedicated devices that can actively monitor and examine the condition of an SSR.

Currently, the flight inspection aircraft is just a known radar target that is recorded by the radar equipment on ground. In the best case, it is equipped with a calibrated transponder installation so that only interrogations of a certain signal level trigger a reply from the transponder. Additionally, the transmit power should be adjusted in order for the SSR to receive distant replies at a defined signal level. The flight inspection aircraft just records its position. After the inspection, both the recorded aircraft position from the FIS and the recorded aircraft position from the SSR are compared and the radar will be assessed for its performance.

While this approach is commonly used and accepted for SSR inspections, it lacks the possibility to assess the compliance of the SSR signals against the specified requirements for those signals [1]. The signals that form the communication between an SSR and the aircraft transponder are made up of impulses that have to obey defined amplitudes, widths and spacings in order to comply with the specifications. Additionally, side lobe suppression is defined to be present all around the radar antenna except for the main beam that rotates at a defined speed in order to only interrogate aircraft in one direction from the radar. Without equipment that checks for those specified parameters, one has no knowledge about the quality of the SSR impulses, the RF-Level of the interrogations at any location between the radar and the coverage border (which in fact is defined by the calibrated sensitivity of the transponder). There is no information about how many valid interrogations reached the aircraft and how often a transponder replied to those. Finally, there is no way to examine impulse trains from a dedicated (Mode S) radar with additional devices such as an oscilloscope in flight.

By using this approach, other signals that are present on the same communication channel (the SSR 1030Mhz uplink band is also used for TCAS as well as all other SSRs that are present in the vicinity of the flight inspection aircraft) can also not be observed and assessed. Degradation of the communication channel can only be recognized in the moment of failure and not beforehand when a possible overload of the channel can be observed over time.

Taking an extreme view, if an ILS was inspected using this same methodology, the assessment would not go further than landing an aircraft using primary instruments and assessing whether the aircraft was able to hit the centerline or not.

This paper presents a different approach to SSR inspections. The SSR is regarded as an additional facility that will be inspected in flight using dedicated flight inspection equipment and processing. Of course, only the interrogation side of the radar communication is checked in the FIS.

TRANSPONDER PULSE DECODER SYSTEM

A Transponder Pulse Decoder System (TPDS) is an approach to incorporate SSR inspection capability into the FIS. It comprises of SSR receiving hardware and FIS software integration.

TPDS Hardware

In order to process the impulses contained in the 1030MHz band, a dedicated receiver is required. An “of the shelf” transponder can be used. However, the transmit functionality must be disabled in order to not interfere with the primary transponder of the aircraft. In addition, some minor modifications must be performed in order to get the baseband or video signal for further processing.

Processing of impulse based signals, with impulses occurring randomly and impulse widths under one microsecond, can only be done while constantly monitoring the signal. Dedicated hardware that contains fast Analog-to-Digital (A/D) conversion and a real-time processing device is best suitable for this task. When we talk about “fast” A/D conversion and “real- time processing”, one has to have in mind that these terms are only relative measures compared to other conversion- and processing-devices inside a FIS. When it comes to the availability and the cost for such hardware, it is safe to say that it is available at very low cost compared to an overall flight inspection system.

The kind of data processing that is most appropriate for this application is “stream processing”. The digital data stream that is constantly “flowing” from the A/D converter has to be processed sample by sample in order to not miss any event that may be an impulse of an interrogation. Once an impulse event is recognized, it has to be determined if this impulse is valid according to the specifications in [1]. Furthermore, it has to be investigated if this impulse is a member of an SSR interrogation and if so, if the timing specifications for that interrogation are met. After an interrogation is positively identified, the presence of side lobe suppression has to be checked. Impulses have to be marked as P1, P2, P3 etc. and finally have to be transferred to the FIS software for recording, graphical visualization and report evaluation.

The digital processing hardware that is most suitable for such a task is a Field Programmable Gate Array (FPGA). With such a device, it is possible to implement any digital circuitry defined by a Hardware Description Language (HDL). It is possible to create a digital circuit that is fully customized for the purpose of transponder impulse recognition, verification and interrogation decoding on a stream of digital data samples. Additionally, logic for a standard data interface such as UART and internal calibration logic can be implemented.

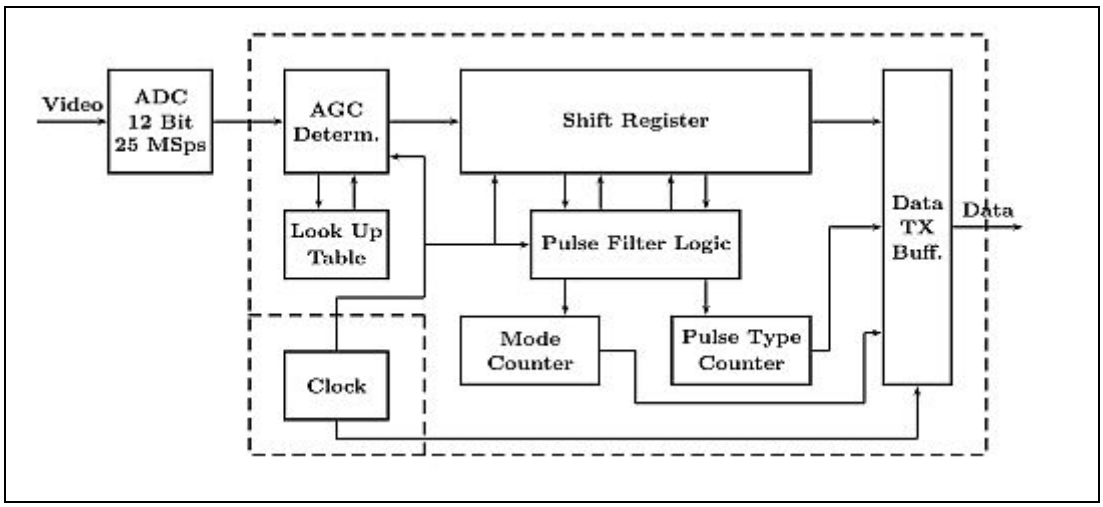

Figure 1 Block Diagram of a Transponder Pulse Decoder Box.

Figure 1 shows the block diagram of a Transponder Pulse Decoder Box (TPDB), which represents the processing part of the TPDS. The dashed box represents all components that are within the FPGA or, in the case of the clock, a mandatory FPGA part. The A/D Converter is in the same housing of the TPDB but is not a part of the FPGA.

The "Video" line connects to the "receive only" transponder and the "Data" output connects to the FIS.

Once the system is powered up, the TPDB transmits every impulse that was contained in the video signal to the FIS along with additional information so that the FIS software can display the information in graphics, alpha numerics and reports. The data interface can be designed with an impulse throughput of about 30000 impulses per second.

In addition to the pure impulse processing, the TPDB also performs some statistics processing by providing counters for all interrogation modes that sum up over a defined period. This way, it is easier for the FIS software to present hit rate and signal in space information to the operator.

For enabling Mode S message decoding, it is required to connect the transponder internal Differential Phase Shift Keying (DPSK) signal to a digital input of the TPDB.

The purpose of this DPSK decoding as well as the hit rate and field strength measurement is explained in the TPDS FIS software section.

Figure 2 shows a manufactured TPDS ready for installation into an aircraft.

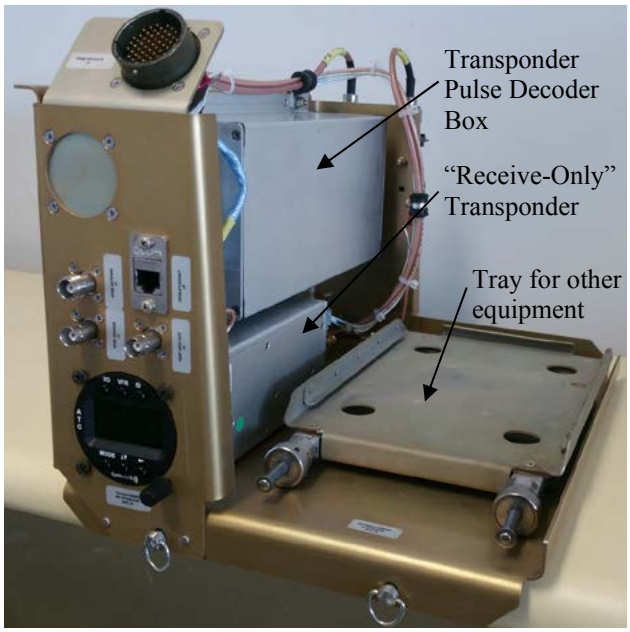

Figure 2 Transponder Pulse Decoder System (TPDS)

TPDS FIS Software

In the FIS software, raw data from navigation receivers is processed and combined against position reference parameters, calibration values and tolerance requirements. Unit transformations and additional calculations like mean value computation can be configured and automatically processed once required. Each measured parameter can be graphed against different references (such as time, distance or azimuth) as required for supporting the Flight Inspector to assess the condition of a NavAid.

Reports with automatically calculated results are prepared once an inspection is finished.

All these parameters and configurations can be configured in detail and because of the availability of recorded raw data, everything can be replayed and even reprocessed after the flight is completed.

Flight inspection software can compare the current inspection results with a facilities history in order to recognize any degradation in a signal received from the ground.

By providing a receiver for the SSR signal, all these FIS software features can also be applied to 1030MHz uplink signals.

TPDS Impulse Graph

SSR signals are impulses of a very short time and SSR interrogations are made up from these impulses, which are spaced apart by defined time intervals.

In the FIS software, an impulse graph is designed to display all impulse events accumulated over a certain period. This gives a visual summary of the signal activity on the 1030MHz uplink band. The impulse graph is initially configured such that the impulses of a whole radar rotation for the currently inspected radar is displayed.

Figure 3 shows an example shot of such an impulse graph. For clarity, impulses of different interrogation modes and/or of different types (P1, P2, etc.) are of different color.

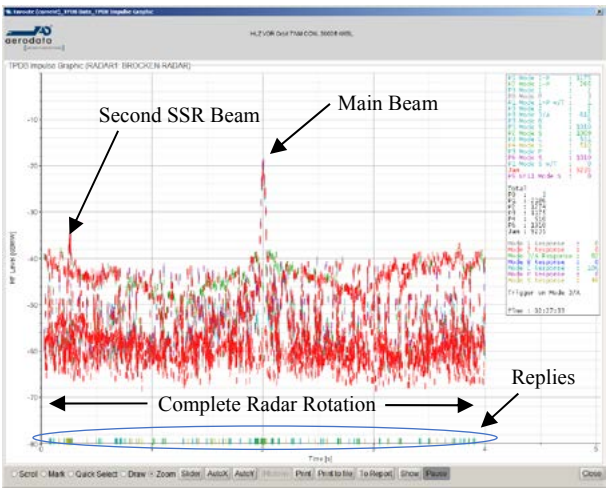

Figure 3 SSR Impulse Graph

The impulse graphic enables the operator to examine all events to a resolution of 40ns. By zooming into an interrogation, it is possible to measure the impulse spacing between P1 and P3 and one can check why the TPDB has possibly marked an interrogation as invalid. Side lobe suppression violations can be recognized as well as the width of the main beam. In order to focus only on one interrogation type, different filters can be applied in order to only see the impulses of interest. The impulse graph display period is configurable from within the FIS software.

The impulse graph is a handy tool to grasp the overall quality of a radar with a glimpse. It enables the operator to judge if the side lobe suppression of a radar is more or less doing what it is supposed to do or how many radars are receivable at the current aircraft position. However, additional parameters should be available that have more of a flight inspection like character and that can be judged by their numerical values against predefined tolerances or expected values.

Special TPDS Parameters

Those parameters are:

- Signal in Space (for coverage measurements)
- Hit Rate per interrogation (for verifying enough interrogations to elicit replies)

Both parameters are available at a 10Hz base. This means that the TPDB accumulates all hit rates and determines the maximum interrogation field strength for each mode for the last 100ms (times could be adjusted to special requirements). These raw parameters are used by the FIS software to calculate so-called sample and hold values. These values are e.g. accumulated 100ms datasets from the TPDB over a period of 1.5 times the radar rotation time of the radar of interest. Again, for this parameter, the field strength value is the maximum field strength received during that 1.5 * radar rotation period.

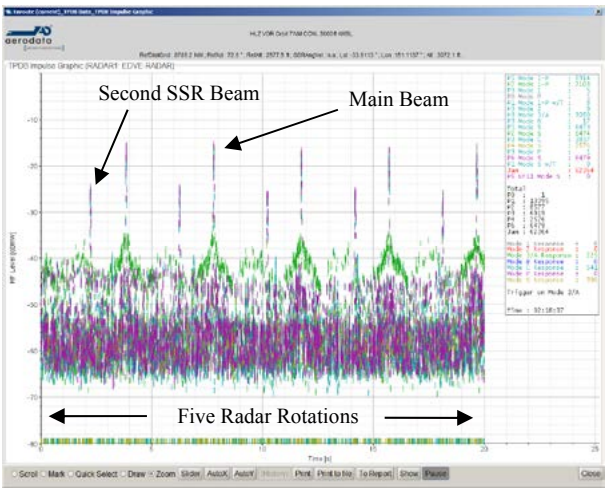

Figure 4 Two SSRs (1)

If we refer to Figure 3, the effect of this sample and hold parameter is to get the maximum field strength of the interrogations of the main beam of the centered radar. Because it holds the maximum field strength value for the last 1.5 radar rotation time, the main beam is measured because it is much stronger than the second visible beam in that plot. This parameter can be used to

measure coverage for the given radar as long as it is the strongest radar in the area.

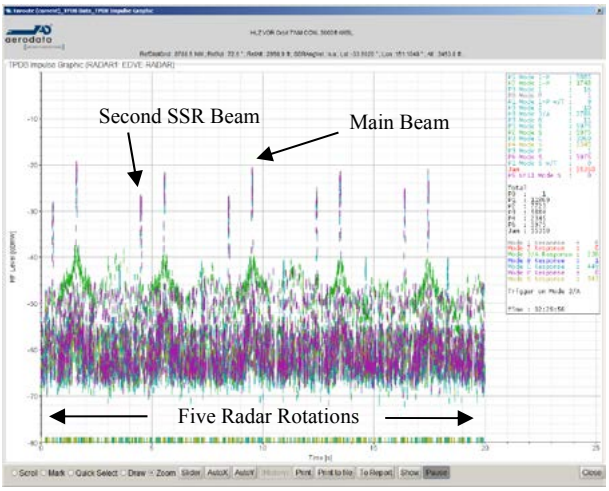

Figure 5 Two SSRs (2)

The situation changes when we refer to Figure 4 and Figure 5. Here, the main beam that initially has a stronger signal strength than the second beam gets weaker while the second beam gets stronger during the inspection. At one point during the inspection the above described algorithms will "lock" onto the second beam which in this case is not the radar that should be inspected.

One can overcome this problem by either switching a radar to a non standard interrogation mode that is only used during radar inspection. This mode will not elicit replies from normal transponders because the impulse spacings will not match. However, the TPDB is able to recognize any predefined impulse spacing and will provide this interrogation as a special flight inspection mode.

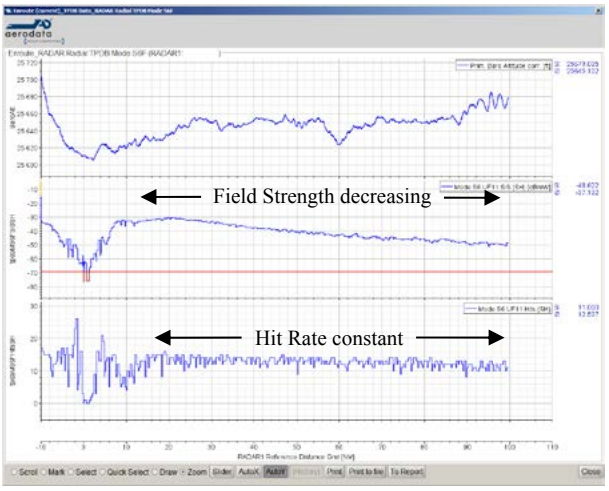

Figure 6 Field Strength and Hit Rate Graph

The more preferable way of filtering a radar is by using the Mode S surveillance and Interrogator Identifier fields in an UF11 message (derived from the transponders DPSK signal). This, of course, will only work with a Mode S capable SSR. With the increase of Mode S equipped radars all over the world, this approach of selecting a radar will become the standard. There will be no need for special impulse spaced interrogations for flight inspection use in the future.

Figure 6 shows an SSR flight inspection radial graph. It displays three parameters plotted against the reference distance to the inspected SSR. The barometric altitude parameter on top is for documenting the flight level of the current radial. The field strength (derived from the above explained sample and hold value) shows how the signal level of the main beam decreases towards the coverage limit line with increasing distance. The hit rate parameter (also derived from the sample and hold mechanism) shows a constant interrogation rate even at greater distances from the station. Again, it is emphasized that in Figure 6, only the radar of interest is displayed, due to the UF11 filtering. Also, only valid interrogations with regard to impulse width, spacing and correct side lobe suppression (in the case of Mode S, sync phase reversal) are displayed here.

Now, the SSR inspection can be carried out similar to a DME inspection, where, instead of a hit rate parameter one would check for squitter and reply rates.

Jam Impulses

By looking at Figure 3, one recognizes that the red colored impulses are very dominate. Those impulses have been classified as Jam impulses. They are events on the transponder video signal that fall closely into the specification of impulses that form a valid interrogation. However, those impulse events are not assignable to any interrogation because their impulse shape or width does not comply with the specified impulse shape or width and/or the impulses do not belong to an impulse group of an interrogation.

Additionally, all interrogations that are side lobe suppressed are marked as Jam since they also are not a considered a valid interrogation.

If, however, the main beam of a radar contains many Jam impulses, it could be a sign of interference that may need further investigation.

Jam impulses are an additional tool to judge the quality of an SSR – transponder link.

Transponder Reply Processing

By connecting the suppression line of the flight inspection transponder or even the primary transponder to the TPDS, it is possible to count the actual reply rate of a standard aviation transponder in a standard aircraft installation. This way, the flight inspection system does not only monitor the 1030MHz band as it sees it, but

also takes the behavior of a real world transponder into account. It can be documented how often a transponder is actually replying to interrogations from the ground and whether this reply rate is in the range of the expected value. For example, if there are too many interrogations from different SSRs, the transponder may not reply sufficiently to the radar under inspection. This would be seen as a null in SSR coverage using the conventional method of SSR inspections, where in fact the issue is overload of interrogations at the input of the transponder and can be identified with the use of the TPDS.

The transponder replies are shown on the impulse graphs in Figure 3 and are marked by the blue circle.

Spectrum Protection Monitoring

Given the above introduction to the Transponder Pulse Decoder System, and its ability to monitor SSR uplink and downlink, the TPDS could be used in other scenarios, such as Spectrum Protection Monitoring. EU Regulation No 1207/2011, Article 6, Spectrum Protection, 1 – 3, demands that:

- SSR transponders should not be "subject to excessive interrogations that are transmitted by ground-based surveillance interrogators", and that the ground based interrogators "are of sufficient power to exceed the minimum threshold level of the receiver of the secondary radar transponder".
- "the sum of such interrogations shall not cause the secondary surveillance radar transponder to exceed the rates of reply per second (…), specified in (…) Annex 10 (…), Volume IV, Fourth Edition".
- "a ground based transmitter (…) does not produce harmful interference on other surveillance systems".

If we compare those requirements with the capabilities of the TPDS, it is apparent that parameters like hit rate, field strength/coverage and reply count are suitable to address the first two requirements of the regulation.

Finally, a Jam analysis could be considered to investigate possible interference problems in the 1030MHz band.

FIS Integration

The TPDS is fully integrated into a flight inspection system, not only as a receiver, that makes it possible to process SSR signals in the FIS software, but it is also able to deliver trigger signals to a FIS Oscilloscope. The FIS Oscilloscope can then be used to investigate the impulse quality of the transponder video signal not only in the digital sense but also in the "old fashioned" analog way. The recognition of a Jam impulse for example could cause a trigger in order to see why the TPDB decided to degrade impulse events to Jam. This gives an additional analysis tool for SSR signals in the air. Figure 7 presents a typical airborne Oscilloscope plot of an SSR interrogation

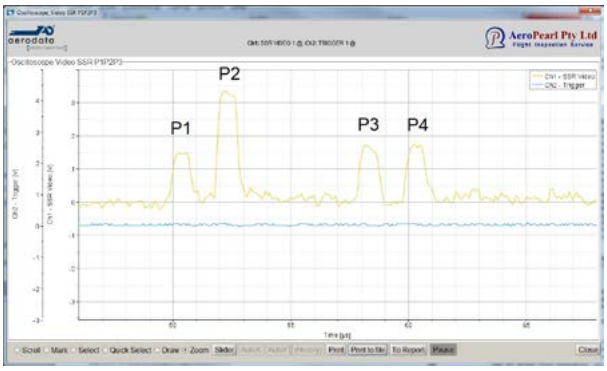

Figure 7 Airborne Oscilloscope Plot of an SSR Interrogation

In addition to connection to an Oscilloscope, the TPDS can also be connected to an LED Panel, Figure 8, which will flash a specific LED each time a valid interrogation is received from the SSR ground station, depending on the interrogation mode received. This can be used by the Flight Inspector to quickly identify what modes are currently being received by the TPDS without the need for opening graphics or alphanumeric pages in the FIS.

Figure 8 TPDS LED Panel

Flight Inspection Missions with the TPDS

Flight Inspection of SSR facilities utilizing the TPDS are flown with the same standard profiles as a standard SSR inspection relying only on GPS data. However, the benefit of having measurement results available to the Flight Inspector in real time means that the performance of the SSR can be assessed earlier in the inspection and runs may be able to be reduced in duration or eliminated completely from the inspection based on this assessment. For example, predefined performance limits can be applied to inner coverage orbits, and if these limits are met the number of outer coverage radials can be reduced. This flexibility during inspections is not available using the conventional inspection methodology.

Standard profiles/assessments performed during an SSR inspection with the TPDS are:

- Inbound/outbound coverage radials;
- Overhead cone checks;

- Coverage/performance Orbits; and
- Impulse assessments (side lobe suppression and main beam levels).

Inbound or outbound coverage radials where nulls in SSR signal strength or hit rate can now accurately be reported and assessed against specified tolerances. Refer Figure 9.

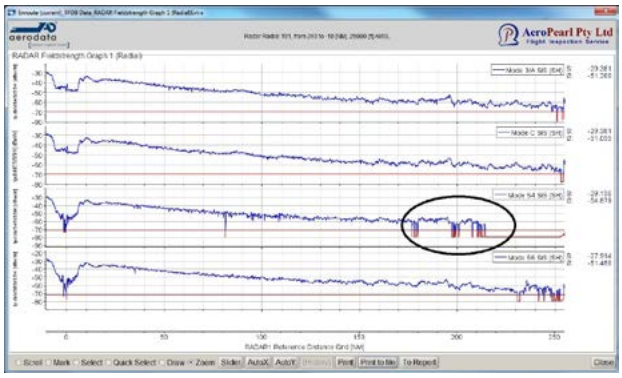

Figure 9 Coverage Assessment Graphic

Additionally, typical RF environmental effects, such as lobing, can now be visualized, Figure 10, along with Overhead cone checks where the performance can now be assessed in much more detail, Figure 11.

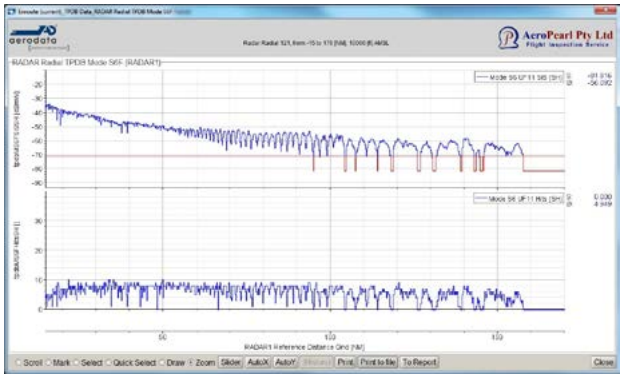

Figure 10 Coverage Radial with Lobing Effect

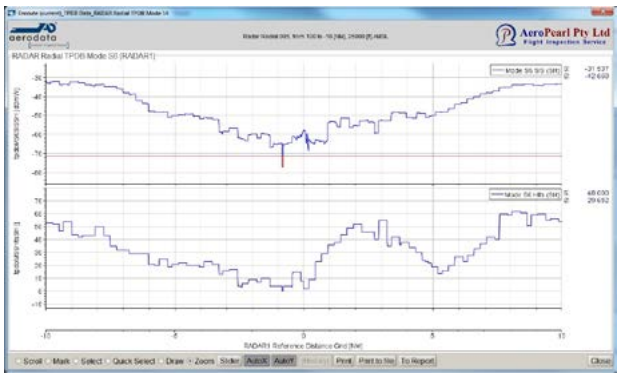

Figure 11 Overhead Cone Check

Areas with increased hit rate can also be identified during coverage radials or orbits and further investigations conducted if excessive interrogations are present. Refer Figure 12.

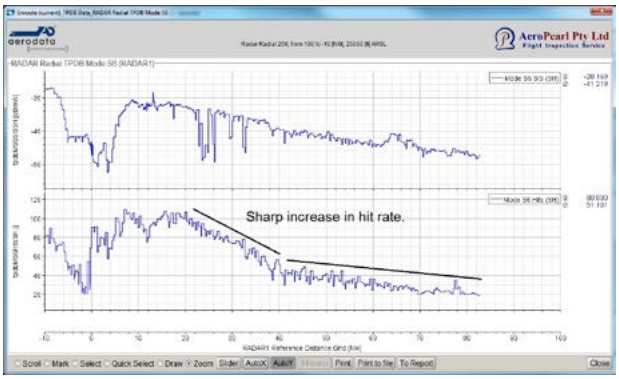

Figure 12 Increased Hit Rate - Possible Area of Concern

Orbits are generally flown around the SSR and the field strength of the SSR around the orbit assessed to identify any potential areas of concern, where coverage distance may be lower than expected. Radials may then be flown at the limit of coverage in these areas of concern.

During orbits the shape of the received SSR beam is assessed to observe the relationship between the side lobe suppression pulses and the main beam using the impulse graphic. Tolerances are applied against the side lobe suppression (P2) pulse using the impulse graphic which should be at least a certain level (6dB for example) below P1/P3 when in the main beam. Refer Figure 13.

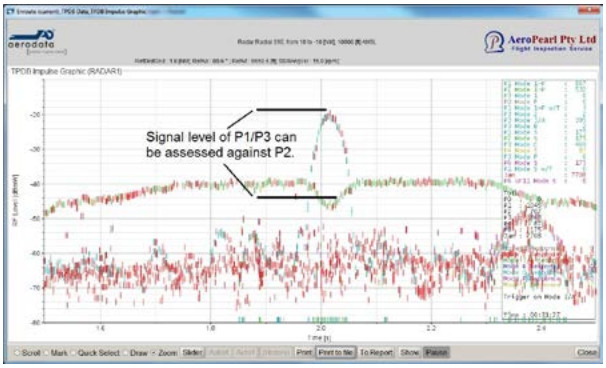

Figure 13 Assessment of Main Beam and SLS

CONCLUSIONS

The introduction of the TPDS to SSR inspections has provided the ability to measure and assess the SSR performance in much more detail than the binary (works or doesn't work) conventional inspection method. This additional information has allowed for more tailored flight inspections and greater transparency of SSR performance, while also allowing for signal assessments to be conducted in flight against the specified requirements [1], which are not being assessed using the conventional SSR inspection method.

FUTURE WORK

In the future, it is planned to reduce the size of the overall TPDS installation dramatically. One approach is to integrate the processing, which is now done in the TPDB, into the receive-only transponder itself. The decrease in size of FPGAs, ADCs and other electronic devices makes this easily possible.

Additionally, it is planned to add the possibility of fine tuning the tolerances for impulse-width and -spacings inside the TPDB (or better, the real-time processing unit) by setting and changing these values in the FIS software and apply them to the real-time processing unit on the fly.

It is also planned to increase the sample rate of the system in order to improve the system performance especially for Mode S chips.

Last but not least, customer requests are always welcomed and can always be incorporated into the system. Being a powerful but relatively new system, many things can surely be added to the overall functionality.

REFERENCES

[1] ICAO, July 2007, International Standards and Recommended Practices, Annex 10 to the Convention on International Civil Aviation, Volume IV, Surveillance an Collision Avoidance Systems, 4th Edition, http://www.icao.int

IFIS2016

Bringing Together Theory and Practice

Session 4

FIS and Aircraft Technology

A Multi-Constellation GNSS Based Position Reference for Flight Inspection

Claus-Sebastian Wilkens
R&D Engineer
Aerodata AG
Braunschweig, Germany
Phone: +49 531 2359-140
E-mail: wilkens@aerodata.de

ABSTRACT

The quality of flight inspection results is highly dependent on the integrity, reliability, and accuracy of the provided reference position solution. For this reason solutions from global navigation satellite systems (GNSS) like the US-American Global Positioning System (GPS) are commonly utilized.

Minimum accuracies of positioning subsystems for flight inspection are defined by ICAO Doc 8071 [5]. The calibration of category I-III instrument landing systems demands accuracies, which can only be provided by algorithms based on the phase measurement of GNSS. These are used by real time kinematic (RTK) or precise point positioning methods.

Although GPS currently has a constellation of more than 30 satellites (depending on location, time of day, and flight maneuvers) the availability of a suitable satellite constellation can still be an issue. The loss of an appropriate satellite reception would possibly lead to the interruption of a flight procedure, which would result in an economic impact in terms of costs and time delays. For this reason it is desirable to include additional GNSS like the Russian GLONASS or in the future the Chinese BeiDou or the European Galileo.

This paper describes the implementation of GLONASS measurements into an RTK module, which is used as a source for a flight inspection reference position. The theoretical considerations regarding the interoperability of GPS and GLONASS are presented. Furthermore, the implementation of the multi-constellation RTK algorithms is described. Finally, the GPS and GLONASS based reference position solution is validated using typical flight inspection procedures.

INTRODUCTION

The flight inspection (FI) of precision flight navigation aids like a category III (CAT III) instrument landing system (ILS) requires the use of a precise position reference system. [5] paragraph 4.3.100 requires the measurement uncertainty to be at least 5 times less than the tolerance of the measured parameter. [10] introduces a guideline for the minimum reference position accuracies for an ILS CAT III flight inspection, which is also used by the Federal Aviation Administration (FAA). Due to the angular nature of the ILS guidance system, minimum accuracies are given as angular values. Thus, for a CAT III ILS, the estimation error (95 %) should be less than 0.015° from the glide path (GP) and localizer (LOC) antennas down to 30 cm in vertical and 60 cm in horizontal direction.

GPS is commonly used as a position reference for flight inspection. Although currently (8 March 2016) 29 satellites (+1 in maintenance and +1 in commissioning phase) are available in orbit (see [16]), depending on location, time, and flight maneuvers, it can still be challenging to receive an adequate number of signals and a good satellite geometry. Thus, it is beneficial in terms of availability and geometry to add measurements from more global navigation satellite systems (GNSS) to the reference position solution. GPS can be complemented by the Russian GLONASS and possibly by future GNSS like the Chinese BeiDou and the European Galileo. Since GLONASS already provides a certified and complete satellite constellation, this paper deals with the implementation of its measurements.

In order to meet the earlier mentioned accuracy requirements, the GPS carrier phase measurement has to be utilized. Although the phase itself can be measured precisely, the estimation of the phase ambiguity requires sophisticated methods like real time kinematic (RTK) or precise point positioning (PPP). RTK methods like precise differential GPS (PDGPS) use a reference ground station receiver and antenna with known position. By double differencing the GNSS measurements from the ground station and the on-board user receiver, several error effects can be eliminated or at least reduced. As long as the distance between reference and user receiver does not increase too much, atmospheric effects from troposphere and ionosphere are comparable at both receiver locations. PPP uses no ground station, but additional corrections, like from commercial and proprietary services

as TerraStar or OmniSTAR in order to achieve an accurate measurement and to estimate the phase ambiguities.

The following chapters are going to deal with the implementation of GLONASS measurements into an existing GPS based RTK solution, which uses the Fast Ambiguity Search Filtering (FASF) [1] method for integer ambiguity resolution.

GLONASS

The Russian Global Navigation Satellite System GLONASS space segment currently (8 March 2016) consists of 22 operational satellites and additionally of 2 satellites in maintenance, 2 under check by the satellite prime contractor, 1 as a spare, and 1 in flight test phase – in total 28 satellites, see [2]. Like the legacy GPS, GLONASS satellites emit signals on the L1 and L2 frequency bands. In contrast to GPS, these signals are not transmitted using the same frequency in the code division multiple access (CDMA) method but use frequencies, which are distributed between the satellites in frequency division multiple access (FDMA). The currently ongoing GLONASS modernization is going to add additional CDMA signals and frequencies to the system. Since until now only one of the new GLONASS-K1 satellites is operational, this paper is going to concentrate on the legacy signals on L1 and L2 for both GLONASS and GPS. More detailed information on GNSS can be found in [4]. The interface control documents for GPS and GLONASS are available in [3] and in [12].

REAL TIME KINEMATIC

RTK uses the carrier phase ϕ in cycles in order to calculate an accurate position solution. The carrier phase range measurement Φ is the distance calculated from the multiplication with the wave length λ.

$$\begin{aligned}\Phi &= \lambda \cdot \phi \\ &= r + dr + c \cdot (dt - dT) + \lambda \cdot N - d_{ion} \\ &\quad + d_{trop} + \epsilon_{\Phi}\end{aligned} \tag{1}$$

The phase range can be modelled similar to [6] from the geometric range r, orbital errors dr, speed of light in vacuum c, satellite clock error dt, receiver clock error dT, carrier phase integer ambiguity in cycles N, ionospheric delay d_{ion}, tropospheric delay d_{trop}, and noise and multipath error ϵ_{Φ}.

Single Differencing

Two receivers of a reference ground station (index *r*) and an exemplary aircraft user (index *u*) share correlated errors, when receiving the same satellite (index *s*). As long as the distance between the receivers is not too large, for instance atmospheric errors are similar. Also, since both receivers use the same satellite signal, the satellite clock error should be the same at both. Thus, by differencing between the two measurements at the receivers, these errors can be reduced significantly. The between-receiver single difference (SD) is indicated by the Δ symbol in equation (1) and illustrated in Figure 1.

$$\Delta\Phi_s^{ru} = \Phi_s^u - \Phi_s^r = \lambda_s \cdot (\phi_s^u - \phi_s^r) \tag{2}$$

$$\begin{aligned}\Delta\Phi_i^{ru} &= \Delta r_s^{ru} + \Delta dr_s^{ru} + c \cdot (\Delta dt_s^{ru} - \Delta dT_s^{ru}) \\ &\quad + \lambda_s \cdot \Delta N_s^{ru} - \Delta d_{s,ion}^{ru} + \Delta d_{s,trop}^{ru} \\ &\quad + \Delta\epsilon_{s,\Phi}^{ru}\end{aligned} \tag{3}$$

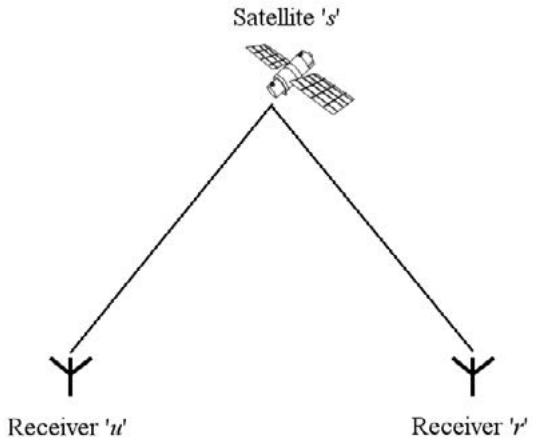

Figure 1. Between-receiver single difference

Similarly, it is possible to calculate between-satellite single differences, as depicted in Figure 2. Usually the difference is calculated from a base satellite (index *b*), which is located at the highest elevation, compared to the other received satellites. In this way, it is possible to remove the receiver clock offset, which is shared by both measurements from the same receiver *u*.

$$\Delta\Phi_{bs}^u = \Phi_s^u - \Phi_b^u = \lambda_{b/s} \cdot (\phi_s^u - \phi_b^u) \tag{4}$$

$$\begin{aligned}\Delta\Phi_{bs}^u &= \Delta r_{bs}^u + \Delta dr_{bs}^u + c \cdot (\Delta dt_{bs}^u - \Delta dT_{bs}^u) \\ &\quad + \lambda_{b/s} \cdot \Delta N_{bs}^u - \Delta d_{bs,ion}^u + \Delta d_{bs,trop}^u \\ &\quad + \Delta\epsilon_{bs,\Phi}^u\end{aligned} \tag{5}$$

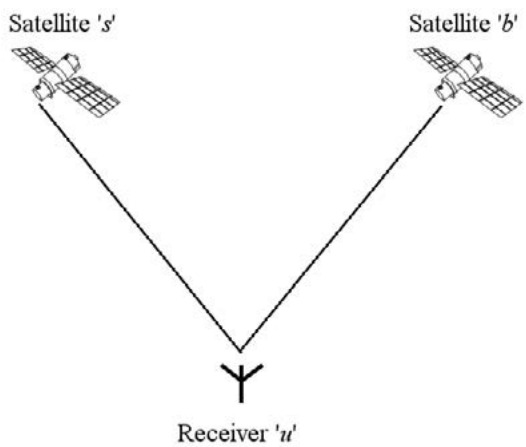

Figure 2. Between-satellite single difference

For now it is assumed, that both satellite measurements use the same wave length $\lambda_{b/s} = \lambda_b = \lambda_s$. This assumption is correct for e.g. GPS, but not for GLONASS.

Double Differencing

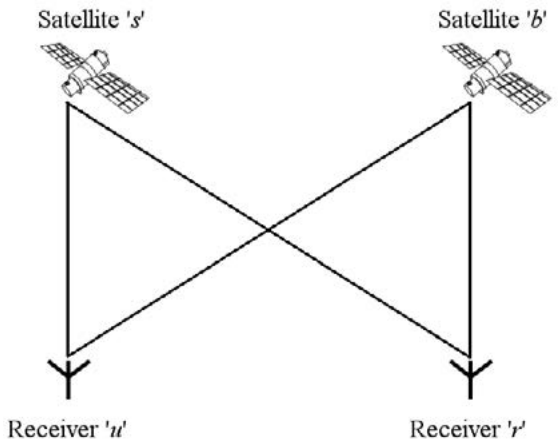

Figure 3. Double difference

In order to benefit from both single differencing methods, the double differences (DD) are introduced, as in Figure 3. For this, the single differences of two receivers or two satellites are differenced. Double differences are indicated by the $\nabla\Delta$ symbols.

$$\nabla\Delta\Phi_{bs}^{ru} = \Delta\Phi_s^{ru} - \Delta\Phi_b^{ru} = \Delta\Phi_{bs}^{u} - \Delta\Phi_{bs}^{r} \tag{6}$$

$$\begin{aligned}\nabla\Delta\Phi_{bs}^{ru} = {} & \nabla\Delta r_{bs}^{ru} + \nabla\Delta dr_{bs}^{ru} + c \\ & \cdot (\nabla\Delta dt_{bs}^{ru} - \nabla\Delta dT_{bs}^{ru}) + \lambda_{b/s} \cdot \nabla\Delta N_{bs}^{ru} \\ & - \nabla\Delta d_{bs,ion}^{ru} + \nabla\Delta d_{bs,trop}^{ru} + \nabla\Delta\epsilon_{bs,\Phi}^{ru}\end{aligned} \tag{7}$$

Thanks to the between-receiver single differencing, the satellite clock error SD Δdt_b^{ru} and Δdt_s^{ru} can be neglected. Similarly the between-satellite single differencing allows neglecting the SD receiver clock errors ΔdT_{bs}^{u} and ΔdT_{bs}^{r}. Thus, the resulting double differences $\nabla\Delta dt_{bs}^{ru}$ and $\nabla\Delta dT_{bs}^{ru}$ can be neglected as well. As long as the baseline between reference and user receiver is not too long, ionospheric and tropospheric errors can be assumed to be similar. Thus, by single differencing between the two receivers, the errors can be reduced significantly. For this reason, the associated DD delays are summarized with the DD noise and multipath error $\nabla\Delta\epsilon_{bs,\Phi}^{ru}$ and the DD orbital errors $\nabla\Delta d\rho_{bs}^{ru}$ to a common DD phase range error $\nabla\Delta\bar{\epsilon}_{bs,\Phi}^{ru}$. The mentioned assumptions lead to a simplified equation for the double differenced phase range.

$$\nabla\Delta\Phi_{bs}^{ru} = \nabla\Delta r_{bs}^{ru} + \lambda_{b/s} \cdot \nabla\Delta N_{bs}^{ru} + \nabla\Delta\bar{\epsilon}_{bs,\Phi}^{ru} \tag{8}$$

In order to calculate a position solution from this equation, the double difference phase integer ambiguity $\nabla\Delta N_{bs}^{ru}$ has to be estimated. This can be achieved by methods like FASF [1] or Least-Squares Ambiguity Decorrelation Adjustment (LAMBDA) [14]. More information on differencing in GNSS can be found in [9].

RTK with GLONASS

As mentioned earlier, GLONASS satellites operate on different frequencies and wave lengths $\lambda_b \neq \lambda_s$. Thus, the earlier introduced simplification of equal wave lengths for both satellites *b* and *s* of between-satellite single differences or double differences is no longer valid for multi-constellation GNSS RTK with GLONASS. This is considered by introducing the different wave lengths into equation (8).

$$\begin{aligned}\nabla\Delta\Phi_{bs}^{ru} = {} & \nabla\Delta r_{bs}^{ru} + \lambda_s \cdot \Delta N_s^{ru} - \lambda_b \cdot \Delta N_b^{ru} \\ & + \nabla\Delta\bar{\epsilon}_{bs,\Phi}^{ru}\end{aligned} \tag{9}$$

Several approaches have been developed in order to compensate for the different wave lengths. [7] proposes the introduction of a mean GLONASS frequency and scaling of the carrier phase observations to it. Unfortunately, the scaling leads to the loss of the integer nature of the phase ambiguities. [11] proposes to keep the integer nature by introducing an auxiliary wave length, of which the used wave lengths are multiples. The drawback of this method is, that due to the resulting very small wave lengths, the resolution of the integer ambiguities is challenging. A short summary of these methods is given by e.g. [18].

[17] introduces a lumped parameter $\nabla\Delta\bar{N}_{bs}^{ru}$ in order to convert equation (9) back to a type similar to equation (8).

$$\nabla\Delta\Phi_{bs}^{ru} = \nabla\Delta r_{bs}^{ru} + \nabla\Delta\bar{N}_{bs}^{ru} + \nabla\Delta\bar{\epsilon}_{bs,\Phi}^{ru} \tag{10}$$

This non-integer parameter incorporates the double difference integer ambiguity and its wave length. In order to compensate for the different signal wave lengths, the base satellite single difference ambiguity is added.

$$\nabla\Delta\bar{N}_{bs}^{ru} = \lambda_s \cdot \nabla\Delta N_{bs}^{ru} + (\lambda_b - \lambda_s) \cdot \Delta N_b^{ru} \tag{11}$$

It can be seen, that for GPS, where $\lambda_b = \lambda_s$, inserting equation (11) into equation (10) would lead to equation (8). A simple approximation for the SD ambiguity is the difference between the SD pseudo range $\Delta\rho_b^{ru}$ divided by the wave length and the SD phase measurement $\Delta\phi_b^{ru}$ (in cycles).

$$\Delta N_b^{ru} = \frac{\Delta\rho_b^{ru}}{\lambda_b} - \Delta\phi_b^{ru} \tag{12}$$

Obviously, this approach is highly dependent on the accuracy of the measured pseudo ranges. Thus, it has to be ensured, that methods for the accurate estimation of the SD ambiguity are used, cf. [8].

Inter-frequency Bias

[13] states, that the hardware and signal processing architecture of a GNSS receiver can introduce frequency-dependent biases in the pseudo range and carrier phase measurements. Since the GLONASS satellites emit the signals on different frequencies, these biases are not can-

celled out by double differencing. Fortunately, the frequency dependent biases are similar for receivers of the same hardware brand and type. Since flight inspection systems (FIS) mostly use the same receiver type in the FIS on board the aircraft and in the DGNSS ground reference station, these biases can be neglected for the presented methods. More details on GLONASS inter frequency biases are given in [13].

EXPERIMENTAL VERIFICATION

In order to evaluate the performance of the presented multi-constellation RTK algorithms, different experiments have been conducted. The general functionality of the presented methods is verified by a short baseline static test. The applicability in flight is then shown using actual flight data. Both experiments have been conducted using two Aerodata AD-GNSS-0100 receivers, which are based on the NovAtel OEM628 GNSS receiver's electronics enclosed in a ruggedized housing for application inside an aircraft and/or flight inspection system. GNSS satellites with an elevation of less than 7.5° have been excluded from the solution.

The following results only describe navigation solutions from the RTK algorithms. Short RTK outages due to e.g. check sum errors are not taken into consideration and excluded from the analysis.

Static Experiment

The static experiment has been conducted with a short baseline of 5.8 m between the two antennas. Both antenna positions had been surveyed earlier for use as a reference during the experiment. The experiment data has been recorded at the Aerodata facilities in Braunschweig, Germany on 25th August 2015 between 14:32 and 17:16 UTC.

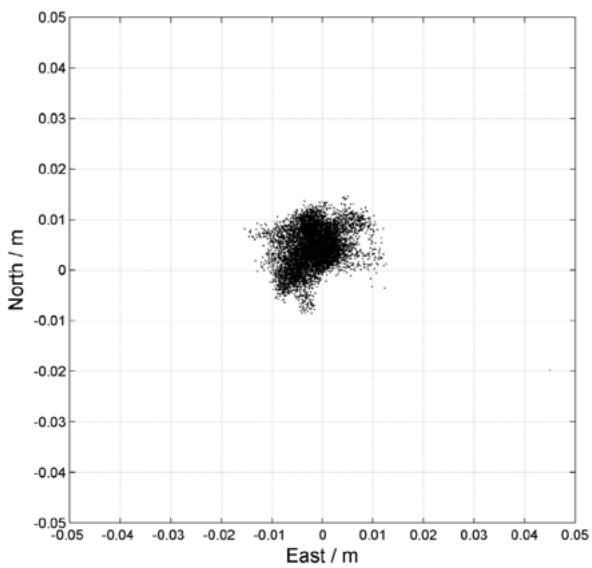

Figure 4. Horizontal deviation from reference of the static experiment

Horizontal accuracy and precision of the static RTK position solution are best seen in Figure 4. Additionally, Figure 6 shows the North, East, Up, and 3D deviations from the surveyed reference position versus time since the start of the measurements. The statistics of the experiment in terms of mean and 95 % deviation from the reference are summarized in Table 1.

Table 1. Accuracy of the static experiment

	Mean deviation	95 % deviation
North	0.4 cm	0.7 cm
East	0.2 cm	0.8 cm
Up	0.2 cm	1.8 cm
3D	1.1 cm	1.0 cm

The results show an accuracy in the range of the actual survey accuracy of the reference position. Furthermore, it can be seen, that the earlier mentioned minimum accuracies for a flight inspection position reference are easily matched.

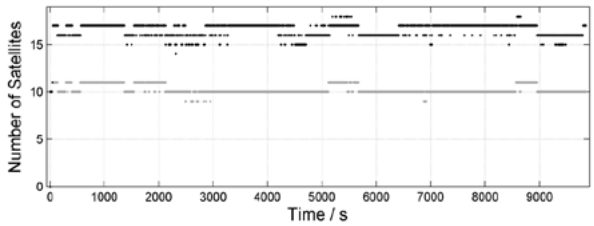

Figure 5. Number of received satellites during the static experiment (gray: GPS, black: GPS+GLONASS)

Figure 5 shows the number of received GPS and combined GPS and GLONASS satellites during the experiment. Most of the time, at least 15 satellites have been available for use in the position solution. This nicely depicts the main advantage of multi constellation satellite navigation – the significant increase in availability.

Flight Experiment

In order to show the applicability of the proposed algorithms in flight inspection, a flight experiment has been conducted in the vicinity of the Research Airport Braunschweig (EDVE / BWE) on 2nd March 2015 between 8:09 and 9:40 UTC. During this experiment, typical FI maneuvers have been flown in terms of four partial orbits and three approaches to runway 26 of Braunschweig airport. The horizontal flight trajectory is shown in Figure 8 in Cartesian coordinates originating at the position of the DGNSS ground station antenna. Additionally, Figure 9 shows the horizontal distance of the aircraft user receiver's antenna to the ground station reference receiver's antenna. It can be seen, that during

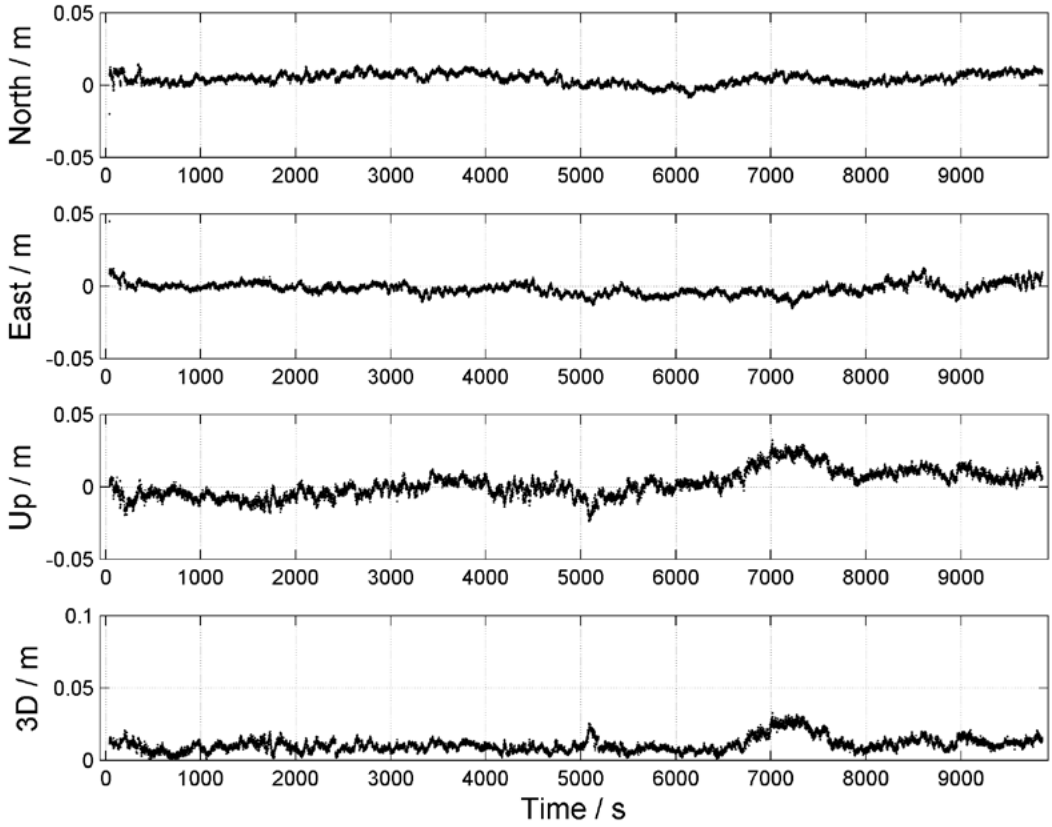

Figure 6. Deviation from reference of the static experiment

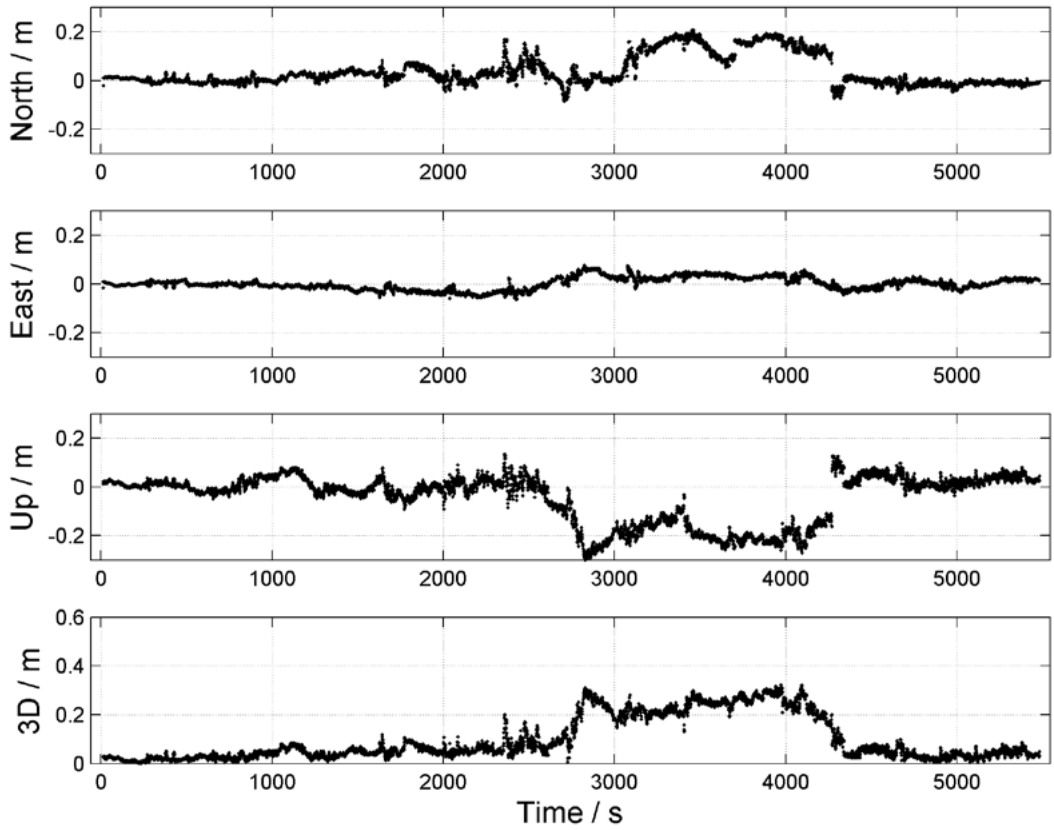

Figure 7. Deviation from reference of the flight experiment

the partial orbits, baselines of 45 to 50 km have been achieved. The maximum baseline for reliable ambiguity fixing is regarded as 10-20 km, see [19].

For the static experiment an earlier precisely surveyed location can be used as a reference. In contrast, the selection of a reference for a flight experiment with estimated measurement accuracies in the area of centi- or decimeters is somewhat challenging. For the presented experiment, a GPS/GLONASS RTK solution calculated by NovAtel's Waypoint GrafNav version 8.60 aided by precise clock and ephemeris corrections is used.

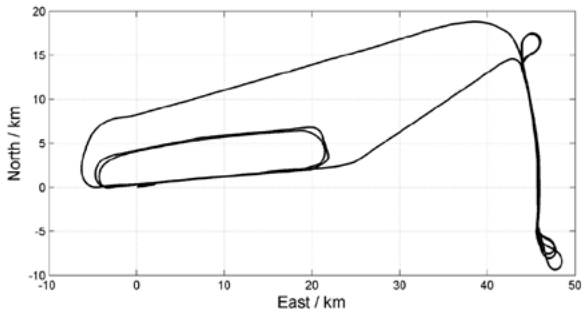

Figure 8. Cartesian horizontal flight path of the flight experiment

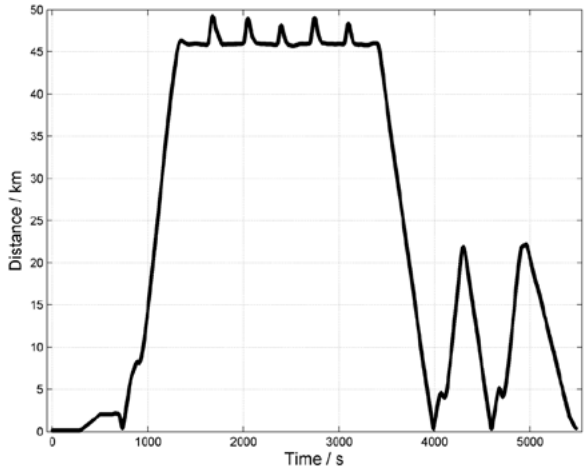

Figure 9. Horizontal distance from the DGNSS ground station

As stated earlier, equation (12) is highly dependent on the accuracy of the SD pseudo range for the ambiguity resolution of GLONASS measurements. In order to increase the accuracy of this process, in the beginning of the RTK calculations, GLONASS ambiguities are only estimated, when a GPS RTK solution has been calculated before.

The achieved accuracies in terms of North, East, Up, and 3D deviations of the presented RTK solution from the reference are shown in Figure 7 versus time since the start of the measurements. The results are summarized in Table 2. It can be seen, that the earlier defined minimum accuracies for a FI position reference system are met. Even the 95 % 3D deviations from the reference meet the minimum vertical accuracy of 30 cm.

It has to be kept in mind, that the reference is also RTK based. Thus, although precise ephemeris and clock corrections are used, the position errors increase with increasing distance from the reference ground station.

Table 2. Accuracy of the flight experiment

	Mean deviation	95 % deviation
North	3.7 cm	12.3 cm
East	0.1 cm	5.0 cm
Up	4.7 cm	19.3 cm
3D	9.8 cm	17.9 cm

The effect of a degrading accuracy with increasing distance from ground reference can be seen in the time series in Figure 7. From a time of 2500 s the shown deviations increase visibly, while the baseline between user and reference antenna is more than 45 km. In the beginning of the long baseline segment of the flight (starting at about 1200 s) the originally fixed integer ambiguities are kept, thus keeping the accuracies at a good level. With a changing satellite constellation and adding and removing of satellites to the solution, the limitations of the long baseline become visible. The reverse effect can be observed after a time of 4000 s, when the baseline decreases significantly during the approaches.

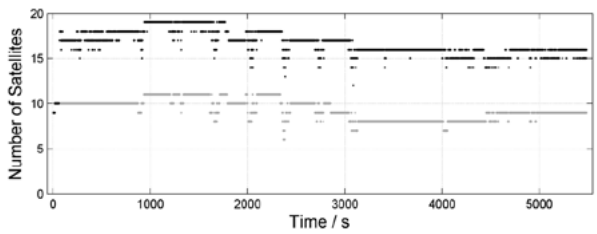

Figure 10. Number of received satellites during the flight experiment (gray: GPS, black: GPS+GLONASS)

One of the main benefits of increased availability due to a high number of received satellites can be observed in Figure 10. Similar to the static test, most of the time, more than 15 navigation satellites can be received. The visible short drops in the number of received satellites happen due to bank angles of partly more than 30° during turn maneuvers – especially at the end of the partial orbits. During these turns, the reception of a couple of low elevation satellites is interrupted by the aircraft fuselage. The number of received GPS satellites drops down to 6. This can become close to unfavorable for RTK solutions with integrity algorithms, since these use the redundancy of measurements. The location of the turns can be easily identified in Figure 8 from the spikes in the long baseline segments of the flight.

CONCLUSIONS

Based on the described experimental results and in comparison with the earlier defined minimum accuracies, it

is shown, that a GPS and GLONASS based multi-constellation RTK solution can be used as a position reference in flight inspection. The benefit of the increased satellite availability can be seen especially during bank maneuvers between the flown FI procedures of the flight experiment. Although a couple of satellites are masked from reception, the RTK solution can still be maintained.

FUTURE WORK

The presented experiments show the general applicability of the proposed multi-constellation RTK solution. Future work is going to deal with an improvement of the robustness and integrity of the of the RTK methods.

Although the experiments already give a good idea on the performance of the algorithms, these are of course not sufficient for a validation of a flight inspection position reference system. Thus, a detailed verification and validation process is going to follow the development and improvement of the multi-constellation RTK position reference.

ACKNOWLEDGMENTS

The author wishes to thank his colleague Mr. Patrick Thomsen for his contribution to the work on multi constellation GNSS during his diploma thesis [15] and for many fruitful discussions on the topic. In addition, the author wishes to thank the FCS Flight Calibration Services GmbH and Mr. Markus Schwendener in particular for the possibility of recording the presented experimental flight data during one of their test flights.

REFERENCES

[1] D. Chen, December 1994, Development of a Fast Ambiguity Search Filtering (FASF) Method for GPS Carrier Phase Ambiguity Resolution, Ph.D. Dissertation, Department of Geomatics Engineering, University of Calgary, Canada, UCGE Report Number 20071.

[2] Federal Space Agency Information-Analytical Centre, 8 March 2016, GLONASS constellation status, https://www.glonass-iac.ru/en/GLONASS/

[3] Global Positioning Systems Directorate Systems Engineering & Integration, 24 September 2013, Interface Specification, IS-GPS-200H, Navstar GPS Space Segment/Navigation User Interface.

[4] B. Hofmann-Wellenhof, H. Lichtenegger, E. Wasle, 2008, GNSS Global Navigation Satellite Systems: GPS, GLONASS, Galileo & more, Springer Wien, ISBN 978-3211730126.

[5] ICAO, 31 October 2002, Manual on Testing of Radio Navigation Aids, Doc 8071, Volume I, Testing of Ground-Based Radio Navigation Aids, 4th Edition with Amendment 1.

[6] A. Leick, 1995, GPS Satellite Surveying, Second Edition, John Wiley & Sons, Inc., ISBN 978-0471306269.

[7] A. Leick, L. Li, J. Beser, G. Mader, 1995, Processing GLONASS Carrier Phase Observations – Theory and First Experience, Proceedings of the 8th International Technical Meeting of the Satellite Division of the Institute of Navigation (ION GPS 1995), Palm Springs, CA, USA, pp. 1041-1047.

[8] R. B. Ong, M. G. Petovello, G. Lachapelle, 2009, Assessment of GPS/GLONASS RTK Under Various Operational Conditions, Proceedings of the 22nd International Technical Meeting of The Satellite Division of the Institute of Navigation (ION GNSS 2009), Savannah, GA, USA, pp. 3297-3308

[9] M. G. Petovello, 2011, The differences in differencing, Inside GNSS, Vol. 6, No. 5, pp. 28-32.

[10] J. D. Powell, T. Walter, E. Kim, U. Peled, December 2007, Use of the Wide Area Augmentation System (WAAS) as a Reference for Flight Inspection, Final Report, FAA Contract AC-05-00695.

[11] U. Rossbach, 2000, GLONASS Double Difference Ambiguity Resolution in Real-Time, Proceedings of the 13th International Technical Meeting of the Satellite Division of the Institute of Navigation (ION GPS 2000), Salt Lake City, UT, USA, pp. 163-171.

[12] Russian Institute of Space Device Engineering, 2008, Global Navigation Satellite System GLONASS, Interface Control Document – Navigational Radiosignal in Bands L1, L2, Version 5.1.

[13] F. Takac, 2009, GLONASS inter-frequency biases and ambiguity resolution, Inside GNSS, Vol. 2, No. 4, pp 24-28.

[14] P. J. G. Teunissen, 1995, The least-squared ambiguity decorrelation adjustment: a method for fast GPS integer ambiguity estimation, Journal of Geodesy, No. 70, Springer Verlag, pp. 65-82.

[15] P. Thomsen, March 2015, Multi-GNSS-Satellitennavigation mittels GPS und Galileo, Diploma Thesis, Technische Universität Braunschweig, Germany.

[16] U.S. Department of Homeland Security - United States Coast Guard Navigation Center, 8 March 2016, GPS constellation status for 03/08/2016, http://www.navcen.uscg.gov/?Do=constellationstatus

[17] J. Wang, 2000, An approach to GLONASS ambiguity resolution, Journal of Geodesy, No. 74, Springer-Verlag, pp. 421-430.

[18] J. Wang, C. Rizos, M. P. Stewart, A. Leick, July 2001, GPS and GLONASS Integration: Modelling and Ambiguity Resolution Issues, GPS Solutions, Vol. 5, Issue 1, pp. 55-64.

[19] L. Wanninger, 16 June 2008, Introduction to Network RTK, International Association of Geodesy Working Group 4.5.1: Network RTK, http://www.wasoft.de/e/iagwg451/intro/introduction.html

ATC-Systems and Wind-Turbines: Status of Numerical Simulations and Flight Measurements - Evaluation and Systematic Results of Examples

Gerhard Greving
NAVCOM Consult
Ziegelstr. 43, 71672 Marbach, Germany
Fax: +49 7144 862561
E-mail: navcom.consult@t-online.de

L. Nelson Spohnheimer
Spohnheimer Consulting
Auburn, WA 98001, USA
Fax: +1 508 526 8273
E-mail: Nelson@SpohnheimerConsulting.com

ABSTRACT

Wind turbines WTs are installed in increasing numbers. Often these are planned close to navigation and surveillance systems. This is in particular for the CVOR/DVOR-systems installed mostly in the country-side. The threatening expectations at the beginning of their appearance especially for the rotating blades are solved by available 3D numerical methodology, increasing theoretical and numerical knowhow and the increasing experience. The authors have published quite a number of papers on that subject also on the last IFIS-conferences. The WTs are neither a mystery nor a subject internationally of research any longer due to the well-founded, available knowhow.

This paper reports on the latest numerical 3D-methodology and theoretical-numerical results for the CVOR/DVOR and the related flight check measurements.

A special emphasis of this paper is on the increasing large number of WTs and the critical issue of the distance to the CVOR/DVOR.

Statistical results for large and numerous WTs are explained and shown which are the basis of the latest update of the ICAO EUR DOC015 document where the maximum ***check*** radius has been reduced for DVOR from a radius of 15km down to 10km. By the statistical evaluation it is shown that the assumption that flight-check measurements would not "catch the worst case" due to the wind direction and rotor blade position, cannot be supported anymore in a relevant way.

It will be even shown and explained that for very large windfarms the wind-direction and the rotor orientation is almost irrelevant for the DVOR due to the averaging complex field superposition effects of many scatterers combined with the system behavior.

The simulated resulting statistical bearing errors are discussed in relation to the applicable ICAO-specifications (Annex 10, DOC8071), in particular for the composition and decomposition of the error components according to the rss-scheme.

INTRODUCTION

The numerical analysis of the effects of Wind turbines on radio based systems has been performed since around year 2000. The first paper of the authors on a major wind-farm has been published on the IFIS 2004 for the VOR-systems and the ATC-radar. The basic simulation principles have not changed since then in a relevant way. By the availability of more powerful computers, the systematic analysis of larger and larger turbines and larger windfarms is possible. More parameter variations can be evaluated, such as studying the asymptotic effects of the wind-direction and the rotor position for large windfarms for the different systems, mainly for

- CVOR/DVOR
- ATC-radar (ASR, MSSR)
- etc.

This paper deals mainly with the cumulative effects of large windfarms on the VOR-system. A new signal processing methodology has been developed for

extremely close objects being in the mutual near field some years ago.

SIMULATION METHODOLOGY; VOR-SYSTEM

The "bearing error" of a VOR is defined by ICAO Annex 10 as to be derived by the VOR-receiver from the "signal in space" (**Fig. 1**). Receiver specifics are not included in the ICAO-specifications.

The simulations consist of 3 major steps (**Fig. 2**):

1. The modelling of the systems and the object
2. The scattering analysis by adequate standardized methodology
3. The system related signal processing

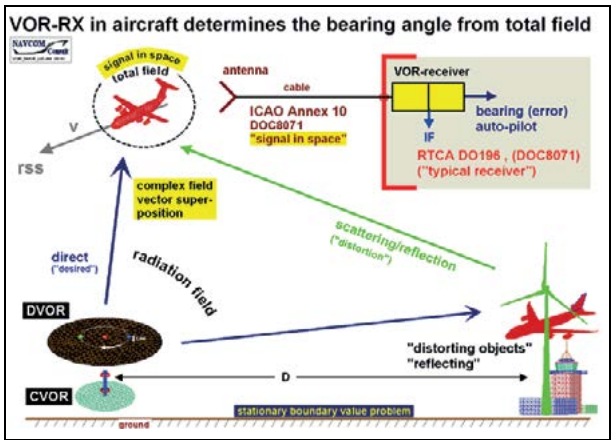

Fig. 1: System and simulation scenario for a CVOR/DVOR

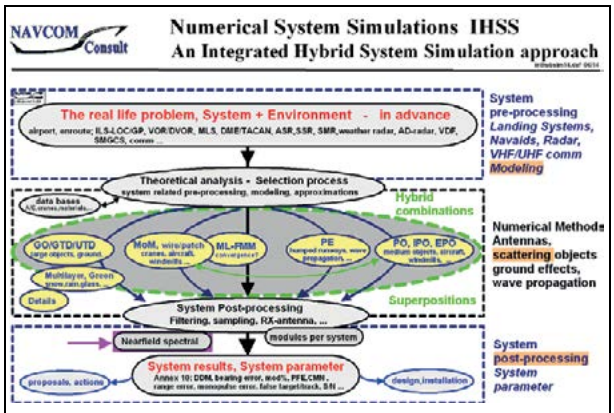

Fig. 2: Signal flow chart of a numerical 3D-simulation in some detail

The modeling and scattering analysis have to be adapted to the wide variety of types and size of the objects – some of which are shown in **Fig. 3** and **Fig. 4** for 3 different very large wind-turbines. The scattering analysis follows the well-established and sufficiently proven simulation and numerical analysis techniques in electro-dynamics which must be applied with the adequate knowhow; but which shall not be reiterated here.

The VOR-system is evaluated on the field-level (**Fig. 1**, **Fig. 2**) which takes into account implicitly the full 3D-scattering of the objects and the terrain as appropriate.

The "system-curves" (**Fig. 5**) are known since the 50th last century. The principle theoretical basics of the CVOR and DVOR are safely and sufficiently known since that time. More than 50 years of extensive operational experience and continuously improved measurement experience are well-known. The improvement of a DVOR compared to a CVOR and related specifics are well-known as well and have been proven many times. However, the "system curves" cannot be used directly for the superposition of the bearing errors of each object, e.g. each WT. The DVOR system curve purpose was just to show the improvement of a DVOR under certain idealized non-operational conditions. The main fundamental errors often made when superposing the "system curves" are

- use of envelope functions
- use of scalar parameters without RF-phases
- use of "scalar omnidirectional scattering patterns" - the scattering of the fields from the objects are in reality 3D and are complex vector quantities use independent of the distance and of the essential point in space (azimuth, elevation).

The large error made when applying scalar-only results is shown schematically in **Fig. 6**. This schematic also explains why in case of many objects the bearing error does not increase linearly with the number of objects.

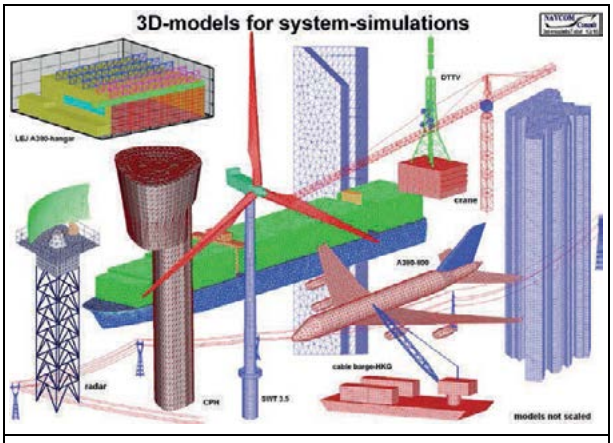

Fig. 3: Examples of modelled 3D-objects for different CNS-systems

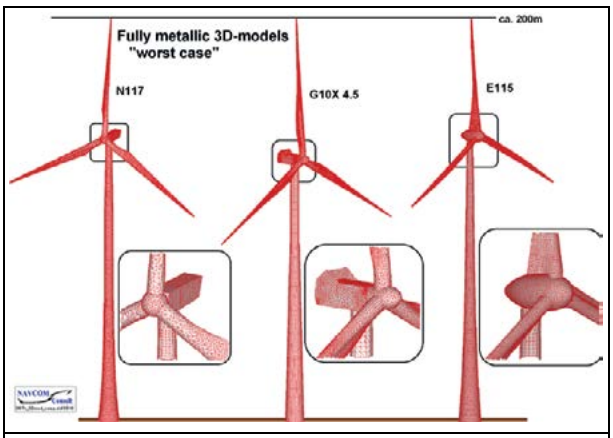

Fig. 4: Three different 3D-models of very large fully metallic wind-turbines (200m class)

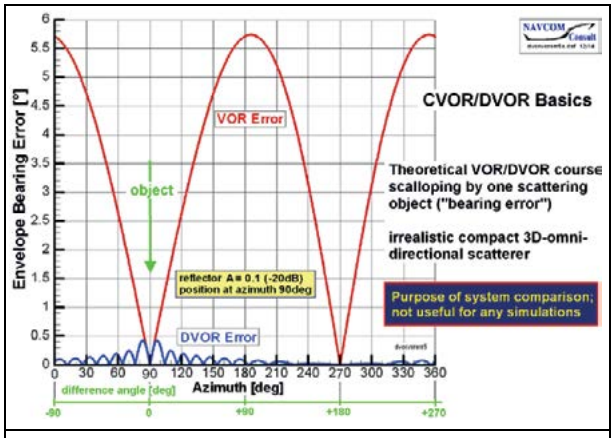

Fig. 5: The well-known basic system behavior of the CVOR/DVOR-system

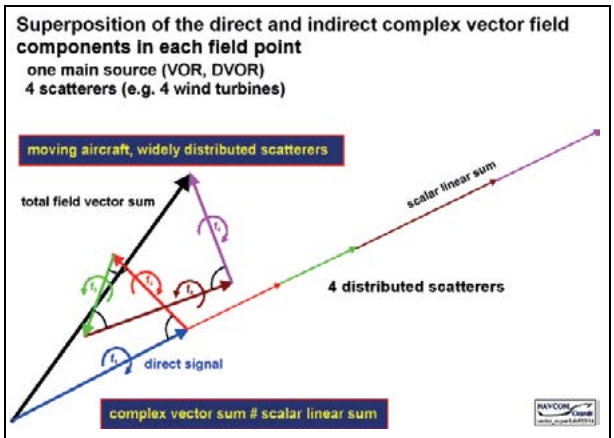

Fig. 6: The complex superposition of field components versus an unphysical linear scalar superposition

RESULTS

Systematic Numerical Results

The following numerical results will show:

- For a **small windfarm**, the potential effects of the different positions of the metallically assumed rotors of 6 large WTs at a minimum distance of 3km. 100 statistical cases for random rotor positions and for one nominal wind direction (±5° random around the nominal direction) are numerically evaluated (**Fig. 7**, **Fig. 8**). It can be seen that the maximum peak error in the defined sector up to 40nm, at 3000ft height varies by about ±15% only while the maxima per case are very rare. For the operationally more relevant lower occurances the spread is smaller. Practically this result means that the service provider and flight inspector do not have to account for potential large undetected bearing errors.

- For a **medium large windfarm** of 16 WTs (**Fig. 9**), 16 wind directions and 100 statistical trials each are evaluated on a partial orbit of 71°. The distance of the windfarm is around 10km to the DVOR. This result served as a basis for the reduction of the check-radius in ICAO DOC015 from 15km to 10km. The bearing errors have been evaluated for the fully metallic 3D-case (**Fig. 10**) the case of the lightning arrestor instead of a full rotor (**Fig. 11**), and for the case of the mast and hub only (**Fig. 12**). As expected the bearing errors are clearly reduced for the case of the lightning arrestor.

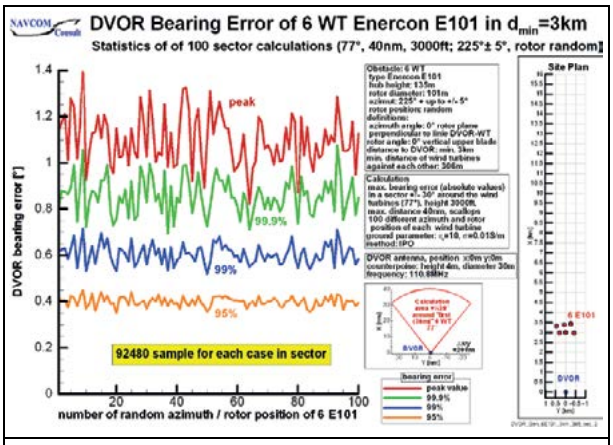

Fig. 7: DVOR bearing error; Small wind farms of 6 large WTs close to a DVOR ; 100 statistical trials for rotor positions

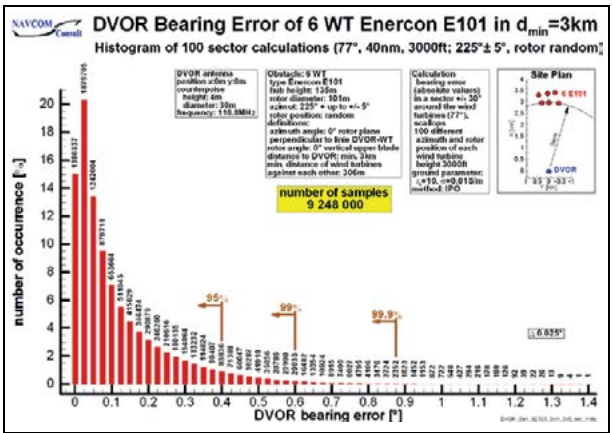

Fig. 8: Histogram statistics of all the results in **Fig. 7**

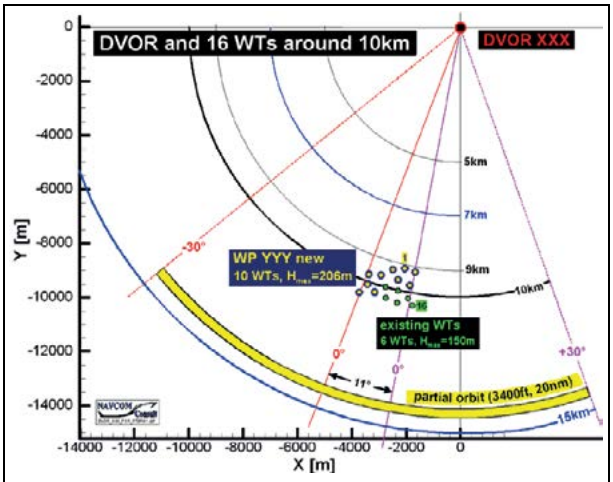

Fig. 9: Layout of medium sized wind farm of 10+6 large WTs in a distance of about 10km

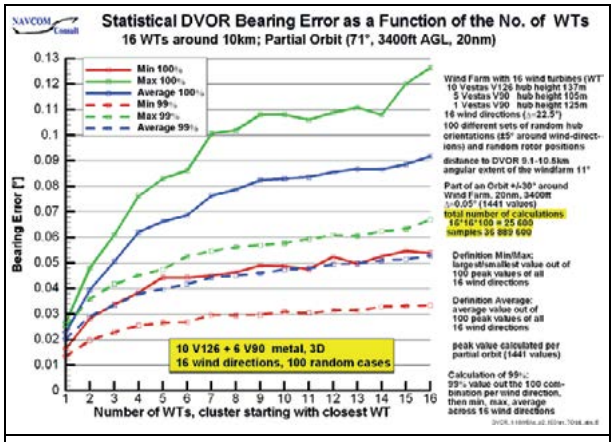

Fig. 10: DVOR bearing error of wind-farm (**Fig. 9**) for up to 16 WTs; 16 wind directions and 100 statistical trials

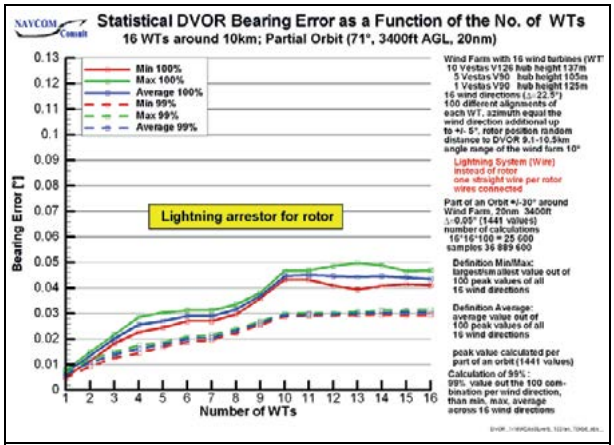

Fig. 11: DVOR bearing error of wind-farm (**Fig. 9**); Lightning arrestor instead of a fully metallic blade

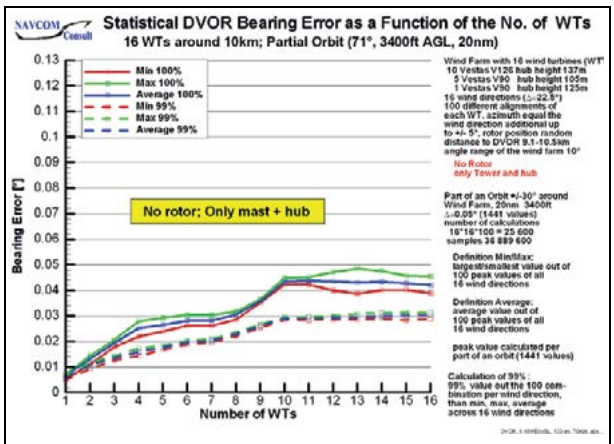

Fig. 12: DVOR bearing error of wind-farm (**Fig. 9**); only mast and hub

It can be clearly seen that the bearing error of larger windfarms does not increase linearly with the number of WTs, but shows some asymptotic behavior. Secondly the fully metallic WT and the rotor is an exaggerated worst-case model because the rotor blades mostly consist of dielectric glas-fibre material and an integrated metallic lightning arrestor. By all that, for larger numbers of large WTs the superposed resulting bearing error is represented more and more first by the metallic lightning arrestor and by the mast and hub sufficiently well – i.e. the additional rotor effects are small. Finally it can be seen that the bearing error is very small (<<0.5°) at the distance of 10km and can never be seen by the flight-inspection measurement and consequently does not harm the navigating user-aircraft at all.

- For a **large windfarm** of 49 large WTs (d_{min}=3km only) the bearing error is simulated on a partial orbit (93.4°; 20nm, 3000ft) and statistically evaluated by 100 random trial cases for the rotor positions for each of the considered 8 nominal wind directions. In total, 73,264,800 field samples have been calculated and evaluated. One can see the increasingly slower increasing effect for increasing number of WTs (**Fig. 13**).

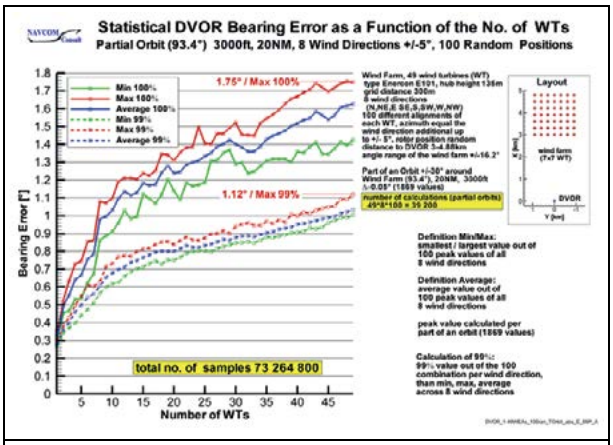

Fig. 13: DVOR bearing error of a large wind-farm for up to 49 WTs; 8 wind directions and 100 statistical trials each

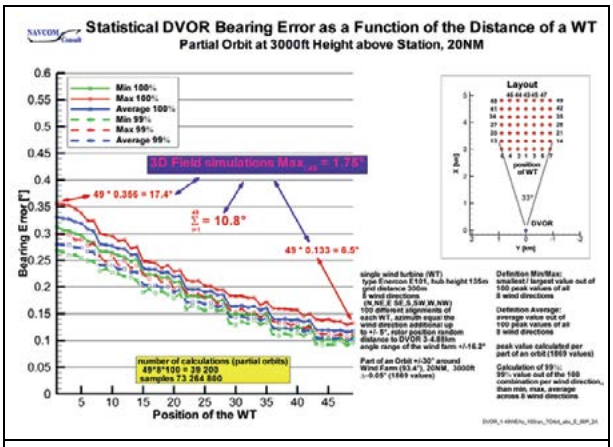

Fig. 14: DVOR bearing error of a large wind-farm each of the 49 WTs; 8 wind directions and 100 statistical trials

In **Fig. 14** the related contributing statistical bearing errors are shown for each of the 49 WTs of different distance. Finally it can be clearly seen the maximum detected extremely rare bearing error of 1.75° (**Fig. 13**) is very much smaller than the summed up (or multiplied) bearing error of all the 49 WTs when scalar addition is inappropriately used (10.5° analog **Fig. 5**; 17.4° for the closest WT and largest error, 6.5° for the

most distance and smallest error). Another use of the DVOR compared to the analyzed conditions (e.g. at much lower height for landing purposes) may change the outcome

- Finally, for a **very large windfarm** of 81 large WTs (d_{min}= 3km; compact cluster), the bearing is calculated on full orbits (10-40nm, 4000ft) - initially for 1 wind direction in **Fig. 15**. The bearing error is confined around the direction of the windfarm which can be deduced qualitatively from the DVOR-system curve in **Fig. 5** (unlike for a CVOR). This is in principle a well-known fact, but it has relevant consequences for increasing number of windfarms and WTs in the vicinity of a DVOR. The very rare maximum peak bearing error is about 1.9° (**Fig. 16**), for a more operationally realistic 99% occurance the max bearing error is ca.1° only.

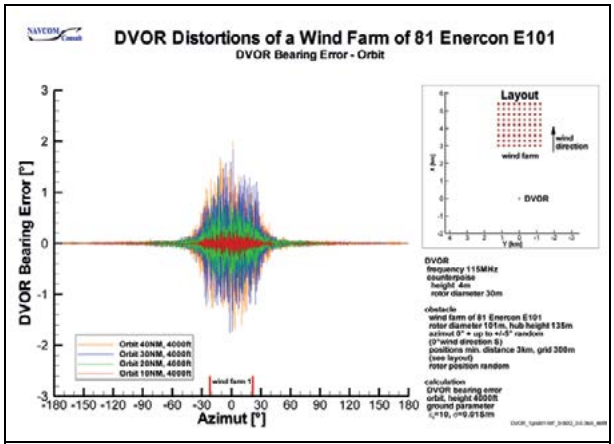

Fig. 15: Bearing error; large wind-farm for 81 WTs; 3km min; orbit 10-40nm, 4000ft; 1 wind direction, rotor random

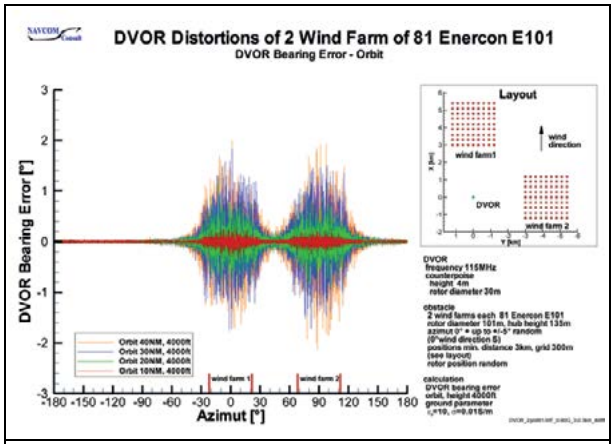

Fig. 16: Bearing error; large wind-farm for 2*81 WTs; 3km min; orbit 10-40nm, 4000ft; 1 wind direction, rotor random

A 2nd identical windfarm is added to the east (**Fig. 16**). It can be clearly seen (as expected on the basis of **Fig. 5**) that the bearing errors of both windfarms of 162 WTs are decoupled and the maximum bearing error does not increase in a relevant way (**Fig. 16**). If the wind direction changes (4 sample directions and 1 windfarm **Fig. 17** and both windfarms and 4 wind-directions **Fig. 18**) the very rare maximum bearing error does not change significantly.

As an overall consequence the result is that another 2 windfarms of 81 WTs could be added, i.e. 324 WTs in total at a minimum distance of 3km, and no significantly increased maximum bearing error would have to be expected. It is reminded that no filtering (bend, scallop) and no 95%-statistics have been applied to these results.

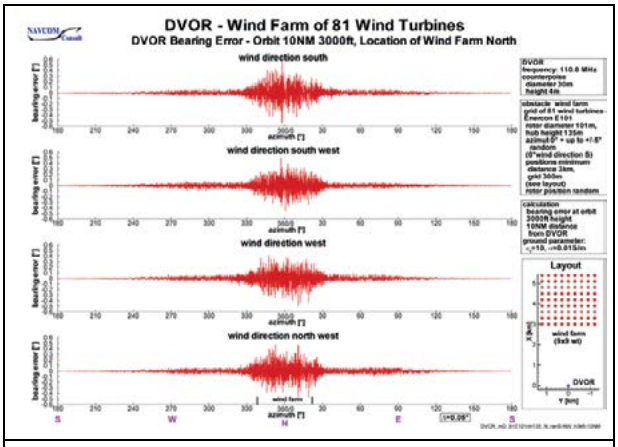

Fig. 17: Bearing error; large wind-farm for 81 WTs; 3km min; orbit 10-40nm, 4000ft; 4 wind directions, rotor random

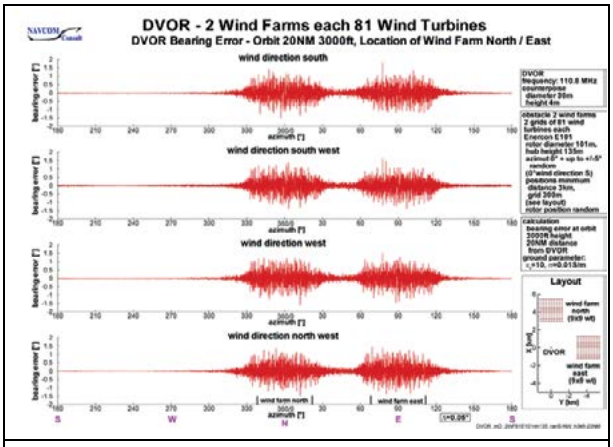

Fig. 18: Bearing error; large wind-farm for 2*81 WTs; 3km min; orbit 10-40nm, 4000ft; 4 wind directions, rotor random

The overall result of these systematic simulations is that the DVOR is relatively resistive against the bearing error effects of wind turbines, and just the large number of WTs is a priori not an argument to expect risky out-of-spec bearing errors in a given case.

Some Flight Inspection Measurement Results

Two examples of DVOR-installations or plannings and related flight-check measurements shall be briefly addressed.

First case: DVOR CRP

A large number of WTs are installed in relatively close distances to the DVOR CRP (**Fig. 19**) - up to ca. 125 WTs within 10km (Status 11/2014) and up to 163 within 15km). The routine flight inspection orbit (10nm, 5400ft) does not show any relevant bearing error effect (**Fig. 20**) – in particular not in the flown height of 5400ft. This is also true for the low-altitude checked radials (not shown).

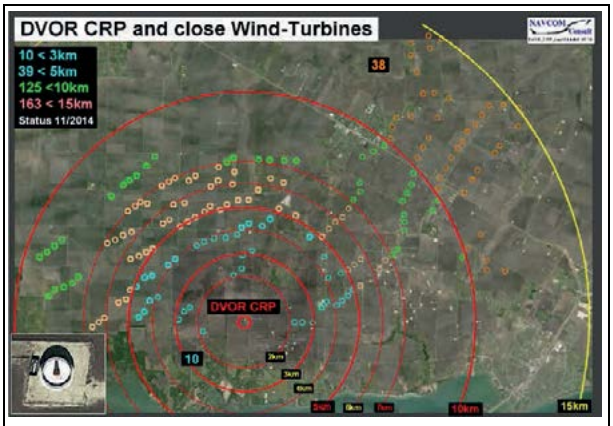

Fig. 19: DVOR CRP; Layout of 163 WTs min up to 15km, 125 WTs up to 10km

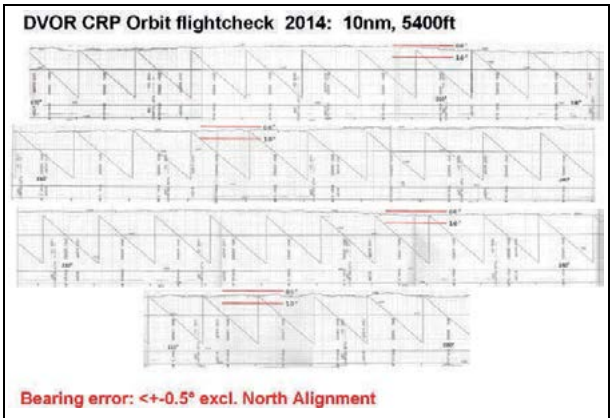

Fig. 20: DVOR CRP Flight Check; Orbit 10nm, 5400ft

Second case: DVOR MIC

Quite a large number of WTs are installed or also planned in the vicinity of the DVOR MIC (**Fig. 21**). Within 5km 52 WTs exist, and 9 very large additional ones are planned, within 10km 72+9 WTs and 114+9 within 15km.

The flight inspection (example from 2010; orbit 20nm, 3500ft; **Fig. 21** top; not all WTs installed) does not show any effect which is technically related to the WTs. The measured effects of the close silo have been simulated by the developed new "near-field spectral approach" (**Fig. 2**) and published also on the last IFIS 2014 ([9]). An excellent agreement has been achieved.

The effects of the 123 WTs (114+9) have been simulated (**Fig. 21** bottom) on almost the same orbit as measured (10nm, 20nm, 3600ft). Very small undetectable bearing errors have been found in the analysis. The azimuthal error distribution is according to the azimuthal distribution of the wind-farms (or wind-turbines).

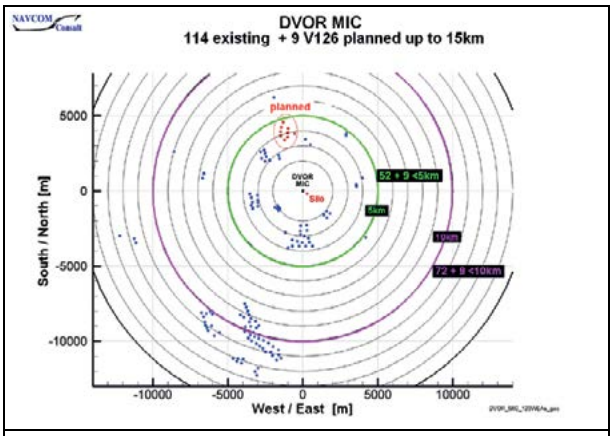

Fig. 21: DVOR MIC; Layout of 123 WTs min up to 15km

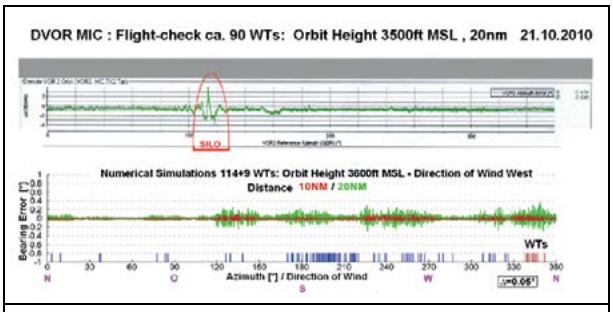

Fig. 22: DVOR MIC; Flight check and simulations (without silo)

FINAL EVALUATIONS; SPECIFICATIONS

ICAO Annex 10 does not define maximum tolerable bearing errors in the coverage volume under the impact of multipath such as the effects of WTs. However, Annex 10 refers to DOC8071 and by that the tolerances layed down in DOC8071 are treated widely as "Quasi-SARPs". DOC8071 defines a limit of ±3.5° for bends and additionaly ±3° for scallops assuming a probability of 95% for the total error including the station error and the given error contribution by terrain effects or existing scatterers. That means explicitly that certain outliers (confined in small space volume or very rare statistical occurance) can be accepted according to the ICAO-tolerance theory.

Existing errors (ground station error excluding the computed resulting north alignment; other bearing errors documented by flight inspection) cannot be added linearly in a scalar manner, but approximately by the rss-superposition. All these error components including the VOR-station itself are just (additional) components in the superposition process shown in **Fig. 6**.

Example: If the flight inspection would show a bearing error of ±1.5° (excluding north-alignment) in some point in space and if the simulations would show a maximum bearing error of ±2°, the resulting bearing

error would yield an rss- figure of ±2.5° which is still far below the DOC8071 limits. The rss-scheme applies for the superposition and the decomposition of VOR-bearing errors.

However, in order to avoid unwanted risky accumulations and take into account unknown effects, often a preliminary limit of ±2° is defined for the evaluation of flight inspection results allowing a lot of margin. Also the errors of a certain development (WTs or other buildings close to the VOR) should not consume the total margin of the acceptable tolerances preventing further developments – even if the actual development would be acceptable relative to the maximum tolerances.

However this paper as well shows by the extensive statistical results that the "feared or expected hidden effects", i.e. the increase of the bearing error by WTs by large factors under certain conditions not seen by flight inspection, is unrealistic.

These final results are in particular applicable for large number of WTs.

CONCLUSIONS; RECOMMENDATIONS

Newly planned WTs in some distance to VOR-navigation systems have to be evaluated in advance before approval by an adequate reliable methodology. This methodology is outlined briefly.

Systematic numerical results and two cases of large number number of WTs (up to 162 WTs within 5km) are shown and discussed. Extensive statistical numerical "trials" show that the earlier expected drastic (linear) increase of the bearing errors under certain combinations of wind-direction and rotor position does not happen for wind-farms. The underlying physics for this behavior is explained, namely the random statistical complex superposition of the error components. By that it is no surprise that flight-inspection does not see relevant bearing errors really caused by WTs. That is not a "problem", but simply the consequence of the real effects of the WTs in the sufficiently large distances of installation. The effects of the WTs simply are hided in the normal measurement noise (e.g. <±0.5°) of the flight inspection measurements

A final recommendation can be given:
"Flight inspectors should not be afraid of a large number of wind turbines" and should not expect major bearing errors a priori in case of many WTs. Tentatively observed effects in the flight-inspection results are most likely not caused by and related to WTs if the WTs are properly analyzed and approved.

ACKNOWLEDGEMENTS

The presented numerical 3D-simulations have been carried out by Mr. Wolf-Dieter Biermann and Mr. Rolf Mundt of NAVCOM Consult.

REFERENCES

[1] ICAO, July 1996, International Standards and Recommended Practices, Annex 10 to the Convention on International Civil Aviation, Volume 1, Radio Navigation Aids, 5th Edition, http://www.icao.int

[2] ICAO EUR DOC015, "European guidance material on managing building restricted areas", Nov 2015

[3] Lo Y.T., Lee S.W. "Antenna Handbook", Vol. I, II; Van Nostrand, NewYork 1993

[4] G. Greving, W.-D. Biermann, R. Mundt "Navigation System Simulations with Integrated Scattering Analysis and Advanced Signal Processing"; ICEAA, Sept 2013, Torino/Italy

[5] G. Greving, "Computer Simulations and 3D-Modelling of Systems and Objects in Aviation - Methodology and Results of Distortion Analysis"; EMS 2012, Malta Nov 2012

[6] G. Greving, N. Spohnheimer Current Issues in Flight Inspection Measurements June, 2010; 16th IFIS Beijing/China, June 2010

[7] Hurley H.C., Anderson S.R., Keary H.F. "The CAA VHF omnirange", Proc. IRE, vol. 47, No. 5, **Dec 1951**, pp. 1506-1520

[8] Anderson S. R., and Flint R. B., "The CAA Doppler Omnirange", Proc. IRE, vol. 47, No. 5, **May 1959**, pp. 808ff

[9] Greving G., Würth H., "A new VOR-antenna in slot technology", 13th EUMW, Nürnberg Sept 1983, pp. 395-400

[10] Odunaiya S., Gomez F. "Doppler VOR performance when located 125-feet above the ground", 12th IFIS, Toulouse, June 2002, pp.119-127

[11] G. Greving, W.-D. Biermann, R. Mundt, Advanced Theory and Results of Classical System Simulations and Related Flight Inspection; 19th IFIS2014, Oklahoma/USA, Juni 2014

[12] G. Greving, N. Spohnheimer Recent Issues in Performance Prediction and Flight Inspection Measurements; 19th IFIS2014, Oklahoma/USA, June 2014

IFIS2016

Bringing Together Theory and Practice

Session 5

Flight Validation of ADS-B and Datalink

Challenges in Complex Procedure Design Validation

Frank Musmann
Dipl.-Ing
Aerodata AG
D-38108 Braunschweig, Germany
Phone: +49 531 2359 341
Fax: +49 531 2359 222
E-mail: musmann@aerodata.de

ABSTRACT

Procedure design of Instrument Flight Procedures (IFP) requires the consideration of many limiting factors such as: terrain, obstacles, environmental constraints and suitability for air traffic management. As a result, instrument flight procedures are more and more based on area navigation (RNAV) or performance based navigation (PBN) which allows a complex flight path definition. The capabilities of modern flight management systems (FMS) enable procedure designers to use new elements for the definition of the procedure path. Typical elements are Radius to Fix (RF) segments for the definition of arcs and the Final Approach Segment (FAS) for the definition of precision approaches with vertical guidance.

This paper highlights some typical undesired effects that can be observed during flight validation of procedures based on RF and FAS. In order to simplify the validation process, software tools and functions have been developed. Based on case examples it is demonstrated how such effects can easily be identified by an automated process.

INTRODUCTION

Any new or modified Instrument Flight Procedure (IFP) is required to be validated before publication. The purpose of the validation is to ensure proper standard and safe operation.

The validation process begins on ground prior to flight. Subject of the pre-flight validation is the correctness and completeness of:

- Procedure charts
- FMS database
- Waypoint coordinates
- Waypoint identifiers
- Waypoint type: fly-by / fly-over
- Tracks between fixes
- Distances between fixes
- Correctness of Final Approach Segment (FAS) datablock
- Suitable path transitions

Only if preflight validation is satisfactory a costly in-flight validation makes sense. Detecting any fail criteria during pre-flight detection can save a lot of money and time.

The in-flight validation focuses on the following subjects:

- Coverage of GNSS signal
- Coverage of SBAS signals
- DME/DME coverage (as required)
- Coverage of conventional Navaids (as required)
- RNP Containment
- Communication Coverage
- Possible interference with navigation signals
- Terrain and obstacle clearance
- Flyability

PROCEDURE PATH DEFINITION

The aim of RNP procedures is to get precise and predictable ground tracks of aircrafts using the procedure. Predictable ground tracks are a precondition for instrument flight routes in mountainous environment and in dense traffic areas.

In order to get predictable ground tracks, first of all the path itself must be defined very precisely. Today's RNP procedures are mainly based on the following path terminators:

- Initial Fix (IF)
- Track To Fix (TF)
- Radius to Fix (RF)
- Final Approach Segment (FAS)

INITIAL FIX (IF)

The Initial Fix (IF) represents the starting waypoint of the procedure and is typically used for naming the procedure:

Initial Fix (TF) [1]

Any Fix is defined by a pair of WGS-84 coordinates and its identifier.

TRACK TO FIX (TF)

Track To Fix (TF) is the great circle connection between two fixes on the WGS-84 ellipsoid:

Track To Fix (TF) segment [1]

Track changes between TF segments can be realized in two ways:

- Fly-by waypoint 
- Fly-over waypoint 

Before reaching a fly-by waypoint the FMS will initiate the turn to intercept the next segment.

At a fly-over waypoint the FMS initiates the turn after overlying the waypoint, and results in much bigger deviation from the path defined by the two TF segments:

Transitions at fly-by and fly-over waypoints

The resulting transition area where aircraft fly on undefined ground tracks is much smaller for fly-by in comparison to fly-over waypoints. Fly-over waypoint should be avoided in order to get more predictable ground tracks. Further, depending on aircraft ground speed and bank limitation this turn anticipation is initiated at different distances from the waypoint. As a result, different aircraft will fly different ground tracks. The size of the transition area can only be limited by speed constraints.

RADIUS TO FIX (RF)

The Radius to Fix (RF) segment allows precise definition of a turned path:

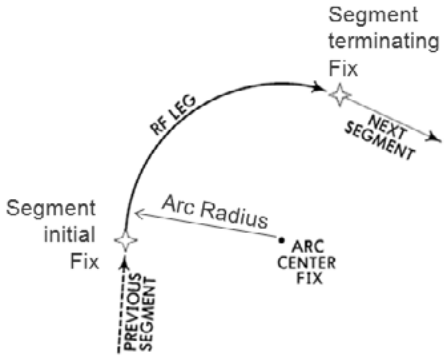

Radius to Fix (RF) segment [1]

According to ARINC 424 specification [1] the RF segment if defined by:

- Segment initial Fix
- Arc center Fix
- Arc radius
- Segment terminating Fix
- Turn direction (CW/CCW)

The required calculations during the procedure design for the determination of the fix coordinates becomes complex, since the arc and the three fixes are not defined on a plane surface but on the WGS-84 ellipsoid.

In addition, the RF turn shall start tangential to the previous segment track and shall end also tangential to the next segment track.

One can easily see that the RF turn path is over specified to a high degree, which can result in inconsistency in procedures based on RF segments. Simplified calculations

for determination of fix coordinates may also lead issues with RF segments.

FINAL APPROACH SEGMENT (FAS)

GNSS based precision approach procedures (e.g. LPV) use a Final Approach Segment (FAS) data block for the definition of the final approach:

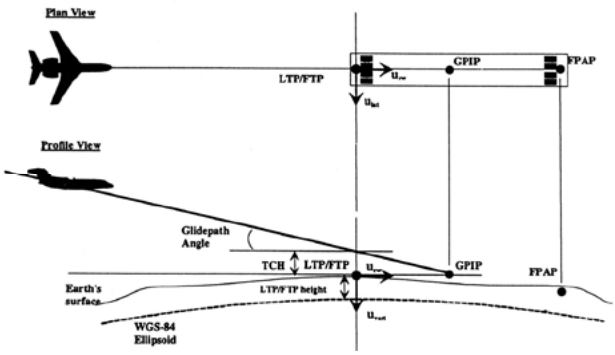

Approach Definition by FAS Data Block [3]

The main elements in the FAS data block are:

- Landing Threshold Point / Fictitious Threshold Point (LTP/FTP) coordinates (including height inWGS-84)
- Flight Path Alignment Point (FPAP)
- Threshold Crossing Height (TCH)
- Glide Path Angle (GPA)
- …

A CRC checksum for the data block content is always published for a FAS in order to detect corrupted data.

All approach construction data refers to the LTP/FTP. The approach is defined "backwards" in a local, Cartesian coordinate system. This could lead to inconsistencies with the previous segment, which is defined on the WGS-84 ellipsoid with altitude constraints in MSL instead of WGS-84 ellipsoid heights.

AUTOMATIC CHECKS AND STANDARDIZATION

In order to have constant quality output from the validation process, the process itself should be standardized and automated to a high extent. This applies to the pre-flight inspection as well as to the in-flight inspection.

Pre-Flight Validation

A lot of time and money can be saved if the aforementioned issues are detected prior to flight.

One would expect that such issues are already detected by the procedure design team during their verification, but in reality there are still a number of cases where incorrect data remain undetected until they are (hopefully) found during in-flight validation.

Since the procedure data must be available to the Automatic Flight Inspection System (AFIS) for the in-flight validation anyway, the idea came up to implement automatic plausibility checks into the AFIS software.

In order to support the pre-flight inspection it is desirable to:

- Have means to identify procedure design errors
- Be alerted if consistency plausibility checks fail
- Have a high level of automation

In-Flight Validation

The flight validation process for a combined validation of GNSS/SBAS procedures including checks for DME/DME coverage and conventional Navaids is a demanding task. Monitoring and controlling all involved elements in flight would simply overload the operator.

In order to standardize the in-flight validation process it is desirable to:

- Have means to select the required tasks for a procedure and the individual segment like:
  - GNSS coverage check required
  - SBAS coverage check required (incl. the definition of primary and secondary SBAS PRN)
  - RAIM algorithm mode
  - RNP containment check required
  - HAL/VAL check required
- Be able to define the above settings in an office environment (Mission Planning)
- For standardization being able to store the above validation setting together with the procedure path in AFIS database.

In the following, elements of such implementation in a modern AFIS are described.

IMPLEMENTATION IN AFIS

In analogy to ARINC424 [1] the AFIS database allows definition of Fixes (waypoints). Any defined waypoint in the AFIS database can be used to define segments of a procedure as TF, RF or FAS segment. The usage of a waypoint in the procedure can be defined as fly-by or fly-over as well as altitude constraints can be assigned. In this way the procedure path, as defined by the procedure design, is loaded (or manually entered) to the AFIS.

The AFIS automatically performs consistency and plausibility checks to the procedure data and outputs alerts to the operator in such case:

- Inbound Track to ALESI not tangent to following RF arc (Delta: 5.2°)
- RF arc not tangent to Outbound Track from LIDMO (Delta: 4.8°)
- RF radius or RF center coordinates do not match ALESI (Delta: 127.33 m)
- FAF not on approach centerline (Delta: 150.54 m)
- FAF not on glide path (Delta: 51.42 m)
- LTP/FTP does not fit to THR coordinates (Lateral Delta: 15.24 m)
- LTP/FTP does not fit to THR coordinates (Vertical Delta: 4.78 m)

Consistency and Plausibility Alerts

For each procedure in the database, settings can be defined that activate a corresponding evaluation task during the validation flight. If an evaluation task is enabled for the procedure, the system automatically provides the corresponding graphics, alphanumeric windows and compiles the data to the report.

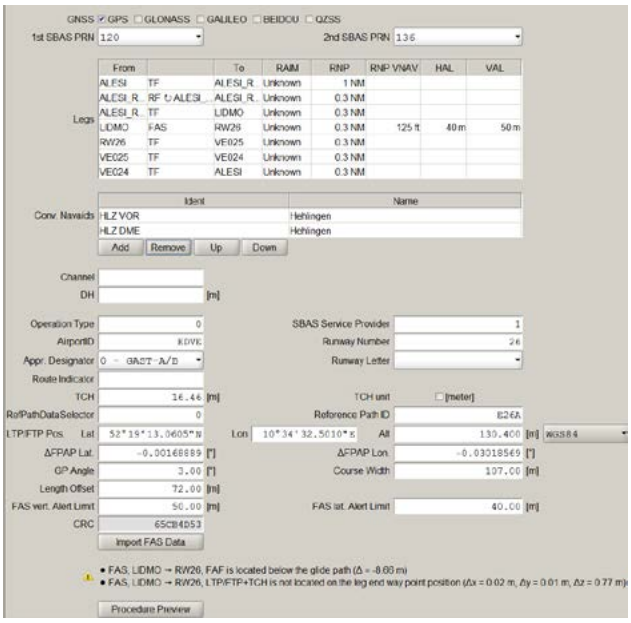

Procedure Settings in AFIS Database

GNSS evaluation

For a GNSS based procedure, select the satellite system that should be analyzed. Currently the following satellite systems can be selected:

- GPS
- GLONASS
- GALILEO
- BEIDOU
- QZSS

The AFIS GNSS receiver (AD-GNSS-0100) with its capability for tracking up to 120 channels provides the corresponding satellite data for the selected systems.

SBAS Evaluation

If SBAS is selected, in addition to the un-augmented GNSS position an SBAS corrected position is provided and analyzed.

The PRN of the primary and secondary SBAS satellite can be defined. Both satellites are analyzed with regards to coverage along the procedure.

Segment Setting

For each procedure leg it is possible to define individually:

- Mode of RAIM (Enroute, Terminal, NPA)
- RNP value
- RNP VNAV
- Horizontal Alert limit (HAL)
- Vertical Alert limit (VAL)

RNP values and alert limits are applied as tolerances for the evaluation and are shown graphically.

Conventional Navaids

Conventional Navaids can be selected to be checked along the procedure. All available receivers of the AFIS can be used for checks of conventional Navaids typically:

- 2 x VOR/ILS
- 2 x DME (or 8 channel DME Scan)
- NDB
- MKR
- VHF-COM
- TACAN (optional)
- UHF-COM (optional)

Each selected conventional Navaid is analyzed regarding coverage, errors, modulation etc. An automatic Report is compiled for each Navaid with reference to the procedure track.

FAS Data Block

The FAS data block is normally imported as CRC wrapped binary file, as provided by the procedure designer. By this the typical errors during manual data entry are eliminated. Alternatively, the data can also be entered manually (not recommended). The AFIS calculates the CRC checksum that can be compared to the published CRC checksum for integrity.

Procedure Preview

For graphical verification the AFIS provides a lateral and vertical preview of the procedure:

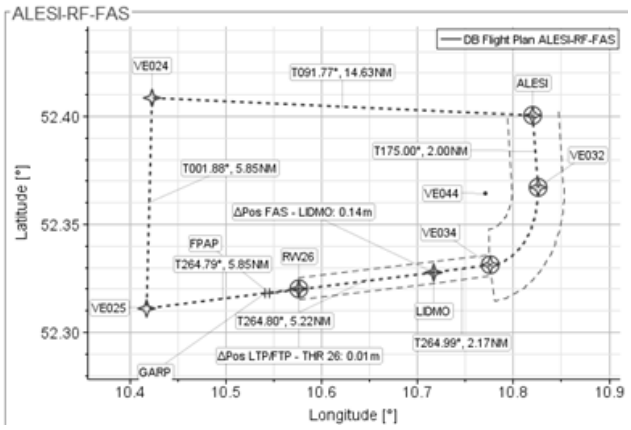

Procedure Preview Lateral

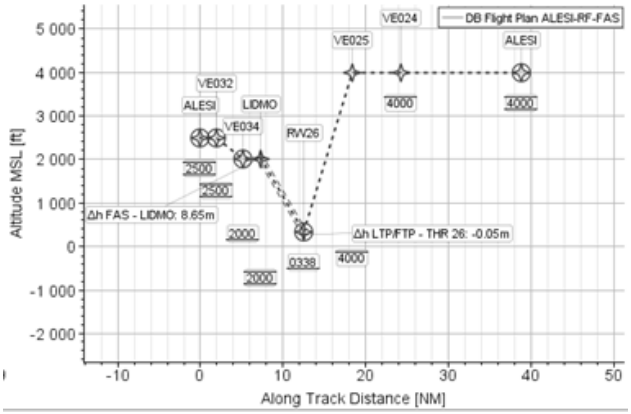

Procedure Preview Vertical

All relevant data are indicated in this preview:

- Fixes with symbols (fly-by / fly over)
- Identifiers
- Tracks between fixes
- Distance between fixes
- FAS data points:
  - LTP/FTP
  - FPAP
  - GARP
- RNP boundaries
- Altitude constraints
- Detected inconsistencies

The Procedure Preview provides also zooming into details of interest. Even smallest detected differences can be graphically analyzed.

Flight Track Simulation

The AFIS integrates a feature which allows to simulate the resulting flight track of different types of aircraft following the procedure. Depending on mass, size and speed of the aircraft, different flight tracks will result.

Currently the following aircraft types can be selected for simulation in AFIS:

- Dornier 128
- Dornier 328
- Airbus A300

EXAMPLE ISSUES FOR PRE-FLIGHT CHECKS

CASE 1: Wrong Coordinates

A typical case is a TF waypoint that is provided with wrong coordinates. Detection in AFIS is simplified by graphical visualization in combination with the calculated tracks and distances.

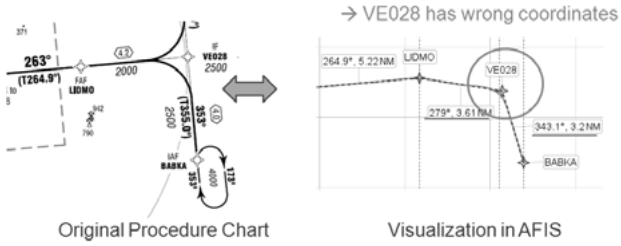

Visualization of Procedure with Tracks and Distances

The wrong coordinates become obvious by:

- Procedure track in graphic
- Distances between fixes
- Track between fixes

CASE 2: Waypoint Type Incorrect

Another typical example is waypoint that is defined as fly-over instead of fly-by:

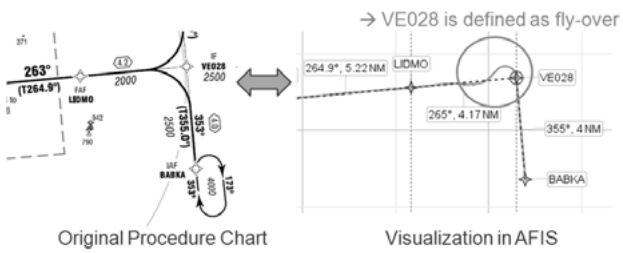

Visualization of Simulated Flight Track

The error becomes obvious by:

- Different waypoint symbol
- The simulated flight track

CASE 3: RF Track Differs From In/Outbound Track

Due to wrong ellipsoid calculations an RF segment path is not tangential to its previous and/or next segments:

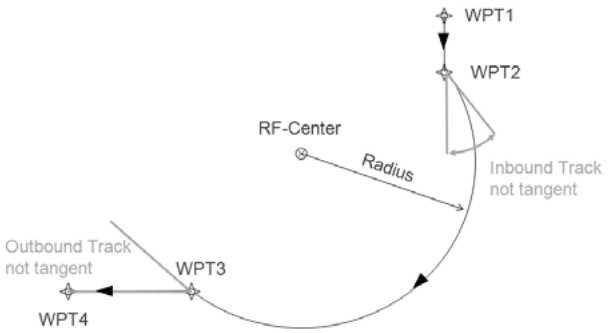

Issues with RF in- and outbound tracks

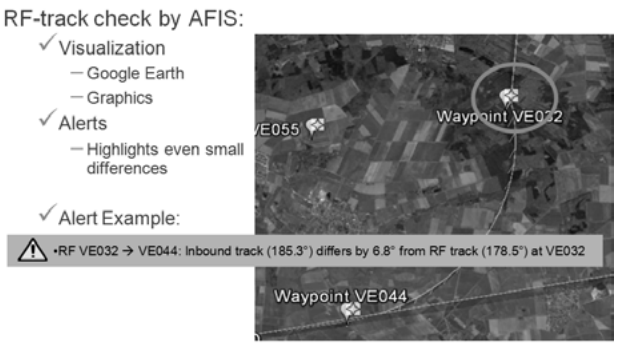

Detection of RF wrong in- and outbound tracks

Such track differences are detected by
- AFIS alert (even small changes)
- Graphical visualization
- Simulated flight track

CASE 4: RF Conflict in Radius and Fixes

Due to wrong ellipsoid calculations the given RF radius does not fit to the constellation of the three involved fixes:

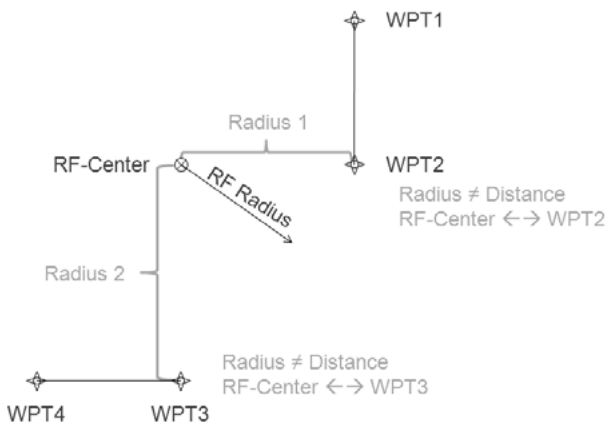

Issues with RF Radius/Center Fix

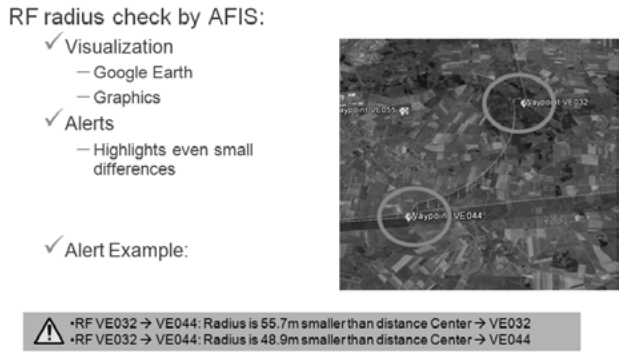

Detection of RF radius issues

Such conflicts are detected by
- AFIS alert (even small differnces)
- Graphical visualization
- Simulated flight track

CASE 5: FAF → FAS Transition Issues

The procedure segments deliver the aircraft forward to the Final Approach Fix (FAF). At FAF, the final approach begins, which is defined by the FAS data block. The FAS approach path is defined backwards from LTP/FTP to the FAF, but might not be laterally or vertically suitable for a smooth transition from FAF:

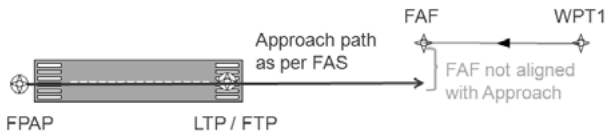

Issues with lateral FAF/FAS transition

Such errors are likely, since at FAF calculations in different coordinate systems merge: All FAS data refers to a local Cartesian coordinate system with its origin in the LTP/FTP, while the previous segment is calculated on the WGS-84 ellipsoid.

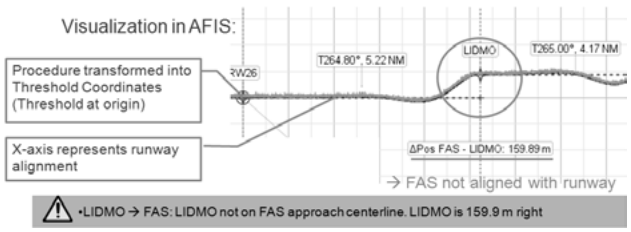

Detection of incorrect lateral FAF/FAS transition

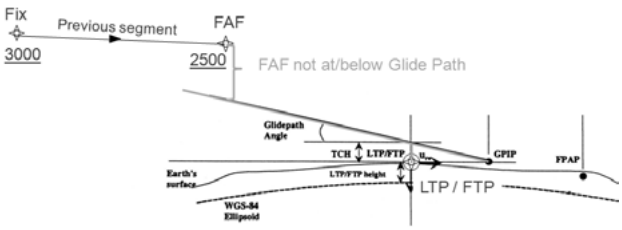

Issues with vertical FAF/FAS transition

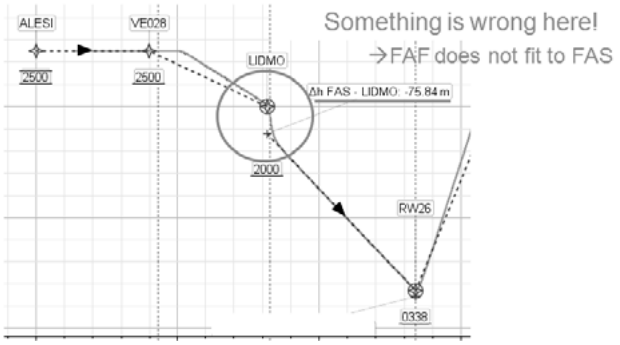

Detection of incorrect vertical FAF/FAS transition

Aircraft arriving at FAF above glide slope is considered as a fail criteria for the procedure, since the glide slope will not be captured by flight director/autopilot.

Such FAF→FAS transition issues are detected by:

- AFIS alert (even small changes)
- Graphical visualization
- Simulated flight track

CASE 6: LTP/FTP issues

The final approach in a FAS data block is calculated with reference to the LTP/FTP. Correctness of the LTP/FTP coordinates are therefore of highest importance. Errors in altitude can occur easily by using wrong coordinate systems (NAD-83 or MSL) or by using incorrect terrain data during the procedure design.

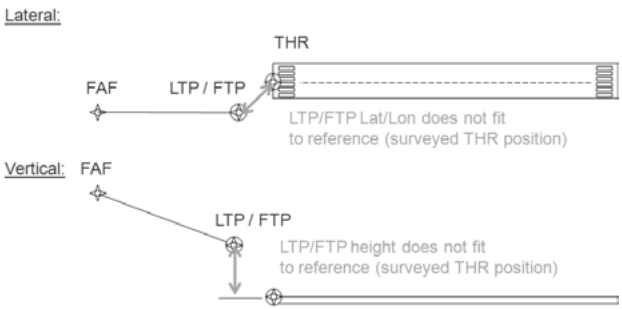

Issues with LTP/FTP coordinate

For flight calibration purpose high precise survey data of the threshold is determined anyway and is available in the AFIS database. This data is totally independent from the data as used by the procedure designer and by this is of highest value for the validation. The AFIS compares the LTP/FTP coordinates against the threshold position as surveyed for flight inspection. Discrepancies are highlighted by alert and visualized laterally and vertically:

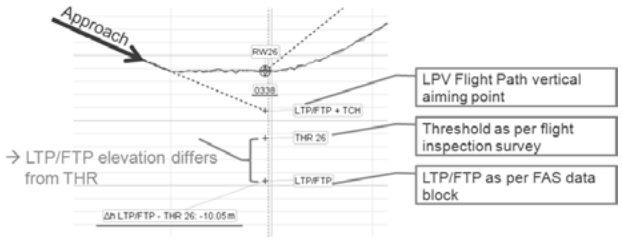

Detection of incorrect LTP/FTP height

FLIGHT VALIDATION OUTPUT

Having the procedure setting for the procedure validation stored in the AFIS database the in-flight validation itself becomes an easy task.

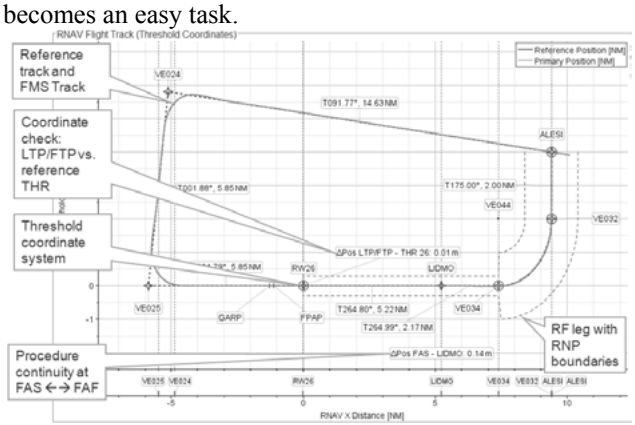

Procedure Visualization in Threshold Coordinates

The AFIS automatically performs the predefined tasks, collects the data and compiles the data for the report.

A few elements of the data provided by AFIS evaluation are shown in the following:

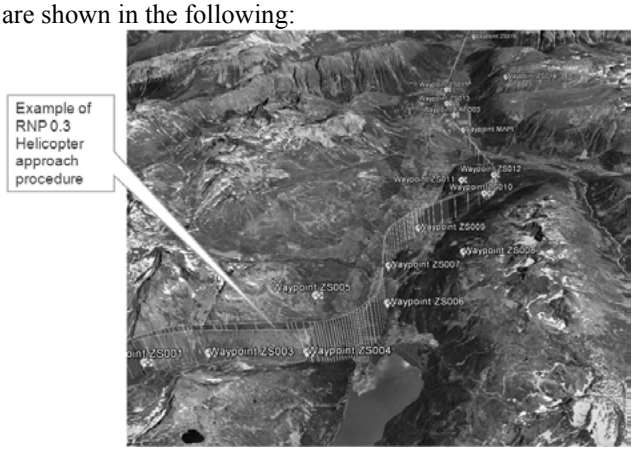

3D Visualization of RNP 0.3 helicopter approach

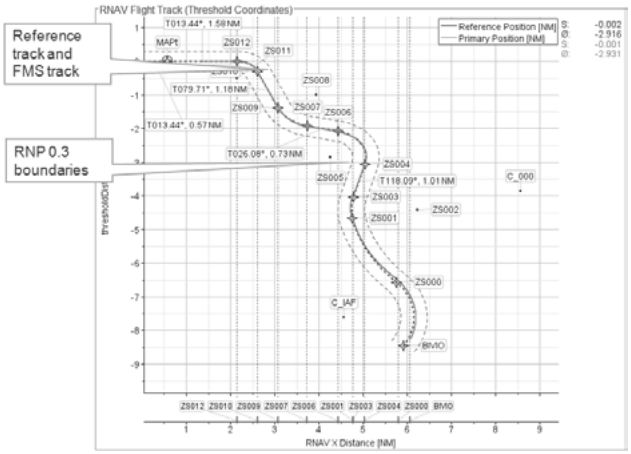

RNP 0.3 Helicopter Approach

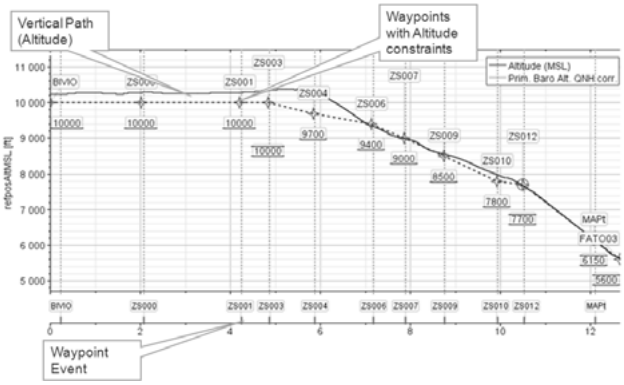

Vertical Profile Graphic

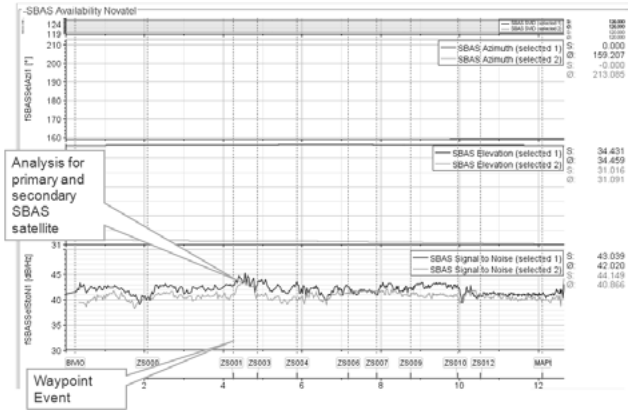

SBAS Availability

If GNSS evaluation selected:

Integrity: GNSS_GPS

		Max VDOP	Max HPL	Max VPL	Max HFOM	Max VFOM	Max ATK Error	Max XTD Error	Max XTD	Min # SV Used	Min C/N0	RAIM Fault Time
			[m]	[m]	[m]	[m]	[NM]	[NM]	[NM]		[dBHz]	[s]
1	1.0	1.8	97	175	9.4	17.5	0.004	0.001	0.056	8	42.6143	0.000
2	1.0	1.8	97	170	9.4	17.5	0.004	0.001	0.061	8	41.7805	0.000

If SBAS evaluation selected:

Integrity: GNSS_SBAS - Primary = 120, Secondary = 126

		Max HDOP	Max VDOP	Max HPL	Max VPL	Max HFOM	Max VFOM	Max ATK Error	Max XTD Error	Max XTD	Min # SV Used	Min C/N0	RAIM Fault Time
				[m]	[m]	[m]	[m]	[NM]	[NM]	[NM]		[dBHz]	[s]
1	1.0	1.8	5	10	1.1	2.0	0.004	0.001	0.056	8	42.6143	
2	1.0	1.8	5	10	1.1	1.9	0.004	0.001	0.061	8	41.7805	
3	1.0	1.8	5	10	1.0	1.9	0.003	0.001	0.027	8	39.5882	
4	1.0	1.8	5	10	1.0	1.9	0.003	0.001	0.013	8	42.8297	
5	1.0	1.8	5	9	1.0	1.9	0.003	0.002	0.023	8	40.4157	
6	1.0	1.8	5	9	1.0	1.9	0.003	0.001	0.015	8	41.5572	
7	1.0	1.8	5	9	1.0	1.9	0.003	0.001	0.012	8	40.0175	
8	1.0	1.8	5	9	1.0	1.9	0.002	0.001	0.006	8	41.6238	
9	1.0	1.8	5	9	1.0	1.9	0.003	0.002	0.016	8	40.2174	

Report Compilation

The output of the flight validation is a comprehensive report that provides a standardized package of data like graphics and alphanumeric tables for each enabled evaluation task.

CONCLUSIONS

Validation of instrument flight procedures is a complex task. In order to ensure a constant quality of the validation output standardization and automation is required.

The flight validation can be simplified and standardized by saving settings for evaluation together with the procedure in the AFIS database.

Leg types like RF and FAS provide potential for inconsistencies and discontinuities.

Many errors or inconsistencies can be detected by an AFIS prior to flight by automatic checks, alerting and features for graphical visualization of the procedure and the relevant points.

The AFIS as described in here can significantly contribute to a standardized validation output with constant quality, independent of individual operator's human performance.

REFERENCES

[1] ARINC 424, Navigation System Database, ARINC Specification 424-20, Published Dec. 2011

[2] ICAO DOC8168, Volume II, Construction of Visual and Instrument Flight Procedures

[3] RTCA-DO229D, Minimum Performance Standards for Global Positioning Systems/Satellite-Based Augmentation System Airborne Equipment, Change 1, February 1, 2013

Approach to Flight Testing of Space-Based ADS-B

Steven R. Bellingham
Manager, Navigation Systems Engineering
NAV CANADA
Ottawa, Ontario, Canada
Fax: +1 613 248 7195
E-mail: Steve.Bellingham@navcanada.ca

ABSTRACT

The Aireon space-based ADS-B system will enter operational service in 2018, following the launches of the 72 satellites of the Iridium NEXT constellation, all carrying ADS-B receiver payloads. The first satellites will begin to provide ADS-B data to support pre-operational testing by the end of 2016.

A comprehensive test program, including a formal flight testing component, will be used to assess and demonstrate the performance and coverage of the Aireon ADS-B system. The fact that the Aireon receivers are installed on orbiting satellites whose footprints move across the Earth's surface at approximately 24,000 km/h adds to the test program an extra degree of complexity not previously encountered with other ADS-B systems.

This paper describes the Aireon space-based ADS-B system, and discusses considerations for flight testing of the Aireon system in context with other facets of the test program.

INTRODUCTION

Since 2008, NAV CANADA has deployed and used ADS-B ground stations to extend its ATC surveillance coverage. In 2012, following stakeholder consultations, the company decided to invest in the Aireon space-based ADS-B program. Once the system is fully deployed, NAV CANADA will be among the first users of the Aireon ADS-B service, to support more efficient routing of oceanic flights over the North Atlantic commencing in 2018.

The first launch of ten Iridium NEXT satellites, carrying Aireon ADS-B payloads, is scheduled for mid-third quarter 2016. On-orbit testing of the ADS-B functionality will commence within two months of the first launch. NAV CANADA will participate in planning and executing various aspects of the test program, including formal flight testing, in cooperation with Aireon and other test partners.

This paper begins with a description of the Aireon space-based ADS-B system, with emphasis on the satellite payloads and their orbit characteristics. It then discusses various inter-related means by which the performance of the system can be characterized and verified, during and after deployment. Attention is drawn to the global coverage of the system and the fast-moving footprints of the individual satellites, which both allow and require some differences in the approach to performance verification in general, and flight testing in particular, as compared to that employed for ground-based ADS-B systems.

Planning for on-orbit performance evaluation is actively underway, but has not yet been finalized. This paper presents the author's perspective at this point in time, and does not claim to represent any official Aireon position.

AIREON SYSTEM

Aireon Mission

The Aireon Space-Based ADS-B system is being developed and deployed to provide a global ATC surveillance capability to complement and supplement ground-based surveillance systems. It will provide service to oceanic and remote airspaces where ground-based surveillance is either impractical or cost-prohibitive, and will offer supplementary or contingency service for areas served by other surveillance systems.

Aireon will also provide a global flight tracking capability based on ADS-B, which will be available without charge for emergency applications through the Aireon ALERT service.

Aireon leverages the opportunity provided by the development of the Iridium NEXT satellites, which will

replace and upgrade the existing Iridium global constellation of Low-Earth Orbit (LEO) telecommunications satellites. All Iridium NEXT satellites will carry Aireon Hosted Payloads.

Aireon Payload

Figure 1 depicts an Iridium NEXT satellite carrying its Aireon Hosted Payload. Each Aireon payload incorporates an antenna array of circularly-polarized patches arranged on five panels. The antenna patches are combined under software control of phase and amplitude to simultaneous form many beams at various orientations. Each individual antenna beam is coupled to one of a bank of 1090 MHz receiver channels, operating in parallel. The combination of the elliptical patterns of the individual beams through the various receiver channels creates a composite "footprint", roughly circular in shape, for each Aireon payload.

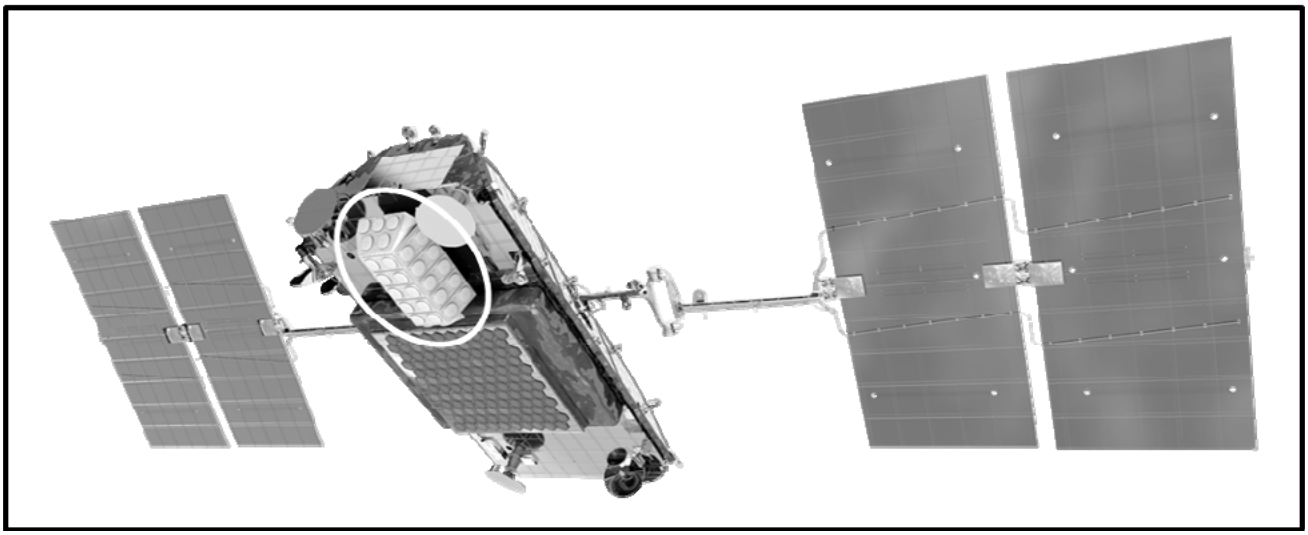

Figure 1. Iridium NEXT Satellite with Aireon Hosted Payload

Constellation Orbit Characteristics

The Iridium NEXT satellites will replace existing Iridium satellites, one-for-one, in the same orbital slots. The constellation will comprise sixty-six operational satellites, plus six on-orbit spares. Additional ground spares are also being produced, to be available for future launch if required.

The satellites will be arranged in six orbital planes, each with eleven operational satellites plus one spare. The circular orbit planes will have near-polar orientation (inclination of approx. 86 degrees), providing global coverage. The orbit altitude will be 780 km above the ellipsoid. Figure 2 illustrates the orbital arrangement of the Iridium NEXT constellation, with notional composite footprints covered by the antenna beams of each Aireon payload.

The orbital period for the Iridium NEXT satellites will be approximately 100 minutes. This translates to a ground speed of roughly 24,000 km/h for the footprint of the Aireon payload. As a result, any given point on the ground (or any given aircraft) will be within geometric line-of-sight of a particular satellite for no more than 15 minutes per pass.

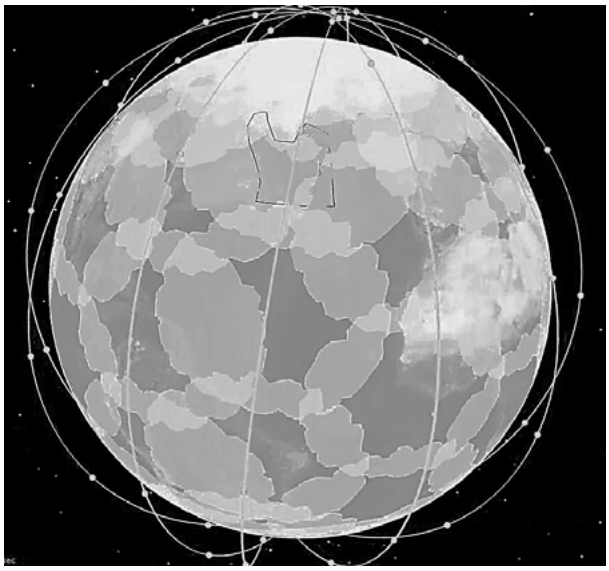

Figure 2. Iridium NEXT Constellation with Notional Aireon Payload Footprints

The satellite orbits will not be geosynchronous, so the ground tracks of satellites will not repeat. As the Earth rotates under the orbital planes, the track of each satellite will shift approx. 25° to the west with each orbit; the next-in-line satellite in the same orbital plane will appear 2.3° west of its predecessor.

Deployment Schedule

The core ground infrastructure for Aireon has been deployed and has completed pre-launch system acceptance testing. Manufacturing and factory acceptance testing of the Aireon payloads is also essentially complete.

The first launch of ten Iridium NEXT satellites, aboard a SpaceX Falcon 9 rocket, is scheduled for mid-third quarter 2016. The first Aireon payload will start relaying ADS-B target data two months after launch, to be followed in quick succession by additional payloads. The constellation will be fully operational by the end of 2017, to support ADS-B surveillance services in 2018.

ADS-B COVERAGE ASSESSMENT

General Framework for Performance Assessment

Any ADS-B system will be designed and tested to meet general specifications and workmanship standards, as well as specific requirements related to its ADS-B services. EUROCAE has recently completed an updated specification for ADS-B ground systems, to be published as Document ED-129B.[1] As stated in [2], "Requirements in ED-129B are broad and detailed, covering areas such as expected ADS-B system modes and states, target processing, capacity, performance, and control and monitoring."

ADS-B Coverage Assessment Criteria

In general, assessment of "coverage" for an ADS-B system means assessment of whether aircraft position updates are consistently provided within the desired update interval throughout a three-dimensional operational coverage or service volume.

ED-129B defines requirements for updates in terms of two parameters: the Probability of Update (PU) and the Probability of Long Gaps (PLG).

The Probability of Update specifies target probability levels for providing position updates within equally spaced update intervals. Both the probability level and update interval are specific to the ATC sector type (e.g. low density en route, high density terminal, etc.). PU is intended to be measured over a grid of geographic cells throughout a service volume, with the PU requirement to be met for each cell.

The Probability of Long Gaps specifies a maximum allowed probability with which the period between successive position updates may exceed n times the update interval specified for PU. Like PU, PLG is also specific to the ATC sector type, but PLG is typically assessed over an entire service volume rather than in individual cells.

Factors Affecting ADS-B Coverage

Factors affecting ADS-B coverage include the following:

a. Line-of-sight between aircraft and ADS-B receiving antenna;

b. Effective radiated power from aircraft – a function of transmitter output power, cable losses and aircraft antenna pattern;

c. Propagation losses;

d. Receiver subsystem performance, in terms of antenna patterns, receiver sensitivity, selectivity, de-garbling and throughput capacity;

e. Interference environment, including 1090 MHz channel occupancy or FRUIT (False Replies Uncorrelated In Time); and

f. Link loading versus capacity, for data output from receiver subsystem.

ADS-B Coverage Assessment Tools

In terms of the tools used to assess ADS-B coverage, ED-129B states that coverage predictions should be modelled with a software tool that considers line-of-sight, power budget, link loading and potential interference. Flight data is required to assess Probability of Update and Probability of Long Gaps. ED-129B recommends the use of flights of opportunity (i.e. regular aircraft traffic) to the extent possible, but notes that dedicated flight test aircraft, particularly when configured for the minimum transmitter power permitted under DO-260B standards [4], can be used to supplement the flight data.

AIREON PERFORMANCE ASSESSMENT

Applicability of ED-129B

The specifications and test cases of EUROCAE Document ED-129B will be applicable to Aireon, albeit with some tailoring to take into account the space-based component and specific surveillance applications. ED-129B will be used as a foundation requirements document for the Aireon system certification program that is being undertaken through the European Aviation Safety Agency (EASA).

Aireon Line-of-Sight Considerations

The composite footprint formed by the set of discrete beams of the Aireon payload antenna array will not be perfectly circular. Nonetheless, it is useful to consider a circular approximation in order to estimate the individual payload performance required in order to provide coverage without any gaps between satellites. The greatest separation between adjacent satellites will occur at the equator. At this latitude, it can be shown that overlapping coverage from Iridium NEXT satellites will be provided by a set of circular footprints

extending 2,200 km great circle distance from each sub-satellite point.

Figure 3 illustrates the relationship between the great circle distance from an Iridium NEXT sub-satellite point to a ground facility or aircraft, the elevation angle to the satellite, and the off-nadir angle from the satellite's perspective. The geometric line-of-sight distance, corresponding to 0° elevation angle, is approx. 3,000 km from the sub-satellite point. (Radio line-of-sight calculations would typically use an Earth model with radius increased by a factor of 4/3, resulting in a greater distance.) The 2,200 km distance to achieve overlap corresponds to an elevation angle of 8°, or an off-nadir angle of 62°.

The fact that overlapping coverage can be provided anywhere using satellites at 8° or higher above the horizon means that line-of-sight will never be an issue for the core Aireon services.

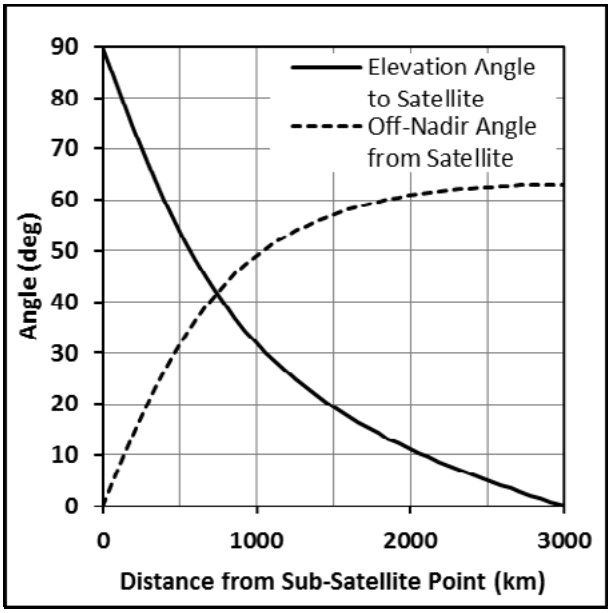

Figure 3. Angles to/from Iridium NEXT Satellite versus Distance from Sub-Satellite Point

Factors Affecting Aireon Coverage

Applying the previous itemized list of factors affecting ADS-B coverage to the particular case of Aireon gives the following:

a. Line-of-sight will not be an issue, as explained above;

b. Effective radiated power from aircraft – reception at satellite will depend on antenna pattern of aircraft top-mounted antenna, although bottom-mounted antenna will also contribute at low elevation angles;

c. Propagation losses will be more significant due to the much greater propagation distances;

d. Receiver subsystem performance has been optimized, particularly in terms of antenna patterns and receiver sensitivity, to account for the greater propagation losses;

e. Interference environment is more complex, due to increased exposure to ground and airborne sources, but mitigated by rapidly moving beam footprints; and

f. Link loading versus capacity for data output from receiver subsystem remains relevant.

Aireon Coverage Assessment Tools

The global coverage of the Aireon space-based ADS-B system and the fast-moving footprints of the individual satellites both allow and require some differences in the approach to coverage assessment for Aireon as compared to that employed for ground-based ADS-B systems. Flights of opportunity and dedicated flight test aircraft are still used, though in somewhat different ways. The role of simulation modelling is much more prevalent. A new role is defined for a calibrated ground-based reference transmitter.

Aireon Simulation Modelling

To deal with the complexities of predicting and analyzing coverage performance for a satellite-based ADS-B system, Aireon has developed a sophisticated simulation model called ASIM (Aireon SIMulator). In addition to handling orbital propagation for the constellation, ASIM exercises detailed models of payload beam patterns and receiver performance, and models aircraft transmitted power levels and antenna patterns. The fidelity of the antenna patterns used by ASIM has been augmented by RF anechoic chamber measurements of the payload antenna array and of various commercially available ADS-B aircraft antennas.

ASIM can model discrete aircraft targets or realistic traffic patterns, including growth projections for ADS-B-equipped traffic. It also models other significant contributors to the FRUIT/interference environment for 1090 MHz, so that message collisions, garbling, etc. can be factored into the simulation. Further descriptions of ASIM are provided in references [2] and [3].

Ground-Based Reference Transmitter

The relationship between the ground tracks of the Iridium NEXT satellites and the size of the Aireon payload footprint is such that every Aireon payload footprint will pass over any given location on the Earth's surface a minimum of four times each day. Furthermore, the number of passes increases with latitude, moving away from the equator.

Installing a ground-based reference transmitter to provide 1090 MHz signals with calibrated output power

and calibrated antenna patterns will allow Aireon to collect data from all payloads over the full range of azimuth and elevation angles. Figure 4 shows the accumulated set of observation tracks for a single Aireon payload over a ten-day period, for a hypothetical transmitter site at 45° latitude (Ottawa). The tracks are plotted in terms of the distance from the sub-satellite point to the ground station and the azimuth angle to the ground station as measured at the satellite relative to its direction of travel.

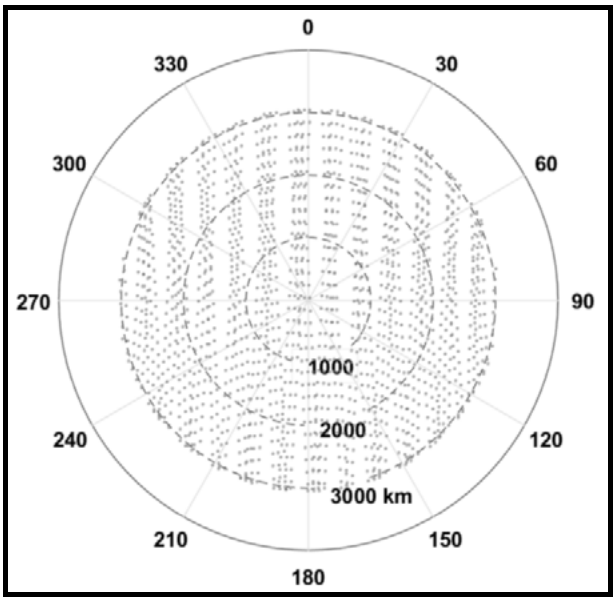

Figure 4. Range/Azimuth Tracks for Line-of-Sight to Ground-Based Transmitter at 45°N

Collection and analysis of receptions of messages from the ground station will allow direct comparison between payloads to establish any initial or future performance differences between them, and to determine the degree to which their footprints are circular.

Flights of Opportunity

Although a calibrated ground-based reference transmitter will provide much information regarding payload performance, it will not provide any information concerning the antenna patterns and performance of the ADS-B-equipped aircraft.

Although a given aircraft will not be airborne at all times, mapping a fixed set of aircraft over multiple flights as seen by successive payloads will allow observation data over tracks similar to those of Figure 4 to be built up over a period of days. Analysis of this data for probability of update will include an extra dimension for aircraft heading relative to the observing satellite, since the aircraft antenna patterns will not be symmetrical.

Analysis of ADS-B message data from flights of opportunity using their positions relative to a moving payload will provide a good understanding of the range of performance in aircraft transmitters and antennas. Analysis of the same data in the more traditional fixed geographic cell structure, on the other hand, will provide insight regarding performance variation between high-FRUIT and low-FRUIT regions.

For some regions where ground-based ADS-B service has been implemented, it will be feasible to directly compare Aireon performance against the ground-based ADS-B data.

ROLE OF FLIGHT TEST AIRCRAFT

Flight Testing of Ground-Based ADS-B

Various papers presented at recent IFIS gatherings have provided excellent information from various perspectives regarding flight testing of ground-based ADS-B systems, addressing flight test capabilities and procedures.[5][6][7][8][9][10]

For the purposes of this paper, which concerns a receive-only 1090ES ADS-B system, flight test considerations related to multilateration and to signals broadcast by a ground system can be set aside. The remaining flight test capabilities and/or flight test procedures for the core ADS-B function as discussed in the referenced papers may then be broadly classified as follows:

a. Demonstrations to air traffic control staff

b. Tests of data content and data integrity

c. Tests of coverage, including update interval

d. Tests to identify interference

Flight Testing of Aireon ADS-B

The service volumes for Aireon ADS-B will in many cases be vast and/or remote, making dedicated test flights covering the extent of the service volume impractical. This is not problematic however, since the overall footprint of the payload and the payload-to-payload variations will be observable using the ground-based reference transmitter and flights of opportunity, as described above.

Dedicated flight test aircraft will still have a valuable, if somewhat different, role to play in assessing Aireon ADS-B coverage. Where these aircraft should prove most useful is in calibrating and validating certain key components of the ASIM simulation model.

At present, flight test aircraft of at least five different aircraft types operated by NAV CANADA, FAA and Aireon are expected to participate in early flight tests of Aireon payload performance. Having a range of aircraft types is beneficial in terms of providing better sampling of various antenna types and of the effects of the airframe on antenna patterns.

In addition to collecting "flights of opportunity" data from the various flight test aircraft during their normal operations, dedicated test flights will also be conducted using specific power and antenna configurations.

Tests at Minimum Transponder Power

The Aireon system is specified to provide nominal performance for aircraft operating with 125 W transponders. The vast majority of aircraft are equipped with higher power units, so setting the output power of the flight test aircraft at a calibrated 125 W level will provide a performance benchmark that will help in power budget simulation and analysis, particularly at the outer edges of the payload footprint.

Tests with Single Aircraft Antenna

The Aireon system is designed to provide surveillance service to aircraft transmitting alternately from each of two ADS-B antennas, mounted top and bottom. Since the satellites will be above the horizontal, the top antenna will be of primary importance. The bottom antenna, however, is expected to be able contribute meaningfully to probability of update at low elevation angles near the edges of the footprint. Reception of messages from the bottom antenna should also allow the Aireon ALERT tracking service to establish at least intermittent tracks for aircraft equipped with only a single bottom-mounted antenna.

SUMMARY

A comprehensive test program will be used to assess and demonstrate the performance and coverage of the Aireon ADS-B system.

EUROCAE Specification ED-129B will be used as a basis for Aireon performance requirements and testing, with some tailoring for the space-based component and for specific Aireon surveillance applications.

Flights of opportunity and dedicated flight test aircraft will be employed in testing the Aireon coverage, though they will be employed in somewhat different ways as compared to in testing of ground-based ADS-B. The role of simulation modelling will be much more prevalent, and a new role is defined for a calibrated ground-based reference transmitter.

FUTURE WORK

With the first launch of Iridium NEXT satellites scheduled for mid-third quarter 2016, much work is actively underway in preparation for the on-orbit performance evaluation program. In terms of topics discussed in this paper, this preparatory work includes development of detailed test plans, augmentation of the ASIM simulation model to facilitate analysis of on-orbit data to assess coverage and other aspects of system performance, and deployment of a ground-based reference transmitter.

Once the first Aireon payload begins delivering aircraft messages, a period of intense effort directed to on-orbit performance testing and analysis, including dedicated flight test activities, will commence.

Formal service acceptance testing for the first operational service volumes will conclude soon after the constellation is completed, to support ADS-B surveillance services in 2018.

REFERENCES

[1] EUROCAE, publication pending, Technical Specification for a 1090 MHz Extended Squitter ADS-B Ground System, ED-129B

[2] German Institute of Navigation (DGON e.V.), April 2016, (M.A. Garcia), Aireon Space Based ADS-B Compatibility and Performance Analysis, ESAVS-2016

[3] IEEE, April 2015, (M.A. Garcia, J. Stafford, J. Minnix and J. Dolan), Aireon Space Based ADS-B Performance Model, IEEE ICNS-2015

[4] RTCA, April 2012, Minimum Operational Performance Standards (MOPS) for 1090 MHz Extended Squitter Automatic Dependent-Broadcast (ADS-B) and Traffic Information Services-Broadcast (TIS-B), RTCA DO-260B

[5] ICASC, June 2014, (T. Heinke), ADS-B, A New Mission for Flight Inspection, IFIS 2014

[6] ICASC, June 2014, (M. Perraut), What We Have Learned About ADS-B and How Do We Stay Under the RADAR, IFIS 2014

[7] ICASC, June 2012, (T. Heinke), Necessities for Flight Inspecting ADS-B and MLAT Signals, IFIS 2012

[8] ICASC, June 2012, (P. Caisso), ADS-B Flight Inspection – The View of French Flight Inspection Unit, IFIS 2012

[9] ICASC, June 2012, (D. McGough, K. Hardina), Methodologies for the Flight Inspection of ADS-B Systems, IFIS 2012

[10] ICASC, June 2012, (A. Graham), Flight Testing for ADS-B and Wide-Area Multilateration, IFIS 2012

ACKNOWLEDGMENTS

The author would like to acknowledge the efforts of the dedicated team at Aireon, their contractor Harris Corp, the FAA, NAV CANADA and other partners, working cooperatively to develop and implement a comprehensive performance verification program for the Aireon space-based ADS-B service.

ADS-B
Experiences in Flight Inspection

Dipl.-Ing.
Thorsten Heinke
Program Manager
Aerodata AG
38108 Braunschweig Germany
Fax: +49 531 2359 222
E-mail: heinke@aerodata.de

Abstract

New technologies concerning safety requirements are arising due to expanding capacity in civil air traffic. One important keystone of new techniques comprised in SESAR, NextGen or CNS/ATM is Automatic Dependent Surveillance Broadcast (ADS-B). It has been developed further and has been upgraded in the past years to fulfill more and more its intended function of supplying situational awareness for safety reasons. ADS-B is used in all new commercial air transport and most general aviation aircraft. The schedule for its mandatory use in aircraft is defined and the final dates are coming closer. The worldwide implementation of ADS-B ground stations for area-wide coverage is steadily increasing and the basic rules for it are set.

The deadlines for the enforcement of ADS-B integration are defined, but the rules for necessaries in-flight verification are not. What needs to be tested and what are the requirements to flight inspect such data in accordance to its sensitivity for flight safety during surveillance? What kind of flight checks have to be performed to uphold the accuracy, integrity or procedure workflow resulting out of the ADS-B technology?

This paper summarizes experiences, practices and requirements regarding the flight inspection of ADS-B systems. It evaluates hard- and software requirements to flight inspect the ADS-B service and it discovers new potentialities in flight inspection missions in regard to the ADS-B technology, while considering the importance for flight safety. The corresponding procedures are examined in detail and evaluated in regard to accuracy, integrity and process workflow.

Introduction

All modern commercial airplanes are equipped with capable transponders using the ADS-B transmission. In the past three different ADS-B techniques were used, explored and analyzed in regard to their advantages and disadvantages.

The first ADS-B technique is the transmission via a separate VHF data link, which requires special equipped VHF radios to fulfill the requirements according to MOPS ED108A. The second technique focuses on the dedicated Universal Access Transceiver (UAT) working in the 978 MHz band. Each aircraft has to be equipped with such unit that complies with RTCA DO-282B and TSO C154c. This technique is mainly used for the lower airspace in the United States. The third method for transmitting ADS-B signals is the extended squitter technique in the 1090 MHz band. It complies with RTCA DO-260B and TSO C166b. The extended squitter method is suitable for the lower and upper airspace and used by all commercial airplanes.

This paper focuses on the extended squitter method for ADS-B as the prevailing system and describes about it new possibilities in flight inspection. It displays the scheduled implementation in aviation in different countries around the globe. The necessary diverging expansion stages are examined in regard to its intended function. The possible new procedures for flight inspection are highlighted and discussed.

Regulations for the implementation of ADS-B

The regulations for the implementation of the extended squitter method for ADS-B are defined and the schedule for its incorporation in commercial air transport is announced in most of the countries with frequent regular commercial air traffic. As an example three implementation deadlines of different civil aviation authorities are listed:

- EASA: NPA 2012-19 defines Extended Squitter (1090 ES) implementation in Europe. The Certification Specifications (CS ACNS) are issued.
    - All IFR General Air Traffic needs ELS.
    - Aircraft above 250 KTS or 5.7t flying IFR need ADS-B Out (DO-260B) and EHS.
    - New Aircraft from 8th of June 2016, retrofit from 7th of June 2020.
- FAA: FAR 91.225/91.227 defines ES and UAT implantation in the US.
    - AC 20-165A and DO-260B compliance required.
    - Implementation for all aircraft flying FL 180 and higher until 1st of January 2020.
- CASA: CAO 20.18 defines ES implementation in Australia.
    - DO-260 compliance required for aircraft flying higher FL 290.
    - IFR forward fit from 6th of February 2014 and all IFR from 2nd of February 2017.

All implementation schedules defining variable stages of introductory phase but in general all focusing on ADS-B as one of the key pillar for surveillance safety in commercial air traffic. This illustrates the important role of flight inspecting this ADS-B technique.

Requirements for ADS-B flight inspection

The general requirement to establish an ADS-B link is to have an airborne segment, which encodes and transmits the necessary data in a special format and a ground segment that receives the data and decodes it. The newest flight inspection systems, like the AeroFIS©, are equipped with state of the art transponders, which are capable to transmit the required data to the ground station. In addition the necessary capable software is included to comply with the newest changes of the defined signal type to manipulate individual transmitted data for flight inspection reasons. The ground stations are equipped with ADS-B receivers to display such data to the radar or ADS-B display operator, dependent on the development stage.

Figure 1: AeroFIS© capable to perform ADS-B flight inspection missions

The flight inspection system comprises a latest revision Rockwell Collins TDR 94 supporting the transmission of elementary and enhanced surveillance and ADS-B messages. Therefore the aircraft is equipped with an additional L-Band antenna for the transponder transmission. Only the newest revision of this transponder complies with TSO C166b and due to this to RTCA DO-260B capable for the transmission of ADS-B.

Figure 2: Suitable ADS-B Transponder latest revision

To operate a non primary transponder on an airborne system special rules have to be followed according to airworthiness standards. The special and advanced design of the certified aircraft installation ensures that not two targets are visible for the ATC controller. The airborne flight inspection transponder is fully controlled by the flight inspection operator, which enables him to submit special test data via the data-link. This assures proper decoding at the ground segment and/or allows the ground station to perform fully autonomous checks with such specialized data. The AFIS computer is connected to the transponder through a digital data connection. The computer submits automatically the necessary dataset required by the transponder for transmitting the desired and requested ADS-B data.

Different stages of expansion

Since the implementation of ADS-B several different stages have been passed through according to its specification. The basic specification in RTCA DO-260 was update to DO-260A, further to Change 1 and 2 of DO-260A and finally to RTCA DO-260B, which is now the current specification. Its deadlines are mentioned above in this paper.

Capability	DO-260	DO-260A	DO-260B	Comments
NUC (Navigation Uncertainty Code)	✓			Baseline
Mode A Code		✓	✓	Support legacy ATC infrastructure
NACp (Navigation Accuracy Code for Position)		✓	✓	Replaced NUC
SIL (Surveillance Integrity Level)		✓		Replaced NUC
NIC (Navigation Integrity Code)		✓	✓	Replaced NUC
Revise SIL to become Source Integrity Level & add: SDA (System Design Assurance)			✓	Clearly separates the reporting to reflect equipment certification levels and navigation source fault detection capability
Revise NIC/NAC/SIL and add GVA (Geometric Vertical Accuracy)			✓	To improve vertical accuracy, decouple vertical from NIC/NAC/SIL and add GVA
Add ADS-B IN bits			✓	Enhancement to show both UAT IN and 1090ES IN receiver equipage
Changes to the Target State Report			✓	To better align with available aircraft data
Offer non-diversity antenna options for small aircraft			✓	Lower cost of equipage for General Aviation
Revise latency requirement (limit extrapolation)			✓	Enhancement
New guidance on how to determine NACv			✓	Fix
New guidance on how to select the best position/state vector sources			✓	Fix
Changes to the Mode A Code transmission rates			✓	Improvements and squitter efficiencies
Redefine TCAS status bits			✓	Fix
Fixes and improvement to NIC reporting and modified surface movement field for airport surface			✓	Improvements for Surface applications

Figure 3: Changes in stages of expansion

Figure 3 shall highlight the tremendous changes in each development stage of the specification of ADS-B. The data, which are transmitted via ADS-B in the last development stage, are grown enormously and influencing more and more the flight safety segment of each aircraft. Therefore the data content of ADS-B becomes further critical for the aircraft itself and for the receiving parties of the signal.

In the past flight inspection missions have focused on three main tasks, while inspecting the receiving ADS-B ground segment:

- Coverage Checks
- Interference Checks
- Data Continuity and Integrity Checks

The flight checks were most likely performed together or in accordance to the regular radar flight inspection tasks.

Nowadays a new mission for flight inspection is conceivable, which investigates the safety critical nature of the complete ADS-B system concerning its future use in programs like SESAR, NextGen or CNS/ATM.

Dataset transmitted according to ADS-B RTCA DO260B

The ADS-B dataset, which is transmitted via extended squitter specified according to RTCA DO-260B is very extensive. The complex design enables future upgrades and further enhancements. Today the mentioned below data are transmitted, at which only the most important datasets are listed. The data list is separated according to known terms of aircraft implementation stage. The terms are described in detail in the EASA certification specification for airborne communication, navigation and surveillance:

ELS – Elementary Surveillance:

- Squawk
- Altitude
- On Ground Status
- Aircraft Identification (Flight Plan or Registration)
- Special Position Indication (IDENT)
- Emergency Status
- Data Link Capability
- Common Usage GCIB Capability
- ICAO 24-bit aircraft address
- ACAS report

EHS – Enhanced Surveillance (Data in addition to ELS):

- MCP/FCU Selected Altitude
- Roll Angle
- True Tack Angle
- Ground Speed
- Magnetic Heading
- Indicated Airspeed or Mach Number
- Barometric Altitude Rate or Inertial Altitude Rate
- Barometric Pressure Setting (QNH)
- Track Angle Rate or True Airspeed

ADS-B Out (Data in addition to ELS and EHS):

- Horizontal Position (fine and course)
- Horizontal Position Quality (NIC, NAC_P, SIL, SDA)
- Pressure Altitude Quality (NIC_{BARO})
- Velocity over Ground (East/West, North/South)
- Velocity Quality (NAC_V, SIL, SDA)
- Geometric Altitude (WGS84)

- Geometric Altitude Quality, respectively Accuracy (GVA)
- Extended Squitter Version
- Emitter Category
- Length and Width of Aircraft
- GPS Antenna Offset

A real data example in Figure 4 shows that not all information is transmitted respectively shown on this webpage.

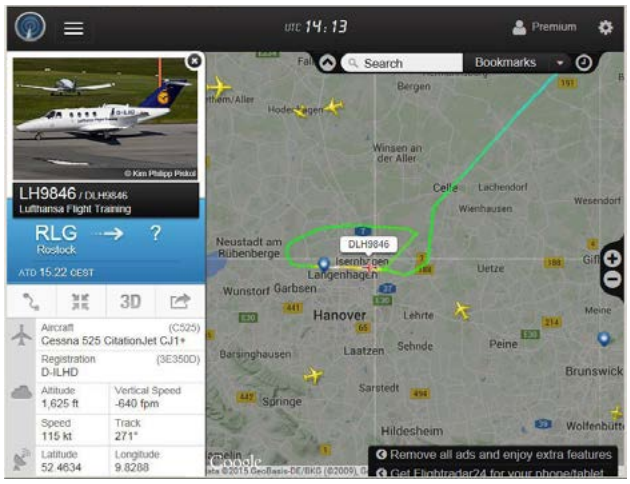

Figure 4: Web page of the ground receiver with ADS-B information

Not all aircrafts are capable of transmitting the complete information. Either this is induced by missing sensors, not connect sensors or due to an old standard of the transponder itself. A set up for such complete installation with all sensors displaying Figure 5.

Figure 5: Aircraft Configuration ADS-B Out

Nowadays a couple of those transponders in general aviation are fully certified according to TSO C166b. Nevertheless, of course the availability of such configurations is growing as we are coming nearer to each individually deadline resp.

ADS-B and flight inspection

In the past the main aspects for flight inspection was to fulfill its tasks according to coverage, interference, continuity and integrity. Modern flight inspection systems are capable to transmit the complete dataset as listed above and can modify this critical data set. This data respectively modified data can be transferred to the ground station to assure correct decoding of the signal and to adjust settings during commissioning. A typical setup for a flight inspection integration of different sensors shows Figure 6.

Figure 6: AFIS Configuration ADS-B Out for calibration purposes.

An example of the flight track on which the desired ADS-B check is monitored and recorded is presented in Figure 7. This graphic and its alphanumeric values are compared automatically to the graphics and recordings of the ground station.

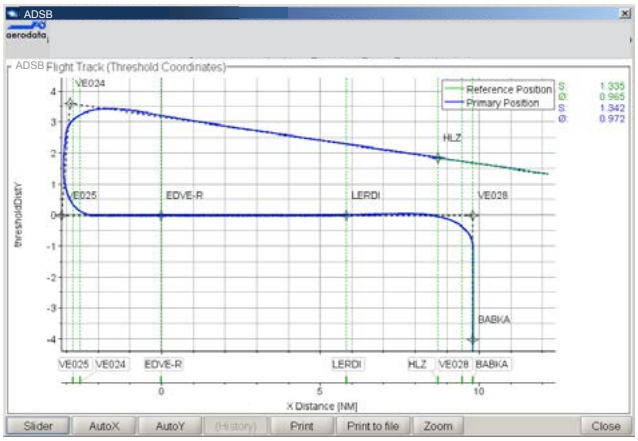

Figure 7: Flight track of flight inspection mission with monitored ADS-B information

In Figure 8 to 11 examples from the AeroFIS© of control pages of the graphical user interface are shown for the ADS-B management. For testing purposes data can be modified to a different value or to the actual pertinent value derived from the primary avionic of the aircraft.

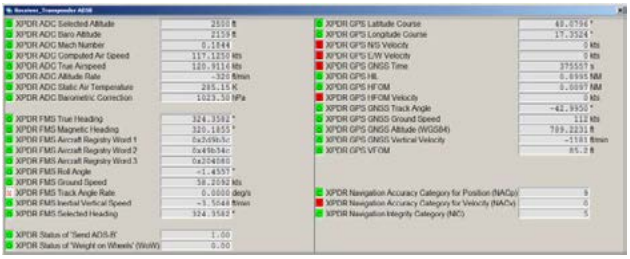

Figure 8: ADSB Out transponder data

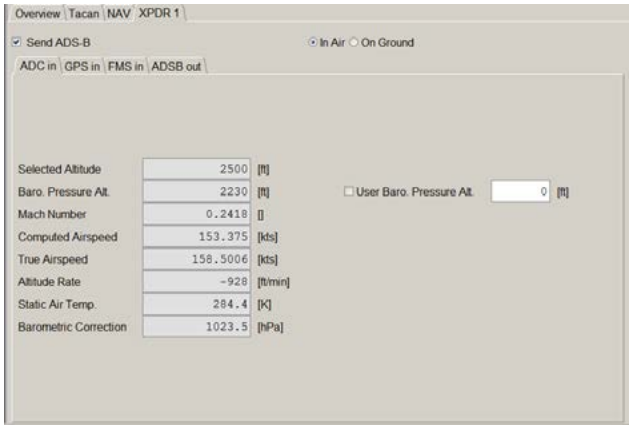

Figure 9: ADC input data

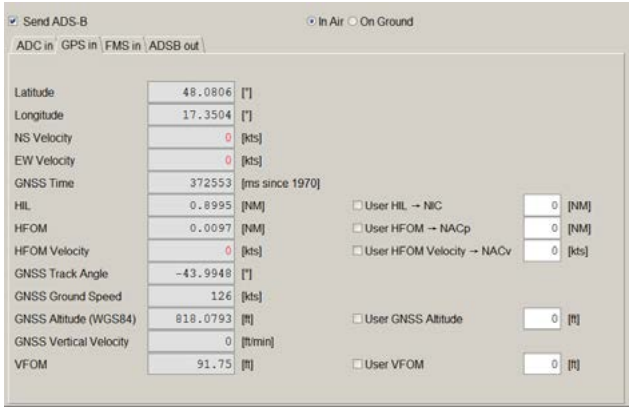

Figure 10: GPS input data

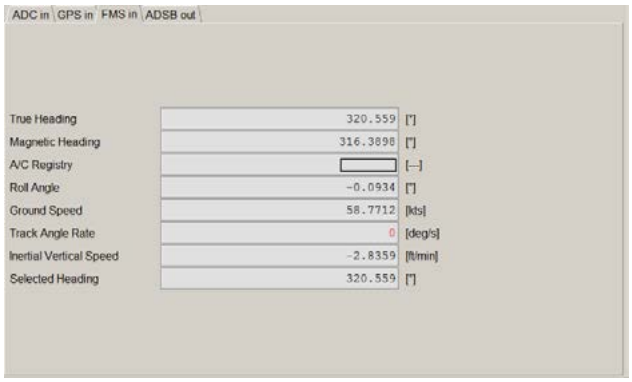

Figure 11: FMS input data

Of course modified ADS-B transmission has to be communicated in advance with ATC and has to follow the regulations of each country. A closer look into the sensitivity of this data and into the growing influence on secure air traffic management and surveillance reveals the growing field of flight inspection regarding ADS-B. The data sets of the above displayed figures could be easily modified by the flight inspection operator, either through a predefined procedure or by simply choosing the typed in value in the text field. Also position critical data can be modified in the airborne flight inspection system. This will allow the receiving ground base to simulate the procedures which are caused by an integrity problem or any other problem of an airliner. Not only the value can be verified, also the routine, the process behind it and the action, which is required to assure the dedicated safety or integrity. As visible in Figure 8 the Navigation Accuracy Category (NAC_P) for the position can be manipulated in parallel. This enables air traffic control to cross check the dedicated recovering procedures. The complete internal path at air traffic management starting with recognizing the error, initiating dedicated procedures and the required action can be verified in regard to its correct function.

Conclusion

Because of the required and intended improvements for the surveillance of aircrafts in aviation regarding air traffic control, and the growing capability of the ADS-B and its key function regarding large programs like SESAR, NextGen or CNS/ATM, it is mandatory to flight inspect the ADS-B ground segment. Flight check of these data including simulate special procedures will become compulsory, if ATC has to relay on these data safety wise and if this safety relevant data is steadily increasing.

The future development for this surveillance, situation awareness and information technique is not easily foreseeable yet. The growing capacity in conjunction with possibilities for ATC improvement will definitely require flight inspection for these new procedures in the future.

References

[1] ICAO Annex 10, Vol IV – Surveillance and Collision Avoidance Systems, Fourth Edition, 2007

[2] ICAO Doc 9871 – Technical Provisions for Mode S Services and Extended Squitter, Second Edition, 2012

[3] EASA Web Page – http://easa.europa.eu

[4] FAA Web Page – http://www.faa.gov

[5] CASA Web Page – http://www.casa.gov.au

[6] Eurocontrol Web Page – https://www.eurocontrol.int

IFIS2016

Bringing Together Theory and Practice

Session 6

Safety Concepts and F.I. Organization Certification

ICASC Document on Standards and Recommended Practises of Flight Inspection & Flight Validation Organisations

Capt Thomas Wede

TransPolar GmbH

Eickhorstweg 11
D - 38110 Braunschweig
Germany

Tel. + 49 - 172 - 430 58 03
e-mail t.wede@transpolar.de

ABSTRACT

The following paper continues from the papers and presentations given at the IFIS 2012 in Braunschweig and the IFIS 2014 in Oklahoma City by the same author, which covered aspects of flight safety on flight inspection and flight validation missions, and ways to mitigate risks associated with flying these particular types of missions. The new paper represents the status of discussions the Operational Working Group within ICASC reached on this topic to this day.

After some detailed discussion among members, both of ICAS in general as well as among the Operations Workgroup of ICASC, this work group is now able to present a first version of an ICASC document that deals with Standards and Recommended Practises of Flight Inspection & Flight Validation Organisations.

The content of the document will be introduced – aspects like Equipment, Theatre of operation, Operation Manuals, Standard Operating Procedures (SOPs), Check Lists and Crew Coordination Concepts – and the recommendations given in the document being elaborated in detail. The main driver behind the proposed standard is explained in more detail:

The idea behind these 2 documents is to enhance safety in our industry by providing a level playing field with regard to operational standards and practises. To that end the paper will introduce an additional tool in the shape of a Contract Annex to Flight Inspection tender documents and contracts, a document that describes the minimum standards any potential bidder for flight inspection and flight validation work should address, with this Annex to be distributed within the industry and all potential customers, again with the ultimate aim to provide a level - and safe! - playing field for all stakeholders.

INTRODUCTION

As the main aspects of this topic are covered in the two documents cited above, this introduction will be kept to a minimum. Attention of the valued reader is drawn to the attached documents "*ICASC Document on Standards and Recommended Practises of Flight Inspection & Flight Validation Organisations*" and "*ICASC Recommended Flight Inspection & Flight Validation Contract Annex*", which are given unde r Appendix A resp. B of this paper.

As the pros and cons of the recommended standards and recommended practices in flight inspection and flight validation operations have been discussed in some detail in the two previous papers and presentations of this author, this paper focusses on the introduction of a proposed new tool, an annex to any new flight inspection and flight validation contract.

CONTRACT ANNEX

The idea of a contract annex picks up on a scheme our colleagues from the International Airborne Geophysics Safety Association (IAGSA) developed over the years, with the latest edition published I May, 2014.

IAGSA faced a challenge similar to our industry, with an operational environment spelling a certain degree of risk, mainly in the shape of low level flying, for a prolonged period of time, at in same cases remote areas of the world with little support in terms of ATC infrastructure or any aviation related infrastructure to start with.

The challenging operational environment of airborne geophysics applications like photogrammetry, aeromagnetic survey, etc., warrants a considerable effort for those organisations that take up on this challenge: due investments in equipment, crewing, training and operational considerations are required to take these challenges seriously.

More often than not operators willing to commit to these investments found themselves in an economically unviable position, as addressing issues like proper equipment, training etc. inevitably invokes a higher cost bases, which in turn commercially favors operators that are not willing to invest in these areas.

When accident numbers rose to level unacceptable to the industry any longer, most of the stakeholders involved agreed to a common set of standards, prescribed in both IAGSA's Safety Manual as well as their published Contract Annex.

The interesting part here to note is that this agreement on common standards did not only cover all operators, but most of all potential customers as well: by agreeing on the aforementioned contract annex, most of the customers in the airborne geophysics environment acknowledged the fact that the risks involved in their particular kind of required services called for a commonly agreed upon standard.

The way of turning this acknowledgment into practical consequences was by first: developing the contract annex and commonly agreeing on the required minimum standards and then second: making this contract annex an integral part of all contracts out for bidding and their associated tender documents. With that move a vitally important level playing field was established for all stakeholders, enhancing safety considerably by not commercially disfavoring operators any more that take issues like proper equipment, crewing and training seriously.

CONCLUSIONS

Apart from a common set of standards and recommended practices, IAGSA's approach of developing these standards being incorporated in any potential contract as a base requirement bears a lot of promise to foster and enhance safety in our industry as well, which is why ICASC is promoting this concept and putting it up for further discussion within our industry.

RECOMMENDATIONS / FUTURE WORK

Future work on the issue of common standards and recommended practices (SARPs) and the proposed contract annex should focus on two aspects:

With the SARPs being recognized by ICASC as a common set of tools, the question to discuss with industry is how to proceed from here: does it suffice to publish the SARPs on the ICASC's webpage, or shall this concept be developed into a full industry-recognized concept by turning it into an officially granted "seal of approval? Who would be "owner" of this concept or the issuer of this approval? And how to address the cost implications that would inevitably go with an approval like this, bearing in mind that in will invoke some form of audit/approval/monitoring process?

The second aspect is the question of how to proceed with the proposed and highly recommended Contract Annex: here, more discussions are required with all stakeholders involved within our industry. Would most of the potential customers of flight inspection and flight validation services be willing to subscribe to a concept like that?

REFERENCES

[1] Thomas Wede, 2012: Flight Safety on Flight Inspection Missions – Past Statistics and Future Strategies
Proceedings of the 17th IFIS, Braunschweig, 2012

[2] Thomas Wede, 2014: Common Standards in Flight Inspection Operations – The Way Ahead to Improve Safety?
Proceedings of the 18th IFIS, Oklahoma City, 2014

[3] International Airborne Geophysics Safety Association, 17/06/2014: Safety Policy Manual

[4] IAGSA Survey Contract Annex Last Revised 29/5/2014 Revision 3

[5] www.iagsa.ca

Appendix A:

International Committee on Airspace Standards and Calibration (ICASC) :

Document on Standards and Recommended Practises of Flight Inspection & Flight Validation Organisations

Vers 1.2

Introduction

Flight Inspection and Flight Validation represents a rather demanding operational environment in aviation. Its very nature translates into a certain amount of risk elements – which are covered in one of the following chapters - that have to be identified, addressed and subsequently mitigated in order to achieve a safe and reliable flight operation.

The tools to mitigate these risks are wide and varied. This document tries to identify these tools, concentrating on the organisational set-up and environment of a flight inspection entity. Each chapter contains ICASC recommendations for addressing risk mitigation. The idea is to arrive at a common set of tools that are useful in achieving the goal of a safe flight inspection flight operation.

A. General Set-up

Objective: paramount to a safe execution of flight inspection missions is a coherent set-up of the organisation, where size, staff numbers, management, equipment, mission profile and theatre of operations are in line, and no ambiguities exist, i.e. staff numbers or other resources insufficient for the intended missions to be flown over the year. Government organisations might have a tendency to be over-bureaucratic and/or underfunded; private organisations might have a tendency to be overly ambitious in economic terms; both tendencies will put unnecessary stress on the organisation and must be avoided.

ICASC Recommendations:

A1. Have a clearly defined set-up, where size, staff numbers, management, equipment, mission profile and theatre of operations are in line with the intended operation, and no ambiguities exist.

A2. Due to the fact that flight inspection missions are time-critical, ICASC recommends to have a back-up solution in place in case the own resources (aircraft, qualified staff) are unavailable.

B. Organisational Set-up

Objective: the organisational set-up, in a way, clearly reflects if an organization is aware of what it is doing and is organizing itself accordingly. The items in questions below go along that line. A clearly defined path of accountability, and a management structure that goes in line with it, are paramount.

ICASC Recommendations:

B1. Establish an organizational set-up that follows the requirements below in a clear and unambiguously manner.

B2. Establish a clear way of communication that set-up, best in a comprehensive Operations Manual OM.

B3. Publish a clearly defined Statement of Work

B4. Establish a clearly defined path of accountability and management structure. Communicate this structure unambiguously

B5. Establish a clearly defined path of responsibilities: Clearly establish asset allocation, position titles, roles and responsibilities, training requirements, as well as Operational Control and Maintenance.

B6. Establish Operational Control and maintain it.

B7. Publish a clearly defined set of rules, procedures and best practises, best laid down in an OM

B7. Establish a clearly defined Change Management / Administration and Program Management Plan in place.

B8. Establish an Emergency Response Plan in place

C. Safety Philosophy / Safety Management System

Objective: A Safety Philosophy, and accompanying Safety Management System (SMS), are the formalized approach of an organization on how to implement safety, clearly defining risk identification methods and tools, risk communication and mitigation strategies, lines of responsibilities and accountability, which are precursors for demonstrating proper organizational risk awareness and increasing overall mission effectiveness. The Safety philosophy of an organization must be a top-down approach, spearheaded by management with a demonstrated and unwavering commitment independent profits and mission success rates. . The SMS should be part an integral part of the OM (preferred option, to avoid

over-complexity), or may be a stand-alone document. The associated Reporting System (RS) does not have to be overly complex with sophisticated forms, as long as it is formalized in one way at all. Just Culture has to be clearly communicated, promoted and executed under all circumstances. Just Culture in the context of aviation means a culture within an entity / organisation that is tailored towards identifying / mitigating risk through an atmosphere of open communication, transparency and non-punitive action, with a clear focus of avoiding / mitigation weak spots within the organisation instead of apportioning blame.

ICASC Recommendations:

C1. Have a Safety Philosophy and a Safety Management System that goes with it .

C2. Live the top-down-approach to safety even in (economically) harsher times.

C3. Encourage a healthy communication on mishaps by a viable Reporting System (RS) and an actively lived Just Culture.

C4. Avoid over-complexity by integrating the SMS into the OM.

D. Flight Operations : Operating Limits

Objective: Operating limits form an essential part of any safety philosophy. The minimum objectives to be covered are set below. It is paramount that the operating criteria be directly related to the organization's mission set. Here, a balance between safety and operational requirements has to be struck: Minima with an excessively high threshold will enhance safety, but will limit the operation up to a point where providing a reliable service to the customer will be impossible. The goal is efficient risk mitigation as there is no way to eliminate risk all together

Again, operating limits have to be accepted by all stakeholders from top down; raising minima and expecting the same productivity output, for instance, will not be a realistic prospect.

Therefore, operating limits should be set after careful study of the operational environment to be expected, equipment to be used and crew qualification considered. The limits have to be open, transparent, clearly communicated and no ambiguities must exist between the organization's ambitions and targets and its operating limits.

ICASC Recommendations:

D1. Have Operating Limits established according to the objectives above.

D2. Operating limits must reflect and bring in line the organization's objectives with mission profile, equipment, and crew requirements, especially in the light of qualification, training, recurrency status and FTLs.

D3. The Operating Limits must reflect the operational environment of the organisation

D4. Have established Flight and Rest Time Limitations (FTLs)

D5. FTLs must reflect individual operational circumstances and requirements of the affected organisation.

D6. Have Weather minima defined

D7. Have Minimum Equipment status and requirements defined

D8. Have defined Crew qualification, training and recurrency standards

D9. Have Airport criteria established

D10. Have defined Security criteria

D11. Have Night Ops specified

D12. Have established a clear, unambiguously method of communicating these limitations, best via OM

E. Equipment

Objective: Picking the proper equipment is an essential factor affecting safety on flight inspection / flight validation missions.

Aircraft: In light of the wide variety of flight calibration missions and theatres of operation, there is no one-size-fits-all solution in picking the right aircraft, however, the selected aircraft type should be able to fly the mission required without restrictions (i.e. fuel load, payload), in order not to pressure crews into accepting risks beyond means of mitigation, just to get the mission done. The aircraft selected must be capable of handling the environmental conditions of the intended theatre of operations (weather hazards, heat, cold, icing conditions, etc.).

The performance of the aircraft selected must be in line with the task at hand, this concept is even more important for Flight Validation missions, where the performance of the validation aircraft must be commensurate with the

performance of the aircraft that will later fly the validated procedures.

The FIS to be used must be commensurate with the task at hand, and must be integrated with fixed aerials that are subject to regular on-aircraft-calibration.

Maintenance Maintenance must be fully integrated into the safety philosophy, executed by appropriately qualified and trained staff, at the proper intervals. The flight inspection aircraft in use should be maintained and upgraded to the current, mission-specific requirements.

The paramount driver behind the Cockpit Environment is the requirement to provide maximum Situational Awareness. Glass cockpits, suitable Flight Management Systems (FMS), interface between FIS and cockpit, TCAS, EGPWS all work towards that goal.

The Environmental System of the aircraft used must be capable of coping with the environmental conditions of the theatre of operation (sufficient cooling, heating, etc.).

ICASC Recommendations:

E1. Aircraft utilised must be in line with mission profile and mission environment.

E2. ICASC recommends multi engine aircraft for flight inspection / flight validation missions.

E3. Aircraft in use should be upgraded, and must be maintained, to the current, mission-specific requirements.

E4. The Maintenance provider must be able to support aircraft in all theatres of operation.

For the benefit of Situational Awareness, ICASC recommends:

E5. Glass cockpits and their associated Moving Map Displays

E6. An interface between FIS and the cockpit, either by utilising the existing avionics or by providing an additional display

E7. a suitable FMS

E8. In case the aircraft is used for Flight Validation Missions as well, the FMS must be capable of handling all relevant ARINC424 formats used on the new procedure under validation, and must be capable of depicting them properly; the autopilot must be capable of following these signals

E9. TCAS

E10. In case an EGPWS is installed, there must be means available to silence it on flight inspection missions in order to avoid nuisance alarms.

E11 The environmental system of the aircraft must be capable of coping with the environmental conditions of the theatre of operation, both in terms of cooling and heating, in order to cater for requirements both of the crew as well as integrity requirements of the FIS Nav receivers.

E12. The FIS must be integrated with fixed aerials, which are in turn subject to regular, on-board calibrations (see chapter F for FIS Requirements)

E13. For Flight Validation Missions, the use of Pre-Production-databases for the relevant Flight Management System FMS is required

F. Crewing

Objective: Defining adequate crew qualification and composition and finding the staff that meet these requirements is an essential part of the overall safety concept of a flight inspection organization.

ICASC Recommendations:

F1. Define crew qualification and skill sets required for the intended mission profile.

F2. As a minimum requirement for commanders, and in line with ICAO Doc 9906 Vol 6, ICASC recommends the following qualifications as a guideline:

- CPL/IR or ATPL
- Current type rating for the type to be flown on mission
- Total flight time > 1.500 hrs
- Command time > 400 hrs
- Flight Inspection Pilot > 2 years

F3. Define adequate selection process

F4. Use adequate tools for the selection process.

F5. Minimum crew on Flight Inspection / Flight Validation missions: 2 pilots, or define applicable means of compliance

F6. Define crew composition.

F7.Define status of Cabin Crew / Nav Aid Inspectors .

G. Operational Status

Objective: A number of flight inspection missions are outside the normal operating envelope of the aviation community (i.e., in some countries, flying below the Minimum Safety Altitude, night flying activities, special Noise Certificates, or waivers stipulating dispense from these Noise Certificates, etc.). In many case this stipulates a requirement for official approval of these kinds of operations.

ICASC Recommendations:

G1. Have Operational status defined and approved by Regulator / Authorities

G2. It is recommended that the affected flight inspection organisation applies for all relevant approvals or "waivers" by the appropriate authorities, to minimize ambiguities and potential risk of violating rules and regulations, which in turn is essential to reduce workload and stress on crews.

I. Quality Management System (QMS)

Objective: A Quality Management System (QMS) is an essential part of any flight inspection organization. Most regulatory frameworks address this requirement – an AOC holder is required to set up a QMS, for instance. A QMS is highly desirable for tracking the performance of, and thus providing integrity for, the flight inspection mission itself, thus providing clarity on issues like ownership of calibration reports, data integrity, and postflight processing.

ICASC Recommendations:

I1. Have a QMS in place, including a relevant Audit program and procedures defining how to act on audit findings.

I2. ICASC recommends the QMS be an integral part of the overall OM of an organization, thus reducing complexity in the organization's documentation.

J. Operations Manual

Objective: The Operations Manual (OM) is the central document of an organisation as it defines all aspects of the flight operation and communicating the way it intends to do business with all relevant stakeholders. Its format, structure and extent, to a certain degree, will be driven by the individual requirements of the regulator in charge of that particular entity.

Numerous layouts and templates for an OM exist within the industry; however, the industry standard is outlined below:

ICASC Recommendations:

J1. Have an OM in place as the central way to document and communicate the scope of work and how to accomplish it.

J2. The OM should be concise and limited to the absolute minimum necessary, in order to avoid over-complexity, which in turn would only create a work atmosphere of ambiguity and unnecessary workload.

J3. The OM must incorporate all operational circumstances organizational operations.

J4. Minimum objects to be covered:

- Organisational set-up
- Responsibilities and accountabilities
- Theatre of Operations
- Aircraft related subjects (Minimum Equipment List (MEL), navigation equipment, etc.)
- Limitations and Minima
- Crewing
- Operational Procedures, Normal and Abnormal
- All weather operations
- Flight and Rest Time Limitations
- Training
- Security

K. Crew Resource Management (CRM) / Team Resource Management (TRM) / Crew Coordination Concept (CCC)

Objective: Crew Resource Management (CRM), and a Crew Coordination Concept (CCC) defines how a crew is to work together, and clearly defines the roles and responsibilities of each crew member. It clearly describes the communication involved in executing these tasks and should be reinforced by Standard Operating Procedures (SOPs) and Checklists (see chapter 11 & 12 of this document). The CRM system, however, does not only define the cooperation between cockpit members, it also should encompass procedures and communication between cockpit and cabin, and it should define the interface between the flight crew and the rest of the company, like tasking / scheduling, management, maintenance, etc. This holistic approach in CRM is of great importance to create a working environment that takes into account all requirements to accomplish the organization's mission profile safely and reliably. It effectively translates into a Team Resource Management (TRM).

ICASC Recommendations:

K1. Have a CRM / CCC in place.

K2. Base it on a holistic approach that does not only cover aspects of flight crew coordination, but all other relevant stakeholders within the organization as well.

K3. CRM should be holistic, = Total Resource management (TRM), i.e. encompasses cabin crew and rest of organization as well.

L. Standard Operating Procedures (SOPs)

Objective: Standard Operating Procedures (SOPs) describe how certain aspects of the scope of work are handled by whom, and at what time. SOPs govern aspects like cockpit work, crew coordination, checklist philosophy, but also issues like how to execute certain calibration profiles, how to schedule tasks, write reports, etc. SOPs should be commensurate with the task at hand. They should be concise, transparent, and whenever possible, be an integral part of the OM.

ICASC Recommendations:

L1. Define SOPs to describe how certain aspects of the scope of work are handled by whom, and at what time within the organization.

L2. Keep SOPs concise and transparent.

L3. SOPs must be in line with other documents, like the OM, CCC, checklists, etc.

M. Checklists

Objective: Checklists form an enormously important part of the operating environment. It is a well-known fact that the manufacturer's checklists, especially when the aircraft in question is certified for single pilot operations, are often less then optimal in a normal aviation environment for reasons of over-complexity and length. These checklists reflect legal and liability issues, which might be well required to keep the manufacturer from harm in legal terms, however, focusing on these legal aspects unfortunately renders these checklists almost useless. As check lists are vital for crew procedural standardization every operator is called upon to design checklists that do reflect its individual needs. Depending on the regulatory environment it might be necessary to get the altered checklist approved by the respective regulator.

ICASC Recommendations:

M1. Define checklists in a way as to reflect the operational environment the specific missions are flown in.

M2. Avoid over-complexity.

M3. The checklists have to be in line with SOPs and other procedures laid down in the OM.

M4. They have to be workable under all circumstances the organization is flying in!

M5. Both Normal and Abnormal / Emergency Checklists should be defined by operator

M6. Checklist philosophy: Do vs. Follow-up Checklists

N. Training & Checking

Objective: The importance of training in aviation in general, and in flight inspection in particular, cannot be overstated. Every flight inspection organization should establish a training scheme, covering both initial as well as recurrent training, and execute it rigourously. This translates into a certain commitment from all stakeholders involved, including management, as training inevitably has cost implications. The training regime should not only cover flight crews, but all other staff members involved in flight operations as well. It must reflect the individual, mission specific requirements, that are not normally covered by a routine training program provided by training organizations.

Aspects to be covered are addressed by the following items:

ICASC Recommendations:

N1. Define and implement training scheme for both initial as well as recurrent training.

N2. Training should be regime described (i.e. in Part D of OM)

N3. Training must reflect and be in line with other organization's documents, like OM, CCC, Checklists, etc.

N4. Training should cover not only crew training, but all pertinent aspects of organization's activities, like OPS, scheduling, etc.

N5. ICASC strongly recommends use of suitable qualified simulators for flight training, both initial as well as recurrent, to the maximum extent possible

N6. Whenever possible, customized training programs should be employed,

N7. Training should always be a tp-down commitment

N8. Training should reflect the equipment to be used

N9. For No-Tech-Training: Cabin Crews should be involved as well

O. Risk Mitigation Strategy

Objective: The Risk Mitigation Strategy of an organisation is a pro-active approach, via a risk assessment, of the individual risks associated with a specific mission, with the goal to arrive at a strategy to minimize or avoid these risks all together. Any risk mitigation strategy shall address the external circumstances of the operation: where do we operate, doing what with whom? How is the terrain, how is the infrastructure (fuel / de-icing / hangar available)? How well is ATC organized, is radar coverage given? Who on a specific mission will be point of contact for the company? Who for the crew? How is the security situation on site / in country? Whenever possible, these data should be collated prior bidding for a tender; marketing or management should try to find out as much information as possible prior committing to a task, in order to reduce crew pressure on site later.

Crew fatigue is another major issue to be addressed: At what point fatigue hits will very much depend on the type of mission flown (for instance, ILS low level work, in general, is more stressful than airway work at high altitudes), the aircraft being used (Cockpit equipment available, space available on board, susceptibility to turbulence, temperature control) and the environment operated in (poor ATC? poor infrastructure, i.e. refueling a major undertaking? Night flying involved?). Thus, geographical and climatological conditions of theatre of operation, length of deployment, transit times and other factors, like aircraft and cockpit equipment or even accommodation should be taken into account when executing a risk assessment and designing a risk mitigation strategy (which, in this case, would be an organization-specific a FTL scheme).

ICASC Recommendations:

O1. Have a Risk Mitigation Strategy in place as a good indicator of one's organization being aware of its mission profile and its associated risk.

O2. It should, as a minimum, have the factors cited above covered.

O3. The external circumstances of operation and associated risk must always be identified.

O4. A Risk Assessment should always be completed prior to bidding for a contract.

O5. As a risk reduction exercise, a FTL scheme should be in place.

Appendix B:

ICASC Recommended Flight Inspection & Flight Validation Contract Annex

Vers 0.2

Introduction

Flight Inspection and Flight Validation represents a rather demanding operational environment in aviation. Flying low or even very low at times, in congested airspace shared by platforms operated at varying airspeeds from ultralight and gliders to heavy airliners, under considerable time pressure to keep the impact of the Flight Inspection mission on the rest of the community as low as possible - this very nature of Flight Inspection and Flight Validation work translates directly into a certain amount of risk elements that have to be identified, addressed and subsequently mitigated in order to achieve a safe and reliable mission outcome.

In providing this level of safety, both the customers of Flight Inspection and Flight Validation services (Customers) as well as the provider of these services, the Flight Inspection and Validation service providers (Contractors) share a responsibility to achieve a Duty of Care to ensure the highest level of safety is achieved on every mission.

In order to achieve this level of safety, this Annex is an integral part of the process for tendering for Flight Inspection and Validation services. This Annex addresses a number of mission specific requirements to which all contractors must adhere. It is based on the safety framework ICASC has developed and defined as the standards in Flight Inspection and Flight Validation operations. Further guidance on this matter may be taken from ICASC webpage under www.icasc.com.

In light of the aforementioned Duty of Care, this Annex serves 2 purposes:

1. It identifies and thus addresses the inherent risk elements of the Flight Inspection and Flight Validation work at hand

and

2. It provides a level playing field for all potential contractors, as adhering to high standards in flight operations inevitably involves a higher cost base by higher expenditure on training, equipment and restrictions on operating parameters

In order to achieve the aforementioned goals of safety, this Annex requires any potential contractor bidding for a specific Flight Inspection or Flight Validation contract to meet the following requirements:

A. General Set-up

The Contractor shall have in place a clearly defined set-up, where size, staff numbers, management, equipment, mission profile and theatre of operations are in line with the intended operation, with no ambiguities.

Due to the fact that Flight Inspection missions are time-critical, this Annex requires to have a back-up solution in place in case the own resources (aircraft, qualified staff) are unavailable.

B. Organisational Set-up

The Contractor shall have in place an organisational set-up that clearly reflects that its organization is aware of what it is doing and is organizing itself accordingly. A clearly defined path of accountability, and a management structure is paramount. Factors to address this requirements are at least, but not limited to

B1. Establish a clear way of communicating its set-up, best in a comprehensive Operations Manual OM.

B2. Establish a clearly defined Statement of Work

B3. Establish a clearly defined path of accountability and management structure. Communicate this structure unambiguously

B4. Establish a clearly defined set of rules, procedures and best practises, Clearly outlined in a comprehensive Operations Manual in an Operations Manual (OM)

B5. Establish a Safety Philosophy and a Safety Management System

B6. Establish an Emergency Response Plan in place

In order to meet the requirements under B., this Annex requires any potential Contractor to operate under an approved Air Operator Certificate (AOC) by its respective Authority, or provide an equivalent level of compliance.

C. Flight Operations

Any potential Contractor for a specific Flight Inspection and Flight Validation Contract shall meet the operational requirements as laid down in the following Annexes chapters:

C1. Operating Limits

The Contractor shall

C.1.1. Establish Operating Limits according to the objectives above.

C.1.2. have his operating limits reflect and align with the organisation's objectives in terms of mission profile, equipment, and crew requirements, especially to include

qualification, training, recurrency status and Flight Time Limitations (FTLs).

C.1.3. have his Operating Limits reflect the operational environment of the organisation

C.1.4. Establish Flight and Rest Time Limitations (FTLs). These FTLs must reflect individual operational circumstances and requirements of the affected organisation.

C.1.5. have Weather minima defined

C.1.6. have Minimum Equipment status and requirements defined

C.1.7. have defined Crew qualification, training and recurrency standards

C.1.8. have Airport criteria established

C.1.9. have defined Security criteria

C.1.10. have Night Ops specified

C.1.11. have established a clear, unambiguously method for communicating these limitations, such as an OM

D.1 Equipment

The Contractor is obliged to meet equipment requirements as follows:

D.1.1. All aircraft utilised must be in line with mission profile and mission environment.

D.1.2. This contract stipulates the use of multi engine aircraft for Flight Inspection / Flight Validation missions.

D.1.3. Aircraft in use are be upgraded, and must be maintained, as best as possible to the current, mission-specific requirements.

D.1.4. The Maintenance provider for the aircraft of the Contractor must be able to support the aircraft in all theatres of operation.

For the benefit of Situational Awareness this Annex requires:

D.1.5. Glass cockpits and Moving Map Displays

D.1.6. An interface between Flight Inspection System (FIS) and the cockpit, either by utilising the existing avionics or by providing an additional display

D.1.7. a suitable FMS

D.1.8. In case the aircraft is used for Flight Validation Missions as well, the FMS must be capable of processing and displaying all relevant ARINC424 formats used on the new procedure under validation, the autopilot must be capable of following these signals

D.1.9. TCAS installed

D.1.10. If an EGPWS is installed, there must be means available to silence it on flight inspection missions in order to avoid nuisance alarms.

D.1.11 The environmental system of the aircraft must be capable of coping with the environmental conditions for all theatres of operation, both in terms of cooling and heating, in order to cater for requirements both of the crew as well as integrity requirements of the FIS Nav receivers.

D.1.12. The FIS must be integrated with fixed aerials, which are in turn subject to regular, on-board calibrations

D.1.13. For Flight Validation Missions, the use of Pre-Production-databases for the relevant Flight Management System FMS is a must.

E.1 Crewing

The Contractor shall

E.1.1. define crew qualification and skill sets required for the intended mission profile.

E.1.2. have a minimum crew on Flight Inspection / Flight Validation missions: 2 pilots, or define applicable means of compliance

E.1.3.define status of Cabin Crew / Nav Aid Inspectors .

F.1 Quality Management System QMS

The Contractor shall

F.1.1 have a QMS in place, including a relevant Audit program and procedures how to act on findings of these audits.

G.1 Operations Manual

The Contractor shall

G1.1. have an OM in place as the central way to document and communicate the scope of work and how to accomplish it. The OM has to be workable under all of the Organisation's operational circumstances , and shall cover, as a minimum, but not limited to, the

- Organizational set-up
- Responsibilities and accountabilities
- Theaters of Operation

- Aircraft related subjects (Minimum Equipment List (MEL), navigation equipment, etc.)
- Limitations and Minima
- Crewing
- Operational Procedures, Normal and Abnormal
- All weather operations
- Flight and Rest Time Limitations
- Training
- Security

H.1 Crew Resource Management (CRM) / Team Resource Management (TRM) / Crew Coordination Concept (CCC)

The Contractor shall

H1.1. have a CRM / CCC in place. Its CRM should be holistic in the sense of a Total Resource Management (TRM) scheme, i.e. encompasses cabin crew and rest of organization as well.

I.1 Standard Operating Procedures (SOPs)

The Contractor shall

L1.1. define SOPs to describe how certain aspects of the scope of work are handled by whom, and at what time within the organisation.

L1.2. SOPs must be in line with other documents, like the OM, CCC, checklists, etc.

J.1 Checklists

The Contractor shall

J1.1. Develop mission-specific/operational environment checklists

J1.2. have the checklists to be in line with SOPs and other procedures laid down in the OM.

J1.4. ensure the Checklist actions are achievable under all expected flight operations and conditions

K.1 Training & Checking

As the importance of training in aviation in general, and in Flight Inspection in particular, cannot be overstated, the Contractor shall

K1.1. define training scheme for both initial as well as recurrent training and adhere to that scheme.

K1.2. develop and implement a training program commensurate with other organisation's documents, like OM, CCC, Checklists, etc. . which does not only cover crew training, but all aspects of organisation's activities, like OPS, scheduling, etc.

K1.3. Contractors are to use suitably qualified simulators (either Full flight Simulators (FFS) or other Flight Training Devices (FTDs)) for flight training, both initial as well as recurrent.

L.1 Risk Mitigation Strategy

The Contractor shall

L1.1. Develop and implement a Risk Mitigation Strategy which encompasses all mission profiles and expected conditions

L1.2. identify the external circumstances of operation and associated risk

IFIS2016

Bringing Together Theory and Practice

Session 7

PBN (SBAS / GBAS / RNP …)

Dynamic Measurement Uncertainty for Runway Fix

Gary A. Flynn
Lead Engineer, Airborne Computer Applications
Federal Aviation Administration
Air Traffic Organization
Flight Inspection Services
Oklahoma City, Oklahoma, USA
Fax: 405 954 4043
E-mail: gary.a.flynn@faa.gov

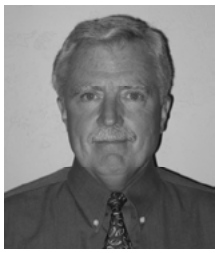

ABSTRACT

This paper describes the method used to compute measurement uncertainty in the airborne survey of latitude, longitude, and elevation of runways used for RNAV (GPS) and RNAV (RNP) approaches.

Measurement uncertainty has traditionally been estimated as a fixed value; however, the uncertainty with RNAV measurements of interest can be large with respect to desired tolerances. The independent error sources for each measurement are determined as a function of flight parameters and GNSS/SBAS conditions. The current conditions are then used to determine the confidence interval for each measurement of runway fix latitude, longitude, and elevation. This provides valuable information to the flight inspection crew regarding the quality of the flight inspection results for each run.

INTRODUCTION

As part of the RNAV inspection development effort, it has become necessary to estimate the dynamic accuracy of Runway Fix Processor (RFP) positioning as well as GPS-based positioning. These two position solutions are combined when measuring runway landmark locations.

This paper will first describe the estimation of the GPS-based positioning accuracy. This will be followed by a discussion of the contributors and magnitudes of the errors associated with the RFP. Finally, these two uncertainties will be combined into an overall assessment of the runway survey accuracy.

It should be noted that, within this paper, all of the error values are to be considered 2σ estimates.

GPS ACCURACY ESTIMATION

The parameter used to evaluate SBAS accuracy is the current vertical protection limit provided by the GPS receiver. The formula used to estimate vertical uncertainty is:

$$e_{SBAS}^{UP} = 0.0417 \cdot VPL + 0.43m$$

Where,

VPL = SBAS vertical protection limit (provided by GPS receiver)

e_{SBAS}^{UP} = Vertical position error, contiguous US (CONUS) average = 4.12 ft

Cross-track uncertainty will be either 60% of vertical uncertainty or 3 ft, whichever is greater.

$$\acute{e}^{XTK} = 0.6 \cdot e_{SBAS}^{UP}$$

$$e_{SBAS}^{XTK} = 3ft \quad |\acute{e}^{XTK} \leq 3ft$$
$$e_{SBAS}^{XTK} = \acute{e}^{XTK} \quad |\acute{e}^{XTK} > 3ft$$

Where,

$\acute{e}^{XTK}$ = VPL-based cross-track position error

e_{SBAS}^{XTK} = Cross-track position error

Along-track uncertainty will be the same as cross-track except an additional 1-ft orthogonal vector will be included to compensate for timing uncertainty.

$$e_{SBAS}^{ATK} = \sqrt{{e_{SBAS}^{XTK}}^2 + 1\,ft^2}$$

Where,

e_{SBAS}^{ATK} = Along-track position error

RFP ACCURACY ESTIMATION - BASICS

Although the FAA estimates uncertainty for both the camera-based and pilot-fix solutions, only the camera-

based solution will be discussed here. This was done in order to hold this paper to a reasonable length.

The following analysis will consider error contributions due to:

- Timing
- Aircraft attitude
- Antenna displacement
- Aircraft sensors

Analysis will evaluate both vertical and horizontal uncertainties.

Timing

In the analysis of any dynamic system, timing is an important factor. RFP timing is based upon the Data Collector/Correlator (DCC) internal clock. GPS-based positioning is based upon Coordinated Universal Time (UTC). Although these are synchronized at the beginning of each run, they will likely drift apart during the run.

The DCC clock has an accuracy of ± 1 ppm with a drift rate of ± 2 ppm every 10 years. If we assume a DCC birth year of 2008, we can estimate the accuracy as follows.

$$\dot{e}_d^t = 1ppm + 2ppm \cdot \frac{(year - 2008)}{10}$$

Where,

$year$ = Current calendar year

$\dot{e}_d^t$ = DCC clock accuracy (ppm)

Our DCC timing uncertainty, at the point in time of runway fix, can be estimated as follows:

$$e_d^t = \dot{e}_d^t \cdot \Delta t$$

Where,

Δt = Flight inspection run duration

e_d^t = Timing uncertainty due to DCC clock

As stated earlier, the DCC clock and the GPS clock are synchronized at the beginning of each run. Ideally, this synchronization would be accurate to the nearest millisecond (DCC clock resolution). This estimation is degraded if the various GPS clock sources do not align or if there are fewer than three GPS clock sources with which to compare.

The estimated accuracy of the synchronization process is described in Table 1. Within the table, the letter "s" represents the standard deviation of the distribution of GPS synchronization times.

Table 1. Synchronization Uncertainty Estimate

Valid GPS Clock Sources	Uncertainty (e_s^t)
0	1000.0 ms
1	3.0 ms
2	s + 1.0 ms
≥ 3	s + 0.5 ms

Simply take the root-sum-squares (RSS) of the DCC clock uncertainty (e_d^t) and the DCC/GPS synchronization uncertainty (e_s^t).

$$e^t = \sqrt{{e_d^t}^2 + {e_s^t}^2}$$

Where,

e^t = Composite timing error

Aircraft Attitude

Aircraft attitude (pitch, roll, and yaw) influences many of the calculations used to determine aircraft location. Because of this, we must quantify the accuracy of these parameters. The Honeywell Model HG2195AB02/03 IRU specified accuracies are: pitch (e_I^θ) and roll (e_I^φ) at 0.05° each, yaw (e_I^ψ) at 0.10° (0.20° for latitude between 60° and 78°, north and south).

As presented within the previous paragraph, IRU attitude error is quite small. However, if we include temporal uncertainty, it could become a little more significant. IRU attitude is provided at a fairly high rate; the Flight Inspection Airborne Processor Application (FIAPA) samples it every 50 ms. Between interpolation-induced error and timing uncertainty, we can estimate a temporal uncertainty of about 20 ms (Δt).

$$e_I^{\dot{\theta}} = \dot{\theta} \cdot \Delta t$$

$$e_I^{\dot{\varphi}} = \dot{\varphi} \cdot \Delta t$$

$$e_I^{\dot{\psi}} = \dot{\psi} \cdot \Delta t$$

Where,

$\dot{\theta}$ = Pitch rate of change

$\dot{\varphi}$ = Roll rate of change

$\dot{\psi}$ = Yaw (heading) rate of change

$e_I^{\dot{\theta}}$ = IRU dynamic pitch error

$e_I^{\dot{\varphi}}$ = IRU dynamic roll error

$e_I^{\dot{\psi}}$ = IRU dynamic yaw (heading) error

In order to simplify some of the documentation found later in this paper, we'll go ahead and combine the two sources of attitude error into a single quantity for each of the three axes.

$$e_I^{\Sigma\theta} = \sqrt{e_I^{\theta^2} + e_I^{\dot{\theta}^2}}$$

$$e_I^{\Sigma\varphi} = \sqrt{e_I^{\varphi^2} + e_I^{\dot{\varphi}^2}}$$

$$e_I^{\Sigma\psi} = \sqrt{e_I^{\psi^2} + e_I^{\dot{\psi}^2}}$$

Where,

$e_I^{\Sigma\theta}$ = Composite pitch error

$e_I^{\Sigma\varphi}$ = Composite roll error

$e_I^{\Sigma\psi}$ = Composite yaw error

Antenna Displacement

When attempting to compare aircraft locations derived from different sensors, we must take into account the physical displacement of these sensors throughout the airplane. Attitude measurements are anchored at the IRU, altitude measurements are anchored at the radio altimeter antenna (or virtual radio altimeter antenna)[1], camera images at the camera lens, and so forth.

When discussing uncertainties associated with these antenna displacements, we split them into three components: forward (a^f), starboard (a^s), and up (a^u).

Given: a_1, a_2

$$\Delta a^f = a_2^f - a_1^f$$

$$\Delta a^s = a_2^s - a_1^s$$

$$\Delta a^u = a_2^u - a_1^u$$

Where,

$a_1(a_1^f, a_1^s, a_1^u)$ = Antenna 1 location relative to aircraft reference point

$a_2(a_2^f, a_2^s, a_2^u)$ = Antenna 2 location relative to aircraft reference point

Δa^f = Antenna 1 to antenna 2 forward displacement

Δa^s = Antenna 1 to antenna 2 starboard displacement

Δa^u = Antenna 1 to antenna 2 up displacement

When considering antenna displacement, we must evaluate both linear error and angular error.

Let's first consider linear error. We can assume that the calculated distance between any two antennas on the aircraft will have an uncertainty of 0.05 feet in each of the three directions (forward, starboard, and up). Since displacement uncertainties are the same for each axis, we can use these same values for along-track and cross-track.

$$e_{A21}^{\uparrow} = 0.05\ ft$$

$$e_{A21}^{\rightarrow} = 0.05\ ft$$

$$e_{A21}^{u} = 0.05\ ft$$

Where,

$e_{A21}^{\uparrow}$ = Linear along-track displacement uncertainty

$e_{A21}^{\rightarrow}$ = Linear cross-track displacement uncertainty

e_{A21}^{u} = Linear up displacement uncertainty

Now let's consider angular error. During the position estimation process, measurements are made relative to different locations throughout the airplane. Although FIAPA attempts to compensate for these differences, there will be a small amount of error due to attitude uncertainty.

Note: Within the formulas developed within this section, we are going to eliminate any terms that yield values less than 0.02 ft (0.24 inch) under the following extreme conditions. Terms determined to be insignificant will be colored red. Simplified formulas, with insignificant terms removed, will utilize the "almost equal to" symbol (≈) and be colored green.

$|\Delta a^f| = 40$ ft

$|\Delta a^s| = 5$ ft

$|\Delta a^u| = 15$ ft

$|\varphi| = 10°$ roll

$|\theta| = 10°$ pitch

$|\psi| = 15°$ yaw

$|\dot{\varphi}| = 3°/s$ … $(e_I^{\Sigma\varphi} = 0.078°)$

$|\dot{\theta}| = 5°/s$ … $(e_I^{\Sigma\theta} = 0.112°)$

[1] Virtual radio altimeter antenna location corresponds to a vertical offset from the physical antenna corresponding to the distance from the antenna to the concrete with weight on wheels. This "virtual" location is used because the altimeter reports zero height when weight on wheels.

$$|\dot{\psi}| = 5°/s \quad \ldots (e_I^{\Sigma\psi} = 0.141°)$$

The formula for calculating the antenna 1 to antenna 2 "up" displacement (A_{21}^u) with no error, but influenced by pitch (θ) and roll (φ), is provided below. Note that yaw (ψ) has no influence on vertical displacement.

$$\begin{aligned} A_{21}^u &= \Delta a^f \cdot sin(\theta) \\ &- \Delta a^s \cdot sin(\varphi)\, cos(\theta) \\ &+ \Delta a^u \cdot cos(\varphi)\, cos(\theta) \end{aligned}$$

Now compute the "up" error by calculating the contributions from pitch, roll, and yaw separately, and then combine them.

$$\begin{aligned} e_{A21}^{u\theta} &= \Delta a^f \cdot sin\left(e_I^{\Sigma\theta}\right) \\ &- \Delta a^s \cdot \left[cos\left(|\theta| + e_I^{\Sigma\theta}\right) - cos\,\theta\right] sin(\varphi) \\ &+ \Delta a^u \cdot \left[cos\left(|\theta| + e_I^{\Sigma\theta}\right) - cos\,\theta\right] cos(\varphi) \\ &\approx \Delta a^f \cdot sin\left(e_I^{\Sigma\theta}\right) \end{aligned}$$

$$\begin{aligned} e_{A21}^{u\varphi} &= -\Delta a^s \cdot sin\left(e_I^{\Sigma\varphi}\right) \cdot cos(\theta) \\ &+ \Delta a^u \cdot \left[cos\left(|\varphi| + e_I^{\Sigma\varphi}\right) - cos\,\varphi\right] cos(\theta) \\ &\approx 0 \end{aligned}$$

$$e_{A21}^{u\psi} = 0$$

$$\begin{aligned} e_{A21}^{u\measuredangle} &= \sqrt{{e_{A21}^{u\theta}}^2 + {e_{A21}^{u\varphi}}^2 + {e_{A21}^{u\psi}}^2} \\ &\approx e_{A21}^{u\theta} \\ &\approx \Delta a^f \cdot sin\left(e_I^{\Sigma\theta}\right) \end{aligned}$$

Where,

$e_{A21}^{u\theta}$ = Up uncertainty due to pitch angle uncertainty

$e_{A21}^{u\varphi}$ = Up uncertainty due to roll angle uncertainty

$e_{A21}^{u\psi}$ = Up uncertainty due to yaw angle uncertainty

$e_{A21}^{u\measuredangle}$ = Up uncertainty due to pitch, roll, and yaw angle uncertainties combined

In order to simplify the calculations for along-track and cross-track uncertainty estimates, we're going to ignore the influence of yaw and then add it in later.

The formula for calculating the antenna 1 to antenna 2 "forward" displacement (A_{21}^f) with no error, but influenced by pitch (θ) and roll (φ), is provided below.

$$\begin{aligned} A_{21}^f &= \Delta a^f \cdot cos(\theta) \\ &+ \Delta a^s \cdot sin(\varphi) \cdot sin(\theta) \\ &- \Delta a^u \cdot cos(\varphi) \cdot sin(\theta) \end{aligned}$$

Now compute the forward error by calculating the contributions from pitch and roll uncertainties, separately. We cannot combine them at this time; we must include the influence of yaw first.

$$\begin{aligned} e_{A21}^{f\theta} &= \Delta a^f \cdot \left[cos\left(|\theta| + e_I^{\Sigma\theta}\right) - cos\,\theta\right] \\ &+ \Delta a^s \cdot sin\left(e_I^{\Sigma\theta}\right) \cdot sin(\varphi) \\ &- \Delta a^u \cdot sin\left(e_I^{\Sigma\theta}\right) \cdot cos(\varphi) \\ &\approx -\Delta a^u \cdot sin\left(e_I^{\Sigma\theta}\right) \cdot cos(\varphi) \end{aligned}$$

$$\begin{aligned} e_{A21}^{f\varphi} &= \Delta a^s \cdot sin\left(e_I^{\Sigma\varphi}\right) \cdot sin(\theta) \\ &- \Delta a^u \cdot \left[cos\left(|\varphi| + e_I^{\Sigma\varphi}\right) - cos\,\varphi\right] \cdot sin(\theta) \\ &\approx 0 \end{aligned}$$

Where,

$e_{A21}^{f\theta}$ = Forward uncertainty due to pitch angle uncertainty

$e_{A21}^{f\varphi}$ = Forward uncertainty due to roll angle uncertainty

The formula for calculating the antenna 1 to antenna 2 "starboard" displacement (A_{21}^s) with no error, but influenced by pitch (θ) and roll (φ), is provided below.

$$\begin{aligned} A_{21}^s &= \Delta a^s \cdot cos(\varphi) \\ &+ \Delta a^u \cdot sin(\varphi) \end{aligned}$$

Now compute the starboard error by calculating the contributions from pitch and roll uncertainties, separately. We cannot combine them at this time; we must include the influence of yaw first.

$$e_{A21}^{s\theta} = 0$$

$$\begin{aligned} e_{A21}^{s\varphi} &= \Delta a^s \cdot \left[cos\left(|\theta| + e_I^{\Sigma\theta}\right) - cos\,\theta\right] \\ &+ \Delta a^u \cdot sin\left(e_I^{\Sigma\varphi}\right) \\ &\approx \Delta a^u \cdot sin\left(e_I^{\Sigma\varphi}\right) \end{aligned}$$

Where,

$e_{A21}^{s\theta}$ = Starboard uncertainty due to pitch angle uncertainty

$e_{A21}^{s\varphi}$ = Starboard uncertainty due to roll angle uncertainty

We have now calculated the forward and starboard uncertainties due to pitch and roll uncertainties. We must now translate these uncertainties to along-track and cross-track uncertainties for each axis (pitch, roll, and yaw) based upon the yaw angle and yaw uncertainty.

The formula for calculating the antenna 1 to antenna 2 along-track displacement ($A_{21}^{\uparrow}$), with no error, but influenced by yaw (ψ), is provided below.

$$A_{21}^{\uparrow} = A_{21}^{f} \cdot cos(\psi) - A_{21}^{s} \cdot sin(\psi)$$

Now compute each component of the along-track error based upon yaw angle. Then combine into a composite along-track error.

$$\begin{aligned} e_{A21}^{\uparrow\theta} &= e_{A21}^{f\theta} \cdot cos(\psi) - e_{A21}^{s\theta} \cdot sin(\psi) \\ &\approx e_{A21}^{f\theta} \cdot cos(\psi) \\ &\approx -\Delta a^{u} \cdot sin\left(e_{I}^{\Sigma\theta}\right) \cdot cos(\varphi) \cdot cos(\psi) \end{aligned}$$

$$\begin{aligned} e_{A21}^{\uparrow\varphi} &= e_{A21}^{f\varphi} \cdot cos(\psi) - e_{A21}^{s\varphi} \cdot sin(\psi) \\ &\approx 0 \end{aligned}$$

$$\begin{aligned} e_{A21}^{\uparrow\psi} &= A_{21}^{f} \cdot \left[cos\left(|\psi| + e_{I}^{\Sigma\psi}\right) - cos\,\psi\right] - A_{21}^{s} \\ &\quad \cdot sin\left(e_{I}^{\Sigma\psi}\right) \\ &= [\Delta a^{f} \cdot cos(\theta) + \Delta a^{s} \cdot sin(\varphi) \cdot sin(\theta) \\ &\quad - \Delta a^{u} \cdot cos(\varphi) \cdot sin(\theta)] \\ &\quad \cdot \left[cos\left(|\psi| + e_{I}^{\Sigma\psi}\right) - cos\,\psi\right] \\ &\quad - [\Delta a^{s} \cdot cos(\varphi) + \Delta a^{u} \cdot sin(\varphi)] \cdot sin\left(e_{I}^{\Sigma\psi}\right) \\ &\approx \Delta a^{f} \cdot cos(\theta) \cdot \left[cos\left(|\psi| + e_{I}^{\Sigma\psi}\right) - cos\,\psi\right] \end{aligned}$$

$$\begin{aligned} e_{A21}^{\uparrow\measuredangle} &= \sqrt{{e_{A21}^{\uparrow\theta}}^{2} + {e_{A21}^{\uparrow\varphi}}^{2} + {e_{A21}^{\uparrow\psi}}^{2}} \\ &\approx \sqrt{{e_{A21}^{\uparrow\theta}}^{2} + {e_{A21}^{\uparrow\psi}}^{2}} \\ &\approx \left\{\left[-\Delta a^{u} \cdot sin\left(e_{I}^{\Sigma\theta}\right) \cdot cos(\varphi) \cdot cos(\psi)\right]^{2}\right. \\ &\quad \left. + \left[\Delta a^{f} \cdot cos(\theta) \cdot \left[cos\left(|\psi| + e_{I}^{\Sigma\psi}\right) - cos\,\psi\right]\right]^{2}\right\}^{1/2} \end{aligned}$$

Where, [2]

$e_{A21}^{\uparrow\theta}$ = Along-track uncertainty due to pitch angle uncertainty

$e_{A21}^{\uparrow\varphi}$ = Along-track uncertainty due to roll angle uncertainty

$e_{A21}^{\uparrow\psi}$ = Along-track uncertainty due to yaw angle uncertainty

$e_{A21}^{\uparrow\measuredangle}$ = Along-track uncertainty due to pitch, roll, and yaw angle uncertainties combined

The formula for calculating the antenna 1 to antenna 2 cross-track displacement (A_{21}^{s}), with no error, but influenced by yaw (ψ), is provided below.

$$A_{21}^{\rightarrow} = A_{21}^{s} \cdot cos(\psi) + A_{21}^{f} \cdot sin(\psi)$$

Now compute each component of the cross-track error based upon yaw angle. Then combine into a composite cross-track error.

$$\begin{aligned} e_{A21}^{\rightarrow\theta} &= e_{A21}^{s\theta} \cdot cos(\psi) + e_{A21}^{f\theta} \cdot sin(\psi) \\ &\approx 0 \end{aligned}$$

$$\begin{aligned} e_{A21}^{\rightarrow\varphi} &= e_{A21}^{s\varphi} \cdot cos(\psi) + e_{A21}^{f\varphi} \cdot sin(\psi) \\ &\approx e_{A21}^{s\varphi} \cdot cos(\psi) \\ &\approx \Delta a^{u} \cdot sin\left(e_{I}^{\Sigma\varphi}\right) \cdot cos(\psi) \end{aligned}$$

$$\begin{aligned} e_{A21}^{\rightarrow\psi} &= A_{21}^{s} \cdot \left[cos\left(|\psi| + e_{I}^{\Sigma\psi}\right) - cos\,\psi\right] + A_{21}^{f} \\ &\quad \cdot sin\left(e_{I}^{\Sigma\psi}\right) \\ &= [\Delta a^{s} \cdot cos(\varphi) + \Delta a^{u} \cdot sin(\varphi)] \\ &\quad \cdot \left[cos\left(|\psi| + e_{I}^{\Sigma\psi}\right) - cos\,\psi\right] \\ &\quad + [\Delta a^{f} \cdot cos(\theta) + \Delta a^{s} \cdot sin(\varphi) \cdot sin(\theta) \\ &\quad - \Delta a^{u} \cdot cos(\varphi) \cdot sin(\theta)] \cdot sin\left(e_{I}^{\Sigma\psi}\right) \\ &\approx \Delta a^{f} \cdot cos(\theta) \cdot sin\left(e_{I}^{\Sigma\psi}\right) \end{aligned}$$

$$\begin{aligned} e_{A21}^{\rightarrow\measuredangle} &= \sqrt{{e_{A21}^{\rightarrow\theta}}^{2} + {e_{A21}^{\rightarrow\varphi}}^{2} + {e_{A21}^{\rightarrow\psi}}^{2}} \\ &\approx \sqrt{{e_{A21}^{\rightarrow\varphi}}^{2} + {e_{A21}^{\rightarrow\psi}}^{2}} \\ &\approx \left\{\left[\Delta a^{u} \cdot sin\left(e_{I}^{\Sigma\varphi}\right) \cdot cos(\psi)\right]^{2}\right. \\ &\quad \left. + \left[\Delta a^{f} \cdot cos(\theta) \cdot sin\left(e_{I}^{\Sigma\psi}\right)\right]^{2}\right\}^{1/2} \end{aligned}$$

Where,

$e_{A21}^{\rightarrow\theta}$ = Cross-track uncertainty due to pitch angle uncertainty

$e_{A21}^{\rightarrow\varphi}$ = Cross-track uncertainty due to roll angle uncertainty

[2] Errors $e_{I}^{\Sigma\theta}$ and $e_{I}^{\Sigma\psi}$ should be replaced with $e_{c}^{\Sigma\theta}$ and $e_{c}^{\Sigma\psi}$ when evaluating camera solution uncertainty.

$e_{A21}^{\rightarrow\psi}$ = Cross-track uncertainty due to yaw angle uncertainty

$e_{A21}^{\rightarrow\measuredangle}$ = Cross-track uncertainty due to pitch, roll, and yaw angle uncertainties combined

To estimate the total antenna displacement uncertainty, we simply compute the root-sum-squares (RSS) of the linear and angular components.

$$e_{A21}^{\uparrow} = \sqrt{{e_{A21}^{\uparrow\_}}^2 + {e_{A21}^{\uparrow\measuredangle}}^2}$$

$$e_{A21}^{\rightarrow} = \sqrt{{e_{A21}^{\rightarrow\_}}^2 + {e_{A21}^{\rightarrow\measuredangle}}^2}$$

$$e_{A21}^{u} = \sqrt{{e_{A21}^{u\_}}^2 + {e_{A21}^{u\measuredangle}}^2}$$

Where,

$e_{A21}^{\uparrow}$ = Along-track displacement uncertainty from antenna 1 to antenna 2

$e_{A21}^{\rightarrow}$ = Cross-track displacement uncertainty from antenna 1 to antenna 2

e_{A21}^{u} = Vertical displacement uncertainty from antenna 1 to antenna 2

RFP ACCURACY ESTIMATION - VERTICAL

Aircraft vertical position relative to the landmark concrete (e.g., runway threshold) is provided via the radio altimeter. Contributors to this uncertainty are described below.

Latency

After a prolonged investigation by Rockwell/Collins, comprised primarily of laboratory testing, they determined that the latency of the radio altimeter measurement has an uncertainty (Δt_{RA}) of approximately ± 100 ms. If we use the uncalibrated velocity provided by the vertical velocity filter and assume it has an uncertainty of ± 20%, due to its latency and accuracy issues, we arrive at the following formula.

$$e_L^u = V_I^u \cdot 1.2 \cdot \Delta t_{RA}$$

Where,

Δt_{RA} = Radio altimeter latency uncertainty (100 ms)

V_I^u = Uncalibrated vertical velocity from Vertical Velocity Filter (derived from IRU integrated vertical acceleration)

Accuracy

The specified static accuracy of the radio altimeter is the greater of 2 feet or 2% of height above ground. Since a calibration of the radio altimeter is performed prior to each flight, we can reduce this lower limit to 6 inches. This becomes subordinate above 25 feet; therefore, we can expect an uncertainty of 2% of height above ground.

$$e_A^u = 0.02 \cdot h_{RA}$$

Where,

h_{RA} = Height above ground measured by radio altimeter

Runway Slope

When sampling height above ground using the radio altimeter, we must ensure that the airplane is over concrete. Ground elevation can deviate from that of the runway considerably when the airplane is located beyond the edge of the runway. This is achieved by using a radio altimeter sample beyond threshold or prior to the end of the runway. This along-track displacement creates a radio altitude error proportional to the distance offset and the slope of the runway at the location of interest.

FIAPA attempts to compensate for this using the average slope of the runway. Unfortunately, the slope can vary considerably over the length of the runway. This variation is unknown. For the purpose of this discussion, let's assume a slope uncertainty of 0.5%. This is equivalent to 6 inches every 100 feet.

Given the groundspeed and time delay/advance, we can calculate this uncertainty as follows.

$$e_m^u = e_m^{\measuredangle} \cdot V_I^h \cdot \Delta t$$

Where,

V_I^h = Uncalibrated horizontal velocity from IRU

$e_m^{\measuredangle}$ = Estimated runway slope uncertainty at location of interest

Δt = Radio altimeter sample delay interval (negative value for runway end)

e_m^u = Estimated radio altimeter height uncertainty due to runway slope uncertainty

Radio Altimeter Composite

The radio altimeter composite uncertainty can be estimated by taking the root-sum-squares of the various components. This value does not include any antenna-to-antenna displacement uncertainty.

$$e_{Ralt}^{u} = \sqrt{e_L^{u\,2} + e_A^{u\,2} + e_m^{u\,2}}$$

Aircraft Antenna Displacement

The height of the radio altimeter must be translated to a different location within the airplane for comparison with the location reported by GPS. Although FIAPA attempts to compensate for this, there will be a small amount of error as described in previous section.

$$e_{AG\acute{R}}^{\uparrow} = \sqrt{e_{AG\acute{R}}^{\uparrow\,2} + e_{AG\acute{R}}^{\uparrow\measuredangle\,2}}$$

$$e_{AG\acute{R}}^{\rightarrow} = \sqrt{e_{AG\acute{R}}^{\rightarrow\,2} + e_{AG\acute{R}}^{\rightarrow\measuredangle\,2}}$$

$$e_{AG\acute{R}}^{u} = \sqrt{e_{AG\acute{R}}^{u\,2} + e_{AG\acute{R}}^{u\measuredangle\,2}}$$

Where,

$e_{AG\acute{R}}^{\uparrow}$ = Along-track displacement uncertainty from radio altimeter virtual antenna to GPS antenna

$e_{AG\acute{R}}^{\rightarrow}$ = Cross-track displacement uncertainty from radio altimeter virtual antenna to GPS antenna

$e_{AG\acute{R}}^{u}$ = Vertical displacement uncertainty from radio altimeter virtual antenna to GPS antenna

RFP Vertical Composite

The composite vertical uncertainty can be estimated by taking the root-sum-squares of the composite radio altimeter uncertainty and the uncertainty due to antenna displacement.

$$e^{u} = \sqrt{e_{Ralt}^{u\,2} + e_{AG\acute{R}}^{u\,2}}$$

RFP ACCURACY ESTIMATION - HORIZONTAL

Insignificant Terms

Within the formulas developed within this section, we are going to eliminate any terms that yield values less than 0.02 ft (0.24 inch) under the extreme conditions listed in the "BASICS" section. Attitude uncertainty will inflate due to camera alignment uncertainty. Expected maximum values are shown below.

$|\dot{\varphi}| = 3°/\text{s}$ $(e_I^{\Sigma\varphi} = 0.078°, e_c^{\Sigma\varphi} = 0.215°)$

$|\dot{\theta}| = 5°/\text{s}$ $(e_I^{\Sigma\theta} = 0.112°, e_c^{\Sigma\theta} = 0.229°)$

$|\dot{\psi}| = 5°/\text{s}$ $(e_I^{\Sigma\psi} = 0.141°, e_c^{\Sigma\psi} = 0.250°)$

Additional limitations, associated with camera-based positioning, are listed below. Terms determined to be insignificant will be colored red. Simplified formulas, with insignificant terms removed, will utilize the "almost equal to" symbol (≈) and be colored green.

$|XTK| = 30$ ft (aircraft cross-track from runway centerline at landmark)

$|h_{AGL}| = 200$ ft (aircraft height above concrete)

Sources of Error

As was the case for vertical uncertainty, along-track uncertainty is dependent upon aircraft attitude uncertainties. These uncertainties are described within "BASICS" section.

$e_I^{\Sigma\theta}$ = Uncertainty of aircraft pitch (reported by IRU)

$e_I^{\Sigma\varphi}$ = Uncertainty of aircraft roll (reported by IRU)

$e_I^{\Sigma\psi}$ = Uncertainty of aircraft yaw (reported by IRU)

These values for attitude uncertainty are exacerbated by any error introduced during the camera alignment procedure.

In addition, there is an uncertainty as to the value of the camera magnification factor (M). Based upon recent analyses of camera-based results, an uncertainty of ± 3% appears to be reasonable.

$$e_M = 0.03 \cdot M$$

Two additional sources of horizontal uncertainty:

- Vertical uncertainty
- Antenna offset uncertainty (from camera lens to GPS antenna)

Camera Attitude Uncertainty

The camera manufacturer's technical manual states that, "all reference lines should be generated to an accuracy of 0.2°." We interpret that statement to indicate that camera pitch, roll, and yaw calibration shall each be accurate to 0.2°.

$$Given: e_c^{\theta} = 0.20°, e_c^{\varphi} = 0.20°, e_c^{\psi} = 0.20°$$

Where,

e_c^{θ} = Camera alignment pitch error

e_c^{φ} = Camera alignment roll error

e_c^{ψ} = Camera alignment yaw error

Combining these values with the IRU attitude uncertainty values, found within the attitude composite error located within the "BASICS" section, we get:

$$e_c^{\Sigma\theta} = \sqrt{{e_I^{\theta}}^2 + {e_I^{\dot{\theta}}}^2 + {e_c^{\theta}}^2}$$

$$e_c^{\Sigma\varphi} = \sqrt{{e_I^{\varphi}}^2 + {e_I^{\dot{\varphi}}}^2 + {e_c^{\varphi}}^2}$$

$$e_c^{\Sigma\psi} = \sqrt{{e_I^{\psi}}^2 + {e_I^{\dot{\psi}}}^2 + {e_c^{\psi}}^2}$$

Where,

$e_c^{\Sigma\theta}$ = Camera pitch uncertainty

$e_c^{\Sigma\varphi}$ = Camera roll uncertainty

$e_c^{\Sigma\psi}$ = Camera yaw uncertainty

Camera Along-Track Spatial Uncertainty

The formula for determining along-track deviation (ΔATK) from the landmark to the camera lens is provided below.

$$\Delta ATK = -h_c \cdot \left\{ tan(\theta_c) \cdot cos(\psi_c) + \frac{tan\left[\varphi_c - tan^{-1}\left(\frac{P}{M}\right)\right] \cdot sin(\psi_c)}{cos(\theta_c)} \right\}$$

Where,

h_c = Height of camera with respect to concrete

θ_c = Pitch angle of camera with respect to level at time of fix

φ_c = Roll angle of camera with respect to zero roll at time of fix

ψ_c = Crab (yaw) angle of camera with respect to ground coordinate system (e.g. runway heading)

P = Pixel displacement from center of sweep (pixels)

M = Magnification factor (pixels)

The formula for each contributor to along-track geometry uncertainty is provided below. An additional uncertainty of 1.0 ft ($e_{c\Delta}^{\uparrow ☺}$) represents the operator's accuracy in locating the landmark as well as the limited resolution of the camera image. The composite uncertainty is also provided below.

$$e_{c\Delta}^{\uparrow\theta} = -h_c \cdot \left\{ \left[tan\left(|\theta_c| + e_c^{\Sigma\theta}\right) - tan(|\theta_c|)\right] \cdot cos(\psi_c) + tan\left[\varphi_c - tan^{-1}\left(\frac{P}{M}\right)\right] \cdot sin(\psi_c) \cdot \left[\frac{1}{cos(|\theta_c| + e_c^{\Sigma\theta})} - \frac{1}{cos(\theta_c)}\right] \right\}$$

$$\approx -h_c \cdot \left\{ \left[tan\left(|\theta_c| + e_c^{\Sigma\theta}\right) - tan(|\theta_c|)\right] \cdot cos(\psi_c) \right\}$$

$$e_{c\Delta}^{\uparrow\varphi} = -h_c \cdot \left\{ \left[tan\left[\varphi_c + e_c^{\Sigma\varphi} - tan^{-1}\left(\frac{P}{M}\right)\right] - tan\left[\varphi_c - tan^{-1}\left(\frac{P}{M}\right)\right]\right] \cdot \frac{sin(\psi_c)}{cos(\theta_c)} \right\}$$

$$e_{c\Delta}^{\uparrow\psi} = -h_c \cdot \left\{ tan(\theta_c) \cdot \left[cos\left(|\psi_c| + e_c^{\Sigma\psi}\right) - cos(\psi_c)\right] + tan\left[\varphi_c - tan^{-1}\left(\frac{P}{M}\right)\right] \cdot \frac{sin\left(e_c^{\Sigma\psi}\right)}{cos(\theta_c)} \right\}$$

$$e_{c\Delta}^{\uparrow M} = -h_c \cdot \left\{ \left[tan\left[\varphi_c - tan^{-1}\left(\frac{P}{M + e_M}\right)\right] - tan\left[\varphi_c - tan^{-1}\left(\frac{P}{M}\right)\right]\right] \cdot \frac{sin(\psi_c)}{cos(\theta_c)} \right\}$$

$$e_{c\Delta}^{\uparrow Ralt} = -e_{Ralt}^{u} \cdot \left\{ tan(\theta_c) \cdot cos(\psi_c) + tan\left[\varphi_c - tan^{-1}\left(\frac{P}{M}\right)\right] \cdot \frac{sin(\psi_c)}{cos(\theta_c)} \right\}$$

$$e_{c\Delta}^{\uparrow} = \sqrt{{e_{c\Delta}^{\uparrow\theta}}^2 + {e_{c\Delta}^{\uparrow\varphi}}^2 + {e_{c\Delta}^{\uparrow\psi}}^2 + {e_{c\Delta}^{\uparrow M}}^2 + e_{c\Delta}^{\uparrow Ralt} + e_{c\Delta}^{\uparrow ☺}}$$

Where,

$e_{c\Delta}^{\Sigma\theta}$ = Camera geometry pitch uncertainty

$e_{c\Delta}^{\Sigma\varphi}$ = Camera geometry roll uncertainty

$e_{c\Delta}^{\Sigma\psi}$ = Camera geometry yaw uncertainty

e_M = Camera magnification factor uncertainty

e_{Ralt}^{u} = Radio altimeter composite vertical uncertainty

$e_{c\Delta}^{\uparrow\theta}$ = Camera geometry along-track uncertainty due to pitch uncertainty

$e_{c\Delta}^{\uparrow\varphi}$ = Camera geometry along-track uncertainty due to roll uncertainty

$e_{c\Delta}^{\uparrow\psi}$ = Camera geometry along-track uncertainty due to yaw uncertainty

$e_{c\Delta}^{\uparrow M}$ = Camera geometry along-track uncertainty due to magnification factor uncertainty

$e_{c\Delta}^{\uparrow Ralt}$ = Camera geometry along-track uncertainty due to radio altimeter vertical uncertainty

$e_{c\Delta}^{\uparrow \circledcirc}$ = Camera along-track uncertainty due to operator's ability to accurately locate landmark on camera image (and camera scan resolution)

$e_{c\Delta}^{\uparrow}$ = Camera spatial along-track uncertainty

Camera Along-Track Temporal Uncertainty

Let's now address two additional sources of error: GPS/DCC timing and camera system timing.

Within the *Timing* topic of the "BASICS" section we describe, in detail, the two sources of GPS/DCC timing uncertainty: DCC clock (e_d^t) and DCC/GPS synchronization (e_s^t).

We must also consider temporal uncertainty systemic to the camera system. In attempting to quantify this uncertainty, we tabulated along-track results from several DGPS runs at two facilities. Results are provided in Table 2.

One goal of this analysis was to identify any bias within the camera system timing and compensate for it, thereby improving our overall accuracy. The results did not uncover any appreciable bias and, consequently, no compensation has been implemented within FIAPA thus far.

The second goal was to estimate any uncertainty due to the camera system timing. We attribute 0.2 ft uncertainty to other sources such as DGPS uncertainty. We must perform an inverse RSS to determine the actual camera system timing error. We will use the standard deviation value of 0.7 ft for this calculation.

$$0.7ft = \sqrt{(0.7ft - 0.2ft)^2 + e_c^{\uparrow t^2}}$$

$$e_c^{\uparrow t} = 0.5ft$$

Table 2. Runway Survey Along-Track Errors using DGPS

Date	A/P	Facility	Dash	GPS	ATK Error (ft.)	
					Threshold	Rwy End
04/21/15	KPWA	17L ILS	001B	RTK Fixed	0.4	-0.7
			002A	RTK Fixed	0.6	-1.4
			004B	RTK Fixed	-0.3	-0.7
	KHSD	17 LTG	002A	Fixed/Float	-1.6	-0.5
			003A	Fixed/Float	-0.6	-0.3
			004A	Fixed/Float	-0.5	-0.5
			005A	Fixed/Float	-0.6	-1.1
			006A	Fixed/Float	-0.7	-0.4
				Average	-0.41	-0.7
				Sample Standard Deviation	0.7	0.4

At 200 fps, this equates to 2.5 ms (e_c^t). This appears to be a reasonable value considering that FIAPA timing and DCC output timing each have a resolution of 1 ms.

These temporal uncertainties can be combined and translated to along-track distance ($e_{ct}^{\uparrow}$) as follows.

$$e_c^{\Sigma t} = \sqrt{e_d^{t^2} + e_s^{t^2} + e_c^{t^2}}$$

$$e_{ct}^{\uparrow} = e_c^{\Sigma t} \cdot V^h$$

Where,

e_d^t = Uncertainty due to DCC crystal

e_s^t = Uncertainty due to DCC/GPS synchronization

e_c^t = Uncertainty due to camera system timing

$e_c^{\Sigma t}$ = Composite temporal uncertainty for camera solution

V^h = Groundspeed

$e_{ct}^{\uparrow}$ = Camera temporal along-track uncertainty

Camera Along-Track Composite

Calculate the camera composite along-track uncertainty by taking the RSS of the spatial and temporal uncertainties.

$$e_c^{\uparrow} = \sqrt{e_{c\Delta}^{\uparrow\ 2} + e_{ct}^{\uparrow\ 2}}$$

Where,

$e_{c\Delta}^{\uparrow}$ = Camera spatial along-track uncertainty

$e_{ct}^{\uparrow}$ = Camera temporal along-track uncertainty

$e_{c}^{\uparrow}$ = Camera composite along-track uncertainty

Aircraft Antenna Displacement

The camera location must be translated to a different location within the airplane for comparison with the location reported by GPS. Although FIAPA attempts to compensate for this, there will be a small amount of error as described in the *Antenna Displacement* topic within the "BASICS" section.

$$Given:\ a_G, a_C$$

$$e_{\overline{AGC}}^{\uparrow} = 0.05\ ft$$

$$e_{AGC}^{\uparrow\measuredangle} \approx \left\{\left[-\Delta a^u \cdot sin\left(e_c^{\Sigma\theta}\right) \cdot cos(\varphi) \cdot cos(\psi)\right]^2 + \left[\Delta a^f \cdot cos(\theta) \cdot \left[cos\left(|\psi| + e_c^{\Sigma\psi}\right) - cos\,\psi\right]\right]^2\right\}^{1/2}$$

$$e_{AGC}^{\uparrow} = \sqrt{{e_{\overline{AGC}}^{\uparrow}}^2 + {e_{AGC}^{\uparrow\measuredangle}}^2}$$

Where,

$e_{\overline{AGC}}^{\uparrow}$ = Linear along-track displacement uncertainty

$e_{AGC}^{\uparrow\measuredangle}$ = Along-track uncertainty due to pitch, roll, and yaw angle uncertainties combined

$e_{AGC}^{\uparrow}$ = Along-track displacement uncertainty from camera lens to GPS antenna

RFP Along-Track Composite

The composite along-track uncertainty can be estimated by taking the root-sum-squares of the camera composite along-track uncertainty and the uncertainty due to antenna displacement.

$$e^{\uparrow} = \sqrt{{e_c^{\uparrow}}^2 + {e_{AGC}^{\uparrow}}^2}$$

Camera Cross-Track Spatial Uncertainty

The formula for determining cross-track deviation (ΔXTK) from the landmark to the camera lens is provided below.

$$\Delta XTK = -h_c \cdot \left\{tan(\theta_c) \cdot sin(\psi_c) - \frac{tan\left[\varphi_c - tan^{-1}\left(\frac{P}{M}\right)\right] \cdot cos(\psi_c)}{cos(\theta_c)}\right\}$$

Where,

h_c = Height of camera with respect to concrete

θ_c = Pitch angle of camera with respect to level at time of fix

φ_c = Roll angle of camera with respect to zero roll at time of fix

ψ_c = Crab (yaw) angle of camera with respect to ground coordinate system (e.g., runway heading)

P = Pixel displacement from center of sweep (pixels)

M = Magnification factor (pixels)

The formula for each contributor to cross-track geometry uncertainty is provided below. An additional uncertainty of 0.5 ft ($e_{c\Delta}^{\rightarrow\text{☺}}$) represents the operator's accuracy in locating the landmark as well as the limited resolution of the camera image. The composite uncertainty is also provided below.

$$e_{c\Delta}^{\rightarrow\theta} = -h_c \cdot \left\{\left[tan\left(|\theta_c| + e_c^{\Sigma\theta}\right) - tan(|\theta_c|)\right] \cdot sin(\psi_c) - tan\left[\varphi_c - tan^{-1}\left(\frac{P}{M}\right)\right] \cdot cos(\psi_c) \cdot \left[\frac{1}{cos\left(|\theta_c| + e_c^{\Sigma\theta}\right)} - \frac{1}{cos(\theta_c)}\right]\right\}$$

$$\approx -h_c \cdot \left\{\left[tan\left(|\theta_c| + e_c^{\Sigma\theta}\right) - tan(|\theta_c|)\right] \cdot sin(\psi_c)\right\}$$

$$e_{c\Delta}^{\rightarrow\varphi} = -h_c \cdot \left\{\left[tan\left[\varphi_c + e_c^{\Sigma\varphi} - tan^{-1}\left(\frac{P}{M}\right)\right] - tan\left[\varphi_c - tan^{-1}\left(\frac{P}{M}\right)\right]\right] \cdot \frac{cos(\psi_c)}{cos(\theta_c)}\right\}$$

$$e_{c\Delta}^{\rightarrow\psi} = -h_c \cdot \left\{tan(\theta_c) \cdot sin\left(e_c^{\Sigma\psi}\right) - tan\left[\varphi_c - tan^{-1}\left(\frac{P}{M}\right)\right] \cdot \frac{\left[cos\left(|\psi| + e_c^{\Sigma\psi}\right) - cos(\psi)\right]}{cos(\theta_c)}\right\}$$

$$e_{c\Delta}^{\rightarrow M} = -h_c \cdot \left\{ \left[tan\left[\varphi_c - tan^{-1}\left(\frac{P}{M + e_M}\right)\right] - tan\left[\varphi_c - tan^{-1}\left(\frac{P}{M}\right)\right]\right] \cdot \frac{cos(\psi_c)}{cos(\theta_c)} \right\}$$

$$e_{c\Delta}^{\rightarrow Ralt} = -e_{Ralt}^{u} \cdot \left\{ tan(\theta_c) \cdot sin(\psi_c) - tan\left[\varphi_c - tan^{-1}\left(\frac{P}{M}\right)\right] \cdot \frac{cos(\psi_c)}{cos(\theta_c)} \right\}$$

$$e_{c\Delta}^{\rightarrow} = \sqrt{e_c^{\rightarrow\theta^2} + e_c^{\rightarrow\varphi^2} + e_c^{\rightarrow\psi^2} + e_c^{\rightarrow M^2} + e_c^{\rightarrow Ralt^2} + e_{c\Delta}^{\rightarrow ☺^2}}$$

Where,

$e_{c\Delta}^{\Sigma\theta}$ = Camera geometry pitch uncertainty

$e_{c\Delta}^{\Sigma\varphi}$ = Camera geometry roll uncertainty

$e_{c\Delta}^{\Sigma\psi}$ = Camera geometry yaw uncertainty

e_M = Camera magnification factor uncertainty

e_{Ralt}^{u} = Radio altimeter composite vertical uncertainty

$e_{c\Delta}^{\rightarrow\theta}$ = Camera geometry cross-track uncertainty due to pitch uncertainty

$e_{c\Delta}^{\rightarrow\varphi}$ = Camera geometry cross-track uncertainty due to roll uncertainty

$e_{c\Delta}^{\rightarrow\psi}$ = Camera geometry cross-track uncertainty due to yaw uncertainty

$e_{c\Delta}^{\rightarrow M}$ = Camera geometry cross-track uncertainty due to magnification factor uncertainty

$e_{c\Delta}^{\rightarrow Ralt}$ = Camera geometry cross-track uncertainty due to radio altimeter vertical uncertainty

$e_{c\Delta}^{\rightarrow ☺}$ = Camera cross-track uncertainty due to operator's ability to accurately locate landmark on camera image (and camera scan resolution)

$e_{c\Delta}^{\rightarrow}$ = Camera spatial cross-track uncertainty

Camera Cross-Track Temporal Uncertainty

Timing inaccuracies do not play a direct role in cross-track uncertainty. They are not considered herein.

Camera Cross-Track Composite

Since timing inaccuracies are not a factor in determining cross-track uncertainty, camera composite cross-track uncertainty is simply equal to the camera spatial cross-track uncertainty.

$$e_c^{\rightarrow} = e_{c\Delta}^{\rightarrow}$$

Where,

$e_{c\Delta}^{\rightarrow}$ = Camera spatial cross-track uncertainty

$e_c^{\rightarrow}$ = Camera composite cross-track uncertainty

Aircraft Antenna Displacement

The camera location must be translated to a different location within the airplane for comparison with the location reported by GPS. Although FIAPA attempts to compensate for this, there will be a small amount of error as described previously.

$Given$: a_G, a_C

$$e_{AGC}^{\rightarrow} = 0.05\ ft$$

$$e_{AGC}^{\rightarrow\measuredangle} \approx \left\{ \left[\Delta a^u \cdot sin\left(e_c^{\Sigma\varphi}\right) \cdot cos(\psi)\right]^2 + \left[\Delta a^f \cdot cos(\theta) \cdot sin\left(e_c^{\Sigma\psi}\right)\right]^2 \right\}^{1/2}$$

$$e_{AGC}^{\rightarrow} = \sqrt{e_{AGC}^{\rightarrow\ 2} + e_{AGC}^{\rightarrow\measuredangle\ 2}}$$

Where,

$e_{AGC}^{\rightarrow}$ = Linear cross-track displacement uncertainty

$e_{AGC}^{\rightarrow\measuredangle}$ = Cross-track uncertainty due to pitch, roll, and yaw angle uncertainties combined

$e_{AGC}^{\rightarrow}$ = Cross-track displacement uncertainty from camera lens to GPS antenna

RFP Cross-Track Composite

The composite cross-track uncertainty can be estimated by taking the root-sum-squares of the camera composite cross-track uncertainty and the uncertainty due to antenna displacement.

$$e^{\rightarrow} = \sqrt{e_c^{\rightarrow 2} + e_{AGC}^{\rightarrow\ 2}}$$

COMPOSITE ACCURACY ESTIMATION

The composite uncertainty can be estimated by taking the root-sum-squares of the GPS and RFP.

$$e^{ATK} = \sqrt{e_{SBAS}^{ATK\ 2} + e^{\uparrow 2}}$$

$$e^{XTK} = \sqrt{e_{SBAS}^{XTK\ 2} + e^{\rightarrow 2}}$$

$$e^{UP} = \sqrt{e_{SBAS}^{UP\ 2} + e^{u2}}$$

CLUMPING

Virtually all of the accuracy uncertainties discussed within this paper are combined using the standard root-sum-squares (RSS) method. This technique ignores the fact that many of these associated errors change very slowly over time. DCC crystal accuracy due to aging is a good example. This phenomenon corresponds to GPS uncertainties as well. SBAS bias can be fairly constant for many flight inspection runs.

Within the temporal perspective in which we operate the aircraft, these errors appear as biases rather than random variations. Unfortunately, we cannot estimate these biases. If we could, we would compensate for them. We can expect that, periodically, a few of these stagnant uncertainties will "clump together" and either give us better-than-average results or worse-than-average results.

It is recommended that the operator be made aware of this phenomenon and evaluate the flight inspection results accordingly.

CONCLUSION

Most would agree that the uncertainties examined within this paper are fairly comprehensive. Many estimates are based upon equipment specifications while others are based upon experience and a little bit of guesswork. Only after these formulas have been programmed into FIAPA and results have been collected and analyzed over a period of several months, will we be able to determine their accuracies and usefulness.

REFERENCES

The content of this paper was taken from the two Engineering Reports listed below. These reports contain additional information as well as examples. These reports are available via Kelly.C.StPierre@faa.gov.

[1] FAA, Flight Inspection Services, 28 March 2016, GPS WAAS Accuracy Assessment, D15-007 GPS Accuracy

[2] FAA, Flight Inspection Services, 20 April 2016, Runway Fix Accuracy Assessment, D15-006 RFP Accuracy

DME SiS Performance and DME/DME Positioning using In-Flight Recorded Data

Valeriu Vitan
Navigation Infrastructure Expert
EUROCONTROL
Brussels, Belgium
Phone: +32 272 4758
E-mail: valeriu.vitan@eurocontrol.int

Klaus Theißen
Product Management
Development RF and Air Navigation Analyzers
Rohde & Schwarz GmbH & Co. KG
Cologne, Germany
Phone: +49 2203 49 51357
Mobile: +49 160 7063234
Fax: +49 2203 49 51462
Email: Klaus.Theissen@rohde-schwarz.com

ABSTRACT

With the broad implementation of Performance Based Navigation, GNSS is becoming an essential infrastructure. Consequently, the role of terrestrial aids is evolving from supporting conventional procedures on a primary and exclusive basis to one that has a complementary function in the context of PBN. Current work in various SESAR (Single European Sky ATM Research) projects revolves around the use of DME/DME (Distance Measuring Equipment) as the main reversionary capability in the en-route and TMA airspace during a GNSS outage in the short and medium term. In the long term, GNSS reversion is addressed in a wider context, considering various solutions supported by advanced terrestrial systems/technologies, referred to as Alternate Positioning, Navigation and Timing (A-PNT). While there are several new technologies proposed to support a future A-PNT solution, DME/DME navigation is still a potential long term candidate to support the positioning and navigation functions due to its large equipage base on the ground and in the aircraft fleet, as well as its two-way ranging principle reducing the required number of ground facilities (a fix is possible with two stations only).However, the DME/DME solution doesn't provide the same accuracy and integrity as the GNSS solution. Although the required performance is clearly specified in various aviation standards, both for the on-board and ground systems, these requirements are based on rather old technology solutions and modern equipment is capable of significantly better performance. Therefore it is important to determine through in-flight measurements the performances achieved by current DME systems and estimate the accuracy of the DME/DME solution. In this context an extensive in-flight data recording and analysis campaign was organized with the contribution of the flight inspection unit of DSNA (Direction Générale de l'Aviation Civile of France), Rohde&Schwarz and EUROCONTROL.

This paper will first explain the functional principle of the level and modulation analyzer R&S®EDS300 and present its technical characteristics, because it was used for measuring and recording the in-flight data. Subsequently the results of the DME SiS flight measurements campaign will be presented and compared with the minimum baseline requirements of the applicable standards. In addition to accuracy performance, received power will also be assessed, as the use of DME at extended ranges is becoming much more significant in the PBN context. The next main topic addressed by the paper will be the estimation of the DME/DME solution accuracy starting from the recorded slant range errors. Finally the paper will briefly address the benefits of a multi-DME positioning algorithm and its potential to support a future A-PNT solution.

DME SIGNAL IN SPACE PERFORMANCE

One first question in what regards the potential of DME to support future A-PNT solutions is what is the actual accuracy achieved by the systems operated today? This question is justified by the fact that DME was introduced and standardized for aviation use many decades ago, on the basis of the technology available at

that time and well before the advent of area navigation computers. Although the manufacturing technology has significantly evolved and improved over time, the DME performance requirements do not reflect this evolution, both for the on-board interrogator and for the ground transponder. Therefore the technical design specifications of modern systems provide a much better performance level than the standardized baseline. In this context, it is important to determine the accuracy and the stability of the DME range information and also estimate the impact on the positioning solution.

It should be noted that a previous analysis of in-flight data collection was performed in USA [1]. Our study makes a similar analysis using data collected in the European environment and compares the results with those presented in [1].A first version of this study was already presented in [DASC]. This paper provides an update and goes into further analysis with respect to achievable area navigation positioning performance.

This study analyses also the peak level of the transponder reply received by the interrogator and compares it with the level predicted based on the Free Space Path Loss (FSPL) link budget and the IF-77 propagation model [2]. Better understanding DME long range propagation is relevant to support the further evolution of DME into an area navigation network.

The device used for data collection, the setup of the In-flight collection campaign and the results of the data processing are presented in the following paragraphs.

Data collection

The DME SiS data collection was performed using the R&S®EDS300 level and modulation analyzer designed for installing and maintaining pulsed, terrestrial navigation systems. The DME/pulse analyzer offers high-precision distance measurements within a range of up to 400 NM for terrestrial, pulsed navigation signals from 960 to 1215 MHz. The R&S®EDS300 can precisely determine peak power and reply efficiency and can identify the ground station being measured. An interrogator with selectable output power (up to 20 W peak) is available for ground measurements, making it possible to acquire the main parameters of the reply pulses. Moreover, a high-power interrogator featuring up to 500 W (peak) can be used for flight inspections. Everything is built into a standard 19 inch housing using 3 height units (HU).

The following list contains the key facts plus some single specifications:

- High-precision measurement of DME and TACAN systems in line with ICAO Doc. 8071, ICAO Annex 10, STANAG 5034 and MIL-STD-291C
- Total peak level deviation < 1 dB
  95 % confidence level
- Receiver acquisition sensitivity –97 dBm
- Distance measurement uncertainty 95 % confidence level:
  - 0.01 NM down to –80 dBm, measurement time ≥ 100 ms/channel (SDME)
  - 0.05 NM from -95 dBm to -80 dBm, measurement time ≥ 100 ms/channel (MDME)
  - 0.03 NM from -80 dBm to +10 dBm, measurement time 5 ms/channel (MDME)
- 0.2° TACAN bearing deviation for input levels ≥ –80 dBm
- Detailed automated pulse shape analysis (rise-, fall-time, pulse spacing, pulse duration)

Furthermore, the R&S®EDS300 offers a "Pulse View" that allows a deeper analysis of the received pulses in the time domain (lin./log.). Several trigger settings can be used. The measurement of

- Rise time
- Decay time
- Pulse spacing
- Pulse duration and
- Peak variation

can be performed manually - by using the marker functions - or automatically.

Multipath propagation occurs due to reflections of the DME signal (e.g. on mountains, buildings and the earth's surface). With the Pulse View the reflected signal components can be measured. Figure 1 shows a DME signal and a reflected signal component (first reflected signal, ~180° out of phase) with an attenuation of ~13.2 dB and a delay of 4.8 µs (Marker 1 – Marker 2):

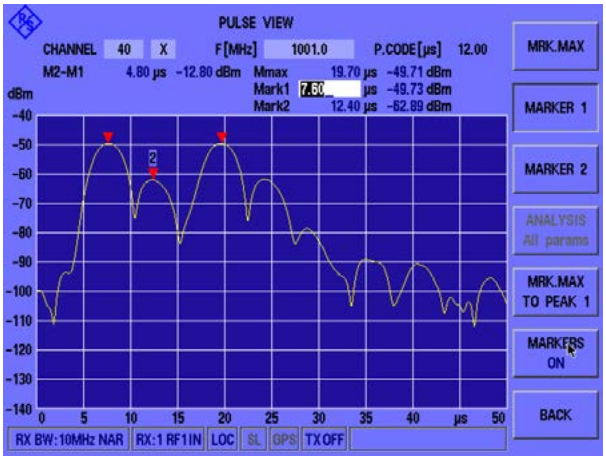

Figure 1. Multipath Analysis with R&S®EDS300 in Pulse-View Mode

The R&S®EDS-K5 multi-DME mode option expands this functionality to include flight inspection measurements and diverse monitoring applications, making it possible to analyze up to ten ground stations within 50 ms. All data can be transmitted to a control system via remote control (LAN), or stored on a USB flash drive (using the data logger).

On board of a flight inspection plane, the suppression bus input/output on the rear of the R&S®EDS300 should be used to protect other receivers aboard when the internal interrogator of the R&S®EDS300 is transmitting and vice versa. This protects the RX input of the R&S®EDS300 when other transmitters on board are temporarily active.

The main parameters stored when measuring in Multi DME mode include: Interrogator status (e.g. detection of valid reply pulses, Search/Track/Memory mode, GPS coordinates) and the main parameters of the transponder reply (peak power level, frequency offset, delay/slant range, pulse spacing, reply efficiency, station ID). The GPS coordinates must be obtained via an external receiver.

Figure 2 shows a screen shot of a measurement of eight DME stations with the multi-DME mode:

SLOT	CHAN	Level [dBm]	PS [µs]	Freq [kHz]	ID Code	Dist [km]	Search/ Track	Reply Eff.[%]
1	42 Y	-46.7	29.988	17.8	GME	10.908	M	95
2	50 X	-63.1	12.005	-7.7	GSW	9.838	T	91
3	40 X	-50.1	11.957	-0.7	OBW	7.963	T	95
4	56 Y	-56.5	30.003	1.0	ONE	9.974	T	96
5	106 Y	-37.9	29.980	0.7	GRM	8.139	T	96
6	109 Y	-47.4	29.998	3.5	ERB	36.211	T	98
7	103 X	-74.6	11.946	-7.4	NLK	33.865	T	89
8	99 X	-71.5	11.942	16.5	BLA	69.437	T	98
9	28 X	-98.9	-.---	-.-	---	--.---	---	---
10	91 X	-100.0	-.---	-.-	---	--.---	---	---

Figure 2. Measurements in Multi-DME mode

A flight inspection software may use the streaming mode or the recurrent query mode of the R&S®EDS300 to acquire and display the measurement results for a test flight. The FI software interprets each time slot and can display it graphically. A typical result of one of the multi DME slots is displayed in Figure 3:

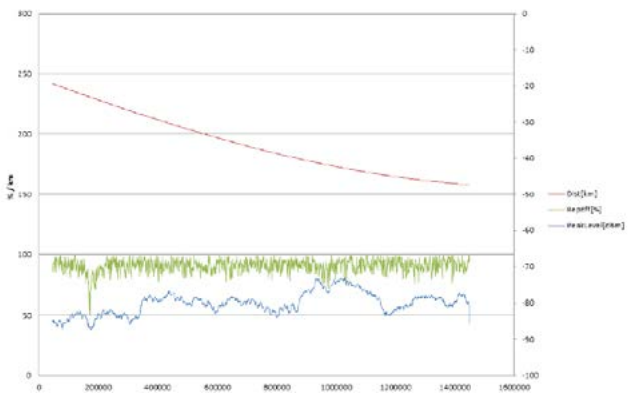

Figure 3. Plots of R&S®EDS300 FI records

The collection of in-flight data was performed by the flight inspection unit of DSNA (Direction Générale de l'Aviation Civile of France), during a regular flight inspection campaign of the VOR facilities. The flights were performed at a low en-route level (FL220) along selected segments of the ATS route network in France and the neighboring countries. The full flight trajectory is presented in Figure 4, together with the locations of all the DME ground stations that were recorded. The total flight time accumulates to more than 50 hours over 8 consecutive days.

For interrogating and recording the reply parameters of these facilities, two R&S®EDS300 test sets were used. The devices were installed in a standard 19 inch rack in the flight inspection aircraft ATR42 (see Figure 5) and shared one DME antenna installed on top of the fuselage. The signal attenuation from the antenna to the input of the receivers was estimated at 4 dB. The overall data recording rate was set to 20 records per second, i.e. 2 records per second for each of the 10 channels. A relative low rate was used (10 times lower than the maximum rate) in order to limit the size of the logs to a reasonable level for post processing.

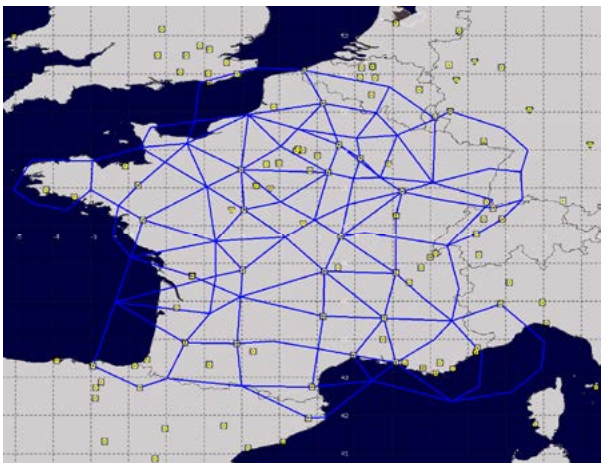

Figure 4. Flight Path and Recorded Stations

Figure 5. R&S®EDS300 Installation in the FI Aircraft

The station tuning plan was defined together with EUROCONTROL prior to this flight campaign. The selection of the ground stations for each flight segment was determined having in view three main objectives:

- Collect data for the validation of usable range predictions at large distances, for potential implementation in DEMETER (EUROCONTROL software tool for infrastructure assessment of DME in support of PBN applications)
- Assess signal level at long ranges and compare with propagation model predictions
- Asses slant range information accuracy to assess performance with respect to current standards

In view of the first two objectives, in general the selection of navaids at the limit of the predicted coverage range due to radio horizon or line of sight obstructions was sought. There is a particular interest in the usability of DME at large ranges, since this has not been studied extensively so far (conventional facility use and associated flight inspection is limited to short ranges) and is becoming more relevant in the context of PBN, also with a view of only having to maintain as few DME stations as possible to provide a sufficient RNAV service. In order to minimize the tuning activity during the flight, the channel selection was maintained in general for 30 to 40 min. Therefore, for some stations and various time intervals the records don't show valid range information due to the absence of valid replies. In other cases, frequent transitions between track search and memory modes were recorded. While the information content of a channel without data is limited (but non-zero), and thus not optimal in that sense, the tuning strategy still allowed collecting a large amount of valid DME records which enabled a large sample statistical analysis from a diverse set of European DME. The dataset includes a large variety of transponder manufacturers and equipment generations.

Range Accuracy Analysis

With the R&S®EDS-K3 GPS synchronization option installed and an NMEA-capable GPS receiver connected, the R&S®EDS300 stores the (D)GPS timestamp and location stamp (coordinates and altitude) for every data set. These data sets also contain the slant range (delay) to the DME stations. However, the slant range errors are not computed in real time and recorded in the data logs. A post processing of slant range and GPS data allows an analysis of the range error. The analysis was performed in a similar way as in the analysis performed by Boeing on USA DMEs data [1] so that the results could be easily compared. The main preprocessing steps are listed below:

- Filter records and keep only data recorded in Track mode
- Estimate reference (true) slant range based on the GPS coordinates of the FI aircraft available in each data record and coordinates of the corresponding ground station
- Compute the slant range error as the difference between the recorded and the reference values
- Compute the mean error and standard deviation values.
- Plot slant range errors, and the mean and standard deviation values vs. reference slant range
- Generate overall error distribution histogram

All "true" slant ranges were computed in the ECEF reference system after converting the aircraft and ground station geographic coordinates to Cartesian coordinates. This same methodology was applied to:

- The full dataset recorded in Track mode
- A dataset in which the first and last 10 sec of a tracking mode period were removed. This "20 sec filter" was applied also in the tests performed by Boeing and is expected to clean the data recorded at the limit of the LoS/coverage areas (where the multipath and diffraction effects could impact the SiS) or before the receiver has achieved a stable Track status.

It should be noted that this section focuses on the analysis of the aggregate dataset which merges all valid records from all stations. The detailed analysis of individual stations performance was out of the scope of this study. Nevertheless, a brief assessment of the accuracy of individual stations and the impact on the positioning accuracy are addressed in the "Real case analysis" section.

The aggregated dataset contains close to 800.000 records. This is considered a relevant amount of data from a statistical analysis perspective. The graphs of the slant range error versus the real slant range are presented in Figure 6: the first graph corresponds to the full data set and the second graph corresponds to the dataset obtained after applying the 20 sec filter. In these plots, the +/- $2\sigma_D$ bounds as defined by the applicable standards are represented by red lines, together with the +/- 2σ values computed based on the recorded data, in 1 NM intervals (dark blue dots). The mean values computed in 1NM intervals are represented with light blue dots.

According to current standards [3], [4] the distribution of individual DME stations errors is assumed to be a normal distribution $e_{Di}=N(\mu_{Di}, \sigma_{Di})$, with zero mean and the standard deviation is estimated as:

$$\sigma_{D_i} = \sqrt{\sigma_{SiS}^{\ 2} + \sigma_{air}^{\ 2}} \quad (1)$$

where:

$$\sigma_{SiS} = 0.05 \text{ NM} \quad (2)$$

$$\sigma_{air} = \text{Max}\ \{0.085 \text{ NM}, 0.00125\ D_i\} \quad (3)$$

D_i = slant range in NM (4)

From the equations above it can be shown that σ_D=0.1NM for ranges up to 68 NM, followed by an increase for higher ranges up to approximately 0.2 NM at 160 NM (as presented in Figure 6).

When analyzing these plots it becomes evident that the standards are conservative and that the achieved range accuracy is significantly better than the required baseline:

- The computed 95% bounds (2σ) are consistently less than 0.1 NM (180 m), less than half than the most stringent standard requirement of 0.2 NM.
- The increase of σ with the distance from the ground station is not confirmed.

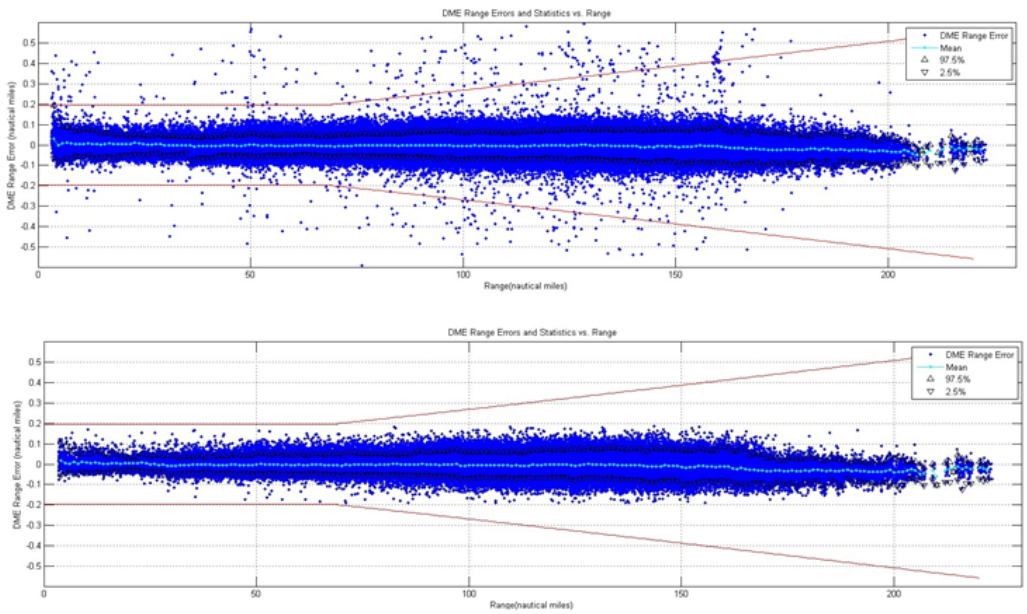

Figure 6. Aggregated Slant Range Error vs. Slant Range: Upper Plot – Full Data Set, lower Plot – 20 Second Filter Data Set

It is also observed that the 20 sec filter cleans out most of the outliers so that practically all measurements are contained within +/- 0.2 NM.

The values that describe the error distribution for the aggregated data are:

- Full data set

  Mean = -0.0038 NM (-7m)

  Standard deviation = 0.0333 NM (61m)

- 20 sec Filter data set

  Mean = -0.0050 NM (-9m)

  Standard deviation = 0.0322 NM (59m)

It can be seen that the filter does not significantly change the characteristics of the error distribution. This means that despite the filter cutting a significant amount of data considering the clearly visible difference between the Figure 6 plots, the difference is statistically insignificant. The histogram generated for the full dataset confirms that the distribution is Gaussian (Figure 7). The shape of the histogram for the filtered dataset is almost identical and therefore not presented.

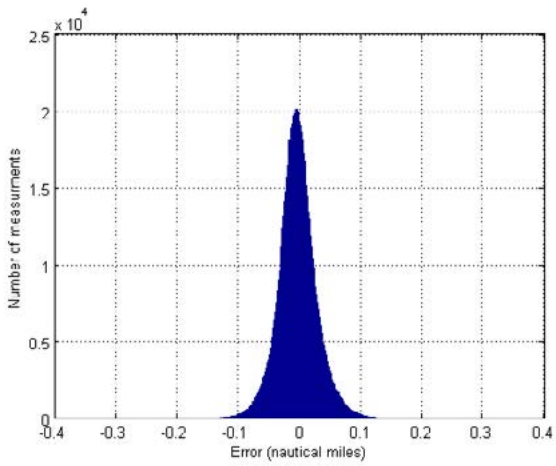

Figure 7. DME Slant Range Error Histogram

The analysis of the individual ground station accuracy confirmed in general the tight standard deviation values derived from the aggregated dataset. However, it was also noted that the mean values are usually higher than the aggregated mean, values close to 0.05 NM (100 m) being computed in several cases. It is not clear though if these relative high biases (but still within the acceptable tolerance limits) are caused by a reply delay offset of ground facilities, incorrect coordinates used in the analysis (or coordinates with limited accuracy resolution) or even due to average multipath effects.

The main conclusion of the analysis is that the results are very similar with the results of the study performed in the US navaids environment [1], and that the achieved accuracy is significantly better than the baseline requirements. Yet some further remarks need to be made:

Our results were obtained with a precision interrogator for which the range measurement uncertainty is significantly better than the standards and slightly degrades only at relatively long distance from the ground station, when the signal level drops below -80 dBm. The error dispersion when using regular TSO C66c [REF] interrogators would most likely be higher. However, according to the specifications of modern receivers with digital signal processing, the uncertainty of range measurements is described by a standard deviation (σ_{air}) on the order of 0.05 NM or better, which is considerably better than the minimum baseline. The following comparison table shows the 95% confidence level of the range error of the R&S®EDS300, and some of the standard interrogators:

Table 1. Range measurement accuracy comparison

R&S EDS300 (MDME)	Rockwell-Collins DME-2100	Honeywell DME-850
0.03 NM -10 to -80 dBm 0.05 NM -80 to -93 dBm	0.1 NM -20 to -83 dBm	0.05 NM+/- 0.1% of range down to -90 dBm

On the other hand, in our tests the error budget includes the un-aided GPS positioning uncertainty which may be in the order 0.01 NM depending on the number of tracked satellites. This error component (not present in the cockpit DME range measurements), slightly degrades the performance level determined using the R&S®EDS300 recorded data.

Last but not least, the ground stations network include a mix of legacy and modern design transponders. Therefore the results are not fully representative for the performances of new design systems which will gradually replace the old systems at the end of their life cycle.

Signal Level Analysis

The signal level measurements were performed without a rigorous calibration. As mentioned above in the data collection description, an antenna mounted on top of the fuselage was used, (specific gain pattern was not determined) and the on-board loss was estimated to 4 dB.

The variation of the recorded peak level of the transponder replies with the distance slant range is shown in Figure 8 (white dots). For better clarity this figure comprises two plots which include following additional information:

- Upper plot

  Blue line: Computed mean value

  Red lines: Computed +/- 2σ values

  Light green line: peak level estimation based on declared EIRP and Free Space Path Loss

  Dark green line: peak level estimation based on declared EIRP and FSPL generated by the FAA implementation of the IF-77 propagation model

- Lower plot

  Red lines: Computed +/- 2σ values

  Magenta lines: IF-77 5% probability (upper) & 95% probability (lower) estimation curves

The mean and standard deviation values were computed on 1 NM intervals. For the peak level analysis, only the high power ground stations were selected (declared EIRP of 37 dBW). When estimating the signal level, the following vertical radiation patterns were used: generic RTCA model [5] for the transponder and generic cosine pattern for the interrogator. The IF-77 estimates were generated using the FAA software application which implements this propagation model [6]. It should be noted that the transponder antenna radiation pattern used with this FAA program (DBS5100A antenna) is slightly different from the generic RTCA model, notably for high elevation angles, which explains the difference between our estimation and IF-77 estimation based on FSPL at low ranges.

After an initial analysis it was found that the mean values of the measured data are constantly lower than the estimated levels by approx. 8 dB. Therefore it was assumed that this is the on-board installation loss, and this loss was taken into account when generating the FSPL estimation curves in Figure 8. While a detailed investigation of this high attenuation is beyond the scope of this paper, it is suspected that the extra 4 dB (the on-board loss was estimated to 4 dB) may be explained by the masking of the direct path by the fuselage, notably at low ranges.

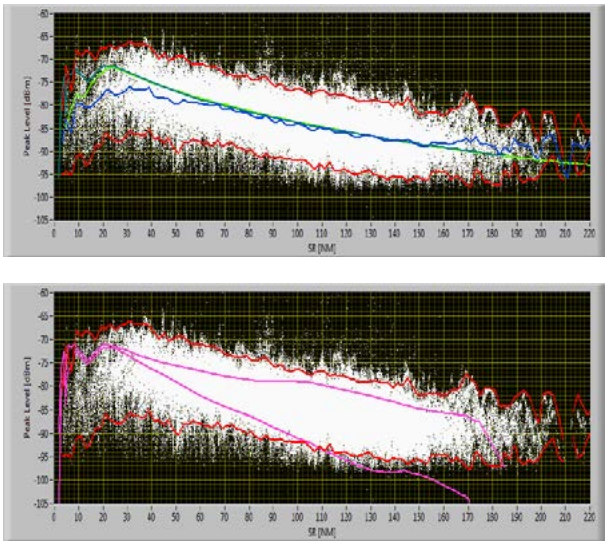

Figure 8. Aggregated Peak Level vs. Slant Range

With the above assumptions on ground stations EIRP, antenna radiation patterns and overall on-board attenuation it is observed that:

- The mean values of the recorded signals match very well the FSPL estimation at ranges between 50 and 150 NM
- At low ranges the mean peak level is lower than the FSPL estimation, by up to 6 dB. This difference could be linked to the location of the antenna on top of the fuselage.
- Beyond 150 NM the mean level becomes higher than the FSPL estimation. However, the number of samples decreases rapidly over this large slant range and the stations recorded at high ranges may transmit with higher power than the declared EIRP considered by the study (e.g. TACAN stations). Additionally, it is highly likely that these stations are installed on high terrain locations since the radio horizon for an altitude of 22.000 feet (flight altitude) is not more than 180 NM.
- The computed standard deviation remains almost constant for all ranges
- The 95% probability estimation generated by the IF-77 model is optimistic at low ranges, and becomes pessimistic beyond 110 NM

The above results are based on the full aggregated dataset. The results clearly show a very high variance of the received peak level in flight conditions at all ranges. The computed standard deviation for the full dataset is equal to 4.8 dB (the FSPL estimation was used as reference). The peak level histogram is presented in Figure 9. Similar to the range accuracy analysis, the 20 sec filter does not have a significant impact on the overall mean and standard deviation values peak level or on the histogram shape (plots not presented).

From this data it can be concluded that DME ranging is clearly possible until at least 160 NM, and maybe even 200 NM.

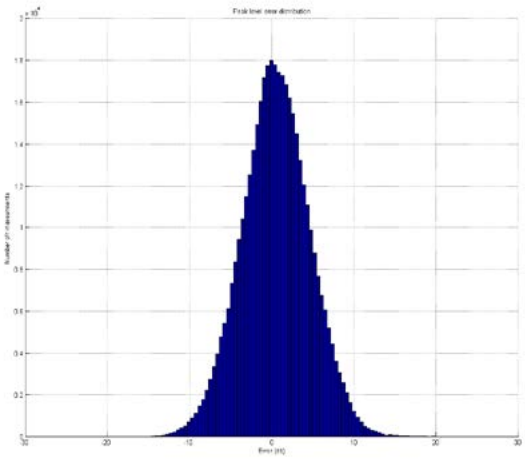

Figure 9. Peak Level Histogram

DME/DME POSITIONING ACCURACY

The analysis of the in-flight data collection showed a much better accuracy of the actual DME slant range information than the requirements baseline. Since this information is used by the RNAV systems to compute the aircraft position it is also interesting to assess the accuracy of the DME/DME solution that can be achieved using the current DME infrastructure. The assessment will address the most common approach used currently: the DME pair approach. It should be noted that a purely DME-based positioning solution will be analyzed, without considering any enhancements using Kalman filters or inertial integration. A brief description of the theoretical principles of the position calculations and error distribution will be presented first. These principles will be applied to the in-flight data records in order to assess the achievable performance.

Theoretical Considerations

The approach used by most of the FMS models in operation today in the DME update mode is based on DME pairs: the ranges from two stations are used to determine two potential position solutions as the intersection of two circles in a local horizontal plane. The ambiguity is typically eliminated based on the latest computed solution.

When the position is computed based on two ground stations, it is assumed ([4], [7]) that the position error has a normal distribution, with zero mean and the standard deviation determined as a function of the individual slant range errors and the subtended angle α_{ij} (as seen from the aircraft):

$$\sigma_{DDij} = \frac{\sqrt{\sigma_{Di}^{\ 2} + \sigma_{Dj}^{\ 2}}}{\sin \alpha_{ij}} \tag{5}$$

It is interesting to note that the DME/DME position is computed only in the horizontal dimension and therefore the theoretical derivation of the solution accuracy indicates that only the horizontal components of the individual DME standard deviation should be used [10], which implies that equation (5) is slightly conservative.

Data Analysis

The slant range data recorded during the flight inspection campaign was used for analyzing the performance achievable by a DME-pair algorithm. It was mentioned above that the R&S®EDS300 unit was set to log two records per second for each of the ten channels. A software application was created to process these records to test all pair combinations, compute and record all valid position solutions. At a maximum, 45 solutions could have been obtained per data record, i.e. $C(10,2)$, therefore only the log saved from the first day was processed to obtain almost 230.000 solutions in total (on average, less than five valid DME ranges out of a possible ten were found in each record). The DME/DME solution was computed in the ECEF (Earth-Centered Earth-Fixed) coordinate system, starting from the stations coordinates, the slant ranges and the aircraft altitude. Due to the fact that the barometric altitude information is not available in the logs, the GPS altitude was used. The position error was computed for each solution using the GPS coordinates as reference. In addition, the subtended angle was computed for the corresponding DME pair. Finally the solution error was plotted versus the subtended angle (Figure 10). In this figure the following curves are also represented:

- Blue line: $2\sigma_{DD}$ limit as per (5), assuming a general slant range standard deviation σ_{Di}=0.1NM, the baseline assumed by the standards, see (1) to (4)
- Red line: $2\sigma_{DD}$ limit as per (5), assuming a general slant range standard deviation σ_{Di}=0.05NM (slightly higher than the standard deviation of the recorded data)
- Green line: $2\sigma_{DD}$ for the computed DME/DME solutions in steps of 2 deg. (over bounds 95 % of the errors)

The results displayed in figure 10 confirm equation (5) which defines σ_{DD} as a function of individual σ_D and the angle subtended by the DME pair. At the same time these results show that (5) returns conservative results when the standard assumptions on the slant range accuracy are used.

The FMS models that use the DME-pair approach select automatically the stations to be used based on specific algorithms defined by each manufacturer. Most of these models limit the acceptable range of the subtended angle to 30-150 deg. which is the minimum baseline defined by [8]. When this limitation is applied in our assessment, the error distribution shown in Figure 11 is obtained. In this case the maximum value of the computed $2\sigma_{DD}$ is 520 m (less than 0.3 NM) which corresponds to the limits of the subtended angle range. It is noted that this accuracy level is significantly superior to that required for the NSE (Navigation System Error) to support RNAV 1 applications, i.e. 0.866 NM [9], which is the most demanding PBN navigation specification which currently explicitly includes the use of DME/DME positioning in addition to GNSS, and should support most if not all en-route and terminal area applications. It should be kept in mind though that this level of performance was obtained using the range measurements of a high accuracy test set (R&S®EDS300). However, these results suggest that when using the current generation of interrogators and transponders, DME/DME navigation can achieve accuracy performance in the area of a 0.3 NM NSE, e.g., able to support RNP 0.5 or better.

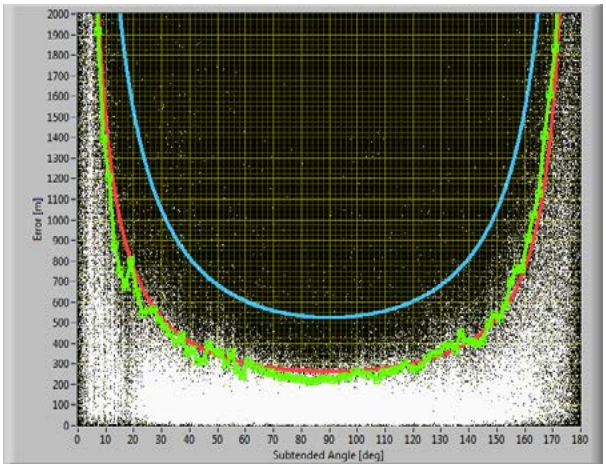

Figure 10. DME/DME Error vs. Subtended Angle

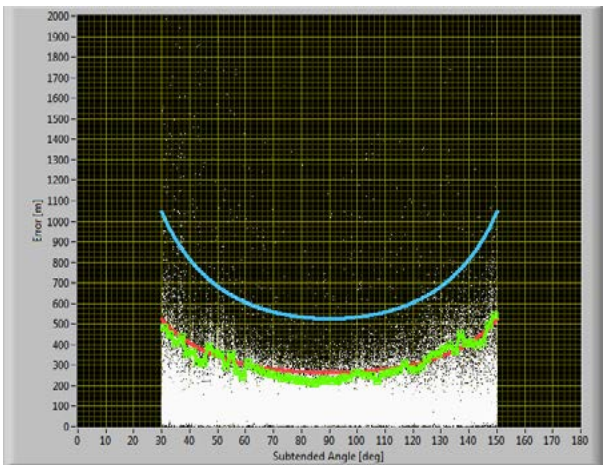

Figure 11. DME/DME Error vs. Subtended Angle (30 to 150 deg.)

PATH FOLLOWING ERROR ANALYSIS

The previous sections have analyzed the DME range and DME/DME positioning accuracy using a statistical approach. In this section we will assess the expected path following errors in the DME/DME mode. This time the analysis is made only on one particular flight segment. While a statistical approach is also possible and would be relevant, it is important first to present a case study in order to analyze the potential issues and their specific causes.

At present there are several software tools available for the assessment of the coverage and the positioning accuracy supported by the DME infrastructure. These tools predict the DME/DME redundancy (number of usable pairs) and the NSE (Navigation System Error) using the baseline geometry restrictions used by FMS's in the navaids selection process, i.e. subtended angle interval and min/max range to the station and the relations (1) to (5) presented above. For the availability and continuity of service, it is desirable to provide full DME/DME redundancy (two independent pairs) in the subject airspace. Additional usable pairs will always improve these parameters; however an excessive redundancy brings only marginal benefits (if any) and leads to increased cost of operation and inefficient use of the spectrum. It can be assumed that the accuracy of the service (NSE) follows the same rule. Indeed, an increased number of facilities, wisely sited, makes that at least one pair with good geometry, i.e. subtended angle not close to the 30/150 deg. limits , is available along the ATS routes defined in a certain airspace. As such, in general the software tools compute and present the best NSE when several usable pairs are available. Yet, this NSE value is based on the assumption that the on-board systems always select the DME pair with the best geometry. Unfortunately, this assumption is invalidated by the evidence collected from flight inspection reports and information available to the authors regarding the selection algorithms used by different RNAV systems. According to this information, some of these systems were designed to minimize the tuning activity, and therefore after acquiring a DME pair, will use it until the geometry constraints are not met, or one of the signals can't be tracked anymore (e.g. the signal level is below the minimum threshold). As a result, it is possible that these navigation systems show EPU values significantly worse than those estimated based on the best DME pair available. It is also possible that the FMS switches shortly to dead reckoning (DR) when a distant station goes out of the Line of Sight (LoS) due to terrain masking, in areas well covered by other closer stations. Such cases have been reported by Flight Inspection crews [10].

In this context, the following questions may arise from the Flight Inspection perspective: how many ground stations should be flight checked when validating an RNAV STAR? Is it sufficient to inspect the signal-in-space received from the closest stations, which provide the best coverage and geometry, or maybe it is necessary to inspect also the more distant stations which provide at least partial coverage for the first legs and which may be tuned when the aircraft starts the procedure? In the case of a SID procedure, the situation is slightly different, since on departure the signals from the closer station will be acquired first because the stations will be in LoS at lower altitudes. Nevertheless, the first pair acquired may not necessarily be the pair with the best geometry, and this pair may be maintained even when better pairs are available.

In order to investigate the potential impact on the navigation accuracy when non-optimal pairs are used, the range data recorded in one particular flight segment was analyzed. This segment, part of an arrival procedure, starts at an altitude of 20.000 feet and ends at around 7.000 feet. Over this leg, 8 MDME channels recorded valid reply data (some of them not for the entire flight time). Details regarding the flight trajectory and the tuned ground stations may be found in Appendix 1. The appendix shows also the plots of the slant range error computed for each station.

The records were first processed as described in the DME/DME accuracy analysis section, to test all pair combinations which respect the geometry constraints, followed by the computation and recording of all valid position solutions and the errors relative to the GPS position. In addition to the absolute error, in this case the lateral deviation from the defined flight path was also computed. These individual lateral errors are shown in Figure 12, using different colors for different DME pairs. From this plot it can be observed that most of the errors are contained within +/- 0.4 NM, but for some parts of the flight and for particular pairs, the error dispersion is higher, so that some outliers are noted close to +/- 0.8 NM. It should be kept in mind that computed solution is based on raw range data: no averaging over a number of samples or other smoothing filters were applied to the slant range measurements. The data was further processed, to estimate the PFE (Path Following Error). For this purpose, a 2nd order low pass filter with a corner frequency of 1.5 rad/s was applied to the position solution (in line with the characteristic defined in ICAO Annex 10 for the DME-P error estimation). The results are presented in Figure 13, in which the plots corresponding to the various pairs can be clearly distinguished.

The magnitude of the lateral PFE is less than 0.3 NM for all potential pair combinations. It can be observed that the plots can be grouped in three main categories. A brief analysis of these categories and the correlation with individual stations range errors is presented below:

- Category #1: PFE less than 0.05 NM over the whole leg. This category includes pairs formed by stations which cover entirely the leg and provide range information with limited mean error and dispersion MDM # 1, 2, 3 and 7).

- Category #2: Negative (right side) mean PFE of around 0.2 NM. This deviation is characteristic for the pairs which include the stations recorded by MDM # 8 and 10, which show a bias of ~0.05, respectively ~0.03 NM
- Category #3: Positive (left side) deviations of up to 0.2 NM, observed between seconds 17.625 and 17.950. This category includes pairs formed with the station recorded by MDM #9. During the first part of the flight this station is at the limit of the LoS which is lost in the second part.

A detailed analysis of the coverage prediction for the recorded stations and the correlation with the measured parameters would require a substantial number of plots due to the descending vertical profile of the flight. Nevertheless, from the error plots presented in Appendix 1 it can be noted that most channels stop recording valid data towards the end of the leg, (mainly due to the low altitude). These figures also show that while the signal is tracked at the limit of the coverage the error dispersion increases significantly and may also show predominant positive or negative "bends", this behavior is most evident for MDM #9.

Overall, the PFE estimation analysis shows that for the analyzed scenario, the lateral flight error due to DME/DME NSE (the FTE component was not considered) remains well below the limit which applies for RNAV 1 applications, i.e. 0.867 NM, for all potential pairs. These results suggest that in this infrastructure environment, even if higher than usual errors are observed for some of the stations, TSE (Total System Errors) of 0.5 NM or even 0.3 NM may be supported (again, irrespective of the DME pair used).

The analysis shows also that while the ground stations may still be tracked, the accuracy of the range data and consequently of the position solution may degrade at the limit of the LoS, even when this happens relatively close to the station due to terrain masking. This highlights the importance of the flight inspection for the facilities which are used close to the coverage limits.

Multi-DME solution

The basic principles for computing a multi-DME solution and the comparison of the specific error distribution to the DME-pair solution error distribution were presented in [11]. In order to further evaluate the potential benefits of this approach, in this PFE analysis the all-in-view solution and the associated errors were computed for the same flight segment. The lateral deviation errors when the position is computed based on all valid ranges recorded in one time slot, is presented in Figure 14. The same low pass filter was applied as for the plots in Figure 13. It can be noticed that this all-in-view solution offers an accuracy better than 0.02NM (~ 40 m) for most of the flight time, with a limited number of peaks which can reach up to 0.06 NM. These peaks are observed when for several consecutive time slots, invalid data is recorded for various MDM channels. It is also observed that the impact of various types of range errors specific to the different stations have very limited impact. One other potential advantage of the multi-DME approach is the possibly to support a "RAIM-like" algorithm to detect and exclude (depending on the number of stations available), the ranges with high errors and ensuring this way a desired level of integrity for the computed solution.

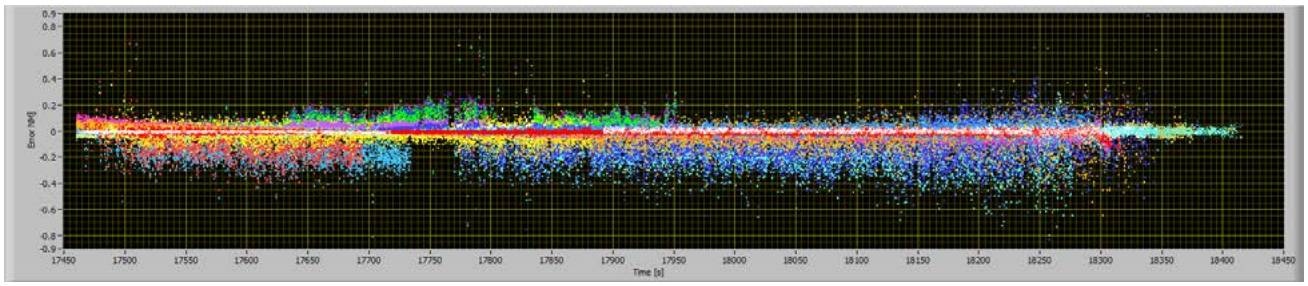

Figure 12. Unfiltered DME/DME solutions

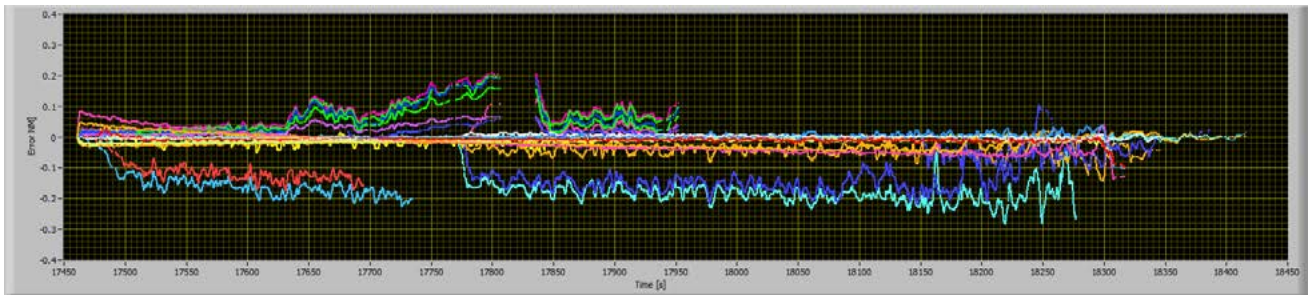

Figure 13. Filtered DME/DME solutions

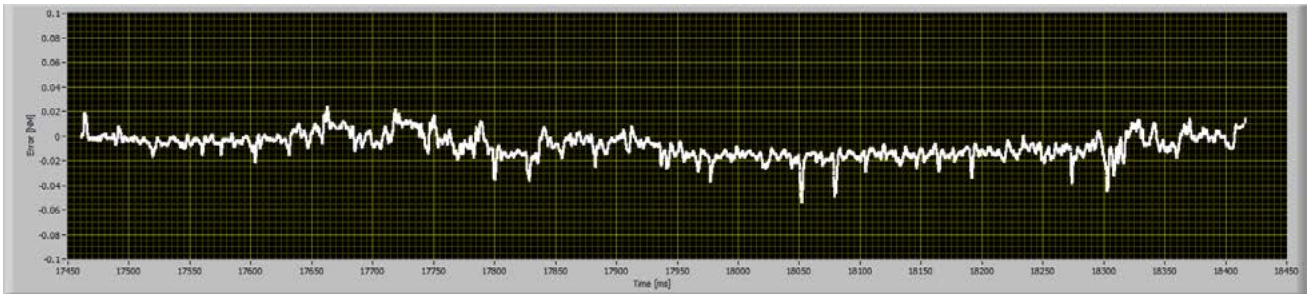

Figure 14. Filtered Multi-DME (all in view) solution

CONCLUSIONS

Building on a significant sample of actual DME ranging performance from many stations across a large European region, achievable RNAV positioning accuracies were derived. Both the DME-specific and the RNAV-positioning standards and assumptions were shown to be excessively conservative with respect to currently achievable performance. This is a problem that the GNSS community is familiar with, since there also actual performance well exceeds the minimum standards, especially when assuming the worst case minimum constellation availability. While it is currently established Air Navigation Service Provider and regulatory practice to only rely on minimum guaranteed performance as reflected in established standards, it may be appropriate to re-think this policy in light of the significant evolution of DME over the years and its use in an application that is well beyond what was targeted by the initial system design. This should be especially true when considering that DME/DME would only be used as a reversionary capability in case of a wide-area GNSS outage, since GNSS-equipage levels are expected to reach near 100 % in the near future. At any rate, careful analysis will need to ensure that DME/DME can actually continue to deliver this impressive performance when needed as the DME network evolves.

While this data demonstrates a relatively high hurdle for new A-PNT technology candidates by being able to provide 0.3 NM accuracy based on only two ground stations (e.g., no point to switch to a new technology if it cannot do better than this), it also points to the limits of achievable performance when excluding any technical improvements which would require an equipment change. A-PNT positioning accuracy performance requirements of 0.3 to 0.1 NM have been suggested, for example to support fixed radius turns (RF-turn) to intercept an ILS Localizer. Trying to push performance of DME/DME down to values around 0.1 NM would require either technical improvements to the DME or an excessive number of ground facilities as well as FMS which all use a multi-DME approach, which is currently not the case. Given that such a stringent requirement is likely to only apply in a very limited region near airports, this is no longer a wide-area outage problem. Consequently, it may be better to relax the A-PNT positioning and navigation guidance requirement to 0.3 or 0.5 NM and be prepared to handle final approach intercepts through ATC assistance using COM and GNSS-independent SUR sensors.

From a flight inspection perspective, it can be concluded that in case of RNAV SIDs/STARs, characterized by a dynamic vertical profile, the in-flight validation is recommended especially when the infrastructure assessment simulations predict multiple transitions in/out of the line of sight for the supporting ground stations. These transitions are not always a quick and clean process, and due to multi-path, diffraction and other propagation effects can be characterized by higher range errors dispersion as well as by error “bends” (equivalent to temporary biases). The analysis also suggests that in such cases it may be relevant to record the SiS from all stations in view (not only those which provide the best geometry) and perform an analysis of the accuracy supported by all potential DME/DME pairs. This analysis, which can be performed in post-processing, is facilitated by the simultaneous recording of a large number of channels (10 channels in case of R&S®EDS300). Nevertheless, the algorithms may be adapted also for flight inspection systems which record fewer channels (in which case data recorded in multiple logs has to be correlated).

ACKNOWLEDGMENTS

The authors are grateful for the support and guidance received from:

Stéphane Garcia, Florence Jacolot, Jean-Claude Bichet, Philippe Labaste, DSNA Flight inspection team, for the collection of in-flight data.

All commercial products mentioned in this paper and any associated intellectual property, copyright or trademark is and remains with their respective owners.

DISCLAIMER

This paper does not contain any official EUROCONTROL position or policy. Furthermore, it does not constitute any endorsement of a particular product.

REFERENCES

[1] Matt Harris, Tim Murphy, Robert W. Lilley, Robert H. Erikson, Performance of Current Distance Measuring Equipment and Implications on Alternative Position Navigation and Timing for Aviation, ION GNSS, September 2012

[2] G. D. Gierhart, M. E. Johnson, September 1983, The IF-77 Electromagnetic Wave Propagation Model, DOTI FAAI ES-83/3, U.S. National Technical Information Service, Springfield, Virginia

[3] ICAO Annex 10, Aeronautical Telecommunications, Volume 1, Radio Navigation Aids, Sixth Edition, July 2006

[4] RTCA DO236C, Minimum Aviation System Performance Standards: Required Navigation Performance for Area Navigation, June 2013

[5] RTCA DO-292, Assessment of Radio Frequency Interference Relevant to GNSS L5/E5A Frequency Band, July 2004

[6] ICAO NSP, Spectrum Sub-Group, IP7, IF-77 Model, May 2010

[7] ICAO Doc 9613, Performance-based Navigation (PBN) Manual, Fourth Edition, 2013

[8] FAA AC 90-100A, U.S Terminal and En Route Area Navigation (RNAV) Operations, March 2007

[9] EUROCONTROL, GUID-114, Guidelines for P-RNAV Infrastructure Assessment, Edition 1.2, April 2008

[10] Valeriu Vitan, EUROCONTROL, DME infrastructure study for LSGS-SION, Switzerland, Navigation Steering Group 17th Meeting, Navigation Infrastructure & GNSS Subgroup, April 2013

[11] Valeriu Vitan, Gerhard Berz, Natalia Solomina, EUROCONTROL, Assessment of Current DME Performance and the Potential to Support a Future A-PNT Solution, DASC, September 2015

APPENDIX 1

DME Range accuracy plots

The following plot shows the position of the ground stations used for the Path Following Error analysis, relative to the analyzed flight segment.

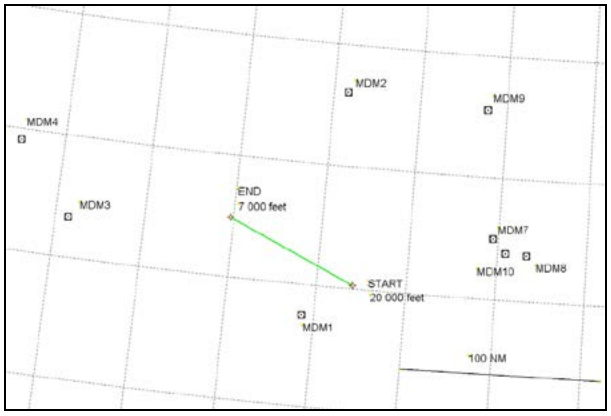

The next plots present the results of the DME range error calculations for the individual stations. For each MDME channel, two plots are presented:

- Left plot shows the slant range error versus time in the specific flight segment
- Right plot shows the histogram of the error distribution

MDME 1

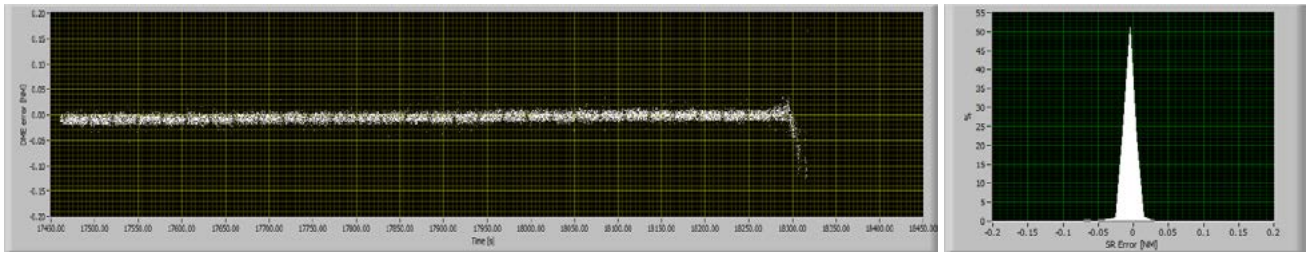

MDME 2

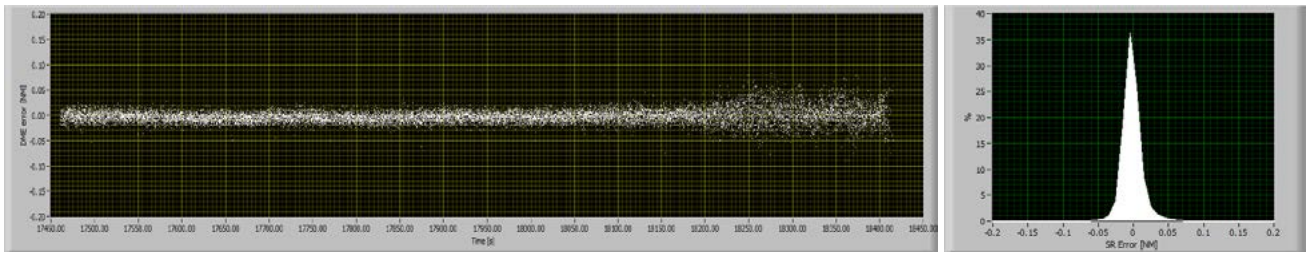

MDME 3

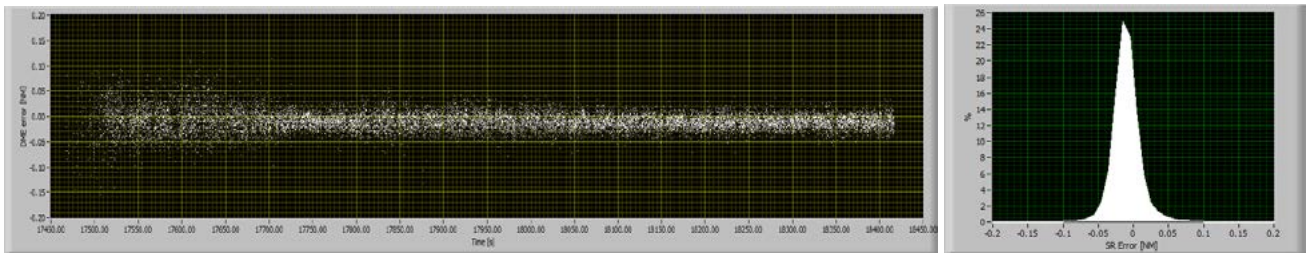

MDME 4

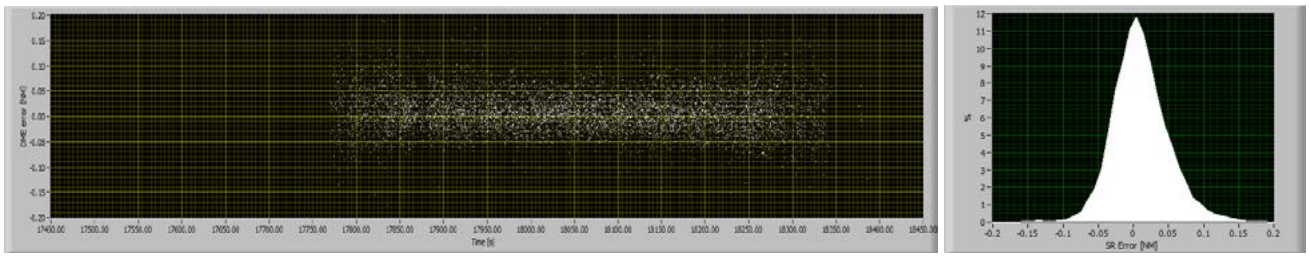

MDME 7

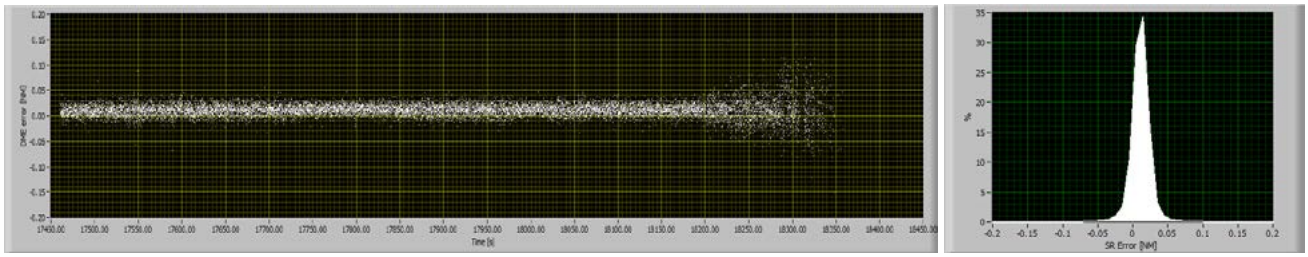

MDME 8

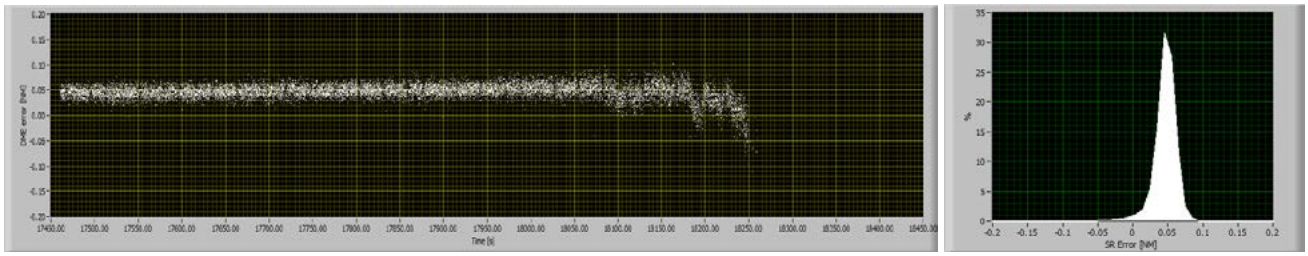

MDME 9

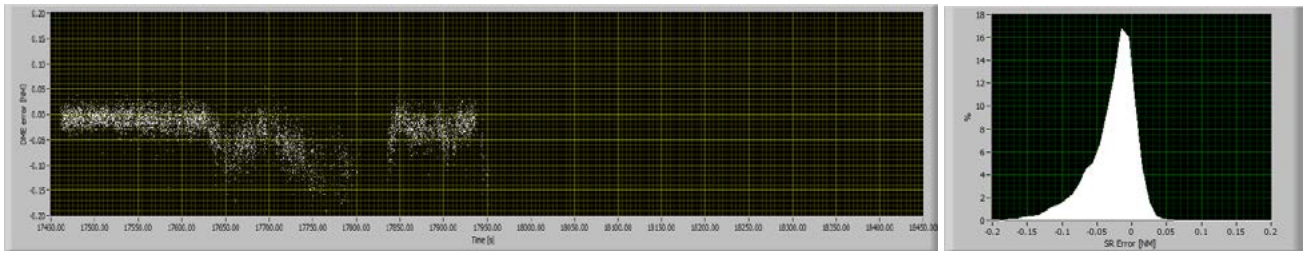

MDME 10

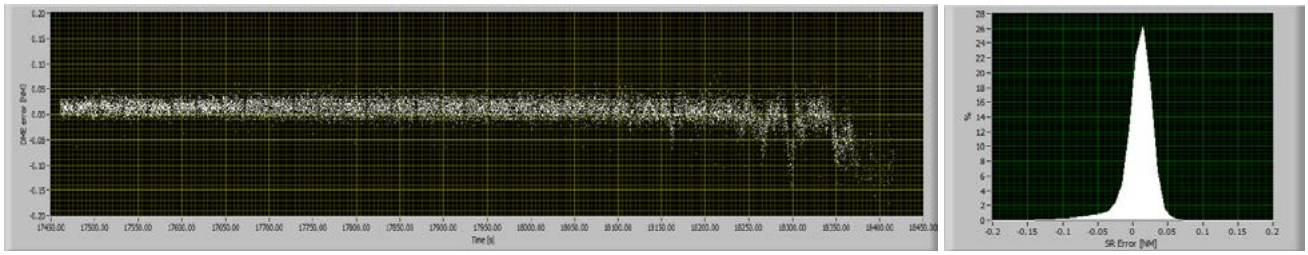

Embedded VDB Emulator for Multi-Mode Receiver Calibration in Flight Inspection System

Pengfei Wang
System Engineer
Aviation Data Communication Corporation
Beijing, China
Fax:+86 10 82339078 ext. 8058
E-mail: figo913@126.com

Xiaofeng Shi
Associate Professor
Beihang University
Beijing, China
Fax: +86 10 82338838
E-mail: shixiaofeng@buaa.edu.cn

Yongchao Wang
System Engineer
Aviation Data Communication Corporation
Beijing, China
Fax:+86 10 82339078 ext. 8058
E-mail: wangyongchao@vip.163.com

ABSTRACT

Ground Based Augmentation System for GNSS (GBAS) is an important trend of next generation landing system in aviation application, called GBAS Landing System (GLS). The flight inspection of Very High Frequency Data Broadcast (VDB) signal then will be an essential function in the future Flight Inspection System (FIS), even in a modern one. The FIS evaluates field strength distribution of VDB signals in the space via flight testing, inspects the guiding deviation of GBAS, and verifies the Final Approach Segment (FAS) data emitted from GBAS ground station.

To guarantee the accuracy and reliability of GBAS inspection, the Multi-Mode Receiver (MMR) in the FIS need to be calibrated periodically, including the output of VDB signal strength and FAS data check. The general options have 1) connecting the same mode VDB transmitter with FIS via an attenuator to calibrate the MMR; 2) outputting VDB signal by VDB modulation module manufactured by Collins and IFR 2051 signal generator. The first option is too expensive and the VDB transmitter has to be programmed which is not easy to achieve, while the second method cannot generate GBAS data and fails to check the FAS data.

An embedded VDB emulator is presented in this paper, which is designed specially for GBAS flight inspection purpose. The emulator is able to provide VDB radio-frequency signal along with simulated FAS data, connecting to IFR2051. Using the emulator, VDB AGC data of MMR can be calibrated on ground, as well as FAS data checking, to ensure the GBAS inspection ability of the FIS. A special interface is developed to configure the VDB emulator real time via USB port, which also can be applied for further extension.

INTRODUCTION

GBAS with aviation standards identified in International Civil Aviation Organization (ICAO) Standards and Recommended Practices (SARPS), Annex 10 on Radio-frequency Navigation provides international standards for augmentation of GPS to support precision landing. The history of these standards can trace back to efforts in the United States by the Federal Aviation Administration to developed a Local Area Augmentation System (LAAS). Many references still refer to LAAS, although the current international terminology is GBAS and GBAS Landing System (GLS).

Local reference receivers located around the airport send data to a central location at the airport. This data is used to formulate a correction message, which is then transmitted to users via a VHF Data Link. A receiver on an aircraft uses this information to correct GPS signals, which then provides a standard ILS-style display to use while flying a precision approach.

The items of GBAS flight inspection is VDB signal strength field measure, ILS-style flight inspection and VDB up-link messages check, which includes Message

Type 1 & 11 - Differential Corrections, Message Type 2 - GBAS Related Data, Message Type 4 - Final Approach Segment(FAS).

In order to periodically calibrate Multi-Mode Receiver(MMR) in the FIS, A VDB simulator is indispensable to generate VDB signal for MMR. Many companies support those kinds of VDB simulator, for instance, Spirent - GSS4150, R&S - SMBV100A and so on. It should be noted that GSS4150 could not work independently but relying on GSS8000 and VDB function is a option of SMBV100A, which key feature is GNSS satellite signal generation. For MMR calibration, it is uneconomical if using GSS4150 or SMBV100A only for calibrating purpose.

The objective of this paper is to designing a embedded VDB emulator with generating VDB signal feature by cooperatively working with IFR2051(Aeroflex) which provides a expansion interface for users to add functionality.

This papaer first addresses the principle of VDB transmitting. The function of IFR2051 signal generator is described. For the rest of this paper, the hardware and software design of VDB emulator are demonstrated detailly. Finally, practical application situation of VDB emulator in FIS calibration is shown.

PRINCIPLE OVERVIEW

VDB Transmitting Principle

For the end of spectrum efficiency, Time Division Multiple Access (TDMA) technique is applied to VHF Data Broadcast (VDB), which is based on a two level hierarchy as shown in Figure 1. Each frame is 500 milliseconds in duration. Therefore, there are two such frames contained in each one-second UTC epoch. The frame is time division multiplexed such that it consists of 8 individual VDB time slots (A-H) of 62.5 millisecond duration.

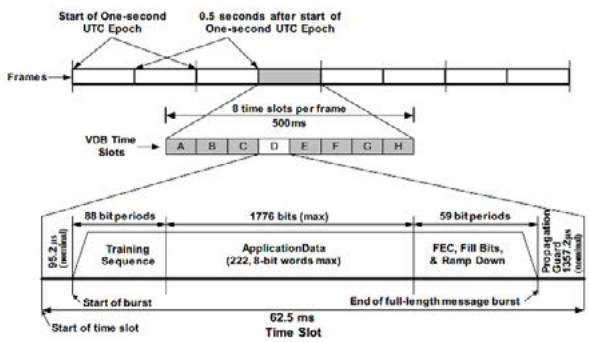

Figure 1. TDMA Timing Structure of VDB

Each VDB burst is contained in a time slot consisting of the data element shown Table 1.

Table 1. Burst Data Content of VDB

Index	Element	Number of Bits
1	Power Satbilization	15
2	Synchronization & ambiguity resolution	48
3	Station slot identifier	3
4	Transmission Length	17
5	Training Sequence FEC	5
6	Application Data	0-1776
7	Application FEC	48
8	Fill Bits	0-2

Symbols are converted to differentially-encoded 8 phase shift keyed (D8PSK) carrier phase shifts as shown in Tabel 2.

Tabel 2. Message Bits & Symbol Phase Shift

Message Bits			Symbol Phase Shift
I_{3k-2}	I_{3k-1}	I_{3k}	
0	0	0	0
0	0	1	$1\pi/4$
0	1	1	$2\pi/4$
0	1	0	$3\pi/4$
1	1	0	$4\pi/4$
1	1	1	$5\pi/4$
1	0	1	$6\pi/4$
1	0	0	$7\pi/4$

As depicted in Figure 2,the principle of VDB transmitting follows the sequence: application data formatting, crc encoding, FEC generation, bit scrambling and D8PSK modulation. In this project, the first four process steps are attained by VDB emulator and the final process step (D8PSK modulation) is achieved in the 2050 series digital & vector signal generator (IFR2051), which is introduced in followed section.

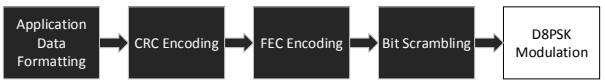

Figure 2. VDB Transmiting Processing Sequence

The Function of IFR2051

The IFR2051 series of digital and vector signal generators covers the frequency range 10 kHz to 2.7

GHz, which are suitable for a wide range of applications including the testing of new digital communication systems. It has an external digital data input port by which digital data of baseband can be feeded to IFR2051.

In digital mode, the IFR2051 signal generator is able to produce a wide array of digital modulation types and in each case the user is free to modify the data rate and filter characteristics to suit individual application needs. For common standards, IFR2051 is already pre-programmed to generate the required modulation format from a single key press and so aid ease of use. As shown in figure 3, IFR2051 is configured to VDR modulation mode the parameters of which include modulation type: D8PSK, symbol size: 3bits, Symbol Rate: 10.5kHz, pulse shaping filter (PSF) type: Nyquist and PSF alpha: 0.60. By the use of PSF, intersymbol interference(ISI) can be eliminated if the symbol rate is arranged like VDB system.

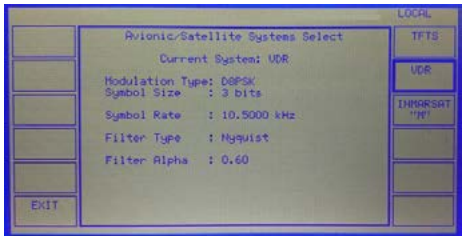

Figure 3. The Confgiuration Screen of IFR2051

The concept of IFR2051 function (D8PSK modulation) is depicted in figure 4. VDB emulator feeds symbol stream (3 bits width) to encoder which converts symbol stream to phase stream. Resampler is used to re-sample phase stream and prepare for pulse shapping filter(PSF). After filter process, by I&Q modulator, D8PSK modulation is typically generated.

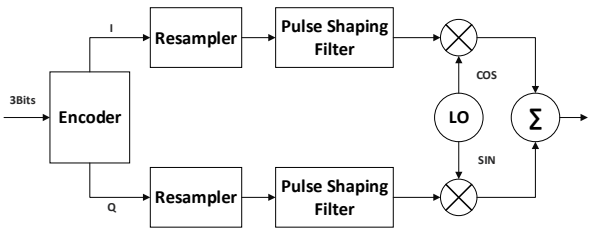

Figure 4. The Concept of D8PSK Modulation

The next question is how to feed symbol stream to IFR2051. A 25-way D-type connector is provided by IFR2051 on its rear panel, by which VDB emulator can apply symbol stream to IFR2051.

In followed section, VDB emulator design is described including hardware design, driver design and software design

HARDWARE DESIGN OF VDB EMULATOR

VDB emulator is USB portable device, the parameters of which can be configured by a special application, including all the message type 4 (FAS data) fields.

Figure 5 shows the VDB emulator which has a 25-way D-type port, an USB port and a spare port.

Figure 5. The VDB Emulator

The hardware structure of VDB emulator is depicted in figure 6. There are four modules in VDB emulator, containing power supply, micro-controller, adapter port for IFR2051 and USB2.0 port. Power supply provide 3.3 VDC power for micro-controller, which is a DC-DC converter circuit. Micro-controller module is the core circuit of this system, the function of which comprises reception of Message type 2 from computer by USB2.0 port, synchronization process for VDB TDMA regulation and communication with IFR2051.

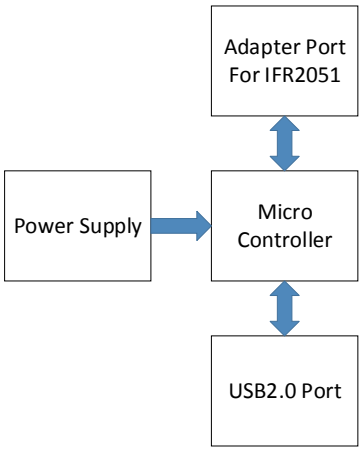

Figure 6. The Hardware Structure of VDB Emulator

Micro Controller Circuit

A 32-bit processer is applied in VDB emulator named STM32, that has 64 Kbytes of SRAM, up to 11 timers, one USB interface and 30 I/O ports. Those resources can satisfy the requirements of message data store, TDMA timing and interface adaption with IFR2051.

The micro-controller circuit is shown in figure 7 as follow.

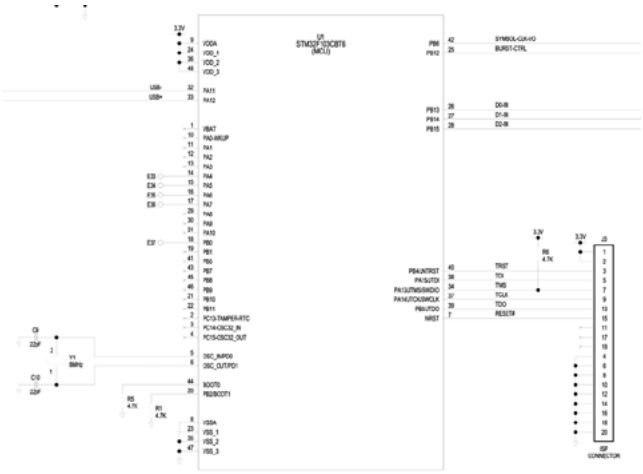

Figure 7. The Micro-controller Circuit

Power Supply Circuit

In power supply circuit, there are two DC/DC convertor chips, HT7550 and REG1117. HT7550 has high input voltage, so it owns the ability of converting 24VDC to 5VDC.

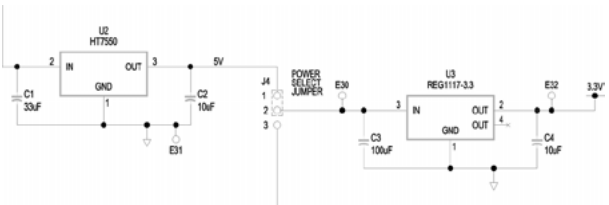

Figure 8. The Power Supply Circuit

Interface Adaption with IFR2051

In this application, IFR2051 is configured to accept external symbol stream in parallel mode drived by internal symbol clock. The used data bus include pin 19, pin 20 and pin 21, the width of which is 3 bits. It should be noted that the burst control input, assigned to pin 11, is used to turn the RF signal on or off with a controlled rise/fall time. The rise and fall time of RF power is internally controlled to occur over 3 symbol clocks to simulate an RF burst of modulated carrier as used in TDMA systems, such as VDB system. The detail timing chart is shown in figure 9.

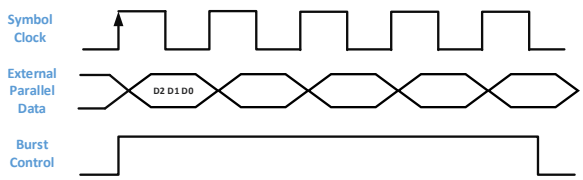

Figure 9. Timing Chart of External Port

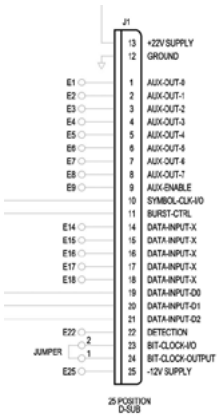

Figure 10. The Adapter Port for IFR2051

SOFTWARE DEGIN OF VDB EMULATOR

Application for VDB FAS Data Configuration

The function of VDB FAS data configuration software includs configuring FAS data content (listed in table 3), encoding CRC and FEC, and strambling data stream.

Table 3. The Content of FAS Data Block

Data Content	Bit Used	Range of Values
Operation Type	4	0
SBAS Service Provider	4	0-15
Airport ID	32	-
Runway Number	6	1-36
Runway Letter	2	-
Approach Performance Designator	3	0-7
Route Indicator	5	-
Reference Path Data Selector	8	0-48
Reference Path ID	32	-
LTP/FTP Latitude	32	± 90.0 °
LTP/FTP Longitude	32	± 180.0 °
LTP/FTP Height	16	-512.0 – 6041.5 m
ΔFPAP Latitude	24	± 1 °
ΔFPAP Longitude	24	± 1 °
Approach Threshold Crossing Height (TCH)	15	0 – 1638.35 m or 0- 3276.7 ft
Approach TCH Units	1	-

Data Content	Bit Used	Range of Values
Selector		
Glide Path Angle (GPA)	16	0 - 90.0 °
Course Width at Threshold	8	80.0 to 143.75 m
ΔLength Offset	8	0 to 2032 m
Final Approach Segment CRC	32	-

The GUI of FAS data configuration software is depicted in figure 11. As listed in tabel 3, all of the data content can be configured. After the FAS data block is organized, it can be downloaded to VDB emulator by USB port.

Figure 11. Application for VDB FAS Data Configuration

GLS CALIBRATION

This VDB emulator is practically used in GLS calibration of China flight inspection system (CFIS). The structure of GLS calibration bench is shown in figure 12, including VDB emulator, IFR2051, MMR930, EHSI and laptop with Arinc 429.

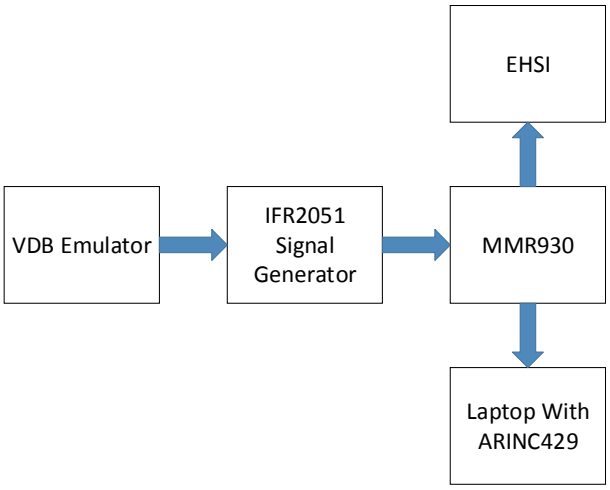

Figure 12. Equipment Structure of MMR Calibration

During the calibration, three virtual airport FAS data blocks is feeded to MMR930. By turning to different channel number, MMR930 can make decision on the selection of FAS data blocks. It should be noted that MMR930 can output reasonable deviation data, although status of those data is No-computed because of no differential correction data.

As depicted in figure 13, the FAS data outputed by MMR930 is shown in the GUI of GLS calibration software. By comparison with the FAS data of VDB emulator, FAS data check function is achieved.

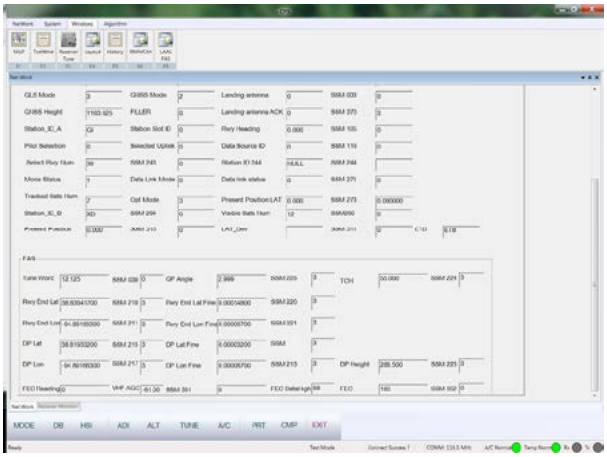

Figure 13. GUI of GLS Calibration Software

CONCLUSIONS

The VDB emulator's practical use is introduced in the paper and shows its valuable potentials in not only GBAS flight inspection but also GBAS equipment improvement.

This equipment can no only be employed for FAS data check. It is possible to extend function by spare interface, such as differential correction data and ground station data. It is proven that this equipment is effective and economical for CFIS.

REFERENCES

[1] ICAO Aeronautical Telecommunications, Annex 10, Volume I, Radio Navigation Aids, Sixth Edition , July 2006

[2] RTCA DO-253C, Minimum Operational Performance Standards for GPS Local Area Augment, December 2008

[3] RTCA DO-246D, GNSS-Based Precision Approach Local Area Augmentation System (LAAS) Signal-in-Space Interface Control Document (ICD), December 2008.

[4] IFR Application Note, Using the External Data Interface on The 2050 Series Digital & Vector Signal Generators, 2009.

[5] IFR Datasheet, 2050 Series Digital and Vector Signal Generator.

Future Flight Inspection of GBAS CAT III Installations

Claus-Sebastian Wilkens
R&D Engineer
Aerodata AG
Braunschweig, Germany
Phone: +49 531 2359-140
E-mail: wilkens@aerodata.de

Patrick Thomsen
Software Engineer
Aerodata AG
Braunschweig, Germany
Phone: +49 531 2359-175
E-mail: thomsen@aerodata.de

ABSTRACT

The term "Ground Based Augmentation System (GBAS)" describes a method for instrument landing based on real-time differential corrections for global navigation satellite systems. Current GBAS approach service type C (GAST-C) installations can be used for approaches up to CAT I conditions. Research and development efforts are presently working towards implementing the GAST-D standard, which will allow approaches up to CAT III conditions. ICAO standards regarding the implementation of GAST-D are being expected for the year 2016. First installations at airports are assumed to become operational in 2019 or 2020.

Before GAST-D installations are being released to public service, a commissioning is mandatory. This in turn requires the availability of appropriate flight inspection equipment and procedures. Current research and development endeavors focus on the implementation of such demands.

This paper presents the fundamental differences between GAST-C and -D systems. Furthermore it provides an overview of the current status of GAST-D developments and standards. Finally, the joint research project MEGA, which deals with the development of a GAST-D capable flight inspection system prototype, is introduced.

INTRODUCTION

The ground based augmentation system (GBAS) is a precision approach system based on global navigation satellite systems (GNSS), which is harmonized by the International Civil Aviation Organization (ICAO). Every aircraft, that is equipped with a GBAS receiver, can use GBAS ground installations at an airport. A GBAS ground station transmits several information messages to approaching aircraft via a VHF data link. These include differential corrections for visible navigation satellites, approach parameters, and integrity information. In this way, aircraft are enabled to follow GNSS based precision approaches. More than 1100 Airbus aircraft have already been delivered, which are GNSS landing systems (GLS) capable, see [2]. Boeing has delivered a fleet of more than 1500 aircraft with GLS activation, see [14].

From the perspective of a pilot or flight control system, these approaches are identical to those of an ILS ("ILS look alike"). Currently, GBAS category I (CAT I) approaches are certified and in operation, e.g. in Frankfurt and Bremen, Germany. These GBAS CAT I approaches are also known as GBAS approach service type C (GAST-C).

Current research and development work deals with the certification of the new GAST-D service for CAT II/III approaches. This service is going to allow aircraft to autoland even during poor visibility conditions. Contrary to ILS CAT II and III approaches, the protecion areas can be reduced in the future, thus increasing the usable airport capacity during adverse weather conditions. Although GAST-D is still to be standardized and certified, experimental ground stations already exist, which transmit a VHF data broadcast (VDB) signal with GAST-D data messages. In Germany, two experimental GBAS ground stations exist at the airports in Frankfurt and Braunschweig, which can be configured to emit GAST-D signals in order to support certification, and research and development works.

In contrast to GAST-C, GAST-D does not cover the approach only, but the complete landing process. This not

only demands stronger requirements towards the navigation system, but also in conjunction with the (auto) pilot. Thus, additional monitoring algorithms are required in order to guarantee the overall performance of the system. The performance of GAST-C installations is primarily defined by the ground stations operation. Additionally, contrary to ILS, GAST-D can be used for taxiing guidance on ground. The taxiing guidance requires reliable coverage on ground.

This leads to fundamental differences regarding the flight inspection, which is necessary for the operation of GBAS ground stations. While GAST-C primarily focusses on the approach of a flight, automatic landing and taxiing guidance also require the inclusion of ground operations into (flight) inspection.

It is the aim of the joint research project MEGA to develop a prototype flight inspection system, which covers the additional requirements for GAST-D ground installations.

GAST-C VS. GAST-D

GAST-D implements additions to the GAST-C standard, which allows CAT I operations. These additions are summarized in [1], which classifies the requirements types as positioning accuracy, integrity risk, continuity risk, availability, and VDB messaging. The following paragraphs give an overview on these requirements towards the GBAS ground subsystem, based on [1]. In these, the term facility approach service type (FAST) is used in order to describe the GBAS ground subsystem similar to the GAST classification.

Positioning Accuracy

The position accuracy is composed of the horizontal and vertical position domain accuracy in an assumed fault-free receiver and the ground subsystem pseudo range accuracy for FAST-C. For FAST-D, the pseudo range correction accuracies have to be improved, in order to support CAT-III approach requirements.

Integrity Risk

The integrity risk is again applied to a fault-free receiver. The ground station transmits integrity parameters, which are used by the aircraft receiver. Furthermore the satellite signal integrity is monitored in order to detect improper operation. In addition to these FAST-C requirements, FAST-D requires a specified performance for range source monitoring and for monitoring of anomalous ionosphere effects. Siting requirements are necessary in order to limit undetected errors by the ground or airborne monitoring. Finally, a specified likelihood probability for ground subsystem components, that could have catastrophic results or effects when failures occur, is proposed.

Continuity Risk

Assuming a fault-free airborne receiver, the continuity of the FAST-C system is defined by the transmission of data being in tolerance, VDB field strength , and the aircraft's achieved position error. FAST-C defines the continuity requirements only as a function of the ground subsystem failures and false alerts. Additionally, requirements on the fault-free detection of the ranging source fault monitoring functions are proposed for FAST-D.

Availability

The availability requirements do not differ between FAST-C and D. It is the air navigation service provider's (ANSP) responsibility to ensure system availability. FAST-D installations have to be backwards compatible to FAST-C requirements and thusly support GAST-C approaches with current aircraft receivers.

VDB Messaging

The VDB RF transmission characteristics and messages are defined by the Standards and Recommended Practices (SARPs). GAST-D is going to transmit additional messages. GAST-C already implements message type 2, which allows the calculation of a 100 second smoothed position solution. The GAST-D message type 11 is going to support the calculation of a 30 second smoothed position solution. These position solutions based on differently smoothed measurements allow for the detection of ionospheric anomalies in the so called dual solution iono gradient monitor algorithm (DSIGMA). Furthermore, GAST-D uses the 30 second smoothed position solution in order to calculate the guidance deviations instead of the GAST-C 100 second smoothed solution, in order to reduce the ionospheric bias effect on the smoothed ranges and deviations.

CURRENT GAST-D STATUS

While GAST-C ground installations have already been implemented and certified at airports, the GAST-D standardization process is still ongoing. According to [9], ICAO is currently working on finishing necessary SARPs. The Navigation Systems Panel (NSP) is scheduled to discuss and if possible endorse GAST-D SARPs in December 2016 for applicability in 2018.

RTCA, Inc. is currently working on the GAST-D related Minimum Operational Performance Standards (MOPS) and Interface Control Documents (ICD). GAST-D updates to the documents DO-246 [11] and DO-253 [12] are planned for early 2017, according to [9]. Similarly EUCROCAE is also working on an update to its MOPS for GBAS ground stations ED-114 [3].

EASA's current rule making plan 2016-2020 includes the rule making task RMT.0680 "Ground-based augmentation system (GBAS) CAT I/II/III". Its objective is the development of the requirements for the use of GBAS to support CAT I/II/III operations, see [4]. The terms of

reference are scheduled for 2016, the decision and completion of the RMT are expected by the end of 2018.

FAA's work on the GAST-D operational approval is currently scheduled to be finished by the first half of 2020, see [6]. For this, the ground equipment system design approval (SDA) is scheduled to be finished by mid-2019. In parallel the GAST-D update for the flight inspection capability is developed. In this process, the acquisition of a GAST-D receiver is scheduled for the first half of 2018 and followed by the aircraft modifications. Currently, no primary or flight inspection navigation receiver with GAST-D capabilities is commercially available. The flight inspection software update is scheduled to be finished with an operational test and evaluation process by the end of 2017.

[9] mentions the overall completion target as 2018-2019. One of the main GAST-D related topics still being worked on is the ionospheric gradient mitigation. Depending on the location of the GBAS installation, it can be challenging to detect changes in the ionospheric delay. For this reason an Ad-Hoc group with more than 30 members from equipment manufacturers, regulators, air navigation service providers, academia, and consultants has been formed to cover this issue with the ionospheric gradient monitor (IGM), see [13].

On the GBAS ground station manufacturer's side, Honeywell is currently developing the SLS-5000 system. The system design approval by the FAA is planned for 2019, see [10]. Indra Navia is currently researching GAST-D using two Normarc 8100 prototype ground stations at Oslo Gardermoen and at Frankfurt airport, see [8]. The latter one uses two VDB stations in order to cover the whole airport area.

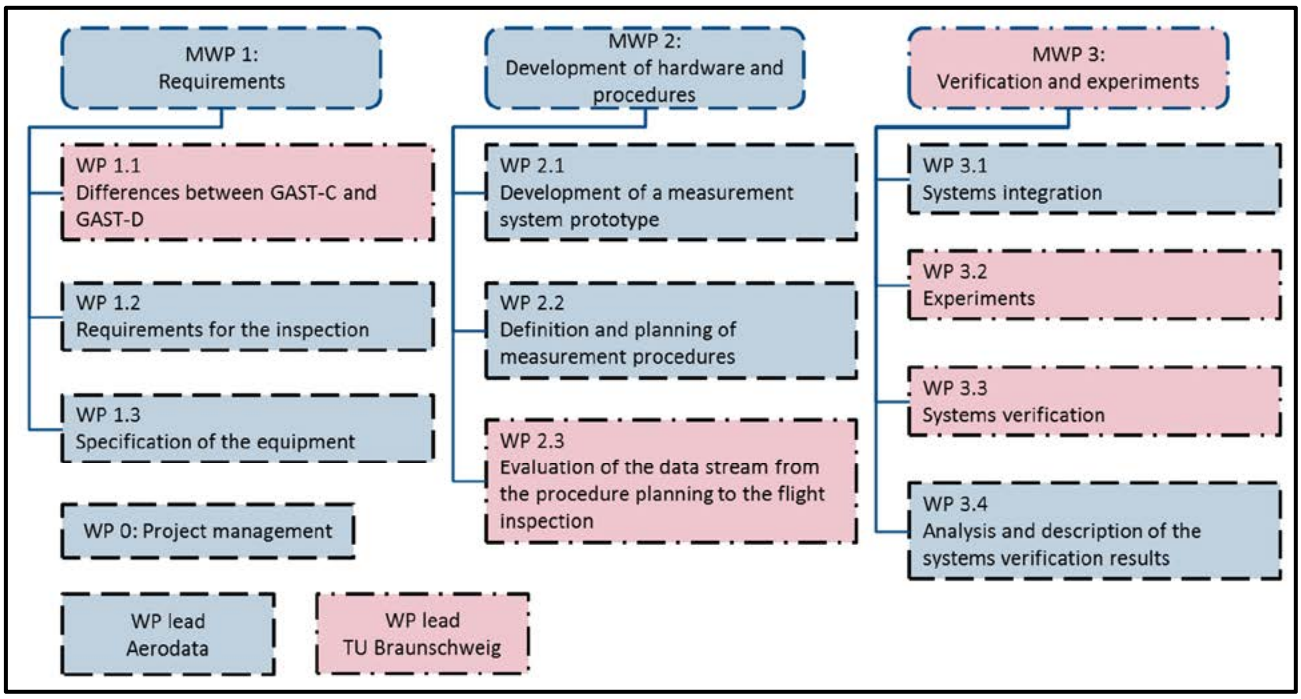

Figure 1. Project MEGA structure

JOINT RESEARCH PROJECT MEGA

The project MEGA "Inspection of GNSS-based CAT-III Approach and Taxiing Guidance Systems" (German: *Vermessung GNSS-basierter CAT-III Lande- und Rollführungssysteme*) aims at developing the aforementioned prototype (flight) inspection system, capable of measuring and calibrating signals from GAST-D ground stations. It is a joint research project with the Institute of Flight Guidance (IFF) of the Technische Universität Braunschweig (TUBS), headed by the Aerodata AG. Both parties are located at the Research Airport in Braunschweig, Germany, which allows an effective and uncomplicated cooperation. Project MEGA consists of two sub projects:

- Flight Inspection System for GBAS Approach Type D (GAST-D), by Aerodata
- Taxiing and Ground Inspection System for GBAS / GAST-D, by the TU Braunschweig

Figure 1 gives an overview on the structure of the project, which is divided into three main work packages (MWP). MWP 1 defines the requirements for GAST-D approaches and taxiing, and the resulting requirements for an inspection. For this, the current GAST-D developments are compared to operative GAST-C standards. The requirements for a (flight) inspection are then investigated based on GAST-D principles and on regulations like a future GAST-D extended version of Doc 8071 (see [5], [7]), which is currently being worked on by ICAO. Further inputs come from conferences and workshops with flight inspection companies. Based on the require-

ments towards a GAST-D flight inspection, the necessary equipment is finally specified. The equipment has to be applicable in road and in flight experiments.

MWP 2 creates an experimental prototype for the inspection of GAST-D installations, based on the before mentioned specifications. For this, the design and documentation of the measurement system are defined. The system is going to consist of a GBAS navigation unit (or a comparable receiver), a position and attitude reference system, and a real-time data acquisition system. The assembly of the prototype is supported and followed by an extensive testing. Furthermore, the necessary measurement methods are developed. These are going to be based on possibly updated documents and regulations, and experiences from GAST-C flight inspection. Finally, from the definition of the measurement methods and regulations, the necessary flight procedures are developed and defined.

Figure 2. Project MEGA logo

MWP 3 utilizes the prototype measurement system and the defined procedures for the generation of exemplary measurement data for the system verification. For this, the prototype system is integrated into TUBS's Dornier Do 128 research aircraft (registration D-IBUF) and into a measurement ground vehicle. In parallel, the measurement methods, procedures, and algorithms are implemented into software. The recorded data from the flight and road experiments is used for the systems verification, by processing it with the methods from MWP 2 under consideration of the requirements from MWP 1.

CONCLUSIONS

GAST-D is going to allow GBAS CAT-III operations. In order to conduct a successful certification and to guarantee a safe operation of GAST-D ground installations, a commissioning and regular flight inspection is necessary. For this reason, a flight inspection system, capable of processing GAST-D signals and procedures, has to be developed and implemented. Supported by the German Federal Ministry of Economic Affairs and Energy, project MEGA is going to develop a FIS prototype incorporating the GAST-D functionality. In this way the development and integration of a GAST-D capable FIS is going to be made available to flight inspection service providers.

FUTURE WORK

The installation and certification of first GAST-D ground stations at airports is assumed to happen in 2019 or 2020. The results of project MEGA will allow for the enhancement of flight inspection system capabilities towards the calibration and commissioning of these installations in time.

ACKNOWLEDGMENTS

The joint research project MEGA is supported by the German Federal Ministry for Economic Affairs and Energy in the framework of the Federal Aeronautical Research Programme V (Luftfahrtforschungsprogramm V).

Supported by:

Federal Ministry for Economic Affairs and Energy

on the basis of a decision by the German Bundestag

Figure 3. Project MEGA is supported by the German Federal Ministry for Economic Affairs and Energy.

Project MEGA is undertaken in close cooperation with the Institute of Flight Guidance of the Technische Universität Braunschweig. The authors wish to thank the institute and in particular Dr. Thomas Feuerle, Dr. Per Martin Schachtebeck, and Mirko Stanisak for their uncomplicated, cooperative work and their fruitful contributions to the joint research project.

REFERENCES

[1] J. Burns, B. Clark, R. Cassell, C. Shively, T. Murphy, M. Harris, etc., 10-20 November 2009, Conceptual Framework for the Proposal for GBAS to Support CAT III Operations, Draft Version 6.5, ICAO Navigation Systems Panel (NSP) Working Group 1 meetings, Montreal, Canada

[2] F. Belloir, 18-21 April 2016, Airbus status, 17th International GBAS Working Group Meeting, Oslo, Norway.

[3] EUROCAE, March 2013, MOPS for Global Navigation Satellite Ground Based Augmentation System Ground Equipment to Support Category I Operations, ED-114A.

[4] European Aviation Safety Agency, 11 December 2015, Rulemaking Programme 2016-2020.

[5] ICAO, 31 October 2002, Manual on Testing of Radio Navigation Aids, Doc 8071, Volume I, Testing of

Ground-Based Radio Navigation Aids, 4th Edition with Amendment 1.

[6] R. Key, 18-21 April 2016, System Design Approval Updates, 17th International GBAS Working Group Meeting, Oslo, Norway.

[7] ICAO, 2007, Manual on Testing of Radio Navigation Aids, Doc 8071, Volume II, Testing of Satellite-Based Radio Navigation Aids, 5th Edition.

[8] L. Lavik, 18-21 April 2016, Indra Navia GBAS Status, 17th International GBAS Working Group Meeting, Oslo, Norway.

[9] A. Lipp, 18-21 April 2016, Status of GAST-D (CAT III) Standards, 17th International GBAS Working Group Meeting, Oslo, Norway.

[10] J. Louwagie, 18-21 April 2016, Honeywell SmartPath GBAS Manufacturer's Update, 17th International GBAS Working Group Meeting, Oslo, Norway.

[11] RTCA, Inc., 16 December 2008, GNSS-Based Precision Approach Local Area Augmentation System (LAAS) Signal-in-Space Interface Control Document (ICD), RTCA DO-246D.

[12] RTCA, Inc., 16 December 2008, Minimum Operational Performance Standards (MOPS) for GPS Local Area Augmentation System (LAAS) Airborne Equipment, RTCA DO-253C.

[13] M. Topland, 18-21 April 2016, IGM Ad-Hoc Status, 17th International GBAS Working Group Meeting, Oslo, Norway.

[14] A. Wilson, 18-21 April 2016, Boeing Presentation 2016, 17th International GBAS Working Group Meeting, Oslo, Norway.

Inside Look at Flight Inspection Airborne Processor Application (FIAPA), RNAV Approach Mode

Brad J Snelling
Airspace System Inspection Pilot
FAA Flight Inspection Services
Oklahoma City, OK
E-mail: brad.snelling@faa.gov

Brad Elliott
Mission Specialist
FAA Flight Inspection Services
Oklahoma City, OK
E-mail: brad.elliott@faa.gov

ABSTRACT

The FAA's latest Flight Inspection System (FIS) software, Flight Inspection Airborne Processor Application (FIAPA), provides new functionality for ground and flight validation of all RNAV type final approach procedures. FIAPA utilizes techniques which work on all RNAV type approaches and presents results in a meaningful format for detecting and reporting data errors which impact the intended final approach course. In the old method, the FIS reported path angle, alignment, and threshold crossing height (TCH) which only provided moderate indications of data errors and few clues for getting bad data corrected. In addition, the old method did not work on RNAV(RNP) approaches at all and only functioned when LPV or LP minima were published on RNAV(GPS) approaches. FIAPA's completely new method addresses the ground and flight validation challenges specific to RNAV procedures. In addition to completion of many ground validation functions, FIAPA presents the results of a flight inspection low approach with an estimate of latitude, longitude, and elevation of both runway thresholds. FIAPA also computes a dynamic measurement uncertainty for the runway fix accuracy. Initial results are showing that the latitude, longitude, and elevation results are far more accurate than previously possible and that the dynamic measurement uncertainty method functions as desired. This paper provides an inside look at how the FIAPA RNAV Approach Mode works, how well it works, and its planned use.

WHY INSPECT FOR DATA ERRORS?

One flight inspection philosophy has been to easily accept confidence in the spatial data coded into new and amended RNAV procedure; however, the possibilities and evidence for data errors remain prevalent. While the day-to-day use of runway spatial data seems good enough, the avionics manufacturers and aviation community are becoming increasingly reliant and trusting of its accuracy. Consider the following example and discussion on the unintended usage of the aeronautical spatial data our ground and flight validation programs are certifying.

Turkish Airlines TK-726 Accident[1]

Figure 1

On 4 March, 2015 Turkish Airlines Flight TK-726 was flying the RNAV(RNP) approach into Tribhuvan

International Airport (Kathmandu) with 224 passengers and 11 crew. The aircraft continued on autopilot below minimums and touched down on the far left edge of the runway with the left main gear off the paved surface. Aircraft damage from the crash was severe, but luckily there were no fatalities or serious injuries. Although the primary factor for this serious aircraft accident was that the pilots continued in weather below minimums, the reason for the crash was due to a spatial data error in the RNAV(RNP) approach. The accident investigation concluded "Therefore, the RNAV (RNP) RWY02 approach coded in the FMS NAV Database applicable at the time of the event took into account the wrong RWY02 threshold." [1] No surveyor made an error, yet an accident still occurred as a result of grossly incorrect approach data. The accident report details the exact sequence of events leading to this data error which was due to both data integrity and resolution issues. Figure 1 shows the difference between the actual threshold and the RNAV(RNP) coded threshold.

Actual Data Quality Requirements

Correct knowledge of both runway thresholds must be identified during the initial survey and propagated at least several times before it ultimately lands in the user's FMS database with high expectations on integrity. The ICAO data quality requirements for the spatial data used to construct all non-precision and precision RNAV approaches is identified in ICAO Annex 15, Appendix 7 and summarized in Table 1.[2]

Table 1 – ICAO Runway Threshold Data Quality Requirements

	Lat/Long	Elevation	Integrity
Non-Precision Approach	1ft	1 ft	10^{-5}
Precision Approach	1 ft	.1 ft	10^{-8}

Unintended Consequences

There is risk in overlooking the ICAO data quality requirement and assuming that flight validation is "good enough" to verify the spatial data. Perhaps this assumption is made because minimums for an approach are high enough, say 300 or 400 feet above touchdown. The risk in this is that we don't actually know how aeronautical data providers and users will ultimately use that data. The HAT for the accident approach above was 360' yet an accident would have been prevented had the data been validated correctly.

Consider the new generation of pilots and proliferation of Synthetic Vision Systems (SVS) which present an artificial display of the real world using best known spatial data. These displays can be so compelling that the pilot may even disregard the actual outside environment, a risk known as attention tunneling. The University of Illinois, supported by the NASA-Ames Research Center looked at the effects of SVS with respect to attention tunneling. They presented one scenario with a runway data error of 500 feet laterally, and the majority of pilots followed the SVS while disregarding the real world.[3]

We see evidence of the same thing in the United States National Airspace System (NAS) where the coded Visual Descent Angle (VDA) presents compelling flight guidance below the Minimum Descent Altitude (MDA). Although the pilot is procedurally required to visually remain clear of obstacles below MDA, pilots are repeatedly compelled to follow this path below MDA, even when doing so results in unsafe terrain or obstacle clearance. This VDA was never intended to be blindly followed below MDA, yet it happens.

EXISTING METHOD – AFIS WAAS MODE

What Data Gets Checked

The existing FIS has a "WAAS Mode" which can provide indirect indicators of spatial data problems, but this has two limitations. First, when problems occur, it is difficult to identify the exact nature of the data error. Since the current FIS does not report results in survey terminology (e.g. latitude, longitude, elevation), the meaning of the results is unclear and they are not useable to report where the spatial data may have gone wrong. Second, this only checks data for procedures where LP/LPV minima are published. The majority of approaches do not have LPV/LP minima or are RNAV(RNP) approaches.

Which Approaches Are Currently Checked

There are currently 14,250 RNAV approach minimums coded and published in the United States.[4] Of those, the FIS has only been used to check the spatial data on 4,257 (30%). This is because the current system is only designed to check the data when LPV or LP minima are published. Figure 2 shows a distribution of Height Above Touchdown (HAT) at minimums for each type of approach, LNAV, LNAV/VNAV, LP/LPV, and RNP. The box shows the only data currently being checked for LP/LPV minima. This shows the volume of approach data that are not getting checked. It doesn't make sense that we would be checking data for LPV with 600 foot HAT and not checking for VNAV data with 250 foot HAT. The new FIAPA approach mode has the capability to check the spatial data for all RNAV approaches.

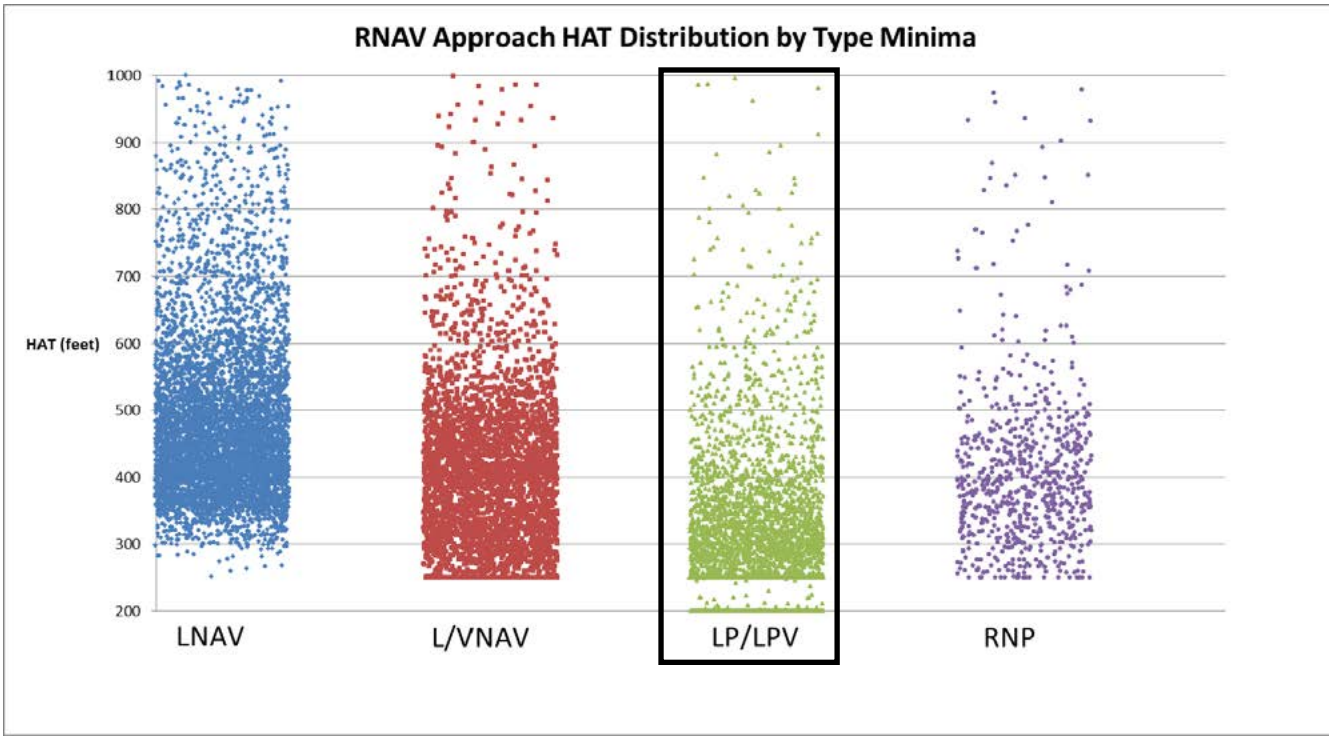

Figure 2 – RNAV Approach HAT Distribution by Type Minima

NEW METHOD – FIAPA RNAV APPROACH MODE

RNAV Mode inputs

In order to prepare for data validation, FIAPA takes inputs from several data sources prior to inspection. RNAV mode has inputs from the AIRNAV and ARINC databases. AIRNAV database contains survey data. AIRNAV data is imported and stored in FIAPA from the official FAA database. An update to the AIRNAV database is provided daily. ARINC data is imported by a custom ARINC file of new and amended procedures or the FAA Coded Instrument Flight Procedures (FAA CIFP) ARINC file. The Custom ARINC file is used for most inspections. The custom ARINC file contains original or amended procedures. FAA CIFP contains published procedures. The custom ARINC file is updated weekly, and the FAA CIFP is updated every 28 days. Multiple ARINC files can be loaded into FIAPA. Selection of the ARINC file for the inspection is completed during the run setup on the Facility tab.

The user enters an airport ID, and FIAPA displays the airport data from the AIRNAV database. The user then selects the runway that the RNAV procedure supports. The selected ARINC file then must be selected. This is where the user will select either the FAACIPF or the custom ARINC database.

Straight-in and circling procedures from the selected ARINC file will be displayed for the entered airport and runway. FIAPA will pull multiple RNAV procedures if the airport and runway supports multiple RNAV procedures. FIAPA inspects multiple RNAV(GPS) and RNAV(RNP) simultaneously.

FIAPA extracts Runway, Final Approach Segment (FAS), Additional Path Point, and FAF to MAP Waypoint data from the selected ARINC file. Figure 3 displays FIAPA AIRNAV and ARINC data.

Ground Validation

While the FAA already has a formal ground validation program, FIAPA is expected to enhance and automate some of what already takes place in ground validation. ARINC data is compared to the survey data in the AIRNAV database. Differences between the runway data and ARINC data are highlighted in red in FIAPA (see Figure 3).

Table 2 displays the FIAPA automated ground validated items. FIAPA is able to verify these items by comparing the data in the different databases.

FIAPA calculates a CRC (for LP/LPV path point records), Final Approach Course, Final Approach Segment, Runway Bearing, Threshold to Missed Approach Point (MAP) distance, and threshold to Final Approach Course (FAC) intersection distance. These items must be verified manually with the procedure documentation, because the procedure documentation is not in a format that can be transferred and compared automatically. Figure 3 shows a sample FIAPA screen where the display, calculation, and validation are displayed to the operator. This screen shows a sample error with magnetic variation and runway bearing.

Table 2 - ARINC Automated Ground Validation

Verified Data	FIAPA Compared Data	
	ARINC	AIRNAV
Runway Data		
Airport Magnetic Variation	Airport Magnetic Variation	Airport Mag.Var.
Runway Bearing	Runway Bearing + (East) or – (West) Airport Magnetic Variation	True Bearing
Runway Length	Runway Length – Threshold Displacement	Landing Length
Threshold Displacement	Threshold Displacement	Is Displaced Selected
Threshold Latitude	Threshold Latitude	Threshold Latitude
Threshold Longitude	Threshold Longitude	Threshold Longitude
Threshold Elevation	Threshold Elevation	Threshold Elevation
LPV/LP FAS Data		
LTP Latitude	LTP Threshold Latitude	Threshold Latitude
LTP Longitude	LTP Threshold Longitude	Threshold Longitude
LTP Ellipsoid	LTP Ellipsoid Height	Threshold Ellipsoid Elevation
CRC Remainder	CRC Remainder	Calculated CRC Remainder

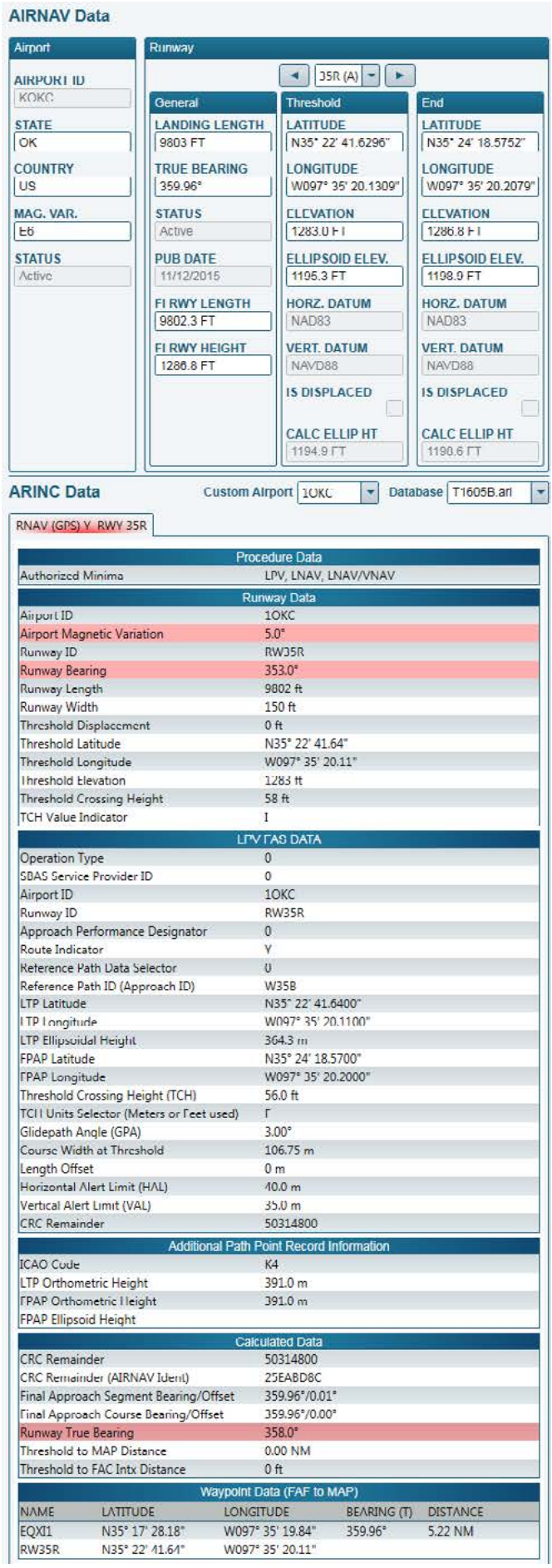

AIRNAV Data

Airport		Runway		
AIRPORT ID: KOKC		35R (A)		
STATE: OK		General	Threshold	End
COUNTRY: US		LANDING LENGTH: 9803 FT	LATITUDE: N35° 22' 41.6296"	LATITUDE: N35° 24' 18.5752"
MAG. VAR.: E6		TRUE BEARING: 359.96°	LONGITUDE: W097° 35' 20.1309"	LONGITUDE: W097° 35' 20.2079"
STATUS: Active		STATUS: Active	ELEVATION: 1283.0 FT	ELEVATION: 1286.8 FT
		PUB DATE: 11/12/2015	ELLIPSOID ELEV.: 1196.3 FT	ELLIPSOID ELEV.: 1198.0 FT
		FI RWY LENGTH: 9802.3 FT	HORZ. DATUM: NAD83	HORZ. DATUM: NAD83
		FI RWY HEIGHT: 1286.8 FT	VERT. DATUM: NAVD88	VERT. DATUM: NAVD88
			IS DISPLACED	IS DISPLACED
			CALC ELLIP HT: 1194.9 FT	CALC ELLIP HT: 1190.6 FT

ARINC Data — Custom Airport: 1OKC — Database: T1605B.arl

RNAV (GPS) Y, RWY 35R

Procedure Data	
Authorized Minima	LPV, LNAV, LNAV/VNAV

Runway Data	
Airport ID	1OKC
Airport Magnetic Variation	5.0°
Runway ID	RW35R
Runway Bearing	353.0°
Runway Length	9802 ft
Runway Width	150 ft
Threshold Displacement	0 ft
Threshold Latitude	N35° 22' 41.64"
Threshold Longitude	W097° 35' 20.11"
Threshold Elevation	1283 ft
Threshold Crossing Height	58 ft
TCH Value Indicator	I

LPV FAS DATA	
Operation Type	0
SBAS Service Provider ID	0
Airport ID	1OKC
Runway ID	RW35R
Approach Performance Designator	0
Route Indicator	Y
Reference Path Data Selector	0
Reference Path ID (Approach ID)	W35B
LTP Latitude	N35° 22' 41.6400"
LTP Longitude	W097° 35' 20.1100"
LTP Ellipsoidal Height	364.3 m
FPAP Latitude	N35° 24' 18.5700"
FPAP Longitude	W097° 35' 20.2000"
Threshold Crossing Height (TCH)	56.0 ft
TCH Units Selector (Meters or Feet used)	F
Glidepath Angle (GPA)	3.00°
Course Width at Threshold	106.75 m
Length Offset	0 m
Horizontal Alert Limit (HAL)	40.0 m
Vertical Alert Limit (VAL)	35.0 m
CRC Remainder	50314800

Additional Path Point Record Information	
ICAO Code	K4
LTP Orthometric Height	391.0 m
FPAP Orthometric Height	391.0 m
FPAP Ellipsoid Height	

Calculated Data	
CRC Remainder	50314800
CRC Remainder (AIRNAV Ident)	25EABD8C
Final Approach Segment Bearing/Offset	359.96°/0.01°
Final Approach Course Bearing/Offset	359.96°/0.00°
Runway True Bearing	358.0°
Threshold to MAP Distance	0.00 NM
Threshold to FAC Intx Distance	0 ft

Waypoint Data (FAF to MAP)

NAME	LATITUDE	LONGITUDE	BEARING (T)	DISTANCE
EQXI1	N35° 17' 28.18"	W097° 35' 19.84"	359.96°	5.22 NM
RW35R	N35° 22' 41.64"	W097° 35' 20.11"		

Figure 3 – Sample Ground Validation Results

Flight Validation (Survey Data Verification)

Survey data used to create the RNAV procedure is verified by completing a 50 foot low approach over the full length of the runway. FIAPA captures GNSS, radio altimeter, aircraft attitude, and television positioning system (or pilot updates) at the threshold and runway end. This data is used to compute an airborne survey of both runway thresholds.

Figure 4 displays sample runway survey results. The results from the inspection include the airborne survey latitude, longitude, and elevation of the runway threshold (THLD) and runway end (RE). The difference between the measured and coded positions are computed as Along Track (ATK) error, Cross Track (XTK) error, and Up error for both runway thresholds. The results contain a percentage that indicates the confidence in the result. When a data error is suspected, this provides a meaningful report for the procedure designer or surveyor to understand the specific nature of the problem.

An achieved TCH error, measured runway length and measured runway bearing error are calculated from the measured runway data. Achieved TCH error and runway bearing error have tolerances, but the runway length does not have a tolerance. The measured runway length is used to indicate errors with the data.

Vertical protection level, horizontal protection level, and carrier to noise values are reported while the aircraft was over the approach end threshold. The protection levels are used to measure the confidence in the results. Carrier to noise ratio is displayed because there is a tolerance of equal to or greater than 30 dB-Hz. Runway and GNSS fix values indicate the sensors used to complete the runway survey validation.

FIAPA has datum conversion capability so that survey verification can be completed on multiple datums using GNSS sensors which output position respect to WGS84 datum. For example, if the AIRNAV horizontal data used for design of an approach was NAD83, FIAPA converts the survey data from WGS84 to NAD83 and displays the ATK and XTK errors relative to NAD83.

As described in Gary Flynn's Dynamic Measurement Uncertainty for Runway Fix 2016 IFIS paper[5], FIAPA also determines a dynamic uncertainty for the ATK, XTK, and Up Error measurements. This uncertainty is then used to assign a statistical confidence that the coded spatial data is within a given tolerance of correct. See Figure 5. If the measured error is less than the tolerance (T) -1.96σ, then there is greater than 95% confidence the error is less than T. If the measured error is greater than T + 1.96σ, there is greater than 95% confidence there is an actual survey error greater than T.

Runway Survey

THLD Atk Err	-0.2 ft / 100%
THLD Xtk Err	-1.3 ft / 100%
THLD Up Err	1.7 ft / 99%
THLD Meas Lat	N36°00'48.75
THLD Meas Lon	W102°32'46.92
THLD Meas EHt	3907.0 ft
RE Atk Err	0.1 ft / 100%
RE Xtk Err	-0.8 ft / 100%
RE Up Err	0.8 ft / 100%
RE Meas Lat	N36°01'52.03
RE Meas Lon	W102°32'47.12
RE Meas EHt	3910.5 ft
VPL	14.4 m
HPL	8.8 m
Achieved TCH Err	1.73 ft
CNR at Threshold	48 dB-Hz
Meas RWY Len	6400.6 ft / 0.3 ft
Meas RWY Brg	359.9° / 0.0°
RWY Fix	Camera
GPS Fix	GPS-4000 [SBAS]

Figure 4 – Sample Flight Validation Results

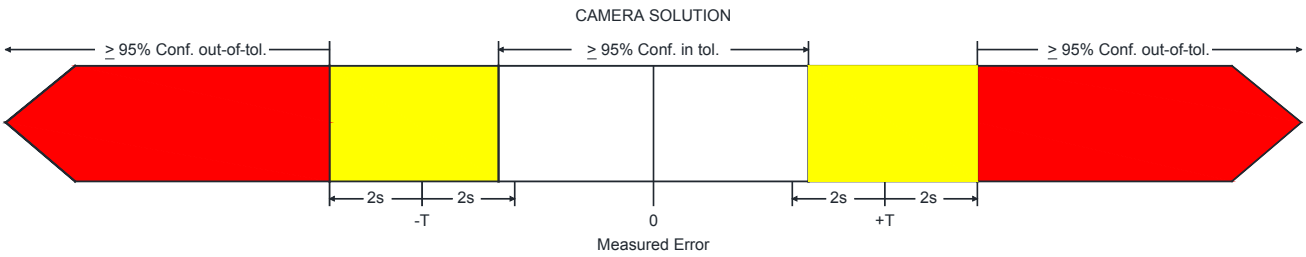

2s = 2-sigma uncertainty computed by FIAPA.
T = RNAV survey tolerance value (±)

Figure 5 – RNAV Result Confidence and Color Coding

RNAV GNSS/SBAS Sensor Inputs

The FAA FIAPA configuration has three GNSS/SBAS sensors available to be used for the survey validation: Rockwell Collins GPS-4000S, Rockwell Collins GNLU-955M, and a Spectra Precision ProFlex 800. FIAPA completes runway survey validation using one sensor per inspection run. All sensor data is logged and can be used to complete a Rerun using a different sensor than the sensor used for the initial inspection.

While the Rockwell Collins equipment only uses GPS augmented with SBAS, the ProFlex 800 is capable of utilizing multiple GNSS constellations including GLONASS and Galileo. The ProFlex 800 is also expected to be capable of utilizing dual frequency GPS L1/L5. The capabilities of the ProFlex 800 should be useful when conducting survey verifications outside SBAS coverage.

There was an unexpected result when updating the aircraft GNSS antenna to be used for GLONASS, Galileo, and L5. The same GNSS antenna is used for inputs to both ProFlex 800 and GNLU-955M; and the antenna divider is powered by the GNLU-955M provided 17dB gain. The new multi-constellation/L5 antenna added an additional 16 dB gain over the old antenna. While this added gain was acceptable to the ProFlex 800, the CNR at the GNLU-955M was lowered approximately 10 dB resulting in sporadic loss of some GNSS satellites. This caused unacceptable fluctuations in the GNSS altitude as individual satellites would come in and out of tracking. By replacing the divider with an unpowered divider, the CNR at the GNLU-955M was restored. Due to the sensitivity of the RNAV Approach Mode to GNSS position and elevation, it was evident in the initial measurement uncertainty results that losing 10 dB from the GNSS signals was unacceptable for stability of the inspection results. All results presented in this paper are with the GNSS antenna divider unpowered.

SPATIAL DATA VALIDATION PERFORMANCE

The FIAPA RNAV Approach mode is still in Operational Test and Evaluation (OT&E), and Operational Approval is anticipated in January 2017. Initial results appear superior to the previous method and are expected to greatly improve flight validation of RNAV spatial data.

To assess measurement uncertainty, the control airport was KOKC where coded spatial data was independently verified and cross checked to be within several inches of correct. Data was collected using the CL-605 on 30 flight inspection low approaches over a 2-day period on all six available runways. Due to the controls in place, any ATK, XTK, or Up Error for these runs was FIS error and not coded spatial data error.

The results presented in Appendix 1 (Figures 6-9) show that the FIAPA RNAV Approach Mode with GNSS/SBAS has performance to provide validation of the coded spatial data to within several feet. The mean survey error is within approximately 1 foot laterally with 2σ values approximately 2 feet. The mean elevation survey error for the departure end is easily within 1 foot with a 2σ values less than 4 feet. The mean elevation survey error for the approach end was about 2-3 feet with similar 2σ values less than 4 feet. We expect to identify and correct the elevation bias for approach end results in future software revisions. The performance achieved in this dataset was using GPS/WAAS as the position reference. Equivalent performance is expected for any areas covered by SBAS. For areas outside SBAS coverage, we expect the performance to reflect uncertainties in the GNSS sensor position/elevation. Multi-constellation GNSS using the ProFlex 800 will help considerably and in the future L5 may even provide worldwide performance equivalent to SBAS. Additional testing and analysis is underway to determine the quality of validation that can be completed when outside SBAS.

When no data errors are present, this performance is sufficient to achieve nearly 100% confidence that the survey data is within tolerance. When spatial data errors exist in the coded data, the presentation of results provides for the ability to identify the source and communicate this to procedure designers and data specialists.

PLANNED USE

The exact survey validation tolerances for operational use have not been finalized yet, but they will depend on whether SBAS coverage is available or not. The expected tolerances within SBAS coverage are 6 feet vertically and 10 feet horizontally. For the small number of our inspections that occur outside of SBAS coverage, we will study the feasibility of using 20 feet vertically and 30 feet horizontally.

FIAPA has the capability to detect and quantify spatial data errors that are much less than would really have any safety impact on some procedures. For example, a 20 foot lateral error would have negligible impact on a procedure with only LNAV minima at 1,000 HAT. For this reason, FIAPA also calculates the realized TCH and procedural alignment with the runway. Tolerances for these will depend on the type of minima: Circling, LNAV, VNAV, LP, LPV, or RNP.

The next problem to solve was how to report known data errors that are small enough not to affect safety of a given procedure but are known to be greater than ICAO survey tolerances. It is helpful to think of the maintenance alert concept used with ILS facilities. When the maintenance limits are exceeded, the inspector has a responsibility to report this to maintenance even though the facility is good enough to remain on the air for operational use. We can apply the same thing with RNAV procedures. Even though the procedure under inspection might be considered "good enough", the inspector still has a responsibility to report the data errors to our data branch because they are known to exceed ICAO data quality requirements. With FIAPA, we now have quantifiable survey type results that can be easily communicated for getting the survey or procedure spatial data corrected.

CONCLUSIONS

FIAPA will be a useful tool to augment and improve the FAA's existing ground validation program.

FIAPA can verify runway survey data for all RNAV approach procedures. This increases the data verified from 30% to 100% of all RNAV approach procedures.

FIAPA displays error results relevant to the survey data. When a data error is suspected, the survey point or points can be discussed in common terms to the survey data. Making it easier to understand and comprehend for the user of the results.

Within SBAS coverage, the FIAPA configuration on FAA aircraft is accurate enough to verify runway survey data to within several feet and with high confidence on the results. This compares to the previous method where any verification was less accurate and only indirect.

RECOMMENDATIONS AND FUTURE WORK

Several months of work remains as the FAA completes development and OT&E on the RNAV approach mode. We expect to continue research and improve in the following areas:

1. Use of ProFlex 800 survey confidence parameters so that this can be the default GNSS sensor for the runway survey.
2. Determine cause and correct the approach end elevation bias.
3. Test and determine expected measurement uncertainty when GNSS+SBAS is not available. What is the optimal use of multi-constellation GNSS?
4. Test cases where 50 foot low approaches are not feasible. How does accuracy suffer and measurement uncertainty increase for higher low approaches at circling type minimums.
5. Stay abreast of developments in using dual frequency L1/L5.
6. When FIAPA begins live inspections in 2017, monitor and collect operational performance over a wider area of regions and airports.

ACKNOWLEDGMENTS

We would like to thank Gary Flynn, Cheng Zhong, Derek Blackford, Reji Zachariah, Todd Edmondson, Ben James, Ryan Mounts, Peter Hill, Samual Burden, Andrew Chandler, Dewayne McMurtrey, Justin Petty, Kelly St. Pierre, Ryan Temple, Stephen Hankins, and Robert Wright of the FIAPA software development team. We would also like to thank Kelvin Hale with the assistance in troubleshooting the powered splitter installation.

Ricardo Carrizosa, Jay Sandwell, and Sergio Molas need many thanks for the hours of operational testing and tracking FIAPA changes.

REFERENCES

[1] Accident Investigation Commission (TC-JOC, A330-303). 6 October, 2015. Final Report on the Investigation of Runway Excursion Accident of Turkish Arilines TC-JOC, A330-303, at TIA, Kathmandu, Nepal on 4th March, 2015.

[2] ICAO, July 2004, Aeronautical Information Services, Annex 15 to the Convention on International Civil Aviation.

[3] University of Illinois, 2004, Eye-tracking and individual differences in off-normal event detection when flying with a Synthetic Vision Display. Lisa C Thomas and Christopher D Wickens.

[4] FAA Website, Satellite Navigation – GPS/WAAS Approaches, April 28, 2016. https://www.faa.gov/about/office_org/headquarters_offices/ato/service_units/techops/navservices/gnss/approaches/

[5] IFIS2016, Dynamic Measurement Uncertainty for Runway Fix, Gary A. Flynn.

APPENDIX 1 – Measurement Uncertainty Data

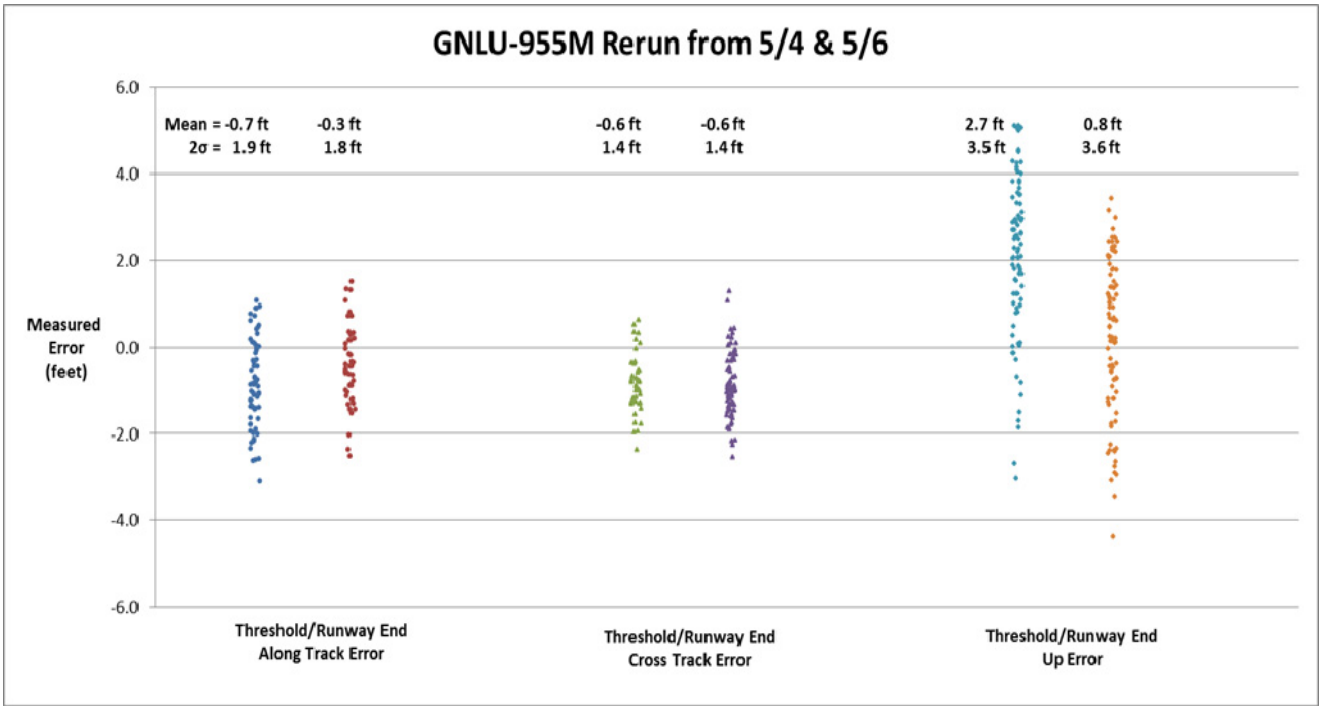

Figure 6 – Survey Measurement Uncertainty using GNLU-955M

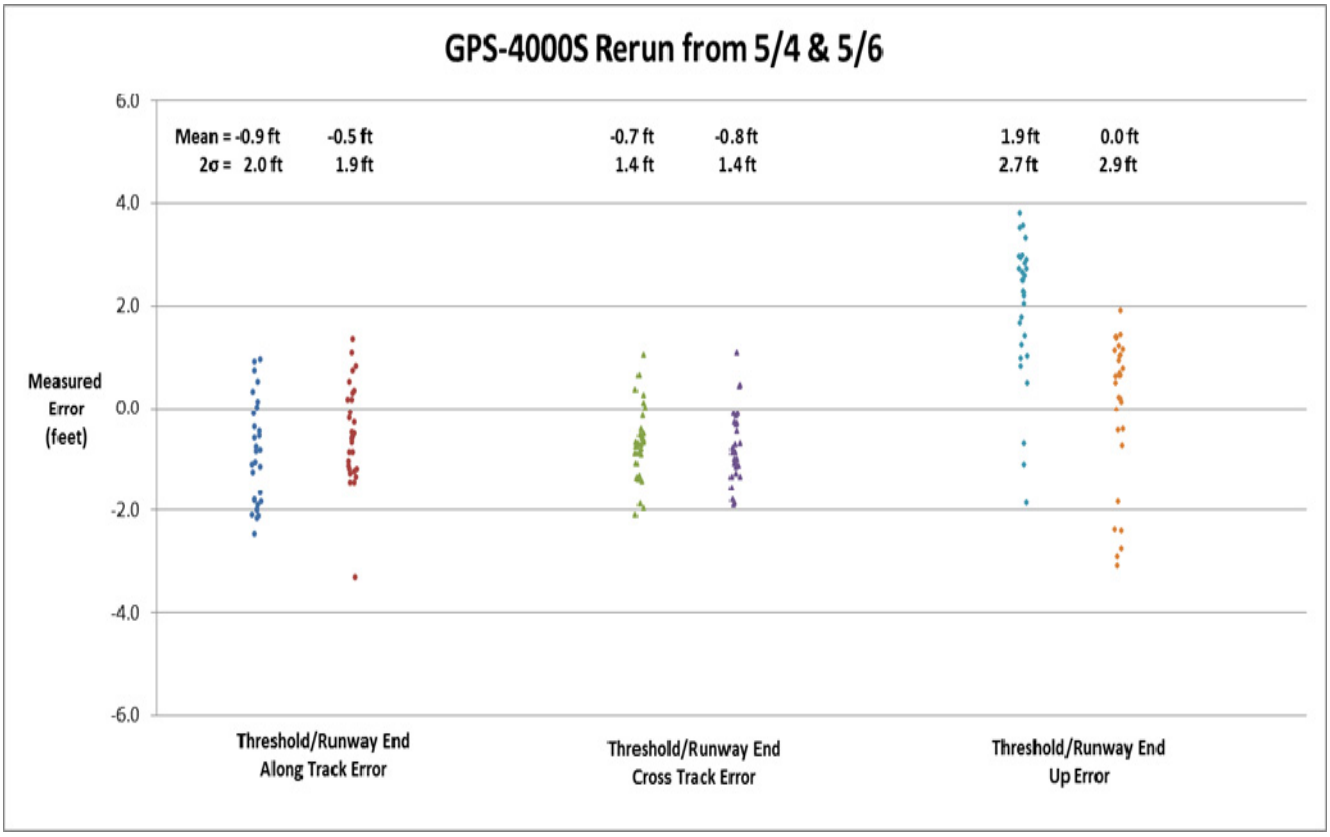

Figure 7 – Survey Measurement Uncertainty using GPS-4000S

APPENDIX 1 – Continued

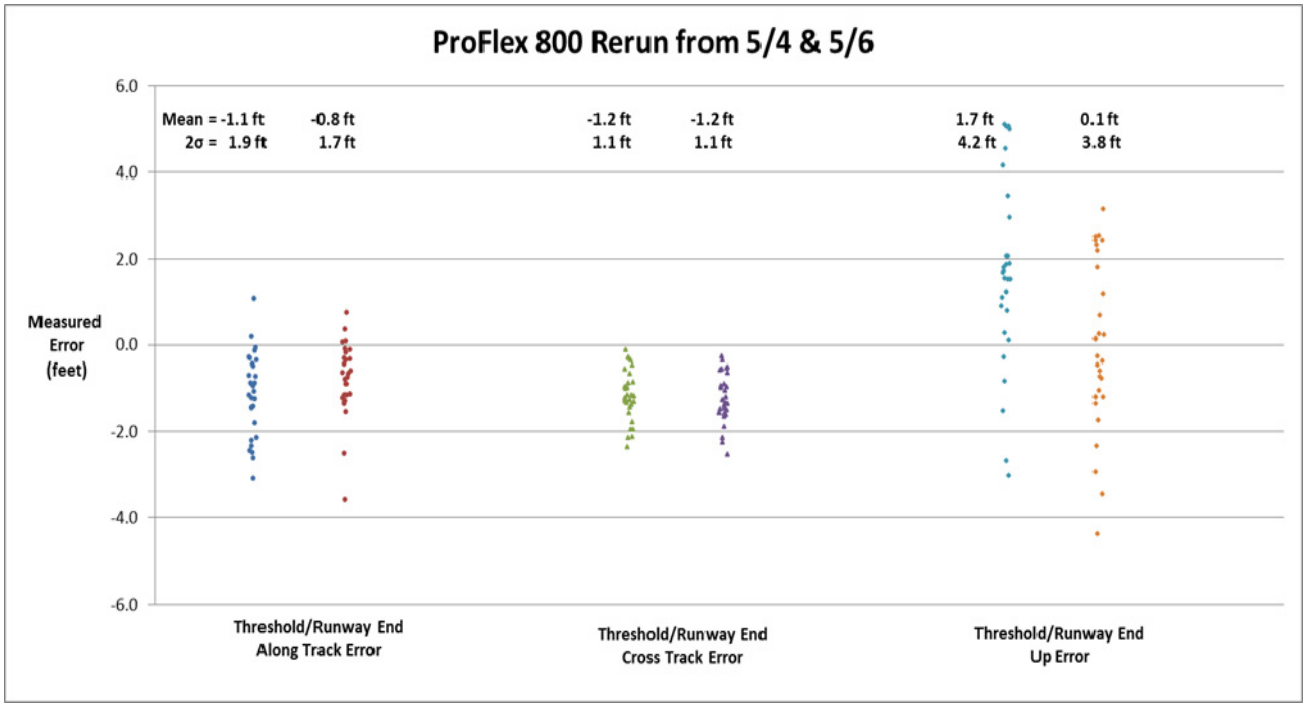

Figure 8 - – Survey Measurement Uncertainty using ProFlex 800

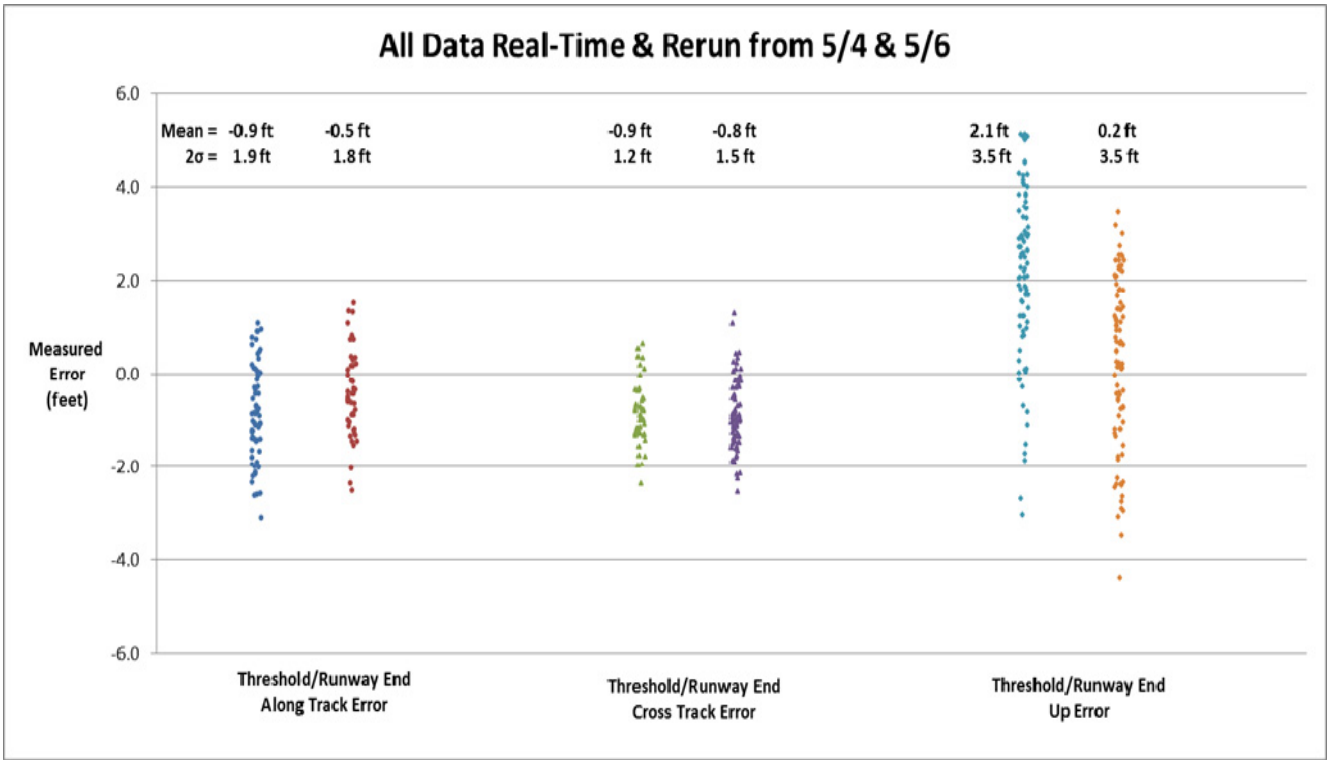

Figure 9 - – Survey Measurement Uncertainty, All Sensors

IFIS2016

Bringing Together Theory and Practice

Session 8

RFI / EMI

Advanced Online GNSS RFI Detection and Investigation

Matthew Bruce
Flight Inspector
FCS Flight Calibration Services GmbH
Braunschweig, Germany
Fax: +49 531 23 777 99
E-mail: brc@flightcalibration.de

Markus Schwendener
Technical Director
FCS Flight Calibration Services GmbH
Braunschweig, Germany
Fax: +49 531 23 777 99
E-mail: swe@flightcalibration.de

Maurizio Scaramuzza
Head CNS Expert Group
Skyguide – Swiss Air Navigation Services Ltd.
Wangen, Switzerland
Fax: +41 43 931 66 19
E-mail: maurizio.scaramuzza@skyguide.ch

ABSTRACT

The potential for GNSS Radio Frequency Interference (RFI) to degrade air-navigation signal quality is well known and the impact becomes more important as the transition to RNAV/RNP based navigation continues.

Building on research presented at the 2014 IFIS [1], this paper describes an "online" implementation of the methodology and techniques presented, additionally incorporating that which was presented at the ION GNSS Conference 2015 [2].

Consideration is also given to aspects such as:

1. "Periodic Inspection" of GNSS Environment during routine ILS inspections at busy airports
2. Online alerting and reporting of results that indicate the presence of an interference source
3. Characterization and localization of interference sources using fixed wing and/or rotary wing Flight Inspection platforms

The implementation in an Automatic Flight Inspection System (AFIS) is discussed and examples of results observed in real-world conditions are analyzed.

INTRODUCTION

Current GNSS interference detection methods provide for a go/no-go indication as to the presence of GNSS inference and are typically performed only during commissioning Flight Inspection/Validation of a new GNSS (GPS) based procedure.

While this method has proven successfully thus far it does have limitations, in particular in the detection of short duration interference (typically < 10 seconds). Short term interference can easily go undetected in flight unless issues such as lost RTK solution or complete loss of GPS are experienced. The use of spectrum analyzers to capture the GPS spectrum is an improvement, however they typically do not allow for continuous monitoring. Use of GPS performance measures, such as Carrier to Noise Ratio (C/No) are effective, but are typically influenced by aircraft attitude which makes interpreting results and online detection difficult.

Doc 8071, Volume 2 [3], states the following at Appendix 3 to Chapter 1, section 4.10:

> *Even with a flight inspection there is no full guarantee that all interference sources have been identified. For example, some sources may be intermittent transmitters or may come from mobile transmitters. Therefore it is recommended that aircraft be equipped with interference sensors (GNSS receivers with interference detection capability producing automatic reports).*

While this consideration is perhaps skewed towards primary GNSS receivers with some kind of alerting function, improved GNSS interference detection techniques have been developed on the basis of that presented at IFIS 2014 [1] and at ION GNSS Conference 2015 [2] and implemented in an AFIS.

The resulting Compensated C/No has proven to be a reliable measure of GPS interference and an online implementation of these techniques into a "C/No Monitor" aids real time detection and reporting of interference. This technology also provides the basis for routine monitoring of the GPS environment during periodic flight inspection tasks such as ILS or VOR inspection and "on opportunity" monitoring during ferry flights.

AFIS SUPPORTED ONLINE GNSS DETECTION

Given the identified problems with existing methods, consideration was given to how the AFIS could be used to better support the detection of GNSS interference online and in real time. The aim was to develop a set of tools available to the Flight Inspector to confidently assess if the GPS environment is free of interference, in flight, and without the need to conduct post-processing or analysis of the recorded data.

GPS antenna pattern correction

The concept of software correction or compensation of antenna pattern for field strength measurement effects has been around for some time. As presented at IFIS 2014 [1], similar techniques can be used to compensate for the influence of a GPS antenna reception pattern on the C/No as measured by a GPS receiver. The result is a Compensated GPS C/No, largely independent of influences from the antenna reception pattern and aircraft attitude, which makes detection of GPS inference easier.

A drawback of the described technique was that the analysis and correction was applied in post-processing, meaning a delay between observation of the interference (by the measurement equipment) and identification of the interference (by the engineer) was present. By this time the opportunity to complete further investigation was lost.

An online implementation of this GPS antenna pattern compensation method was considered to have several benefits:

1. Make real-time identification of GNSS interference easier
2. Use the Compensated C/No values in algorithms to automate GNSS interference detection and/or trigger specific actions when interference is detected
3. Potential to identify and investigate short-duration GNSS interference effects (which may otherwise go unnoticed)

With this in mind the AFIS software was developed to use an antenna model to calculate the Compensated C/No values and present these for visualization and further analysis.

Development of Antenna Pattern

The antenna pattern was derived empirically using the same methodology as presented in [1]. Specific flight profiles were not used to gather data, rather a collection of recordings from approximately 50 hours of routine flight inspection tasks were processed to calculate the pattern.

Processing required calculation of the relative position of each GPS SV with respect to the AFIS GPS antenna and subsequent calculation of a correction factor to give a normalized C/No of 50 dBHz. These correction factors were arranged into to 1x1 degree "bins" across the GPS antenna surface and further processing though averaging and smoothing provided a suitable 3D model for implementation in the software.

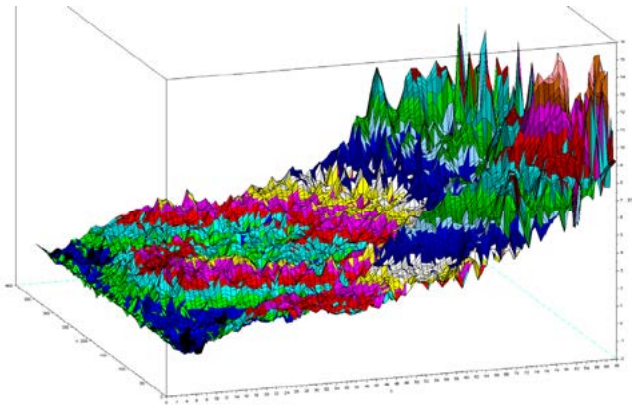

Figure 1 – GPS Antenna Pattern, X – Azimuth (0-360 degrees), Y – Zenith (0-90 degrees), Z – Correction (dBHz)

As a plausibility check the derived pattern was compared with that from the antenna manufacturer, correlation was considered to be acceptable noting that the manufacturer only provides information relating to the antenna gain in elevation and assumes no directionality in azimuth, an assumption that is not valid when considering installation on an aircraft.

For comparison purposes two antenna models were finally generated for software implementation, one being the manufacturer's with gain as presented on that datasheet and one model with derived gain in elevation and azimuth for the aircraft specific installation.

Implementation and Validation

The antenna models were packaged into an existing data format used in the AFIS software for 3D correction of antenna gain in field strength calculations. Data from flights free of GPS interference was "reprocessed" to see how the compensation algorithm performed and if the results were plausible, especially during periods where the aircraft was banked.

From the initial testing it became apparent that use of the empirically derived aircraft specific model provided better results. Azimuth dependent effects, typically affecting SVs at low elevation angles and in the region of the wing and tail structures, could not be considered negligible. Given this finding further use of the standard model was abandoned with focus shifting to refining the aircraft specific model.

The use of the model meant that the C/No of each SV was compensated to a normalized C/No of 50 dBHz, small variations and noise were filtered out through averaging to give an Averaged Compensated GPS C/No which was largely resilient to aircraft attitude while remaining sensitive to simultaneous C/No drops like those seen during periods of GPS interference.

Using this new parameter with a limit on minimum Average Compensated GPS C/No provides the basis for the C/No Monitor and thus the online detection of GPS interference.

False Positives

Reprocessing of previous ILS flight inspection data where no interference was observed showed some peaks and unexpected noise on the Averaged Compensated C/No parameter, however as these were all "positive" they did not trigger false alarms of the C/No Monitor.

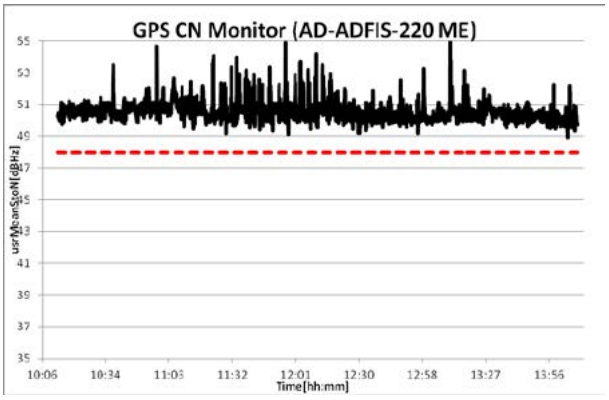

Figure 2 – Typical ILS Flight Inspection (4 hours) Without Observed GPS Interference

Missed Detections

Analysis into the possible rate of missed detections has not been completed, however if we consider the previous implementation as a baseline we can see that the C/No Monitor immediately reduces the probability of a missed detection.

CASE STUDIES

While these examples are from the past they clearly demonstrate the effectiveness of the newly implemented AFIS capabilities.

#1 – HeliFIS: Intermittent short term interference

During post flight evaluation of a helicopter RNAV procedure a C/No ratio irregularity in the region of the missed approach turning fix (MATF) was observed. However, as tracking was not lost on any of the onboard GPS receivers and the irregularity was only observed on one of the two approaches there was no "trigger" to consider further investigation in flight at the time.

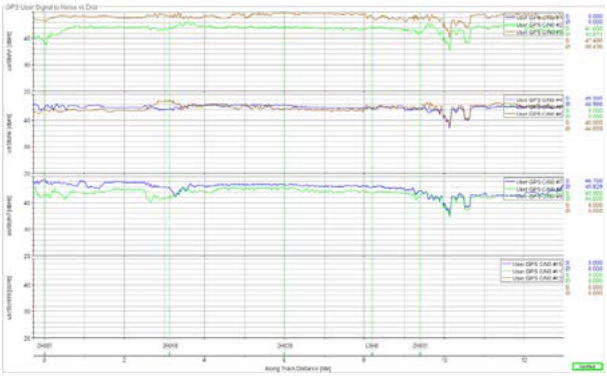

Figure 3 – Conventional C/No Graphic

As can be seen, the conventional graphic shows a drop in all C/No but not one that causes immediate concern. When using the C/No Monitor method the drop is much more obvious.

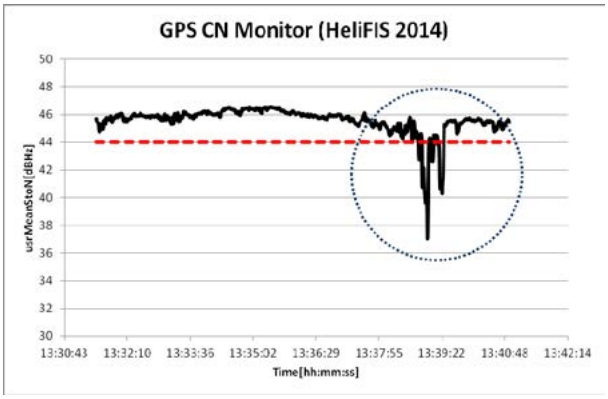

Figure 4 –C/No Monitor Graphic

In April 2016, some two years after the original occurrence and during a VFR departure, the C/No Monitor triggered in the same region.

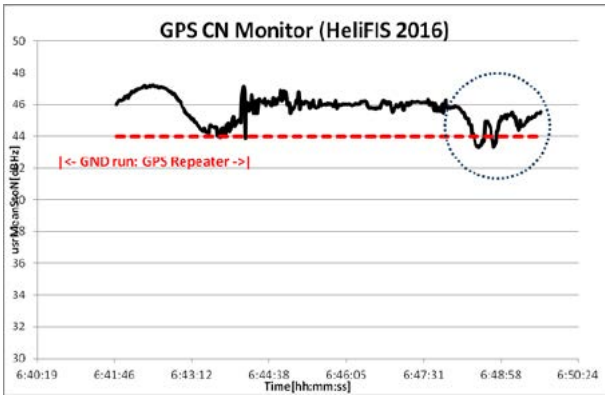

Figure 5– Similar Path, C/No Monitor Graphic

Given the points at which the inference was observed to begin and end, a general region where the interference source may be located can be deduced.

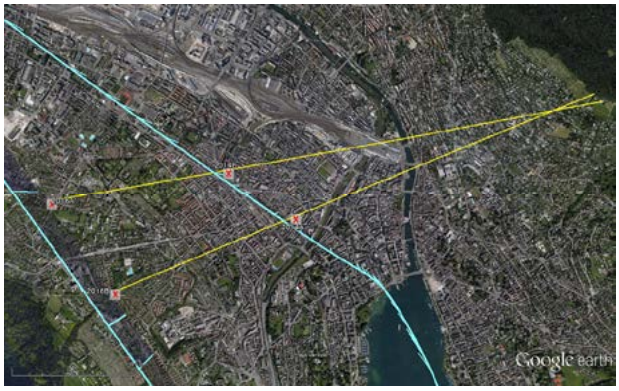

Figure 6 – Possible Location of Interference Source

The source of this interference is yet to be located, however the authorities have been provided with useful information to start their investigation.

#2 – ILS calibration: Short term interference

During routine flight inspection of the ILS at a military airfield a complete loss of GPS was observed on the AFIS receiver. Pilots reported seeing no loss of GPS, however later analysis revealed that Primary GPS was lost, but as the FMS reverted to DR mode for these 1-2 seconds it effectively went unnoticed.

GPS was lost at a point abeam the Precision Approach Radar (PAR) installation, approximately at the mid-point of the runway. Troubleshooting at the time, which included temporarily removing power to the PAR, was unable to positively identify the source of the interference.

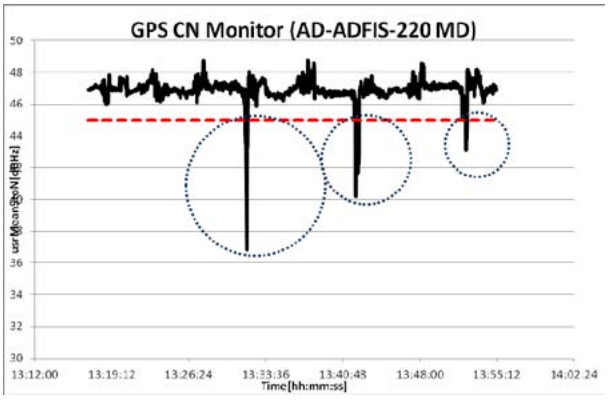

Figure 7 – Interference During Low Pass

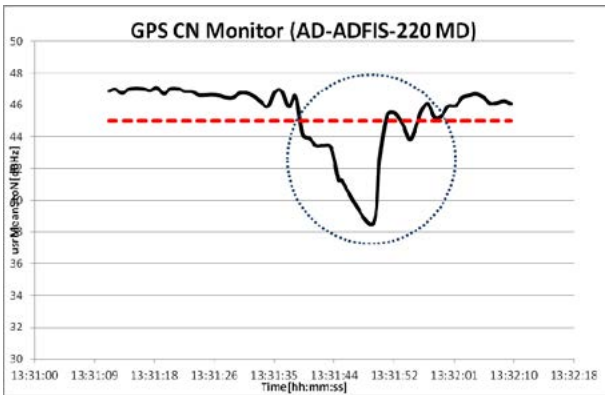

Figure 8 – Expansion of Interference (10 Sec / 80m)

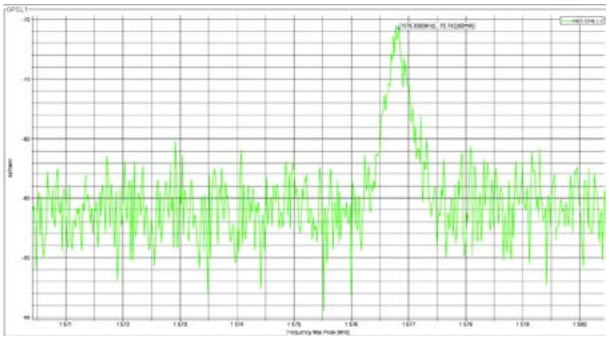

Figure 9 – Spectrum Plot

Figure 10 – Location of Interference

The source was traced to a faulty GPS antenna which was part of the PAR installation, which, due to an internal failure, was transmitting a CW signal near to the L1 frequency.

#3 – ILS calibration: Scattered interference

Crews reported several losses of GPS RTK during an ILS flight inspection in different locations around the airport. While post evaluation of the flight discovered suspicious C/No behavior during the entire flight, the source of the interference could not be detected and was not observed during subsequent ILS inspections at this location.

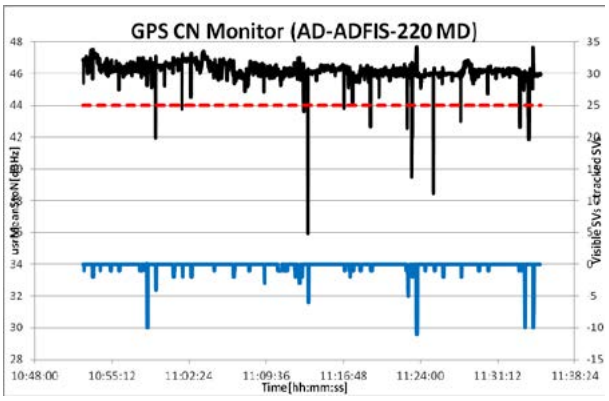

Figure 11 – Several Losses of RTK

As seen on the second trace, even though the C/No was clearly disturbed it was not sufficient for all satellite tracking to be lost.

AIRBORNE INVESTIGATION

Once interference is observed the primary objective is normally to positively identify the source so that it can be suppressed. However, a Flight Inspection aircraft is typically not equipped to complete this task and often the responsibility for this mission (and hence the necessary tools and experience) lies with Federal Radio or Spectrum Management Authorities.

In this case the aim of the Flight Inspection crew should be to quantify if/how the interference poses any threat to the procedures that rely on GNSS, and to gather as much information as possible on the characteristics of the interference to aid further investigation by the responsible authorities.

A spectrum analyzer (SPA) and suitable antennas for signal reception, are important tools for capturing the characteristics of the signal suspected of causing interference however the characteristics of the measurement system must be understood.

Spectrum Analyzer Settings

A balance must be found in the configuration as compromises between Span, Resolution/Video bandwidth and Sweep Time have an influence on the minimum detectable signal. In general, settings which improve sensitivity of the SPA increase the sweep time, however this can often be controlled independently at the expense of accuracy. Taking advantage of this to reduce the sweep time to 1 second, normally leads to the SPA operating in an un-calibrated state.

For our purposes this is of no consequence since the exact level of the interference signal is of little interest, however its presence and general characteristics are; and with a low sweep time we can take more samples in a short period of time. This not only increases the probability if detection for a short duration or highly localized interference source, but may also provide useful information for locating the source as relative changes in amplitude can be referenced to aircraft location to deduce a location.

GPS Antenna Frequency Response

The frequency response of the antenna also impacts on whether or not the signal is detectable with the SPA. By using a SPA with tracking generator and a suitable horn antenna as a transmitting source the frequency response of the GNSS antennas installed on a Flight Inspection aircraft were measured.

The results show that some antennas are better suited to the job of searching for interference signals than others.

Figure 12 - Typical AFIS GPS Antenna (L1, L2)

This dual frequency antenna would strongly attenuate any signals outside of the L1 or L2 band, so would be suitable for searching for in band interference but not out of band interference.

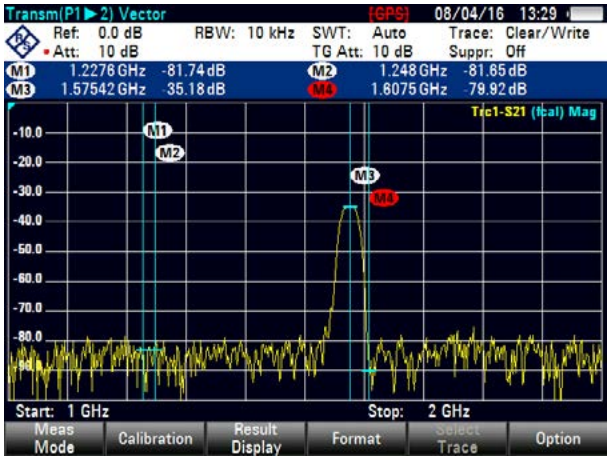

Figure 13 - Typical Primary GPS Antenna (L1)

Again, the strong filter effects most likely from the pre-amplifier, would make an antenna like this suitable for searching for in band interference but not out of band interference.

Figure 14 - Typical Multiband GNSS Antenna (L1, L2, L5, Omnistar, GLONASS)

This multiband GNSS antenna may provide little resilience to interference when connected to a GNSS receiver but provides a great frequency response for both in and out of band interference detection.

Figure 15 - Typical Passive L-Band Antenna

A standard, passive L-Band antenna provides a relatively flat frequency response as expected, however to measure this it was required to remove 40 dB of attenuation from the test setup. This means the antenna is 40-50 dB less sensitive than a standard GNSS antenna, limiting its usefulness for detecting low power interference sources such as personal privacy devices.

GNSS Antenna Location

GNSS antennas installed on top of the aircraft can have limited usefulness when localizing inference, which typically comes from below the aircraft. For this reason it has become typical to install the antenna intended for connection to a monitoring receiver, such as a SPA, on the bottom of the aircraft so that it is "downward facing".

The antenna pattern data shows that GPS antenna performance is strongly affected by elevation angle. When mounted on the bottom of an aircraft this means that interference signals coming from the side will be attenuated and it may be difficult to capture a useful spectrum of the inference unless near to overhead the source. While this has a certain disadvantages, using a standard L-Band antenna with a more useful reception pattern, would mean losing at least 40dB of sensitivity.

Given these considerations, the benefits of using a dedicated GNSS antenna for this purpose outweigh the relative disadvantages of using the next best alternative. With further knowledge of the relative frequency responses we can also see that it is beneficial to use a Multiband GNSS antenna for this purpose as the wide frequency response allows for effective detection of out of band interference sources.

Search Patterns

It should be stressed that the primary focus of these search patterns is to improve the chances of characterizing the interfering signal, not necessarily to locate the source.

Two radials at 90° to each other and of length ± 5NM over the point where the interference is suspected is a simple yet effective search pattern. A distinct advantage of this pattern is that by describing the profile in terms of heading and distance it is normally easy to relay intentions to ATC, which can be important when the detection occurs in flight and warrants immediate investigation before further briefings are possible.

A pattern such as this can show the relation between C/No and location, which is important to know when assessing the potential impact of the disturbance. Additional radials can easily be flown parallel to the initial radial, and if sufficient radials are flown a grid pattern is eventually formed, which will likely provide the authorities with a very good starting point for locating the source so that it can be suppressed.

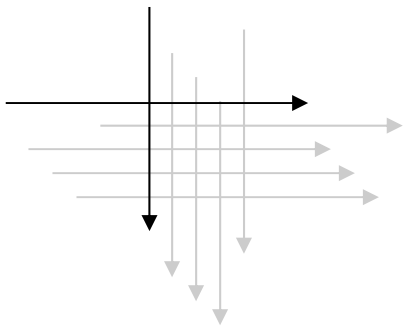

Figure 16 – Simple Search Pattern

Adaptation of Complex, Search and Rescue type search patterns, such as a Creeping Line or Expanding Square would also be useful in assessing the extent of an interference source's impact, however prior coordination with ATC for such "non-normal" maneuvers would be required.

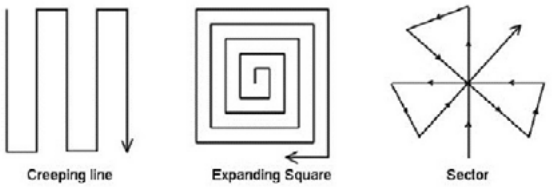

Figure 17 – Complex Search Patterns [4]

Rotary wing platforms offer significant advantages in this scenario, with reduced speed and tighter turns, not to mention the ability to hold over a defined position, all of which allow for increases in sample rate with respect to position.

PERIODIC INSPECTION OF GNSS ENVIRONMENT

During ILS, VOR or NDB periodic flight inspections the aircraft typically spends a lot of time at low altitude, normally less than 3000ft above ground. These low altitudes provide the best conditions for the detection of GNSS interference sources, and given the typical ILS flight inspection periodicity of 6 months, changes in the GNSS environment can be identified quickly.

GNSS based approaches at the airport will share similar final approach profiles to any ILS, VOR or NDB approach, and as such measurements completed in the background during these periodic inspections could constitute a periodic inspection of the GNSS environment without additional flying, important in busy airspace.

This periodic inspection should be seen as an important step towards ensuring the availability of published GNSS procedures.

Applicable Tolerances

From the performance of the C/No Monitor during cases of known interference the following tolerances can initially be derived for this specific configuration of GPS receiver, antenna, and normalization algorithm:

Average Compensated C/No	Interference
> 50 dBHz	Nil Observed
> 45, < 50 dBHz	Probable
< 45 dBHz	Present

Note that secondary effects, such as loss of RTK or primary GPS, should be used to confirm or quantify the impact of the interference.

Reporting

Consideration will need to be given to how the results from such a periodic investigation are documented. One possibility would be for the AFIS to generate a simple report, tabulating the time and location of instances where the C/No dropped below pre-defined limits.

The report could be generated when the monitoring makes any detection in the background and of course specifically included as part of the Flight Validation Report for GNSS based procedures.

FURTHER DEVELOPMENT

While implementation of the C/No Monitor provides a significant step forward in real time detection of GNSS interference, consideration has been given to further AFIS enhancements to build on this functionality.

Automation Based on C/No Limits

The C/No Monitor could be used to automatically trigger specific software actions when exceeding specified limits.

For example, if Average Compensated C/No dropped to a level indicating *probable* interference, the software could automatically make a spectrum analyzer measurement in the GPS L1 and GPS L2 bands, recording also the Latitude, Longitude and Altitude at the time of the measurement. An important requirement on the AFIS for this capability would also be a navigation solution based on multiple sensors (such as IRS, DME/DME) such that a temporary loss of GNSS can be compensated for and have minimal influence on the positional accuracy.

An automatically generated report would combine information relating to the detection (time, minimum value of Average Compensated C/No, aircraft, duration of detection) and the spectrum measurement for further distribution as required.

If the Average Compensated C/No dropped further, for example into the range where interference is considered certain, the software could additionally provide alerts to the Flight Inspector and generate a simply search pattern centered on the point of detection for the purposes of further investigation.

Continuous Monitoring

Currently the C/No Monitor is only active during calibration tasks, however it would be useful for it to be running at all times from AFIS start-up to shutdown.

While this will generate a lot of recording data the alert of possible interference will be available during ferry flights (in particular during take-off and landing) or in between calibration tasks.

This would provide the Flight Inspector the opportunity to conduct further investigation as warranted and could also lead to an AFIS generated "end of week GNSS interference" report, listing the locations where *probable* interference was detected along with information relating to each detection such as time, minimum observed Average Compensated C/No, duration and a spectrum measurement.

Predicted Vs. Observed Performance

Consideration may be given to further developing the capabilities to include alerts when achieved GNSS performance is not in-line with predicted performance. This would act as an additional indication of a potential interference.

An example would be for the software to detect when the observed constellation, including geometry and expected SVs, is different to one calculated from received almanac data. If for example there were to be 10 SVs in view and only 4 SVs are available, a further indication of GNSS interference or unexpected shielding is available without total loss of GNSS tracking.

Another possibility would be for the FIE to conduct a RAIM prediction for the expected duration of the next procedure, similar to that completed in an FMS before a GNSS approach. It is worth noting that a RAIM alert itself is not cause for concern, as this is simply the FMS stating that the GNSS conditions (number of SVs, geometry) are not suitable for application of RAIM algorithms. However if this RAIM alert is not expected through forward prediction it may be useful as an indicator of interference or shielding.

Interference Visualization

Consideration could also be given to exporting the flight track in Google Earth™ compatible KML format with traffic-light style color coding corresponding to the level of observed GPS interference, for example the following legend could be implemented:

Average Compensated C/No	Color
> 50 dBHz	Green
> 45, < 50 dBHz	Orange
< 45 dBHz	Red

This data, unlike the raw flight inspection data and associated plots, could be easily distributed to and interpreted by 3rd parties without the need for specialized training or tools.

Visualization of the data in this format could also provide clues as to the source of the interference and be useful in planning any follow up investigation activities.

Further Development of Antenna Pattern

In order to develop a more accurate antenna model, further consideration would need to be given to factors such as:

1. Varying power output from each GPS SV
2. Atmospheric effects

Specific flight profiles may also need to be developed and flown, where necessary by multiple aircraft in a close timeframe, to ensure a common baseline.

Initial experience shows that the compensation function works quite well but that there are some unexpected variations in Average Compensated C/No, in the order of 3-5 dB, during turns and subsequent changes in heading.

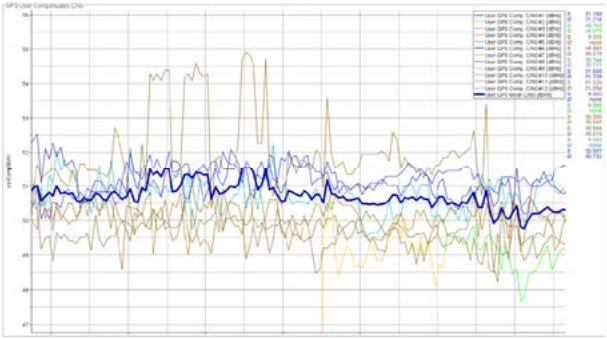

Figure 18 – Azimuth Induced Variations in Average Compensated C/No

While it will never be possible to completely eliminate these effects, it is suspected that some azimuth data in the model is causing overcompensation of the C/No value and that refining the model with additional data from dedicated flight profiles and smoothing processes will improve performance.

Experience gained through further and longer term use of software will drive development of the antenna pattern as warranted.

Important to note is that the goal of any further development will be to reduce the risk of false-positives from the C/No Monitor and not to measure GPS C/No with a specified accuracy.

CONCLUSIONS

From the development and implementation of the C/No Monitor we can make the following conclusions:

1. Implementation of a C/No Monitor provides a useful tool for online detection of GNSS interference such that an appropriate response (such as further investigation) can be considered and carried out in real time
2. Implementation of a C/No Monitor provides a suitable means of compliance with the recommendations of Doc 8071 Volume 2
3. A C/No Monitor provides the basis for Periodic Inspection of the GNSS environment, which can be completed "in the background" of normal Flight Inspection activities and without the need for additional flying
4. Similar techniques to those presented here for GPS could be used to monitor other GNSS signals, such as Galileo, GLONASS or BeiDou for evidence of interference in real time

RECOMMENDATIONS

Based on the experience with the C/No Monitor thus far the following recommendations are offered for consideration:

1. A GNSS C/No Monitor should be considered as "minimum equipment" for all AFIS designs
2. Requirements and guidance material relating to airborne GNSS interference detection, both from a technical capability and reporting perspective should be further defined

FUTURE WORK

The algorithms and functionalities presented in this paper will continue to be refined by FCS, skyguide and Aerodata as operational experience builds. An important future development will be derivation and implementation of the antenna model in preparation for civil use of L2 and L5 frequencies and adaptation of the C/No Monitor such that interference on these frequencies can be identified.

ACKNOWLEDGMENTS

Mr. Manfred Webers (FCS Technical Department) lead the analysis required to develop the GPS antenna models used in the on-line algorithms, and along with the programming efforts of Mr. Volker Logemann (FCS Flight Inspection Department) generated the necessary basis for this research. The AFIS OEM, Aerodata, were able to quickly develop the software in-line with FCS' specifications and implement this new technology.

REFERENCES

[1] M. Scaramuzza, H. Wipf, M. Troller, H. Leibundgut, R. Wittwer, and S. Rämi, 2014. GNSS RFI Detection in Switzerland based on Helicopter Recording Random Flights. IFIS 2014, Oklahoma City, USA, Proceedings.

[2] M. Scaramuzza, H. Wipf, M. Troller, H. Leibundgut, S. Rämi and R. Wittwer, GNSS RFI Detection: Finding the Needle in the Haystack. ION GNSS Conference 2015 Tampa, Florida, Proceedings.

[3] ICAO, 2007, Manual on Testing of Radio Navigation Aids, Volume 2, Testing of Satellite-based Radio Navigation Systems, Doc 8071, 5th Edition

[4] www.researchgate.net/profile/Piotr_Kopacz/publication/284488044/figure/fig19/AS:299219312234515@1448350851904/Figure-20-Planar-SAR-patterns-creeping-line-expanding-square-and-sectror-search.png, Accessed 2 May 2016

Localization of GNSS RFI Transmitters Using Digital Surface Models

Maurizio Scaramuzza
Dr. sc. techn. ETHZ
skyguide, Swiss Air Navigation Services Ltd.
CH-8602 Wangen bei Dübendorf, Switzerland
Fax: +41 43 931 66 19
E-Mail: maurizio.scaramuzza@skyguide.ch

ABSTRACT

GNSS radio frequency interference (RFI) is increasingly becoming an important topic with the growth of applications based on these systems. Furthermore, safety critical applications exposed to RFI might lead to unacceptable performance degradations. In a first step it is therefore crucial to develop the capability of detecting potential GNSS RFI. In a second step it is necessary to develop the ability of localizing the GNSS RFI transmitter.

Related to the first step, a methodology for the detection of potential GNSS RFI was presented at the IFIS 2014 in Oklahoma City, OK [1], and at the ION GNSS+ 2015 in Tampa, FL [2]. This method is primarily based on GPS L1 Carrier to Noise Power Ratio (C/N_0) measurements recorded onboard of helicopters.

Concerning the second step the advantage is taken that the helicopters are flying at low altitudes above ground level. Consequently it is expected that these aerial vehicles are only partially affected by interference sources due to terrain shadowing effects. This circumstance can be utilized to draw conclusions on the potential location of the GNSS RFI transmitter. To do so, digital surface models, electromagnetic signal propagation models and GNSS signal degradation information is used in order to confine the location of the GNSS RFI transmitter.

After a short recapitulation on the methodology used to detect potential GNSS RFI, an approach for GNSS RFI transmitter localization is presented.

INTRODUCTION

The method for the detection of potential GPS RFI consists in installing mini quick access recorders (mQAR) on board of two dozen helicopters and collecting data during a period of several years. The helicopter fleets are operated by Rega, the main Swiss Helicopter Emergency and Medical Service (HEMS), and by the Swiss Air Force (SAF). Daily missions of those two operators are used for data recording, so there is a random coverage of large parts of Switzerland. Since those helicopter missions are all flying at low altitudes (90% of flight time below 500m AGL), it is expected that they have a higher probability of being exposed to ground based RFI than commercial fixed wing operations.

For RFI detection it would be advantageous to record parameters such as the receiver's Auto Gain Control (AGC) or the power spectrum density within the L1 band, but only data on the ARINC 429 bus is available and therefore the only recorded parameter relating to the GPS signal quality are the C/N_0. These are then normalized based on GPS satellite azimuth and elevation angles as well as roll, pitch and yaw angles of the helicopters. To do so it is necessary to know the expected $C/N_{0,exp}$ at each GPS signal incidence angle at the receiver antenna. This was empirically derived by assessing over 200 hours of recorded data of each helicopter, resulting in an antenna pattern as depicted in Figure 1. For more details refer to [2].

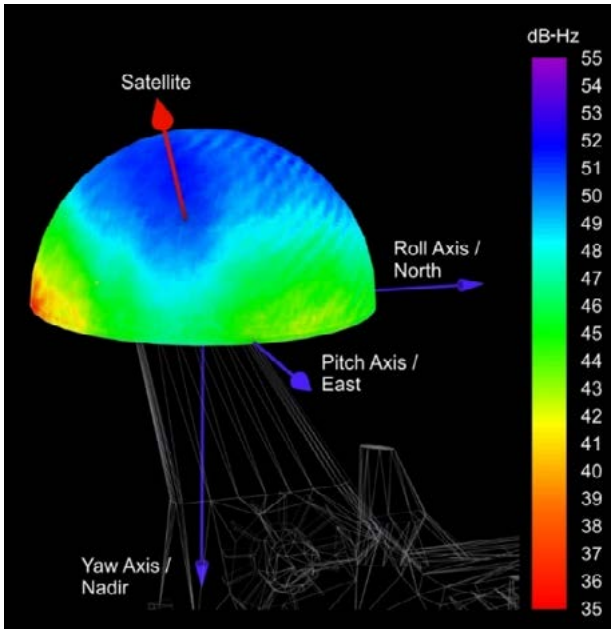

Figure 1: GPS antenna pattern on top of a helicopter fin describing the $C/N_{0,exp}$. The red arrow indicates the direction towards an arbitrary GPS satellite (incidence angle of GPS signal).

Finally, the normalized GPS signals are statistically assessed for the determination of potential RFI. Only GPS L1 C/A signals are taken into account, but with a few modifications this method can be adapted to any GNSS providing pseudo range services. This method has shown, based on assessments of over 6000 flight hours, that C/N_0 degradations due to potential GPS RFI of a few dB can be detected. One example is shown in Figure 2, where the C/N_0 ratios of all tracked satellites were similarly affected by a potentially interfering signal.

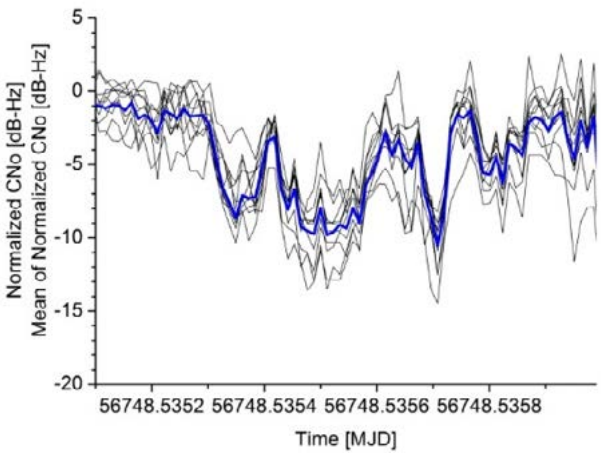

Figure 2: Situation where a potential RFI might be present. The thin black lines represents the normalized C/N_0 of each tracked satellite where the bold blue line is derived by averaging the normalized C/N_0.

Within the assessed period, degradations of normalized C/N_0 were observed at different locations. A repeatedly degraded C/N_0 at the same location is a strong indicator for a static RFI source in the vicinity of the flight paths. One of these areas is shown in Figure 3. Its size is 5km by 4km. The colored dots indicate a mean degradation of the C/N_0 of at least -3dB. Underlaid is a shaded relief map derived from a digital surface model (DSM). Two main flight routes are visible in this area. The degradations on the right route reach values down to -18dB, while they do not decrease below -8dB on the left route. Attention has to be paid to the left route where the degradation systematically rises to values higher than -3dB at certain locations. One assumption for this behavior is that the helicopters might be shadowed from the RFI transmitter by obstacles, namely the terrain (including vegetation and buildings). This effect is the point of origin of this study. The concept is to trace back to the interference source by assessing the attenuation of the interfering signal caused among others by shadowing effects of the terrain and obstacles on ground.

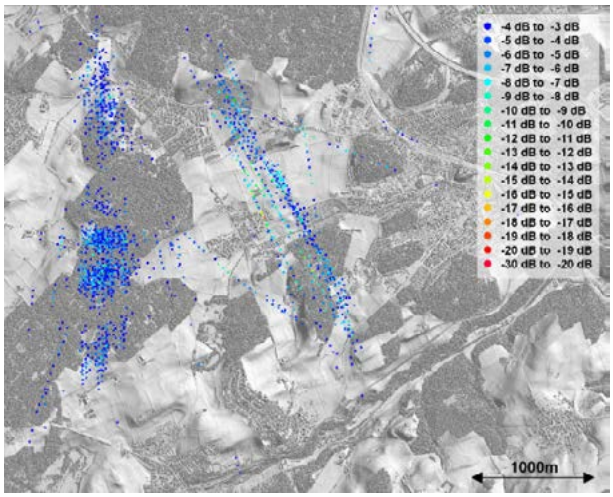

Figure 3: An area where the C/N_0 is repeatedly degraded indicating a potentially present RFI source.

CONCEPT FOR RFI TRANSMITTER LOCALIZATION

The concept for the localization of the RFI transmitter is to estimate the EIRP (Equivalent Isotropically Radiated Power) of this source based on the degradation of the C/N_0. It is obvious that different gains and losses of the interfering signal between RFI transmitter and GPS antenna have to be taken into account. Defining an arbitrary RFI transmitter position in the proximity of the affected flight paths allows to estimate the EIRP. In the most probable case the selected RFI transmitter position is incorrect and therefore the estimated EIRP varies from the effective EIRP. If a set of n affected helicopter positions is defined, which will further be denoted by the index i, then a set of $EIRP_i$ is estimated. The closer the arbitrary defined RFI transmitter position is to the real RFI transmitter position, the smaller is the variance of

$EIRP_i$. If additionally a set of m arbitrary RFI transmitter positions is defined, further denoted by an index j, then the problem can be reduced to find the jth RFI transmitter position with minimum variance of $EIRP_i$, i.e.

$$min_j\{Var(EIRP_i)_j\}, i = 1..n, j = 1..m \quad (1)$$

RFI EIRP ESTIMATION

The effective carrier power to noise ratio $C_S/N_{0,eff}$ including an interfering signal can be approximated analytically by equation (2). An extensive treatment of following equation is given in [3].

$$C_S/N_{0,eff} = \left(\frac{1}{C/N_{0,exp}} + \frac{C_I/C_S}{QR_C}\right)^{-1} \quad (2)$$

where

$C_S/N_{0,exp}$: expected carrier to noise power ratio of received GPS signal inside the receiver without any interfering signal,

C_I/C_S: interfering to received GPS signal power ratio inside the GPS receiver

Q: interference resistance quality factor

R_C: chip rate of the Binary Phase Shift Keying (BPSK) code

The $C_S/N_{0,exp}$ is known through the empirically derived GPS receiver antenna pattern (see Figure 1). Analytical derivation of the dimensionless parameter Q is given in [3]. Q is approximately equal to 1 for CW (Continuous Wave) interfering signal at the L1 carrier frequency of 1.57542 GHz and increases when the CW frequency is shifted away, meaning that the GPS signal is then less affected. Q reaches values larger than 2 for a white noise like interfering signal. Finally, for the C/A code, R_C is equal to $1.023 \cdot 10^6$.

The EIRP of the RFI is derived based on equation (2) (see [3]) and expressed in dB-Hz yields

$$(C_S/N_0)_{eff,dB} = -10log_{10}\left[10^{-\frac{(C_S/N_0)_{exp,dB}}{10}} + \frac{10^{\frac{(C_I/C_S)_{dB}}{10}}}{QR_C}\right] \quad (3)$$

The round bracket followed by the index dB denotes, that the unit is dB. It follows

$$(C_I/C_S)_{dB} = 10log_{10}\left[QR_C\left(10^{-\frac{(C_S/N_0)_{eff,dB}}{10}} - 10^{-\frac{(C_S/N_0)_{exp,dB}}{10}}\right)\right] \quad (4)$$

Now, the measured degradation of the C/N_0 as shown in Figure 2 is brought into relation on the right side of equation (4). The left side of this equation can be expressed according to [3] as follows:

$$(C_I/C_S)_{dB} = (I_H/S_H)_{dB} + (G_{H,I})_{dB} - (G_{H,SVi})_{dB} \quad (5)$$

where

I_H/S_H: interfering to GPS signal power ratio at the helicopter GPS antenna input

$G_{H,SVi}$: helicopter GPS antenna gain towards i^{th} GPS satellite

$G_{H,I}$: helicopter GPS antenna gain towards interfering source

According to [4], the GPS signal power S_H at the helicopter GPS antenna for satellites of Block II to IIR is in the range of -158.5dBW to -156.5dBW. Both GPS antenna gains $G_{H,SVi}$ and $G_{H,I}$ can be omitted, as these parameters are already contained within the GPS antenna pattern for $C/N_{0,exp}$. The equations solved for I_H yield

$$(I_H)_{dB} = 10log_{10}\left[QR_C\left(10^{-\frac{(C_S/N_0)_{eff,dB}}{10}} - 10^{-\frac{(C_S/N_0)_{exp,dB}}{10}}\right)\right] - (S_H)_{dB} \quad (6)$$

The EIRP at the RFI source is therefore

$$(EIRP)_{dB} = (I_H)_{dB} - (G_I)_{dB} + (L_{FSPL})_{dB} + (L_{DIFF})_{dB} + (L_{POL})_{dB} + (L_{FE})_{dB} \quad (7)$$

Where

G_I: RFI antenna gain towards helicopter

L_{FSPL}: free space path loss of interfering signal

L_{FIDD}: diffraction loss of interfering signal at the terrain and obstacles

L_{POL}: loss due to polarization mismatch

L_{FE}: loss due to receiver front end filtering

The RFI antenna gain G_I is unknown. A first approximation could be to assume a dipole antenna where the antenna gain can be derived. Another approach could be to assume a range of antenna gains and to derive a minimum and maximum EIRP based on the extremal values of this gain range. For instance, if an RFI dipole antenna is assumed, then a polarization mismatch between the linearly polarized RFI antenna and the right hand circularly polarized (RHCP) GPS antenna is present. This loss is taken into account within the parameter L_{POL}, which in this case would be 3dB. In case the interfering signal is out of band, a loss caused by the receiver front end filtering L_{FE} has to be taken into

account. For the further discussion it is assumed that an in-band interfering signal is present yielding L_{FE} = 0dB.

The signal free space path loss L_{FSPL} is derived according to [5]

$$L_{FSPL} = 20log_{10}\left(\frac{4\pi d}{\lambda}\right) \quad (8)$$

where λ = 0.19m for the GPS L1 frequency. It is important that the distance d between RFI transmitter and GPS receiver antenna is derived from the arbitrarily selected RFI transmitter position as discussed in the chapter on the concept for RFI transmitter localization.

The loss caused by the signal diffraction L_{DIFF} is approximated by the Bullington method, which is an extension of the knife-edge loss method. This method is described and recommended in [6] where an automatic process is needed and in a situation where the terrain and obstacle profile is well known. The advantage of this method is the simple implementation in the simulation software used for this paper. However, it is also known that this method has the tendency to underestimate the diffraction loss.

The arbitrarily defined RFI transmitter locations are arranged in a grid with regular distances (e.g. 5m), and for each grid point the EIRP is calculated for each helicopter position with a degraded C/N_0. Therefore, for each grid point a set of n EIRP values is derived. The standard deviation of the EIRP values is used in order to find the correct RFI source position. The lower the standard deviation value, the closer the arbitrary position is to the correct RFI transmitter position. Nevertheless, outliers have to be expected, and hence more appropriate variables could be used as well, such as quantiles.

DIGITAL TERRAIN AND SURFACE MODELS

The calculation of the diffraction loss requires digital terrain models (DTM), or digital surface models (DSM), respectively. Today DTMs with a resolution of 1" or 3" in latitude and longitude are common, and in some cases freely available (e.g. Shuttle Radar Topography Model, SRTM). However, due to the relatively short distances between the RFI transmitter and the helicopter paths combined with obstacles (vegetation and buildings) with heights above ground of up to 30m or more, it is advantageous to rely on surface instead of terrain models. Further, higher horizontal resolutions lead to more accurate results.

Following DTM and DSM are at the disposition within this study

- DTM with 25m horizontal resolution (DHM25)
- DSM with 20m horizontal resolution (DOM20)
- DSM with 0.5m horizontal resolution (DOM-ZH)

where the DOM-ZH is used for the calculations and the other two are used for comparison of the results only. Figure 4 depicts the differences in resolution for these different digital models for an area of 500m by 500m containing buildings at the border of a small village (left), a farm house (middle/right), cultivated land (right) and forest (rear left). It is clearly visible that the high resolution surface model offers a great advantage for signal propagation calculation purposes.

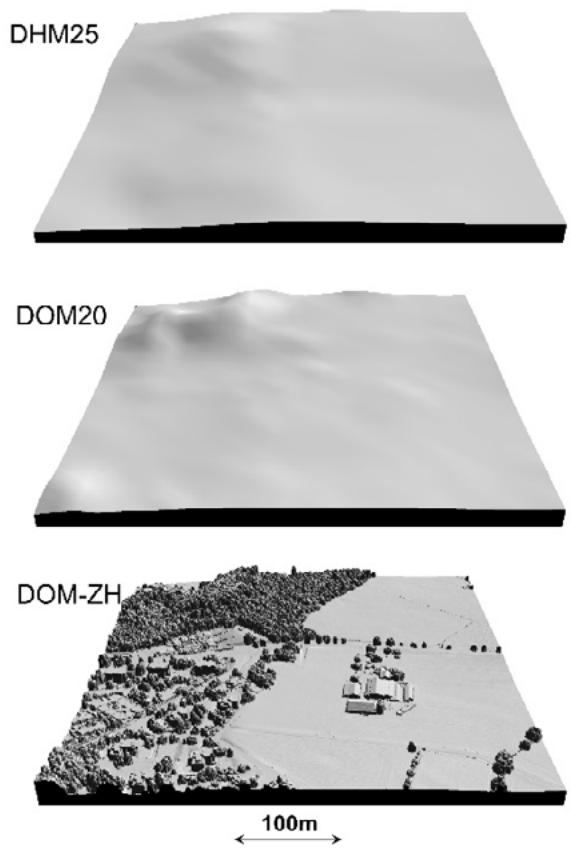

Figure 4: Comparison of one digital terrain model (top) and two digital surface models (middle and bottom) with different horizontal resolutions.

RESULTS

The situation depicted in Figure 3 is used as a test case. Some data is filtered in order to keep calculation time at a reasonable level. Only two flights are used, one for each route. Out of these two flights, only every tenth degraded C/N_0 is used, resulting in 17 samples (see black crosses in Figure 5). The grid space for the arbitrarily defined RFI transmitter locations is set to 5m. It is assumed that the RFI antenna is static and located 2m above the surface. The profile sampling for the signal diffraction estimation is set to 2m. For the RFI transmitter a half wavelength dipole antenna is assumed. Further, the RFI signal is assumed to be a CW within the GPS L1 band. The alternation of these RFI input parameters are discussed too.

The simulation result in Figure 5 shows that the potential location of the RFI transmitter can be dramatically confined to a few spots (red areas). These are the areas where EIRP's standard deviation is low, i.e. below a few mW. The areas with values larger than 10mW to 15mW are clipped.

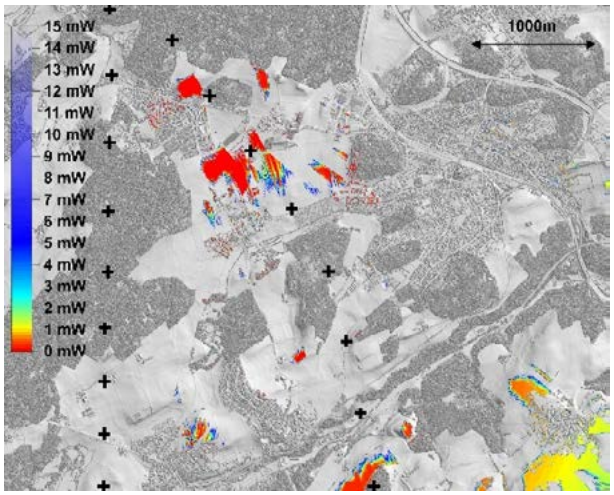

Figure 5: Potential areas where the RFI transmitter could be located.

Care has to be taken on the fact that very small areas of the size of buildings can be identified as potential RFI transmitter location as well (see Figure 6). This is due to the fact that the roofs of these buildings are more exposed to the flight paths than the nearby ground surface. Finally, artefacts can be detected within the forest. This is mainly due to the irregular shape of the DSM in this area. A screening with the help of a Geographic Information System (GIS) in order to find installed transmitting antennas in this area has shown, that only one of these antennas is located within the forest. Therefore, in a first step, the forest can be neglected as a search area for the RFI source.

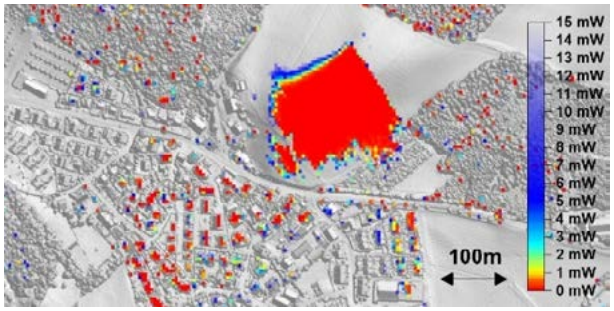

Figure 6: Detailed view of the left top part of Figure 5 showing the ability to identify single buildings as potential RFI transmitter location.

Variation of input parameters is performed in order to show that the result is only marginally affected by improper assumptions. This behavior can be explained by the fact that only the minimum standard deviation of the EIRP is assessed, but not the EIRP itself.

Two cases are discussed: Firstly, the assumed altitude of the RFI antenna over ground is increased from 2m to 5m. By consequence the RFI antenna will affect a larger area. Thus the area with the potentially correct position of the RFI transmitter increases, which is visible in Figure 7. However, when comparing this result with that in Figure 5, it can be seen that the area of interest is only slightly increased. This effect is advantageous in order to minimize the risk of searching the RFI transmitter in improper locations when assuming incorrect altitudes of the RFI antenna.

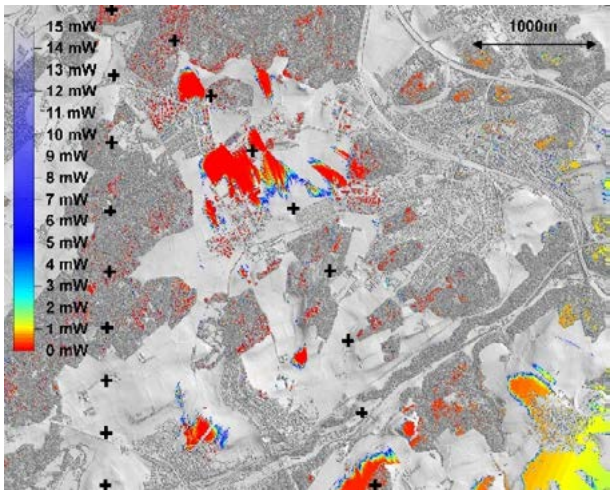

Figure 7: Potential areas where the RFI transmitter could be located. In this case the assumed altitude of the RFI antenna over ground is increased from 2m to 5m.

The second case assesses inappropriate assumption on the RFI signal characteristics, e.g. polarization of the interfering signal or out of band instead of in-band interference. To do this, an additional constant loss of 6dB is taken into account in equation (7). The assumed altitude of the RFI antenna over ground is set to 2m. This adaptation systematically affects the calculated EIRP. Nevertheless, the size of potential areas containing the RFI transmitter is only marginal affected, as can be seen in Figure 8. The range where the potential RFI transmitter could be located has to be increased. This is visible when comparing the right bottom part of the Figures 5 and 7.

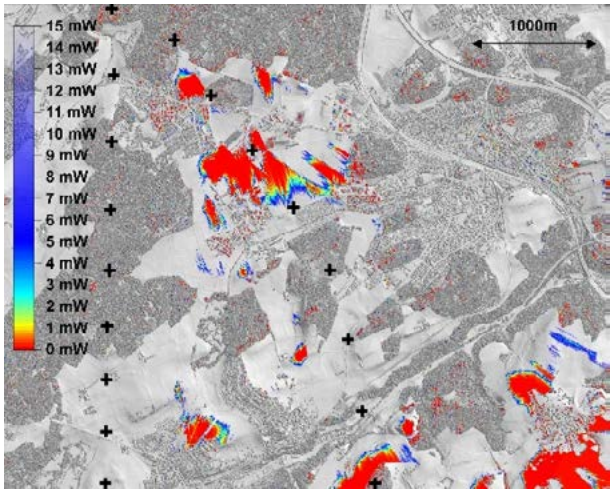

Figure 8: Potential areas where the RFI transmitter could be located. In this case the assumed altitude of the RFI antenna over ground is increased from 2m to 5m.

Finally, the impact on the results depending on selection of DSM and DTM is shown. Figure 9 depicts the result when applying a DTM with 25m horizontal resolution (DHM25) and within Figure 10 a DSM with 20m horizontal resolution (DOM20). The advantage of high resolution DSM is clearly visible when comparing these results with that in Figure 5. Even with similar horizontal resolutions (20m to 25m) a DSM has an advantage compared to a DTM.

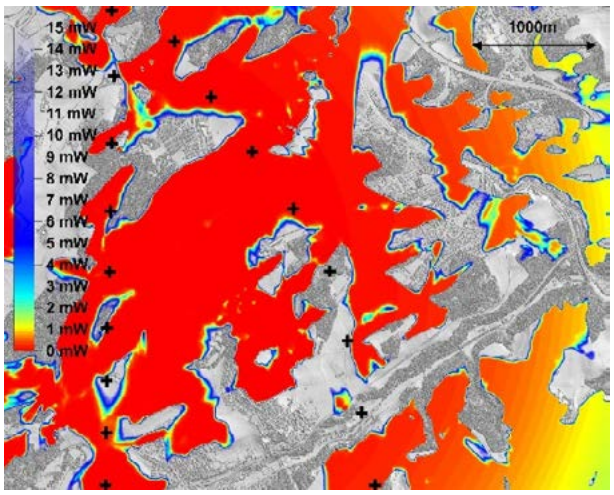

Figure 9: Simulation results when using a DTM with 25m horizontal resolution instead of a DSM with 0.5m horizontal resolution.

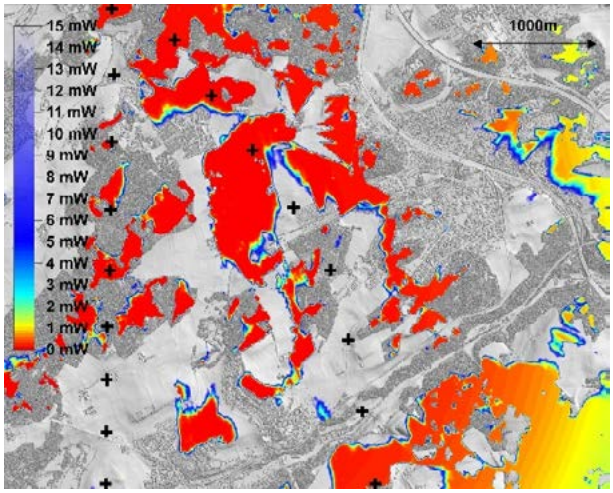

Figure 10: Simulation results when using a DSM with 20m horizontal resolution instead of a DSM with 0.5m horizontal resolution.

CONCLUSIONS

A method has been described which allows to confine the search area of a RFI transmitter site. This is based on the comparison between expected and effective C/N_0 while taking advantage of high resolution digital surface models. Following conclusions are deduced from this study:

a) The described method allows to reduce the search area of a RFI transmitter site to a large extent.

b) The use of high resolution digital surface models improve the result quality by several factors.

c) To a certain degree the results are not affected by inadequate assumptions on the RFI transmitter characteristics.

RECOMMENDATIONS

It is recommended to apply the presented method in order to reduce the search area of a static RFI transmitter and consequently to reduce the time to localize the RFI transmitter.

FUTURE WORK

Additional analysis will be performed on the signal diffraction loss models. Processing time and result quality shall be reasonably balanced.

The antenna pattern for the expected C/N_0 will be assessed more in detail for negative angles. Currently only limited data is available for each helicopter. Improvement of this parameter is particularly important

when the helicopter flies close or over the RFI transmitter.

After having assessed the impact of the RFI transmitter in the spatial domain it is important to assess the temporal domain too. This additional information is crucial when attempting to localize the RFI transmitter on-site.

ACKNOWLEDGMENTS

Special thanks go to CHIPS and the Swiss Federal Office of Civil Aviation for the financial support of this project within the frame of the applied research and development programme for implementation of future navigation applications in Switzerland. Contributions to this study were done by P. Truffer, G. Aschwanden, H. Wipf, and M. Troller (skyguide), H. Leibundgut (REGA), S. Rämi, and M. Bertschi (Swiss Air Force), and R. Wittwer (armasuisse).

REFERENCES

[1] M. Scaramuzza, H. Wipf, M. Troller, H. Leibundgut, R. Wittwer, and S. Rämi, 2014, GNSS RFI Detection in Switzerland based on Helicopter Recording Random Flights, Proceedings of IFIS 2014, Oklahoma City, USA.

[2] M. Scaramuzza, H. Wipf, M. Troller, H. Leibundgut, S. Rämi and R. Wittwer, GNSS RFI Detection: Finding the Needle in the Haystack, Proceedings of ION GNSS Conference 2015 Tampa, Florida.

[3] P. Ward, J. Betz, and C. Hegarty, Interference, Multipath, and Scintillation, Chapter 6 in book 'Understanding GPS – Principles and Applications', 2nd Edition, Artec House, 2006.

[4] US DoD, Navstar GPS Space Segment/Navigation User Interfaces, Interface Specifications IS-GPS-200H, Global Positioning Systems Directorate, Systems Engineering & Integration, 24.9.2013.

[5] ITU, Calculation of Free-Space Attenuation, Recommendation, ITU-R P.525-2, 1994.

[6] ITU, Propagation by Diffraction, ITU-R P.526-13, 2013.

GPS Jammer Localization Using Unmanned Aerial Vehicle

Adrien Perkins
Ph.D. Candidate
Stanford University
Stanford, California, US
E-mail: adrienp@stanford.edu

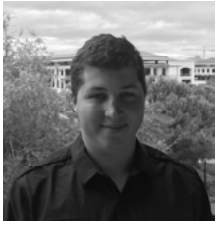

Per Enge
Professor
Stanford University
Stanford, California, US
E-mail: penge@stanford.edu

ABSTRACT

The aviation industry has and continues to benefit tremendously from the efficiency and safety improvements provided through the prevalence of GPS technology. However, as GPS technology becomes more ubiquitous and relied upon for all phases of flight, the potential risk posed by GPS jamming devices increases. In an effort to combat these risks and mitigate the effects of interference in the vicinity of an airport, this paper presents the design of a system called Jammer Acquisition with GPS Exploration and Reconnaissance (JAGER) which is an multirotor unmanned aerial vehicle (UAV) sensor platform capable of rapidly and autonomously localizing the source of a jamming device.

The urban environment near many major airports poses a challenge for quickly localizing a jammer through ground based methods. Our approach to localization uses a UAV as a mobile sensor platform operating well above the noise and multipath rich environment near the ground to make bearing observations of the jamming signal at dynamically chosen positions in order to optimally locate the source of the jammer.

The three main elements making up the system to localize a GPS jammer described in this paper are the sensing and measurement system, the path planning system and the navigation system. For sensing and measurements, JAGER relies on the maneuverability of the multirotor platform to be able to use simple antenna configurations, such as a directional antenna, to determine the bearing to the signal source from specific locations. Using the bearing observations, a closed loop navigation controller determines the next action to most quickly locate the source of the jammer.

Using bearing observations, JAGER is able to use different path planning methods to determine the best route for localization of the jammer. In this paper we will describe and show experimental results of the use of two different path planning methods: a simple greedy method following the direction of strongest signal and a more complex approach that models the problem as a partially observable Markov decision process (POMDP) which results in a near optimal path for localization. The benefits and challenges faced by each of the different methods will be explained for different jamming scenarios including multiple or moving jammers.

In addition to localizing the GPS jammer, the navigation system must be able to successfully navigate in the GPS denied environment. Our approach to denied navigation with JAGER is to leverage vision, low cost inertials and the many signals of opportunity present near an airport to navigate in the denied environment in and around the jammer.

JAGER is a fully integrated mobile sensor platform capable of autonomously locating the source of a GPS jammer in the urban environments present near many major airports designed to quickly mitigate the risks posed by a GPS jammer placed in the vicinity of an airport.

INTRODUCTION

The concern over radio frequency interference (RFI) of safety critical applications is not a new one. The vulnerability of GPS to jamming has already led the Federal Aviation Administration (FAA) to pursued different technologies for RFI detection and localization [1].

To help mitigate the risks posed by GPS jammers, we are developing an unmanned aerial vehicle (UAV) capably of autonomously localizing the source of a GPS jammer. The system we are developing, JAGER (Jammer Acquisition with GPS Exploration and Reconnaissance), is being designed with a target application of supporting airports in localizing sources of jamming that could interfere with airport operations and pose a threat to the safety of commercial aviation.

Existing Solutions

An existing solution of note to localizing RFI sources is the Aircraft RFI Localization and Avoidance System (ARLAS), which used a small, manned airplane with a patch GPS antenna on the roof [2]. Using this antenna, and the banking motion of the aircraft, ARLAS was capable of creating a bounding area of the source of RFI from determining at what regions the roof mounted GPS antenna picked up the interference.

ARLAS unfortunately suffers from coupling between sensing and navigation, meaning that in order to make a measurement, the plane needed to bank and therefore change the trajectory of the aircraft. This coupling leads to tradeoffs between trajectory and sensing, leading to longer search times.

JAGER

Our approach to the jammer localization problem uses a multirotor UAV to be able to quickly navigate and sense its environment for rapid localization. JAGER is built on a commercially available octocopter platform, the DJI S1000, which has been modified to be a test platform for various systems, including the one presented in this paper [3]. For localization of a GPS jammer, the vehicle is equipped with several different subsystems, illustrated in Figure 1.

At the autopilot system's core is the open source Pixhawk autopilot system running the PX4 firmware that has been modified to work with the path planning and navigation systems to autonomously execute the desired path and measurements [4]. The path planning system is comprised of an Odroid-XU4 ARM based computer that is the decision making heart of the system. It processes all the sensor measurements, makes the high level decisions for the next observation location and reports the location of the jammer when finished. Finally, the navigation system will be using infrared imaging and signals of opportunity processed by an Intel NUC computer at its core. This system processes all the imaging and signal of opportunity to determine an estimate for JAGER's location, which is fed to the autopilot system to assist with the autonomous navigation.

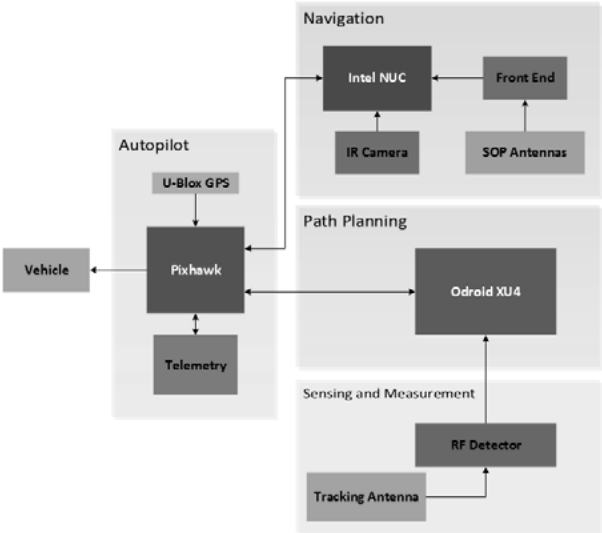

Figure 1. JAGER System Diagram.

Through the use of an agile, multirotor UAV, we hope to overcome the limitations posed by existing RFI localization techniques. The airborne nature of a UAV allows it to fly well above the noise that can plague ground based systems, and the ease of rotation of a multirotor can be leveraged to make measurements and observations without having to alter its flight path. This solution also aims to be easier to deploy, have a lower cost, and provide faster response times than a manned system.

SENSING AND MEASUREMENT SYSTEM

The primary observation that is used in the path planning system is the bearing to the jammer, however in order to determine bearing, we need signal strength measurements. Therefore the primary sensor onboard JAGER is a directional antenna and radio capable of measuring signal strength at a given heading. With a collection of signal strength measurements generated by rotating at a specific location we can recreate the gain pattern of the antenna, which can then be used to determine the bearing to the signal source.

In this section, the antenna configuration and sensing equipment will be described along with several different bearing calculation methods and their different advantages and drawbacks.

Sensing

Signal strength measurements of the jamming signal are made with a directional antenna and a radio frequency (RF) detector. In flight testing, due to legal constraints, a Wi-Fi router has been used a proxy for a GPS jammer, therefore in this case the antenna is a directional WiFi antenna and the signal strength measurements are being

made with an RN-XV WiFly module capable of returning the received signal strength indicator (RSSI) value. However, the frequency of operation makes no difference to the resulting methods of calculating bearing from a set of measurements, therefore when JAGER will be tested with GPS jammers, the same methods will be used. Currently, the directional antenna being used has a beamwidth of about 60 degrees and a true gain pattern as shown in Figure 2.

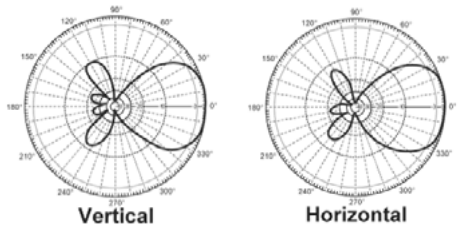

Figure 2. Directional Antenna Gain Pattern [5].

The antenna is mounted like shown in Figure 3 on JAGER. This allows maximum forward field of view, but does create an empty region just below the vehicle. However, this void below the vehicle is not a concern as one of the goals of the navigation system is to avoid approaching the jammer more than is necessary to minimize operational time in the GPS denied environment, therefore getting a maximum field of view outwards is more advantageous.

Figure 3. Directional Antenna Mounted on Underside of UAV with Antenna Main Lobe Shaded.

The orientation of the antenna creates three different classes of measurements based on the distance to the jammer: near, ideal and far. When near the jammer, measurements are very noisy and therefore the resulting gain patterns are nearly unusable. In the ideal case we get gain patterns that look almost identical to the true gain pattern, which result in very good bearing estimates. Far from the jammer, we are limited by which of the bearing calculation methods we can use, and the precision is also reduced. Finally, beyond the sensitivity of the sensor, we get no valid measurements.

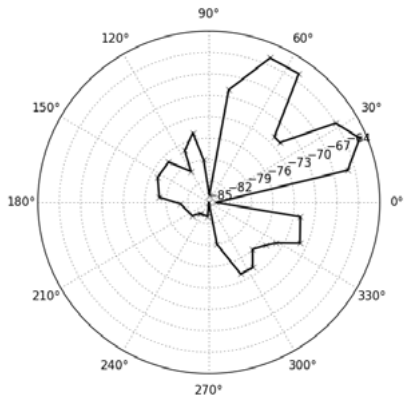

Figure 4. Gain Pattern for Direction Finding Antenna.

The directional antenna being used is by far the simplest configuration, and has worked well so far. However, we are also exploring the use of several different antennas such as the addition of an omnidirectional antenna to normalize measurements or two directional antennas to make a direction finding antenna. An example of the direction finding antenna pattern can be seen in Figure 4. Note that with a direction finding antenna a sharp null created in the center can potentially allow for more precise bearing measurements to be calculated.

Measurements

The signal strength measurements themselves are only used as a way to get bearing information. We do not use the signal strength as an indicator of range, due to its notoriously unreliable performance due to effects from the surrounding environment such as multipath and fading [6]. This poor range performance has also been illustrated in our flight testing, shown in Figure 5. In this figure, the maximum signal strength measured at each of the locations have been plotted in different colors ranging from strongest (lightest in color) to weakest (darkest in color). Note that the color does not fade nicely with distance as one might expect if signal strength was a good metric of distance. Furthermore, notice that close to the signal source the measurements get worse due to the fact that the vehicle is overhead of the signal source and no longer has the jammer in the main lobe of the antenna. For all these reasons, signal strength is not a reliable metric of distance, and therefore the main observation is the bearing calculated from a set of measurements at a specific location.

Figure 5. Signal Strength Measurements at Various Bearings and Distances.

Bearing Calculation

Given a recreated gain pattern, two different techniques have been used to be able to calculate the bearing to the signal source. The first method is a modification of simply using the heading of the maximum received signal strength as the bearing, which has been used on UAVs in prior research [7]. The modification used here, a method we call Max3, smooths out noise along the main lobe of the gain pattern by determining the bearing to be the halfway point between the two -3dB crossing points of the gain pattern (this is the point where the main lobe begins to drop off quickly) [8]. These points are illustrated in Figure 6.

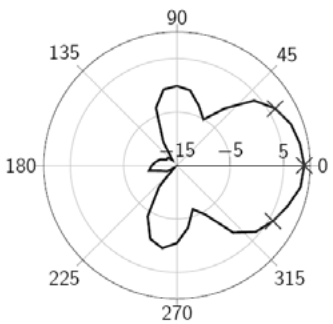

Figure 6. Depiction of Max3 Bearing Method.

The second method used is cross-correlation, which compared the measured pattern with a known "truth" pattern for the antenna. This method has also been used previously to determine bearing on a rotating robot in previous research [9].

The main disadvantage of cross-correlation is that the reliance on a known gain pattern makes it more difficult to get accurate bearings very far from the signal source. Far from the jammer, the gain pattern created, shown in Figure 7, no longer resembles the true gain pattern. At these distances the Max3 method performs significantly better.

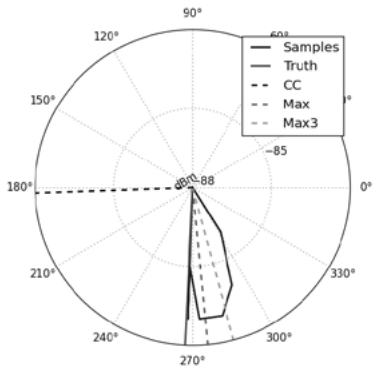

Figure 7. Measured Gain Pattern Far from Signal Source.

However, at ideal distances from the signal source, both method perform very well, an example which is shown in Figure 8. In this case the advantage with cross-correlation is that it is able to provide a cross-correlation coefficient which is a measure of confidence in the calculated bearing. This provides additional information that can be used in the path planning system.

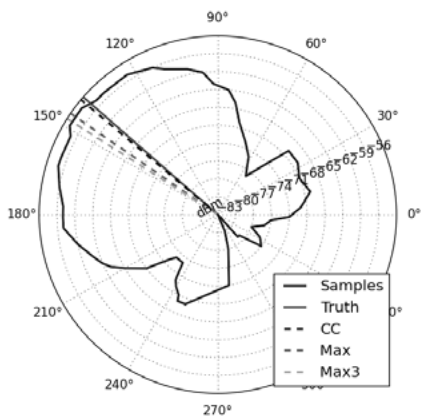

Figure 8. Measured Gain Pattern at Ideal Range from Signal Source.

Overall these methods of determining bearing from a set of measurements have proven to be sufficiently accurate to be able to quickly localize a signal source. Both of these methods, at an ideal distance, have standard deviations of about 13 degrees, and far from the signal source, the Max3 method still fairs decently with a standard deviation of about 22 degrees.

Near the signal source, both bearing determination techniques suffer greatly due to the noise of the measurements, shown in Figure 9. As will be shown later in the path planning section, this greatly affects the decisions made by the POMDP based path planner, as it strives to avoid the areas near the signal source, where it will not be able to get reliable measurements.

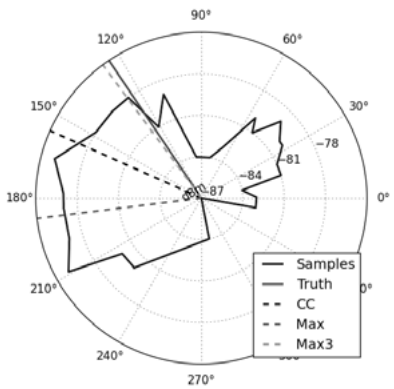

Figure 9. Measured Gain Pattern Near Signal Source.

PATH PLANNING SYSTEM

JAGER's path planning system focuses on determining, in real time, the next best location for making a bearing observation. Given that each observation provides information to the location of the signal source, getting the right collection of observations allows JAGER to localize the signal source as quickly as possible.

In this section of the paper, the partially observable Markov decision (POMDP) based method used by JAGER will be demonstrated and motivated by the performance of a simple greedy method for path planning.

Greedy

In order to establish a baseline for comparison, a simply greedy method was used as a path planner. This method is the closest approximation to how a human might do localization: keep moving forward in the estimated bearing direction until you pass the signal source and the bearing becomes the other way around. Now because we don't have continuous bearing observations, and JAGER must stop to make those measurements, we take this approach and discretize it into a set of steps. To make some slight improvements in the method to speed things up, we used a variable step between the observations. This means that the algorithm will move in the direction of the calculated bearing with a variable step size. The step size used is determined using equation 1. In this equation, δ is the tolerance in bearing similarity, α is the step increase factor, s is the step size and b is the calculated bearing.

$$s_{t+1} = \begin{cases} \alpha * s_t & if\ |b_t - b_{t-1}| < \delta \\ s_0 & \end{cases} \quad (1)$$

As can be seen, this effectively increases the step size by a factor of α if the current and previous observations are within some tolerance. Or more intuitively, if the signal source is still in the same direction last time we checked, then keep going in that direction and go even further before making another measurement as we are surely on the right track.

The baseline was able to successfully localize the signal source consistently in all of the flight tests performance. An example flight path taken can be seen in Figure 10. This method takes on average 4 steps to reach the vicinity of the jammer, and then another 4 or 5 steps to be able to crisscross the signal source's location to have a reasonable certainty that the signal source is at that location.

Figure 10. Flight Path of Greedy Path Planning.

Partially Observable Markov Decision Process

The more optimal method of localization is based on a partially observable Markov decision process (POMDP). The POMDP takes in a set of observations, and from that create a belief distribution for where the signal source could be. From here, the algorithm determines the optimal action, which in this case is where to make the next observation. This process is repeated online until the jammer has been successfully localized.

For this method, the world that the vehicle is operating in needs to be discretized into a grid. The grid that is used is one with cells 10 meters on a side, as being able to localize the signal source within a 10x10m square is

enough to be able to greatly minimize the search for the ground team.

When the POMDP approach was executed from the same starting location as the greedy method, the localization took a mere three steps and four measurements to find the signal source, as can be seen in Figure 11. The final belief state is overlaid with the location accurately determined to be the darkest cell. There are a handful of light cells, but those all had negligibly small probabilities.

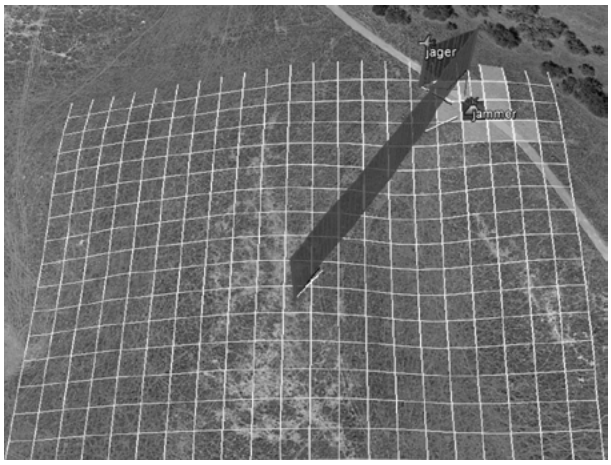

Figure 11. Flight Path of POMDP Path Planning with Overlay of Final Belief State.

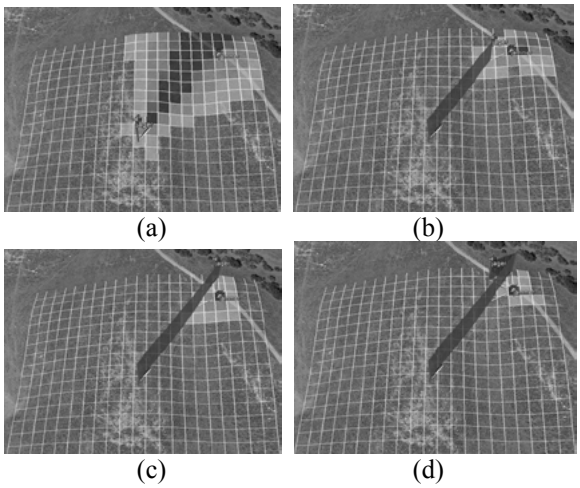

Figure 12. POMDP Belief State at Each Step.

Figure 12 shows the internal belief state of the location of the jammer between all of the observations made by JAGER during the localization. The cells with the highest probability are in dark red and then fade from there. Notice that with the POMDP based path planner, JAGER makes much larger steps than seen in the greedy method and does not always move towards the signal source. This is due to the fact that in order to minimize the spread of the belief, a measurement that is to the side of the belief distribution can be a lot more effective than going towards the jammer itself. When the measurement model with the additional noise near the jammer is taken into account, the resulting effect of maintaining enough distance from the signal source, shown in Figure 13, is much more pronounced.

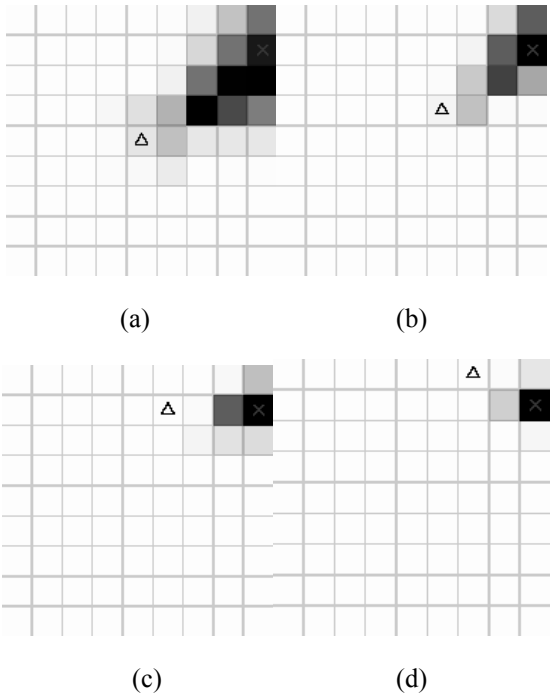

Figure 13. Path Planning with High Noise Near Jammer.

NAVIGATION SYSTEM

As with most autonomous systems, the open source hardware that powers JAGER by default relies on GPS position for navigation, which will need to be substituted for the duration of time that JAGER find itself in the jammed environments. The navigation system being developed will provide an approximate location of the vehicle in the environment using signals of opportunity and vision.

For JAGER, we have three main goals for our navigation system: low cost, robustness to time of day, and robustness to weather. These conditions come out of a need to be able to operate at any point in time. Since we are designing for operation at an airport, where the impact of a GPS jammer would need to be taken care of immediately to be able to minimize the impact to flight operations, it is important for JAGER to have a robust navigation system.

This navigation problem is defined as a simultaneous localization and mapping (SLAM) problem, a problem that has become increasingly popular for autonomous navigation. Some examples are indoor and outdoor rover navigation [10], indoor UAV navigation [11], and outdoor UAV navigation [12]. The SLAM problem is one of both creating a map of the environment the vehicle is moving within and determining the location of the vehicle within that map. While JAGER is not necessarily explicitly trying to map the environment, it

does indeed need to generate a map of key features that can be used to then localize JAGER within that map.

A lot of research recently has focused on the visual SLAM (vSLAM) problem with the use of both stereo-vision cameras [13] and monocular vision cameras [11]. For JAGER, we will have a visual sensor, but we will also leverage signals of opportunity that come in great variety near airports. We have previous shown the ability to post process the location of a UAV to within 10s of meters [3].

The SLAM problem we are solving is better known as bearing only SLAM. The traditional SLAM definition has both range and bearing to features in the map as an observation, but in this case, bearing will be the only observation. This again is due to the fact that we can very easily rotate the vehicle and get bearing estimates to features around the vehicle, while range requires stereo-vision cameras and a ranging metric for the signals of opportunity. As we have seen for the WiFi measurements, signal strength, the simplest metric, is not the best indicator of range. While there are other possible techniques for determining range, most add unnecessary complexity to the system.

Of the vSLAM techniques, the majority use visual-spectrum cameras, which suffer performance loss at night and in inclement weather conditions (e.g. fog). For this reason JAGER will be equipped with an infrared (IR) camera. IR cameras will give the navigation system the necessary robustness to be able to operate day or night and are able to provide more detail than visible spectrum cameras in other low light conditions such as fog and rain [14].

Four the specific target environment and application of JAGER, there are very useful simplifications that can be made. For example we can leverage the fact that we can take off from a known point that is ideally far from the jammer such that we have GPS when we start. This means that for the duration of time that JAGER is operating outside of the denied environment, the system is able to build a map more reliably and accurately. Therefore, once in the denied environment, JAGER can rely heavily on features that are very well known within the map, while at the same time continuing to build the map.

Furthermore, the path planning algorithms can be tuned to tradeoff some optimality for navigation support by keeping JAGER far enough from the denied environment to be able to maintain a GPS position for as long as possible.

CONCLUSIONS

With JAGER, we have successfully demonstrated, through flight testing, the ability to autonomously rapidly localize a signal source using a UAV and a POMDP based path planning algorithm.

We have demonstrated the capability of determining bearing from a set of signal strength measurements reliably and accurately enough to successfully and rapidly localize a signal source.

Finally we have outlined the development of a navigation system that represents the problem as a bearing SLAM problem that will use IR vision and signals of opportunity to both build a map of the environment and localize JAGER when in the denied environment around a GPS jammer.

FUTURE WORK

So far all JAGER flight tests have been performed with the goal of localizing a WiFi signal at no more than 150m away. However, in the coming months, JAGER will be tested with GPS jammers at significantly greater range.

JAGER is an ongoing project and we are continuing to refine the sensing modality to be able to reduce the time for a measurement and observation. Currently we only use the measurements during a rotation, however the localization process can be sped up by being able to also use the measurements being made while traveling from one observation location to another. In order to do this, we are working on estimation algorithms that will provide bearing estimates given the measurements in flight.

The navigation system being developed is also still heavily being tested and refined. The biggest challenge is the ability to robustly track features in IR imagery in real time. There are many existing methods for visual imagery, however IR imagery poses additional challenges that are still being explored.

ACKNOWLEDGMENTS

The authors would like to gratefully acknowledge the Naval Postgraduate School for providing an unmatched space to be able to perform test flights of the JAGER system at the Joint Interagency Field Experimentation events.

The author would also like to thank the Stanford Center for Position Navigation and Time (SCPNT) and its members for supporting this work.

REFERENCES

[1] M. Geyer and R. Frazier, 1999, FAA GPS RFI Localization Algorithm, Proceedings of the 12th International Technical Meeting of the Satellite Division of The Institute of Navigation, Nashville, TN.

[2] E. M. Geyer and B. M. Winer, 1997, Airborne GPS RFI Localization Algorithms, Proceedings of the 12th International Technical Meeting of the Satellite Division of The Institute of Navigation, Nashville, TN.

[3] J. Spicer, A. Perkins, L. Dressel, M. James, Y.H. Chen, S. Lo, D.S. De Lorenzo and P. Enge, May 2015, Jammer Hunting with a UAV, GPS World, pp. 30-38

[4] Pixhawk, PX4 Autopilot Project, https://pixhawk.org/

[5] L-com, HyperLink Wireless 2.4GHz 9dBi Radome Enclosed Wireless LAN Yagi Antenna Datasheet

[6] Savvides, A., Han, C.C. and Strivastava, M.B., July 2001, Dynamic fine-grained localization in ad-hoc networks of sensors, Proceedings of the 7th annual international conference on Mobile computing and networking (pp. 166-179), ACM

[7] S. Venkateswaran, J. T. Isaacs, K. Fregene, R. Ratmansky, B. M. Sadler, J. P.Hespanha and U. Madhow, 2013, RF Source-Skeeing by a Micro Aerial Vehicle using Rotation-Based Angle of Arrival Estimates, American Control Conference (ACC), IEEE

[8] A. Perkins, L. Dressel, S. Lo, and P. Enge, Sept 2015, Antenna Characterization for UAV Based GPS Jammer Localization, Proceedings of the 28th International Technical Meeting of The Satellite Division of the Institute of Navigation, Tampa, FL

[9] J. Graefenstein, A. Albert, P. Biber and A. Schilling, 2009, Wireless Node Localization based on RSSI using a Rotating Antenna on a Mobile Robot, Proceedings of the 6th Workshop on Positioning, Navigation and Communication

[10] K. L. Ho, and P. Newman, 2007, Detecting loop closure with scene sequences, International Journal of Computer Vision 74.3: 261-286

[11] A. Davison, I. Reid, N. Molton, and O. Stasse, 2007, MonoSLAM: Real-time single camera SLAM, Pattern Analysis and Machine Intelligence, IEEE Transactions on 29.6: 1052-1067.

[12] M. Bryson, and S. Sukkarieh, 2005, Bearing-only SLAM for an airborne vehicle, Australasian Conf. Robot. Autom (ACRA 2005), Sydney, Australia

[13] T. Lemaire, C. Berger, I. K. Jung, and S. Lacroix, 2007, Vision-based slam: Stereo and monocular approaches, International Journal of Computer Vision, 74(3), 343-364

[14] W. Maddern and S. Vidas, 2012, Towards robust night and day place recognition using visible and thermal imaging, RSS 2012: Beyond laser and vision: Alternative sensing techniques for robotic perception (2012)

IFIS2016

Bringing Together Theory and Practice

Session 9

Safety Concepts and F.I. Organization Certification

How we manage the flight inspection aircraft at peak hour

Christophe Nadal
Tower manager Roissy Charles de Gaulle
DSNA
France
Fax: +33 0174 378 709
E-mail: christophe.nadal@aviation-civile.gouv.fr

Stephane Veysseyre
ATSEP radio navigation Roissy Charles de Gaulle
DSNA
France
Fax: +33 0174 378 709
E-mail: stephane.veysseyre@aviation-civile.gouv.fr

INTRODUCTION

The aim of this presentation is to explain, in a non-exhaustive way, how Air Traffic Safety Electronics Personnel (ATSEP) and Air Traffic Controller Officers (ATCO) manage the flight inspection in the world busiest airports.

To preserve a high level of safety and a minimum of incidents, due to faulty ground devices, flight inspections are compulsory. Obviously, the bigger the airport, the more often inspection flights are scheduled, checking and validating all the ground systems (ILS, VOR…). Those flights have a non-negligible impact, in terms of safety and the way of working especially for the main airports.

So let's see how ATCO and ATSEP deal with these flight inspections in the middle of a high density IFR flights while maintaining the requested spacing between them.

ORGANIZATIONAL MANAGEMENT

- **Rules**
  - International rules

The airports with the densest traffic are all located in countries signatory to the Convention on International Civil Aviation (Chicago convention). So they follow the rules enacted by ICAO in the annex 10.

In the ICAO Doc. 8071, the flight inspections' periodicity, for an ILS, is 6 months with a maximum of 9 months afterwards the ILS is shut down.
Nevertheless, countries (and sometimes airports) are allowed to derogate the annex 10 if an established procedure, described in the appendix 13, has been ratified by the national authority. Indeed, the biggest airports generally have many systems to check (several runways, VOR, RNAV approaches...) and local Air Navigation Service Provider (ANSP) try to reduce the flight inspection's periodicity by using specific method.

  - Local examples

Paris Charles de Gaulle:

In Paris Charles De Gaulle (CdG), a document called PROCedure de Mise En Service et de Suivi des stations sol (PROMESS) enacts the rules to follow in order to perform flight inspection once a year with a maximum delay of 16 months between 2 on the same ILS (18 months with a VOR).

Chicago O'Hare:

In Chicago airport, all the desired amendments of the annex 10 are done according to an established procedure National Airspace System Change Proposal (NASCP). Once this proposal has been validated, amendments are described.

To respect local rules reducing the flight inspections' periodicity, extra ground measurements must be done. This means from ATC point of view, additional runway closure involving impact on the traffic and the way of working.

Nevertheless, the impact of the runway closure is less heavy while only ground measurements are done. Indeed, the runway closure generally lasts 2 hours (instead of 4 hours for a complete flight inspection) and ATCO must not separate the flight inspection aircraft from the commercial ones. This procedure is well-known from all the actors and is not stressful.

FLIGHT MANAGEMENT

➢ Pre-tactical management

In the most important airports, there are no seasonal effects, and the traffic structure is similar from one month to the other (obviously Met conditions can change traffic structure punctuality). Peak hours are generally well known, then, to avoid incidents between the flight inspection aircraft and the arriving and/or departing IFR aircraft to/from the airport, air traffic control authorities chose slots to close the runway(s) between two main peaks.

In the biggest airports, like Chicago, the capacity of the field is very high all day long, so for safety reasons, they have to plan their flight inspections during the night between midnight and 4 am.

The following graph illustrates the traffic structure in CdG, the blue line represents the departures and the red one the arrivals.

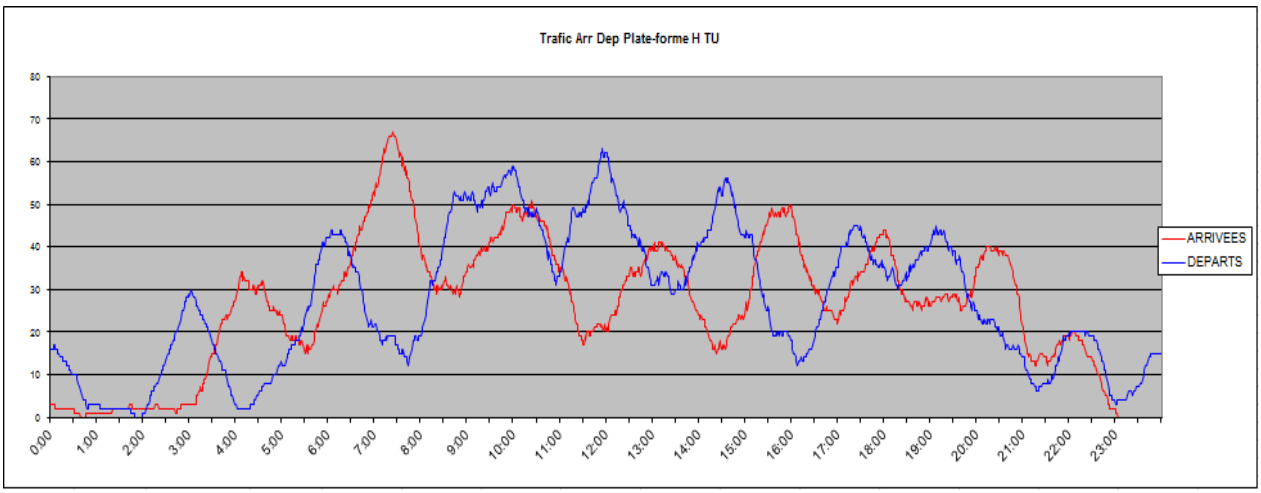

Figure 1. TRAFFIC STRUCTURE IN PARIS CHARLES DE GAULLE

So pre-tactical planning is realized. The most important point is to check the period of validity of the previous ground and in-flight measurements on all the field systems.

Few weeks before these deadlines, a yearly plan is enacted describing when the flight inspections will take place. At this time, the peak hours' notion is not evoked. Once the first plan is confirmed by all the participants (Flight inspector, ATSEP and ATCO), a second one is enacted between ground engineers (ATSEP) and air traffic control in order to realize the ground measurements before the planned flight inspections (ground measurements have a restricted time validity of 1 month). It's only when this second planning is accepted that ATC identifies the slots allocated for the ground measurements. Indeed, to perform them, a runway closure for all commercial flights is required in order to let a truck measure the ground facility. Then, if this runway is used in single mode i.e. for departures, we will choose a period of time during which the number of departures expected doesn't reach a peak, but in this case arriving traffic can be very important. This approach is the same if it's a mixed mode runway, but in this case, ATC study previsions of arriving and departing traffic.

Nonetheless, these slots can be amended tactically, indeed bad Met conditions, emergencies and so on can generate lots of delays and a huge complexity to handle an important traffic with a closed runway. These

problems alter the traffic structure and initial slots allocated.

- **Tactical management**

First of all, a team briefing or a phone conference ensures that all the staff involved (ATCO, ATSEP, flight inspector, pilots and airport representative) received the necessary information.

The ATSEP and the flight inspector present what they must check during the week, their constraints, but also what they would do in case of extra time. ATCO confirms the expected slots. The Met conditions determine what ILS will be calibrated.

We also plan, if necessary, how to perform taxiing measurements and how many ground engineers' teams are available and if it' s possible to calibrate the localizer (LOC) and the glide path (GLD) at the same time or separately.
The aim of this briefing is also to ease the handling of this specific flight according to the airport's conditions.

What's more, the first day of the week, Met services have quite good forecasts for the weekly airport configuration. We usually calibrate the ILS in the same configuration as the airport. If a runway change is expected, the other ILS of the runway is calibrated. Obviously, if we don't have another option the flight inspection can be managed in counter configuration, but these situations are very difficult to manage so we try to avoid them as much as possible.
Met services also indicate the ceiling and visibility, these elements are fundamental for the flight inspection's pilots and indicate whether the flight will be possible or not.
For instance, in Chicago, the flight inspection comply with the VFR rules so if the VMC conditions are not met, the flight is cancelled and planned for another day.

These elements are compiled in a briefing document describing the procedure as clearly as possible. This document contains the following information: which runway is going to be calibrated, the runway closure time, the traffic consequences, the regulations, the flight inspection aircraft trajectories, its altitude, its call sign, the type of aircraft and on which frequency it will be controlled.

However, ATC can be affected in a number of ways: if the flight inspection aircraft has to make taxiing measurements on the runway, if it needs to backtrack, if we can keep on crossing the runway while it performs approaches, does the commercial traffic maintain the Cat III holding point or the Cat I before crossing and so on.

This document is given to the tower manager and all involved personal, see following example in CdG.

CALIBRATION 09R CDG

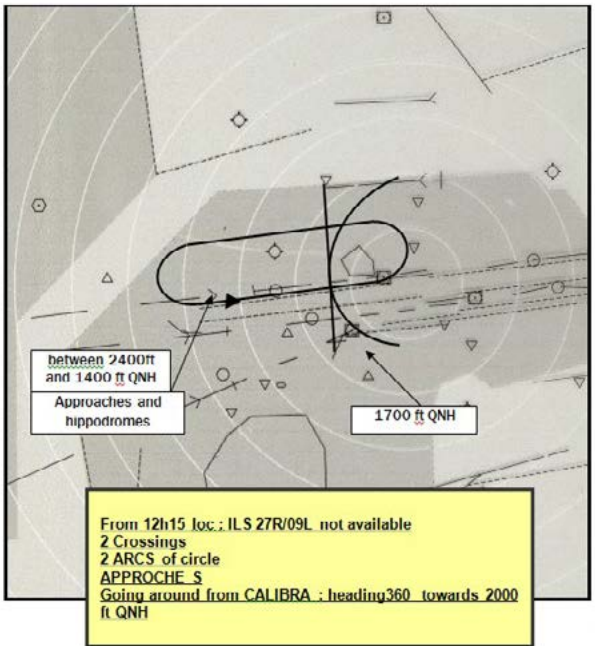

SOCIETY	CALIBRA
DATE	16 juin 2016
HOUR	12H15 14h 15h 17h00 loc
AIRCRAFT TYPE	BE20
FREQUENCY	MAGALI or JULIEN sur 126.57
TOWER MANAGER	▪ ATIS : Flight inspection in progress
NORTH TOWER CONTROLLER	▪ Runway 09R/27L used in single mode ▪ Lining ups possible on the 09R ▪ No take off when flight inspection a/c from 5Nm final until it goes around
SEQUENCER	▪ LOAD the runway 08R (arrivals) ▪ Runway 09R/27L used in single mode
SOUTH TOWER CONTROLLER	▪ No consequences
LE BOURGET	▪ When arc of circle and crossing axis - no take off ▪ Coordonate all VFR trafic
DEPARTURE	▪ Le Bourget departures only with the agreement of controller in charge of the flight inspection

Figure 2. Typical briefing document

- **During the flight inspection**

  - From ATSEP side

At the beginning of the flight inspection Ground engineers (ATSEP) position themselves in the GLD or/and LOC shelters, they turn the DGPS beacon on, in order to control the flight inspection aircraft's trajectory is perfectly accurate. They also contact the tower manager to indicate him when the ILS will be off duty for the commercial flights.

Then, ground engineers set the equipment into the appropriate mode for each flight measure and analyze the data. They keep a permanent radio contact with the flight inspector to communicate their data and to decide if additional measures or additional flight inspections are necessary. This information is generally transmitted by the pilot towards the ATC, in order to start predicting the runway re-opening time.

ATSEP check if the collected data conform to the regulation (for instance PROMESS in CdG) and if necessary they reconfigure the ground facility. This highly critical operation must be accurate and quick:

- Accurate so as to reduce the number of additional flight measures,
- Quick in order to comply with the duration decided during the team briefing usually 4 hours.

Sometimes it is necessary to realized measures from a radio navigation equipped truck on the runway. For instance, this type of situation can occur if an aircraft technical failure is suspected. Of course this kind of decision is rare and carefully thought because it involves a non-expected runway closure and a strong impact on the traffic.

However, the most difficult decision to take is to postpone a flight inspection given that the quantity of work provided to organize this operation. Such situation will occur for instance if a technical failure on the facility or the aircraft is detected and cannot be solved immediately.

At the end of the flight inspection, the equipment is set on duty for commercial flights as soon as possible. A certificate of conformity is cosigned by the flight inspector and the ground engineers. This document extends the validity of the equipment performance category (CAT I, CAT II, CAT III …).

  - From ATCO side

From an ATC's point of view, this part is the most critical, indeed even if the commercial traffic is less important, arriving and departing traffic are still flying around the airport and are very close to the flight inspection aircraft. Obviously, if commercial flight predictions are wrong for any reasons, we can decide to stop the flight inspection if the safety is impended. Most of the time we avoid stopping it, because this could lead to a situation where the ILS measurements validity is compromised and then the ILS approaches would be forbidden.

To calibrate a full ILS, a flight inspection generally lasts 4 hours. This can be done in the same slot (if the aircraft has enough fuel) or split into several slots. In Charles de Gaulle airport, the flight inspection is divided into two slots of two hours.

After take-off, ATC decide in real time which measurements are going to be performed according to the surrounding traffic, and before the end of the measurement ATC decide on the next branch and plan for the missed approach. We coordinate this information with all the others ATCOs so they can decide how they will manage their own flights, and the in flight engineer transmits the information to the ground staff. Most of the time we try not to constrain the others ATCOs because inspection flight aircraft flying close to the airport without following standardized route generates a lot of stress amongst them. Indeed, their planning is disturbed by an unusual flight and it generates unusual constraints. For example, a tower controller will not be able to clear for take-off while the flight inspection's trajectory is potentially not separated from that of departures'. According to the conception of the airport and how far the calibrated runway is from other runways, new complications can arise. What's more frustrated commercial pilots put the pressure on ATCOs.

If the traffic is too dense, the flight inspection flight can be vectored somewhere in the vicinity of the airport, to hold few minutes until the traffic has cleared.

At the end of the slot, we check with the in-flight engineer to see if everything has been done and if not, what remains to be done.

What's more, we check with ground engineers to ascertain when runway operations will turn back to normal. This information is transmitted to ATC managers who decide when the runway will be operational, and when departing and/or arriving traffic will be able to use it.

CONCLUSION

To conclude, we can say that the good management of flight inspection in the busiest airports relies on human factors. The knowledge of the constraints of each participant, and a quick responsivity are essential to cope with unexpected events. In CdG airport, ATC authorities decided few years ago to specialize 4 local ATCOs in flight inspection management. These specialists receive a special training in the ground operation and work in close cooperation with the ATSEP involved in flight inspection.

The flight inspection procedure has given us useful insight and improved knowledge increasing the level of safety and reducing the number of incidents.

REFERENCES

[1] ICAO, July 1996, International Standards and Recommended Practices, Annex 10 to the Convention on International Civil Aviation, Volume 1, Radio Navigation Aids, 5th Edition, http://www.icao.int

[2] FAA, 31 October 1995, Siting Criteria for Instrument Landing Systems, Order 6750.16C

[3] DSNA, 20 June 2012, PROMESS (Procédure de mise en service et de suivi des stations sol ILS)

Safety Management System customized for a Flight Inspection Organization

Andrea Gioia
First Officer and Safety Officer
ENAV S.p.A.
Rome, Italy
E-mail: andrea.gioia@enav.it

ABSTRACT

As the aviation world has become more and more competitive, profit has turned into one of the biggest concerns for the operators that, in a complex environment, have to constantly face new questions. In this scenario it is inevitable to ask if it is possible to keep the same level of safety without increasing the costs. Even more challenging, is it possible to improve safety performance reducing the budget? Implementing a safety management system can effectively improve both safety and business.

This paper will try to explain how this is not only possible but also desirable even for small organization.

It will describe how to identify the key roles and establish the procedures needed to create a SMS, give an overview of the hazard identified and of the mitigation action taken. It will present real life scenario such as bird strike, night operation and adverse weather operation based on the experience gained in one flight inspection organization.

INTRODUCTION

A flight inspection organization deals with safety more than others do in the aviation business. Not only it has to maintain high safety standards within, as most of the activity is performed at low altitude and in high-density environments, it also has to grant safety as an outcome of its work.

Having to implement a Safety Management System (SMS) can be a very challenging task especially for a small organization, on the other hand can be very rewarding both for the operation and for the business. It should not be a matter of fulfilling a regulation requirement, on the opposite, as it will be discussed later, it should be part of the core business of the company. The commitment of the organization is essential to be successful.

The SMS can possibly be very complex; however, it is important to notice that it has to fit the real needs and complexity of the organization. Even more important, it has to be a real benefit for the operations.

This paper will try to describe some general principle as well as a real life experience gained in one flight inspection organization.

THE "DILEMMA OF THE TWO P": PRODUCTION VERSUS PROTECTION

As the aviation world has become more and more competitive, profit has turned into one of the biggest concerns for the operators who, in a complex environment, have to constantly face new questions. In this scenario it is inevitable to ask if it is possible to keep the same level of safety without increasing the costs. Even more challenging is the question of whether it possible to improve safety performance while also reducing the budget?

"A misperception has been pervasive in aviation regarding where safety fits, in terms of priority, within the spectrum of objectives that aviation organizations pursue, regardless of the nature of the services that aviation organizations might deliver. This misperception has evolved into a universally accepted stereotype: In aviation, safety is the first priority." The ICAO Safety Management Manual (SMM) warns against this safety stereotype and, in doing so, raises a question: If not at the first place, where does safety stand in our organization? This question may seem prosaic, but it is important to go over the answer every now and then, as it always is a good safety indicator. Even though Flight Inspection is guarding aviation safety, it still has to face production constraints in order to be competitive and

remain within the company's budget or on the market. The financial management of an organization has the important role of collecting and analyzing all the possible information from inside the company and from specific market indicators to optimize the production costs. The Safety Management does something very similar in order to increase safety. To this extent, "the management of safety is just another organizational process that allows aviation organizations to achieve their business objectives through the delivery of their services. Safety management is, therefore, just another core business function that must be considered at the same level and with the same importance as other core business functions" (SMM). It is interesting to notice that the ultimate person responsible for both the finance and the safety of the organization is the Accountable Manager. He not only has to grant production, but he also allocates resources for protection. In addition, not only is safety at the same level of other functions, but it cooperates with them to fulfill the core business. Whether it may be simple to imagine the relationship between the safety office and the training department or the quality management, it would not be easy to see the connection these departments have to the financial department, as they appear in opposition to each other. However, this is not the case. The company's finance can get a great advantage by managing and mitigating the risks related to flight inspection. A well-structured safety management system can be presented to the insurance company to get a discount on the premium at the end of the year. It is a bit more difficult to demonstrate a reduction in the costs related to hazard mitigation because a hazard, by definition, is only a potential cost.

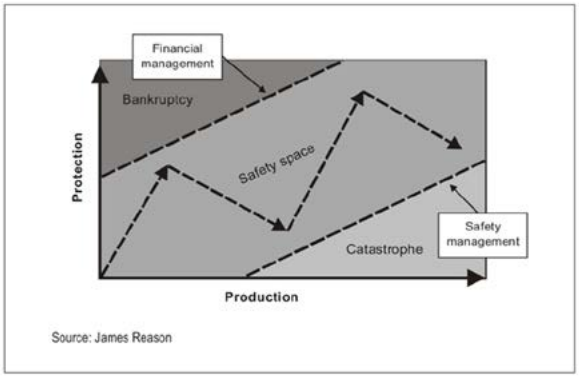

Figure 1

Figure 1 helps one to understand that a straight line cannot represent the relationship between production and protection but as a sinusoid that moves within a safety, space defined by financial needs on one side and safety constraints on the other side. An excess of protection will lead to bankruptcy, but the opposite, no safety constraints, will end in catastrophe. The ultimate goal of the safety management system is to keep one flight inspection organization between these two excesses.

THE TOOLBOX

To help understand what a safety management system is, the ICAO SMM compares it to a toolbox "that contains the tools that an aviation organization needs in order to be able to control the safety risks of the consequences of the hazards it must face during the delivery of the services for which the organization is in business. What an SMS does for an organization is to provide a toolbox that is appropriate, in size and complexity, to the size and complexity of the organization." (SMM)

Even though there are certain rules to be followed, the organization can write its own set of rules and procedures. It is very important that an organization implement a SMS that really fits its needs. This procedure should not be too complex; otherwise, it will be impossible to perform all tasks required. But neither should it be too simple, which would allow something to be missed along the way. It would be impossible to cover all the aspects and the regulation requirements; however, I would like to share some steps that we followed in our organization.

The first tool that helps to create a SMS is the Safety Management Manual of the organization. Since this document has to be approved by the local State Civil Aviation Authority, it is a good idea to share the process with them in order to work in the right direction from the beginning. It should contain the company's safety policy, which will be described in more detail later on. It should define the key role such as the Accountable Manager, the Flight Operation Postholder, the Safety Manager, the Quality Manager, and the Training Manager, or any other Postholder that may apply to a specific organization and describe what each position is accountable for and the process of cooperation and communication between each function of the company. In a small organization, some of these roles may be covered by a single person or not required at all. It is, however, important to explain the procedures that the top management of the organization has to follow in order to fulfill the safety objective.

The Safety Review Board (SRB) is certainly one component of this procedure. All the Postholders should be member of the board and meet at least once a year, or whenever a safety-related event dictates, in order to verify the safety "health" of the organization, review the safety objectives and the hazards previously identified and, if needed, institute one or more safety action group (SAG). A SAG is usually under the responsibility of one of the Postholders and has to face a specific objective indicated by the SRB. The SMM should also contain all the procedures and forms related to the System Safety Assessment including the hazard identification and evaluation process, an example will be discussed at the end of the paper.

Safety Reporting should be an important chapter in the manual; not only it is a regulation requirement, but each report has the potential to discover a new hazard that was not yet identified. Based on our experience, mandatory

reports mostly deal with technical related problem, if this is the case, fixing the component solves the problem. In addition and in collaboration with the training department, we reviewed our training program according to the real technical failure we encountered. In one case, we performed a briefing for the crew on an air data failure occurred during a flight. The briefing included a list of suggestions to deal with this event. A few weeks later, this failure happened again to a different crew that, in the analysis of the event, reported to have taken a great advantage from the suggestion received in the briefing. In a small group, it is not always easy to share experience, during the International Flight Inspection Symposium in 2014 our organization has presented the results of a Cockpit Resource Management program dispensed to our crew. After a two years period we are even more convinced that, in addition to other results, it has strongly contributed to improve our safety culture. Improving human resources will certainly create a better climate to discuss safety related events. Safety is everybody's responsibility and this was a big step forward in this direction.

Safety Policy

The first page of the organization's safety management manual should contain the safety policy. "The implementation of a safety management system by an organization should be endorsed by the most senior level of management within the organization" (CAP 728) because safety is primarily a top-down process. The Safety Policy is the manifesto of the organization: it defines the strategy to the management of safety and the overall safety objective. It would be desirable to mention the company's commitment to the "just culture" as all individuals within the company should understand that the objective is to increase safety and not to allocate responsibilities. In a large organization, the safety policy is particularly important as it can possibly be the first bridge between the management and the front-line employee. On the other hand, the management of a small organization may have more opportunities to share time with the rest of the group. This time should be used to demonstrate the true commitment and adherence of the organization to the safety policy and will strongly improve motivation at all level of the organization.

Safety Accountability and Responsibility

In order to be effective, a "safety management system depends upon individuals understanding and accepting their delegated responsibility within the organization. Accountability for safety belongs to all levels of management and the attainment of satisfactory safety performance requires the commitment and participation of all members of the organization" (CAP 728). In other words, a safety management system requires the identification of structures and procedures for which the management is accountable; however, the safety management only works if every person, according to his role, feels responsible to make the system work. Safety is everybody's responsibility. In a small flight inspection group, where everybody knows each other very well, it may be harder to report a safety problem. Even though safety culture does not cost any money, it does cost a lot of effort to build, and only one mistake can destroy it. The organization should avoid pointing fingers. In fact, the opposite is true. Personnel should be encouraged to discover unmanaged hazards. Some companies have created small gadgets to reward proactive behavior; however, most of the time, appreciation is the best reward.

The practical drift

An organization should always be aware of the practical drift. When a system is designed the outcome is tested and analyzed to define the baseline (or ideal) system performance. Once the system becomes operational, however, the real-life outcome (or operational performance) differs from the baseline performance expected; this process is referred to as practical drift. "A practical drift from the baseline performance to operational performance is unavoidable in any system, no matter how careful and well thought out its design planning may have been." (SMM) In a complex environment as the aviation business in general and fight inspection in particular the factors that can introduce deviations from the baseline performance are potentially infinite; new components, technology that does not operate as predicted, weather change, procedures that cannot be executed as planned just to name a few.

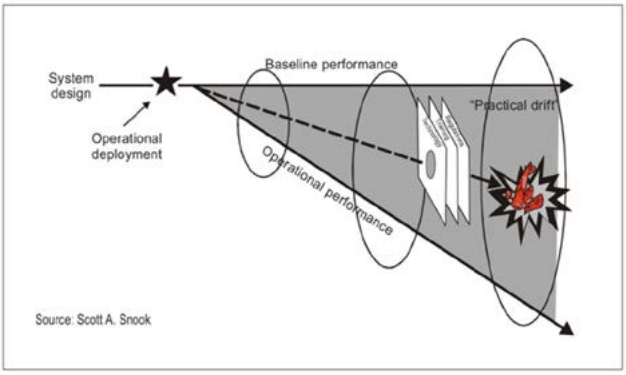

Figure 2

Figure 2 shows that if operational performance deviation are not managed can possibly lead to an accident. It should be taken into account that practical drift is a result of everyday life operation so it is easy to understand that hazards should be re-evaluated from time to time as operation continue. A well-structured safety risk management is the best tool to meet this goal.

SAFETY RISK MANAGEMENT

Risk is a very common word in everyday life; however, each individual has a personal perception of danger. "Safety risk management is a generic term that encompasses the assessment and mitigation of the safety risks of the consequences of hazards that threaten the capabilities of an organization, to a level as low as reasonably practicable (ALARP)."(SMM) In terms of safety, the risk related to a hazard has to be assessed taking into account the severity of the consequences and the probability that the event takes place. Therefore, the first step is to identify hazards related to the peculiar operation of the company.

Hazard Identification

"A Hazard is defined as a condition or an object with the potential to cause injuries to personnel, damage to equipment or structures, loss of material, or reduction of ability to perform a prescribed function."(SMM) Procedures and operating practices are essential to our job, however, not following the right procedure can lead to a reduction in safety therefore they are also a hazard that has to be managed.

Hazards can be identified in many ways but, in my opinion, the safety reporting system should be the first and most reliable source. Sharing experience with other organizations can also be very helpful and this is part of the objectives of this work.

In our flight inspection organization, we have identified a list of hazards related to or that have a major effect on operation. Human performance: for example communication between the cockpit and the flight inspection operator is essential during the mission, however, in high-density traffic condition, can possibly lead to a missed communication with Air Traffic Control that could result in a near midair collision. Birds: since many airports in Italy are very close to the sea, birdstrike is very high in probability therefore on top of our hazard identification list. Terrain: most flight inspection profile bring close to terrain rising the risk of controlled flight into terrain (CFIT). Aircraft performance: this hazard is in part related to the consideration already discussed for terrain and, in addition, to face the complex environment of operation, the capability of the aircraft to increase or decrease speed according to other traffic and to be able to properly heat or refrigerate the cockpit and the cabin. Night operation: during night-time it is not always possible to maintain visual separation from terrain and obstacles, as they may not be lighted properly. Weather: obviously no flight inspection operation are allowed in adverse weather, weather minima for flight inspection operations have been defined and included in the Operation Manual (OM). As it was mentioned before, hazard have to be updated from time to time and this is the perfect example. We recently started to provide flight inspection services in the Middle East and had the first experience of a real big sandstorm. Also in this case it is evident that no flight inspection is possible but this hazard was added to the list and assessed. The result was a new chapter in the OM related to sand storm operations. Even though this is not the complete list, it may be a good starting point.

Safety Risk Probability

"Safety risk probability is defined as the likelihood that an unsafe event or condition might occur."(SMM) Once again, the safety reporting can be of great help to assess probability. An isolated occurrence will be present only once in the safety database, on the opposite many occurrences will require a frequent evaluation. Other factors that may help in the evaluation are the numbers of person involved, how much a certain equipment is used or if there are similar equipment or components with the same defect. ICAO SMM defines safety risk probability according to the following table.

	Meaning	Value
Frequent	Likely to occur many times (has occurred frequently)	5
Occasional	Likely to occur sometimes (has occurred infrequently)	4
Remote	Unlikely to occur, but possible (has occurred rarely)	3
Improbable	Very unlikely to occur (not known to have occurred)	2
Extremely improbable	Almost inconceivable that the event will occur	1

Safety Risk Severity

"Safety risk severity is defined as the possible consequences of an unsafe event or condition, taking as reference the worst foreseeable situation." The loss of a human life is obviously not acceptable and will always produce an avoidance outcome of the assessment. Other factors, however, such as property or financial damage, environmental impact and media communications that may damage the image of the company should be evaluated. ICAO SMM defines safety risk severity according to the following table.

Severity of occurrence	Meaning	Value
Catastrophic	— Equipment destroyed — Multiple deaths	A
Hazardous	— A large reduction in safety margins, physical distress or a workload such that the operators cannot be relied upon to perform their tasks accurately or completely — Serious injury — Major equipment damage	B
Major	— A significant reduction in safety margins, a reduction in the ability of the operators to cope with adverse operating conditions as a result of increase in workload, or as a result of conditions impairing their efficiency — Serious incident — Injury to persons	C
Minor	— Nuisance — Operating limitations — Use of emergency procedures — Minor incident	D
Negligible	— Little consequences	E

Safety Risk Tolerability

Risk tolerability can be defined as the final assessment that combines severity and probability in order to decide if the risk is acceptable, acceptable based on risk mitigation or unacceptable. The safety risk matrix reported below is a very useful tool in order to explicit the result of the safety risk assessment.

Risk probability		Risk severity				
		Catastrophic A	Hazardous B	Major C	Minor D	Negligible E
Frequent	5	5A	5B	5C	5D	5E
Occasional	4	4A	4B	4C	4D	4E
Remote	3	3A	3B	3C	3D	3E
Improbable	2	2A	2B	2C	2D	2E
Extremely improbable	1	1A	1B	1C	1D	1E

The Process of safety risk management

The process of risk management should be described and documented in the safety management manual of the organization. In addition to the four step so far described, hazard identification, risk analysis according to probability and severity, risk assessment on tolerability, the organization should define the level of risk that it is willing to accept and the mitigation action to be taken to remain within this level. Keeping records on all phases of the process is essential to meet regulations requirements and to review the process if needed.

A block diagram like the one below can also be inserted in the manual to clarify the process.

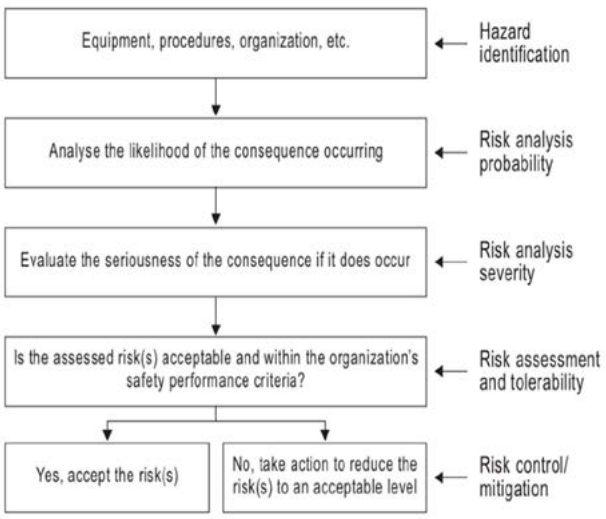

Night–time operations

In highly congested airports, it may be convenient to perform flight inspection during the night-time when the traffic volume is lower. To maintain safety risk within acceptability, some requirements have been introduced in the OM. Flight inspection activity at night should be conducted according to IFR rules, however, for all the profiles that are outside the normal containment areas of the published procedures a visual approach clearance may be asked by the crew if condition permits. Familiarization during the daytime with the airport and surrounding environment is required to the crew. A safety assessment involving the Flight Operation Postholder, the Crew Training Postholder, the Safety Manager and Standard Office is required. An assessment is required for each flight inspection exercise, however a list of airports, with peculiar characteristics, where night-time operations are forbidden was included in the OM The assessment should contain, at least, information regarding all relevant airport and airspace data, as well as evaluation of all relevant obstacle both natural and man-made, they should be highlighted on a chart attached to the assessment. In addition, the Standard Office will provide a revised flight inspection checklist that should include all the suggestions contained in the safety assessment. It has also been decided that some flight inspection profile such as crossover at 6 NM, 150 µA and 180 µA fly up are not allowed, crossover at 17 NM and 25 NM are allowed but the altitude has to be raised by 1000 ft, 75 µA below path is allowed only if offset guidance is provided by the autopilot and, finally, the PAPI serving the associated runway should be available.

Bird Strike Assessment

So far, we have discussed a lot of theory and I know this will not help to convince your Accountable Manager to invest any money in the safety department. As mentioned before, the first step in order to implement a good Safety Management System is to identify safety hazards related to your operations and to analyze their consequences in terms of probability and severity.

I will describe some consideration regarding a safety assessment conducted on bird strike. The initial risk was evaluated 4C. Based on our safety database, it has occurred only twice in the last six years therefore the probability has been considered occasional. Severity was evaluated Major not only based on the criteria so far described, but using an estimate on the cost that this event could potentially produce. It is possible to evaluate hazards according to their economic impact on the organization. In this example, we could consider that a bird strike would ground the aircraft for an average of one week and could calculate how much it will cost to keep the aircraft on the ground in terms of additional maintenance and delay on the flight inspection schedule. Even though it is not possible to give real numbers, just as an example of the process, the average flight time for

one aircraft in seven days can be considered 20 hours, if the company sells each hour for 3000 Euro it means a potential loss 120000 Euro. An additional 20000 Euro could be considered for additional maintenance and parts replacement. The delay in the flight inspection schedule should also be estimated, taking into account the size of the organization, a flight inspection operator with only one aircraft will be more effected than a larger one, and in this case, it will be estimated in 10000 Euro. Therefore, the total potential cost of a bird strike can be assessed in 150000 Euro and considered Major.

In order to manage this risk to a lower level the organization can introduce a number of mitigation action. In our case, in conjunction with the training department, it was organized a briefing to the crew to increase awareness, illustrate the possible damage and some safety recommendation. Since 60% of bird strike occurre below 50 ft and the majority of it below 500 ft, the first recommendation was to remain below this altitudes for as little as possible using, for example and if condition permits, the level run instead of the 75 µA profile to calculate the Glide Path width. According to the Bird Strike Annual Report provided by the Italian Civil Aviation Authority, the number of bird strikes increase significantly between 07:00 a.m. and 09:00 a.m. The graph shows the relation between number of impacts and time of the day.

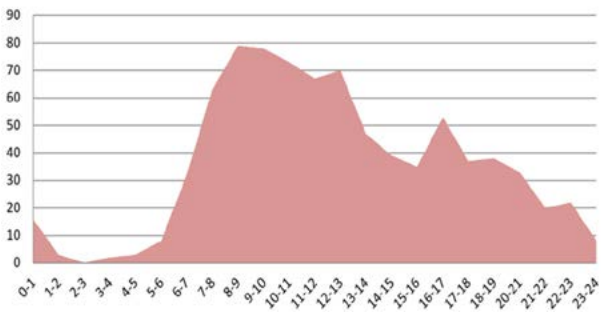

As a result of this statistics, both the operation office and the crew have been briefed not to schedule any flight during this time in airports located close to the sea. As a result, to the mitigation actions described the probability was lowered to a value of 3 and the total risk was managed to 3C. In addition, the total risk was estimated to be lower by 30% that result in a potential saving of 45000 Euro.

CONCLUSIONS

The Safety Management System can effectively help the organization to reduce risks associated with operation.

Although it is “also” a regulatory requirement, the organization should decide to implement a SMS to improve Safety and business through a process of integration between all functions of the company. As discussed, ICAO recommends that the SMS should be part of the core business of the organization.

The outcome of well-structured SMS will be the reduction of potential costs related to the consequences of the hazards identified. Paraphrasing an old aviation way of saying, it is much better to discuss about potential savings than to deal with a real accident.

IFIS2016

Bringing Together Theory and Practice

Session 10

RFI / EMI

Improving In-Flight Localization of GNSS RFI Sources

Gerhard E. Berz, Pascal Barret
EUROCONTROL
Brussels, BELGIUM
E-mails: gerhard.berz@eurocontrol.int
pascal.barret@eurocontrol.int

Brent Disselkoen, Michael Richard
Rockwell Collins
Cedar Rapids, Iowa, USA
E-mails: brent.disselkoen@rockwellcollins.com
michael.richard@rockwellcollins.com

Todd Bigham
Federal Aviation Administration
Oklahoma City, OK, USA
E-mails: todd.bigham@faa.gov

Vincent Rocchia, Florence Jacolot
Direction des Services de la Navigation Aerienne
Toulouse, FRANCE
E-mails: vincent.rocchia@aviation-civile.gouv.fr
florence.jacolot@ aviation-civile.gouv.fr

Okko F. Bleeker
ADSE BV
Hoofddorp, The NETHERLANDS
E-mail: okko.bleeker@adse.eu

ABSTRACT

The need to ensure the continuous availability of Global Navigation Satellite Systems (GNSS) continues to increase along with the implementation of PBN and ADS-B. For this purpose, a Radio Frequency Interference (RFI) Mitigation Plan is being developed by Eurocontrol, which includes a comprehensive set of preventive and reactive measures to limit vulnerability to RF interference. Among the reactive measures is the need to be able to detect, locate and eliminate an RFI source in a timely and efficient manner. A cooperative concept is foreseen for this purpose, where aerial capabilities aim to quickly identify the approximate location of an RFI source. This should allow dispatching ground measurement vehicles to a limited search area, ensuring a good chance that the precise location of the source can be identified and lead to successful enforcement action. Limiting the time of exposure to an RFI source will then make an important contribution to mitigating GNSS vulnerability to RFI.

However, currently, only very few flight inspection or other aerial work platforms are equipped with RFI localization capabilities with the sensitivity required to detect GNSS interference sources. Another problem is that if an aircraft flies into an area of GNSS interference, its own positioning capability may be impacted, affecting both aircraft navigation and the ability to fix the position of RFI sources. In order to both maintain ownship position while looking for RFI sources and improve the speed and accuracy of RFI source localization capabilities, the use of a GNSS CRPA is being evaluated. A CRPA is a Controlled Radiation Pattern Antenna, which can dynamically modify the gain pattern and either form beams of positive gain towards the satellite signals being received, or steer nulls (negative gain) towards the interference sources. The CRPA is expected to both preserve GNSS positioning while also providing at least an azimuth angle towards the source of the interference. If the latter is integrated with an AHRS (Attitude and Heading Reference System), only a few lines of position pointing towards the RFI source could provide a fast indication of the probable ground location.

The paper proposes an operational concept and reports on the conducted technical studies and test campaigns. The studies include consideration of installation options on typical flight inspection aircraft, such as if the CRPA should be installed on top or on the bottom and other system integration challenges. It will quantify detection capability in terms of angular resolution and ranges. Finally, the paper will provide an assessment of the CRPA capability in comparison with other options, and discuss potential future work.

INTRODUCTION

GNSS is an essential enabler for many aviation applications which rely on either accurate position or time synchronization. While the idea of “sole means” GNSS is disappearing, it remains challenging to match the performance and coverage of GNSS with terrestrial systems. This is why aviation is working on Alternate Positioning, Navigation and Time (A-PNT) in order to cope with the potential for a wide-area GNSS outage.

Current navigation aids are clearly part of the options in the short term. But due to their potential performance shortcomings, the availability of GNSS must be maximized. Corresponding responsibilities for States have been recognized at the 12th ICAO Air Navigation Conference [1]:

> *Recommendation 6/8, Planning for mitigation of GNSS vulnerabilities:*
>
> *That States assess the likelihood and effects of GNSS vulnerabilities of in their airspace and apply, as necessary, recognized and available mitigation methods.*

Among the three principal vulnerabilities of GNSS, constellation performance issues, space / solar weather and RFI, RFI is the one where observability on the ground is often limited. The GNSS Manual, ICAO Doc 9849 [2], further specifies:

> *7.11.3.1 Air Navigation Service Providers must be prepared to act when anomaly reports from aircraft or ground-based units suggest signal interference.*

While the protection of radio services from interference is a State responsibility typically assigned to a telecommunications agency or such of a State government, it is in the interest of an ANSP to be able to request help and enforcement action from the telecommunications regulator in an efficient manner. Even if not prescribed explicitly, it will be obvious to the flight inspection community that corresponding detection and localization capabilities could be a significant asset towards being "prepared to act".

As a part of its SESAR contribution, EUROCONTROL has developed an "RFI Mitigation Plan" as a guidance framework with the objective to maintain risks to GNSS and the associated operations at tolerable levels [3]. Upon further review, the ICAO Navigation Systems Panel plans to include the document as an appendix in the GNSS Manual. Additional guidance on RFI test capabilities will also be considered in the further work on ICAO Doc 8071, Vol II [4]. The activity described in this paper is one of several efforts being undertaken with the aim to develop such material.

RFI MITIGATION PLAN CONTEXT

As intentional RFI is a security issue, the nomenclature from aviation security has been used to define the mitigation plan terminology: there are many threats, but not necessarily all of them translate into risks. Threats are thus sort of dormant risks, which, if left to develop unmitigated, could develop into risks to aviation. The mitigation process is to monitor threats, assess risks, and then implement whatever mitigation is suitable to stop threats from developing into risks. Three successive stages have been identified where such barriers can be applied:

1. Prevent transmission of RFI, mostly through radio regulatory actions and coordination;
2. Prevent interruption of positioning and navigation capabilities despite the presence of RFI. This is achieved at the avionics level by making sure receivers can tolerate some RFI as well as redundant capabilities;
3. If a service interruption cannot be avoided, ensure that other CNS capabilities provide continued safety while being able to detect, locate and eliminate an RFI source efficiently.

This third barrier is where flight inspection can play a significant role. However, it should be noted that this role is not limited to risk mitigation only. Aerial measurement capabilities can also play a role in threat monitoring by getting data on RFI emissions that are too weak to pose operational risks, and facilitate risk assessment by providing a reliable reference of the impact of such signals on an aircraft in flight.

EVOLVING ROLE OF FLIGHT INSPECTION

The evolution of conventional navigation aids towards a supplementary capability to support PBN alongside GNSS is expected to lead to a reduction of most NDB and a significant number of VOR facilities [5]. Meanwhile, it is hoped that the network of DME stations will be optimized over time, which should include more stand-alone transponders than before [6]. While this confirms a somewhat reduced but nonetheless clear long term future for terrestrial navigation aids, GNSS capabilities must be developed. This must be done judiciously, since it is recognized that for most GNSS-related issues, ground based recording, testing and analysis makes a lot more sense than using expensive flight test time.

Similar to the subject of flight validation, airborne GNSS signal in space testing must also not necessarily rely on traditional flight inspection capabilities. Other aerial work capabilities can be used, and it is hoped that over time, data from regular aircraft operations and event recording systems can be used at least for threat monitoring purposes [7]. However, as soon as a significant RFI occurs, purpose-built aerial detection and localization capabilities are hard to beat. Given that aviation is carrying the risks related to RFI and telecom regulators are unlikely to have such capabilities, this naturally points to the experience and resources of flight inspection aircraft and their crews.

In a past RFI case in Sidney [8], it has been further confirmed that even if a significant amount of ground based RFI sensors are available, local building shadowing can make it very difficult to impossible to

detect and locate an RFI emitter. While Airservices Australia managed to approximate the location of the source relatively quickly using ADS-B data, this is not expected to be efficient for all operational environments. Most of all the case illustrated that aircraft-provided data can be superior to ground data, and that even a rough aircraft-based localization can greatly assist in increasing the efficiency of ground-based localization and ultimately, RFI source elimination efforts. Consequently, aerial RFI localization capabilities should be seen as one element with unique strengths in an overall cooperative process.

EVOLVING NATURE OF CNS SIGNALS AND RFI SOURCES

GNSS is also a manifestation of the transition from the typically analog signals of conventional navigation aids to digital ones. The predominance of analogue signals remains very obvious when looking at current flight inspection systems. One common characteristic of digital signals is their better use of a frequency channel by spreading the carrier energy such that distinct carrier or subcarrier tones become difficult to observe. Unfortunately, RFI sources have kept up with this development and now most commonly employ swept CW signals [9] which are easy to produce but still look essentially like broadband signals. Because GNSS is a multi-modal system not uniquely used by aviation, a new type of RFI threat is becoming a lot more common: intentional RFI, which is not directed at aviation, but may nonetheless have an impact on aviation. Because there is no direct intent to harm aviation, the nature of these signals and RFI scenarios can become rather diverse and unpredictable. Furthermore, given the prevalent and ubiquitous nature of GNSS, the number of potential RFI threats is more significant and will evolve more dynamically than aviation capabilities.

In the absence of direct reporting by the aircraft, GNSS signal quality also suffers from an observability problem. A recent effort from EUROCONTROL to collect GPS outage data as reported by pilots [7] revealed that a small but nonetheless surprising number of outages which could potentially be linked to RFI occur on a regular basis, even during en-route operations. The data allows the conclusion that while GNSS RFI does have a substantial threat potential, this has nonetheless so far not translated into significant risks. To ensure that mitigation efforts can maintain this low risk situation, it is necessary to increase the observability of threats, so that they can be detected before they grow into risks. For flight inspection, this implies that it would be useful to increase the sensitivity of RFI source detection commensurate with the digital nature of GNSS and consistent with the power levels which can impact receivers.

Another particular challenge comes from the specification of an interference mask for GNSS. Other navigation systems do not have such a mask, or even any kind of minimum signal to noise ratio standard. The mask represents a realistically achievable interference environment based on a study of the U.S. radio environment [10]. It has been adopted as a global benchmark in Annex 10 [11] where receivers experiencing signals above the mask may not produce misleading information, but may stop operating. However, in practice, little is known about by how much typical receivers exceed the minimum masks. Some tests have reported a margin as significant as 23dB to CW and 10dB to broadband signals [12]. This means that an RFI which may not bother one type of receiver at all may be a significant problem for another, limiting the possibility to rely on observed receiver performance. It also implies that signal in space effects should be detectable at the low levels of the ICAO receiver RFI mask.

For flight inspection, it can be concluded from all the aspects described above that there is a desire to increase the detection and localization capabilities of narrow and wide band signals operating in GNSS frequency bands, and for such capabilities to work in conjunction with other RFI detection and localization methods as part of an overall vulnerability mitigation process.

MOTIVATION FOR THE USE OF CONTROLLED RADIATION PATTERN ANTENNAS FOR RFI LOCALIZATION

Military forces have developed significant anti-jam capabilities which allow continued operation in difficult signal environments. Due to cost and complexity, it is excluded that regular air transport aircraft will ever equip with such technology. However, the situation is different for aerial work antennas, where a CRPA could make sense provided that it outperforms current RFI localization methods at a reasonable price. In military applications, the exact location of the RFI source may be of a secondary nature, as long as desired signal tracking can be maintained. However, by steering a null (negative gain) towards the angle of arrival of an undesired signal source, a line or sector of possible source positions can be obtained. The use of a GNSS-specific antenna is expected to provide the required sensitivity, while being able to profit from the “military off the shelf” development. When further integrated with standard flight inspection sensors such as an Attitude and Heading Reference System (AHRS) and additional geolocation software, this approach has the potential to increase the reliability, accuracy, and speed of geolocation while reducing operator effort and flying time. An additional potential benefit is the preservation of own-ship position when flying into an area of significant RFI.

The suggested use of military technology brings with it the question on how such use could be authorized. CRPA antennas and associated antenna electronics

manufactured in the United States fall under ITAR, the International Traffic in Arms Regulation. For "official uses", it is possible to obtain licenses for foreign use of products covered by ITAR. According to received preliminary information, this should be possible in the case of using CRPA's on flight inspection aircraft for RFI source detection and localization. Furthermore, several other States and research institutes have developed CRPA's, limiting reliance on U.S. industry suppliers. While it is recognized that this is a solvable but nonetheless cumbersome issue, the approach taken by the project was to first seek to evaluate the possible benefit that could be obtained from using a CRPA before worrying too much about the ITAR issue.

A study was conducted by EUROCONTROL in the frame of a SESAR Project on GNSS, including a contract with Rockwell Collins for a feasibility study of the CRPA RFI localization concept. Additionally, the French (DSNA/DTI) and U.S. FAA Flight Inspection service supported the project with their expertise and in-kind contributions. The FAA conducted an overflight with a regular direction-finding equipped aircraft to allow a direct comparison between the CRPA approach and other, non-GNSS specific, commercial off the shelf (COTS) solutions. With this combination of partners, all needed expertise was available to further develop and assess the CRPA RFI geolocation concept. It should be noted, however, that this combination of project partners does not imply any endorsement of a particular organization, product or supplier by anyone.

TECHNOLOGY OPTIONS ASSESSMENT

Current, common GNSS CRPA's come in either 4 or 7 element variants. CRPA's always require antenna electronics for further processing of the RF inputs, and perform either nulling (steering negative gain towards RFI sources) or beamforming (steering positive gain towards GNSS satellites), or both. The most performant system is a 7 element CRPA in combination with digital beam-former antenna electronics. Rockwell Collins also has the most experience in testing and calibrating this system. The 7 element CRPA has a diameter of 36cm (14 inches), which is of some concern for installation on a typical flight inspection aircraft such as the Beech King Air. But for a feasibility study it makes sense to first evaluate the most performing option – if there is unnecessary margin the solution can always be simplified afterwards.

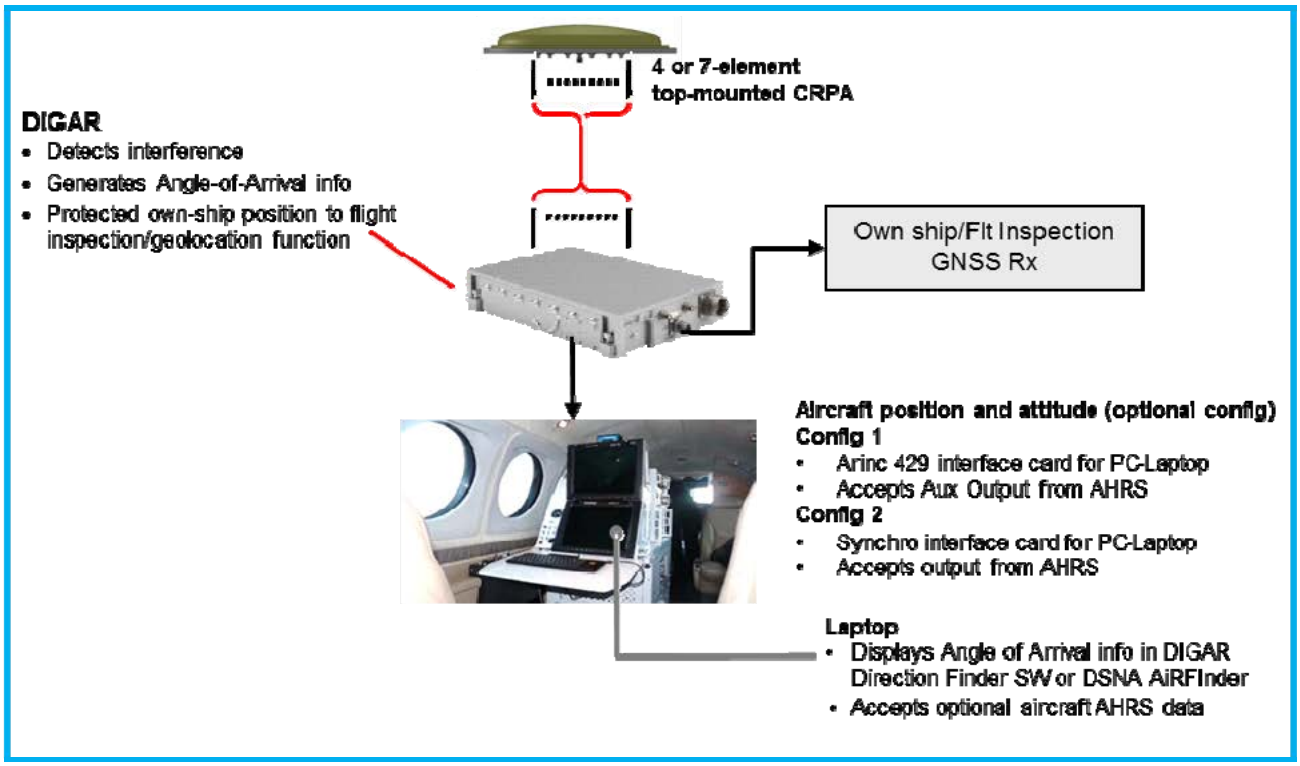

Figure 1: System Configuration

Another key question is the mounting of the antenna either on the top or on the bottom of the fuselage. A top mounted antenna corresponds to the normal installation location when visibility of satellite signals is to be maximized, while attenuation of ground based RFI sources at low elevation angles is a benefit. A bottom mounted antenna on the other hand would maximize exposure to RFI sources while making GPS reception difficult to impossible. Distributed (some elements on top, some on bottom) and linear arrays were also considered but rejected as too complex. The top mounted solution was retained due to the experience with military anti-jam performance suggesting that RFI localization performance would be sufficient while retaining the benefit of stable own-ship position. Consequently, a key element of the assessment focused on how to best use aircraft banking to facilitate geo-localization.

SYSTEM DESCRIPTION

As shown in figure 1, the CRPA is connected to the DIGAR, which stands for Digital Integrated GPS Anti-Jam Receiver. As there is one RF cable per CRPA element, it is useful to install the DIGAR as close as possible to the CRPA. The standard military production DIGAR contains not only the antenna electronics but also the receiver including baseband processing. For civil purposes, either a civil receiver would need to be integrated into the DIGAR or alternatively, a single RF output is available to connect a standard civil GPS receiver. The DIGAR will also feed angle of arrival information into a detection software. The software provided by Rockwell Collins for this purpose is called the "DIGAR Direction Finder Software". This may be integrated further into more generic direction finding capabilities, such as the "AiRFInder" used by the French flight inspection service.

The direction finder software provides angle of arrival information with respect to the antenna / aircraft reference frame. In order to provide a geolocation capability, this needs to be combined with ownship position and aircraft attitude. As most flight inspection aircraft are equipped with an Attitude and Heading Reference System (AHRS), this is not expected to be a problem. The available project resources did not allow developing this full integration, so testing was done using the direction finder display only. The AHRS would need to provide 10 – 50 Hz updates with an error of not more than ±2 degrees. The AHC-3000 from Rockwell Collins meets these requirements. Figure 2 shows an example of the direction finder output. The lighter areas show where the antenna electronics produce negative gain, while the darker areas represent stronger positive gain. The red dot indicates that a potential jammer has been identified. In this example, the source location is at about 280 degrees of azimuth with respect to the aircraft nose.

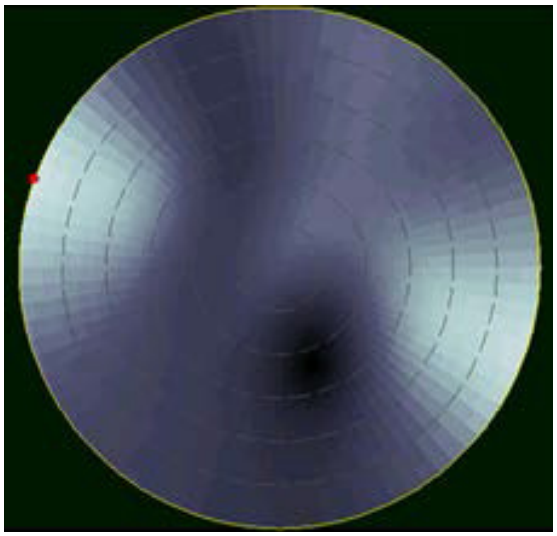

Figure 2: Excerpt from Direction Finder Polar Display of RFI Signal Angle of Arrival

Correct detection probability will depend on the sensitivity threshold and associated false detection probability being considered acceptable. It is expected that a visual localization may still be possible at carrier to noise density ratio variations below those needed to produce the red dot here, especially if the visible ambiguity can be removed through some aircraft maneuvering. It can be inferred from the system description that once the full integration is accomplished, the provision of a direct output using only a few lines of position to find a probable RFI source location in terms of approximate lat/long coordinates should be straightforward.

ANTENNA WAVEFRONT SIMULATOR TESTING

A well-calibrated simulator capable of feeding the 7 RF inputs was used to assess detection performance for different flight patterns near an RFI source. The tested patterns include a rectangular, a circular and an oscillating, S-shaped trigger and hunt trajectory. A variety of different encounter scenarios in terms of power levels and free space path loss were tested. Power levels were adjusted to produce a 1dB reduction in the carrier to noise density ratio (C/N0). Both a continuous wave (CW) jammer at the L1 center frequency and a broadband (BB) jammer were simulated (using a 20 MHz-wide PSK signal). Figure 3 shows an example of achieved detection accuracies in both azimuth and elevation angle.

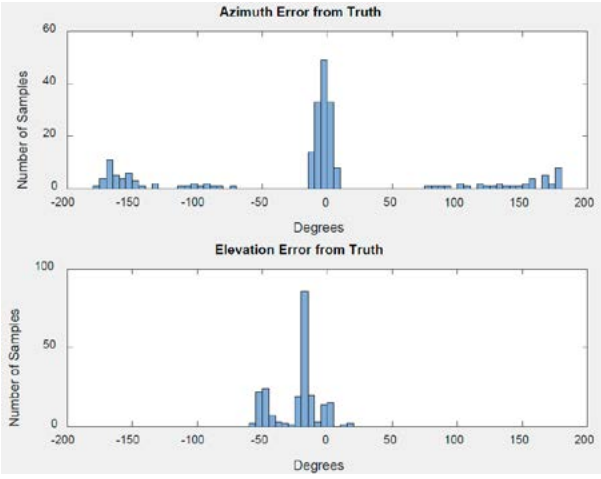

Figure 3: Example Result of Angular Detection Performance Histogram

While there is a strong peak within ±10 degrees of azimuth, there are also significant outliers. For the elevation (note the normalized scale) however, the main peak is thinner with even stronger sidelobes. Due to the installation of the antenna on top of the aircraft fuselage, the simulation results indicate that the elevation angle output is not very useful for detection. The time series result for the azimuth is given in figure 4, where it can be seen that there are many good detection matches but also some "sympathetic nulls" that move in the opposite direction of the ground track truth reference (circled in grey). It is expected that with additional software processing, these sympathetic nulls can be filtered out.

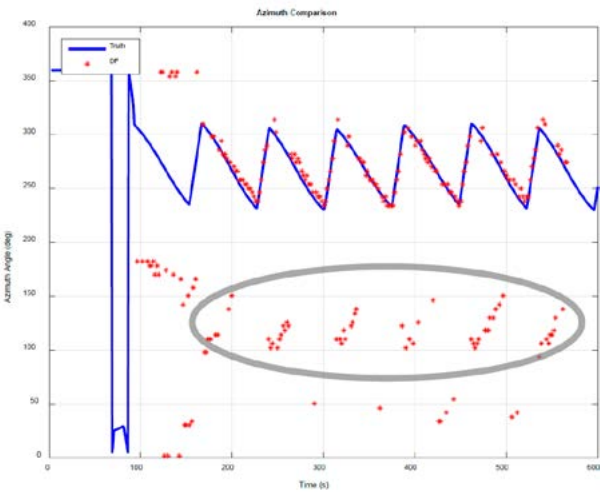

Figure 4: Azimuth Time Series Result Corresponding to Figure 3

For all tested scenarios (assuming additional filtering), azimuth detection capability was better than ±10 degrees (one standard deviation), and in some cases as accurate as ±2 degrees. There was no significant difference between CW and BB results. As could be expected, simulated aircraft banking significantly improved detection capability. Consequently, the use of orbits seems to be the best search strategy. The simulator testing used a figure-eight pattern with one of the orbits passing over the interference source.

LIVE SKY VAN TESTING

Rockwell Collins has an authorization to broadcast RFI test signals at the GNSS L2 frequency. Previous work showed that the results at L2 can be applied equally to L1. Figure 5 shows the test area, including a -100dBm signal level boundary. The jammer was installed on a tripod and fed by a signal generator using a normal GPS antenna (FRPA, fixed radiation pattern antenna). Locations B and C were used to both calibrate the RFI level and as check points for the van trajectory. The test van included a fixture that allowed a tilting of the CRPA by 30 degrees from zenith to either side. The van is shown in figure 6, and a schematic of the tilt fixture in figure 7. It can be seen that this set up creates a realistic RFI path that arrives with an elevation slightly below the horizon at the unit under test. Two sets of tests were performed: one where the van drove straight into or out of the area of interference in order to determine overall equipment sensitivity, and varied paths in order to quantify angular detection performance. Again, both CW and BB RFI signals were evaluated.

Figure 5: Live Sky Test Area

Figure 6: Test Van

Not surprisingly, elevation angle results turned out not to be very reliable given the below horizon signal path. But azimuth errors were slightly greater than obtained during the wavefront simulator testing (±12 degrees, one sigma). This can be attributed to both multipath and a less accurate heading truth reference. Taking these additional factors into account, the results are very consistent. Tilting the antenna by 30 degrees towards the RFI source significantly improves azimuth resolution (to about ±8 degrees) while also reducing sympathetic nulls. When the tilted antenna points away from the RFI source path, azimuth accuracy will decrease, which is considered helpful in avoiding false detections.

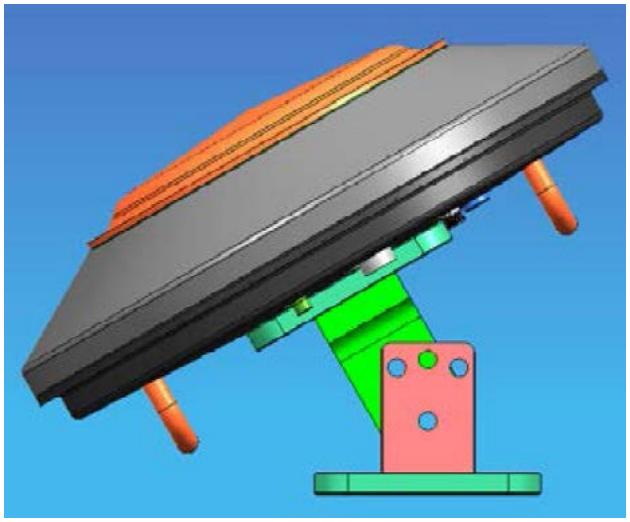

Figure 7: CRPA with Tilt Fixture

SUMMARY OF ROCKWELL COLLINS TESTING

Even if a good bit of integration work remains necessary to produce a production-ready system for flight inspection aircraft, the approach shows promise. Further testing, especially using an actual aircraft installation is recommended. Installation of a 7-element CRPA will be challenging on a typical Beech King Air, but possible. Antenna calibration requirements are expected to be manageable with a standard network analyzer. To avoid further complications with export regulations, the use of a separate civil GNSS receiver is recommended. The overall system is at this stage still on the costly side.

While a 4-element CRPA could be used, this was estimated to double or triple angular azimuth detection errors and reduce the detection distance, and consequently not likely to be worth the additional cost. While smaller 7-element CRPA's than the one used are available, their performance would need to be assessed.

For a top-mounted CRPA, aircraft banking is essential to ensure good performance. This could increase the amount of airspace required for detection and thus lead to operational complications. Furthermore, since the aim is to increase detection sensitivity in order to geo-locate weak power sources such as Personal Privacy Devices (PPD), maintaining own-ship position is not really all that critical, as it can be managed by maintaining an appropriate distance from the RFI source if needed. Both DSNA and FAA consequently recommend using a bottom-mounted CRPA. In addition to adding another 10dB of detection sensitivity on average and reducing the need for maneuvering, it may restore the utility of the elevation output; thereby potentially further reducing search time. Either way, it will be useful for flight inspection aircraft to have alternate positioning capabilities to GNSS both for aircraft guidance and the flight inspection truth reference system.

The tested system required a 15dB stronger signal to transition from detection to localization. However, this is dependent on the accepted false alarm rate. A tunable procedure can be envisaged where the software is accepting a higher false alarm rate at first to maximize search capability and moving to a lower alarm rate to confirm suspected RFI source locations later. Both the potential of the additional filtering software and any human-machine interface aspects (fully automatic detection versus an inspector-assisted approach based on interpretation of the direction finder display visual indications) would need to be further evaluated.

COMPARISON OF CRPA APPROACH WITH GENERIC CAPABILITIES

The two common options for in-flight detection of RFI sources in any relevant frequency band are the use of either a spectrum analyzer or, if available, a direction finder. The spectrum analyzer approach depends on connection to a suitable antenna, preferably with some directionality. In this way, the aircraft can be maneuvered to point the antenna either towards or away from the RFI source. Normally there is very little directivity, making this a challenging search. A direction finder is a significant improvement. A commonly installed direction finder is the Cubic DF-4400. Figure 8 shows the L-band antenna array used by the DF-4400 as installed on the bottom of the aircraft.

Figure 8: Cubic DF-4400 Antenna Array

Traditional spectrum analyzers are built for laboratory use and do not fare very well when used by aircraft in flight, having to detect very low signal levels requiring a long sweep time. However, newer generation analyzers with a good GNSS-specific pre-amplifier (as often used in ground test vans with GNSS RFI detection capability), using digital sampling with a fast A/D converter could still provide a very useful capability. However, this subject is considered to be out of scope of the current discussion, and the paper will focus on comparing the CRPA approach with a standard direction finder. While Cubic no longer manufactures the DF-4400, alternate products with equal or better performance are available on the market at reasonable prices.

The FAA Flight Inspection service conducted complementary flights during the Rockwell Collins live sky van testing. The flights included orbits and a direct overflight of the RFI source. This was complemented by additional laboratory calibration to ensure that results could be compared. This paper has waited up until now to provide sensitivity results of the CRPA approach because they are more meaningful in comparison with a generic direction finder capability. It should be noted that since test data is only available for a top mounted CRPA, the comparisons here are made for the preferred bottom mounted CRPA using engineering estimation.

The key finding was that while direction finding capability was quite comparable between the CRPA-system and the DF-4400 for CW, the CRPA-system outperforms the DF-4400 by a significant margin when encountering broadband signals. This is considered to be a significant improvement given the expected nature of RFI sources. During the FAA overflight, the aircraft did not manage to detect the broadband signal. Consequently, the values given here are reconstructed from laboratory analysis. Table 1 compares the estimated achievable sensitivities.

Table 1: Comparison of Direction Finding Sensitivity

[dBm]	DF-4400	CRPA System	CRPA System
Antenna Mounting	Bottom	Top	Bottom
Narrowband	-120	-115	-125
Broadband	-99	-115	-125

In view of the stated limitations of the data analysis performed, these values need to be interpreted with caution. But in general it can be concluded that the direction finding sensitivity of the CRPA-system is relatively insensitive to the encountered modulation of the RFI signal, and that the bottom-mounted CRPA system does outperform the DF-4400 system by a small margin in the CW case and by a large margin in the broadband case. How many additional dB's can be gained by both approaches through further optimizations is of course a matter of potential future analysis. The performance improvement of the CRPA system does come at a cost, as could be expected.

INTERFERENCE DETECTION PRIOR TO LOCALIZATION

Before the search for an RFI source can begin, it needs to be detected. Normally it should be easier to detect an RFI source than to locate it, since direction finding requires a certain signal strength to obtain bearing information. However, given the directionality of DF arrays, this may not necessarily be true. Another potential factor is the potential reliance on a spectrum analyzer to detect RFI, which may not achieve the corresponding noise floor, especially when using a broad scan across a wide frequency range. As mentioned, the direction finder system needs about a 15dB difference between detection and localization ability. Figure 9 shows the detection ranges for the top-mounted CRPA system for a given ground based emitter while the aircraft altitude is assumed at 2000ft AGL. The bottom mounted system would improve the minimum detection threshold further. But given that 15dB can translate into quite a significant difference in terms of free space path loss distance, concepts for efficient direction finding once an RFI source is detected will also deserve further attention.

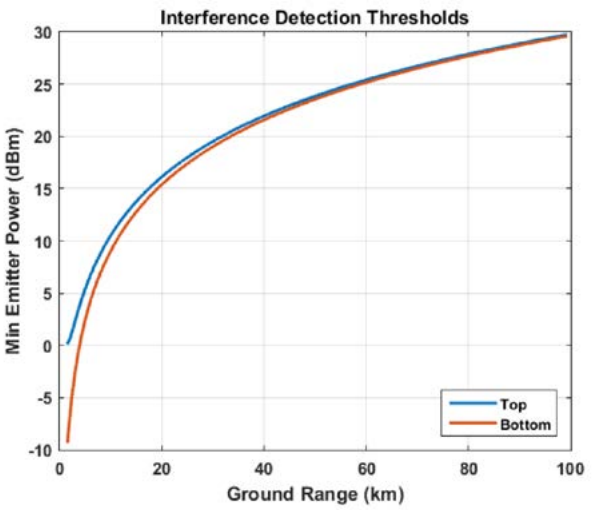

Figure 9: Detection Ranges for Top-Mounted CRPA System

HUMAN FACTORS ASPECTS

During the FAA overflight, the broadband RFI couldn't be detected by either the spectrum analyzer in use or the DF-4400. Part of the challenge was using the right equipment settings. For the DF-4400, it was found that best performance could be obtained for detecting broadband RFI when using the FM wide mode of demodulation. Similar findings were obtained for the use of the spectrum analyzer, where specific skills are necessary to use the equipment to its fullest capability. Similar issues are expected when having to interpret the display of a CRPA-based system. This means that regardless of the RFI source geo-location approach used, specific training should ensure that flight inspectors have the greatest chance of success in finding RFI sources.

CONCLUSIONS

This paper explained the motivation for flight inspection organizations to improve their capabilities in geo-locating GNSS RFI sources. An approach using a CRPA antenna and corresponding antenna electronics and processing software was presented, and demonstrated to be superior to current, generic direction finding capabilities, especially with respect to broadband signals. Maintaining own-ship position in the presence of RFI was found to be a secondary objective when looking for the expected weak signal sources, and the use of a bottom-mounted CRPA system is preferred. A number of issues need to be further analyzed, such as the additional filtering needed to eliminate sympathetic nulls.

RECOMMENDATIONS

In light of the potentially very significant benefit that can be achieved when employing aerial work aircraft in cooperation with ground based capabilities, flight inspection organizations are recommended to further study all aspects of GNSS RFI geo-location and improve their capabilities. Such capabilities are expected to limit the exposure time to RFI cases and allow a more efficient deployment of ground based spectrum enforcement resources. These studies should include the improvement of detection and localization equipment, and the development of corresponding operational procedures for both the flight crew and flight inspectors.

ACKNOWLEDGMENTS

The Eurocontrol-funded contract with Rockwell Collins is part of the Eurocontrol contribution to SESAR Project 15.3.4, “GNSS Baseline” and the GNSS RFI Vulnerability Mitigation Task.

All commercial products mentioned in this paper and any associated intellectual property, copyright or trademark is and remains with their respective owners.

DISCLAIMER

This paper does not contain any official EUROCONTROL, SESAR, FAA or DSNA position or policy. Furthermore, it does not constitute any endorsement of a particular product, or a statement of any kind relating to any future procurement activity.

REFERENCES

[1] ICAO, 29 November 2012, Report of the Committee to the Conference on Agenda Item 6, 12th Air Navigation Conference, AN-Conf/12-WP/162, Montreal

[2] ICAO, 2013, Global Navigation Satellite System (GNSS) Manual, Doc 9849, 2nd Edition

[3] ICAO, December 2015, Insertion of RFI Mitigation Plan into GNSS Manual, 2nd Meeting of the Navigation Systems Panel, Working Paper 36, Montreal

[4] ICAO, 2007, Manual on Testing of Radio Navigation Aids, Volume 2, Testing of Satellite-Based Radio Navigation Systems, Doc 8071, 5th Edition

[5] ICAO, 4 April 2016, Adoption of Amendment 90 to Annex 10, Volume I, Attachment H of Amendment 90, State Letter AN 7/62.2.1-16/23

[6] G. Berz and V. Vitan, 16-20 June 2014, Evolution of Terrestrial Navigation Aids as a Consequence of PBN Implementation, Proceedings of the 18th International Flight Inspection Symposium, Oklahoma City, USA

[7] G. Berz and P. Jonas, 18-19 November 2015, GNSS RFI Mitigation: Overall Context and CNS Links, 8th EUROCONTROL CNS Team Meeting, Information Paper 3, Brussels

[8] ICAO, April 2015, GPS Interference Event – Sydney, Australia, 1st Meeting of the Navigation Systems Panel, Information Paper 23, Montreal

[9] T. Kraus, R. Bauernfeind, B. Eisfeller, September 2011, Survey of In-Car Jammers: Analysis and Modelling of the RF Signals and IF Samples (Suitable for Active Signal Cancellation), Proceedings of ION GNSS, Portland, Oregon

[10] RTCA, March 2008, Assessment of Radio Frequency Interference Relevant to the GNSS L1 Frequency Band, DO-235B

[11] ICAO, July 1996, Radio Navigation Aids, International Standards and Recommended Practices, Annex 10 to the Convention on International Civil Aviation, Volume 1, 6th Edition

[12] SESAR Joint Undertaking, April 2016, GNSS RFI Vulnerability Report, Deliverable 11 of Project 15.3.4, GNSS Baseline Study

19th International Flight Inspection Symposium (IFIS)

Belgrade, Serbia, 13-17 June 2016

Critical impact given by the interference from LTE to the implementation of flight inspection in JAPAN

Kazuya. Oguro
Flight Inspector
Japan Civil Aviation Bureau
Tokoname-City, Aichi, Japan
Fax: +81 569 38 1354
E-mail: oguro-k05j7@mlit.go.jp

ABSTRACT

Currently in Japan, flight inspection demand for new flight procedure establishments is increasing with increase of the air traffic. Our four old flight inspection aircraft has been renewed so that JCAB can establish efficiently a large number of the advanced PBN procedures including RNP-AR and can evaluate new ATC surveillance system that called MLAT or Wide Area MLAT (WAM).

As a result, our new flight inspection aircraft are equipped with GNSS positioning system as more precise positioning system to perform flight inspection in the wider area than before. Especially, in case of an evaluation for WAM, such sub-meter position accuracy will be needed beyond 100nm from the facility.

But mobile communication service providers in JAPAN are using the L band (1.5GHz) frequency communications as mobile network all over JAPAN, and it has been becoming a threat to our using GNSS positioning service.

Now we are struggling for the implementation of robust flight inspection under this severe condition.

INTRODUCTION

In recent years, the volume of information that each mobile communication company treats has become so a lot with increase of individual users. The frequency resources with which the network is connected are needed, as a result the communication network is going to be assigned to many frequency bands. Long Term Evolution (LTE) is one of the communications which more frequency bands will be needed all over the world from now on in particular.

On the other hand, a frequency band of the broadcast service of the satellite reinforcement information by using Geostationary Satellite (GEO) belongs to L-BAND.

Seemingly in JAPAN, it seemed to be arranged in neutralizing frequency allocation, but it wasn't for us.

JCAB keeps offering of highly precise flight inspection services to users in associate with ATS performance in JAPAN at all times. Especially using such GNSS service by the new aircraft to the implementation of flight inspection is effective into wider area than before. Therefore we will manage to lead that issue to the solution immediately.

It is not the point in this issue. The TV camera system as independent positioning function is the most irrelevant one to the RF interference that needed slightly big fleet and equipped with IRS and Camera itself. If this impact would be greater than we expected, we might be consider necessity of the diversity system.

The purpose here is to introduce the impact as one of case studies that flight inspection will be affected by LTE communications. And we show the influential degree to the L-band GNSS service by LTE communication service. In addition, we introduce effectiveness of the Band Pass Filter (BPF) and reinforcement of Low Noise Amplifier (LNA) as countermeasures.

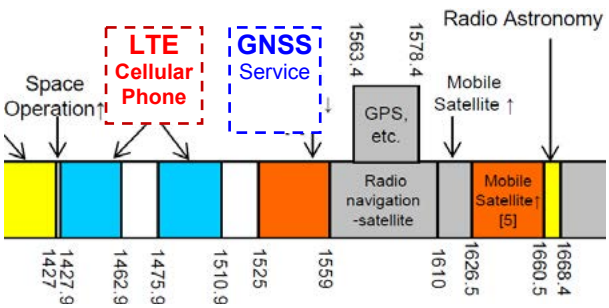

Figure 1. JAPAN Frequency allocation

IDENTIFY THE INTERFERENCE

During evaluation of new flight inspection aircraft, it was difficult to specify that the cause is derived from LTE radiation while we can recognize that GNSS service has been degraded, and we had to spend long time for it.

Interference is generally to be manifested itself as jamming, noise and crosstalk. In such case, we can find easily its origin by the observation of frequency spectrum, because it cause that operational center frequency may be affected or overridden by something close frequency.

The frequency of GNSS Service is about 30 MHz away from the center frequency of interference source. In case of this time none of harmonic content and none of parasitic radiation were also observed.

Of course, each mobile communication company which handle with LTE band shall keep to operate strictly by ITU regulations of their stations, and also the operation of stations with the high quality maintenance is accomplished, and because there are almost no cases that an unnecessary signal is radiated, it's also fact that there were no cases that we consider as interference source.

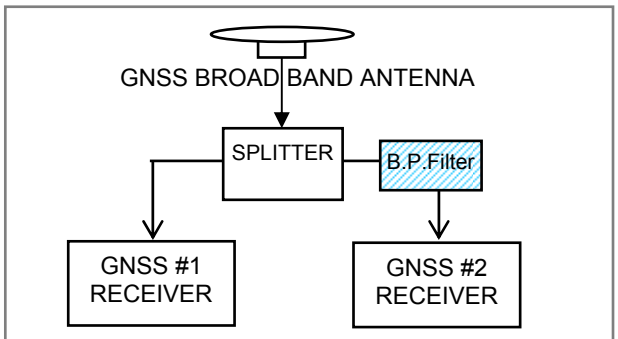

Figure 2. Ground Test of Broad Band Antenna & FILTER（Under LTE radiation）

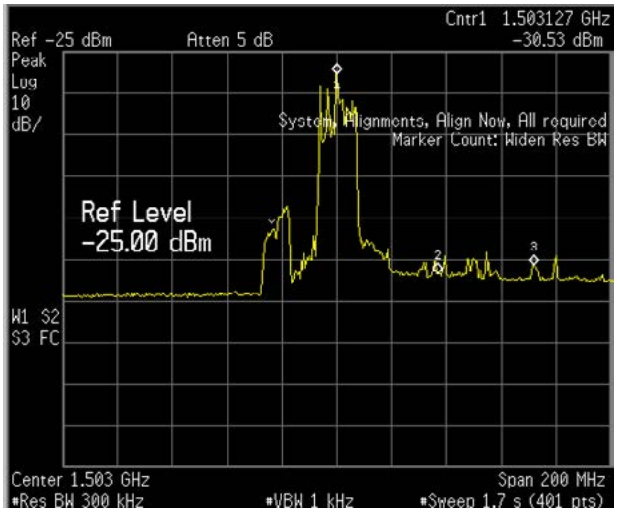

Figure 3. GNSS Receiver #1 ANT. IN spectrum CTR Freq.1,503 MHz

During repeating the thing which takes low approach to the airport in the evaluation of the new aircraft, the level of C/No of GPS, SBAS, GNSS reinforcement service and a frequency spectrum observation of 1.5GHz band, that LTE has appeared as interference source may be correct expression.

It may be one by which it can't be said that LTE may be placed with interference source from the above.

The Improvement of the receiver sensitivity

It isn't a so much difficult thing to consider the measure which is after that if interference source could be specified, whether the countermeasure can be made something effective separately.

At first, as the departure to breakthrough of this difficulty, we have paid attention to the C/No of GPS L1 that received throgh the broad band GNSS antenna. Then we tried to inspect how level of C/No can be affected, how degree of LTE radiation can be excluded and how degree of improvement of position accuracy can be managed under LTE radiation emvironment by the composition on the ground indicated Figure 2..

Each equipment of composition are as follows;

- Both two GNSS receivers are the same as using Ground Reference Station of RTK.
- Filter attenuation ; ≧30dB @ 1495.9-1510.9MHz
- GNSS Antenna; Broad GNSS Frequency Tracking and LNA installing

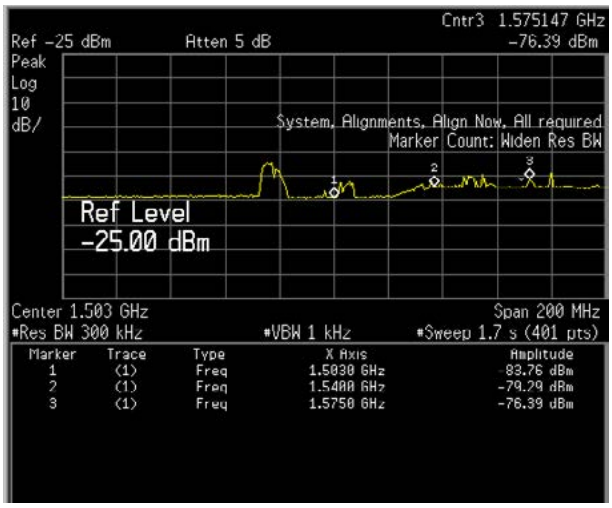

Figure 4. GNSS Receiver #2 ANT. IN spectrum（+ FILTER）CTR Freq. 1,503MHz

Under the environment that the antenna was put itself in strong LTE radiation, and the GPS signal from the identical antenna is divided into two receivers at splitter equally.

The filter which excludes LTE BAND21 signal was inserted in #2 receiver and the comparison was performed at the same time.

Observed results are as follows;

Received spectrum through the GNSS Antenna;
Figure 3. and **4.**

- GPS L1⊿C/No [dB] =
  C/No(GNSS#2) [dB] - C/No(GNSS#1)[dB];
  Figure 5.

- Estimated Error 1 σ （Horizontal）[m];
  Estimated Error 1 σ （Vertical） [m];
  Figure 7.

The plot on Figure 5. is the C/No difference between GNSS#1 on the orbit by the time course of GPS PRN1 and #2. From this result, we can find out that L1 C/No is improved roughly 3 dB by insertion of the filter to the receiver input under LTE radiation.

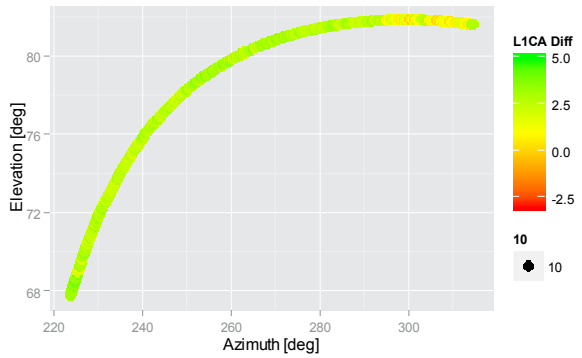

Figure 5. GPS PRN1_L1⊿C/No [dB] = C/No(GNSS#2) [dB] － C/No(GNSS#1)[dB]

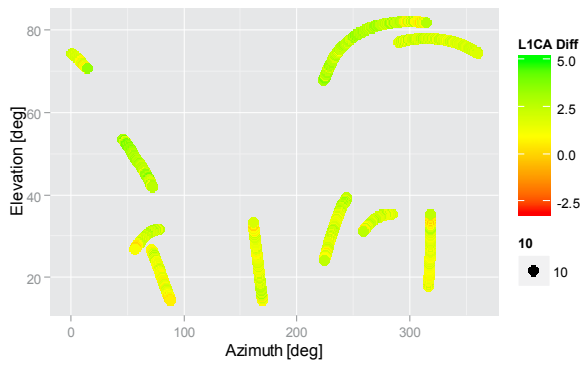

Figure 6. OBSERVED GPS PRNs_L1⊿C/No [dB]

The plot on Figure 6. shows improvement of 2 or 3 dB for all PRNs.

From two plots of Figure 7, we can presume that improvement of C/No is reflected into improvement of the SPS position estimation of GPS receiver.

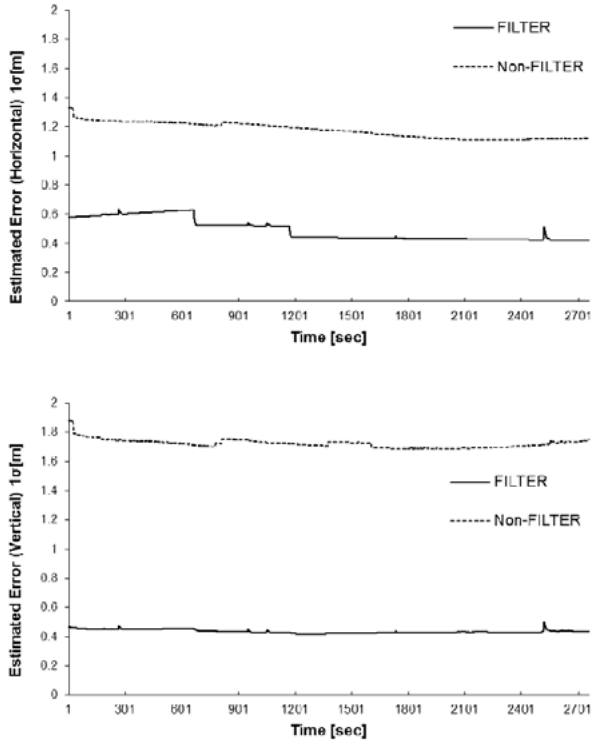

Figure 7. Estimated Frror (Horizontal and Vertical)

Developing Flight Inspection Interference Monitor

While not depending on the location and time it can't keep GNSS Positioning Service means that Flight Inspection System doesn't grasp the position of the our own aircraft correctly, and implementation of many inspection would become difficult.

It has not been clear that uncontinuity of GNSS service might be derived from powerful LTE radiation since we have started the evaluation of new flight inspection aircraft.

We have tried to check the cause about whether uncontinuity of GNSS Service is something to come to malfunction of equipment or a physical problem of a cable or an antenna, etc. while evaluating the system of course.

On the way to performing this process we have been focusing different flight altitude, different airport location and radiation outside L-band on the interference. And we had been grasping the tendency of GNSS service degrade-ration gradually while also suspecting the interference.

And so, we have watched some parameters that are C/No, Eb/No, Age of correction and the field strength of LTE radiation. It was possible to relate uncontinuity of GNSS Service to LTE radiation by accumulating and analyzing these data of parameters during flight and above-mentioned ground test.

JCAB has developed Flight Inspection Interference Monitor (FIM) to make its relation clear and then evaluated this issue by using this monitor fully.

To utilize more FIM, it would be estimated the impact of the interference by observing the input of field strength of LTE to fuselage antenna and GNSS service's Eb/No. And we has been able to estimate the threshold that uses GNSS Service as flight inspection positioning source finally.

Evaluation @ OUR HOME , CHUBU Centrair International Airport using Flight Inspection Interference Monitor

This monitor works to express acquired data successively by our Flight Inspection Aircraft.

Related parameters are as follows and showed on the FIM window as each graphs. Please refer to **Figure 8.**

Background is the Map of Chubu Centrair International Airport.

LTE (BAND21) specrum[dBm] is the left side on the FIM window.

Aircraft Altitude[FT] is the upper right on the window.

GNSS Service Eb/No[dB] is the middle right on the window.

Age of Correction[second] is the lower right on the window.

Moving MARKs is aircraft track and show the strength of GNSS service Eb/No [dB] being classfied by colour.

Under FIGURE 8.～14. show images that from Spot OUT to Takeoff.

It's possible to make a correlation of related parameters clearly.

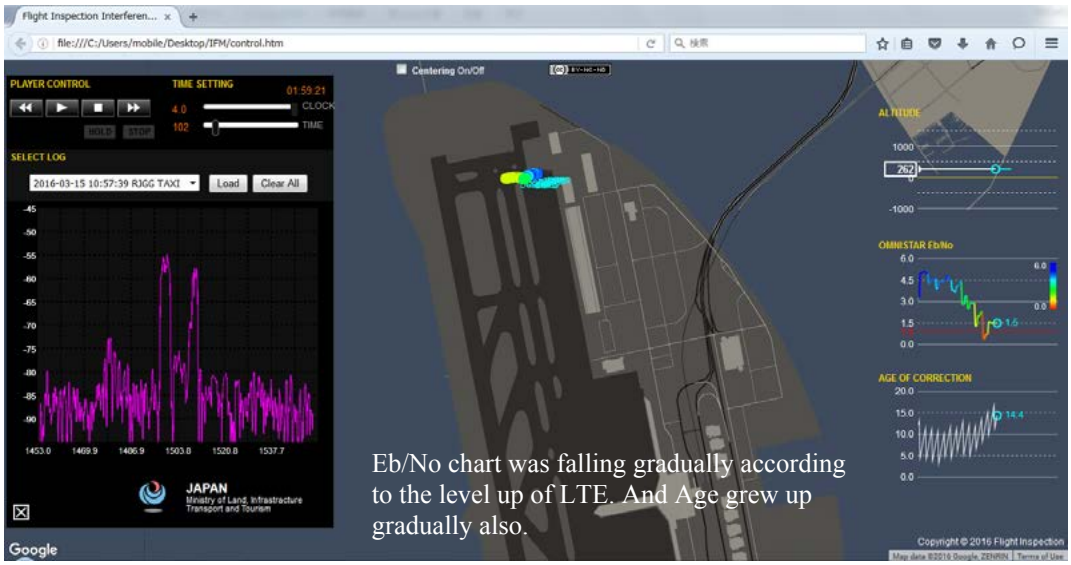

Figure 8. The aircraft spotted out from our office.

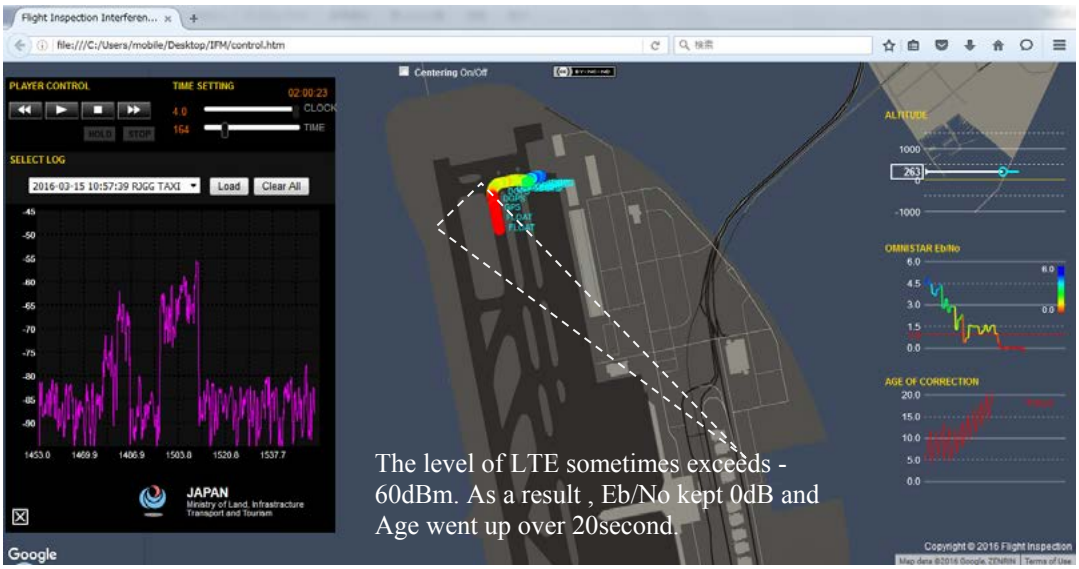

Figure 9. The aircraft taxied down on A-TWY.

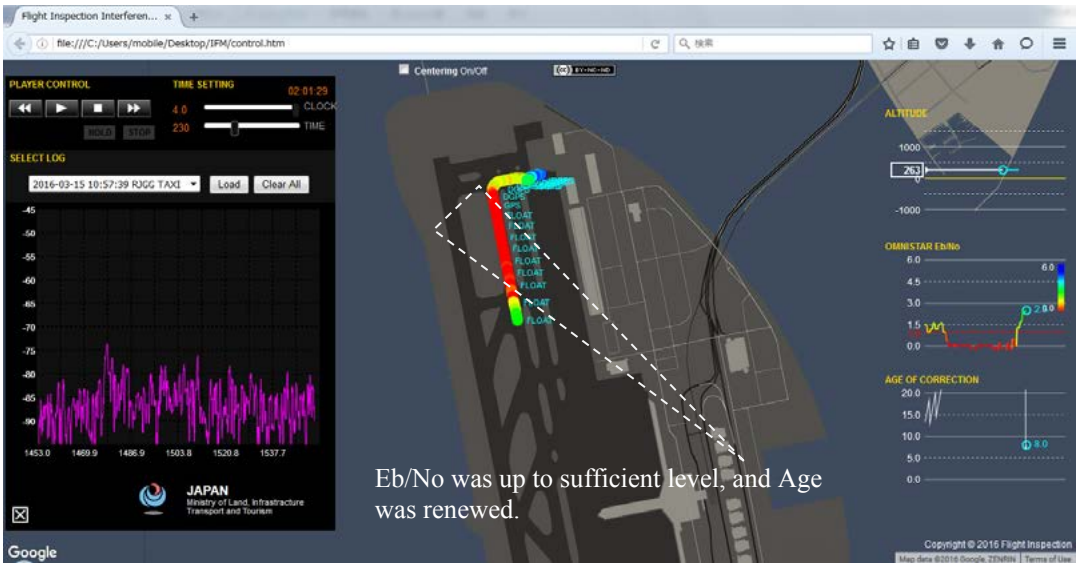

Figure 10. The aircraft proceeded on A-TWY and located out-sight from the LTE station and wasn't affected at LTE.

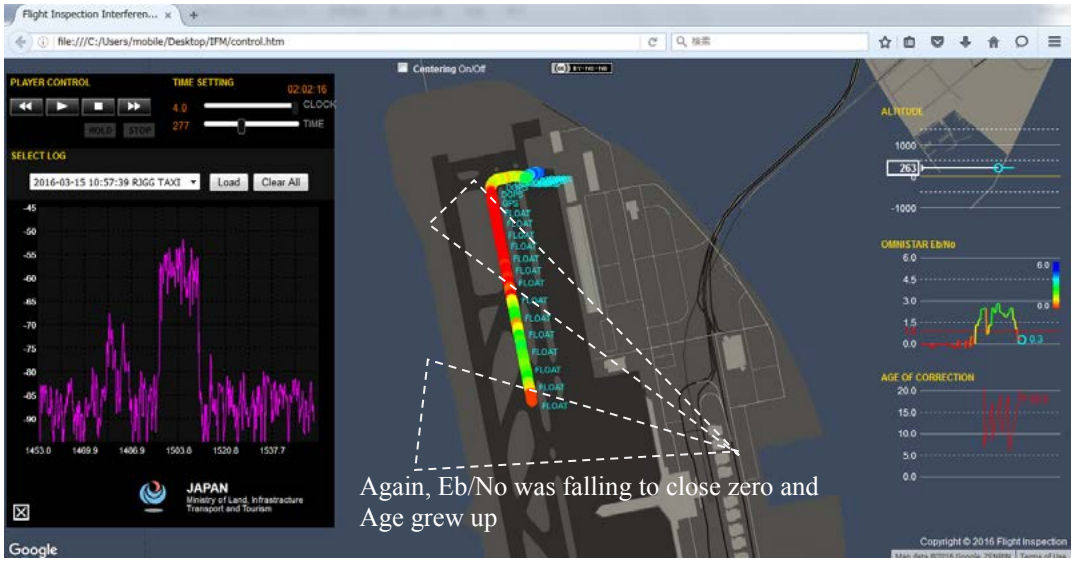

Figure 11. The aircraft was close to LTE station and was under the LTE radiation again.

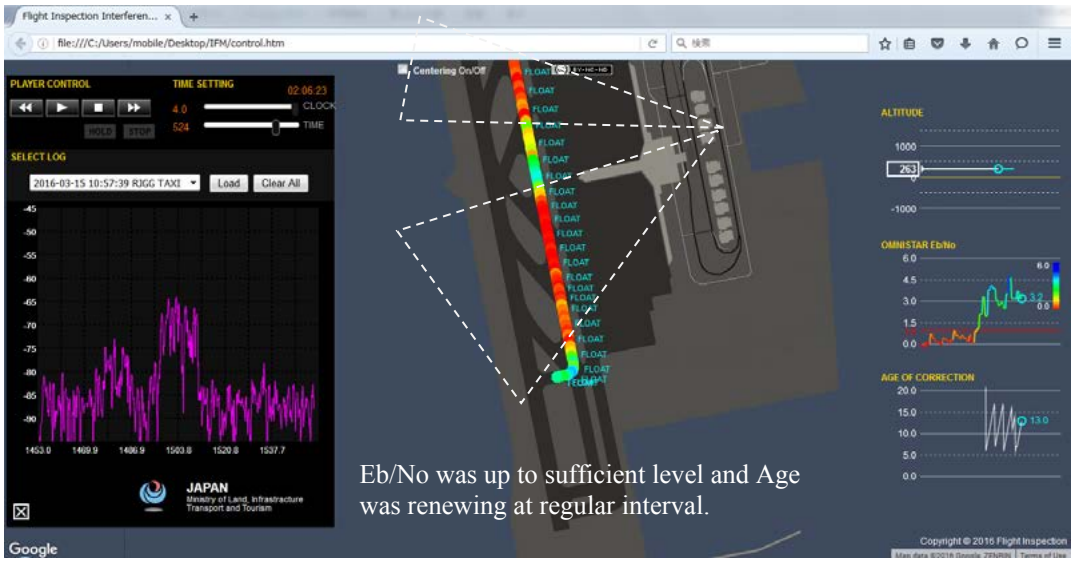

Figure 12. The aircraft was close to take off position and entered into out-sight from the LTE station.

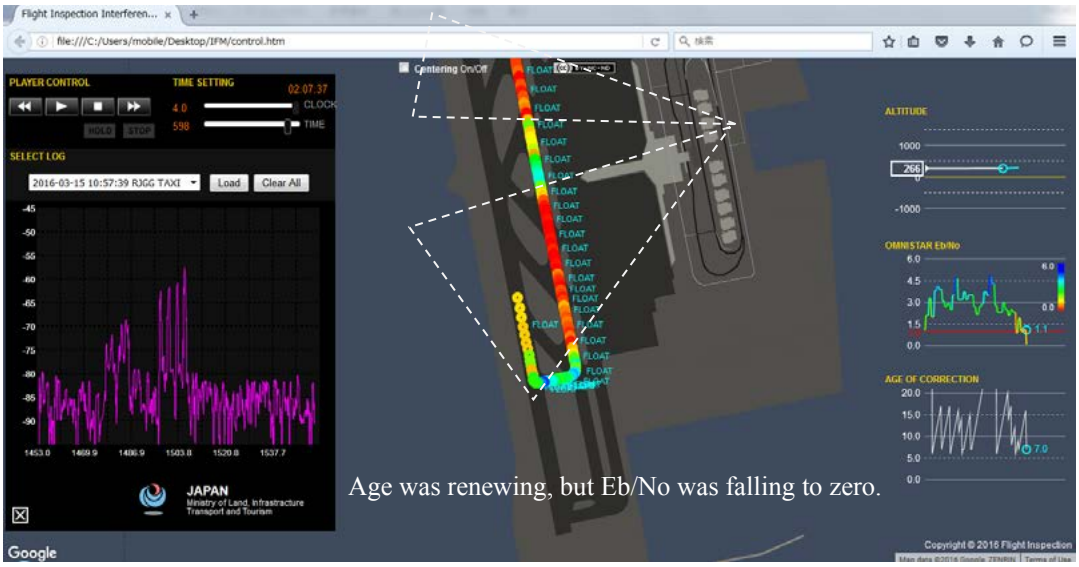

Figure 13. The aircraft started rolling and re-entered into intereference zone.

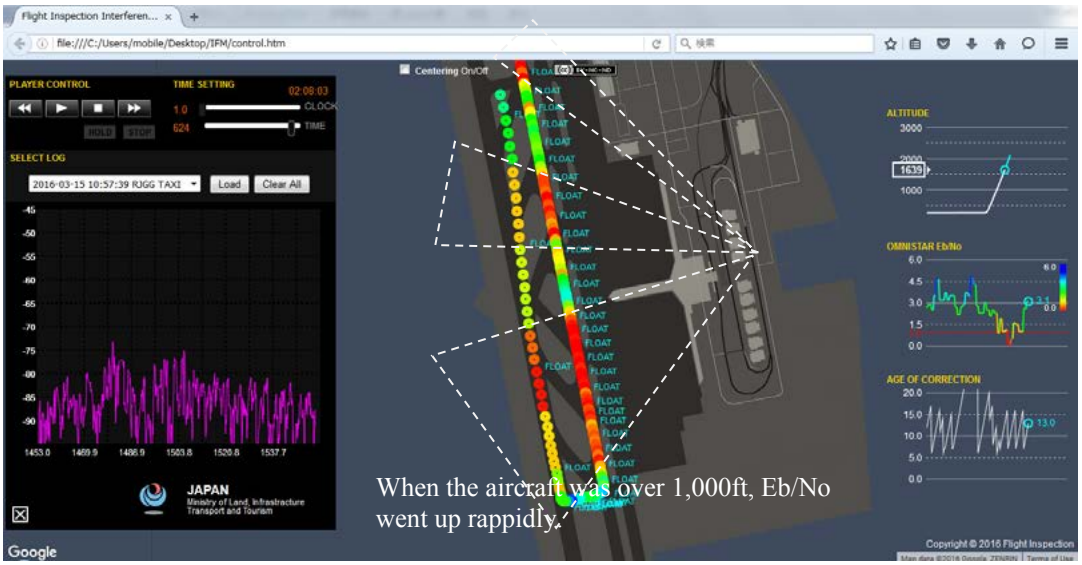

Figure 14. The aircraft was taking off and clibming.

ANALYSIS

For investigation mentioned above, we are now able to see the relation between Eb/No and C/No of our aircraft GNSS receiver as follows,

C/No[dB] = 33.8 + Eb/No [dB] **Figure 15.**

*Eb/No is known as Signal-to-noise ratio per bit.

GNSS Service isn't formed as reinforcement service under the condition of "Eb/No < 1dB".

We can be fairly certain that Eb/No improved by excluding LTE BAND frequency by FILTER installation and improving GNSS C/No when it was also based on a result of the ground test, the receiver selectivity improves, if DIGITAL LINK is to become stable, and the service level of the position accuracy becomes stable.

Also it is obvious that even if BPF was inserted in the latter part of an antenna under LTE powered radiation, Low Noise Amplifier (LNA) of antenna inclusion was saturated, and that C/No may become 0db. Therefore a perfect measure of LTE won't be only by equipment of FILTER, and development of the antenna in which FILTER specialized in LTE was included is going to be wished for.

On the other hand, one of the profits we got through this evaluation can make impact to a position error according to its level of strength and the range of interference clearly during this struggle, and then we could establish operational index of the GNSS service which can judge that a flight inspection was possible by that.

That is to say that we can settle clearly by approach to the runway at which airport GNSS Service can be used for a flight inspection by flying once around the airport.

It is necessary, at this point, to explain that our index can be adopted only for using our aircraft in connection with LTE of BAND21 in JAPAN.

But such evaluation process is helpful when estimating LTE which becomes a threat to GNSS service in each country.

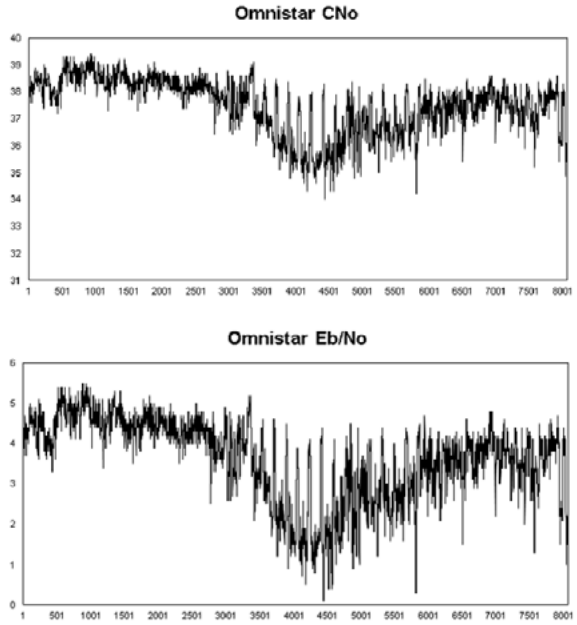

Figure 15. GNSS Service Eb/No vs C/No

CONCLUSIONS

The mobile communication using LTE for which band 21 put it in Japan, and is a certain threat to GNSS Service frequency users. But it's the current state that the person who catches this with a threat is limited by a minority to an agricultural enterpriser and a surveyor very much including us.

Therefore it'll be also apparent from now on that it's difficult even making narrow it's threatening area as well as taking this threat from the root. Because a mobile communication in case of emergency is something indispensable for the Japanese who has experienced a big earthquake disaster, addition of LTE stations by mobile companies is obvious, and LTE coverage can get expansion and no reduction.

From the above, now that GNSS Positioning Service is employed as a flight inspection tool, it becomes important to get along with this threat.

By using GNSS positioning service as implementation of robust flight inspection:

a. Installation of a BPF against LTE frequency

b. Installation of an antenna with improved LNA

c. to evaluate the impact correctly and to recognize own threshold of operation

d. none of operation beyond threshold

e. preparation of Back UP system（ex. GPS RTK, TV-camera system, theodolite mission performance, etc.）

FUTURE WORK

Installing a band pass filter between an antenna and a receiver or using an antenna which improved LNA function are both effective countermeasures to the interference under LTE radiation, but we realize that these will be not perfect one by expansion of LTE network and appearance of more high power LTE station in JAPAN.

And GNSS service interruption will often occur close to the runway where LTE station located nearby. It means that Age is not renewed. And in this area, most precise aircraft position would be required for calculation of ILS parameters or validation of FINAL APCH phase.

Therefore we have to estimate the impact of interruption of Age during flight, and will establish the tolerance of interruption of the Age as uncertainty of the inspection. It is the focus of efficient utilization of GNSS positioning service.

ACKNOWLEDGMENTS

I would like to acknowledge and thank Kenji Uehara for developing of Flight Inspection Interference Monitor. Kenji is the Air Navigation Services Engineer at the JCAB's Technical Management Center.

Signal-in-space Measurements using Microcopters

19th International Flight Inspection Symposium (IFIS) 2016, Belgrade, Serbia

Jochen Bredemeyer
FCS Flight Calibration Services GmbH
Braunschweig, Germany
E-mail: brd@flightcalibration.de

Thorsten Schrader
Physikalisch-Technische Bundesanstalt (PTB)
Braunschweig, Germany
E-mail: Thorsten.Schrader@ptb.de

ABSTRACT

An unmanned aerial system (UAS)-based measurement process to supplement conventional flight inspection of terrestrial navigation aids is described. In contrast to typical flight inspection with an aircraft, the platform allows quasi-stationary hovering in critical areas with extended observation times, without using expensive manned helicopters to carry measurement equipment and antennas.

A microcopter carries the payload which consists of a short linear antenna and a highly miniaturized, FPGA-based large bandwidth receiving/recording system. In contrast to conventional methods, the raw band pass signal-in-space covering the complete channel bandwidth is sampled at a high data rate, and is directly recorded without any pre-processing whatsoever. This preserves maximum opportunities for any signal post-processing to extract all essential parameters of interest. Among typical flight guidance parameters such as DDM, the nature of scatterers can be shown in the time and frequency domains. All data is synchronized in time with the flight vector gained from an advanced on-board position system.

The paper describes experiences gained with the system, and provides first measurement results obtained from ILS localizer and VOR facilities.

INTRODUCTION

Absolute field strength and signal-in-space (SIS) measurements have been performed by using manned helicopters, aircraft or ground vehicles with extendable masts where necessary. Also helium-filled balloons and blimps have been used in the past. Drawbacks of their operation are high costs, fast movement (no repetitive measurement samples can be taken at the same spot), limited maneuverability, long setup time, or, in case of a mast, limited air space to be covered. Now, with the availability of unmanned aerial systems (UAS) such as microcopters a versatile and comparatively cost-effective platform can be deployed for such purposes. Fields of application such as aerial photography, infrared spectroscopy and thermometry, surveillance, inspection and service, surveying, etc. are partly already firmly established with many small companies offering these services. However, these platforms also offer several features that drastically improve the effectiveness of SIS measurements. Here, the UAS is used for precision electromagnetic field and signal measurements of CNS facilities defined in ICAO Annex 10 [1]. This is a task which cannot be assessed sufficiently by conventional flight inspection (FI), and is beyond of the procedures defined in DOC8071 [2].

In the current WERAN project (German abbreviation for “Measuring the potential interaction of wind turbines with terrestrial navigation and radar systems” – [3] – supported by

the Federal Ministry of Economic Affairs and Energy on the basis of a decision by the German Bundestag [grant: 0325644A]), the potential interaction between wind turbines and terrestrial navigation / radar systems is investigated. The frequencies of interest span across the rather wide frequency range of 200kHz to 5GHz. The measurements presented in this paper were performed employing the measurement platform developed in the WERAN project.

DESIGN OF A MEASUREMENT SYSTEM

Among the numerous design requirements for the microcopter (here: octocopter) designated "PTBee" (cp. Fig. 1, 2) a few stand out:

- smooth pre-planned and highly precise operation, also in adverse (e.g. windy) weather conditions
- Electromagnetic Compatibility (EMC) issues
- necessity to calibrate the receiving antenna factor
- various electrical requirements
- quick exchange of batteries

Electromagnetic Compatibility (EMC) issues were of particular importance. On the one hand, motor speed controller switching and high motor lead and battery currents have the potential to cause internal EMC problems such as affecting the magnetic sensor controlling the yaw angle, but also to cause interference with the fields to be measured, especially at frequencies up to a few hundred MHz. On the other hand, it is intended to fly in electromagnetically saturated environments, e.g. at airports or in the vicinity of a radar. Therefore, shielding against high power RF external sources is a basic requirement to protect the UAS itself. This shielding will also reduce inherent emissions from the UAS. Since payload weight and dimension is limited on all flying platforms, the shielding has to be of light weight. To reach the defined safety limits, all electronic instrumentation need to be encapsulated by the shielding, including motor controllers, flight and navigation controllers, data sampling/storage unit and batteries. To prevent overheating of the now internal electronics, a mesh shielding was designed that allows for some air flow. Another advantage of the mesh shielding is that the internal barometric pressure sensor of the UAS contributing to the height information relative to the ground level is not affected.

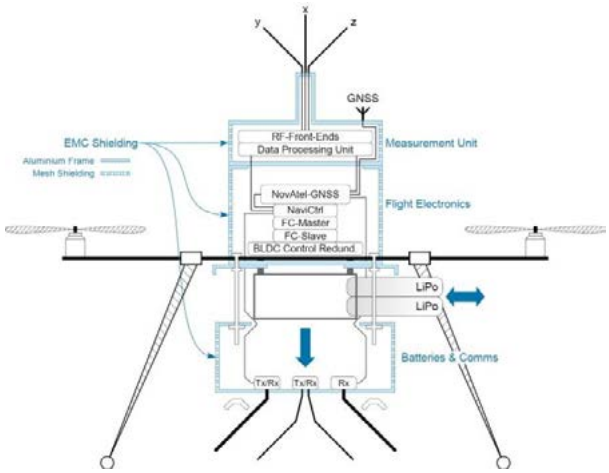

Fig. 1: Mechanical setup of the UAS with the battery tray opened

A low-weight aluminum frame with top and bottom plates and with mesh inserts forms the outer body of the shielding that takes all of these conditions into account. The top plate also serves as mounting pad for the different sensing heads and the GNSS antenna. The inner part of the bottom plate can be unlocked and released, thereby providing access to the battery compartment. A quick exchange feature was designed for the shielded battery. The outer ring of the lower plate serves as support for the antenna of the remote-control receiver, the downlink for the flight status to be received by a smartphone application, and the uplink for a potential differential navigation correction signal. All input and output signal paths are filtered using narrowband band pass filters.

Fig. 2: Photograph of electromagnetically shielded octocopter.

PRECISION NAVIGATION USING RTK

The navigation capabilities include a state-of-the-art NovAtel OEM615 global navigation satellite receiver [4] (GNSS: GPS+EGNOS, GLONASS) and ground differential correction transmitter to enable precise localisation of the UAS. Platform stability is granted by hybridization of GNSS with

motion and rotation sensors of an inertial navigation system (INS). This forms a real-time kinematic (RTK) capability at a sensor update-rate of 20Hz that controls the eight rotors.

A major advantage of such UAS is their ability to approach predefined waypoints (WP) (cp. Fig. 3), a point in space (WGS84 format horizontally and height above ground), and to trigger some action when the WP has been reached. A software tool [5] uses geo-referenced satellite images as maps to define the WPs. Once defined, the WP data is transmitted to the UAS with all necessary parameters such as horizontal and vertical (ascending/descending) speed, waypoint radius (WPR), dwell time at the waypoint, steering of the UAS towards a fixed cardinal direction or towards one or a set of predefined points of interest (POI). After the automatic start procedure, the microcopter moves to the first WP. The predefined WPR between 1 m and 10 m determines the region in space around a WP, where the navigation controller assumes that the given waypoint has been reached.

Fig. 3: Flight track with waypoints (WP) and point of interest (POI)

During its operation the UAS transmits the current position of the UAS including the altitude above ground, the time stamp, and the validity of the measurement data using another radio link. This flight log data can be displayed in real-time on an Android-based smartphone, for which an application has been written.

SIGNAL RECEPTION AND PROCESSING

RF front-ends and antennas

A variety of linear antennas has already been developed for different frequencies and applications. For simplicity, the radiation pattern of each antenna should be as close as possible to an ideal, electrical short, linear antenna [7]. Since the radiation pattern is not ideal, a model for real antennas has been developed. The signal of the real antenna is modelled as a superposition of the signals of an ideal isotropic and an ideal linear antenna. The parameters for this model are again determined through calibration in a known electrical field.

At a later stage it is intended to measure the field strength of three probes where each probe is sensitive for one field component in an orthogonal system. Hence, the data processing unit is capable to sample up to three received signals at full coherence. This allows to calculate the electrical field vector. Consequently, scalar or two-dimensional measurements are also possible.

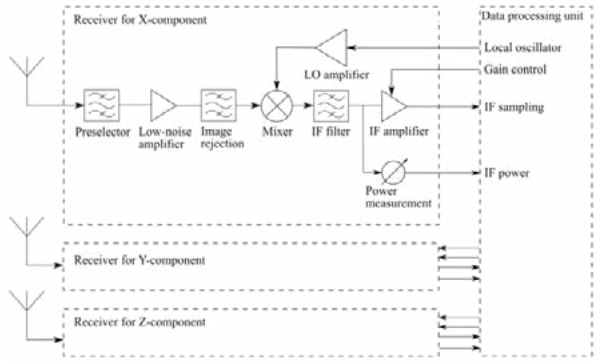

Fig. 4: Block diagram of the RF frontend.

For the various CNS radio bands different RF frontends can be connected to the data processing unit in a modular fashion using the same electrical and mechanical interface (Figure 4).

Signal processing

The RF signal is amplified, filtered and down-converted to an intermediate frequency (IF) using a local oscillator (LO) signal from the data processing unit. The IF signal is then filtered by a Surface-Acoustic-Wave (SAW) filter to suppress undesired mixing products and adjacent RF channels. The IF signal is sampled and stored by the data processing unit using a fast analog-to-digital converter (ADC) and a solid-state disc (SSD) as mass storage device. All further signal analysis that is required to demodulate the signal's content is performed in post-processing using software-define radio (SDR) algorithms after the data has been copied from the SSD. Working on the raw band pass samples allows a maximum of flexibility to derive the relevant information from the signal-in-space. This post-processing is performed through specific algorithms implemented in the C++ language.

An embedded processor hosted on a FPGA-based design manages the data streams from various sources. Fully time-synchronized position information is obtained from the RTK and recorded as well.

To ensure a high dynamic range a digital automatic gain control (AGC) drives variable gain amplifiers (VGA) in the IF section. Highly integrated amplifiers are used for the receiver providing sufficient overall gain, low noise figure, and high bandwidth. The entire system is fully phase-coherent: A single, stable crystal oscillator drives all frequency-dependant components such as ADC clock and LOs.

Undersampling technique

According to the Nyquist criterion the sampling frequency needs to be twice the signal bandwidth to prevent aliasing:

$$f_S > 2\Delta f \qquad (1)$$

Undersampling corresponds with the use of a sampling frequency which is less than the highest frequency present in the signal. In Figure 5 (taken from [5]) this principle is illustrated in the frequency domain. Signals below $0.5f_S$ are located in the so-called first Nyquist Zone (NZ), see (A). Sampling these signals preserves their original carrier frequency. The number of NZ increments by every $0.5f_S$. Frequencies higher than half the sampling rate are folded back into the 1st NZ. Hence, a signal located in any higher NZ will give an image in the first NZ (B, C). No signal information is lost except for the value of the original carrier frequency f_C. An additional frequency reversal occurs if signals are located in even Nyquist zones (B).

If equation

$$f_S = \frac{4f_C}{2NZ-1} \qquad (2)$$

Applies, then the image of f_C is safely placed in the center of the first NZ (= 0.25 f_S) [6].

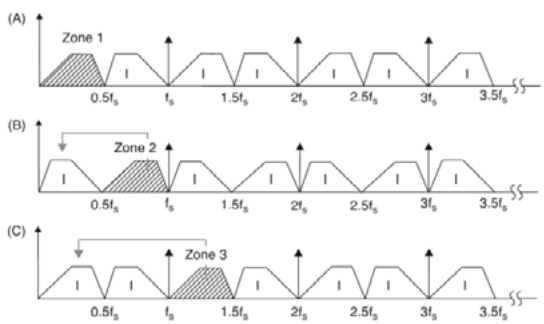

Figure 5: Nyquist zones and frequency translation [6]

The primary function of an anti-aliasing filter is to ensure that the band of sampled signals must not overlap any multiple of $f_S/2$, i.e. it is limited to a unique Nyquist zone. For this purpose, a steep SAW band pass filter is placed in the receiver's IF section. The ILS LOC/VOR RF frontend offers a 70MHz IF. After further amplification on the digitizer board, this signal is then initially sampled at 95MHz. This converts the IF into the second NZ, resulting in an image in first NZ at 25 MHz. A chain of FIR (Finite Impulse Response) decimation band pass filters inside the FPGA then reduces the sampling rate dramatically by the factor of 54, but finally it remains well above twice the channel bandwidth of VHF navigation facilities (<25 kHz) when stored on the SSD.

FLIGHT TESTS AND RESULTS

First tests were performed to receive VHF RF channels using a single horizontally polarized short dipole as shown in Figure 9.

ILS LOC

At Braunschweig airport (EDVE) trials to receive the ILS 2F-localizer were performed. These flights took place while hovering above the threshold of runway 26. Since the raw band pass signal is recorded, the specific signal contents of course and clearance components can be shown separately. As an example, the LOC frequency spectrum at high resolution at a specific point in flight time for both signal components is shown in Figure 6. A sliding window over the band pass signal defines the number of ADC samples that feed a Short-Time Discrete Fourier Transformation (STDFT) that visualizes the spectrum.

On centerline the CRS signal is significantly stronger than CLR (ratio >20dB, height dependant), therefore signal-to-noise ratio of CRS is also higher which can be read from the curves.

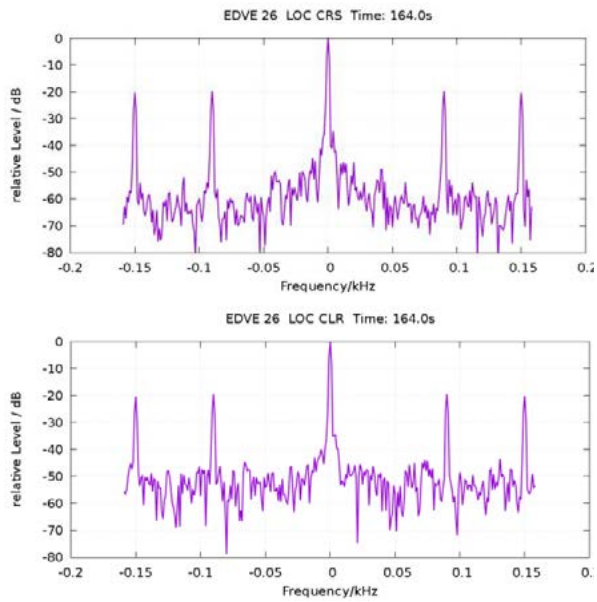

Figure 6: Spectrum of Localizer Course and Clearance gained from band pass signal

In the time domain, the DDM can be derived from the band pass signal by simply demodulating the 90Hz and 150Hz tones using appropriate SDR algorithms.

During a hovering maneuver perpendicular to the centerline at threshold 26 the computed DDM of the right half sector (mod. 150Hz > mod. 90Hz) is given by Figure 7. The left Y-axis gives the displacement angle of the microcopter position against centerline (purple curve), whereas the right Y-axis depicts the DDM.

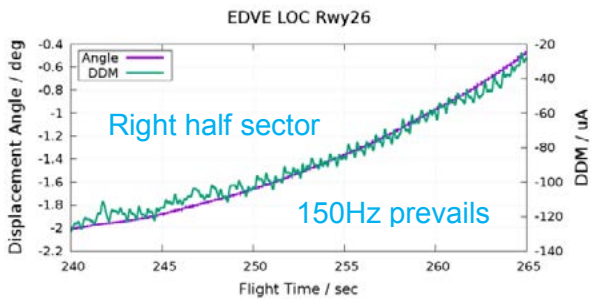

Figure 7: Unfiltered raw DDM of right half sector during hovering flight at THR perpendicular to centerline

A non-linear increase of the raw unfiltered DDM (green) curve can be observed since the flight path was perpendicular to the centerline and not a part of an orbit.

Doppler VOR

Using the data gained from microcopter flights, also radiations from VOR facilities can be assessed showing a large amount of details that conventional flight inspection cannot provide.

In case of a Doppler VOR, it is now possible to fully separate the signals from the center antenna (30Hz AM reference) and the sideband antennas (SBO, 30Hz FM azimuth dependant).

The SBO signal will be analyzed by measuring the frequency deviation of the 9960Hz carriers. As well known, a full 360° turn of the SBO gives one period of a 30Hz oscillation. In Figure 8 the X-axis of the diagram has 50 time slots which corresponds to current DVOR facilities in Germany that have 50 sideband antennas. Within these time slots, the application of the STDFT results in the FM frequency deviation up to 480Hz (left Y-axis) and the amplitude (right Y-axis). Actually, Figure 8 shows a reference curve with a synthesized VOR signal in a lab, which is done for calibration purposes. The 30Hz tone curve deviates from a perfect sine since the number of samples per time slot and therefore the resolution of the STDFT is limited (here: ~1200). Over the period, the amplitude reveals some variances within 0.5dB. This is also due to the resolution limitations across the very short slot observation time of 1/(30*50)sec = 0.67msec .

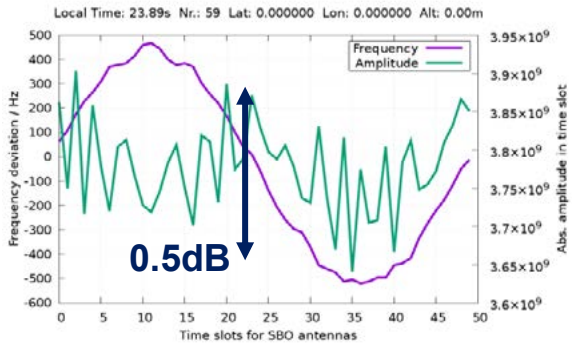

Figure 8: VOR 30Hz SBO frequency deviation in 50 time slots

Figure 9: Reference measurement on ground close to DVOR HLZ

Next, a real signal-in-space of 'DVOR Hehlingen' (HLZ) was recorded on the ground close to the transmitter as shown in Figure 9.

During a 30Hz period, the SBO radiation takes place from the different antenna positions above the counterpoise. A significant variation of the field strength over one full rotation is expected. This behavior is shown in Figure 10: The signal strength varies over roughly 6dB and reveals two significant maxima and minima. In fact, the diagram shows an overlay of the Lower sideband and the Upper sideband antenna. So there are always two opposite antennas which have nearly the same radiation characteristics from the receiver's point of view.

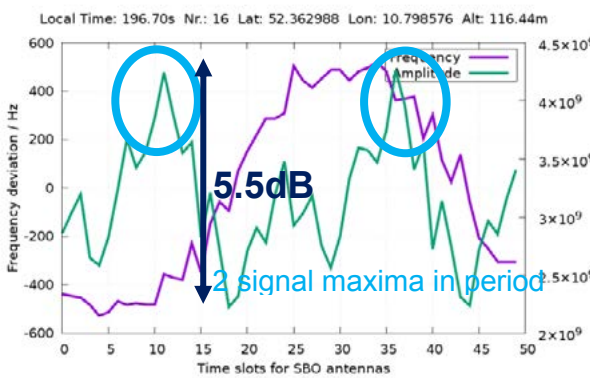

Figure 10: Characteristic Doppler shift and level of DVOR SBO antennas on ground

Even more interesting is the course of the 30Hz tone derived from the frequency deviations. A significant distortion becomes apparent in this unfiltered view (purple curve). The time slots are not synchronized to the antenna numbers, and within one time slot not a single SBO antenna but a mixture of two of them is active due to the SBO blending modulation. But it can be clearly observed that the increase and the decrease of the frequency deviation within 480Hz does not consist of monotone steps. From one slot to another, instead alternating step-ups and step-downs are present in the unfiltered curve. Applied to numerous succeeding pictures of the 30Hz Doppler rotations, comparable to a motion picture, these diagrams always show the same characteristics.

However, in a navigation receiver the 30Hz tone that must be precise in phase will be reconstructed by band pass filtering to ensure the well-known DVOR performance.

These VOR measurements in the lab and on ground provide an overview of the expected performance, before some more degrees of freedom are introduced by the hovering octocopter platform. These measurements were subsequently carried out in the surrounding of DVOR HLZ. In Figure 11 the received center antenna signal level (purple, left Y-axis) and the flight altitude (WGS83, right Y-axis) over flight time at a specific point (constant radial) is shown during the octocopter ascent. At 120sec, a significant level variation becomes visible. These notches are due to the vertical pattern of the DVOR center antenna over the counterpoise and terrain. An example of the already introduced switching behavior of the SBO antennas at free line-of-sight to the DVOR is given by Figure 12. Frequency and amplitude curves show similar characteristics as already seen on the ground (cp. Fig. 10).

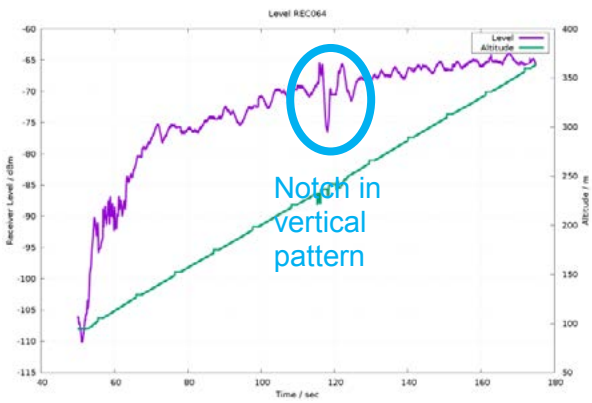

Figure 11: DVOR signal level of vertical octocopter flight

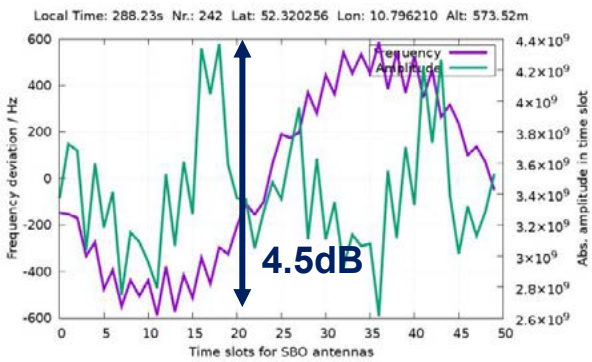

Figure 12: SBO switching as signal-in-space during octocopter flight

Moving the octocopter to a position where the Fresnel zone of free space radiation is affected by a rough edge (forest), some anomalies occur in the signal-in-space as shown by the frequency deviation diagrams: In Figure 13 the Doppler frequency steps (purple) vary much more from the known course in free space or on ground. Especially in slot 25, a strong positive frequency step (marked) to +250Hz occurs. Simultaneously, there is a significant decline in signal amplitude, so that the overall dynamic increases to 8.5dB, compared to 4.5dB in Figure 12.

As more of these anomalies occur in numerous succeeding 30Hz Doppler rotations, the more the phase is affected and slightly shifted. This will eventually contribute to a bearing error as experienced by an aircraft using the DVOR for navigation.

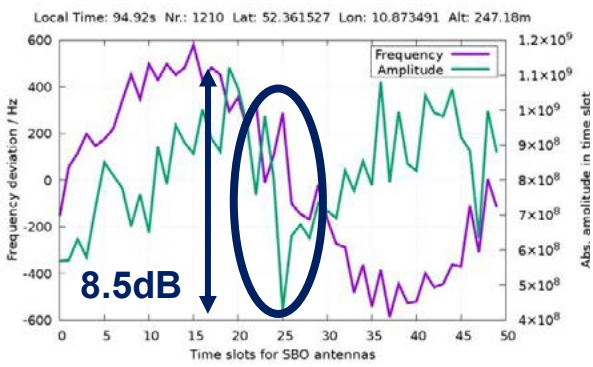

Figure 13: Anomalous SBO switching received in some slots due to multipath propagation

All in all, this shows the complexity and the differences in radiation of the single SBO antennas of a Doppler VOR.

It is the purpose of this new measurement equipment to reveal these signal-in-space anomalies which in turn will for example allow to precisely locate the nature of the source of a Navaid's signal degradation.

GBAS

As the receiver is suitable for VHF navigation band, a useful application may also be the measurement of the GBAS signal-in-space. Just for testing purposes, the transmitter at Braunschweig airport (117.95MHz) was recorded as a band pass signal. Using the STDFT, a spectrum of the signal around the center frequency was computed that is shown in Figure 14. Since the GBAS transmission is time-slotted (16 slots/sec) and the observation time for the spectrum was 1sec, the result for one specific slot may vary. Existing data can be used to synchronize the beginning of a time slot with demodulated D8PSK contents, but this was not done for this paper. Future application may derive the absolute field strength and the bit error rate at specific positions in air space.

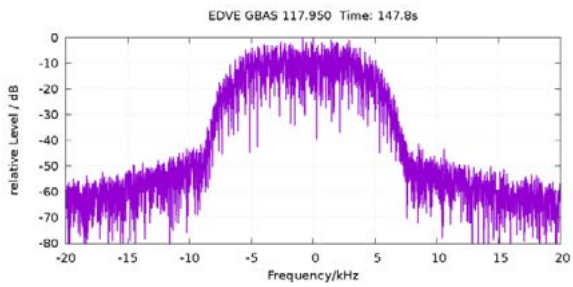

Figure 14: IF spectrum of GBAS during octocopter flight

CONCLUSIONS

A new method based on a UAS octocopter platform was introduced to measure the signal-in-space of Navaids and GBAS. The successful, technologically highly challenging design and integration a small commercially available UAS with an FPGA based high bandwidth multi-channel recording system, calibrated antennas, high-performance receivers and the design elements necessary to operate the octocopter in the vicinity of wind turbines and NAV or radar systems provides a so far unknown high level of insight into RF signal behavior and propagation-related interaction with the topographic context of the ground installation. Due to their small size and hovering capability such systems are well suited to supplement conventional flight inspection. Especially where prolongued observation times of the SIS are required and/or conventional aircraft are unable to reach the measurement positions of interest, the UAS described will allow to obtain the relevant data.

The precision flight paths along predefined waypoints were provided by a real-time kinematic localization system with 20 Hz update rate. The experience so far is that even in heavy wind conditions the octocopter was stable and safe to operate.

The system still has a preliminary design status and further flight tests and design work will be required to achieve all initial design requirements and to fully explore the potential of this new and exciting technology.

UPCOMING WORK

Implementing full three-channel usage will further extend the capabilities to obtain a 3D field vector representation of the measured signals.

A process will be developed to calibrate the overall platform and its antenna factors to SI units, thus allowing a transition from (relative) receiver levels to absolute field strength values.

Further validation measurements using reference dipoles on the open area test site of PTB will improve the confidence in the overall results and the specified operational measurement uncertainty, in compliance with the introduction and usage of specified uncertainties according to [8].

REFERENCES

[1] ICAO Annex 10, Volume I, Radio Navigation Aids, Sixth Edition, July 2006

[2] ICAO DOC 8071, Volume I, Testing of Ground-based Radio Navigation Systems, Fourth Edition – 2000

[3] Schrader T.; Bredemeyer J.; Stupperich C.; Garbe H., "WERAN – Interaction of Wind Turbines with Terrestrial Navigation / Radar Systems," in Electromagnetic Compatibility (EMC), 2015 IEEE International Symposium on, WS14 "Unmanned Aircraft Systems – EMC and Applications," 16-22 Aug. 2015

[4] NovAtel, "Positioning Modes of Operation," Application Note, Rev. 1, 24 Oct. 2013

[5] HiSystems, http://www.mikrokopter.de, 2015

[6] Zumbahlen, H. (Ed.): Linear Circuit Design Handbook, Analog Devices, 2008

[7] Balanis, C.:"Small Dipole" in Antenna Theory, 3rd ed., Hoboken NJ, John Wiley & Sons Inc., 2005.

[8] JCGM 100:2008. Evaluation of measurement data — Guide to the expression of uncertainty in measurement (GUM)

IFIS2016

Bringing Together Theory and Practice

Session 11

Flight Inspection Standards

A Brief History of Flight Inspection System Technology

Larry Brady

Airfield Technology, Inc.
Olathe, Kansas USA
E-mail: Lbrady@airfield.com

ABSTRACT

This paper provides a brief history of flight inspection system technology, starting with the earliest days of pilot-only assessment, progressing through analog instrumentation and visual ground position checkpoints up to modern, computer based systems using digital receivers with small measurement uncertainties and centimeter level positioning systems.

INTRODUCTION

The need for flight inspection began with the introduction of ground-based navigation aids (navaids). The earliest navaids served exactly the same purposes then as now: to assist pilots in navigating between desired locations (the enroute phase) and approaching and landing at the desired destination (the terminal phase).

Prior to the establishment of any formal navaid infrastructure pilots relied on visual landmarks to determine their position, sometimes augmented with road maps and conventional land navigation. The remaining constraint then, as it is today, was limited visibility most often caused by darkness and/or clouds.

As is usual in the development of any technology, financial and military concerns were the driving factors behind finding a better way to navigate an aircraft.

Although the inventions of the telegraph (1832) and telephone (1860) and their subsequent and widespread use had remarkably changed the way people communicated, paper remained a formidable and required necessity for business and politics. There was also some semblance of security still afforded by placing a wax seal on the outside of an envelope that was not afforded by the wired methods.

One of the earliest non-military applications for which aviation was intensely promoted and would quickly become a household term was: “Airmail”.

EARLY VISUAL NAVIGATION AIDS IN USA

Fire

The earliest ground-based navigation aid was also one of mankind’s earliest adaptations… Fire! As early as 1919 the U.S. Army Air Service began using bonfires to assist pilots in navigating at night.

Airways Beacons

During the 1920’s and 1930’s the United States government built an extensive infrastructure of lighted airways mainly to support the fledgling airmail service.

Figure 1. Airways Beacon, circa 1930 (public domain)

In the USA these airways beacons were installed on 15 meter towers spaced approximately 25 to 40 kilometers apart. They were visible for approximately 60 kilometers in clear weather.

These airways consisted of fixed course lights and rotating beacons, and later included spotlights to indicate wind direction. Directional arrows constructed from concrete identified and pointed the way for daytime operations.

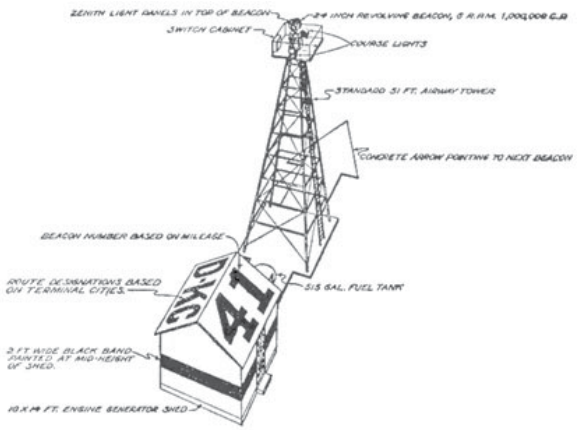

Figure 2. 1931 - Airways Beacon Installation (public domain)

Radio voice communications were being developed and put into use during this same period of history. This was critically important in order to get current weather information to the pilots.

Regularly scheduled airmail operations at night started in 1924 and by 1933 there were approximately 29,000 kilometers of airways and 1,500 beacons installed in the USA.

EARLY RADIO NAVIGATION AIDS IN USA

Four-Course Radio Range

In 1929 the Four-Course Radio Range was made the national standard in the USA. With this system the pilot listened to an audio signal to navigate. An alternating Morse code signal of "A" (dot-dash) and "N" (dash-dot) was heard on either side of the course, and on-course a continuous tone was heard. In addition an identification signal was broadcast every 30 seconds.

The four-course radio range was quickly adopted by the government and a large infrastructure was installed throughout the country.

Check pilots were required to inspect the signals to confirm they provided adequate coverage and proper alignment. Formal flight inspection of the airways equipment was established in the USA in 1932.

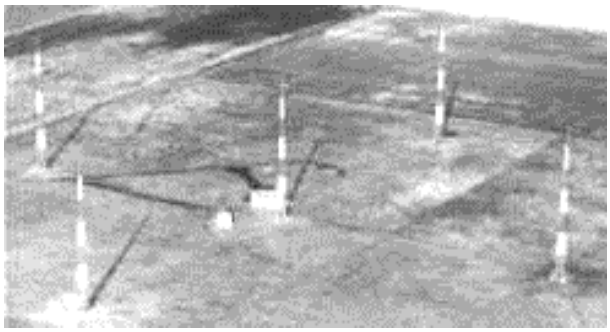

Figure 3. The last remaining US four-course radio range system in Northway, Alaska was removed from service in 1979 (public domain)

Automatic Direction Finding (ADF) and Non-Directional Beacons (NDB)

Heinrich Hertz discovered radio direction finding in 1888 when he found that an open loop wire antenna had directional properties. Other milestones included:

- 1902: John Stone patents first direction finding system
- 1904: Lee de Forest patents improved direction finder
- 1909: Ettore Bellini and Alessandro Tosi patent improved direction finding system
- 1919: Frank Adcock patents an improved direction finding antenna

In 1931 the US Army Air Corps began testing a primitive radio compass that used commercial stations as the beacon. Manually operated loop antennas allowed for aircraft-based direction finding (homing).

Between 1939 and 1946 William Lear received a series of patents for radio compass advances which led to development of the Automatic Direction Finder (ADF) and Radio Magnetic Indicator (RMI). This set the stage for implementation of an NDB navaid infrastructure.

Figure 4. Lear Radio Compass (public domain)

INTRODUCTION OF VHF AND UHF RADIO NAVIGATION AIDS

Instrument Landing System (ILS)

In the 1930's development of various types of radio navaids for approach and landing proceeded in the United Kingdom, Germany and the USA.

The ILS as we know today derived from the SCS-51 Instrument Landing System, which owes a portion of its technology to the British Standard Beam Approach (SBA). The SBA did not have a glide path component but did introduce outer, middle and inner markers to indicate distances, approach fixes and crossing heights.

In 1939 the USA Civil Aeronautics Administration (forerunner of the FAA) began development work at the CAA Experimental Station in Indianapolis, Indiana on what would become the standard Instrument Landing System.

Following World War II representatives from 52 states met in the USA at Chicago in an early attempt to find common ground on aviation standards. On 7 December 1944 the "Chicago Convention" was signed, leading to the establishment of ICAO on 4 April 1945.

In October 1945 ICAO recommended ILS as the standard approach aid and formally approved it in 1949.

Figure 5. Circa 1940 – Early ILS equipment (from Chester Watts collection)

Much of the radio navigation development work in Germany used lower frequencies. Nevertheless the technology developed in the various states had a lot in common. The indicator instrument shown below is clearly an ancestor of Course Deviation Indicators (CDI).

Figure 6. 1943 - Luftwaffe AFN 2 indicator (public domain)

VHF OmniRange (VOR)

FAA initiated development of VOR in 1937 and the first equipment was delivered 1944. World War II delayed widespread installation until the late 1940's and early 1950's. The first VOR was commissioned in 1947 and the first "Victor" airways were established in 1950.

Figure 7. Circa 1950 – Early VOR ground equipment installation (from FAA archives)

EXAMPLES OF PREVIOUS GENERATION FLIGHT INSPECTION SYSTEMS

United States CAA / FAA

At the CAA Indianapolis station a Boeing 247-D aircraft was modified to add flight inspection equipment to support the ILS development work.

In addition to the flight inspector's instrumentation an auxiliary set of instruments was installed for demonstration purposes, and a couch was placed along one side for observers.

ILS and other navaids still under development were demonstrated to delegates to the then provisional ICAO during this time period.

The Boeing 247D, tail number NC-11, was retired in 1952 and put on display in the Smithsonian Air and Space Museum.

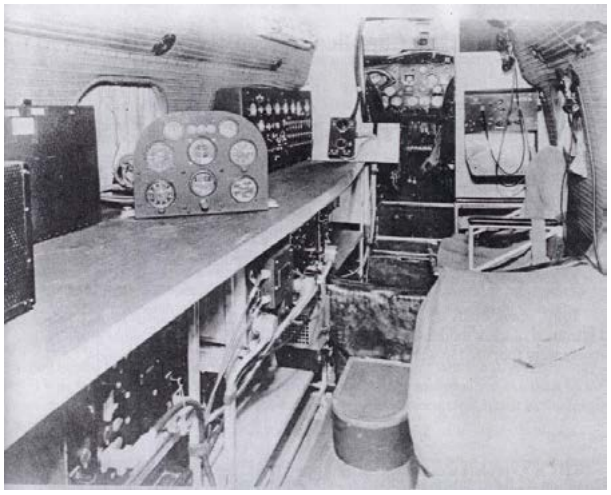

Figure 8. 1940's USA CAA flight inspection equipment and demonstration instrumentation (from Chester Watts collection)

Figure 9. 1940's USA CAA Boeing 247D flight test aircraft (from Chester Watts collection)

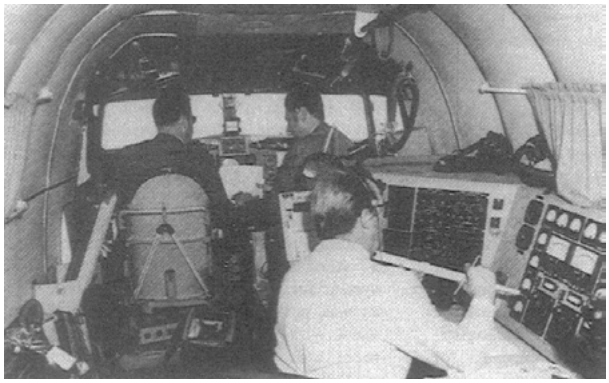

Figure 10. FAA flight inspection equipment installed in DC-3 aircraft (from FAA history office)

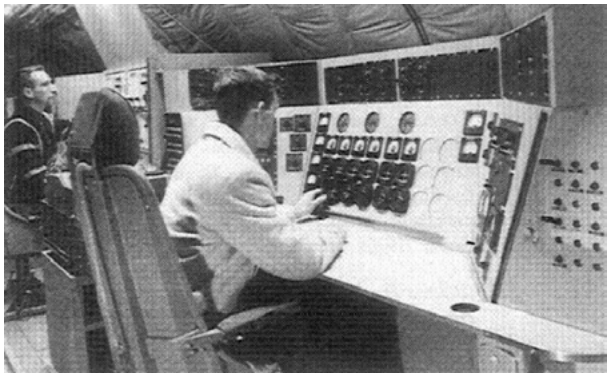

Figure 11. FAA SAFI flight inspection system installed in C-135 aircraft (from FAA history office)

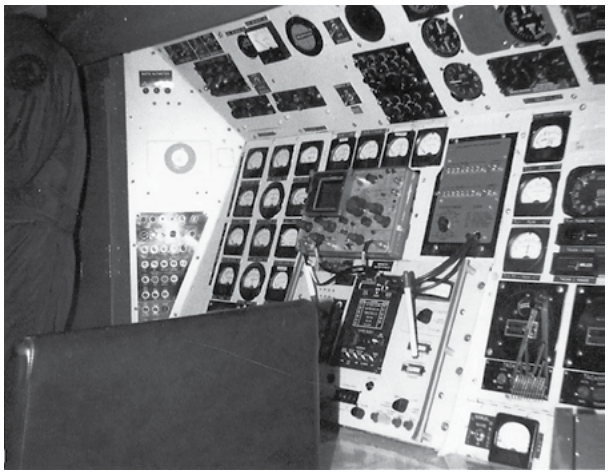

Figure 12. 1986 – USAF flight inspection system installed in C-140A Jetstar (note 10-point dividers) (from USAF Flight Check Facebook Page collection)

United Kingdom CAFU

Figure 13. Circa 1952 UK CAFU flight inspection equipment installed in Dove aircraft (from Flight International magazine archives)

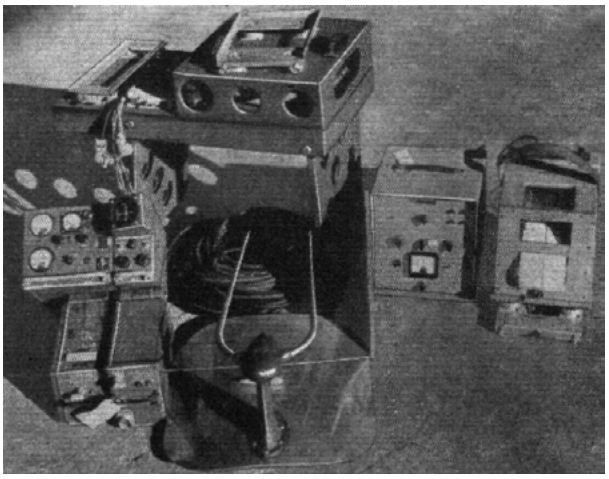

Figure 14. 1952 UK Portable flight inspection system weighing approximately 50 kg (from Flight International magazine archives)

Figure 15. UK CAFU FIS installed on Avro HS-748 aircraft (from Jim Fuller collection)

Figure 16. UK CAFU FIS installed on Avro HS-748 aircraft (from Jim Fuller collection)

Australia Department of Civil Aviation

Figure 17. Circa 1954 Australia DCA flight inspection equipment, port side surveyor's station (courtesy Civil Aviation Historical Society, Inc.)

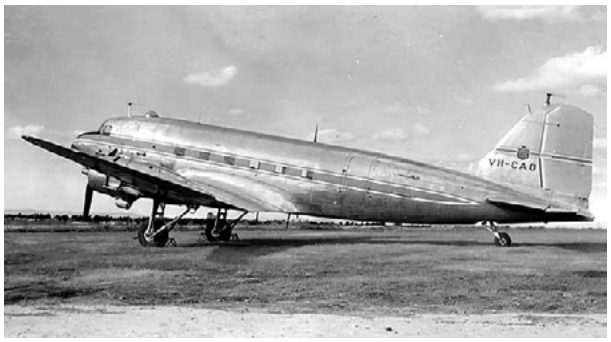

Figure 18. 1954 - Australia DCA flight inspection DC-3 which began life as a C-47A (courtesy Civil Aviation Historical Society, Inc.)

…

Figure 19. Circa 1954 Australia DCA flight inspection equipment, starboard side surveyor's station (courtesy Civil Aviation Historical Society, Inc.)

Figure 20. Airservices Australia flight inspection equipment installed in Fokker F28 (courtesy Civil Aviation Historical Society, Inc.)

New Zealand Civil Aviation Branch / National Airways Corporation

The New Zealand authorities operated a locally constructed flight inspection system on-board a Fokker F27 aircraft from 1971 through 1991.

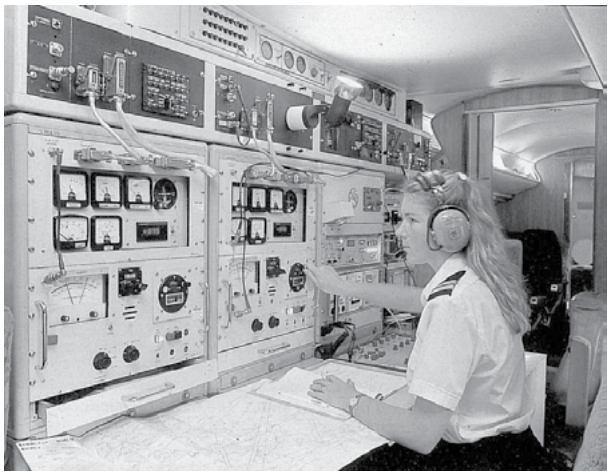

Figure 21. Circa 1985: Airways Corporation of New Zealand locally manufactured flight inspection equipment (from Carole Thompson collection)

FLIGHT INSPECTION AVIONICS SENSORS

General Trends

Avionics sensors for flight inspection have followed the same general trends of improving technology as most electronics devices:

- Vacuum Tubes (Valves)
- Transistors
- Integrated Circuits
- Microprocessors
- Digital Signal Processing

Ground/Air System Development

The development of most conventional ground-based radio navaids (ILS, VOR, DME, TACAN) by necessity was through a "system approach" in that simultaneous design of both ground and airborne components was required. The first flight inspection avionics sensors, as well as the navaid ground equipment, were still prototypes during the initial development efforts.

As the navaid systems were approved and put into use it was typical that avionics sensors used for flight inspection varied only slightly from production units. It was common to add outputs to the avionics in order to monitor additional receiver parameters during flight inspection.

Divergence of Ground / Airborne Designs

The standards established for ground navaids and avionics were essentially conventions based on the initial development results.

As the technology matured for each type of navigation aid, the designers and manufacturers of the ground equipment and avionics, who worked at different companies, would come to rely on the standards and communicate less with each other.

When a manufacturer would introduce some new technology to the ground or airborne equipment, although the change might satisfy the existing standards there still could be unintentional and detrimental results.

In some cases this divergence led to problems; some examples are listed below and have been documented in previous IFIS papers by others:

- ILS transmitter carrier frequency synthesis and residual frequency modulation
- IF bandpass ripple in LLZ receivers
- DDM normalization algorithms in ILS receivers

Avionics Selection

Development of fully custom avionics sensors for flight inspection would be a very expensive process. Therefore standard manufacturer avionics designs have been used in two ways for flight inspection:

- Modify a standard avionics sensor to extract additional required signals for flight inspection and apply signal processing.
- Commission an avionics manufacturer to modify a standard avionics sensor to transmit flight inspection parameters digitally.

Some widely used examples of manufacturer modified avionics sensors for flight inspection include:

- Rockwell-Collins 51RV(x)
- Bendix / Honeywell RNA-34(x)

It is worth noting that both of these commonly used flight inspection versions have discontinued in recent years.

Multi-Mode Receivers (MMR)

In the early 2000's the avionics manufacturers promoted the concept of "Multi-Mode Receivers (MMR)" which integrated the primary required onboard avionics functions needed for navigation and landing into a single box. The main selling points were that the MMR would reduce aircraft operating costs by (1) reducing overall size and weight and (2) simplifying and speeding up line-level maintenance. Certain MMR avionics have been adapted by some FIS manufacturers.

Navaid Ground Test Equipment as Avionics Sensors

Over the past decade or so certain pieces of test equipment which were designed primarily as navaid ground test equipment have been adapted for use as flight inspection avionics sensors.

While this shows some promise there are certain tradeoffs which should be carefully studied and considered before relying on this type of equipment as the primary avionics sensor for flight inspection. Some FIS have used the test equipment in conjunction with TSO certified avionics sensors in order to take advantage of the additional functions while retaining a certified sensor for reference.

POSITION REFERENCE EQUIPMENT

The position reference for flight inspection is critical as it provides the "truth source" for aircraft position so the signals received from the navaids may be evaluated for accuracy and coverage.

Visual Reference

The earliest method was visual positioning of the aircraft with respect to some known waypoint. This of course is useful only for azimuth navaid evaluation.

Prior to widespread use of GPS for flight inspection the ground checkpoint method was commonly used for inspection of enroute navaids and other coverage checks beyond the range of ground tracking capabilities.

FAA still authorizes localizer alignment inspections for any ILS Category using a visual reference. From FAA 8200.1 par 15-11f(4):

> ***Localizer.*** *The use of a theodolite, AFIS, or RTT is not required for any inspection on a localizer sited along runway centerline, regardless of category, providing performance can be satisfactorily evaluated by flying a visual centerline track.*

Tapeline

This method determines aircraft position relative to the navaid being inspected using time and distance calculations. Altimeter readings and local barometric observations are used to calculate vertical angles.

Theodolite (Manual Operation)

Theodolites have been an intrinsic part of commercial aviation since the beginning as they were used with "pilot balloons" to measure winds aloft.

In the manual method of flight inspection with a theodolite the operator tracks the aircraft in real-time during the flight inspection run. The azimuth and/or elevation angles to the aircraft are recorded either on the ground or in the aircraft (depending on the method used).

Theodolite (Analog)

The Radio Telemetering Theodolite (RTT) was introduced around 1970 and provided a method for indicating and recording a continuous angular position in the aircraft via a radio telemetry link.

In a common RTT implementation potentiometers with 20 turns were coupled to the azimuth and elevation shafts of the theodolite. The pots were connected to an external RTT transmitter device. The RTT transmitter generated an ILS type signal based on the potentiometer position and transmitted it to the aircraft, typically at a carrier frequency of 329.00 MHz[1]

Figure 22. 1974 - USAF Theodolite operator during TACAN flight inspection at Bergstrom AFB (from USAF Flight Check Facebook Page collection)

[1] The most commonly used flight inspection data uplink frequency worldwide is 329.00 MHz. This is a standard ILS test channel (paired with localizer 108.10 MHz) that can be selected by all ILS receivers. This frequency was originally selected so a standard, off-the-shelf glide slope receiver could be used in the flight inspection system to receive, detect and output the RTT signals.

The theodolite operator adjusted the calibration of the RTT transmitter so that its reference "width" matched that of the ILS component being tested (LLZ or GP). It was centered on localizer centerline or at the glidepath angle. This allowed the use of basic analog circuits in the airborne equipment to compare the position reference (RTT) with the raw ILS receiver indication (deviation) using a Differential Amplifier circuit to measure the ILS error independent of small flight technical errors (aircraft flight path displacement from nominal). This method is the source of the term DIFF for the ILS error indication (in microamperes) which is used almost universally in ILS flight inspection.

Theodolite (Digital RTT)

The analog RTT equipment was subject to numerous equipment errors including drift with temperature and operator calibration error.

Improvements in the 1980's replaced the potentiometers with optical encoders and used digital circuits to measure the theodolite angles. Digitally modulated telemetry signals were also employed which provided better system integrity.

Photography

For some period the UK FACU used photography as a rudimentary position reference. Please refer to the paragraphs on Cameras in the section about Data Recording Devices later in this paper.

Laser Tracker

Laser trackers were employed primarily to remove the human error element inherent in manual tracking. Some laser trackers were able to measure distance also, thus providing three dimensional position.

As an optical device laser trackers suffer from the same visibility limitations as a theodolite. Clouds, rain, and smoke can interfere with laser tracker operation. Laser trackers also require special reflectors to be installed on the aircraft and these require careful maintenance and regular cleaning.

Infrared Trackers

Infrared trackers also were employed to remove the human error element inherent in manual tracking.

The UK FACU employed an infrared tracker as a position reference for inspecting ILS in the 1970's. This was an infrared device designed by the UK Ministry of Defence for tracking guided missiles.

Another infrared device originally designed for missile tracking was used by several organizations for ILS flight inspections. Several versions of this product were produced from the 1970's through the 1990's. The concept for this device originated in France and was further refined in the Netherlands.

Figure 23. Infrared tracking device used for flight inspection in UK (from Jim Fuller collection)

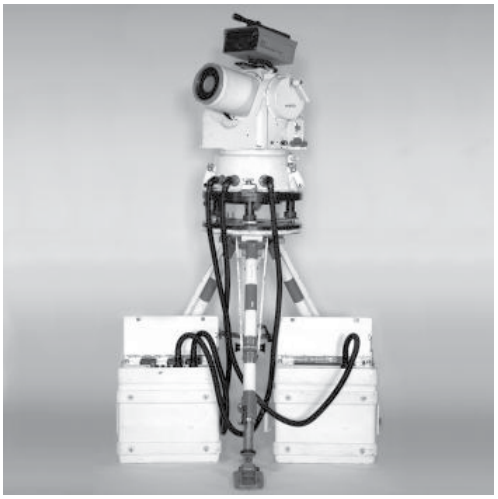

Figure 24. Infrared tracking device of French origin and Netherlands development (from Nicolàs de Hilster collection)

Multiple DME Triangulation

Some flight inspection organizations have used triangulation position fixing using multiple DME's. This method is limited in accuracy and therefore is only useful for less accurate requirements such as inspection of enroute navaids. It is sometimes used as an update source for inertial navigation based position reference systems.[2]

[2] ICAO Doc 8071 specifies DME reply delay measurement uncertainty for ground test equipment is ±1 µs. This equates to an actual DME range uncertainty of 150 meters (based on two-way radio propagation).

Inertial Navigation Units (INU)

Some flight inspection systems use inertial navigation units (INU) as the aircraft position reference. INU's calculate aircraft position using a double integration method. Instantaneous acceleration data from the INU sensors (accelerometers) are integrated over time to calculate velocity data, which are integrated over time to calculate position data.

The position calculation can only be as accurate as the known initial conditions, which are typically established at the runway threshold (where ILS flight inspection uncertainty requirements are most demanding). The calculation process has to be done after the initial conditions are established so there is a delay after an ILS approach while corrected data are calculated.

The method to establish the initial conditions for the integration algorithm has developed over the years. The first systems relied on an event switch pressed when the aircraft passed over the threshold and a radio altimeter measurement. This method was not very accurate and was later modified to use cameras to identify the runway end markings and also in some cases with laser height measurements.

While having the advantage of not requiring any ground equipment to be carried or setup at the local site, it is difficult for an INU based position reference system to meet ICAO 8071 requirements for ILS flight inspection measurement uncertainty near the runway threshold.

ICAO Doc 8071 specifies a measurement uncertainty for Category III glidepath of 0.009° for a 3.00 degree path angle. Calculating the associated vertical displacement indicates that a vertical position uncertainty of approximately 5 cm is required at the runway threshold.

GPS / DGPS

Currently the state of the art in position references for flight inspection is GPS and DGPS. These systems provide high accuracies (small uncertainties), excellent availability and all weather capability. With Real-Time Kinematic (RTK) phase-tracking DGPS systems it is normal to achieve position accuracies at the centimeter level.

For approach type inspections requiring high accuracy a local DGPS ground reference station is normally set up at the airfield. Some flight inspection operations have multiple ground reference stations which are sent ahead and setup by the navaid maintenance engineers before the inspection. In this way the aircraft does not need to land before starting the inspection.

One potential drawback to a GPS based position reference is radio interference. However, it is suggested that if this is the case then locating and eliminating the interference source would be a higher priority than the flight inspection mission.

Commercial SBAS

There is a commercially available SBAS (Satellite Based Augmentation System) which provides DGPS corrections over an L-band satellite data link. Originally developed to position oil drilling platforms at sea, the system has been adapted to other uses including precision farming and mining applications.

For flight inspection applications this system was found to have limitations that make it not too useful. The system requires approximately 20 minutes for the initial acquisition period in order to obtain a useful high accuracy position fix. Unfortunately if the datalink from the satellite is lost (for example while banking the aircraft) the acquisition period must start over again.

Attitude and Heading Data

In order to meet the ICAO 8071 measurement uncertainty requirements for position reference it is necessary to consider and compensate for the relative positions of the receiving antennas with respect to the position reference system origin.

For example, the GPS antenna is not located at the same position as the ILS Localizer or Glidepath antennas on the aircraft. The DGPS position reference system will provide a very accurate position for the GPS antenna, but to obtain the required measurement uncertainty it is necessary to calculate the relative positions of the Localizer and Glidepath antennas. This "coordinate transformation" calculation (sometimes termed "lever arm correction") requires accurate aircraft attitude and heading data.

Attitude and heading data are also required by the flight inspection system for applying antenna calibration data in order to measure accurately navaid power density (field strength) according to ICAO recommendations.

Heading data also is used in some FIS for automatic evaluation of NDB bearing indications. However, considering the accuracy of an NDB this might be a case where the phrase "measure with a micrometer, mark with chalk, and cut with an axe" applies.

USER INTERFACES

The user interface technology used in modern flight inspection systems has followed general trends in other industries and therefore the subject will not be discussed in this paper.

The foregoing photos provided of earlier generation flight inspection systems compared to modern equipment clearly illustrate the advances in user interface technology.

SIGNAL PROCESSING

The general FIS system architecture remains the same today as it was in the beginning: avionics sensor, signal processing, displays/indicators and recording devices.

Analog Signal Processing

In the earliest FIS equipment signal processing was basic and consisted primarily of analog amplification installed between the avionics sensors, displays (meters) and recording devices (chart recorders).

The purpose of the analog amplifiers was twofold: (1) buffering in order to prevent the external equipment from adversely affecting the internal avionics circuit functions, and (2) scaling of the avionics internal voltages/currents to easily understandable engineering units for the flight inspectors.

In the early generation flight inspection systems maintaining accuracy in the DC amplification circuits which used vacuum tubes (valves) was problematic and special instrumentation grade equipment was required.

Modern systems still require analog interface circuitry, whether located internal or external to the avionics sensor. The signal scaling requirements are somewhat different in today's systems; in addition to providing the desired accuracy another main objective is obtaining the optimum resolution from analog-to-digital convertors over the required dynamic range.

Timing and Data Synchronization in Modern FIS

In the early FIS designs the various analog sub-systems were connected together and timing synchronization was mainly dependent on cumulative low-pass filtering characteristics. The pen-type chart recorder was a significant contributor to the overall system frequency response.

Modern FIS collect data from multiple sources, mainly from various digital sub-systems. Most, if not all, of the various sub-systems operate asynchronously.

It is necessary that data from the avionics sensors are precisely synchronized with the position reference data. Otherwise time skew errors can occur which will contribute to the system measurement uncertainty.

This subject was discussed in detail in papers presented by this author and others at the IFIS 2010 in Beijing.

Digital Signal Processing (DSP)

Conventional navigation converters using analog circuits to measure ILS deviation and modulation had inherent instability due to component variations over the operating temperature range. The bandpass filters and other circuits contained resistors and capacitors whose values would change with temperature.

For ILS signals shifting of filter center frequencies and changes in passband ripple over temperature resulted in DDM and SDM variations.

By using DSP technology it is possible to reduce the analog hardware to a single A/D converter. The navigation converter circuits are replaced with DSP software and temperature variations are eliminated. This type of DSP technique is considered the most accurate method for measuring ILS deviation and modulation.

DATA RECORDING

It is important that the results of a flight inspection or procedure validation are permanently recorded to allow analysis and comparison of data after a run is completed. It is useful to have a record for quality control auditing and trend analysis. In the case of litigation recorded data is invaluable to provide evidence that all established procedures have been followed and reasonable care has been taken.

Pencil and Paper

This was indeed the first method of data recording during flight inspection. A pencil sharpener was a critical piece of equipment, and a careful observer may have noticed these installed near the operator console in early flight inspection aircraft.

Chart Recorder (Pen-Type)

The introduction of chart recorders to flight inspection between 1945 and 1950 allowed a continuous recording of parameters and thus was an improvement over the purely manual method. When first introduced chart recorders had only a single channel.

Figure 25. Early pen-type chart recorder (public domain)

The earliest pen-type chart recorders were temperamental under the best of conditions, and even more so when operated in environments like an aircraft cabin of that generation.

The FAA had made the early chart recorders available to other flight inspection organizations around the world. Apparently they were so messy during flight that some agencies believed FAA was sending them their rejects!

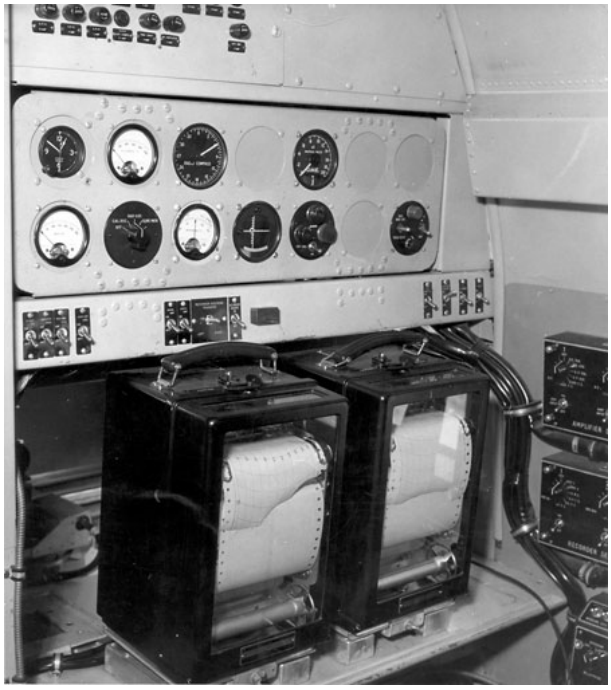

Figure 26. Circa 1954 –Australia DCA flight inspection dual equipment chart recorders (courtesy Civil Aviation Historical Society, Inc.)

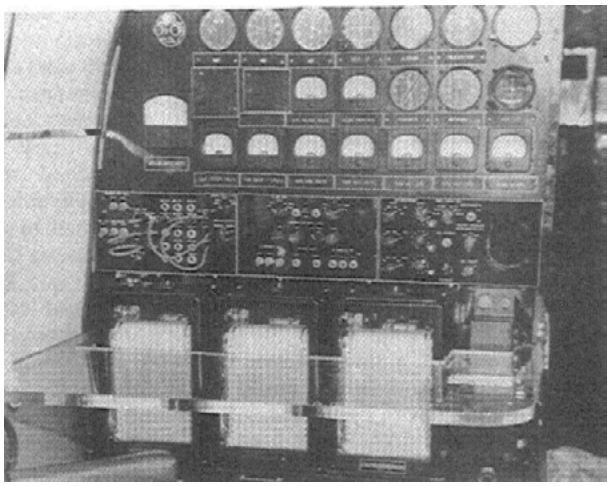

Figure 27. FAA chart recorders in DC-3 aircraft (from Ed Davies collection)

The chart recorder was part of the system calibration. A known input signal (for example 75 µA fly up) would be injected into the FIS receiver and the recorder gain adjusted so that a fixed number of divisions were indicated on the chart.

The charts were annotated and analyzed by the flight inspector during the inspection flight. Shown below is an annotated chart recording from an Ohio University flight inspection system.

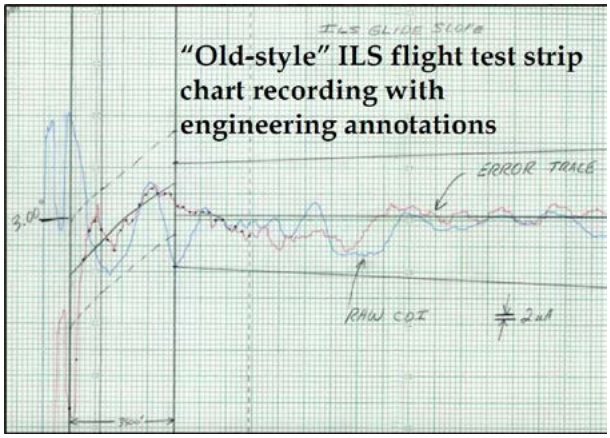

Figure 28. Circa 1983: Chart recording of ILS Glidepath (courtesy Ohio University Avionics Engineering Center)

Cameras

Some flight inspection organizations require the pilots to take photos of airfield lighting in order to document and backup their real-time visual observations.

In the early 1950's the UK FACU used cameras to create synchronous records of aircraft position and received navaid indications:

> *"The Doves, Princes and later the HS748's, all used the F.. camera which photographed marker boards on the ground. This camera was synchronised with an F.. 35mm camera in the cockpit which took simultaneous photos of the Instrument panel in order to help with the assessment of the calibration."*

Dot-Matrix Printers

In the 1980's some of the early computer-based FIS used dot-matrix printers as the real-time data recorder. This technology required custom software drivers to interface the FIS computers to the printers.

Chart Recorder (Thermal, Multi-Channel Digital)

Chart recorder technology was greatly advanced during the 1980's and 1990's with thermal, multi-channel digital units becoming the norm for flight inspection. The later generations of these recorders included as many as 32 channels, internal signal scaling and data logging capabilities.

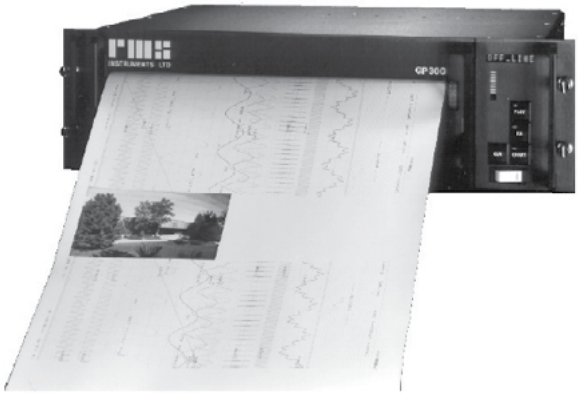

Figure 29. Advanced modern chart recorder (from Onorio Rocca collection)

Computer Non-Volatile Memory

By the 1990 virtually all new FIS design used some form of computer configured as a custom data acquisition system. Since then it has been common to store the flight inspection data on some form of non-volatile memory. Roughly in chronological order the memory devices have included:

- Magneto-Optical Drive
- Floppy Disk Drive
- Hard Disk Drive
- Solid-State Drive
- USB Memory Sticks

REFERENCES

Chester B. Watts, Jr. "Instrument Landing System Scrapbook, Landing Blind over the years 1940 to 2003", 2005

Thompson, Scott. "The History of Flight Inspection in the United States of America", 1990

Martyn Wills, "Perspective on Technology in Flight Inspection", Final Proceedings of 8th International Flight Inspection Symposium, 1994

James Fuller, "Safety Was No Accident – History of the UK Flight Unit", 2012

Larry Brady. "Timing Synchronization and Uncertainty in Flight Inspection Systems" International Flight Inspection Symposium, 2010

ICAO Doc 8071

ICAO Annex 10

FAA 8200.1

College Park Aviation Museum
http://www.collegeparkaviationmuseum.com

The Evolution of Airway Lights and Electronic Navigation Aids
http://www.centennialofflight.net/essay/Government_Role/navigation/POL13.htm

The Airways Museum & Civil Aviation Historical Society (Australia) web site
http://www.airwaysmuseum.com/

John Schamel. "The Development of Night Navigation in the U.S." web page
http://www.atchistory.org/History/nightnav.htm

World Heritage Encyclopedia, Automatic Direction Finder web site
http://www.gutenberg.us/articles/automatic_direction_finder

Nick A. Komons. "Bonfires to Beacons: Federal Civil Aviation Policy Under the Air Commerce Act, 1926-1938"
https://babel.hathitrust.org/cgi/pt?id=mdp.39015013920528;view=1up;seq=7

Wikipedia. "Low-frequency Radio Range"
https://en.wikipedia.org/wiki/Low-frequency_radio_range

Wikipedia. "Radio Direction Finder"
https://en.wikipedia.org/wiki/Radio_direction_finder

YouTube. "Navigation in the 1940s: The Four Course Radio Range"
https://www.youtube.com/watch?v=p-VqtNY8vpw

Charles Wood. "On The Beam" internet page.
http://www.navfltsm.addr.com/ndb-nav-history.htm

USAF Flight Check – Facebook Page
https://www.facebook.com/search/top/?q=air%20force%20flight%20checks

History of Flight Inspection in Canada
http://www.icasc.co/history/history-of-flight-inspection-in-various-countries/canada/

UAVs and Flight Inspection: should we brace for impact?

Fabrizio Maracich
Senior Captain
Crew Training Manager
Head of FIV STD
ENAV S.p.A.
Rome, Italy
E-mail: fabrizio.maracich@enav.it

ABSTRACT

ICASC understands that many Flight Inspection and Validation (FIV) Service Providers are discussing approaches to investigate the use of Remotely Piloted Aircraft Systems (RPAS), or UAVs, as a way to reduce costs by minimizing aircraft flight time, either in the domain of Flight Inspection or Procedure Validation. It is the purpose of this paper to analyze pros and cons, evaluate the regulatory framework, safety, legal liabilities, airspace constraints, logistics and organizational needs, technical issues, staffing and training, etc. As each of these items are considered and evaluated, data for the development of a tentative Business Case become available to provide managers with enough information and supporting evidence for a decision making process.

Finally, an "Evaluation Matrix" is proposed and probable "challenges" are discussed, including the need of risk mitigation features.

A TOOL FOR ANALYSIS

All the considerations and evaluations that form the core of this paper are meant to provide a list of things to be considered when analyzing the possibility of RPAS operation for FIV purposes. Flight characteristics, flight control laws, different levels of autonomous flight capabilities are not part of this study. If they are mentioned, it is for the purpose of providing a high level Concept of Operations.

Most of the regulations are left in the hands of individual States, and an analysis of each existing regulation on the matter is clearly out of the scope of this paper, nevertheless the points to be considered are always the same. In the end the driving factor is always technical first (can we do that?) and then economical (is it worth it? What are the benefits? Can we build a business case for this?).

INTRODUCTION AND BACKGROUND

Commercial pressure and budget constraints are usually big motivators to look into new levels of technology, in the ongoing quest to find better and more efficient solutions to common needs. FIV, being a highly technological activity, requiring very skilled, well trained personnel, specially equipped aircraft, laboratory equipment and dedicated technical staff for aircraft/system maintenance and instrument calibration, with all the associated financial requirements, is the ideal target for a study on cost reduction and efficiency improvement. Traditionally the search for better efficiency, both in the technical and in the financial domain, passed through better AFIS equipment, more efficient aircraft, outsourcing of certain maintenance tasks and a better use of human resources. Combining multiple checks in one single run, for example, drastically increased the general efficiency, reduced flight time, and increased aircraft availability to fulfill other tasks, allowing for more revenues to be collected, and so on.

The next logical step, given the technology available today, looks natural: why not using UAV/RPAS to perform FIV tasks?

Over three years ago, a group based in Spain published their findings on this topic, (Remote Flight Inspection Using Unmanned Aircraft, C. Barrado et alt., JOURNAL OFAIRCRAFT, Vol. 50, No. 1, January–February 2013). The study, which is very interesting, did have some fundamental flaws, lacking almost entirely operational considerations and analysis on logistics. Nevertheless the paper has many interesting points and form a good study base for further analysis.

TECHNICAL FEASIBILITY

Military aviation forces worldwide have demonstrated without doubt how valuable an asset the unmanned systems are. The technical feasibility of such a system, specifically tailored for FIV needs, is certainly within the domain of the possible. It is not clear, at the moment of the writing of this paper, what are the technical solutions preferred for the mission package. Given the huge spectrum of available systems, from small and very light platforms, to airliner-sized platforms, the most efficient mission package/platform combination is still an argument for speculation. At least two distinct solutions can be devised at present, one being the use of a fully developed and integrated AFIS in an appropriately sized platform, and the other being a smaller platform, equipped with a defined mission package depending on the specific needs.

Signal in space analysis and related datalink requirements, as well as command and control datalink requirements and ATC communication requirements will be discussed in a dedicated chapter.

TYPE OF OPERATION

Directly connected with the type of RPAS used is the type of the operation. With the term "operation" it is intended the action range of platform, that can be used locally (e.g. crated after each use and sent to another location, or stored locally awaiting the next use), regionally (e.g. transferred in flight from one location to another, usually within the same State or bordering States) or globally (e.g. capable of being transferred in flight to any location in the world) - not part of this analysis. Due to the trajectories that need to be flown, it is assumed that all the FIV operations with RPAS are BVLOS operations (beyond visual line of sight), with all the associated regulatory and technical requirements as described in ICAO DOC 10019 (Ref. 4).

ASSOCIATED LOGISTICS

Depending on the type of operation, the logistical needs might be simple or extremely complex. A platform, independently from its capabilities, will require assistance at the departure point and at the arrival point, refueling/recharging, maintenance, etc. Crating, un-crating, assembly and disassembly will require dedicated personnel. Logistical support must be established to deliver the RPAS where it is required, together with the necessary personnel. This can be done directly (by an equipped van, for example) or through a parcel service. In this case personnel will proceed to the location with other available means of transportation and the equipment will be delivered to them. Special consideration must be given to delivery as air freight of the RPAS to the area of operations. Fuel and/or batteries might be considered Dangerous Goods. Consideration must be given to command and control equipment, mission equipment, fuel/batteries. If the FIVSP (Flight Inspection and Validation Service Provider) has been approved to transfer in flight the RPAS then personnel must be dispatched to both departure and arrival points to do the appropriate actions (maintenance, servicing, refueling/recharging, etc.). Consideration should be given to airside entry requirements for the members of the support team if the operation has an airport as its base. Part of the logistics is also the command and control network in case of regional operation. This will require redundant datalink capability and secure transmission capability. If the RPAS requires a runway for takeoff and landing, then a suitable alternate should be considered. Personnel may, or may not, be required at the alternate. Detailed analysis is required to assess the best options. Considering that all the intended operations are BVLOS a centralized command and control center might be the most economically efficient solution. This will allow for pilots and system operators to stay in one site, dispatching only technical support staff on location. Other options might be advisable, depending on the specific operation.

Special care must be dedicated to the coordination effort, including overflight permits, ATS coordination, and coordination with National CAAs. FIV is an international activity and many FIVSP operate in different continents at the same type. This will require dedicated personnel (we can consider them as Flight Dispatcher) or the use of third party services.

COMMAND AND CONTROL CAPABILITIES

The necessary datalink capability is within the boundaries of existing technology. Security will be addressed later on, in a separate chapter. Satellite datalink looks promising and should be the preferred command and control enabler (figure 1). Redundancy must be provided. Other types of datalink, based on ground based relay must be carefully evaluated. There is a good chance that electromagnetic line of sight could be compromised when performing certain type of maneuvers. VHF or UHF datalink might not be a viable option in most of the cases. When dealing with the level of performance required for this kind of operations, including the availability of broadband data communication, possibly via satellite relay, the cost involved are not to be underestimated.

Regarding flight commands, a RPS, Remote Pilot Station (this can be considered the "cockpit"), is needed. Depending on the type of RPAS, the complexity of the operation and the airspace in which the operation take place, more than one pilot might be required. A mission system RPS is also needed, with a dedicated system operator.

The level of sophistication of both RPSs is related to the complexities of the operation, the type of RPAS and the class of airspace the RPAS is flown into.

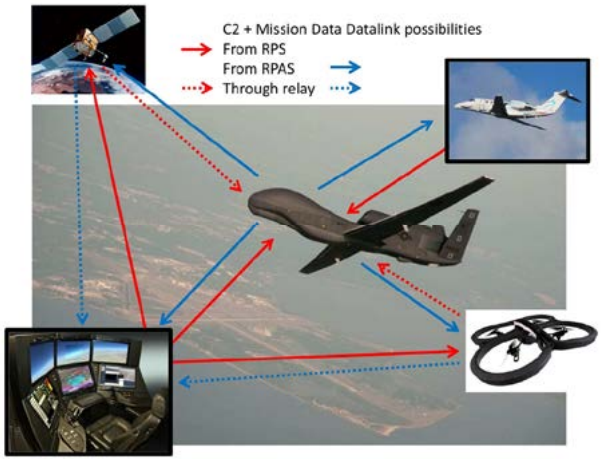

Figure 1

There are other options emerging in the C2 domain, including the use of cellular data network. This can be used by lower end platforms to further reduce the cost and provide C2 BVLOS, in theory. Aeronautical certification of such a network remains to be evaluated, as well as other technical challenges, including having priority in managing RPAS C2 inputs, to minimize latency, over other commercial/leisure data exchanged by the general public.

PERSONNEL REQUIREMENTS

This can be one of the key elements in defining the economic viability of any related business cases. It is difficult to define a standard requirement, though some assumptions can be made.

Simple local operation may require as few as one person, acting both as pilot and system operator. The person would also have to be qualified for basic maintenance and servicing tasks, as well as crating, un-crating and assembly and disassembly of the RPAS they are operating.

More complex operations may require 4 or more persons as basic crew.

Consideration should be given to the organization (FIVSP) structure. Depending on the dimension of the operation, such as number of RPAS in service, geographical distribution of the activity, frequency of flight operations, training, maintenance, calibration of mission packages, administration, sales and marketing, data analysis and management, the minimum staff can be determined.

National CAAs may have specific requirements regarding staffing, according to the certification issued to the operator (FIVSP).

THE PLATFORM

What are the minimum dimensions of the RPAS that satisfies the intended requirement?

First of all it is necessary to define the mission package specifications. Many options are available, and the range of possibilities goes from single task mission packages to fully integrated systems. Then the performance level must be identified, including endurance and range specifications. Finally command and control features must be decided, including the need for broadband data communication channel and redundancy features. Given the task to be performed, the performances are quite demanding. It is possible to assume that small RPAS are not suitable for the job.

Flight time should be measured in hours, certainly not in minutes, with all the consequences in terms of mass and complexity of the platform. Electrical propulsion might not be a viable option. Mission package can range from few kilograms to hundreds of kilograms, imposing proportionally bigger RPAS. 4-6 hours endurance at cruise speed at low altitude is probably the best option.

Considering the constraints discussed above, it is unlikely to design a viable platform with a total mass below 500-750 kilograms, while fulfilling all the specifications for a simple, single task mission. If a fully integrated AFIS system is mandated, then the expected mass may easily raise to the 1000 kilograms range, and up.

Operating speed range should also constitute an important part of the overall specifications of the platform. Normal speeds in the 160-200 KIAS range, with dash capability to 250 KIAS, are recommended.

It is understood that most of the flight profiles will be flown in autopilot mode. Certain military platforms have autonomous takeoff and landing capabilities, mitigating the risk of incidents during these delicate phases.

Discussion on antenna placement is provided in a dedicated chapter.

MISSION PACKAGE AND POWER REQUIREMENTS

Given the miniaturization level reached by today's equipment, it is possible to minimize mass and dimensions of the Flight Inspection System. Single task mission packages might be eventually developed, but attention should be given to the overall efficiency of the system. For example, an ILS package should always include Markers and DME capabilities. Electrical power available must be sufficient to operate the intended mission package at its most demanding conditions, on top of providing power for all the other flight related operations. Datalink and voice communication equipment (if required, see "Operations" chapter) must be considered, as well as video cameras as required. Top of the line installations, like the military counterpart, may boast a full range of capabilities, providing vastly improved efficiency and flexibility, including the capability to change the type of mission once already in flight, at the cost of a much more complex organizational structure and with all the associated costs. In a perspective view, even if initially this solution might look more expensive, the increased efficiency, vastly improved mission flexibility and a potentially better distribution of the resources geographically, may lead to this outfit as the model of choice.

The detailed capabilities of the mission package are not discussed in details, because this is out of scope, but it should be understood that for mission package we do define, as a minimum, the following technical features:

a) positioning system with appropriate level of accuracy (truth system)

b) one or more receiver, specially developed/modified to collect the necessary parameters for FI purposes,

c) appropriate computational devices, with real time capability preferred,

d) digital recording device,

e) broadband datalink if real time operations are intended (see "Datalink Technical Challenges", below),

f) antenna system with known characteristics,

g) voice communication capability (usually at least two VHF radios are required, UHF eventually)

h) power supply.

VISUAL AIDS CHECKS MISSION PACKAGE

RPAS are well suited for this kind of check. PAPI can be assessed with pinpoint accuracy and with minimal restrictions imposed to the airspace and airport operations. Runway and Approach lights can be easily surveyed. A relatively small RPAS can be equipped to fulfill the task (see Picture 4). Electro-optical equipment of very high quality and resolution will be required, with a precise positioning system (RTK, OMNISTAR, STARFIRE, etc.). An evaluation should be made about cost effectiveness, for most of this checks can be done associated to other tasks (PAPI can be associated to an ILS check, for example). Technically it looks very promising.

ANTENNA PLACEMENT

For the RPAS in the lowest mass range the required antennas could be part of the interchangeable mission package. All radiation patterns must be known. Proper ground plane for these antennas may be difficult to obtain. For those RPAS in the highest part of the mass scale, antennas should be placed as part of the basic design, considering proximity to other antennas. In smaller platforms it might became impossible to obtain the performance required. Datalink transmissions in the UHF (or VHF) range could interfere with FIV antennas, and special consideration has to be taken in the design to avoid interference. A case by case study is required. Furthermore ILS and DME antennas might be incompatible in a small RPAS, forcing a single task mission package (ILS only, DME only, etc.). Communication equipment in the VHF or UHF band might be required, further complicating the issue for small RPAS. This is another domain where an in depth analysis is certainly necessary.

FIV METHODOLOGY

As a basis of the evaluation, it is considered that all the FIV flights are conducted in accordance to ICAO Annex 10, ICAO DOC 8071 and ICAO DOC 9906. All flight maneuvers are to be performed as recommended by ICAO documents and State regulations.

REGULATORY ASPECTS

This part deals specifically with the aspects related to the peculiarities of FIV activities, and general regulatory aspects will not be discussed. Links to appropriate material are provided at the end of this paper. At present many States have devised authorization schemes for Commercial RPAS operators. The main difference is that FIV activity takes place exactly where the normal RPAS operations are forbidden. Depending on the State regulation, those limitations may range from 2 to 5 miles from an airport, not above 400 feet, not allowed in controlled airspace,

etc. Independently of the relevant State regulation, one thing is clear: an RPAS cannot be flown close to an airport, which is exactly what we need to do. That means that some change of the rules is required, either to use technology (and regulatory effort) to integrate RPAS in civilian airspace, including controlled airspace, or to segregate the airspace during FIV activities. The latter is not an advisable solution. Another regulatory requirement that needs to be considered is related to the overflight of cities or populated areas. There are limitations in the analyzed regulations that may force the RPAS operator to use multi engine platforms in order to obtain a waiver to overfly cities and other sensitive areas.

Regarding the FIV itself, there are certain parts of the activity that must be conducted by a Pilot, like Flyability assessment and Procedure Validation (ICAO DOC 8071 Vol. 1 and 9906 Vol. 5). It is extremely unlikely that those requirements will be removed anytime soon. Nevertheless certain tasks related to FI can be performed with an RPAS, so the key element might be integration of FIV aircraft with FIV RPAS.

OPERATIONS

While certain flight operations will be conducted outside controlled airspace, a great deal of them will be within controlled airspace. Local operations may start and finish at any suitable location, nevertheless communication with local ATC should be considered as a mandatory requirement. If the flight is entirely outside controlled airspace, cellphone coordination over a recorded line could be acceptable, but not so if the flight is supposed to penetrate controlled airspace or operate along IFP and/or in proximity of one or more airports, unless the airspace has been segregated. Capability to contact ATC on the appropriate VHF or UHF frequency should be considered as a mandatory requirement. Radio communication is also required to exchange information, or requests to perform adjustments, with the Navaid ground engineer.

Regional operations may require IFR flights from one location to another, and of course full integration between RPAS and all other aircraft in civilian airspace. The rule making process is in its infancy, but this may provide, in the long term, the best results in terms of efficiency and operational flexibility.

It is of paramount importance to consider that procedures must be developed to cope with LOST LINK/LOST COMM situations. General concepts for these procedure, during which execution of pre-selected navigation trajectories is autonomously conducted by the RPAS, must be reported in the Operations Manual of the FIVSP. Specific procedures, implemented case by case, must be notified to local ATC well in advance of the intended operation.

No operation should be initiated unless a briefing has been held between the operator and all the other involved stakeholders (local ATC, local CAA office if required, Airport Authority, etc.).

Emphasis should be placed in defining weather minimums for the operation. If the airspace is segregated, then the technical capabilities of the RPAS/OM limitations dictates the minimums. If the airspace is not segregated then is recommended to use VMC as the minimum, to give other traffic the possibility to visually maintain clearance in case of pre-programmed LOST LINK/LOST COMM procedures being activated.

Another operational issue is related to the time needed complete a given task. As an example we can consider an ILS/DME FI. The total flight time may vary according to specific requirements, so as a baseline the Italy's ENAV standard has been considered. For a periodic FI of an ILS/DME the average flight time is 2h15' with an average ground speed of 200 knots, accounting for a total air distance of 450 nautical miles. Most the available RPAS, including high end military platforms, cannot cope with this average speeds. Only a handful of the most powerful ones can match the speed and range, but are not designed for low altitude operations. Others are meant to operate at low altitude, but the speed range is limited. Finmeccanica's Sky-Y, with a cruise speed of almost 170 KTAS, an acceptable endurance and a 200+ kilograms payload, is a good example of the possibilities that might be exploited. The speed and endurance range of the various quad-, esa- or octo-copter is such that they can hardly be considered as a viable option. With speeds of 20-50 KTAS the time constraint applied to the airspace is simply not acceptable.

SAFETY

There is general concern about RPAS operations. Data collected mainly in the US shows an alarming number of incidents (so far), with about one third of the total being classified as serious incidents. In the period from 17th of December, 2013 to September 12th, 2015, the FAA received 921 reports, 35.5% of which posed a concrete risk of collision, including 158 cases (17.2%) where the closest point of approach was estimated to be below 200 feet., and more than 90% of the events happening in an airspace within which RPAS operations were forbidden (either above 400 ft. AGL, or in proximity of an airport). The trend is showing worsening safety data, with 519 events reported in a five months period starting from August 21st, 2015 and ending January 31st, 2016 (Bard College, ref. 1, complemented with data retrieved from the Bard College website on April 14th, 2016). 103 of these events had a reported closest point of approach below 200 feet., about 19.8%. The percentages are in line with the ones of the preceding period. 36.2% were classified "close encounters", where a concrete risk of collision

exist, while 91.9% of the total sightings happened above 400 ft. and/or within proximity of an airport.

During January 2016 the FAA has received reports of 93 events, confirming the upward trend (official FAA data, retrieved from website http://www.faa.gov/uas/media/UAS_Sightings_report_21Aug-31Jan.xlsx).

In Italy there have been 18 events reported in 2015 (in some occasions the airmiss term was technically improper, for the crew that did the report was still on the ground, taxiing out for departure, and in another case the report came from airport personnel on the ground. Another interesting case was a report from an authorized State Police drone that spotted, through its own onboard surveillance devices, an unauthorized drone in close proximity. ANSV, Rapporto Informativo 2015, ref. 2). The 23rd of December, 2015, in a very high profile incident, a relatively big camera drone fell on the ground very close to a skier during the world championships in Madonna di Campiglio. The operation was unauthorized. As a result of the ensuing enforcement action all drones operations, except authorized Police/Military drones, are forbidden during public events.

In the UK, on 17th of April, 2016, a "small drone" collided with a British Airways Airbus A320 approaching London Heathrow International Airport. Fortunately the aircraft landed safely with negligible damage, and after a technical check was immediately released to service.

These are examples coming from only three States, but the picture that these data provide clearly indicates the need for an action, or a series of actions, to educate people, enforce regulations and monitor operations.

The risk of a midair collision, or of a collision with the ground, must not be underestimated. Serious damages or loss of lives may result from these events. Mitigations are required to keep the risk at an acceptable level. These mitigations might include multi engine RPAS, ballistic parachute recovery systems, etc. An RPAS used for FIV mission will not be small, and a mass of few kilograms falling to the ground is surely deadly.

NASA recently announced the beginning of FT4 testing phase (Flight Test 4) for Detect and Avoid technology (DAA), using theirs Predator B. The test schedule requires 15 flights and more than 270 encounters. These encounters will consist of flying several piloted aircraft, (intruders), approaching with different geometries NASA Armstrong's Predator B remotely piloted aircraft. NASA's, Honeywell's and US Air Force's aircraft will participate (Ref. 3).

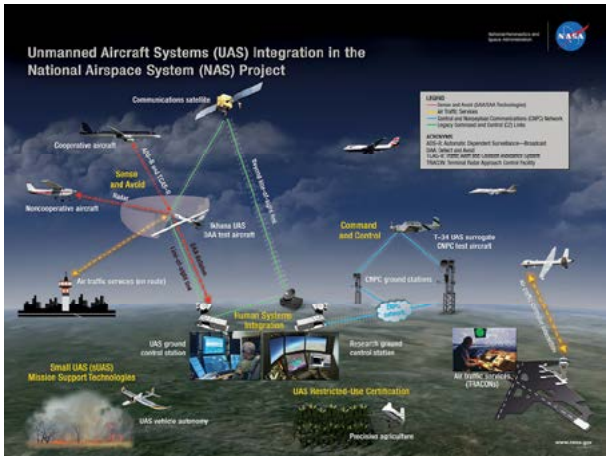

Figure 2 (NASA)

Failures must be accounted for, including automatic recovery capability failure. Pilot incapacitation, though not as serious as in a manned aircraft, should be considered. Defining all the failure modes and corresponding mitigations is not the purpose of this paper, nevertheless the point is extremely important and warrants further detailed studies in the future.

Picture 1

SECURITY

Command and control signals, as well as data exchanged for FIV purposes, must be secured against any kind of external interference, including natural and unlawful interferences. The fact that mission packages and the RPAS itself can be delivered on location by a commercial parcel service poses a lot of security issues. The equipment will remain outside the control of the operator for days and this poses a security threat. Procedures must be in place to assess the integrity, security wise, of hardware and software at the location of un-crating and reassembly. Same goes for the mission package. Another security issue is related to operator's personnel. A flight crew is security screened

every time it begins duty at the airport. Not necessarily so for RPAS operations, that may be conducted at any suitable location close to the Navaid to be checked. Even in case of ILS checks, the operator may find more convenient to base its operation close to the airport, but not necessarily at the airport. Also security issues will warrant a detailed study in the future.

LIABILITY ISSUE

It is clear that a defined responsibility must be attributed. The operator should be responsible for all the aspects of the operation, except cases of negligent/reckless conduct by the RPAS pilot. Insurance coverage of the appropriate level must be mandatory. Regulatory actions (ICAO, FAA, EASA and national CAAs) are already providing a set of rules defining responsibility. We are confident that this will be expanded and refined in the near future.

AIRSPACE USE

According to current regulations the only way to conduct a FIV operation with an RPAS, provided the flight profiles are those foreseen in ICAO DOCs 8071 and 9906, is through segregation of the airspace. There is no other possibility. Unless the RPAS are fully integrated with manned aircraft in all classes of airspace, there are serious doubts that segregating the airspace will be viewed as an efficient option. Night operations can be an answer to avoid delaying commercial traffic, but this may require technological and procedural mitigations, and human resources considerations as well.

DATALINK TECHNICAL CHALLENGES

Datalinks for FIV data exchange and datalinks for command and control must not interfere. Proper positioning of the required antennas has been discussed above, but bandwidth requirements need to be considered, as well as transmitter power requirements.

Transmitting FIV raw data is hardly a possibility. The bandwidth required can be in excess of 16 Mbit/s and warrants the use of very sophisticated, heavy, in relative terms, and expensive systems. On the other hand elaborated data for the same type of check, when properly optimized, may require only a more manageable 80 Kbit/s or even less. Range, and thus transmitter power, is another issue. Considering that certain tasks are performed at distances that may reach more than 50 nautical miles, and executed BVLOS, the issue is absolutely important. Unless a satellite link capability is provided to the RPAS there are checks that are precluded. One interesting option, to mitigate the huge cost of a satellite relay network, could be the use of multiple low cost RPAS used as airborne relay. Strategically positioned in terms of altitude and location might provide the coverage needed to complete most of the FI checks. If this is case, then existing datalink transmitters in the 5-10 W power range can do the job, though a latency issue might again arise.

USE OF DATALINK FREQUENCIES

Frequencies are assets managed by each State. An operator (of any kind, from aeronautical stations to television networks) uses the frequencies that are assigned according to a government concession. There is a finite number of frequencies that can be assigned. FIVSP that intend to use RPAS internationally must consider also the issue of having allocated datalink frequencies in each State, if this is required.

ECONOMICS

Estimating in details the cost structure of a developed FIVSP that does everything using RPAS is literally impossible at this stage. The industry is still in its infancy. Certification for FIV use is not defined, but there are requirements for pilots and for Navaid Inspector and FIV Pilots. The cost of the platform and mission packages can vary so widely, but in any case they will be relatively expensive. Even the simplest of the mission packages, with a dedicated FI receiver, datalink capability, antenna system, etc. will cost in the range of hundreds of thousands Euros. A fully equipped RPAS with all the goodies may be worth easily 10 million Euros.

Integrating a fleet of RPAS with existing FIV aircraft is a possibility, and probably the only way to start looking into the concept. At the beginning, though, the overall costs are going to increase significantly due to a need to invest in the RPAS and all the associated equipment and mission packages, in parallel with normal operations.

Logistics costs will become the center of any cost control exercise, especially if the operation is based on small RPAS. Platform, all the required mission packages and ancillary equipment as well as personnel must be moved all the time from one operating location to another. In a different scenario, with more capable platforms, the operation may be conceived as a manned aircraft operation, requiring less efforts on the logistical side.

Personnel cost is strictly connected with the number of RPAS that operator intends to use. Reliability figures are not established for this type of operation, but we can assume a tentative 85% dispatch reliability. For each RPAS there could be the need to establish a number of "Go Teams", similarly to what is done in the rest of the aviation transportation industry, where usually between 2 and 3.5 crew are assigned to each aircraft. This will

allow for a good human resource management scheme in terms of schedule. It should be noted, however, that there are no set flight time limitations for RPAS pilots, and probably the operator will try to obtain commercial advantages utilizing a maximum duty time scheme instead, in order to maximize RPAS flight time.

OPERATING SCENARIOS

If FIV has to be conducted according to current ICAO provisions, then certain operations are not viable, such as Instrument Flight Procedures Validation, at least for that part where human evaluation is required. We have analyzed a number of scenarios, but basically they all come down to two main families:

a) operations that start and end in the same location, usually where the Navaid is located

b) operations that originate from a main base not necessarily close to the Navaid, and that may end at the same main base or at other bases

Scenario type (a) can be sub-divided into:

1) use of local RPS

2) use of remote/centralized RPS

Scenario type (b) requires clearly a centralized RPS.

It should be noted that when the operation is not fully centralized logistics can be quite an effort.

Picture 2

Picture 3

Picture 4

Picture 5

Picture 6

Picture 8

Picture 7

EVALUATION MATRIX

It is clear that what drives the efforts of the proponents of RPAS use for FIV purposes is the quest for efficiency. Costs must go down drastically to support any research and development exercise. Examining ICAO DOC 10019 in details, however, may provide a better insight. There are some technological enablers not yet fully developed and not yet certified, like DAA equipment, same applies to C2 link specifically developed for the task, and so on.

This simple matrix is only a "container" for the major indicators. Each box should be further expanded into a full Business Case analysis. One of the main issues in dealing with cost analysis is that the variables, when rules are not defined and certification standards are not yet available in the basic technical areas needed for this type of operation, are such that the end results, depending on the initial assumptions, can vary easily by one order of magnitude.

MATRIX		
	BASELINE FIV AIRCRAFT	RPAS
Acquisition cost		Includes RPS and all ancillary equipment
AFIS acquisition cost, including integration		Mission package or integrated AFIS
Pilots and AFIS Operators Maintenance Dispatchers		

Administration and other support personnel		
Direct operating costs	Fuel, handling and all expenses connected to ops	Fuel, handling and all expenses connected to ops
Indirect costs, including financial cost of ownership, insurances and all other costs		
Expected life cycle costs, normalized over a standard period of time		
Hourly productivity coefficient, based on baseline aircraft, per type of FIV mission and ferry, if allowed	1	*

* Productivity coefficient is very important. If, for example, the coefficient is 0.22 due to speed and mission package limitations, then to be convenient to operate an RPAS for that specific mission the overall cost per hour must be less than one fifth of the baseline aircraft. This is not purely an economic efficiency marker, and other considerations might prevail to decide if it is feasible to operate an RPAS or not, including the utilization time of the airspace. In fact a coefficient of 0.22 means also that if one hour of flight of the baseline aircraft is required to complete the task, almost five RPAS flight hours are required to complete the very same task. This may prove to be the more limiting factor if the airspace must be segregated and commercial air operations suspended or restricted.

CONCLUSIONS

The concept of using remotely piloted platforms to fulfill FIV requirements is very interesting and holds good promise for the future. However, RPAS operations are probably premature at this time, due to the lack of uniform international regulations and certification standards, including ATM/UTM integration in non-segregated airspace, nevertheless the time has come to seriously assess the possibilities.

The regulatory framework associated with FIV operation, at present, does not allow for the use of RPAS to cover all the requirements. Therefore, if and when certain FIV operations are proven to make sense economically but are outside the current regulations, the regulatory aspects will have to be addressed and changed, if it is possible without any degradation in safety.

Economics do not clearly show that the use of RPAS will bring savings and improve the efficiency of FIV operations, but again, this may depend on the fact that the range within which these evaluations are being made are so wide that it is extremely difficult to assess a baseline. This is a direct consequence of the lack of a common regulatory framework. If ANNEX 10 and DOC 8071 are to be applied as they are today, then it might be extremely difficult to propose a credible business plan that takes advantage of RPAS use. When considering cost of research and development, systems integration, certification, RPAS AFIS development, and all the associated ancillary research work on command and control, datalink, etc., and all the cost for RPS, then acquisition cost of these systems might easily reach, or even surpass, the cost of a fully equipped, manned aircraft. Military programs may be used to define baseline cost of R&D and certification, with appropriate adjustments.

Personnel need to be dispatched and travel expenses considered. Depending on the size and cost of the airborne vehicles, the RPAS may have to be disassembled, crated and sent to the next location, uncrated, re-assembled, tested and prepared for flight again. And people will follow. This would become a time consuming, and money draining, effort. Visual Aid checks can also be performed using an RPAS. This looks promising, even if these checks are often combined with other checks, making them very cost effective. In any case this is an interesting area of study, as it may lead to an unprecedented level of efficiency in terms of quick response, provided the RPAS is always available at the airport.

We are positive about future developments, and within a 10 to 15 years window we will certainly see experiments and possibly flight trials to really assess the viability of the RPAS in the FIV domain. It must be kept in mind, however, that as long as aircraft are manned, certain aspects of FIV should be assessed by manned, specially equipped FIV aircraft, with specialized aircrew. ICAO has recently published a dedicated Manual, ICAO DOC 10019 (Ref. 4). This manual will be expanded in the future, and hopefully a common international regulation regarding system certification will follow that will open the door for some use of RPAS, while not degrading safety in any way.

REFERENCES

Ref. 1 Bard College, “Drone Sightings and Close Encounters: An Analysis”, Dan Gettinger, Arthur Holland Michel, 2015, plus data retrieved 19th of April,2016 from official website http://dronecenter.bard.edu/

Ref. 2 ANSV "Rapporto informativo sull'attività svolta dall'ANSV e sulla sicurezza dell'aviazione civile in Italia nel 2015", retrieved from official website http://www.ansv.it/

Ref. 3 NASA News, retrieved from official website 26th of April, 2016. http://www.nasa.gov/centers/armstrong/features/flight_test_series_4.html

Ref. 4 ICAO DOC 10019, Manual on Remotely Piloted Aircraft Systems (RPAS), First Edition, 2015

ACKNOWLEDGEMENTS

The author wishes to acknowledge the contribution given by all the Members of ICASC.

ABBREVIATIONS AND ACRONYMS

AFIS Automatic Flight Inspection Systems

ATC Air Traffic Control

ATM Air Traffic Management

BVLOS Beyond Visual Line of Sight

C2 Command and Control

C2 Link Command and Control Data-Link

DAA Detect And Avoid

FI Flight Inspection

FIV Flight Inspection and Validation

FIVSP FIV Service Provider

ICAO International Civil Aviation Organization

IFR Instrument Flight Rules

KIAS Knots Indicated Air Speed

KTAS Knots True Air Speed

LOST LINK/LOST COMM a situation in which datalink or voice communication is lost due to technical failure, external disturbances (interferences, jamming, spoofing), or operational error

Navaid Navigational Aid

OM Operations Manual

R&D Research And Development

RPAS Remotely Piloted Air System

RPS Remote Pilot Station

UAS Unmanned Aerial System

UAV Unmanned Aerial Vehicle

UHF Ultra High Frequency

US United States

UTM Unmanned Traffic Management

VHF Very High Frequency

VMC Visual Meteorological Conditions

FIGURES AND PICTURES

Figure 1 – Platform, Remote Pilot Station, Datalink block scheme.

Figure 2 – NASA integration of UAS in the National Airpsace System

Picture 1 – RPAS crashing at Madonna di Campiglio.

Picture 2 – EADS Harfang

Picture 3- Finmeccanica SKY-Y

Picture 4 – Terra8 Drone, used as an example of RPAS that might be capable of certain FIV missions, like PAPI and other visual aid checks.

Picture 5 – Example of a RPS: centralized system installed at main operating base (from www. droneinsider.net)

Picture 6 – Portable RPS (from www. dronetecnology.eu)

Picture 7 – Portable RPS (from www.dronebase.it)

Picture 8 – Parrot AR Drone, APP for Smartphone (from http://www.parrot.com/fr/produits/ardrone-2/)

IFIS2016

Bringing Together Theory and Practice

Further Publications

RADAR performance through SSFT in the solution of Helmholtz wave equation

Bruno Michel Marcondes Alves
Flight Inspection Pilot
Department of Airspace Control
Rio de Janeiro, RJ, Brazil
Fax: +55 21 2101-6420
E-mail: alvesbmma@decea.gov.br

ABSTRACT

The primary radar detection involves a series of parameters determining the range at which an aircraft would be presented to ATC. That's the reason why the Flying Inspection of Radar systems becomes different from other NAVAIDS, establishing itself as a way to check statistically, from the ground, the Radar performance in a real scenario. This scenario which basically depends on: weather conditions, surface of the region of interest, electromagnetic and physical characteristics of the aircraft and the radar system itself. Due to the floating performance, inherent in a primary detection system, every day the detection of targets of opportunity are used to supplement the checklist requirements.

However, different types of aircraft in varied and constantly changing weather conditions and surfaces around the radar can result in unreliable detection ranges, possibly lower than expected, requesting flight inspection for verification of the radar.

On the other hand, literature presents a number of mathematical models for radar performance prediction. Models that assume physical and mathematical properties able to represent the behavior of a radar system in the region of interest.

In this context, this article proposes the application of the mathematical model that is based on the algorithm Split-Step-Fourier-Transform for the solution of the plane wave equation of Helmholtz, computationally implemented, in evaluation of the radar performance in a real scenario. In this way, it is possible to predict the radar performance with adequate reliability, both for homologation inspection and for periodic reviews.

INTRODUCTION

Doc 8071 [1] has a number of methods for evaluation and technical and operational performance of surveillance systems testing, and say that a proper verification of the performance of these systems is performed using an appropriate combination of detection opportunity to traffic or dedicated aircraft , recorded data or simulated , BITE (built-in test equipment) and RTQC (real time quality control).

The same document also emphasizes that, in general, the evaluation required determining system performance is categorized by coverage, accuracy, detection performance and resolution.

The radar coverage, focus of this work is defined as the three-dimensional volume of space in which the system holds specific values of detection performance, accuracy and resolution. The coverage should be expressed in terms of distance, azimuth and altitude.

The main task in this assessment are the detections made in the inspection procedure in flight called vertical coverage. In this procedure, the inspection of aircraft performs nose-on and tail-on procedures, always bearing radar antenna reference, varying flight altitudes. This radial should be free of clutter, dense traffic and populated areas, and influences created by line-of-site.

However, other sectors may have different performances in coverage because, depending on weather conditions and relief variations, different targets would be detected at different distances and/or altitudes.

Therefore, this work demonstrates the ability to predict the performance of a radar system from proper mathematical modeling, considering the weather, relief variations, characteristics of the target and the radar system.

This makes it possible to implement a software tool for assisting engineers and maintenance ATC staff in evaluating performance of various types of radar systems, this making the process less cost and less dependent on the flight inspection.

In general, the wave equations have closed form solution for simple cases, for example, linear variation or bi-linear refractive index with height [2].

Aproximate equations seek to facilitate the solution of complex problems spread through numerical techniques. The reduction of the Helmholtz equation from elliptical to parabolic, through proper approximation, and the solution to this equation through numerical algorithm SSFT (split-step Fourier Transform) is called the parabolic wave equation method. This method provides a complete solution without great cost computational front of the other methods [3].

The use of the tropospheric propagation method was presented for the first time by Dockery in 1988 [4] and is applied to the propagation of radar signals [5], considering the effects of rough surfaces, including scattering and diffraction associated with terrain variations [6].

However, this method has some disadvantages, among them, the main one is the need for robust computing resources to applications involving high frequencies, high altitudes and distances.

Initially the main characteristics of the troposphere, and then the structure of the main phenomena that affect the propagation in the microwave range are displayed. The next item the refractive index is defined in function of meteorological parameters and propagation mechanisms are described in anomalous atmosphere. Set the refractive index, the wave equation solution is presented as the proposed allocation.

TROPOSPHERIC PROPAGATION

By propagating in the troposphere, electromagnetic waves are influenced by weather effects, obstacles and the earth's curvature.

In the troposphere occur the main weather effects, such as fog, rain, clouds, temperature variation, pressure and humidity. Considering the range of EHF frequencies, as well as dispersion, still occur the reflection, diffraction, tropospheric scattering, absorption and refraction.

The phenomena of reflection, absorption and refraction are described in detail in order to contribute to the understanding of the article.

Reflection

When a wave passes from one medium to another, part is reflected back to the same middle, and another part is refracted in the following way. The power of the reflected wave is determined by the reflection coefficient. This coefficient depends on the transmission frequency, polarization, incident angle and the roughness of the reflecting surface.

For shallow incidence angles and flat surfaces (i.e. calm seas), the typical values of the reflection coefficient is close to unity, that is, the reflected wave intensity is close incident wave.

With increasing wind speed, the surface becomes rougher and decreases the coefficient [7].

Two considerations should be highlighted when the reflection occurs. The first refers to the different distances covered by the same issue. The second relates to signal phase changes according to polarization of the incident wave.

The direct and reflected waves travel different paths and, therefore, there will be the phase difference between the two signals when crossing at a designated place. When two waves arrive at the same point in phase, constructive interference they generate. If they arrive out of phase, destructive interference is caused.

In addition to the effect caused by the different path, signal phase change may occur at the time of reflection by changing the reflected wave. For grazing angles, vertically polarized waves do not undergo phase changes upon reflection, since the electric field tends naturally to remain perpendicular to the reflecting surface.

For horizontally polarized waves there is a change of 180 degrees phase, because the electric field at the site of reflection is always zero, occurring phase inversion. For polarizations with vertical and horizontal components, there is a change in tilt or rotation direction of the reflected wave.

Absorption

Absorption is the change of the form of energy due to existing elements in the atmosphere. It has more influence at high frequencies, especially in certain ranges, when there is resonance with the molecules of water and oxygen. In these cases, the molecules absorb the radiant energy transforming it into vibration and heat. In situations such as in the presence of clouds and rain, related absorbing water vapor is even greater.

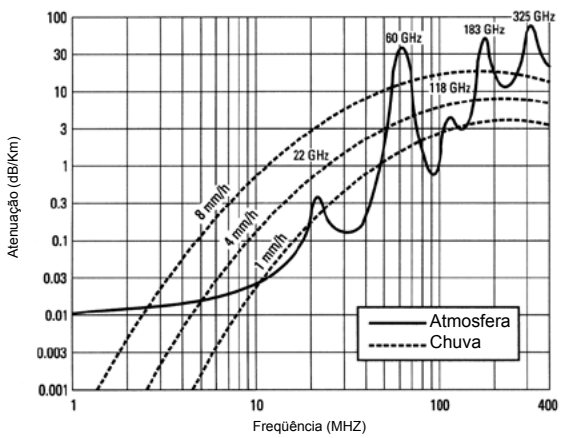

Figure 1. Attenuation at sea level by absorption [8]

Refraction

Refraction is a phenomenon that changes the trajectory of an electromagnetic wave. It occurs when a wave passes from one medium to another obliquely and finds

in this new medium a different propagation speed of the previous speed.

In the troposphere (portion of the atmosphere that extends from the surface to approximately 40,000 ft) normally occurring pressure changes, humidity and temperature with altitude and thus variation in the density of the air, so that the waves do not propagate into rectilinear path.

The frequency of the incident wave does not change and has always concordant phases.

Refractive index in the Troposphere

Electromagnetic waves propagating in the troposphere are refracted and scattered due to the refractive index variations. By definition, the index of refraction presented as follows: $n = \sqrt{\varepsilon_r} = c/\upsilon$, where ε_r is the dielectric constant of the troposphere, c is the speed of light in vacuum and υ is the speed of the wave in the medium in question.

The variation of tropospheric refraction index occurs due to molecules constituting the air, especially oxygen, nitrogen, carbon dioxide and water vapor. Changes in the value of n result of polarization imposed on the wave by these molecules, thanks to quantum molecular resonance [8].

The deviation value of n is very close to the unit , and its typical value on the Earth's surface is 1.00003. Therefore, it has become desirable to define the N parameter called refractivity and described as follows:

$$N = (n-1)\cdot 10^6 \qquad \text{Eq. 1}$$

The index N is dimensionless and for convenience is measured in units N. In general, the refractivity decreases with height, as it is influenced by the weather conditions of the atmosphere, defined as [9]:

$$N = \frac{77.6\,p}{T} - \frac{5.6e}{T} + \frac{3.732\cdot 10^5 e}{T^2} \qquad \text{Eq. 2}$$

Where P is atmospheric pressure in hPa, T is temperature in Kelvin, and e is the partial pressure of water vapor in hPa. For the range of microwave frequencies, the troposphere can be considered as an isotropic and non-dispersive medium [10].

Propagation in standard atmosphere

Standard propagation mechanisms are those that are associated with a structure called standard atmosphere, and shall apply to the propagation on a flat surface or slightly rough. The normal or standard atmospheric condition is characterized by the exponential decrease of the index n to the height (from the surface to approximately 1 km, decrease can be approximated to linear) [7]. This standard atmosphere model was set for computational convenience, being based on average local (usually continental regions) taken for long periods and has properties similar to real atmosphere. The standard atmosphere should not be considered as the condition most frequent since there are regions with climatological characteristics that provide frequent training anomalous propagation conditions. In a standard atmosphere pressure, temperature and humidity decreases exponentially as a function of height z above the surface. For reference atmosphere defined by the International Telecommunications Union [11], we have:

$$N(z) = 315\ \exp(-0.136\,z) \qquad \text{Eq. 3}$$

Where z is given in kilometers.

For propagation in the microwave range, the standard atmosphere used is called "atmosphere 4/3 ". This is the average refraction of electromagnetic waves observed at the portion of the atmosphere that extends from the ground to approximately 600 m, with a linear decreasing function of time in refractivity h. $\frac{dN}{dh} = -39\ /\ km$.

With this, gradient electromagnetic waves run along a trajectory curve rather than a straight line. The radius of curvature of the trajectory taken by the wave, launched a low elevation angle, in a standard atmosphere is defined by the following equation:

$$\xi = -\frac{dh}{dn} = 25{,}600 \approx 4\cdot a \qquad \text{Eq. 4}$$

Where a is the radius of the Earth (≈ 6371 km).

A useful tool to examine their effects on gradients and spread, as well as facilitating the identification of tropospheric ducts consists in the transformation of spherical to flat earth by means of the modified refractivity. This index, denoted by M, has its gradient dM/dh, to negative values of dN/dh smaller than -57 Nkm^{-1} [7].

$$M = N + 0{,}157\,z \rightarrow \qquad \text{Eq. 5}$$

$$M = N + 0{,}048\,z \rightarrow \qquad \text{Eq. 6}$$

z (height) in ft.

In the transformation of spherical to flat land ($k \rightarrow \infty$) by M, instead of N, the curvature radius is modified, preserving the relative curvature between the radius and the earth [10].

This transformation adjusting the wave equation in cylindrical coordinates for the condition of the flat earth, substituting the refractive index n for the modified refractive index m, by the relation:

$$m(x,z) = n(x,z)\exp(z/a) \cong n + z/a \qquad \text{Eq. 7}$$

Where $0 \leq n$ -1 << 1 e z << a.

Anomalous propagation in atmosphere

The anomalous propagation mechanisms in the troposphere (containment, super-refractive and sub-refractive) are associated with the abnormal occurrence of gradients in the refractive index. It is considered normal gradient between -79 Nkm^{-1} and 0 Nkm^{-1}. Within this range a radio wave will bend down with a smaller curvature than the radius of Earth, is classified as a normal condition or standard propagation.

The following figure illustrates the profile of each of the conditions of anomalous propagation:

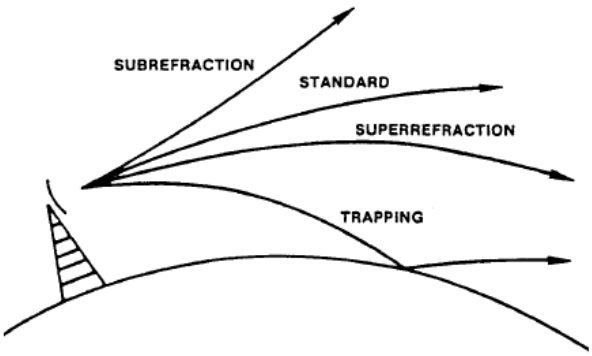

Figure 2. Trajectory of relative wave conditions of anomalous propagation [7]

REFRACTIVE INDEX MODEL IN TROPOSPHERE

As the air temperature, humidity and pressure varies with altitude, one can quantitatively determine the refractive index of the atmosphere from the weather code used in radio probes.

This type of weather message has great availability on the Internet and for various periods of the day. The code indicates the altitude where there are moisture inversions and / or air temperature, which, as seen above, are the causative parameters of inversions in refractivity and thus affect the propagation of electromagnetic waves.

The description of the radio message poll indicated in this work is presented in detail by Alves [12] in 2008. However, Equation 2 describes the final calculation of the refractive index.

Calculation of absorption

The effects of absorption are due primarily to the presence of molecules of gases, water vapor and particles in the atmosphere. For the frequency, range of interest to molecular absorption related to gas should be only to oxygen [11]. In the troposphere and the temperature 15°C, this attenuation is expressed by the following equation [13]:

$$\gamma_0 = 10^{-3} \cdot \left(\frac{6{,}09}{\left(\frac{f_{MHz}}{1000}\right)^2 + 0{,}227} + \frac{4{,}81}{\left(\frac{f_{MHz}}{1000} - 57\right)^2 + 1{,}5} + 0{,}00719 \right) \cdot \left(\frac{f_{MHz}}{1000}\right)^2$$

Eq. 8

Where f_{MHz} is the frequency in MHz.

To account for the temperature variation must make correction given by [13]:

$$\gamma_1 = \gamma_0 \cdot [1 + 0{,}01 \cdot (T - 15)]$$

Eq. 9

Where T is the air temperature at the surface in degrees Celsius.

The absorption by water vapor is described by [13]:

$$\gamma_w = (t_1 + t_2 + t_3 + 0{,}0021 \cdot abs_{hum} + 0{,}5) \cdot \left(\frac{f_{MHz}}{1000}\right)^2 \cdot \frac{abs_{hum}}{1000}$$

Eq. 10

Where abs_{hum} is the absolute humidity near the surface (g/m^3), defined below, and t_1, t_2 and t_3 are temporary variables defined by [14]:

$$abs_{hum} = \frac{UR \cdot e_s}{T \cdot R_v} = \frac{e}{T \cdot R_v}$$

Eq. 11

$$t_1 = \frac{3{,}6}{\left(\frac{f_{MHz}}{1000} - 22{,}2\right)^2 + 8{,}5}$$

Eq. 12

$$t_2 = \frac{10{,}6}{\left(\frac{f_{MHz}}{1000} - 18{,}33\right)^2 + 9}$$

Eq. 13

$$t_3 = \frac{8{,}9}{\left(\frac{f_{MHz}}{1000} - 325{,}4\right)^2 + 26{,}3}$$

Eq. 14

The total absorption in dB/km can then be defined as:

$$gas_t = (\gamma_1 + \gamma_w)$$

Eq. 15

Set the refractive index and absorption can enter them in the propagation model of the parabolic equation, through the Split-Step Fourier algorithm, and analyze the behavior of electromagnetic wave in this medium.

TROPOSPHERIC PROPAGATION PREDICTION MODEL THROUH PARABOLIC WAVE EQUATIONS

As the wave equations have physically consistent and closed solution for simple cases, approximations of these equations were developed, enabling efficient numerical techniques and low computational cost, applicable in

solving complex problems of propagation in the troposphere.

The reduction of the Helmholtz equation, the elliptical shape to a satellite from a suitable approximation followed by a numerical solution method is called the parabolic equations. This process provides a full wave solution and low computational cost when compared to other prediction methods [3].

Modeling and numerical solution

The scalar wave equation (Helmholtz equation) three-dimensional for electric or magnetic Ψ field is shown below:

$$\nabla^2\Psi + \beta_f^2\Psi = 0 \qquad \text{Eq. 16}$$

Where β_f is the phase constant and $\beta_f^2 = \omega^2\mu\varepsilon$ (ω is the angular frequency, μ is the magnetic permeability, and ε is the electrical permittivity). For non-magnetic means ($\mu = 1$) and n being the refractive index of the medium and $k = (2\pi / \lambda)$ wave number in vacuum, it follows that $\beta_f^2 = k^2n^2$ that applied to 16 provides:

$$\nabla^2\Psi + k^2n^2\Psi = 0 \qquad \text{Eq. 17}$$

Taking advantage of the transformation of spherical flat earth to [10], using the modified refractive index m for n, and considering the azimuthal symmetry can simplify the analysis. Therefore, the equation 17 becomes:

$$\frac{\partial^2\Psi}{\partial z^2} + \frac{\partial^2\Psi}{\partial x^2} + \frac{1}{x}\frac{\partial\Psi}{\partial z} + k^2m^2(x,z)\Psi = 0 \qquad \text{Eq. 18}$$

This is a partial differential equation in two dimensions containing second derivatives with respect to x and z. For propagating at angles close to the horizontal, the variation of Ψ function is slow in x and z, which does not occur with phase. Therefore, it is possible to separate the function of the other two, "amplitude" and "phase" (Split) [15]:

$$\Psi(x,z) = \mu(x,z)\exp(ikx) \qquad \text{Eq. 19}$$

Substituting 18 in 19, are obtained:

$$\frac{\partial^2 u}{\partial z^2} + \frac{\partial^2 u}{\partial x^2} + 2ik\frac{\partial u}{\partial x} + \frac{1}{x}\frac{\partial u}{\partial z} + k^2\left(m^2 - 1\right)u = 0 \qquad \text{Eq. 20}$$

As interest is far fields from the source, at least 100λ (in this case $\lambda = 0.15$) from the source, it follows that $x >> 1$ (in this case $x > 750$ m for a radar with LP 5 µs - characteristic search radar) thus $x - 1 \approx 0$ in 19. According Kuttler & Dockry 1991 [15], one can assume that u varies slowly in x, suggesting that also ε varies gently x. Thus, the approximation below can be considered:

$$\left|\frac{\partial^2 u}{\partial x^2}\right| << 2k\left|\frac{\partial u}{\partial x}\right| \qquad \text{Eq. 21}$$

The effect of this approach, known as parabolic approximation is to neglect the spread retro field, limiting the use of the method of propagation studies with low elevation angles. This restriction is not severe since, in this case, the electromagnetic energy is spread predominantly without retro scattering [15]. With this consideration, equation 20 reduces to an elliptical parabolic, since only the first derivative with respect to x remains, as follows:

$$\frac{\partial^2 u}{\partial z^2} + 2ik\frac{\partial u}{\partial x} + k^2\left(m^2 - 1\right)u = 0 \qquad \text{Eq. 22}$$

In short, equation 22 is valid only under the following conditions:

- Field to be calculated is far from the source, $x >> 100\lambda$.
- The change $\partial u / \partial x$ is slow enough so that they use the approximation of Eq. 28. The second condition is satisfied in the troposphere and spread within the limit of 15°-20° from the horizontal [5]. For studies of propagation in pipelines this is not a severe condition, because only the radiated energy within a few degrees, one or two, the horizontal will be guided into the duct and radiated energy at higher angles enter the structure, but not be trapped in the duct [16].

Solução numérica da equação parabólica: Split-Step Fourier

The advantage of reducing the wave equation for a parabolic elliptical shape is useful to provide a numerical solution to the propagation model. The resolution of an elliptic equation as 27 require specification of the boundary conditions in the closed two-dimensional domain. The solution of the field at each point depends on the neighboring fields. Thus, a considerable computing capacity becomes necessary, as a system of simultaneous equations is calculated [5].

Already the parabolic equation 22 has an open boundary condition, and you can solve it using a technique of steps (step). The initial distribution of the field u (0, z) is specified on the left contour. The solution ($0 + \Delta x$, z) can be obtained according to the initial field and boundary conditions in the lower and upper limits of the open domain. The solution goes a step forward in x, reducing the computational loss with respect to the case of elliptic equation. Figure 7 illustrates the condition for the case of open contour:

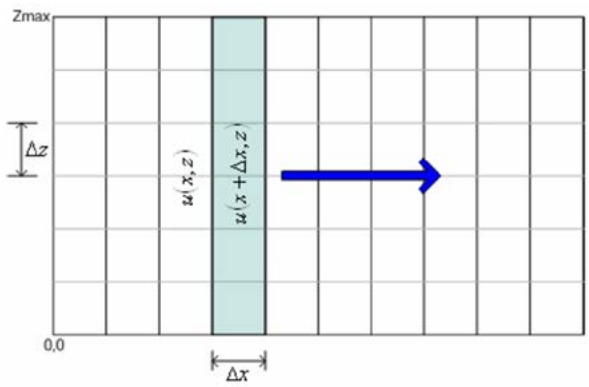

Figure 3. The solution of the field at (*x*+Δ*x*, *z*) is a function of the field *u*(*x*, *z*) [2]

The retro scattering is ignored because the field x is not affected by structures at $x + \Delta x$. To facilitate further development, the equation 22 can be shown as:

$$i\left[\frac{\partial^2}{\partial z^2}\cdot\frac{1}{2k}+\frac{k\left(m^2-1\right)}{2}\right]u=\frac{\partial u}{\partial x} \qquad \text{Eq. 33}$$

Thus, we define the operators A and B:

$$A=\frac{k}{2}\left[m^2(x,z)-1\right] \qquad \text{Eq. 24}$$

$$B=\frac{1}{2k}\frac{\partial^2}{\partial z^2} \qquad \text{Eq. 25}$$

Substituting A e B in 23, are obtained:

$$i\left[B(z)+A(x,z)\right]u(x,z)=\frac{\partial u}{\partial x} \qquad \text{Eq. 26}$$

The index m in A must initially be considered constant (will be explained later in this consideration). In this case, the equation 26 may be integrated with respect to x, as shown 27:

$$\frac{du}{u(x,z)}=i\left[A(x,z)+B(z)\right]dx \rightarrow \int_x^{x+\Delta x}\frac{du}{u(x,z)}=\int_x^{x+\Delta x}i\left[A(x,z)+B(z)\right]dx$$
Eq. 27

Therefore, the expression for the value of the field at $x+\Delta x$ can be presented as:

$$u(x+\Delta x,z)=\exp\left[i\Delta x(A+B)\right]\cdot u(x,z)$$
Eq. 28

Observing the property of exponentiation, equation can be separated as a product of two exponential, one in the function and the other function in B. The expression 28 can be rewritten:

$$u(x+\Delta x,z)=\exp(i\Delta xA)\cdot\exp(i\Delta xB)\cdot u(x,z)$$
Eq. 29

As B contains a second order differential operator, the term $\exp(i\ \Delta x\ B)\ .\ u(x, z)$ must be calculated using the Fourier transform of the spatial domain z and spectral domain p:

$$\exp(i\Delta xB)\cdot u(x,z)=\Im^{-1}\left\{\Im\left[\exp(i\Delta xB)u(x,z)\right]\right\}$$
Eq. 30

The transform variable $p = k\ sin\ (\theta)$ is the wave number in the z direction, θ being the angle to the horizontal.

As the exponential 29 is a series of powers in $\partial^2/\partial z^2$, the Fourier results in $-p^2$ [17]:

$$u(x+\Delta x)=e^{\frac{ik\Delta x\left(m^2-1\right)}{2}}\Im^{-1}\left\{e^{\frac{-i\Delta xp^2}{2k}}\Im\left[u(x,z)\right]\right\} \qquad \text{Eq. 31}$$

The term was defined considering 31 m constant, but in the case of our study, it will be used even when m is not constant. The use of this equation in regions where m is variable presents a proportional error to Δx the frequency to the refractive index gradient. According Slingsby (1991) [3] & Levy and Craig (1991) [5], the solution converges reducing the value Δx.

Boundary conditions

To start the integration is necessary to know the field at $x = 0$, or $u\ (0, z)$. This field can be obtained by inverse Fourier transformed in space p of the antenna radiation pattern for far field. The space translation Fourier theorems frequency can be used to vary the height of the antenna and pointing your diagram in the vertical plane. The radiation pattern of the antenna can be defined numerically or analytically [18].

This work is an antenna employed with standard Gaussian radiation, which analytically is defined by:

$$u(0,z)=\exp\left[\frac{-(z-z_0)^2}{g^2}\right] \qquad \text{Eq. 32}$$

And z_0 is the height of the antenna and g is the antenna beam aperture function. This factor is defined by the following equation [7]:

$$g=\frac{\frac{\log 2}{2}}{\left(\sin\frac{BW}{2}\right)^2} \qquad \text{Eq. 33}$$

Where BW is the antenna aperture angle related to the 3dB points of the main lobe of the antenna.

Given a solution (x, z) in the solution $(x + \Delta x, z)$ can be obtained by 31 since they have the boundary conditions defined top and bottom.

The use of discrete transforms means that the field needs to be artificially limited z, i.e., the condition $z \rightarrow \infty$ must be approximated by a boundary condition $z = z_{max}$ and an abrupt cut would result in strong reflections, for the condition upper contour would act as a perfect conductor.

One proposed solution would be satisfactory as set z_{max} twice the height of interest and applying a Hanning window [19] [2] in this extended region, ensuring the absorption of energy before z_{max} [5].

The use of the Fourier transform requires knowledge of the field below and above $z=0$. For a perfectly conducting surface, the boundary condition is $u(x, 0) = 0$ for horizontal polarization and $\partial u / \partial z = 0$ for vertical polarization. As the surface of the calm sea has reflection coefficient close to -1 for small elevation angles [20] as shown by Balvedi, 2006 [2] , you can use the theory of images [21] , according to which the boundary conditions to conductive surfaces can be satisfied if u is odd or even in relation $z = 0$, respectively, for horizontal and vertical polarization .

For this work was considered the sea as a perfectly conducting surface without losses to the range of microwave [2] and vertical polarization (characteristic of an air surveillance radar).

Computational implementation

Split-Step Fourier algorithm is directly implemented in MatLab®. Transformed are approximated by discrete amounts by means of Fast Fourier Transform - FFT.

First, one must determine the maximum propagation angle, θ_{max}. It is noteworthy that the parabolic approximation is only valid for low elevation angles, i.e. until 15°-20°.

Chosen θ_{max}, the step width z can be calculated:

$$\Delta z \leq \frac{2\pi}{2\,p_{máx}} \rightarrow \Delta z \leq \frac{\pi}{k \sin \theta_{máx}} \qquad \text{Eq. 34}$$

Since L is variable, the number of samples in z is defined:

$$L \geq \frac{2h}{\Delta z} \qquad \text{Eq. 35}$$

Where h is the height of the interest region and L for convenience should be a power of two. According to the Nyquist theorem, the number of samples S in the space p (field angle), which determines the size of the FFT should be twice the number of samples in z-space. Therefore:

$$S > 2L \qquad \text{Eq. 36}$$

The p in step size can be calculated by:

$$\Delta p = \frac{2\pi}{S\Delta z} = \frac{\pi}{L\Delta z} \qquad \text{Eq. 37}$$

So that $\Delta p \Delta z = \pi / L$ [17], the space p is set for:

$$p = S\Delta p \qquad \text{Eq. 38}$$

The step size in x, Δx, should be small enough so that errors are avoided that arise when considering constant m in the equation 31. The value of Δx used in the simulations is 400 m [4], which guarantees a result coherent.

Computational implementation of the prediction method

The method of parabolic equation was used to calculate the factor F, which is usually used for radar applications. This factor is defined by [7]:

$$F = \frac{E}{E_0} \qquad \text{Eq. 39}$$

Where E is the value of the field at a given point in space, including the standard effects of antenna radiation and E_0 is the value of the field at this same point in space conditions for isotropic antenna. The result of the parabolic equation is the electric field Ψ and thus the factor F is calculated by [10]:

$$F = 20 \log_{10} |\Psi(x,z)| - 10 \log_{10}(x) - 10 \log_{10}(\lambda) \qquad \text{Eq. 40}$$

The program was developed according to the features listed above. The expression 31 is the basis of the computational algorithm.

Initially it is necessary to determine the distance to be analyzed, the maximum height considered and the frequency of operation. The Δx and Δz steps should be established: taking up the operating frequency and the maximum angle of the spread Δz calculation is straightforward and step in Δx is based on the slightest mistake. Given the value of Δz, the value of L (z-space samples) is calculated and S (samples in the space p, or the FFT size) is twice the sampling rate z.

The left boundary, $x = 0$, represents the field coming from the antenna. In this case, the antenna function is opening the pair of far field of the Fourier described by the equation $f(z) = \exp[-g \,.\, (z - z_a)^2]$. This pattern refers to Gaussian radiation pattern.

For a vertically polarized wave and considering the surface of the calm sea as a perfectly reflective medium (reflection coefficient -1) formed the image field without phase shift (even symmetry).

The upper contour absorbs all the energy from the lower region, as an abrupt cut would make this a perfect conductor interface generating reflections. To avoid this effect was defined as the maximum height twice the desired, applying in this region a Hanning filter [2].

The domain of the implemented program is:

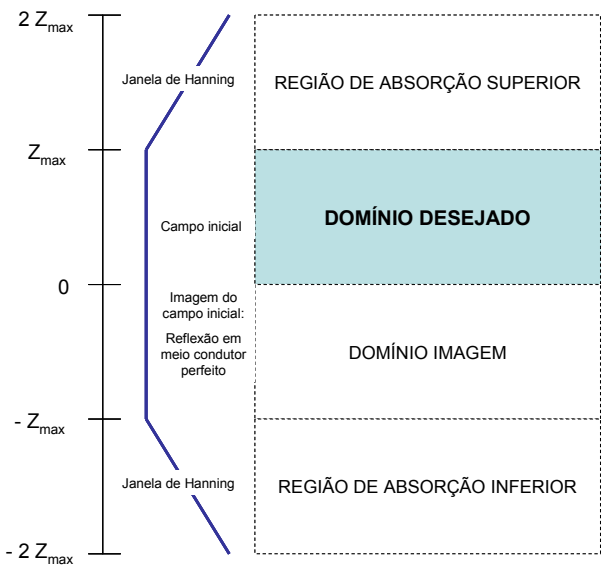

Figure 4. Domínio completo do modelo [2]

To implement this propagation model in the RADAR equation can follow the traditional method, including the effect of modifying the propagation equation of free space [5]. Thus was introduced the propagation factor (F) and atmospheric loss factor (L_a), as shown below [5]:

$$P_r = \frac{P_t G^2 \sigma \lambda^2}{(4\pi)^3 r^4 L} \cdot \frac{F^4}{L_a} \qquad \text{Eq. 41}$$

Where P_r is the received power, G is the maximum antenna gain, σ is the RCS (Radar Cross Section) of the target, λ is the wavelength, r is the distance between the RADAR and the target and L is the system loss.

The F factor considers the losses related to the pattern of the antenna radiation and the effects of propagation, since the L_a factor involves the effects of oxygen absorption and water vapor. Losses inherent in the F factor are considered the result of the parabolic equation while L_a is calculated by absorption equations presented in this work.

The L factor is other losses, such as noise figure, thermal noise and losses assumed the system. These losses are calculated by the following equation:

$$L = 10 \cdot \log_{10}\left(\frac{\kappa T}{\tau}\right) + N_f + L_s \qquad \text{Eq. 42}$$

Where κ is the Boltzmann constant (1,38 10^{-23} Joules/Kelvin), T is the temperature in Kelvin of the equipment, τ is the pulse width in µs, N_f is the noise figure in dB and L_s represents loss of the system.

It notes that from this point we have the target characteristics (RCS), radar equipment characteristics, surface conditions and weather.

ANALYSIS OF THE SOLUTION IMPLEMENTED

In this topic, shows of the radiation patterns generated by the programming implemented are demonstrated, in part, the ability of this solution. These diagrams show the same profile for a single azimuth, elevation on the vertical axis and distance on the horizontal axis and the color legend representing the values of the F factor.

Graphs were generated for pre-established conditions, which are: standard atmosphere (figure 5), limited surface duct at 200 meters [8] (figure 6) and high duct between 50 and 200 meters [10] (figure 7). Alves, in 2008, annexed the routines implemented in the published work.

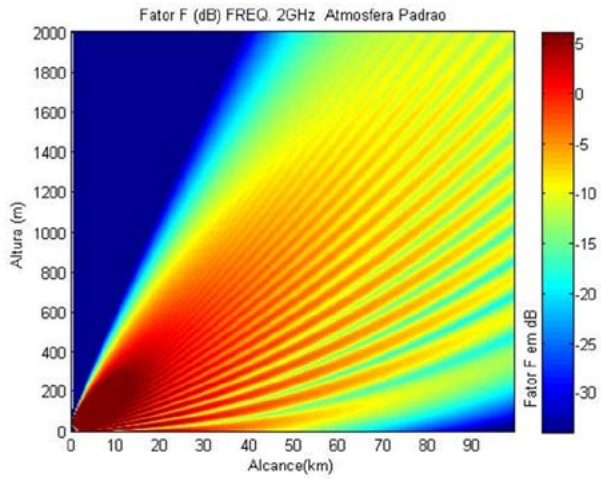

Figure 5. F factor.
Standard atmosphere.

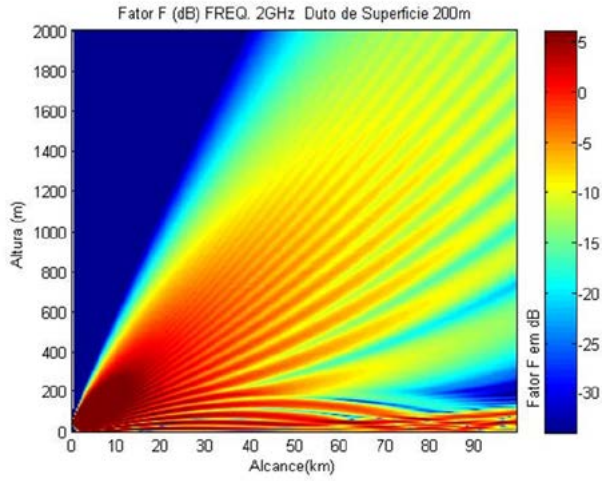

Figure 6. F Factor.
Surface duct limited to 200m.

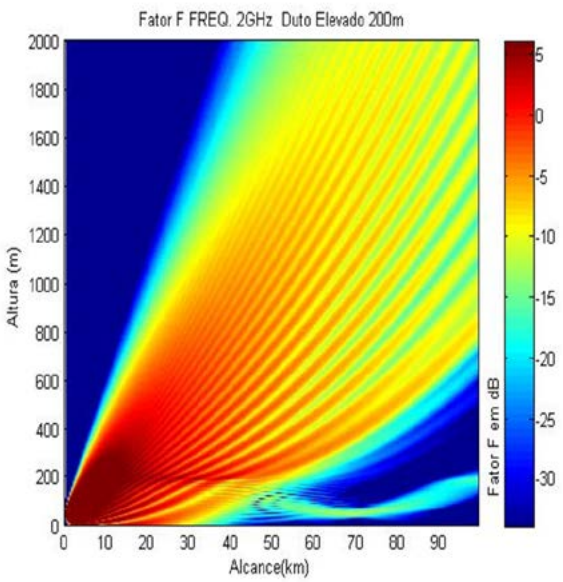

Figure 7 – F Factor.
Elevated duct between 50 and 200m.

Absorption related to oxygen and water vapor, presented in this article, have not been implemented due to the difficulty of programming.

As seen in the above figures, the radiation pattern is changed due to the refractive index, with different values of *F* for each position in space. Can also been seen the constructive and destructive patterns for the multipath, which arise from reflections on the surface. The upper area, just above the emitter (region highlighted by blue color - low intensity of *F*), does not correspond to the blind cone of radar system. This is because the algorithm used to implement features constraint for larger angles of propagation.

One proposed solution would be the implementation of the Split-Step Fourier Solution algorithm for Wide-Angle. In this other way to approach, the Split-Step solution emitter modeling undergoes changes allowing for higher angles of propagation, above 25º [22].

CONCLUSIONS

In this article, it was found that the radar performance evaluation is performed using a suitable combination of detection opportunity traffic or dedicated aircraft, recorded or simulated data BITE (built in test equipment) and RTQC (real time quality control).

It was also found that the assessment is carried out from parameters such as coverage, accuracy, detection performance and resolution.

The Flying Inspection procedures check the coverage on a marking, which is selected seeking the best electromagnetic propagation region. However, other sectors may have different performances in coverage because, depending on weather conditions and major variations, different targets would be detected at different distances and / or altitudes.

In this context, this work demonstrates the ability to predict the performance of a radar system, for all azimuths from appropriate mathematical modeling, considering the weather, terrain variations, characteristics of the target and of the radar system. It should be noted that the detection performance is also considered from the inclusion of *F* factor in radar equation.

This type of tool can also contribute to a radar site performance evaluation or in the face of changes in the system, as well as assessment of performance over the life of the equipment.

Therefore, such a computational tool helps as a decision aids for maintenance engineers and ATC staff in assessing the performance of various types of radar system, such as simulation tool and prediction of radar detection requirements. Consequently, it is possible to reduce the cost of this activity and allow less reliance on targets of opportunity and / or exclusive flight inspection.

FUTURE WORK

Indeed, the solution implemented yet lacks several developments, such as correlating to apply on the *F* factor graph of radar equation, introduction of roughened surfaces for interaction with the terrain, including attenuation caused by oxygen and vapor water as well as the use of wide-angle solution to cover the whole region of interest.

REFERENCES

[1] ICAO, 1998, Manual on Testing of Radio Navigation Aids, **Doc 8071**, Volume 3, Testing of Radar Surveillance Systems, 1st Edition.

[2] BALVEDI, Gláucia Costa. **Efeitos dos dutos troposféricos na propagação e recepção de sinais GPS**. 2006. 103f. Dissertação (Mestrado em Telecomunicações) – Instituto Tecnológico de Aeronáutica, São José dos Campos.

[3] SLINGSBY, P. L. Modelling tropospheric ducting on VHF/UHF propagation. **IEEE Transactions on Broadcasting**, v. 37, n. 2. p. 25-34, jun 1991.

[4] DOCKERY, G. D. Modeling electromagnetic wave propagation in troposphere using the parabolic equation. **IEEE Transactions on Antennas and Propagation,** v. 36, n.10, p.1464-1470, out. 1988.

[5] CRAIG, K. H.; LEVY M. F. Parabolic equation modeling of the effects of multipath and ducting on RADAR systems. **IEE Proceedings – F**., v. 138, n. 2, p. 153-162, abr. 1991.

[6] AWADALLAH, R. S. et al. Modeling RADAR propagation in three dimensional environments. **Johns Hopkins Technical Digest**, v. 25, n. 2, p. 101-111, 2004.

[7] PATTERSON, W. L. et al. **Engineer's refractive effects prediction system (EREPS)**. San Diego: NRDA, 1994. (NRDA TD 2648)

[8] HALL, M. P. M.; BARCLAY, L. W.; HEWITT, M.T. **Propagation of radiowaves**. London: The Institution of Electrical Engineers, 1996. 446p.

[9] ISAAKIDIS, S. A.; XENOS, T. D. Parabolic equation solution of tropospheric wave propagation using FEM. **Progress in Electromagnetic Research**, PIER 49, p.257-271, 2004.

[10] LEVY, M. F. **Parabolic equation methods for electromagnetic wave propagation**. London: The Institution of Electrical Engineers, 2000. 349f.

[11] BOITHIAS, L. **Radio wave propagation**. London: North Oxford Academic Pub., 1987. 330p.

[12] ALVES, Bruno Michel Marcondes. **Modelos de Propagação para Aplicação em Sistemas RADAR**. 2008. 98f. Monografia (Curso de Especialização em Análise do Ambiente Eletromagnético) – Instituto Tecnológico de Aeronáutica, São José dos Campos.

[13] SPAWAR, Space and Naval Warfare Systems Center. **Software design description for the advanced propagation model CSCI, version 2.1.04**. San Diego, CA, 2006. 438 p. (Technical document 3214)

[14] SAPUCCI, Luiz Fernando. **Estimativa do vapor d'água atmosférico e avaliação da modelagem do atraso zenital troposférico utilizando GPS**. 2001. 193f. Dissertação (Mestrado) – Universidade Estadual Paulista, Presidente Prudente.

[15] KUTTLER, J. R.; DOCKERY, G. D. Theoretical description of the parabolic approximation / Fourier Split-Step method of representing electromagnetic propagation in the troposphere. **Radio Science**, v. 26, n. 2, p. 381-393, mar. 1991.

[16] CRAIG, K. H. Propagation modeling in troposphere: parabolic equation method. **Electronic Letters,** v. 24, n. 18, p. 1136-1139, set. 1988.

[17] BARRIOS, A. E. A terrain parabolic equation model for propagation in the troposphere. In: **IEEE Transactions on Antennas and Propagation**, v. 42, n. 1, jan. 1994.

[18] LEVY, M. F. Transparent boundary conditions for parabolic equation solutions of radiowave propagation problems. **IEEE Transactions on Antennas and Propagation,** v. 45, n.1, p.66-72, jan. 1997.

[19] HANNAH, B. M. **Modelling and simulation of GPS multipath propagation**. 375f. 2001. Tese (Doutorado em Filosofia) - The Cooperative Research Centre for Satellite Systems, Queensland University of Technology, Brisbane.

[20] CINTRA, R. S. C. et al. Inclusão de dados ATVOS no sistema de assimilação de dados GPSAS do CPTEC. In: SIMPÓSIO BRASILEIRO DE SENSORIAMENTO REMOTO, 12., 2005, São José dos Campos. **Anais XII Simpósio Brasileiro de Sensoriamento Remoto**. São José dos Campos: INPE, 2005. p.2917-2924

[21] BALANIS, C. A. **Advanced engineering electromagnetics**. Nova York: Wiley, 1989. 981p.

[22] KUTTLER, R. J. Differences between the narrow angle and wide angle propagators in the split-step Fourier solution of parabolic wave equation. **IEEE Transactions on Antennas and Propagation**, v. 47, n. 7, p. 1131-1140, jul. 1999.

Flight Testing of Localizer Coverage in China and Analysis on Typical Cases

Liu. Shuming
Flight Inspector
Flight Inspection Center of CAAC
Chaoyang District, Beijing, China
Fax : + 0086-010-64542800
E-mail: cficlsm@163.com 409849193@qq.com

Liu. Tong
Director
Inspection Department
Flight Inspection Center of CAAC
Chaoyang District, Beijing, China
Fax: + 0086-010-64542800
E-mail: ltzhlsm@sina.com

ABSTRACT

Flight testing of localizer (LOC) coverage is a very important profile of ILS flight inspection, which provides the ILS Flight Procedures designers and the aircraft pilots with the available localizer signal-in-space coverage area and it also determines the localizer's restriction area caused by insufficient signal strength or hazard terrain.

The purpose of this paper is to introduce how Flight Inspection Center of CAAC (CFIC) conducts localizer coverage check and the newest periodic inspection rules China Flight Inspection Center (CFIC) issued for the increasing "long final[1]" ILS Approach Procedures. The writers also analyze the cause of the "restriction" conclusion through four typical cases.

INTRODUCTION

This paper makes an introduction of the flight testing of LOC coverage in China from three aspects as follows: the coverage area, signal strength and flight method.

Coverage Area

International Civil Aviation Organization (ICAO) Annex 10, Volume 1 *Radio Navigation Aids* [1] defines the Standard Service Volume (SSV) of LOC as follows:

1. *46.3 km (25 NM) within plus or minus 10 degrees from the front course line;*
2. *31.5 km (17 NM) between 10 degrees and 35 degrees from the front course line;*
3. *18.5 km (10 NM) outside of plus or minus 35 degrees if coverage is provided;*
4. *Such signals shall be receivable, to the distances specified, up to a surface extending outward from the localizer antenna and inclined at 7 degrees above the horizontal.*

Similarly, as the guidance on the flight testing of ground based radio navigation systems, ICAO Doc 8071 has the same requirements.

Civil Aviation Administration of China (CAAC) specifies the SSV of LOC the same as ICAO Annex 10 except that the area outside of plus or minus 35 degrees is not required, as Figure 1 shows.

For most airports, only a small part of the SSV of LOC is used by the ILS approach procedure. Most of the other area of the SSV of LOC is used to provide the aircrafts with an accurate indication under some other circumstances, such as holding patterns or flight directed by the Air Traffic Control (ATC).

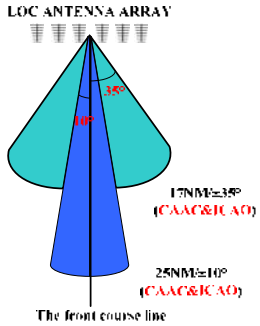

Figure 1. The SSV of LOC Defined by CAAC

[1] "Long final" in this paper means the ILS procedure whose intermediate approach fix (IF) is more than 17 nautical miles (NM) far away from the LOC antenna array.

Signal Strength

Tolerance

Table I-4-7 in ICAO 8071, volume 1, chapter 4 [2] specifies that *the signal strength of LOC should not be less than* $40\mu V/m$ $(-114\ dBW/m^2)$; likewise, ICAO Annex 10, Volume 1 3.1.3.3.1 requires that "*the field strength shall be not less than 40 microvolts per meter (minus 114* dBW/m^2*)*".

Different form the definition mentioned above, the *Flight Inspection Rule MH 2003-2000* issued in the year 2000 [3] by CAAC states that:

Within the scope of 17NM far away from the LOC antenna array, plus or minus 35 degrees from the LOC course line and 25NM far away from the LOC antenna array, plus or minus 10 degrees from the LOC course line, the identification code is correct and clear, the course signal is stable and the signal strength shall be not less than 5 μV *(-93* dbm*).*

The units of the LOC's signal strength measured by the flight inspection systems of CFIC are in dbm .ICAO 8071 volume 1 4.3.35 states that :

Adequate coverage for modern aircraft systems may be defined by a signal level of 5 microvolts.

Next, let us find out the conversion relationship between the different power units through theoretical analysis and calculation.

Conversion Relationship

The signal transmitted by the LOC antenna array is horizontally polarized, of which the carrier frequency is between 108~112MHz. It has the time-varying electric field $\boldsymbol{E}$ and magnetic field $\boldsymbol{H}$. The direction of $\boldsymbol{E}$ and $\boldsymbol{H}$, and the direction of the LOC signal propagation obey the right-hand rule. The Poynting vector $\boldsymbol{S}$ [4] is defined as:

$$\boldsymbol{S} = \boldsymbol{E} \times \boldsymbol{H} \ \left(W/m^2\right)$$

The unit of $\boldsymbol{S}$ is W/m^2, and the direction of $\boldsymbol{S}$ is along the wave's direction of propagation. Thus, $\boldsymbol{S}$ represents the power per unit area (or power density) carried by the wave.

As the propagation medium of the LOC signal, air is a lossless medium. The Poynting vector $\boldsymbol{S}$ in space is $\boldsymbol{S} = \vec{k}\frac{|\boldsymbol{E}|^2}{\eta}$, of which $\vec{k}$ is the unit vector along the propagation direction, and η is the characteristic resistance of electromagnetic wave propagation medium, as for air,

$$\eta = \eta_0 = 120\pi\ \Omega \approx 377\Omega$$

Apply the above formula to the definition in ICAO 8071 and ICAO Annex 10, the corresponding power density of the signal whose field strength is $40\mu V/m$ is :

$$S = \frac{(40*10^{-6})^2}{377}\ W/m^2 = 4.244\times10^{-12}\ W/m^2$$

Convert the unit of power density to Decibel

$$S = 10\log 4.244\times10^{-12} = 10\times(-11.37)\ dBW/m^2$$
$$\approx -114\ dBW/m^2$$

Nowadays all the input impedance of aviation navigation receiver is 50Ω. For 5 μV input level , the input power is:

$$P = \frac{V^2}{R} = \frac{(5\times10^{-6})^2}{50} = 5\times10^{-13}W$$

Convert the unit to dbm

$$P = 10\log\frac{P}{1000} = 10\times\log(5\times10^{-3})\ dbm$$
$$\approx 10\times(-9.3)dbm = -93dbm$$

The length of the LOC antenna added to the flight inspection aircraft of CFIC is about 20cm, as shown in figure 2, whose parameters are listed in figure 3. Compared with the approximately 3m wave length, the time-varying current on the antenna can be regarded as uniform, for the $40\mu V/m$ $(-114\ dBW/m^2)$ field strength, the output voltage of the antenna is about $V \approx EL = 40\mu V/m\times0.2m = 8\mu V$. Even if the gain of the antenna reaches $-2dB$ at worst, regardless of the loss on transmission cables, the input voltage level of the navigation receiver is about

$$V_{in} = 8\mu V\times10^{(\frac{-2}{20})} \approx 8\mu V\times0.8 = 6.4\mu V > 5\mu V$$

The calculations above indicate that, the requirements for LOC signal strength in Flight Inspection Rule MH 2003-2000 is in accordance with ICAO 8071 and ICAO Annex 10.

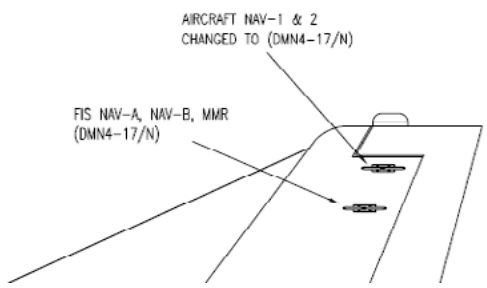

Figure 2. Flight Inspection System Antenna of the Flight Inspection Aircraft

Currently, the onboard flight inspection system set $-93dbm$ to be the tolerance of LOC signal strength.

SPECIFICATIONS	
Electrical	
Frequency Range	
VOR/LOC	108 - 118 MHz
Glide slope	329 - 335.3 MHz
VSWR	5.0:1 max
Gain	0 ±2 dB
Impedance	50 Ohms
Polarization	Horizontal
Radiation Patterns	
VOR/LOC	Omnidirectional
Glide slope	Forward Pointing
Lightning Protection	dc short

Figure 3. Parameters of the LOC Antenna

Flight Method

During a LOC coverage test, the flight inspection aircraft flies a circular arc at the minimum coverage height (MCH). The radius of the arc, which is the distance from the LOC antenna array is 17NM. The arc starts at -35°and ends at +35°.

A 25NM/±10° arc flight test at the height of minimum coverage height (MCH) is conducted additionally for a commissioning test. Figure 4 shows the flight method.

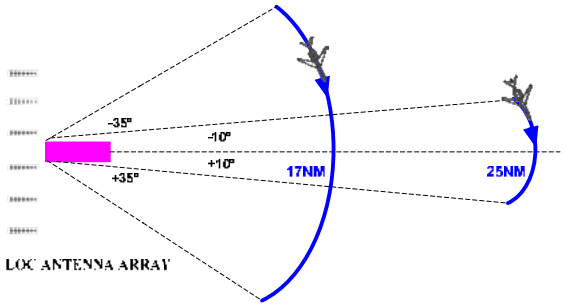

Figure 4. Flight Method of the Flight Test of LOC Coverage

The height of the flight test is extremely important, which affects the conclusion of the LOC coverage to a large extent and it also determines the flight safety of the inspection aircraft. The flight test of LOC coverage is conducted at the minimum coverage height (MCH). Once the MCH is set, the flight height cannot be changed during the flight testing. The MCH varies between different airports and different ILS procedures. CFIC defines MCH as the highest of the three heights below:

1) The height of 600m (2000ft) above the elevation of the threshold.

2) The height of 300m (1000ft) above the elevation of the highest point within the intermediate and final approach protection areas.

3) The height of intercept point of the glide-path of the ILS approach procedure.

During a commissioning test, the LOC coverage test should be conducted under the power-alert status.

RULES CFIC ISSUED FOR LONG FINAL ILS PROCEDURES

The number of high elevation airports increases continuously in China these years. Compared with the plain airports, the air density is lower and the aircraft engine power decreases in the high elevation airports, so the aircraft's mobility also decreases. Meanwhile, the wind speed and wind direction is changeable near the high altitude airports, so turbulence and wind shear is frequently seen. For these reasons, the ILS procedures of the high elevation airports mostly have a long final. Airports in the mountainous areas may also have a long final ILS procedure due to the poor clearance condition to enable the aircraft to descend at an appropriate height.

As for the long final ILS procedures, the LOC coverage test CFIC conducted without checking the 25NM/±10° arc in the past is not sufficient to support the procedures. In order to further ensure the rigor of the flight test and make sure that the LOC signal coverage is able to support the flight procedures, CFIC issued a new rule *Notification on Perfecting the Periodic Flight Test Method on LOC Coverage*. Owing to space reasons and in order to introduce the notification better, this paper summarizes the notification as shown in table 1.

Table 1. Summary of the Notification

Test / Scope	17NM/±35°	25NM/±10°*	IF/±10°*
IF <17NM	C, P	C	
17NM <IF< 25 NM	C, P	C, P	
IF> 25 NM	C, P		C, P

NOTE：1、C=Commissioning P= Periodic

2、*If the procedure covers more than ±10°, a test on the expanded LOC service volume should be conducted based on the actual angle to make sure that the tested area includes all the ILS procedure.

Now all the LOC coverage tests in China are conducted according to the notification mentioned above. It makes the LOC coverage test more elaborate and it also provides the equipment maintenance engineers, the ILS flight procedures designers, the aircraft pilots and the air traffic controllers with the most reliable reference about the LOC coverage.

RESTRICTION ON THE LOC COVERAGE

Restriction on the LOC coverage is most common among the ILS restrictions and all the equipment maintenance engineers and administration departments pay very close attention to it. This paper makes introduction of the importance and causes of the restriction on the LOC coverage.

Importance of Restriction

The restriction conclusion in the flight inspection reports marked the area where the LOC signal is out of service. Some of the conclusions restrict the distance range while the others restrict the angle range.

The importance of the restriction is just like "mine clearance", the flight test aircraft flies at a super-low-altitude to find out the hazardous areas where the LOC signal is unusable, which provides the ILS flight procedures designers and the aircraft pilots with the most reliable, direct and effective reference.

Causes of Restriction

The restriction conclusions vary from equipment to equipment, but the causes of restriction focus on two points: 1.the equipment itself 2.terrain.

Restriction caused by the equipment itself is uncommon, which usually appears during a periodic test. For example, ageing of the LOC antennas, loose contact of the cable plug and transmitter's own problems may all cause a restriction. The alignment of the LOC course line will be abnormal at the same time and the monitor may even alert. The restriction caused by the equipment itself is easy to find and get rid of.

Restriction caused by terrain is most common. One situation is shown in figure 5, a mountain whose elevation is 1200m lies 15 degrees right of the LOC front course, 17NM far away from the LOC antenna array. If the aircraft conducts the 17NM /±35° arc test and flies at 800 meters high MCH, due to the mountain, the aircraft cannot accomplish the whole 17NM /±35° arc, which causes a distance restriction or an angle restriction to the LOC.

For an angle restriction, the conclusion may be:

The LOC signal beyond (-) 10° right of the front course line is unusable (taking the radius of turning circle into account).

For a distance restriction, if 14NM is sufficient for the ILS procedure and if the aircraft can conduct a 14NM/±35° arc test, the conclusion may be:

The LOC signal beyond 14NM far away from the LOC antenna is unusable.

The other kind of restriction caused by terrain is shown in figure 6, the elevation of the obstacle is acceptable on the 17NM /±35° arc, but somewhere inside the area lays a high mountain which shields the LOC signal when the aircraft, the mountain and the LOC antenna are in a straight line. If the mountain is so high and huge that the LOC signal cannot diffract, then the signal strength of the flight inspection system received may be less than -93 *dbm* , and an angle restriction will follow.

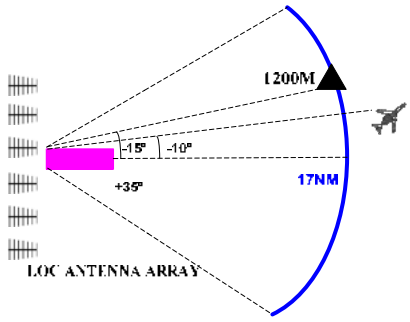

Figure 5. Restriction Caused by Terrain (1)

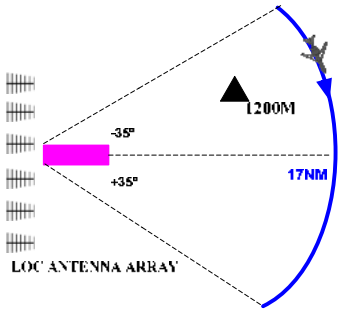

Figure 6. Restriction Caused by Terrain (2)

Many maintenance engineers worries a lot at the mention of "restriction". The restriction conclusion often provides the ILS flight procedures designers, the aircraft pilots with the terrain information inside the SSV of the LOC. The restriction conclusion on the LOC has a positive significance when it is not caused by the equipment itself and when the restriction does not affect the ILS procedure.

CASES ANALYSIS

This paper analyzes the causes of the LOC coverage restriction, the LOC coverage flight test on the long final ILS procedures and especially the calculation of the minimum coverage height (MCH) through 4 cases as follows.

Case 1

During a LOC commissioning flight inspection, the signal strength was found to be insufficient when the aircraft conducted the 17NM/±35° arc LOC coverage test. However, no obvious high obstacle was discovered by the flight inspection crew inside the 17NM area. The power of the transmitter could be increased and the LOC's coverage was restricted to 13NM, which was able to support the ILS procedure.

After the commissioning flight inspection, the airport took the coverage restriction seriously. They first eliminated the possibility of the equipment itself, then a hill laid on the side the runway was suspected to shield the LOC signal, and the hill was removed later.

The writer attended the surveillance inspection 3 months later. At the maintenance engineers' request, the

crew rechecked the LOC coverage. The signal strength was satisfied during the 17NM /±35° arc test. A 25NM /±10° arc test was added for changing the restriction conclusion but the signal strength was out of tolerance, finally, the signal strength was sufficient in the 20NM / ±10° arc test and the restriction conclusion changed to:

The LOC signal beyond 20NM far away from the LOC antenna is unusable.

Case 2

The signal strength was found to be insufficient when the aircraft conducted the 17NM/ ± 35° arc LOC coverage test during a LOC commissioning flight inspection. The airport was located in plain area, the terrain was good and the equipment itself was working in normal condition. Through analysis, the maintenance engineers doubted that the LOC antenna was not erected highly enough, so they raised the LOC antenna by 1 meter, and the LOC signal strength met the requirement.

Further analysis, the earth surface seems to be horizontal, but indeed the earth is a sphere and human being's eyes cannot feel its radian. As shown in figure 7, if the LOC's antenna is erected too low, the obstacles inside the SSV shield the LOC signal more easily, the signal strength is weakened, and thus the LOC antenna should be erected higher.

Figure 7. The Signal Strength Weakened by the Radian of the Earth

Case 3

Figure 8 shows the 16# ILS procedure of an airport in the mountainous area of southwestern China. The writer participated in a periodic inspection of the ILS in 2015.

The IF point is 19NM far away from the threshold, so besides the 17NM /±35° arc test, a 25NM /±10°arc is required during periodic test according to the *Notification On Perfecting the Periodic Flight Test Method on LOC Coverage*.

When calculated the minimum coverage height (MCH), we got

1) The threshold elevation + 600m = 1150m

2) The height of intercept point of the glide path = 1280m

If the aircraft flies at 1280m, the LOC signal is easily shielded by the mountains, what is more, the terrain between 19NM and 24NM far away from the threshold is so rough that the aircraft cannot fly at 1280m in the area. However, if the test radius is less than 19NM, the procedure cannot be used because that means the LOC signal does not support the ILS procedure.

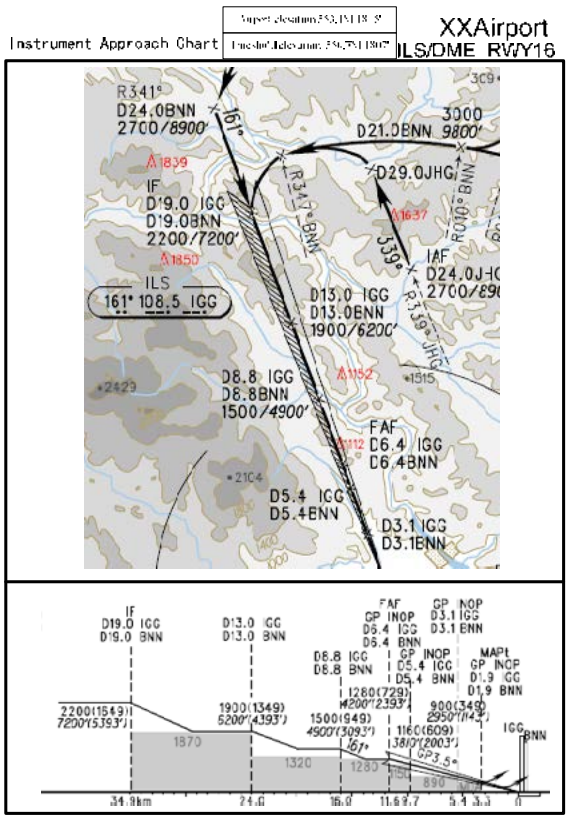

Figure 8. The ILS Procedure of a Mountainous Airport

Finally, the writer checked the elevation of the highest point within the intermediate and final approach protection areas. There are altogether 5 obstacles involved in the approach chart; they are the 1839m, 1637m, 1152m, 1112m and 1850m mountains marked with red font in the chart. The 1839m mountain is far beyond the IF point so it is outside of the intermediate approach segment, and it was not taken into account when calculating the MCH.

In ICAO Doc8168 *Procedures for Air Navigation Services – Aircraft Operations*, Volume 2 -*Construction of Visual and Instrument Flight Procedures* [5], the width of the intermediate and final approach areas are defined as follows:

The intermediate segment:

The total width at the beginning of the intermediate approach segment is defined by the final total width of the initial approach segment. It tapers uniformly to match the horizontal distance between the Obstacle Assessment Surface (OAS) X surfaces at the Final Approach Point (FAP).

For obstacle clearance purposes the intermediate approach segment is usually divided into a primary area bounded on each side by a secondary area.

The primary area is determined by joining the primary initial approach area with the final approach surfaces (at the FAP). At the interface with the initial approach segment the width of each secondary area equals half the width of the primary area. The secondary area width decreases to zero at the interface with the final approach surfaces.

The initial approach segment area for this procedure is also divided into a primary area and a secondary area in Doc8168. The half width of the primary area at IF is 2.5NM and the secondary area is 2.5NM as well at IF.

As for the final approach segment, the protection area of the final approach segment is determined by the Obstacle Assessment Surface (OAS), which is decided by the category of the ILS and the size of the aircraft, etc.

The OAS consist of six sloping plane surfaces (denoted by letters W, X, Y and Z) arranged symmetrically about the precision segment track, together with the horizontal plane which contains the threshold, The geometry of the sloping surfaces is defined by four linear equations of the form z = Ax + By + C.

The calculation of the OAS is very complicated and this paper does not cover the details, the readers can refer to Doc8168 for more information.

Figure 9 shows the protection area of the ILS procedure.

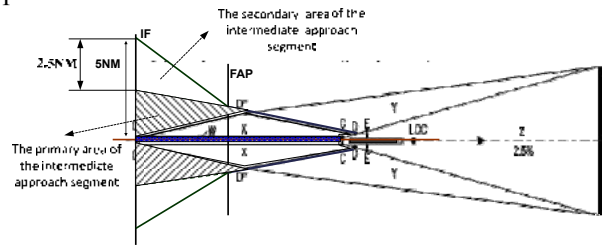

Figure 9. The Protection Area of the ILS Procedure

Based on the definition mentioned above, it can be measured with a ruler (The proportion of the approach procedure chart is 1:500000) that the 1850m high mountain is in the protection area of the intermediate approach segment of the ILS procedure. Table 2 shows the segments that the five mountains related to from the *Aeronautic Information Publication* of the airport, from which we can see that the 1850m high mountain is a controlling obstacle of the RWY16 intermediate segment.

Table 2. Segments the Five Mountains Related to

	Location（Relative to the airport reference point）		Elevation (m)	Controlling Obstacle and the Segment related to
	Magnetic Bearing（Deg）	Distance(m)		
1	332	14478	1112	Controlling obstacle of the RWY16 intermediate segment step-down fix
2	001	33200	1637	Controlling obstacle of the RWY16 initial segment
3	**327**	**35500**	**1850**	**Controlling obstacle of the RWY16 intermediate segment**
4	332	43200	1839	Controlling obstacle of the RWY16 initial segment
5	348	20200	1152	Controlling obstacle of the RWY16 intermediate segment

Finally, the writer selected 1850+300 =2150m to be the MCH, and the aircraft checked the LOC coverage at 2150m high, the signal strength was sufficient.

Case 4

Figure 10 is the sketch of an ILS procedure with step-down fix, and the ILS belongs to an airport located in a mountainous area. According to this procedure, the aircraft intercepts with the LOC course and carries on a step-down descent until intercepting the glide path.

When checking the LOC coverage, the inspector found that the MCH was just the height of the FAF, however, the terrain was very rough in the area beyond 11NM far away from the threshold, where there are several obstacles higher than 700m. The inspection aircraft could barely conduct a 14NM /±35° arc coverage test, and it had to fly over a 600m high mountain during the test, which made the flight test more difficult and more dangerous.

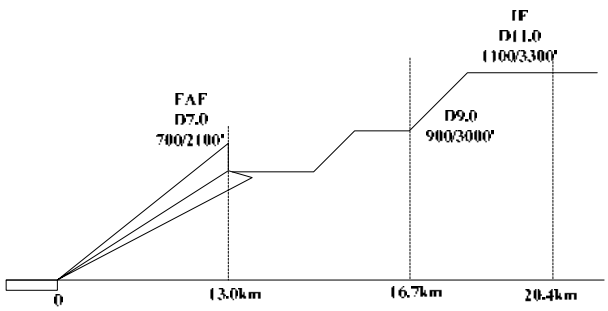

Figure 10. The ILS procedure with step-down fix

The ILS passed the inspection and when the inspectors reviewed the mission, they suggested that the procedure to be optimized as shown in figure 11, which has the following advantage:

1. To raise the intercept height of the glide path from 700m to 1100m, thereby the MCH is raised as well, which will not only increase the efficiency of the subsequent periodic test, but also make the flight test safer and expand the restricted coverage of the LOC

2. To replace step-down descent with continuous descent, this will reduce the workload of the pilots during the approach.

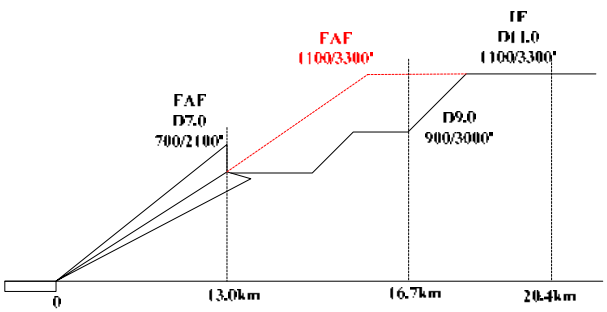

Figure 11. The Optimized ILS Procedure

However, the optimized procedure moves the FAF further away from the runway threshold, which enlarges the final segment. This will increase the procedure designers' work on computing the OAS. What is more, because the minimum obstacle clearance (MOC) of the primary area of the intermediate segment is 150m which is different from the OAS, the new OAS maybe penetrated by the obstacle in the original intermediate area and this is not permitted. Under this circumstance, the glide slope angle could be raised if the height of FAF must be raised. The highest glide slope angle permitted is 3.5° .

CONCLUSION

Flight testing of localizer (LOC) coverage is a very important profile of ILS flight inspection, this paper analyzed the causes the restriction on the LOC coverage through practical cases. The majority of the restriction conclusions are caused by terrain and they are not easy to eliminate or ameliorate. To eliminate or ameliorate the restriction, a huge economic cost is involved. Under the premise that the restriction does not affect the procedure, the restriction on LOC has its positive meaning and we suggest a neutral attitude be took up towards the LOC restriction.

Meanwhile, this paper introduced the flight test method of the LOC coverage of the long final ILS procedure in China and made an analysis on how to calculate the MCH.

REFERENCES

[1] ICAO Annex 10 Fifth Edition-1996
[2] ICAO Doc 8071 Fourth Edition-2000
[3] Flight Inspection Rule MH 2003-2000 MH2003-2000
[4] Fawwaz T. Ulaby. APPLIED ELECTROMAGNETICS [M] .PEARSON 2010
[5] ICAO Doc 8168 OPS/61 Fifth Edition-2006

Notes

Notes

Notes

Exhibitors

Exhibitor

SAFRAN

Sagem Defense Securite

Exhibitor

ROHDE&SCHWARZ

Rohde & Schwarz Gmbh & Co. KG

Exhibitor

ENAV

Enav S.p.A.

Exhibitor

CGX

CGX Aero

Exhibitor

RMS INSTRUMENTS
Data Recording Systems

RMS Instruments

Exhibitor

RADIOLA AEROSPACE

Radiola Aerospace Limited

AIRFIELD TECHNOLOGY

Building the world's best flight inspection and procedure validation systems

www.airfield.com

Airfield Technology, Inc.
12897 West 151st Street
Olathe, Kansas 66062 USA
Tel +1 913 780-9800

UNIFIS 3000 / 2000

SBAS, GBAS, ADS-B, Datalink FANS 1/A, PBN, IFP

COCKPIT INTERFACE

MFD, FMS, A/P, FPL upload, Tablet / WIFI, Adv. guidance

ACCURACY

DGPS RTK, OmniSTAR, UNICAM, DRTT

CONSOLE

Low weight composite, Certified, Easy installation

CONNECTED

Downlink / Uplink / Remote control (UAS)

Norwegian
Special Mission

PERFORMANCE

Real time, ED-109 SW QA, Innovative HMI, Remote access, Adv. reports

www.nsm.aero

Sponsors

IFIS Signature Sponsor / Exhibitor

aerodata®

[precision in special mission]

Aerodata AG

Gala Dinner Sponsor / Exhibitor

Norwegian Special Mission

Norwegian Special Mission

Gala Entertainment Sponsor / Exhibitor

AIRFIELD TECHNOLOGY

Airfield Technology

Breakfast Sponsor

AeroPearl

AeroPearl Pty Ltd

Coffee Break Sponsor / Exhibitor

FCS Flight Calibration Services

skyguide

FCS & Skyguide

Coffee Break Sponsor / Exhibitor

IDS INGEGNERIA DEI SISTEMI

IDS – Ingegneria Dei Sistemi

Supporting Organization

ICAO · OACI · ИКАО

ICAO

Supporting Organization

International Committee for Airspace Standards and Calibration

ICASC

Many thanks to our 2016 Sponsors and Exhibitors, who lent their support with such respect and courtesy and their admirable role in making this year's IFIS a success. Special thanks to all our speakers, who contributed so graciously their time to be with us; and to the support stuff, all friends and colleagues whose efforts and talent ensured an outstanding event.